AGARD

ADVISORY GROUP FOR AEROSPACE RESEARCH & DEVELOPMENT

7 RUE ANCELLE 92200 NEUILLY SUR SEINE FRANCE

AGARD REPORT No. 712

Special Course on Subsonic/Transonic Aerodynamic Interference for Aircraft

NORTH ATLANTIC TREATY ORGANIZATION

DISTRIBUTION AND AVAILABILITY
ON BACK COVER

NORTH ATLANTIC TREATY ORGANIZATION

ADVISORY GROUP FOR AEROSPACE RESEARCH AND DEVELOPMENT

(ORGANISATION DU TRAITE DE L'ATLANTIQUE NORD)

AGARD Report No.712

SPECIAL COURSE ON SUBSONIC/TRANSONIC AERODYNAMIC INTERFERENCE FOR AIRCRAFT

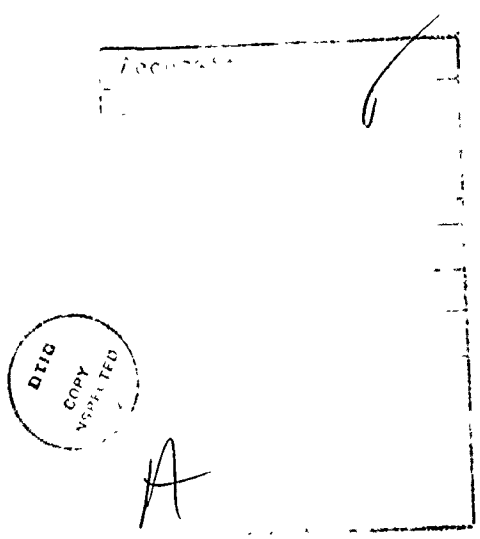

The material assembled in this book was prepared under the combined sponsorship of the Fluid Dynamics Panel, the von Kármán Institute and the Consultant and Exchange Program of AGARD and was presented as an AGARD Special Course at the von Kármán Institute, Rhode-St-Genèse, Belgium on 2–6 May 1983 and at Wright-Patterson AFB, Dayton Ohio on 16–20 May 1983.

THE MISSION OF AGARD

The mission of AGARD is to bring together the leading personalities of the NATO nations in the fields of science and technology relating to aerospace for the following purposes:

- Exchanging of scientific and technical information;
- Continuously stimulating advances in the aerospace sciences relevant to strengthening the common defence posture;
- Improving the co-operation among member nations in aerospace research and development;
- Providing scientific and technical advice and assistance to the North Atlantic Military Committee in the field of aerospace research and development;
- Rendering scientific and technical assistance, as requested, to other NATO bodies and to member nations in connection with research and development problems in the aerospace field;
- Providing assistance to member nations for the purpose of increasing their scientific and technical potential;
- Recommending effective ways for the member nations to use their research and development capabilities for the common benefit of the NATO community.

The highest authority within AGARD is the National Delegates Board consisting of officially appointed senior representatives from each member nation. The mission of AGARD is carried out through the Panels which are composed of experts appointed by the National Delegates, the Consultant and Exchange Programme and the Aerospace Applications Studies Programme. The results of AGARD work are reported to the member nations and the NATO Authorities through the AGARD series of publications of which this is one.

Participation in AGARD activities is by invitation only and is normally limited to citizens of the NATO nations.

Published July 1983

ISBN 92-835-0332-5

Printed by Specialised Printing Services Limited
40 Chigwell Lane, Loughton, Essex IG10 3TZ

PREFACE

The course was a follow-up to an AGARD Fluid Dynamics Panel Syposium on Subsonic/ Transonic Configuration Aerodynamics held in Neubiberg (Munich) in May 1980. As in the symposium the emphasis of the course was on the configuration optimization in the transonic regime where both military and commercial aircraft must cruise efficiently and where military aircraft must maneuver in an agile but stable manner. The course material was updated and presented in a more structured fashion emphasizing the fluid dynamic interference mechanisms that are the keys to the optimization. In addition, some aspects of subcritical interference were also covered, including those arising in the takeoff and landing phase of the flight with high lift devices deployed.

SPECIAL COURSE STAFF

Special Course Director — Dr H.Yoshihara
Boeing Company, M/S 3N-19
P.O. Box 3707
Seattle
Washington 98124
USA

LECTURERS

Professor A.Jameson
57 Hemlock Circle
Princeton
New Jersey 08540
USA

Mr J.Slooff
NLR
Anthony Fokkerweg 2
1059 CM Amsterdam
Netherlands

Dr R.Whitcomb
46 Lakeshore Drive Apt. 1B
Hampton
Virginia 23666
USA

Mr I.Rettie
Boeing Company, M/S 7993
P.O.Box 3707
Seattle
Washington 98124
USA

Mr A.B.Haines
Chief Executive
Aircraft Research Association
Manton Lane Bedford MK41 7PF
UK

Dipl. Ing. G.Krenz
VFW-GmbH
Hunefelstr. 1 5
D-2800 Bremen 1
Germany

Mr A.Vint
Principal Aerodynamicist
British Aerospace PLC
Warton Division
Preston, Lancashire
UK

Mr Ph.Poisson-Quinton
Director, International Cooperations
ONERA
29 Avenue de la Division Leclerc
92320 Châtillon
France

LOCAL COORDINATOR

Professor J.Wendt
Von Kármán Institute for Fluid Dynamics
Chaussée de Waterloo 72
B-1640 Rhode-Saint-Genèse
Belgium

AGARD REPRESENTATIVE

Mr R.H.Rollins, II
Fluid Dynamics Panel Executive
AGARD
7 rue Ancelle
92200 Neuilly-sur-Seine
France

CONTENTS

* Paper not available at time of printing.

SUBSONIC/TRANSONIC AERODYNAMIC INTERFERENCE FOR AIRCRAFT-INTRODUCTORY REMARKS

by
H. Yoshihara
The Boeing Company
P. O. Box 3707, M/S 3N-19
Seattle, WA 98124
USA

SUMMARY

These introductory remarks provide examples of important subsonic and transonic fluid dynamic mechanisms that make up interference concepts used in aircraft optimization. The rationale for the lecture topic selection and the course outline are then given.

1.. INTRODUCTION

Aerodynamic interference in aircraft is defined as the change in the flow over given elements of the configuration due to the presence of one or more of the other elements. Interference can arise, for example, locally between the aft camber portion of an airfoil and the forward portion, or more globally between the nacelle/pylon and the wing. In practice interference considerations are tied closely to the optimization of aircraft. Of particular importance is the transonic regime where crucial performance requirements arise for both military and commercial aircraft. Here interference effects are magnified by the sensitivity of the flow to perturbations, particularly with shock waves present. Unfavorable interference in the transonic regime can have intolerable consequences, but also skillful design can lead to favorable interference.

Aerodynamic interference is however pervasive over the entire operating spectrum of the aircraft. In the present lectures, in addition to the transonic interference, we shall consider some aspects of subcritical interference arising for example in the takeoff and landing phase of the flight with high lift devices deployed. There are important interference effects in the supersonic regime, but we shall not consider these in the present lectures.

In the remaining portion of these introductory remarks, we shall first briefly review an important fluid dynamic ingredient in interference; namely, the manner in which perturbations propagate within the flow field. Examples of important interference are next given starting from the optimization of airfoils and extending to aircraft configurations which will be covered more thoroughly in the lectures. The organization of the lecture course is then briefly outlined.

2. PROPAGATION OF PERTURBATIONS

A key element in interference is the manner in which a perturbation introduced at one point on the configuration propagates and influences the flow at other points. The nature of the propagation of disturbances is well known in subsonic and supersonic flow. In a subsonic flow a perturbation introduced for example at a point on a planar airfoil will influence the flow at all other points, the magnitude of the influence geometrically attenuating in the well known fashion. In the supersonic case such a perturbation is confined to the downwind Mach wave along which the disturbance is unattenuated.

In the transonic case the propagation is more complex, but it can be deduced from the subcritical and supersonic cases described above. In Figure 1 an expansion perturbation introduced at point A propagates along the Mach wave AB to the sonic line. Here it is reflected as a compression perturbation along the Mach wave BC. At the airfoil surface the compression perturbation is reflected as a compression perturbation which then propagates into the shock wave at point D.

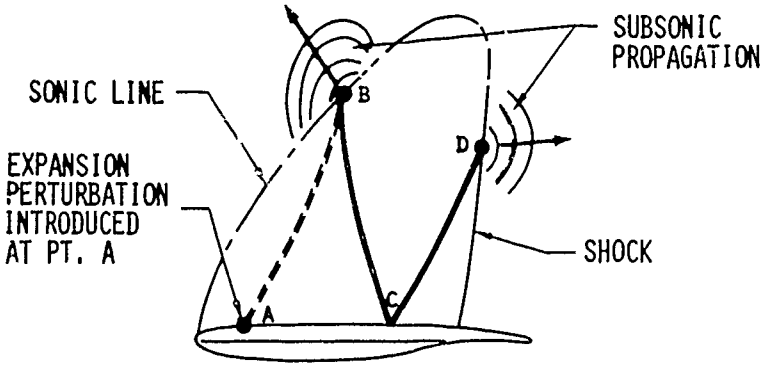

Figure 1. Transonic Propagation of a Perturbation

At point C the perturbation magnitude is doubled by the reflection. At points B and D where the perturbation impinges on the sonic line and the shock wave, subcritical disturbances are excited which then propagate, though weakly, to all points of the flow including points along the airfoil upstream of the original perturbation point A. The original expansion perturbation has thus resulted in a compression perturbation of double strength at a downstream point C and a perturbation of the shock at point D, and therefore to its displacement.

The propagation of perturbations in the three dimensional case as for a swept wing would follow generally that described above for the planar case with however some modification of the attenuation and the region of influence of the perturbation due to the additional dimension.

Thus consider the case of the swept wing of constant chord. On the left side of Figure 2 is first shown the case of a yawed wing of infinite span where the flow is planar in planes normal to the leading edge. On the right side of Figure 2 is shown a swept wing of finite span formed by truncating the yawed wing and imposing a plane of symmetry. Here the planar flow shock has distorted to the forward shock, and a new shock, the rear shock, has appeared. The latter is a product of the interference due to the forcing of the yawed wing streamlines to be aligned with the symmetry wall. At the wing surface this distortion of the streamline has generated compression bicharacteristics which have coalesced to form the rear shock. Inversely one can consider a contouring of the symmetry wall guided by the yawed wing streamlines to largely eliminate the rear shock. Such far-reaching influence as seen here is an important element in transonic interference.

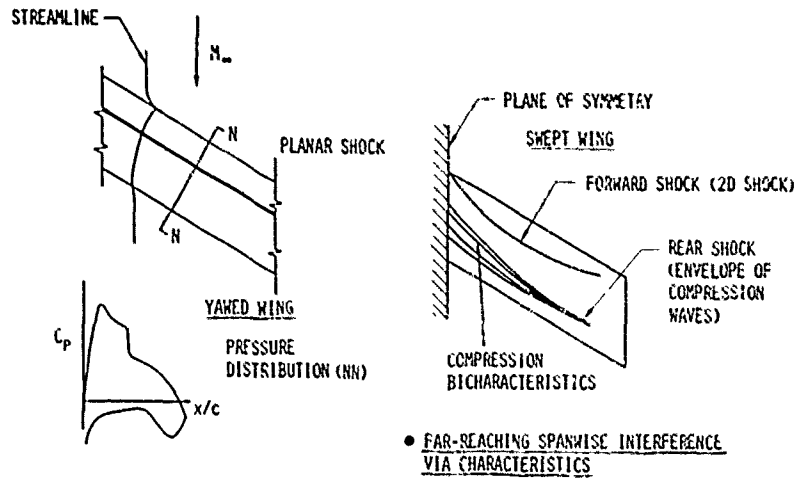

Figure 2. A Spanwise Interference

There is another mode of propagation of strictly three dimensional character carried out via the trailing vortex system. Here a perturbation at a given point alters the span loading. This in turn changes the downwash and therefore the effective angle of attack at neighboring span stations leading to a pressure distribution change. We shall give a number of examples in the next section where this mechanism arises.

3. EXAMPLES OF INTERFERENCE

In this section selected cases of interference at subsonic and transonic Mach numbers will be given to illustrate the wide variety of fluid dynamic phenomena that enter practical interference considerations. Consider first the simplest case of an isolated planar airfoil addressing the problem of minimizing the drag for a given lift and thickness ratio. From the inviscid point of view the formal solution to this optimization problem is well known; namely, a shockless airfoil derived for example from a hodograph solution. To be useful the resulting shockless airfoil must be modified to compensate for viscous effects. The difficulty is that this cannot be accomplished by simply compensating for the displacement thickness of the boundary layer. Let us first recall that the drag is the integral over the profile of the pressure times the local slope. In the above case the pressure is generated by the compensated shape plus the displacement thickness that is by the original hodograph shape. The dilemma is that the shockless pressures act not on the above hodograph shape, but on the compensated shape underlying the displacement thickness (Figure 3). The drag is therefore not zero. There is of course the further difficulty that negative ordinates for the compensated airfoil will arise near the trailing edge, and there is no direct way to compensate for the effects of the near-wake.

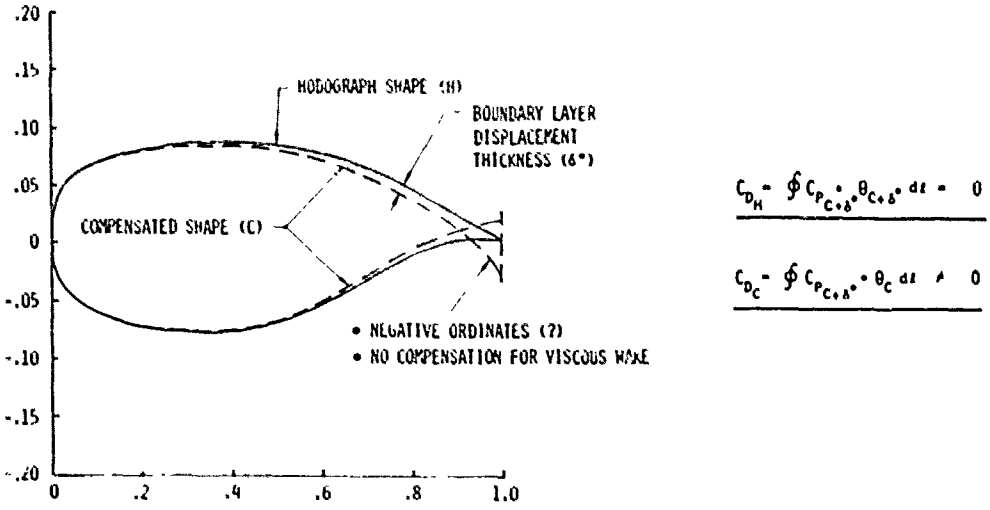

Figure 3. Compensation for Viscous Effects for Shockless Airfoils

The above difficulties might be circumvented on a numerical level by using an inviscid design code (pressure distribution prescribed instead of the airfoil slopes) supplemented with a boundary layer and wake code. Shockless airfoils with near-zero drag in real flow might then be evolved by a successive approximation procedure, for example, starting from a hodograph solution.

There is finally the difficulty of validating such a shockless and "dragless" design in a wind tunnel test. On several occasions it was necessary to adjust the angle of attack (in some cases the Mach number as well) to recover the "shockless" pressure distribution. If such an adjustment of the angle of attack is attributed to wind tunnel wall interference, and there is clearly no assurance of this, then the drag should be based on the corrected angle of attack and not measured by an uncorrected balance reading. In the past shockless airfoils have been possibly unfairly assessed in this manner.

Another approach to the airfoil optimization for cruise lifts is due to Dr. R. Whitcomb who proposed an aft-cambered airfoil with a "benign shock." His rationale was to keep the airfoil essentially at zero angle of attack and incorporate an aft camber to induce a loading on the upstream "aligned" portions of the airfoil. A wedging displacement effect of the post-shock boundary layer was used to prevent the sliding of shock down the aft camber to maintain a benign shock, a rare instance of a favorable effect due to shock/boundary layer interaction. The upstream influence of the aft camber here can be considered a favorable chordwise interference effect. Aft camber will produce an aft loading. Moderation in the use of aft camber may be required from the consequences of the resulting pitching moment as well as from other off-design considerations.

In the relatively simple case of the planar airfoil we see that the optimization problem was by no means clearly resolved. Here the complicating aspects of the viscous interactions, the impact of sometimes ill-defined off-design constraints, and our inability to carry out reliable wind tunnel tests are responsible for this unsatisfactory situation. This situation unfortunately is symptomatic of transonic optimization generally.

The second planar case considers the interference between the elements of an airfoil with high lift devices. The objective here is to maximize the lift at subcritical velocities. Such a problem is meaningful only for a real flow since the lift is limited by viscous separation. The favorable interference arising in the case with a leading edge slat is shown in Figure 4 where the upper surface pressure distribution on the base airfoil with and without the slat and the upper surface slat pressures are sketched. Here the slat has induced a downwash in the leading edge region of the base airfoil greatly reducing its suction peak and correspondingly delaying leading edge separation. The base airfoil in turn has produced a favorable interference on the slat by inducing increased velocities with upwash in the neighborhood of the slat trailing edge. This then permits a trailing edge pressure recovery on the slat with a greatly reduced aft upper surface pressure gradient thereby delaying aft separation on the slat. For more general high lift configurations, for example with aft flap elements added, the mutual interference described above would carry over between any two neighboring elements.

Interference effects between inviscid and viscous flows as found above are not uncommon. Another recently revived example is the tailoring of the pressure distribution to delay boundary layer transition which will be covered by Dr. Whitcomb later. Other examples arising in complex configurations are described below.

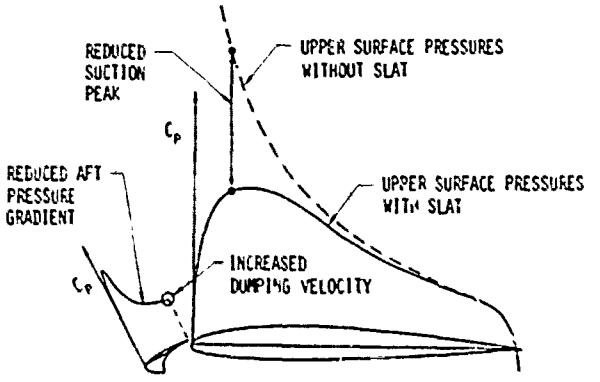

Figure 4. Favorable Interference for a Slatted Airfoil

Consider now the interference problems arising for a high aspect ratio swept wing in the transonic regime. At the cruise lift it is relatively straightforward to avoid severe unfavorable interference and achieve reasonably good lift to drag ratios by eliminating significant isobar and shock unsweeping by appropriate wing washout and thickness and camber variations.

Difficulty with such swept wings however arises at lifts beyond the cruise value where the tendency of swept and tapered wings to load up in the outboard region continues to persist leading to outboard shock-induced separations. For a given lift the appearance of extensive separation in the outboard region will shift the wing loading to the inboard more upstream portion of the wing generating a noseup pitching moment. In addition the resulting increased wake downwash downstream of the inboard wing leads to a more negative lift on the tail and to a further increase in the nose-up moment. This combination leads to pitchup which results in an undesirable stick-force lightening and in more severe cases to a longitudinal instability of the aircraft.

The cure for pitchup in principle is clear. One simply prevents the above lateral shift of the spanwise loading by either delaying outboard separation or by hastening inboard separation. The challenge is to implement this without undesirable side effects.

In connection with the outboard separation, a subtle but frequently occurring interference mechanism arises at the inboard edge of the separated region through the local reduction of the spanwise loading by the separation. Here trailing vortices are generated which decrease the effective angle of attack inboard of the separation and increases it outboard. This then stabilizes the separation pattern, delaying its spread inboard. Inversely if the separation is eliminated for example by vortex generators, the above trailing vortices will be removed, bringing back separation on the inboard side.

As the final example let us consider the interference of the nacelle/pylon and powered jet on the wing/fuselage. Such interference has recently been aggravated in the case of an underwing installation of large diameter high bypass turbofan engines. Here considerations of landing gear length, center of gravity positioning, and nacelle/pylon flutter have necessitated mounting of the engines in much closer proximity to the wing than for previous smaller less fuel-efficient and noisier engines.

In all engine installations an important interference effect is the local loss of the loading. In the transonic case this will lead to a drag increase when the angle of attack is increased to make up the lift loss. The resulting bucket in the spanwise load distribution can have a favorable interference effect. Here the alteration of the trailing vortices will result in a reduction of the local effective angle of attack on either side of the lift-loss bucket moderating any adverse shock-induced separations present.

In the transonic case there is another important consequence of the close coupling, namely, the choking of the flow between the nacelle/pylon/powered jet and the wing lower surface giving rise to detrimental shocks and shock/boundary layer interactions. Proper contouring of the configuration therefore assumes increased importance not only in the shaping of the nacelle/pylon, but in the local redesigning of the wing.

In the past it was sufficient to contour the nacelle and pylon to fit the subscritical streamlines of the wing/fuselage without modifying the wing. In the transonic case with closely coupled engines, the above procedure is no longer adequate. Unfortunately, the necessary transonic computer code to handle the complete configuration with a powered jet exhaust plume is still in development. The present alternative is therefore to start with the streamline fitted configuration, with however the streamlines determined by an available transonic wing/fuselage code, and then refine this baseline design in the wind tunnel. Here local leading and trailing edge camber modifications must be considered.

The large turbofan engines have also led to unfavorable interference at subcritical high lift conditions with high lift devices deployed. In the case that the leading edge slat is sealed against the nacelle and pylon a significant reduction of the maximum lift results. It is caused by the contamination of the boundary layer in the forward regions of the wing by the separated flow from the nacelle and pylon channeling up the corner formed by the slat, pylon, and nacelle (see Figure 5). The contamination then leads to a premature stall of the wing.

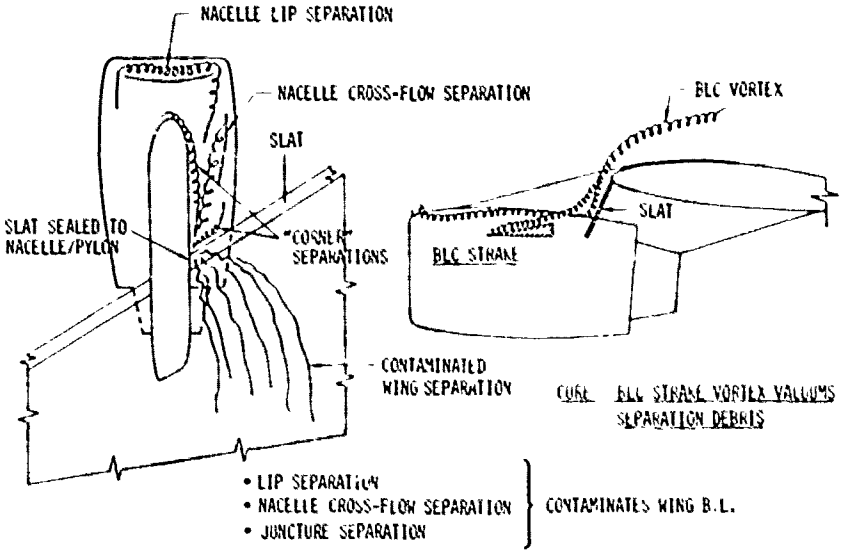

Figure 5. Adverse Viscous Interference at Subcritical High-Lift Conditions

A satisfactory cure for the above difficulty is the addition of a strake at an appropriate location on the nacelle (Figure 5). Such a strake generates a powerful leading edge vortex which siphons off the low energy boundary layer flow on the nacelle, pylon, and slat transporting it downstream well above the wing upper surface.

The above examples are but a sampling of important interference effects arising at transonic speeds. Omitted, for example, is a whole class of interferences which arise in fighters at maneuver lifts where vortices generated upstream by separations on the fuselage, canards, or strakes interact with the wing or tail to cause both favorable and unfavorable interference. These cases will be covered in the lectures.

4. ORGANIZATION OF THE LECTURES

As in the examples of the last section, interference effects to be covered in the present lecture series will be linked closely to specific aircraft performance objectives. Considerations of interference in the optimization process will therefore be undertaken constrained by overall vehicle requirements.

Important interference effects were seen to envolve fluid dynamic phenomena far too complex to be analyzed by existing computational methods. A direct optimization is therefore out of reach. Optimal configurations must be sought by a search process wherein experience is used both to eliminate detrimental gross fluid dynamic features as strong shocks and boundary layer separations and to promote favorable interference. It is therefore not surprising that the end design is not unique.

The lecture course has been divided into three parts. The first part (Lectures 1 to 5) forms background material describing the computational and testing tools. In describing the numerical methods complex algebraic details are omitted whenever they distract from the essential features of the methods. The first part concludes with a review of the overall design process where the compromised gross features of the aircraft are evolved, based upon its overall performance requirements, which defines the starting point for the optimization.

Lectures 6 to 14 cover the wide range of interference phenomena arising in the optimization of both military and commercial aircraft. Here the emphasis will be on describing the relevant fluid dynamic mechanism that drives the optimization. Lectures here are intentionally duplicative, so that alternative approaches toward a given design goal can be demonstrated.

The third part on the last day will cover advanced innovative interference concepts in aircraft design. The near-term applications will be for military aircraft where such concepts are pioneered and thoroughly developed before being applied to commercial aircraft. Such subjects as powered lift, aeroelastic tailoring, swept forward wings, variable geometry and novel weapons carriage will be among the topics to be discussed.

COMPUTATIONAL METHODS FOR SUBSONIC AND TRANSONIC AERODYNAMIC DESIGN

by

J.W. Slooff

Head, Theoretical Aerodynamics Dept.,
National Aerospace Laboratory NLR
Amsterdam
The Netherlands

SUMMARY

An overview is provided of computational methods that can be used in solving the design problem of aerodynamics; i.e. the problem of finding the detailed shape of (parts of) configurations of which the gross geometric characteristics have already been determined in a preliminary, overall design process, and that, subject to certain constraints, have to meet given aerodynamic requirements.
Attention is focussed on methods for solving the classical inverse problem of aerodynamics and on approaches using optimization techniques. Both methods limited to subsonic flow utilizing panel method technology as well as methods based on finite difference/volume formulations for compressible, transonic flow are covered.
In conclusion a discussion is presented of the relative merits of the various computational approaches to the problem of aerodynamic design.

CONTENTS

1. INTRODUCTION

In the process of aerodynamic design one can, traditionally, distinguish two phases (Fig. 1). The first phase, that of PRELIMINARY DESIGN, consists of a parametric study in which the major design variables such as general dimensions, wing loading (C_L), basic wing planform, etc. are fixed. During the second phase, that of DESIGN DEVELOPMENT or DETAILED DESIGN the geometry of the wing and other configuration parts is worked out in detail.

It is primarily this second phase that represents the market for the now decade-old technical/scientific discipline that we call COMPUTATIONAL FLUID DYNAMICS (CFD). However, it must be expected that, with computing speeds and algorithm efficiency still increasing continuously, computational aerodynamic methods will also intrude gradually in the phase of preliminary design.

By far the greater part of the effort invested in CFD over the past 10 to 15 years has been in developing methods and computer codes that solve the direct problem of aerodynamics, i.e. the problem of determining the flow about a given shape at given incidence, Mach and Reynolds number. This has greatly improved the possibilities for the early, but admittedly approximate, aerodynamic ANALYSIS of airplane configurations. However, the greatest potential of CFD, when suitably adapted, is probably in the possibility of directly computing shapes that will produce prescribed aerodynamic characteristics. In this DESIGN mode, computational aerodynamic methods are really complementary to wind-tunnel testing, [1].

The purpose of this lecture is to review such design-type of computational methods for subsonic and transonic flow. The review will be limited to methods that can be used or, at least in principle can be extended for use in situations involving aerodynamic interference. For this reason methods for single airfoils based on conformal mapping principles and hodograph methods will not be covered. For those interested in conformal mapping methods references [2] to [5] provide suitable entry. A review of design methods for transonic flow, including hodograph methods, has recently been given in chapter 5 of [6] and [7].

In the following sections we will first present a classification of computational aerodynamic design methods. This will facilitate a systematic description of the various methods that can be found in the literature. The most important of these, (from the point of view of this author) will be discussed in some detail. The discussion will be concluded by a comparison of the possibilities and limitations of the various approaches, leading to certain suggestions for improving the applicability and efficiency of aerodynamic design methods.

For a good understanding of the material presented it is essential that the reader be familiar with at least the principles of current CFD techniques for subsonic and transonic flow. It will also be helpful if he is familiar with the principles of the calculus of variations and optimization techniques.

2. CLASSIFICATION OF COMPUTATIONAL AERODYNAMIC DESIGN METHODS

Computational aerodynamic design methods can be categorized according to various criteria corresponding with different viewpoints. The aerodynamic designer will be inclined to distinguish by the flow regime (subsonic, transonic) in which the methods are applicable as well as by the geometrical capabilities (2-D airfoils, wings, bodies, etc.). A matrix of existing computational aerodynamic design methods following this classification, with numbers of listed references, is given in table 1. Note that there are several "holes in the market".

With respect to geometric capabilities an important aspect of design methods is the extent to which direct control can be executed over the geometry (in addition to the indirect control that can be excercised through e.g. the pressure distribution). Because design methods can give rise to the problem that the geometry required to realize given aerodynamic characteristics may not be acceptable from the point of view of the structural engineer, some form of explicit control over the geometry is highly desirable. This, ofcourse, is particularly important in the case of airplane modification studies, where certain parts of the geometry may be modified and others must be kept fixed. It is indicated in table 1 which of the existing methods offer the possibility of excercising direct control over the geometry. Distinction is made between the possibility to keep parts of the geometry fixed (mixed analysis/design problem) and the possibility to allow the geometry to vary only within certain constraints.

Next let us have a look at design methods from the point of view of the computational aerodynamicist. We may then distinguishes three classes of formulations viz. (Tab. 2):

1. Inverse methods This category contains methods for solving the classical inverse problem of aerodynamics, i.e. that of determining the detailed shape of a body that will produce a given pressure distribution.
2. Indirect methods Indirect methods are characterized by the fact that, in principle, the designer has direct control over neither aerodynamic quantities such as lift, pitching moment and pressure distribution nor over the geometry. Rather than specifying such quantities directly, the designer has to manipulate a number of (generally non-physical) parameters and see what comes out of it. The hodograph and fictitious gas methods are in this category. In this lecture we will consider the fictitious gas method only.
3. Aerodynamic optimization methods This category is characterized by the use of automated design procedures in which an optimization algorithm and a fluid dynamics solver are linked together to, directly, minimize a given aerodynamic object function, such as drag.

Another possible division of design methods is by the mathematical and numerical flow model that is used. The present discussion will be essentially limited to inviscid, potential flows. The modeling of viscous effects will be touched upon whenever appropriate, but will be discussed in more detail in another lecture of this series. The potential flow model is usually adequate for design calculations, which generally involve no, or only weak shock waves. Methods based on the Euler equations, to the author's knowledge, are not (yet) used in design-type calculations.

Potential flow methods restricted to subsonic flows that can be described by the linear Laplace or Prandtl-Glauert equation are generally of the PANEL METHOD variety[8]. I.e. they use discretized surface distributions of sources, doublets, vorticity etc. Methods that can also deal with (non-linear) transonic flow situations utilize Finite Difference (FD), Finite Element (FE) or Finite Volume (FV) discretizations of the flow field.

Because aerodynamic design problems are non-linear by neture, at least in the boundary conditions, they must be solved by iteration. Hence, aerodynamic design methods, inverse methods in particular, can also be distinguished by the way in which the problem is linearized in each iteration step. In this respect we may distinguish between methods in which the problem is linearized analytically and, from the outset, is formulated as a sequence of linear boundary value problems (b.v.p.) and methods which directly address the full non-linear boundary value problem. With the iterative linear b.v.p. formulations numerical discretization takes place after the (analytical) linearization of the problem. With the non-linear b.v.p. formulation the full non-linear problem is discretized, resulting in a system of non-linear algebraic equations. The latter are then solved by means of some standard (iterative) solution method for non-linear algebraic equations [9].

Although the non-linear b.v.p. approach, in principle, is the most general of the two, most existing methods employ the iterative linear b.v.p. formulation. Reasons for this are:

1. The fact that the conditions for uniqueness and solubility of linear b.v. problems are generally better known than those of non-linear problems.
2. Methods and computer codes for linear b.v. (flow) problems are already available in most cases and can readily be implemented in program systems for the iterative linear approach.

In the following sections we will describe the main characteristics of a fairly large number of aerodynamic design methods that are known to the author. Some of these cannot (yet) be found in the literature. The purpose of this description is to provide the back-ground for a discussion of the possibilities and limitations of the various approaches. Since these (the possibilities and limitations) are a direct consequence of the way in which the design problem is formulated it is most convenient to follow the classification of table 2.

3. INVERSE METHODS

3.1 General aspects

In the inverse problem of aerodynamics the detailed shape is to be determined of a body of which the gross geometrical and main load characteristics are already known from a preliminary design process. The detailed geometry is to be determined such that, for a given Mach number, the body will produce a given pressure distribution. This "target" pressure distribution is chosen in agreement with the main load characteristics adopted in the preliminary design process. Because the shape of fuselage-type bodies is generally determined by other than aerodynamic requirements, inverse methods are usually directed towards obtaining the detailed shape of airfoil or wing-like bodies.

In incompressible or (linear) subsonic flow the inverse problem is non-linear in the boundary conditions only. In transonic flow the problem is non-linear in both the boundary conditions and the flow equations. Due to the non-linearity of the boundary conditions, the inverse problem is fundamentally more complicated than the analysis problem. This is already so in the case of 2-D incompressible flow, as pointed out by Lighthill[10] and Woods[11], and more recently by Volpe and Melnik[12]. In particular it has been demonstrated by Lighthill, using conformal mapping techniques, that a unique and correct solution to the inverse problem of 2-D, incompressible flow does not exist unless a number of additional conditions in the form of certain integral constraints are satisfied. Lighthill formulated these integral constraints in terms of the zero lift velocity distribution (q_o) and the angular coordinate θ in the plane obtained by conformally mapping the airfoil to a circle, viz.

$$\int_{-\pi}^{\pi} \log q_o \, d\theta = 0 \tag{3.1}$$

$$\int_{-\pi}^{\pi} \log q_o \cos\theta \, d\theta = 0 \tag{3.2}$$

$$\int_{-\pi}^{\pi} \log q_o \sin\theta \, d\theta = 0 \tag{3.3}$$

The velocity distribution q is, of course, readily related to the pressure distribution through the isentropic relation

$$C_p = \frac{2}{\gamma M_\infty^2}\left\{\left[1+\tfrac{1}{2}(\gamma-1)M_\infty(1-q^2)\right]^{\gamma/\gamma-1}-1\right\} \tag{3.4}$$

(or the equivalent for incompressible flow).

The first of the conditions (3.1)-(3.3) is a consequence of the fact that q_o is required to be an analytical (i.e. non-singular) function, that takes the unit value at infinity. If the free-stream velocity is taken to be different from unity, the right-hand sight of Eq. (3.1) takes a value different from zero. Equations (3.2) and (3.3) together express that the airfoil to be mapped to the (closed) circle be closed (zero trailing edge thickness) and that the specified velocity distribution is consistent with the specified circulation. Woods[11] has pointed out that similar constraints are also required in the mixed design problem in which the pressure distribution is prescribed for some parts of the airfoil and the shape is prescribed for other parts. Volpe and Melnik[12] have pointed out that the role of constraints and the question of correct formulation of the inverse problem have never been properly addressed for (2-D) compressible flows and that, as a consequence, most existing inverse methods for transonic flow are not well formulated. For 3-D flows the situation is still more unsatisfactory. To the author's knowledge the question of proper formulation has not been addressed even for incompressible flows. This, however, has not prevented the development of useful inverse procedures.

The problem of non-linearity in the boundary conditions is avoided when the boundary conditions are satisfied in the wing mean plane, as in classical thin wing or transonic small perturbation (TSP) theory. The inverse problem then can be reduced to a Dirichlet boundary value problem for the perturbation velocity potential ϕ.

The additional conditions to be satisfied for a proper formulation of the inverse TSP problem are not known. However, we do know these conditions for the limiting case of incompressible flow from the classical thin airfoil and thin wing theories. For a good understanding of the inverse problem it is useful to consider these first.

In thin airfoil theory[13], the symmetric (thickness) and antisymmetric (lifting) parts of the incompressible flow are described by the following integral relations

$$u_t(x,\pm 0) = \frac{1}{2\pi} \oint_0^1 \frac{[\![w(\xi)]\!]_{0^-}^{0^+} \, d\xi}{x-\xi} \tag{3.5}$$

$$w_\ell(x,\pm 0) = -\frac{1}{2\pi} \oint_0^1 \frac{[\![u(\xi)]\!]_{0^-}^{0^+} \, d\xi}{x-\xi} \tag{3.6}$$

In these expressions u_t is the chordwise perturbation velocity due to thickness and w_ℓ is the perturbation velocity normal to the z-axis due to lift. They can be expressed as the chordwise (ϕ_x) and normal (ϕ_z) derivatives of the perturbation velocity potential. $[\![w]\!]_{0^-}^{0^+}$ and $[\![u]\!]_{0^-}^{0^+}$ denote the jumps in normal and chordwise velocity across the slit ($0 \leq x \leq 1$, $z = 0$) where the airfoil boundary conditions are satisfied. With the linearized boundary conditions, $[\![w]\!]_{0^-}^{0^+}$ and w_ℓ are related to the airfoil geometric quantities as follows

$$[\![w]\!]_{0^-}^{0^+} = 2\frac{dz_t}{dx} \tag{3.7}$$

$$w_\ell = \frac{dz_c}{dx} - \alpha \tag{3.8}$$

where the subscripts t and c refer to thickness and camber, respectively, and α is the angle of attack.

In the direct problem, with the geometric properties (3.7), (3.8) given, (3.5) must be considered as an integral expression for u_t and (3.6) as an integral equation for $[\![u]\!]_{0^-}^{0^+}$. Equation (3.6) is the classical integral equation of lifting surface theory. It is known that equation (3.6) does not have a unique solution, unless an additional condition is satisfied; the reason being that there exists a non-trivial solution of the homogeneous equation. In thin airfoil theory the Kutta condition

$$[\![u(x=1)]\!]_{0^-}^{0^+} = 0 \tag{3.9}$$

together with its implication of a jump in velocity potential extending from the trailing edge to downstream infinity is the additional condition that guarantees a unique (and indeed physically relevant) solution.

In the inverse problem the situation is exactly opposite. We then have the situation that equation (3.6) represents an integral expression for determining the camber and incidence from the specified load distribution $[\![u]\!]$, while (3.5), with (3.7), represents an integral equation for the unknown thickness distribution.

Since the integral equation (3.5) of the inverse thickness problem is the same as that (3.6) of lifting surface theory we must also specify an additional condition to be satisfied in order to have a well-posed problem with a unique solution. The relevant choice to be made for this additional condition is of course the closure condition:

$$\int_0^1 [\![w(\xi)]\!]_{0^-}^{0^+} d\xi = C \tag{3.10}$$

requiring that the airfoil be closed (C = 0) or have a given trailing edge thickness (C > 0). With C > 0 there is a net source flow trailing behind the airfoil.

It can be shown that in the mixed boundary value problem, in which the velocity distribution is prescribed over part of the slit and the geometry over the remainder, both a condition fixing the circulation and the closure condition must be enforced in order to obtain a problem with a unique solution. It is emphasized that without satisfying, either explicitly or implicitly, the necessary additional condition(s) any numerical scheme is bound to fail. Corresponding additional conditions must be satisfied in the case of 3-D (thin) wing flow. Note, that in thin airfoil theory as described above the airfoil shape can be determined directly, without iteration.

At this point it is instructive to notice that the Kutta condition (3.8) together with the closure condition (3.9) represent the equivalent in thin airfoil theory of Lighthill's constraints (3.2) and (3.3). While these conditions are necessary and sufficient for a unique solution they do not guarantee a valid solution. For a uniformly valid (that is non-singular, [14]) solution in thin airfoil theory, the airfoil must be cusped at both ends. In other words, the additional constraint

$$w(x = 0,1) = 0 \tag{3.11}$$

must be imposed on the solution of the inverse thickness problem. Evidently (3.11) is the thin airfoil equivalent of Lighthill's constraint (3.1). We will call equations (3.1), (3.11) the regularity condition.

As pointed out by Volpe and Melnik[12], Lighthill's constraints, or rather the equivalent of those, must also be satisfied when the boundary conditions are linearized about a given (non-planar) approximation of the airfoil that is being sought. In the latter case the inverse problem can be solved as a sequence of Dirichlet boundary value problems for the velocity potential with the geometry updated through the normal velocity W resulting after each Dirichlet step (Fig. 2a).

The distribution of the surface potential required for the Dirichlet boundary condition is obtained by integration of the target velocity distribution, i.e.

$$\Phi = \Phi_o(s = 0) + \int_{s=0}^{s} q(s')ds' \tag{3.12}$$

The constant of integration Φ_o in (3.12), fixes the average level of the potential at the airfoil relative to that at infinity and through this the total net mass flux from the airfoil to infinity. Hence Φ_o can be used to satisfy the equivalent, for thick airfoils, of the closure condition (3.10).

At this point a remark must be made with respect to the boundary conditions at infinity. For panel methods these are of little concern because they are satisfied implicitly by the elementary source and doublet/vortex solution. In transonic FD/FE/FV methods they must be imposed explicitly at the outer boundary of the computational domain. For a properly formulated analysis method with Neumann boundary conditions in the near-field, (airfoil surface), the far-field boundary condition must be of the Dirichlet type, with allowance for a jump in potential corresponding with the circulation around the airfoil. Conversely, methods utilizing Dirichlet-type near-field boundary conditions should have Neumann-type far-field boundary conditions, with allowance for an integral mass flux constraint corresponding with the required amount of trailing edge openness of the airfoil. In none of the transonic inverse methods that can be found in the literature this point is dealt with adequately. It was, however, (partly?) recognized by Volpe and Melnik[12].

Volpe and Melnik also argue, that in order to obtain a proper stream surface, we must require the solution to contain a branch point or dividing streamline. This, in general, requires a stagnation point. This last requirement can also be brought-up as follows. Note, that since

$$q^2 = U^2 + W^2 \tag{3.13}$$

the normal velocity W resulting from the solution of the Dirichlet problem, must be small with respect to U (and q), or, in other words

$$W \ll U,q \tag{3.14}$$

This implies the requirement

$$W(s_o) = 0 \tag{3.15}$$

where $s_o = s(U = 0)$. Equation (3.15), of course, is the equivalent of the regularity condition (3.11). As discussed in [12], the implication of this requirement is that a free parameter such as the magnitude of the free stream or a free parameter in the target pressure distribution must be introduced.

In three dimensions the question of well-posedness of the inverse problem does not seem to have been addressed properly even for incompressible flow. One aspect is that the 3-D equivalents of Lighthill's constraints have not been formulated. Apart from this there are strong indications that the 3-D inverse problem is ill-posed, in the sense that small differences in specified pressure distribution may lead to large differences in geometry. The point was first noted in [1]. An example taken from [55] has been reproduced in figure 3.

Related aspects of the 3-D inverse problem, in particular when formulated in terms of a sequence of Dirichlet problems with geometry corrections based on calculated normal velocity distributions, are the following:

The conversion of specified pressure or velocity distribution into specified velocity potential is fundamentally more complicated than in 2-D flow. Assuming the normal velocity to be sufficiently small the conversion is described by the equation

$$\Phi_\xi^2 + \Phi_\eta^2 = q^2(\xi,\eta) \tag{3.16}$$

ξ, η being orthogonal curvilinear coordinates on the (approximation to the) wing surface. The problem of finding Φ is similar to one in three-dimensional boundary layer computations, [15], in which the boundary conditions at the edge of the boundary layer require the knowledge of the velocity components of the outer inviscid flow while only the pressure distribution is given. It leads to an initial value problem with either the potential or both velocity components at the leading edge given as initial conditions. Because of the hyperbolic nature of this initial value problem, the characteristics of which are the streamlines, the solution may contain discontinuities manifesting themselves in "intersecting streamlines" or limit lines (Fig. 4), unless the prescribed pressure distribution and/or the initial conditions satisfy additional requirements. Clearly such discontinuities are not acceptable in the inverse problem*). However, it is not evident how they should be avoided. Presumably one should either avoid to linearize the full non-linear problem in such a way that the solution of initial value problems is required at intermediate steps or one should choose the initial conditions (Φ or direction of q at the leading edge) such that discontinuities are avoided.

The problem of correcting the geometry when the normal velocity (W) is known from the solution of the Dirichlet problem is closely related to the problem of computing the displacement thickness of a 3-D boundary layer. It follows from a discussion by Lighthill[16] that, assuming the displacement δ to be small, δ is determined by a quasi-linear first-order equation of the type

$$\frac{\partial}{\partial\xi}(\rho U\delta h_\eta) + \frac{\partial}{\partial\eta}(\rho V\delta h_\xi) = \rho W\, h_\xi h_\eta \tag{3.17}$$

In (3.17) ξ, η are orthogonal curvilinear coordinates and h_ξ, h_η metric coefficients. Note that the streamlines are also the characteristics of (3.17). Hence the remarks given above with respect to the determination of Φ from (3.16) are also relevant for the determination of δ from (3.17).

The difficulties described above are circumvented, to some extent, in iterative-Neumann or residual-correction type of formulations of the inverse problem (Fig. 2b). In such formulations the residual, that is the difference between the actual and required pressure distribution, is determined in each iteration step, by means of an analysis (Neumann) code and a correction to the geometry, driving the residual to zero, is obtained from some (simplified) inverse procedure. It will be clear that in this case the closure and regularity conditions must be satisfied in the simplified inverse procedure.

The third category of inverse methods (non-linear boundary value problem approach, Fig. 2c) directly addresses the full non-linear problem. This should, of course, also be formulated such that the closure and regularity conditions are satisfied.

In the following sections we will discuss a number of examples of inverse methods from the various categories in some detail.

3.2 Methods based on thin airfoil theory

Subsonic flow models

An example of an early panel method containing a design option is that of Woodward[17,18] (1967). In this method the flow about a wing-fuselage configuration is simulated by means of (Fig. 5):

- line source and doublet distribution along the fuselage axis, to simulate fuselage volume and camber effects
- constant source density panels in the wing mean plane, representing wing thickness
- constant "pressure (difference) panels", i.e. constant bound vorticity panels with their associated trailing vorticity, to represent wing lift effects
- constant bound vorticity panels on a (cylindrical) part of the fuselage around the wing-fuselage intersection, to model interference effects.

The method can be considered to provide an approximate solution for the problem of linearized subsonic or supersonic flow about thin wings mounted on a fuselage of simple shape. In the analysis mode, the strengths of the vorticity panels is determined by solving a system of linear equations that results from satisfying the boundary condition of tangent flow at discrete vorticity panel control points. It is now known[8,19] that such a discretization scheme is numerically unstable when the panel mid-points are selected as control points. Woodward, empirically, circumvented this problem by positioning the control points at 95 % of the central panel chord. In the design mode the method is used to compute the wing twist and chordwise camber slopes $\frac{\partial Z_c}{\partial x}$ that, in the presence of the fuselage, and for a given wing thickness, will sustain a prescribed spanwise and chordwise lift distribution. The camber surface itself is obtained by integration

$$Z_c(x,y) = Z_o(y) + \int_{x_{\ell e}(y)}^{x} \frac{\partial Z_c(\xi,y)}{\partial\xi}\, d\xi \tag{3.18}$$

where $Z_o(y)$ is an integration constant which, within the limitations of linearized theory can be chosen freely.

Utilizing the relation

$$\Delta C_p = 2\left(C_{p_{up}} - C_{p_{th.}}\right) \tag{3.19}$$

between lift distribution ΔC_p, upper surface pressure distribution $C_{p_{up}}$ and pressure distribution due to wing thickness $C_{p_{th.}}$, the design mode can also be used to design the camber surface for a given upper surface pressure distribution and given wing thickness distribution.

In the design mode the strengths of the wing vorticity panels are related directly to the prescribed load distribution. Only the strengths of the fuselage vorticity panels have to be solved for. Note that in this "inverse lift" problem the closure and regularity conditions do not appear and that the Kutta condition is satisfied implicitly by the vorticity panels. However, due to the linearized (thin wing) boundary conditions, the results are not valid at the leading edge of wings with round-nosed airfoil sections.

*) In the boundary layer case the discontinuity may be indicative for a separation line, with the discontinuity representing the "footprint" of the associated vortex sheet in the outer inviscid flow.

Design options similar to those described above are also available in the early Boeing subsonic wing-fuselage code A236, as communicated briefly by Rubbert in [8]. An example of application can be found in [18]. A summary of the capabilities is reproduced in figure 6. The method differs from Woodward's in the sense that on the fuselage, which can be of arbitrary shape, the exact boundary conditions are satisfied. This is realized through constant density source panels on the fuselage surface. Wing lift effects are modeled by the vortex lattice variant (Fig. 7) of constant density (normal) doublet panels.

According to [8], the method also contains the option to do the inverse thickness problem. However, in the present author's experience, the discretization scheme used (constant density source panels) is unstable, in the sense of [19], when tangential velocity boundary conditions are applied. This would be so even if a closure condition were enforced, which is not mentioned. Hence, there is some doubt whether this option is useable.

A further notable feature of the method is that it contains a Riegels type of leading edge correction. The purpose of such correction is to remove the singularity of solutions of thin-wing theory at the leading edge of wings with round-nosed airfoil sections. For background of the Riegels type of leading edge correction see, e.g., Weber[21] or Van Dyke[14].

The NLR linear subsonic inverse code, [22] combines several features of the Woodward I and Boeing A230 codes, as indicated in figure 8. As in the Boeing code, the fuselage surface is covered with constant density source panels. Wing lift effects are modeled through Woodward constant pressure panels with, however, the control points at the panel centers. This discretization scheme, while unstable in combination with analysis-type boundary conditions, is stable (in the sense of [8], [19]) in combination with the design-type boundary conditions utilized here.

Wing thickness effects are modeled through constant density x-doublet panels (doublet axis in free stream direction). It can be shown, [22], that this is equivalent to line source/sink segments with equal but opposite strength along the leading and trailing edges of a panel. In analogy with the vortex lattice method this is called a source lattice method. In contrast with the constant source density panel, this discretization scheme is stable in combination with design type boundary conditions at panel center control points. A further attractive feature of the scheme is that the closure condition (3.10) is satisfied implicitly for each chordwise strip of panels.

A unique feature of the NLR code is that it also contains means for explicit control over the geometry, in particular with respect to wing twist, (maximum) thickness, leading edge radius and trailing edge angle. Required values for these quantities may be specified at all span stations. The extra equations modeling these geometric requirements are added to the system that represents the pure aerodynamic problem. The resulting total system of equations is over-determined and is solved in a weighted least squares sense utilizing the formulation of transposed matrices. The designer may choose different weights for the upper and lower surface pressure distributions and geometry requirements. The option may be used to satisfy the regularity condition or, more in general, to avoid shapes that are undesirable from the point of view of full scale wing structures. It may also be used to satisfy wing thickness requirements resulting from multi-disciplinary, preliminary design considerations.

In NLR practice the code is never used in stand-alone mode but is part of a more comprehensive computer-program system for the design of thick wings through a residual-correction formulation. The latter will be discussed in section 3.4.

Apart from the thin-wing type methods discussed above, the literature also contains a number of methods, [23], [24] which, utilizing vortex lattice modeling, are directed towards optimizing the twist and camber of thin lifting surfaces for minimum induced drag. These lifting surfaces may be multiple and mutually interfering. Fuselage effects, however, are not modeled. While such methods are not inverse methods in the actual sense of the word they do allow or even require the specification of chordwise lift distributions, the spanwise distributions being determined by means of an optimization process (see also section 4).

Transonic flow

Transonic flow with thin-wing boundary conditions is, classically, described by means of transonic small perturbation (TSP) theory. As we shall see in the following survey inverse TSP methods are generally less well developed than their subsonic counterparts. This is reflected in particular in the limited geometric capabilities and the almost common lack of control over closure. The situation is primarily a result of the fact that, due to the non-linearity of the TSP flow equations, the surface as well as the space around the configuration must be discretized. In addition, the lift and thickness problems can no longer be dealt with separately.

Early work on a mixed direct/inverse method for transonic airfoil design, based on transonic small perturbation theory and utilizing a relaxation type of finite difference technique has been reported by Steger and Klineberg[25]. These authors have studied the problem of an airfoil in transonic flow with given leading-edge geometry with the pressure distribution specified over the remaining portion of the chord. A perturbation velocity potential formulation was used in the leading-edge region and a first-order equation system

$$\frac{\partial F}{\partial x} + \frac{\partial w}{\partial z} = 0 \quad \text{(continuity)} \tag{3.20}$$

$$\frac{\partial u}{\partial z} - \frac{\partial w}{\partial x} = 0 \quad \text{(irrotationality)} \tag{3.21}$$

in the remainder of the flow field (Fig. 9). F was chosen according to the Guderley-Von Karman formulation of TSP theory. Steger and Klineberg do not mention and, apparently, do not explicitly satisfy the necessary additional condition (closure) required for uniqueness. However, at the same time, rather than specifying u directly as a boundary condition in the finite difference relaxation process, they utilize an iterative procedure in which, successively,

i) a complete relaxation sweep is performed with direct (analysis) boundary conditions for an estimate of the required geometry

ii) an improved estimate for the geometry is obtained from the irrotationality condition (3.21) by, successively;

ii.1) replacing $u(z = 0)$, on the slit (Fig. 9) in the finite difference expression for $\frac{\partial u}{\partial z}$ $(z = 0)$, by the required surface value of u.

ii.2) chordwise integration of $\frac{\partial w}{\partial x}$ to yield

$$w_{\pm} = \frac{dZ_{\pm}}{dx} = \int_{x_1}^{x} \frac{\partial w}{\partial x}(\xi, z = \pm 0)d\xi + C_1$$

$$= \int_{x_1}^{x} \frac{\partial u}{\partial z}(\xi, z = \pm 0)d\xi + C_1 \qquad (3.22)$$

and

$$Z_{\pm} = \int_{x_1}^{x} w_{\pm} dx + C_2 \qquad (3.23)$$

the constants of integration C_1 and C_2 being used to enforce continuity in Z and $\frac{dZ}{dx}$ at x_1, where the new shape is joined to the fixed leading-edge geometry.

Although a convergence proof for the procedure is not given, the process does converge apparently. Not in the least, according to the authors, because they maintained consistency between the numerical formulation of direct and inverse boundary conditions, and presumably also because a Neumann type boundary condition is satisfied in each relaxation sweep. Note, that there is no control over the trailing-edge gap, and that the angle between the free stream and the reference coordinate system is held fixed (Fig. 9), implying that the orientation of the given leading-edge geometry with respect to the free stream is also fixed.

While the examples presented by Steger and Klineberg are of a fairly academic nature, Langley[26] of ARA, utilizing a similar iterative procedure, but a (non-conservative) Murman and Krupp[27] type perturbation velocity potential formulation through the entire flow field, succeeded in carrying the inverse TSP method to appreciably more practical levels of application. The latter is reflected in the fact that Langley arranged his program to have various options. For example the upper surface and lower surface, aft of a fixed leading-edge geometry, may be altered simultaneously or separately; alternatively the pressure distribution may be specified over the upper surface and the thickness distribution may be kept constant. The latter option was incorporated in order to avoid problems like negative or too large trailing-edge thickness which, as in the Steger/Klineberg approach, may result from the absence of control over airfoil closure. It is interesting to note that Langley, in [26], reports the failure of attempts to solve the inverse problem directly by enforcing the Dirichlet boundary condition for ϕ

$$\phi(x) = \int_{x_1}^{x} u(\xi)d\xi + \phi(x_1) \qquad (3.24)$$

on the slit (reason why he switched to the "indirect" inverse approach in which successive analysis-type calculations are made with regular updating of the airfoil shape through the irrotationality condition). The additional conditions associated with the inverse problem are not mentioned in [26]. Hence, it seems likely that the failure was caused by not satisfying the necessary additional conditions, resulting in a wrongly posed problem.

Both Steger and Klineberg[25] and Langley[26] stress that the crux of the design problem is the treatment of the airfoil boundary conditions. In Langley's method the Neumann boundary condition is implemented by substituting the given surface slope $\frac{dZ}{dx}$ for ϕ_z in the finite difference expression

$$(\phi_{zz})_{i,j} = \frac{2}{(\Delta z)^2}\left(\phi_{i,j+1} - \phi_{i,j} - \Delta z(\phi_z)_{i,j}\right) \qquad (3.25)$$

for ϕ_{zz} at the (j^{th}) mesh line coinciding with the slit (Fig. 9). The cross-derivative $\phi_{xz} = \frac{\partial u}{\partial z}$ in the expression (3.22) for the geometry update is approximated by

$$(\phi_{xz})_{i,j} = \frac{1}{2\Delta z}\left\{-3(\phi_x)_{i,j} + 4(\phi_x)_{i,j+1} - (\phi_x)_{i,j+2}\right\} \qquad (3.26)$$

with $(\phi_x)_{i,j}$ replaced by the required velocity.

It should be noted that the geometry update procedure, equation (3.26) in particular, implies continuity of ϕ_x in the z-direction, but not necessarily in the x-direction. In terms of the general discussion of section 3.1 this means that the regularity condition is not satisfied. The analysis calculation on the other hand does imply continuity of ϕ_x because of the finite difference approximation for ϕ_{xx}. This numerical inconsistency could, presumably, have a negative effect on the convergence of the iteration process and, apparently, shows up as a local oscillation in the resulting pressure distribution at the point x_1 where the fixed leading edge geometry meets the remaining, new shape (Fig. 10).

It is further worth noting that Langley reports that substantial underrelaxation (0.1 to 0.3) is required in updating the surface slopes through the irrotationality condition and that 150-300 fine grid iterations, preceeded by a similar amount on two successive coarser grids, are required for convergence.

In a later effort at ARA by Forsey and Carr briefly reported by Lock[28], the problem of not being able to successfully enforce the Dirichlet-type boundary condition was apparently overcome. At the same time the method was extended to 3-D wings. An example of application is given in figure 11.

Use of the "indirect" inverse technique (as well as failure of the "Dirichlet technique") has also been mentioned by Schmidt et al.[29] and Schmidt and Hedman[30]. In the latter paper the closure problem is crudely disposed off by rotating the lower surface around the airfoil section leading-edge point.

Inverse methods based on TSP formulation which do utilize Dirichlet boundary conditions (except, again, in the leading-edge region, where a fixed shape is assumed), have been studied by Shankar et al.[31,32]. In [31], a non-conservative, transonic similarity form

$$[K - (\gamma+1)\phi_x]\phi_{xx} + \phi_{\bar{z}\bar{z}} = 0 \qquad (3.27)$$

of the 2-D Guderley-Von Karman TSP equation is used. K being a transonic similarity parameter and $\bar{z}$

representing a stretched coordinate. In the leading-edge region the Neumann boundary condition is implemented as in Langley's method. This leads to the following difference equation being solved at the airfoil grid points where the shape, i.e. $\phi_{\bar{z}}$ is prescribed

$$\left[(K-(\gamma+1)\phi_x)\phi_{xx}\right]_{i,j} + \frac{2\phi_{i,j+1} - 2\phi_{i,j}}{(\Delta\bar{z})^2} = \frac{2(\phi_{\bar{z}})_{i,j}}{\Delta\bar{z}} \tag{3.28}$$

The non-linear term, as usual, is approximated by central differences at elliptic points and by upwind differences in hyperbolic points. At the design-portion of the airfoil grid points, the Dirichlet boundary condition is implemented as

$$\phi_{i,j} = \phi_{i-1,j} + u_{i-\frac{1}{2},j}(x_{i,j}-x_{i-1,j}) \tag{3.29}$$

$u_{i-\frac{1}{2},j}$ being the required velocity, specified at half-mesh. Equation (3.29) enforces continuity of ϕ at $x = x_1$. The level of ϕ in the design portion is updated during each relaxation sweep. After the relaxation process has converged, the new airfoil slope is computed from the exact inverse of equation (3.28), i.e.

$$(\phi_{\bar{z}})_{i,j} = \frac{\Delta\bar{z}}{2}\left[(K-(\gamma+1)\phi_x)\phi_{xx}\right]_{i,j} + \frac{1}{\Delta\bar{z}}(\phi_{i,j+1} - \phi_{i,j}) \tag{3.30}$$

In this way full consistency between the analysis and design formulations is achieved, thereby avoiding, presumably, local oscillations at the analysis/design junction x_1 of the kind observed in figure 10. As mentioned earlier the finite difference procedure, and the difference formula for ϕ_{xx} in particular, implies continuity of ϕ_x at x_1 on both upper and lower surface. Hence, the regularity condition is satisfied. It is suggested here, that these two, implicit, additional conditions also serve to fix the circulation and trailing edge openness and thereby the uniqueness of the solution. As in the Steger and Klineberg[25] and Langley[26] procedures this does not leave room for control over the trailing-edge thickness. However, it would seem possible to, additionally, exercise control over trailing-edge closure by introducing the orientation of the fixed leading-edge geometry with respect to the free stream as an additional free parameter.

In [32] Shankar et al. have extended their approach to 3-D wings in the presence of a body. The approach was taken to modify the existing 3-D Bailey-Ballhaus TSP analysis code as extended by Mason et al.[33]. The 3-D code utilizes fully conservative differencing.

The 3-D design examples presented in [32] suffer severely from the absence of control over trailing edge thickness. Several suggestions are given for, fairly crude, remedies for this situation, such as rotating the lower surface about the leading edge. However, the possibility mentioned above, to control closure through introduction of an additional free parameter which represents the orientation of the fixed leading edge geometry with respect to the free stream, is not considered.

In a further paper[34] Shankar, now considering Dirichlet boundary conditions over the whole of the chord, addresses the closure problem by varying the constant of integration in equation (3.24), or, in other words, by varying the potential at the leading edge. In particular he uses the following procedure:

(1) Compute the flow field for a given starting geometry with the purpose of providing a first estimate for the potential ϕ_{LE} at the leading edge
(2) Compute the potential on the wing plane from (3.24), (with $x_1 = x_{LE}$).
(3) Solve the Dirichlet problem for the difference equations by means of line relaxation.
(4) Determine the trailing edge gap t_{TE} from equation (3.10) and the derivative $\partial t_{TE}/\partial\phi_{LE}$; determine correction $\Delta\phi_{LE}$ from

$$\Delta\phi_{LE} = t_{TE} \Big/ \frac{\partial t_{TE}}{\partial\phi_{LE}} \tag{3.31}$$

(5) Repeat steps (3) and (4) until closure is achieved.

Note that the determination of the n^2 derivatives $(\partial t_{TE})_j/(\partial\phi_{LE})_m$ (n is the number of span stations) is very costly since each requires another Dirichlet problem to be solved. For this reason a simplified procedure is used involving only a small fraction of the gradient matrix elements $\partial t_{TE}/\partial\phi_{LE}$. Clearly, there is a need for more efficient procedures that enforce closure. As we shall see in the next section one possibility seems to be to update the leading potential after each relaxation sweep.

3.3 Iterative methods utilizing Dirichlet-type boundary conditions

In this section we will discuss methods that, basically, solve for the non-linearity in the boundary conditions by means of an iterative process of the type of figure 2a.

Subsonic flow models

Design options utilizing Dirichlet-type, or rather tangential velocity boundary conditions on thick, lifting geometries are contained by the Boeing PANAIR System, [35], [36]. The PANAIR system utilizes linear source and quadratic doublet distributions on flat panels that can be used in combination with various types of boundary conditions (Fig. 12a). The doublet/design network can be used for the design of thin camber surfaces. The source/design network is used for the design of thick geometries. It can be used in combination with other types of network to solve complete design problems as well as mixed analysis/design problems in which part of the geometry is fixed (Fig. 12b). As such it is highly versatile. In the source/design network the closure condition is imposed explicitly; the linear source distribution provides the additional free parameter necessary for this. The regularity condition, however, is not considered.

A rather extreme example illustrating the consequence of not satisfying the regularity condition in a mixed analysis/design problem is presented in figure 12. The solution, obtained after three iterations is clearly singular at the points where the fixed and free parts of the geometry are matched. This would be the case in all mixed analyses/design problems with arbitrary prescribed pressure distributions. Similarly, the solution would be singular at the stagnation point in complete design, requiring some form of local smoothing of the designed geometry.

A 3-D example [36] of a mixed analysis/design problem using PANAIR has been reproduced in figure 14. The example illustrates that the method is capable of (approximately) recovering, after 2 iterations, the geometry of a shape the pressure distribution of which was taken as "target". Note that in this case the regularity condition is satisfied automatically through the particular choice of the pressure distribution.

In the example of figure 14 the problem, mentioned in section 3.1, of converting the given pressure distribution into a distribution of velocity potential or velocity components was circumvented by specifying the tangential velocity components to have the direction of the velocities of the modified (starting) geometry and the magnitudes of the velocities of the original geometry (which is to be recovered). A consequence of this choice is that the original geometry cannot have been recovered exactly, unless the velocity directions on the modified and original geometries were identical.

References [35], [36] do not provide details about the procedure utilized for updating the geometry from the normal velocity components in each iteration.

A method for the design of multiple airfoils with given pressure distribution has been described by Ormsbee and Chen[37]. The method, based on earlier work of Oellers[38], differs from the majority of inverse methods in the sense that a formulation in terms of stream function ψ rather than velocity potential is utilized. As a consequence the approach is fundamentally limited to two-dimensional flows.

The integral equation to be solved in this method is of the type

$$\psi = z(s)U_\infty \cos\alpha - x(s)U_\infty \sin\alpha - \frac{1}{2\pi}\oint \gamma(s')\ln r(s,s')ds'$$

$$= \text{constant} \qquad (3.32)$$

where s is the arc length along the airfoil, z(s) and x(s) are the airfoil coordinates and $\gamma(s')$ represents a surface vorticity distribution. In the iterative process chosen $\gamma(s')$ is set equal to the local (prescribed) velocity (as it should be in the converged solution) and z(s) is calculated directly for fixed x(s) in each iteration step. The discretization scheme chosen employs flat panels with constant vorticity. Control points are chosen at panel centers.

It is worth noting that the use of vorticity distributions only implies that the closure condition is satisfied implicitly. Another consequence is that only airfoils with zero trailing edge thickness are admitted. The stream function formulation, presumably, implies that also the regularity condition is implicitly satisfied. This might explain the authors' remark that "specification of γ on the entire airfoil results in overspecification of the problem and reasonable answers may not be obtained". They also communicate the experience that "special care is (must be?) taken in specifying the velocities near the leading and trailing edges". This suggests that the method may not be fully properly formulated in the mathematical/numerical sense.

The method can be used for the design of single as well as multiple airfoils with fixed gap and overlap between components. The latter, according to the authors, "can cause a nonconverging iterative process if the specified velocity at the trailing edge of the forward element is inconsistent with the high velocity peak on the flap".

Examples of single and two-element airfoils designed for high lift with attached flow have been reproduced in figure 15.

Transonic flow

The first reported effort to solve the full potential transonic lifting 2-D inverse airfoil problem is that of Tranen[39]. Broadly speaking Tranen's method can be considered as a version of the Garabedian-Korn[40] analysis method with the Neumann boundary condition on the airfoil surface replaced by a Dirichlet boundary condition. In the Garabedian-Korn method the quasi-linear form of the full potential equation is solved in polar coordinates ω,r in a computation plane obtained by mapping the region exterior to the airfoil onto the interior of a unit circle. Non-conservative differencing with simple upwind bias in the supersonic zone is used and the resulting non-linear system of equations is solved by means of SLOR.

The distribution of the surface potential required for the Dirichlet boundary condition in Tranen's method is obtained by integration of the target velocity distribution, viz. Eq. (3.12). While in the original analysis method the velocity components are calculated by means of central differences at the mesh points themselves, Tranen, in specifying the surface potential in the Dirichlet problem, found that for a stable discretization it is necessary to specify the pressure (velocity) at half-mesh and to determine Φ through integration, using an expression of the type

$$\Phi_i = \Phi_{i-1} + (U.f)_{i-\frac{1}{2}}\,\Delta\omega \qquad (3.33)$$

f being the mapping modulus. (Note that a similar strategy was followed by Shankar[32], see Section 3.2.) In Tranen's method the constant of integration determining the level of the surface potential can either be fixed or can be used to control closure. In the latter case a correction $\delta\Phi_o$ to the surface potential level is applied after each relaxation sweep. The magnitude of this correction is taken to be proportional to the net mass flux Q (transpiration) through the airfoil surface, i.e.

$$\delta\Phi_o = \varepsilon.Q \qquad (3.34)$$

with

$$Q = \int_0^{s_{max}} \rho V\, ds \qquad (3.35)$$

where V is the velocity component normal to the surface (radial direction). The value of the proportionality constant ε has been determined empirically. However, utilizing the fact that the potential of a source (in incompressible flow) equals Q $\ln \tilde{r}$ ($\tilde{r}$ being the distance to the source in the physical plane) it should also be possible to determined ε theoretically.

Tranen's way to control closure is probably more efficient than that of Shankar[34], described in the preceding section; the reason being that Tranen's procedure does not require the numerical determination, through additional Dirichlet problems, of the derivative $\partial t_{TE}/\partial\Phi_{LE}$ prior to update of the potential but corrects the potential after each relaxation sweep.

It can be argued ([12], see also section 3.1) that the Dirichlet problem in Tranen's method is not properly posed because of the far-field boundary condition that is used and that the inverse problem as a whole is not well formulated because the regularity condition at the stagnation point is not imposed. The latter is reflected in the way the new airfoil shape is determined. The latter problem requires two steps:

i. determination of the normal velocity V from the Dirichlet solution
ii. determination of the displacement of the stagnation streamline (integration of new surface slopes).

In determining the normal velocity V at the surface mesh points from the Dirichlet solution Tranen utilizes the usual central difference expression, [40]

$$V_{i,j=1} = \frac{1}{r_{i,1}} \cdot \frac{1}{2\Delta r} \left[\phi_{i,2} - \phi_{i,0} \right] \tag{3.36}$$

with the potential in the dummy point (i,0), inside the airfoil (outside the unit circle in the computational plane) determined by satisfying the difference form of the flow equations in the surface mesh points. As described in the preceding section a similar procedure was adopted by Shankar[32] for the TSP equation.

The fact that Tranen does not enforce proper branching of the surface streamline is reflected in particular in the procedure for the determination of the displacement of the "stagnation streamline". The displacement δ of the new surface, relative and normal to the old shape is determined by quadrature using the mass conservation expression

$$\delta_i = \frac{1}{\rho_i U_i} \left[\rho_{i-1} U_{i-1} \delta_{i-1} + \frac{\rho_i V_i + \rho_{i-1} V_{i-1}}{2} \Delta s \right] \tag{3.37}$$

U_i, V_i etc. are determined by means of central differences of the type (3.36). However, at the trailing edge V is set equal to zero by extrapolation from upstream grid points. At the same time some smoothing procedure is required at the grid points nearest to the "stagnation point" (i.e. the point where U, but not necessarily V, is equal to zero) where the integration is started.

As a result of the improper formulation of the inverse problem and the necessarily required adjustments to the surface displacement Tranen requires a direct (= analysis) calculation to check the resulting pressure distribution. A flow chart of the complete design procedure is reproduced in figure 16. Note that the procedure exhibits aspects of a residual-correction type of formulation (Fig. 2b).

Convergence is considered to be obtained when the pressure distribution output by the analysis program is sufficiently close to the prescribed pressure distribution from the previous inverse case. Although convergence in the proper mathematical sense is not guaranteed in Tranen's procedure, examples such as reproduced in figure 17 suggest that engineering requirements can be met in two or three inverse - direct iterations.

Approaches similar to Tranen's have been followed by Volpe[41] and Arlinger[42] in developing inverse methods for two-element airfoil systems in two-dimensional transonic flow. Methods of this type are useful in the design of transonic manoeuvre devices.

In both methods the infinite physical domain is mapped into a computational domain consisting of the finite annular region between two concentric circles. In this plane the main airfoil is mapped into a circle of unit radius and the slat or flap into a circle with smaller radius. In this computational plane finite differences and SLOR are used to solve the full potential equation. The relative position of the elements is fixed during the iteration cycles.

In Volpe's[41] method Dirichlet boundary conditions must be applied on the entirety of both or either one of the airfoil elements. The level of the potential on each of the elements is taken from an analysis solution for a starting geometry. The resulting trailing edge gap must be accepted as it is or can be corrected "manually". As in Tranen's method the regularity condition is not imposed.

Arlinger's[42] method accepts mixed Neumann/Dirichlet boundary conditions in much the same way as in Shankar's[31] inverse TSP method, discussed in section 3.2. As in [31] the regularity condition is satisfied at the junction of the fixed and free parts of the geometry, but there is no control over closure.

A more fundamental (but not necessarily more practical) approach to the 2-D inverse single airfoil problem for the full potential equation has been taken by Volpe and Melnik in [12]. The fundamental difference with Tranen's[39] procedure is that Volpe and Melnik satisfy the regularity condition, i.e. their solutions represent proper stream surfaces. They do so by allowing the magnitude q_∞ of the free stream to vary in such a way that, in Tranen's terminology, V = 0 where U is specified to be zero. In this way they succeed in solving the "pure" inverse problem by a sequence of Dirichlet problems with no need, at any stage, for a direct solution over the current airfoil contour. However, they do not control closure in the sense that a given trailing edge thickness is designed for.

The formulation and solution of the Dirichlet problem in Volpe's[12] method differ from Tranen's in a number of technical but not insignificant details. The most important of these are:

- the "circle plane" finite difference technique is based on Jameson's[43] (non-conservative) rotated difference scheme and mapping procedure rather than those of the Garabedian-Korn method[40]
- the constant of integration fixing the surface potential is chosen arbitrarily but a source term σ ln r is subtracted from the potential. The source term is also represented in the far-field boundary condition and allows for a net mass flow through the boundary as well as for mass generation at shock waves introduced by the non-conservative differencing.
- After each relaxation sweep both the free stream velocity q_∞ and the source term σ are corrected in order to enforce V = 0 at the leading edge stagnation point and at the trailing edge. Hence there is no room for control of closure and whatever trailing edge gap results from the computation is accepted.
- After each Dirichlet problem the perturbation slope

$$\delta\theta_{i,j=1} = \tan^{-1} \frac{V_{i,j=1}}{U_{i,j=1}} \tag{3.38}$$

is used to determine the corrections to the mapping modulus that will drive the approximate airfoil surface to become a streamline. Upon convergence the inverse mapping from the unit circle to the converged airfoil shape is carried out using the known mapping modulus and airfoil slopes.

A point of concern with respect to Volpe's method is that substantial underrelaxation must be applied to the changes in airfoil shape in order to ensure convergence of the design process. In spite of this the number of Dirichlet cycles required for convergence is fairly large, being of the order of 15. This should be compared with the 2 to 3 cycles, which, apparently, are required in Tranen's approach. We will return to this point shortly.

A remark must be made first with respect to the treatment of the trailing edge. It is recalled that the target surface pressure (velocities) are specified at half-mesh and the circulation fixed by integration. At the same time, after satisfying the difference equations, the velocity components are calculated

at the mesh points themselves by means of central differences. As a result, U at the trailing edge is not necessarily zero. Hence there is no complete consistency with the direct solution where the circulation is fixed by requiring U to be zero at the trailing edge. In the inverse method a small correction to the circulation of $O(h^2)$, h being the mesh width, will in general be sufficient to drive U exactly to zero at the trailing edge.

Having noticed that in general, $U \neq 0$ at the trailing edge one may conclude that $\delta\theta$ (equation (36)) will also in general remain bounded. Hence the question arises whether the source term σ should be used to drive $V \to 0$ at the trailing edge. An interesting alternative would seem to be to use σ for control over the trailing edge gap instead. Some control, if necessary at all, over the boundedness of $\delta\theta$ at the trailing edge could be exercised through a (small) correction of $O(h^2)$ to the circulation. There is reason to believe that the use of the source term σ to control closure might also improve the convergence characteristics. The argument being that the value of σ is completely determined by the total integrated net mass flux through the surface and depends only very weakly on the normal velocity in one particular (the trailing edge) point.

A distinctly different approach to (2-D) transonic flow computations (both analysis and design) has been taken by Carlson[44]. Instead of using a body conforming finite difference mesh in the circle plane, Carlson uses (stretched) Cartesian coordinates in the physical plane. As a consequence special complicated difference formulae must be used to satisfy the airfoil boundary conditions in both the analysis and design mode.

From the design point of view Carlson's method, while based on full potential theory (non-conservative), is very similar to the small perturbation formulation of Shankar[31]. In both methods a mixed boundary value problem is solved with the leading edge shape or a greater portion of the airfoil fixed and the pressure prescribed over the remaining portion ($x/c > .06$). As in Shanker's method the orientation of the given leading edge shape with respect to the free stream is fixed and there is no actual control over airfoil closure. Closure can be obtained only by adopting a sharper or blunter nose shape.

From the numerical point of view the analysis and design formulations of Carlson are not completely equivalent. As a result there is no perfect agreement between direct and inverse calculations.

A point worth mentioning is further that, rather than determining the new geometry after convergence of the mixed boundary value problem, the geometry is updated after every ten relaxation sweeps. In combination with successive grid refinement Carlson found this to be the most economic procedure.

The first inverse method for 3-D transonic potential flows is that of Henne[45]. Henne's method can be considered as the 3-D equivalent of Tranen's[39] 2-D method. The Jameson-Caughey FLØ22 wing code[46] has been modified to accept Dirichlet boundary conditions. Figure 18 presents a simplified scheme of the procedure.

Henne does not address the complete 3-D problem of determining the velocity components, and hence the surface potential, as mentioned in section 3.1. Instead, the surface value for the potential in the Dirichlet problem is obtained by "streamwise integration of the velocity at constant span stations". This could mean that the contribution of the spanwise velocity component to the surface pressure is neglected. The spanwise variation of the surface potential at the leading edge is reported to be used as a parameter for trailing edge closure. However, [45] does not provide details. Details about the determination of the surface displacement from the normal velocities are given neither. Nor is mention made of any additional (regularity) conditions enforcing proper branching of the stream surface at the leading edge.

As in Tranen's[39] case Henne's method requires direct analysis computations to check whether the design goal has been achieved. Similarly it is doubtful whether the scheme will converge in the proper mathematical sense. However, the examples of application presented in [45], one of which is reproduced in figure 19, indicate that convergence in an engineering sense can be obtained in 2 to 6 inverse cycles. To this author's knowledge the method is probably the only 3-D transonic inverse method that has been used in a production-type environment.

A somewhat unusual scheme for the 3-D conversion of a given pressure into a Dirichlet-type boundary condition is utilized by Shankar[47] in an effort to modify the FLØ30 finite volume wing-fuselage analysis code[48] into a design code. Starting out from the analysis solution for a suitable estimate of the required geometry Shankar applies a correction to the surface value of the potential in each relaxation sweep. This correction is determined from the isentropic relation for the density

$$\rho = \left[1 - \frac{\gamma-1}{2} M_\infty^2 (q^2-1)\right]^{\frac{1}{\gamma-1}} \tag{3.39}$$

This is linearized to read

$$d\rho = -\rho^{2-\gamma} M_\infty^2 . |q| . d|q| \tag{3.40}$$

or

$$\rho^{(n+1)} - \rho^{(n)} = -\rho^{2-\gamma} M_\infty^2 . |q^{(n)}| . (|q^{(n+1)}| - |q^{(n)}|) \tag{3.41}$$

Utilizing the isentropic relation

$$\rho = \left\{ C_p \frac{\gamma}{2} M_\infty^2 + 1 \right\}^{1/\gamma} , \tag{3.42}$$

equation (41) can, in general curvilinear coordinates, be rewritten as

$$\left(U^{(n)} \frac{\partial}{\partial \xi} + V^{(n)} \frac{\partial}{\partial \eta} \right) \delta\Phi = \frac{\left(\rho^{(n)}\right)^{\gamma-2}}{M_\infty^2} \left[\rho^{(n)} - \left\{ C_{p_t} \frac{\gamma M_\infty^2}{2} + 1 \right\}^{1/\gamma} \right] \tag{3.43}$$

In (3.43) U and V are the contravariant surface velocity components. C_{p_t} is the "target" C_p-distribution. Equation(3.43), in discretized form, is solved for the correction $\delta\Phi$ to the surface potential. Note that the procedure is related but not identical to one in which the direction of the surface velocity is kept fixed but the magnitude updated.

Using the contravariant velocity component W, computed at half a mesh from the wing surface, the

geometry is corrected, without control over closure, after each relaxation sweep. The author of [47] is not very clear, however, on the precise procedure and communicates the opinion that a better procedure to update the wing coordinates, including control over closure should be included.

Remarks like the latter seem to indicate that we have only just begun to tackle the 3-D inverse problem for transonic flow. Considerable effort will be required before we will arrive at well founded, reliable engineering tools of practical significance.

3.4 Residual-correction or iterative Neumann-type methods

In this section methods are described that are based on an iterative process of the type depicted by figure 2b.

Subsonic flow

An engineering type of inverse method directed in particular towards multi-element high-lift airfoil design has been described by Beatty and Narramore[48], The method is based on the Douglas-Neumann (Hess[50]) second-order potential flow method with parabolic surface elements and linear source and vorticity distributions. The earlier idea of Wilkinson[51] is used of determining the (additional) vorticity distribution along the mean line of the airfoil (element) that is necessary to remove the difference between the actual and required upper surface velocities (Fig. 20a). This vorticity distribution is used to calculate the required change in slope of the mean-line elements. The original thickness is then wrapped around the new camberline to determine the new configuration. The latter, in turn is analyzed with the direct mode of the program. A simplified flow chart is reproduced in figure 20b. According to [49], between 5 and 15 iterations are needed for convergence which is considered in an engineering sense only.

The method is capable of dealing with configurations on which the upper surface pressure distribution is specified on one or more elements and the geometry of the remaining elements is specified. The lower surface pressure distribution must always be accepted as it is. The relative location of the leading edge of each airfoil element remains fixed with respect to the trailing edge of the airfoil immediately upstream. An example of application is reproduced in figure 20c.

The method also has limited capabilities for solving the mixed boundary condition problem that is typical for high-lift system design. When used as such, changes in the mean-line in the region where the shape must be kept fixed are simply disregarded. Also the change in lower surface shape associated with the change in mean-line is disregarded.

An approach similar to that described above has been used by Fornasier[52] in constructing a program system for the design of 3-D wings with given thickness and given upper surface pressure distributions. The system contains a vortex lattice method for calculating the required change in camber surface and the MBB Panel Method[53] for checking whether the actual upper surface pressure distribution is sufficiently close to the desired one.

A residual-correction formulation for 3-D wings, [22], employing the thin wing inverse method of Fray and Slooff described in section 3.2 and the NLR Panel Method[54] for arbitrary (thick) configurations has been in use at NLR since 1974. A flow diagram of the method has been reproduced in figure 21. The linear (thin wing) inverse method is used to determine the geometry corrections that are needed to drive the difference δC_p between the actual and required pressure distribution to zero. The thick wing panel method is used for determining the residual δC_p.

The method is used for the design of thick wings with given pressure distribution on both upper and lower surface in the presence of a fuselage and/or other configuration elements of fixed geometry. An essential feature for convergence is the Weber/Riegels leading edge correction. A unique feature, as mentioned already in section 3.2, is that explicit control can be exercised over the geometry while approaching the required pressure distribution as close as possible. This option has proven to be of great value for avoiding undesirable geometries.

An example of application of the method is given in figure 22. Shown is the result of the redesign with and without geometry constraints of the (inner) wing of a wing-fuselage configuration. The starting geometry of the wing was obtained by a wing-alone design for the same target pressure distribution. Other examples may be found in [55].

An approach to the mixed analysis/design problem that, in principle, can be used for general 3-D configurations or parts thereof has been studied by Malone[56]. Malone formulates the problem in terms of minimizing the least squares object function

$$E = \left\{ \sum_{i=1}^{n} w_i \left(C_{p_{t_i}} - C_{p_i} \right)^2 \right\}^{\frac{1}{2}} \quad , \; i = 1(1)n \tag{3.44}$$

through variation of the normal velocity W_j, $j = 1(1)m$, at a selected number of surface points. The minimization of E through variation of the W_j is done numerically by means of a steepest descent method [57]. For this purpose the problem is first linearized around a starting geometry, providing starting values $E^{(o)}$ and $C_{p_i}^{(o)}$. Then, a vector is constructed with components. δW_j such that $E^{(o)} + \delta E = E^{(o)} + \sum_j \frac{\partial E}{\partial W_j} \delta W_j$ takes a minimum value. This requires the determination of the derivatives $\frac{\partial C_{p_i}}{\partial W_j}$. These derivatives are determined numerically by means of finite differences and an analysis type panel method. The panel method, Hess'[54] method in this case, is used to compute the variations δC_{p_i} due to a sequential perturbation δW_j of the normal velocity at panel centers. This requires m panel method solutions with fixed influence coefficients. The derivatives are used to construct the gradient vector representing the direction in the design-variable space in which the decrease of the object function is maximal. The optimization algorithm then determines the step-length in this direction that will minimize E, after which a new gradient and step-length search is executed. This sequence is repeated (of the order of 5 times) until a further decrease of E is no longer significant. Then the W_j are used to correct the geometry in a 2-D, stripwise fashion, after which the whole process is repeated (Fig. 23) for the new estimate of the geometry. About six "outer" iterations are needed for "reasonable" convergence.

As described in [56], the method does not have control over closure and the regularity condition is not satisfied. This might be one reasone for the fact that the author of [56] observes that "local pressure

deviations near the leading and trailing edge are evident". It would seem possible, however, to improve the method in this respect by imposing constraints on W_j in the minimization problem through the introduction of feasible directions.

The approach, as sketched, is interesting because (when the closure problem has been solved) it is one of the few that offers a possibility for the design of local regions of aircraft geometry, such as wing-body fillets or landing gear pods. It also has the advantage that the analysis code can be replaced relatively easily by a better one if it comes available. A drawback, shared with other methods utilizing numerical optimization (section 4) is that the method is relatively costly; about 30 x K panel method solutions being required if K is the number of design variables. Note, however, that only about 6 of these require the calculation of new influence coefficients, the most costly part of panel methods.

Transonic flow

A simple, but apparently effective residual-correction type of approach toward the 2-D transonic inverse airfoil problem has been described by Davis[54]. In this method the FLO6 analysis code [60] is utilized to determine the actual pressure distribution for the latest geometry. The residual δC_p is the driver for a simple, perturbation type of surface modification (inverse) routine. For the latter Davis has taken transonic wavy-wall formulae. These relate the required change in pressure to a change in surface curvature when the local Mach number is <1 and to a change in surface slope when $M_{loc} > 1$. The perturbation slopes and curvatures are then integrated to yield ordinate modifications.

Due to the local perturbation character of the wavy-wall formula the method can be used only for local modifications to the pressure distribution of an existing airfoil. [59] presents results for upper surface contour modifications only, with no control over the trailing edge gap. About 20 iterative cycles are needed for convergence.

While, from the design point of view, the possibilities of Davis' method are limited to local modifications, an advantage of his approach is that only modest development efforts are needed to obtain a working code; the reason being that the (complicated) analysis code is retained in its original form and only the (simple) geometry correction package must be developed.

An approach related to that of Davis[54], but with appreciably wider design capabilities has been realized in the NLR INTRAFS program system, [61]. This system combines the 2-D version of the subsonic thin wing inverse code of [22] and an inverse supersonic wavy-wall formula with the Boerstoel[64] TRAFS fast solver analysis code. A flow diagram is depicted in figure 24. The method can be used for the complete design with full closure control of 2-D airfoils in transonic flow, with or without shock-waves. As a unique feature it retains the possibilities of [22] for explicit control over leading-edge radius, (maximum) thickness and trailing-edge angle.

Figure 25 presents an example of the design of an airfoil with a weak shock, starting out from the NACA 0012 airfoil. Convergence to engineering accuracy is obtained after about 10 iterations. The experience is that shock-free airfoils may require upto 25 iterations before convergence is obtained in terms of pressure distribution, but appreciably less when wave drag is taken as the criterium.

Another possibility for solving the inverse problem through the use of an analysis method, has been studied by McFadden[63]. In [63] a modified version of the Bauer-Garabedian-Korn-Jameson (BGKJ) circle plane relaxation program[43] with non-conservative rotated difference scheme, and a functional relationship involving the mapping and the velocity distribution along the airfoil surface in the physical and computational planes are used in an iterative sequence. In each iteration a functional relationship of the type

$$\frac{ds}{\partial\omega}^{(n+1)} = \frac{1}{q(s(\omega))} \frac{\partial\phi}{\partial\omega}^{(n)} \qquad (\omega, r = 1) \tag{3.45}$$

is used to obtain a better approximation to the mapping function of the required airfoil. In (3.45) s is the arc length along the airfoil and ω the angular coordinate in the circle plane; the mapping is essentially determined by $\frac{ds}{d\omega}$. $q(s)$ is the required velocity distribution and $\phi^{(n)}$ is the potential on the airfoil surface as obtained from the preceding BGKJ relaxation solution.

Note that, upon convergence, equation (3.45) leads to the identity

$$q(s) = \frac{\partial\phi}{\partial s} = \frac{\partial\phi}{\partial\omega} \quad (\omega, r = 1) \frac{d\omega}{ds} \tag{3.46}$$

Note also that the procedure bears some resemblance to the "indirect" inverse TSP formulations discussed in section 3.2. In the latter, the irrotationality condition (3.21) plays the same role as equations (3.45)/(3.46) in McFadden's approach.

Further noteworthy features of McFadden's method are that

- the (iterative) relaxation process and the outer iterations for the geometry are intermingled
- on fine meshes an additional artificial viscosity term that suppresses the formation of shock waves is required for convergence (which takes 200-700 relaxation cycles). As discussed in [63] the undesirable effects of this limitation can be overcome largely by a suitable design strategy
- in order to avoid singular behaviour of (3.45) at the stagnation point ($q = 0$) a special treatment, implying modification of $\phi^{(n)}$, is incorporated
- while the analysis routine requires M_∞ and q_∞ to be given (the latter is set equal to unity) the critical velocity c^* must be chosen in the design program. M_∞ is determined from the isentropic relation

$$\frac{1}{2}\left(\frac{c^*}{q_\infty}\right)^{\frac{\gamma+1}{\gamma-1}} = \frac{1}{2}\,\frac{1}{(\gamma-1)M_\infty^2} \tag{3.47}$$

- instead of setting q_∞ equal to unity, the free stream velocity, as in Volpe's[12] method, comes out as a result of the design calculations. However, rather than using q_∞ to eliminate the stagnation point singularity, q_∞, in McFadden's approach, is used to minimize the functional

$$I = \int_0^{2\pi} \left[\left(\phi_s^{(n)}\right)^2 - \frac{q(s)}{q_\infty^{(n)}}\right)^2\Big]^2 d\omega \tag{3.48}$$

While a motive for this particular choice is not given, the result seems to be that the overall thickness of the new airfoil is approximately the same as that of the starting airfoil.

- there is no control over closure. The trailing edge gap must be accepted as it is or must be manipulated through changes in the target pressure distribution. An alternative possibility would seem to be to use q_* to control the trailing edge gap rather than to minimize (3.48).

An example of application of McFadden's method has been reproduced in figure 26. The example is interesting in that it illustrates the fact that a smooth surface pressure distribution does not necessarily lead to a shock-free flow or even a flow with low wave drag; the shape of the sonic line as well as the figure for wave drag (40 counts) indicate the presence of a shock wave in the flow field that weakens and vanishes as it approaches the airfoil. Note that [68] contains several useful guidelines for the choice of "target" pressure distributions in relation to low wave drag.

A modified version of the method, known as the Modified Mapping Modules (M³) method is operational at Grumman Aerospace.

A residual-correction type of formulation for 2-D wings in transonic flow has been described briefly by Garabedian and McFadden[64],[65] (see also Miranda[66]). The method utilizes a version of the H[illegible] analysis code, [46], in combination with a relationship between geometry correction and pressure residual of the type

$$a_2 \frac{\partial^2(\delta S)}{\partial X_1^2} + a_1 \frac{\partial(\delta S)}{\partial X_1} + a_0 \delta S = a\, \delta q^2 \tag{3.49}$$

Here, $S(X_1,Y_1)$ defines the wing surface in the sheared parabolic coordinate system (X_1,Y_1,Z_1) of the FL30 code, δS and δq^2 denote the geometry corrections and surface velocity (squared) residuals, respectively. a, a_0, a_1 and a_2 are parameters "selected to accelerate convergence", [65]. Details are not provided in [64], [65], [66]. Note, however, that the first and second terms of (3.49) are related to curvature and slope modifications, respectively. This suggests that the approach is related to that of Davis[54] for 2-D airfoils.

In order "to avoid questions of closure and other complications with the geometry", [64], Eq. (3.49), at each iteration step, is solved subject to the constraint that $\delta S \geq 0$. As a result the wing surface is modified only where the local speed is sufficiently high.

An example of application is presented in figure 27. An interesting feature of the method is the determination (and visualization) of wave drag through spatial integration of the artificial viscosity term of the discretization scheme. Further details about the method are to be found in [67].

3.5 Nonlinear boundary value problem formulation

Here we will describe methods that follow iterative schemes of the type of figure 2c or variations thereof. As we shall see, in most of the methods of this category the inverse problem is formulated as a minimization problem.

Subsonic flow

Utilizing panel method technology an approach based on minimizing a functional of the type

$$E = \sum_{i=1}^{n} \left(U_i - U_{t_i}\right)^2 \tag{3.50}$$

has been described in a series of publications by Bristow[68],[69],[70]. In Eq. (3.50) U_i represents the actual tangential velocity at a panel control point i and U_{t_i} the corresponding "target" value. In order to yield a stream surface E must be minimized subject to the constraint that the normal velocity V is zero.

In [68] the problem is solved for bodies of revolution utilizing flat panels with constant source density. The problem variables are the source densities σ_i and the panel slopes α_i. Minimizing E requires that the first variation of E is zero which is the case when

$$\frac{\partial E}{\partial \sigma_j} = 2 \sum_{i=1}^{n} \left(U_i - U_{t_i}\right) \frac{\partial U_i}{\partial \sigma_j} = 0 \qquad j = 1(1)n \tag{3.51a}$$

and

$$\frac{\partial E}{\partial \alpha_k} = 2 \sum_{k=1}^{n} \left(U_i - U_{t_i}\right) \frac{\partial U_i}{\partial \alpha_k} = 0 \qquad k = 1(1)n \tag{3.51b}$$

with the constraint

$$V_i = 0 \qquad\qquad i = 1(1)n \tag{3.52}$$

U_i and V_i are expressed in terms of σ_j and α_k by means of aerodynamic influence coefficients $A_{ij} = A_{ij}(\alpha_i,\alpha_j)$ and $B_{ij} = B_{ij}(\alpha_i,\alpha_j)$

$$\left.\begin{aligned} U_i &= \sum_j A_{ij}(\alpha_i,\alpha_j)\sigma_j + \cos\alpha_i \\ V_i &= \sum_j B_{ij}(\alpha_i,\alpha_j)\sigma_j - \sin\alpha_i \end{aligned}\right| \tag{3.53}$$

the terms $\cos\alpha_i$, $-\sin\alpha_i$ stemming from of the component of the free stream velocity. Note, that because σ and α are related through the stream surface constraint (3.52) the equations (3.51a) and (3.51b) are <u>not</u> independent. Bristow chooses to use (3.51a).

Equations (3.51a) and (3.52) with (3.53) represent a system of 2n non-linear equations for 2n unknowns σ_j, α_k. In order to solve this system Bristow linearizes (3.51a) and (3.52) around a starting solution $U_i^{(o)} = U_i(\alpha_i^{(o)}, \sigma_i^{(o)})$ obtained by solving the analysis (Neumann) problem for a starting geometry. This leads to the linear system

$$\left.\begin{aligned} &\sum_{i=1}^{n}\left(U_i^{(o)}+\delta U_i-U_{t_i}\right)\frac{\partial\delta U_i}{\partial\sigma_j}=0\\ &\delta V_i=0\end{aligned}\right| \qquad (3.54)$$

where

$$\delta U_i=\sum_j A_{ij}^{(o)}\delta\sigma_j+\sum_j\frac{\partial A_{ij}}{\partial\alpha_j}\delta\alpha_j\,\sigma_j^{(o)}-\sin\alpha_i^{(o)}\,\delta\alpha_i \qquad (3.55)$$

and

$$\delta V_i=\sum_j B_{ij}^{(o)}\delta\sigma_j+\sum_j\frac{\partial B_{ij}}{\partial\alpha_j}\delta\alpha_j\,\sigma_j^{(o)}+\cos\alpha_i^{(o)}\,\delta\alpha_i \qquad (3.56)$$

The influence coefficients and their derivatives are calculated analytically. After solving (3.54) for $\delta\sigma$ and $\delta\alpha$ the geometry is updated through $\delta\alpha$ and a new starting solution is created through the solution of a Neumann problem for the corrected geometry. Hence, the iterative process can also be considered to be of the type of figure 2b.

It is worth mentioning that Bristow, through further approximations, manages to eliminate $\delta\alpha$ from the system (3.54). This, although of practical importance, is not essential. Of more fundamental importance is the fact, that with the constant source density and mid-panel control point discretization the (square) system of equations (3.54) does not leave room for imposing the closure condition. Moreover, as we have seen earlier, this discretization scheme is basically unstable in the sense of [19]. The first problem, i.e. that of closure, is solved by Bristow by introducing the closure condition as an additional constraint to the minimization problem through the technique of Lagrange Multipliers. The problem of instability is overcome by means of an elaborate smoothing operation involving the use of "substitute elements". In spite of this the author reports that "an inability to converge" may be apparent. This might also be due to the fact that Bristow does not address the regularity condition. Underrelaxation in updating the geometry is used to improve convergence. As indicated by the example reproduced in figure 27 about 10 iterations are needed for convergence.

Basically the same approach was used by Bristow[69,70] in developing an inverse method for 2-D multiple-element airfoils, culminating in the MAAD program system, [70]. The main differences with the preceding method for axisymmetric flow are the following.

- The method utilizes constant or, optionally, linear source distributions and linear vorticity distributions on flat panels. The source and vorticity distributions are related according to Green's third identity [71]*). This implies that the source strength is directly related to the normal velocity through

$$V_i=\sigma_i-\sin\alpha_i \qquad (3.57)$$

  and the vorticity strength to the tangential velocity through

$$U_i=\cos\alpha_i+\tfrac{1}{2}\gamma_i \qquad (3.58)$$

  This greatly facilitates the analytical elimination of the $\delta\gamma_i$ and $\delta\sigma_i$ from the final system of equations (the equivalent of (3.54)) that is to be solved; only the $\delta\alpha_i$'s remaining as independent variables.
- The squared residuals in the object function (3.50) are weighted through the arc length of the relevant panel.
- Both complete inverse and mixed analyses/design problems, with the shape of certain parts of the geometry fixed, can be dealt with.

An example of application of the MAAD program has been reproduced in figure 29. Shown is the reconstruction, in 5 iterations, of the so-called Williams flap (a configuration obtained through a conformal mapping procedure).

The multiple airfoil mixed analysis/design problem has also been studied by Labrujère[72,73,74]. Labrujère formulated the problem in terms of minimizing a functional of the type

$$E=\sum_{p=1}^{q}\sum_{i=1}^{n}\left\{w_{t_{p,i}}\left(U_{p,i}-U_{t_{p,i}}\right)^2+w_{n_{p,i}}V_{p,i}^2+w_{g_{p,i}}\left(Z_{p,i}-Z_{p,i}^{(o)}\right)^2\right\}\Delta S_{p,i} \qquad (3.59)$$

In (3.59) U and V, again, represent the tangential and normal velocity, respectively. The $Z_{p,i}$'s represent coordinates, in a local coordinate system, of the p^{th} airfoil element geometry that is being solved for and the $Z_{p,i}^{(o)}$'s represent a starting or "target" geometry. The $w_{t_{p,i}}$, $w_{n_{p,i}}$ and $w_{g_{p,i}}$ represent (positive) weighting coefficients. $\Delta S_{p,i}$ represents the panel length.
Surface doublet distributions μ_i only are used to model the flow. Note that this implies that the closure condition is satisfied implicitly, but that the airfoil elements must have zero trailing edge thickness.

E, Eq. (3.59), is minimized by varying:
- the doublet strengths $\mu_{p,i}$,

and, as far as required and admitted by the designer,
- the angles α_p between the local and reference coordinate systems (Fig. 30)
- the coordinates of the origins of all but one of the local coordinate systems
- the $Z_{p,i}$'s.

The system of non-linear equations resulting from setting the first variation of E equal to zero is solved by means of Newton's method. The aerodynamic influence coefficients and their derivatives with respect to the geometry variables are calculated analytically. For the latter purpose use is made of the small curvature expansion technique of Hess[50].

The choice (3.59) for the object function and in particular the possibility to manipulate the weighting coefficients w_t, w_n and w_g has a number of interesting consequences.
1. By choosing $w_t = 0$ the problem reduces to a Neumann problem for $Z^{(o)}$
2. With $w_n = 0$ a Dirichlet problem for $Z^{(o)}$ is obtained.

*) A different choice was made in [69]

3. $w_g = 0$ represents the pure inverse problem.

The latter option is never used in practice for two reasons. The first is that, in order to impose the regularity condition w_g must be $\neq 0$ at or near the stagnation points ($U_i = 0$). Secondly, in case of multiple airfoils, the pure inverse problem may be ill-posed when the airfoil elements are completely free to move. (When the airfoil elements are sufficiently far apart their relative position is no longer important.) Note further, that in principle the solution obtained through the minimization of (3.59) may exhibit "leakage" ($V_i \neq 0$). In practice this can be suppressed by choosing a sufficiently high value for w_n.

While pioneering the approach sketched above Labrujère considered various types of doublet distributions and surface representations, [72], [73]. In the final "production" version of the method (the NLR MAD Program System, [74]) quadratic representations are used for both doublet distribution and geometry. The velocities are calculated at panel centers. The program has further been embedded in a bigger system, together with the "viscous" analysis method of Oskam[75], providing a possibility for the allowance for viscous effects.

An early (test) example of Labrujère's method, taken from [73], is presented in figure 31. Shown is the reconstruction of an airfoil-flap configuration with fixed overlap. Three Newton iterations were required for convergence.

Transonic flow

Inverse methods for transonic flow that directly address the non-linear boundary value problem do not exist at present. The main reason is that the analytical determination of the derivatives that are needed for constructing the gradient of the residual is virtually impossible. Methods minimizing object functions of the type of (3.50) by means of numerical optimization techniques will be discussed in section 4.

4. DIRECT DESIGN BY MEANS OF (NUMERICAL) OPTIMIZATION

In this section we will discuss methods, involving the use of aerodynamic analysis methods in combination with a (numerical) optimization algorithm, that directly address the problem of optimizing a chosen aerodynamic quantity, such as drag. The linear (vortex lattice) based methods for the minimization of induced drag, [23], [24], already discussed in section 3.2, can also be considered to belong to this category. However, they utilize the technique of Lagrange multipliers rather than numerical optimization.

While applications of the direct numerical optimization approach have seen the use of various aerodynamic codes, only one single feasible directions/gradient optimization algorithm, developed by Vanderplaats[76], seems to be used almost exclusively, in particular in combination with transonic flow codes.

The approach is fairly recent (1974, Hicks et al.[77]), owing its existence entirely to the availability of large and fast computer system. Because of the excessively large computational requirements, at least in 3-D, the approach is sometimes referred to as "design by brute force". Nevertheless it holds great potential for the future. A reappraisal of the technique has been given recently by Hicks[78]. Several chastening experiences are also reported in [86].

A generalized flow diagram of the design - by - numerical - optimization technique is presented in figure 32. Inherent to the numerical optimization approach are the choice of an aerodynamic object function F that is to be minimized, a number of quantities to be constrained G_j and the choice of a set of design variables. The object function can be the drag or any other suitable aerodynamic quantity. The constraints can be of aerodynamic or geometric nature; e.g. C_L and/or t/c greater than a specified value. The design variables are taken to be the coefficients A_i of a number of shape functions

$$Z = Z_o + \sum_{i=1}^{n} A_i . f_i \qquad (4.1)$$

describing (modifications to) the starting wing geometry.

The process begins by perturbing, in sequence, each of the shape function coefficients A_i. The resulting n shapes are analyzed by means of the aerodynamic program (determination of F and G_j's) and the derivatives $\frac{\partial F}{\partial A_i}$, $\frac{\partial G_j}{\partial A_i}$, or rather the difference quotients $\frac{\Delta F}{\Delta A_i}$, $\frac{\Delta G_j}{\Delta A_i}$ are determined. The next step is the formation, by the i^{th} optimization program, of the gradient $\overline{\nabla F}$ and the determination of the direction of steepest descent of F, in the n-dimensional space formed by the basis vectors $\overline{A_i}$, while satisfying the constraints. The optimization program then executes a number (typically 3) of steps in this direction, with another aerodynamic analysis performed at each step, until either a constraint is met or F attains a minimum. In the first case, or when the minimum of F is lower than the previous minimum, the process is repeated; new gradients are determined, etc.. When the latest minimum of F is equal to or higher than the previous one the process is terminated.

The optimization process described above requires typically 10 complete cycles or, in other words, 10(n+3) analysis calculations, [79]. This immediately illustrates the weakest point of the numerical optimization approach. In order to keep the computational effort required within reasonable bounds one has to put severe limitations on the number n of design variables, in particular in 3-D flow. The problem is enhanced by the fact that for acceptable convergence of the optimization process it is necessary to avoid "numerical noise" in the partial derivatives of the object function, [81], [82]. This requires that the relaxation process in each analysis calculation must be continued until the residual has reached a level beyond that which is often customary in "normal" analysis calculations. It also appears to exclude the use of analysis codes with simple boundary layer corrections, [78]. The reason for the latter is that the airfoil aerodynamic quantities do not vary consistently enough when boundary layer and potential flow are coupled in the weak interaction sense.

One way to reduce the number of analysis calculations required in 3-D applications is to evolve the design variables in a series of steps, [84]. For example by first designing the upper surface, section by section, going from root to tip and then the lower surface. Clearly it is also very important to select a starting geometry having aerodynamic characteristics which are already close to the target. This asks for an information systems/data base approach. With previous experience stored in the data base, the latter can be searched for the most suitable starting solution. As described in [79] the data base approach can also be used to speed-up the convergence of numerical optimization by at least a factor two. With the results of all preceding geometry perturbations stored it is possible to construct higher partial

derivatives of the object function and utilize higher order gradient methods.

With the severe limitations on n, the choice of the shape functions is of utmost importance. The choice should be directed towards describing a sufficiently wide class of practical solutions. While simple polynomial expressions were used in early applications [77], [80], of the numerical optimization concept, a more sophisticated class of shape functions describing more local geometry modifications was used in later applications, [81], [82], [83]. However, as discussed in [84], there is a need for still better shape functions with even more localized curvature variations. In fact it can be argued, following arguments similar to those used by Davis[59] in selecting the geometry correction formulae in his residual-correction type of inverse method, that while curvature based shape functions are suitable for areas with subcritical flow, slope based shape functions might be more appropriate in areas with locally supersonic flow. In general it can be stated that the design variables must be chosen carefully for each individual optimization problem. Not in the least because the choice also affects the convergence of the optimization progress, [79].

While the choice of the design variables is of great practical significance, the choice of the object function, in conjunction with the choice of the aerodynamic and geometric constraints, is of more fundamental interest. In two-dimensional transonic applications, [77], [79], [80], [81], it has been customary to select the wave drag as the quantity to be minimized, subject to constraints on, e.g., airfoil thickness or volume, lift and/or pitching moment. Although it is clear that constraints are necessary in a meaningful drag minimization problem it is by no means clear how exactly the problem should be formulated in order to guarantee a unique solution. The problem is illustrated by figure 33, taken from [79]. Shown are the results of two drag minimization runs with identical free stream conditions and identical constraints on lift and airfoil volume. Only the starting solutions differ. As illustrated by the figure the two resulting airfoils are totally different in shape. Clearly the problem, as formulated, has more than one, local minimum and neither of the two necessarily represents the absolute minimum.

Figure 33, the airfoil on the right in particular, also illustrates another problem of direct (inviscid) wave drag minimization. In the absence of (direct) control over the pressure distribution the solution may acquire unrealistically high pressure gradients, such as near the upper surface trailing edge.

A strong point of the numerical optimization approach is the possibility of selecting object functions and constraints suitable for multi-point designs. An example of a two-point design problem directed towards the design of airfoils with low drag creep can be found in [81]. Low speed airfoil design applications are considered in [85]. It is also entirely possible to consider, e.g. transonic drag minimization and low-speed stall requirements simultaneously.

While the direct minimization of (inviscid) wave drag is feasible in two dimensions, it is not, at present, in the case of three-dimensional wings. Several unsuccessful attempts in this direction can be found in the literature, [82], [83], [84]. The main reason for this failure is the lack of accuracy in the determination of the pressure drag with the currently available 3-D codes and the limited number of mesh points. Another problem would seem to be that the problem of uniqueness in three dimensions is even more severe than in two dimensions. The accuracy problem might be overcome when more efficient algorithms and/or more computer power (vector machines) allow the number of mesh points to be increased. The uniqueness problem would probably require the introduction of more constraints or more sophisticated object functions.

Because of the difficulties just mentioned most 3-D applications [83], [84], of design-through-numerical-optimization have seen the use of the pressure distribution type of object function

$$F = \sum_{i=0}^{N} \left(C_p - C_{p_{target}} \right)_i^2 \qquad (4.2)$$

When used in this mode, design-by-numerical-optimization is an extremely expensive substitute for the inverse approach described in the preceding section. While the latter is absolutely feasible on currently available general main frame computers, the former, requiring an order of magnitude more computer time, is absolutely not, at least in an industrial environment. On the other hand, inverse design through numerical optimization does have the advantage that direct control over the geometry can be excercised through the application of constraints. The latter possibility is absent in most of the inverse methods discussed in section 3, at least for transonic flow.

The technique of numerical optimization has also been used by Lamar[87] in the exploratory design of optimal camber surfaces for slender (low aspect ratio) wings with leading edge separation. For this purpose the CONMIN optimization code[76] was coupled with a vortex lattice method supplemented with the leading edge suction analogy of Polhamus[88].

Summarizing the discussion on design by numerical optimization, it may be said that the potential possibilities of the approach are enormous with, at present, unique capabilities such as multi-point and constrained design. However, the approach is also unique in terms of required computer resources. Substantial improvements in both flow optimization code algorithms and/or computer efficiency, relative to current general standards, are required before numerical optimization in 3-D wing design can be used on a routine basis.

5. SPECIAL METHODS: FICTITIOUS GAS CONCEPT

A special class of methods, directed in particular towards the modification of existing shapes for the purpose of eliminating transonic wave drag, is formed by those based on Sobieczky's fictitious gas concept, [90]. As discussed in [89], the fictitious gas methods are closely related to the Sobieczky-Eberle hodograph methods. Both are based on the concept of the elliptic continuation of the subsonic part of a mixed subsonic/supersonic flow field into the supersonic zone by modifying the pressure-density (or velocity - density) relation. However, instead of working in the hodograph plane the fictitious gas method utilizes a direct (analysis) transonic potential flow method in which the pressure (velocity)-density relation is modified locally whenever $M_{local} > 1$.

The modified analysis code is used to compute the fictitious gas flow about a given base configuration, the transonic wave drag characteristics of which, at given angle of attack and Mach number, have to be improved. When the solution to the fictitious gas flow problem is known, the correct supersonic flow field inside the sonic surfaces is determined by solving an initial value problem with the initial data given on the sonic surface. The new correct flow inside the sonic "umbrella" defines a new stream surface that is tangent to, and has the same curvature as, the stream surface (contour) at the intersection of the

sonic surface and the original body. In this way a part of the original body is modified and indeed in such a way that, at the same conditions of Mach number and angle of attack a transonic shock-free flow is obtained. Hence, the fictitious gas method should be considered as a shock-free redesign method[91].

An appealing feature of the fictitious gas method is that, in principle, any available 2-D or 3-D analysis code may be modified, and used to solve the elliptic part of the problem. In 2-D, Sobieczky et al.[90] use Jameson's FLØ6 code[60], while in another application of the concept Eberle[92] uses a 2-D version of his finite element method. Applications in 3-D have seen the use[90,93] of a Bailey-Ballhaus type of transonic small perturbation code as well as [91], [94] the more advanced Jameson-Caughey full potential FLØ22 and FLØ27 codes. As demonstrated in [95], [96] it is also possible to utilize analysis codes including viscous-inviscid interactions.

In two dimensions[90,92] the initial value problem in the supersonic part of the flow field may be solved by means of either a characteristics methods in a hodograph-like working plane or by a finite difference marching procedure[97]. In 3-D a marching procedure is used, going inward from the sonic surface by successive surfaces of constant density for the full potential equation or constant longitudinal flow speed u for the small perturbation equation.

An important point to note is that the (re)design problem as sketched above does not always have a useful solution. This is associated with the character of the initial value problem to be solved in the supersonic part of the flow field. In the 2-D hodograph plane the problem is well posed and the solution is readily found. However, as mentioned earlier, the solution may not be useful because of the appearance of limit lines in the transformation from the hodograph to the physical plane. Limit lines or surfaces may also appear directly when the marching procedure is used[90,93]. If they appear, a next attempt towards a physically meaningful solution may be made by using a "more elliptic" fictitious gas law. An additional complication in 3-D is that the initial value problem for the supersonic domain seems to be ill-posed[90,93]; i.e. small changes in the initial data will cause large changes in the solution elsewhere. As a consequence the marching procedure, or, indeed, any numerical method, is unstable in principle. However, the instability appears to be manifest only when spanwise gradients are large, and, apparently, is of little consequence for moderate to high aspect ratio wings[93]. Note that as discussed in section 3.1 the 3-D inverse problem is also "ill-posed".

Some examples of application of the fictitious gas method are reproduced in figures 34 and 35. Figure 34, taken from [90], shows the (inviscid) shock-free redesign of the NACA 64A10 airfoil at a Mach number of 0.72 and 0.4 degrees angle of attack. Note that the modified airfoil is somewhat thinner and has a 10 % lower lift coefficient. An illustrative 3-D example, taken from [95] has been reproduced in figure 35. Shown is the result of the shock-free redesign of a 15.7° swept wing built-up from GA(W)-2 type airfoil sections. This type of airfoil is known to have good low speed $C_{L_{max}}$ characteristics, but as indicated by the figure, the high speed characteristics at M = 0.8 are poor. Also shown is the result of a shock-free redesign at M = 0.8 which has not affected the first 9 % of the airfoil chord. Because of the latter it can be expected that the new wing will also have a good low speed $C_{L_{max}}$.

Examples such as this serve to illustrate the point that the fictitious gas method is a viable tool for the shock-free redesign of a given wing in the final stages of the aerodynamic design process. However, because of the fact that a suitable basic shape is required from the outset, additional tools such as those described in the preceding sections are required if the complete aerodynamic design of a wing or airfoil is the objective.

It seems appropriate at this point to comment on the, apparently, still wide-spread misconception that, from an engineering point of view, shock-free flows are less interesting than other supercritical airfoil flows. This is so, it is argued, because the best L/D for a given Mach number is always obtained with a weak shock present and also because of the large aerodynamic center shifts that would be produced by shocks occurring at slightly off-design conditions.

Although the statement that $(L/D)_{max}$ is obtained when a weak shock is present is correct, at least for a given geometry, this does not necessarily make "shock-free" designs less attractive. This is so first of all because the problem of aerodynamic design is generally to find a shape that, subject to certain constraints, maximizes L/D (or rather minimizes D) for <u>given lift</u>. This is a different optimization problem than that of finding the best L/D for a <u>given shape</u>. A second reason is that "shock-free" designs very seldom turn out to be really shock-free in practice. Due to inappropriate boundary layer modelling, wind tunnel wall interference and aeroelastic distorsion, most if not all shock-free designs exhibit weak shock waves at and around the design C_L and Mach number in the wind tunnel or atmospheric flight environment. Shock-free designing must therefore be viewed as one (of several) possible means to design for flows with small or negligible wave drag for a certain range in C_L and Mach number. The reader is referred to the Round Table Discussion contained by [98] for a recent discussion on the issue. The possible problem of rapid shifts with Mach number of the aerodynamic center is not confined to shock-free designs. Such rapid shifts occur on most advanced and many conventional airfoils in transonic flow. Airplane designers have learned to live with it, with Mach trim compensators found on most commercial jet transports.

6. CONCLUDING REMARKS

Having discussed the possibilities and limitations of several approaches in aerodynamic design, the question may be raised which, if any, of the various techniques is to be preferred. As usual with such questions a general and definitive answer cannot be given. The answer will depend on the particular circumstances that apply and will vary from case to case.

There also appears to be divergence of opinion on the matter: In [86] one author states (p. 383) that "Because of their relative simplicity and computational efficiency, coupled with (these) weaknesses, inverse methods seem best suited for initial wing design. Some other technique is then required to produce an optimized design". Another author communicates the opinion (p. 439) that "Direct optimization appears to be well suited for early design iterations involving large geometry changes subject to design constraints. Later refinements can probably be accomplished more efficiently with an inverse solution". Who is right?

If a choice between the various possibilities is to be made table 3 may be of some help. The table illustrates the point that if a general design method for complete wings is required the fictitious gas

method does not suffice. Neither do, of course, residual-correction type of inverse methods with only local redesign capabilities, such as [59], [64]. In this author's opinion an inverse approach allowing global wing design as well as local design modifications is, at present, the best compromise, numerical optimization being to expensive. Subsonic codes having this capability are those of [56], [70], [74] and (possibly) that of [35]. To the author's knowledge they do not exist for transonic flow, with the possible exception of [42].

The most serious limitation of most existing inverse methods is that it is not possible to impose constraints on the geometry. Efforts should be directed towards developing inverse codes having such capability, in particular for transonic flow. Existing codes having this capability are those of [22], [61], [72-74], and to some extent, [70], (see table 1).

Another problem with inverse methods is that the specification of the target pressure distribution puts a heavy burden on the aerodynamicist. As an example, for transport aircraft, the target pressure distribution must be chosen such that, at least at the design condition, boundary layer separation is avoided and that drag is minimized while obtaining an acceptable geometry. At the same time the choice should lead to acceptable off-design characteristics.

That the problem is not at all trivial, e.g. in relation to wave drag minimization, is illustrated by figure 26, showing that a suitably looking shock-free surface pressure distribution may not be suitable for the minimization of wave drag. Another example of this kind is presented in figure 36 which was taken from [64]. The figure on the right presents the result of an inverse (McFadden's) method; the resulting airfoil carries a wave drag of 38 counts. The figure on the left, on the other hand, presents the nearest shock-free solution (zero wave drag) as obtained with a hodograph method. Note that the latter result could also be obtained by means of the fictitious gas method. As mentioned, the fictitious gas could be a useful tool for the final elimination of the wave drag from a design that has already been taylored in all other respects.

It is conjectured that most if not all of the limitations of inverse methods could be avoided through an approach which we will call inverse numerical optimization. In this conjectural scheme (Fig. 37) the design variables are parameters describing the pressure distribution rather than the geometry. The optimization algorithm is used to optimize a target pressure distribution, e.g. with the objective to minimize the drag. Using the latest available estimate of the geometry this can be done relatively cheap through an induced drag (Trefftz plane, [99]) routine, a boundary layer code and a pressure drag routine. With the target C_p-distribution established the new geometry can be determined by means of an inverse code. Subsequently the off-design characteristics can be determined by means of an analysis code. The process is repeated when the new geometry differs significantly from the previous one or when a geometry or off-design constraint is met. In the latter cases (new) constraints will have to be imposed on the values of the parameters describing the pressure distribution. Information from all the previous iterations can be used to determine these new values.

It is the author's opinion that an approach of the type sketched above, is worthy of further investigation, in particular when embedded in an information systems/data base approach, [100].

7. REFERENCES

1. Slooff, J.W.; "Wind-tunnel tests and aerodynamic computations, thoughts on their use in aerodynamic design", AGARD CP. No.210, Paper 11, 1976.
2. Eppler, R.; "Direkte Berechnung von Tragflügelprofilen aus der Druckverteilung", Ingenieur-Archiv XXV, Band 1957, pp. 32-57.
3. Van Ingen, J.L.; "A program for airfoil section design utilizing computer graphics", AGARD/VKI Lecture Series, 1969.
4. Arlinger, B.; "An exact method of two-dimensional airfoil design", SAAB TN67, 1970.
5. Strand, T.; "Exact method of designing airfoils with given velocity distribution in incompressible flow", J. Aircraft, Vol. 10, pp. 651-659, 1973.
6. Holst, T.L., Slooff, J.W., Yoshihara, H., Ballhaus Jr., W.F.; "Applied computational transonic aerodynamics", AGARD-AG-266, 1982.
7. Slooff, J.W.; "Computational procedures in transonic aerodynamic design", Lecture presented at ICTS Short Course on Computational Methods in Potential Aerodynamics, Amalfi, Italy, 1982. (Also NLR MP 82020 U).
8. Hess, J.L., Johnsson, F.T., Rubbert, P.E.; "Panel methods", Notebook, AIAA Professional Study Series, 1978.
9. Ortega, J.M. and Rheinboldt, W.C.; "Iterative solutions of nonlinear equations in several variables", Academic Press, N.Y., 1970.
10. Lighthill, M.J.; "A new method of two-dimensional aerodynamic design, ARC R&M 2112, 1945.
11. Woods, L.C.; "The design of two-dimensional airfoils with mixed boundary conditions, Quart. Appl. Math. Vol. 13, pp. 139-146, 1955.
12. Volpe, G. and Melnik, R.E.; "The role of constraints in the inverse design problem for transonic airfoils, AIAA Paper No.81-1233, 1981.
13. Ashley, H. and Landahl, M.T.; "Aerodynamics of wings and bodies", Addison-Wesley Publ. Company, Inc., Reading, Mass., 1965.
14. Van Dijke, M.; "Perturbation methods in fluid mechanics", Academic Press, N.Y., 1964.
15. Der Jr., K. and Raetz, G.S., "Solution of general three-dimensional laminar boundary layer problem by an exact numerical method", IAS Paper No. 62-70, 1962.
16. Lighthill, M.J.; "On displacement thickness", J. Fl. Mech. 4, p. 383, 1958.
17. Woodward, F.A.; "Analysis and design of wing-body combinations at subsonic and supersonic speeds", J. Aircraft, Vol. 5, No. 6, pp. 528-534, December 1968.
18. Woodward, F.A., Tinoco, E.N. and Larsen, Y.W.; "Analysis and design of supersonic wing-body combinations, including flow properties in the near field - Part I - "Theory and Application", NASA CR-73106, August 1967.
19. Oskam, B.; "Stability analysis of panel methods", unpublished NLR Memorandum (AT-82-002 U), 1982.
20. Rubbert, P.E. and Saaris, G.R.; "Review and evaluation of a three-dimensional lifting potential flow analysis method for arbitrary configurations", AIAA Paper 72-188, January 1972.
21. Weber, J.; "The calculation of the pressure distribution on the surface of thick, cambered wings and the design of wings with given pressure distribution", ARC R&M 3026, 1957.

22. Fray, J.M.J. and Slooff, .W.; "A constrained inverse method for the aerodynamic design of thick wings with given pressure distribution in subsonic flow", AGARD CP. No. 285, paper 16, 1980.
23. Feifel, W.M.; "Optimization and design of three-dimensional aerodynamic configurations of arbitrary shape by a vortex lattice method", NASA SP-405, 1976, pp. 71-88.
24. Lamar, J.E.; "A vortex-lattice method for the mean camber shapes of trimmed noncoplanar planforms with minimum vortex drag", NASA TN D-8090, June 1976.
25. Steger, J.L. and Klineberg, J.M.; "A finite difference method for transonic airfoil design", AIAA J., Vol. 11, No.5, pp. 628-635, May 1973.
26. Langley, M.J.; "Numerical methods for two-dimensional and axisymmetric transonic flow, ARA Memo 143, 1973.
27. Murman, E.M. and Krupp, J.A.; "The numerical calculation of steady transonic flow past thin lifting aerofoils and slender bodies", AIAA Paper No. 71-566, 1971.
28. Lock, R.C.; "Research in the U.K. on finite difference methods for computing steady transonic flow" in: Symposium transonicum II, Springer Verlag, 1976.
29. Schmidt, W., Rohlfs, S. and Vanino, R.; "Some results using relaxation methods for two- and three-dimensional transonic flows", Lecture Notes in Physics, Vol. 35, pp. 364-372, 1975.
30. Schmidt, W. and Hedman, S.; "Recent explorations in relaxation methods for three-dimensional transonic potential flow", ICAS Paper 76-22, 1976.
31. Shankar, V., Malmuth, N.D. and Cole, J.D.; "Computational transonic airfoil design in free air and a wind tunnel, AIAA Paper No.78-103, 1978.
32. Shankar, V., Malmuth, N.D. and Cole, J.D.; "Computational transonic design procedure for three-dimensional wings and wing-body combinations, AIAA Paper No.79-0344, 1979.
33. Mason, W., McKenzie, D.A., Stern, M.A. and Johnson, J.K.; "A numerical three-dimensional viscous transonic wing-body analysis and design tool", AIAA Paper No. 78-101, 1978.
34. Shankar, V.; "Computational transonic inverse procedure for wing design with automatic trailing edge closure", AIAA Paper No. 80-1390, 1980.
35. Johnson, F.T.; "A general panel method for the analysis and design of arbitrary configurations in incompressible flows", NASA CR3079, May 1980.
36. Johnson, F.T. and Rubbert, P.E.; "Advanced panel-type influence coefficient methods applied to subsonic flows", AIAA Paper 75-50, January 1975.
37. Ormsbee, A.I. and Chen, A.W.; "Multi-element airfoils optimized for maximum lift coefficient", AIAA J., Vol. 10, No. , pp. 1620-1624, December 1972.
38. Oellers, H.J.; "Die Inkompressibelen Potentialströmung in der ebener Gitterstufe", Jahrbuch 1962 WGLR, pp. 349-353.
39. Tranen, T.L.; "A rapid computer aided transonic airfoil design method", AIAA Paper No. 74-501, 1974.
40. Bauer, F., Garabedian, P. and Korn, D.; "Supercritical wing sections", Springer Verlag, 1972.
41. Volpe, G.; "Two-element airfoil systems design: An inverse method", AIAA Paper No. 78-1226, 1978.
42. Arlinger, B. and Schmidt, W.; "Design and analysis of slat systems in transonic flow", ICAS paper, 1978.
43. Bauer, F., Garabedian, P., Korn, D. and Jameson, A.; "Supercritical wings sections II", Springer Verlag, 1975.
44. Carlson, L.A.; "Transonic airfoil analysis and design using Cartesian coordinates", J. Aircraft, Vol. 13, pp. 369-356, May 1976.
45. Henne, P.A.; "An inverse transonic wing design method", AIAA Paper No.80-0330, 1980.
46. Jameson, A. and Caughey, D.; "Numerical calculation of the transonic flow past a swept wing", ERDA R&D Rept. COO-3077-140, Courant Institute, New York University, 1977.
47. Shankar, V.; "A full potential inverse method based on a density linearization scheme for wing design", AIAA Paper No.81-1234, 1981.
48. Caughey, D. and Jameson, A.; "Progress in finite volume calculation for wing-body combinations", AIAA J., Vol. 18, No. 11, November 1980, pp. 1281-1288.
49. Beatty, T.D. and Narramore, Y.C.; "Inverse method for the design of multi-element high-lift systems", J. Aircraft, Vol. 13, No. 6, June 1976.
50. Hess, J.L.; "Higher order numerical solution of the integral equation for the two-dimensional Neumann problem", Comp. Meth. Appl. Mech. Eng., Vol. 2, 1973, pp. 1-15.
51. Wilkinson, D.H.; "A numerical solution of the analysis and design problems for the flow past one or more aerofoils or cascades", ARC, R&M 3545, 1967.
52. Fornasier, L.; "Wing design process by inverse potential flow computer programs", in: The Use of computers as a design tool, AGARD CP. No. 280, 1979.
53. Kraus, W. and Sacher, P.; "Das Panelverfahren zur Berechnung der Druckverteilung von Flugkörpern in Unterschallbereich", ZFW, Heft 9, September 1973, pp. 301-311.
54. Labrujère, Th.E., Loeve, W. and Slooff, J.W.; "An approximate method for the calculation of the pressure distribution on wing-body combinations at subcritical speeds", AGARD CP. No. 71, Paper 11, 1970.
55. Slooff, J.W. and Voogt, N.; "Aerodynamic design of thick supercritical wings through the concept of equivalent subsonic pressure distribution", NLR MP 78011 U, 1978.
56. Malone, J.B.; "An optimal-surface-transpiration subsonic panel-method for iterative design of complex aircraft configurations", AIAA Paper No. 81-1254, 1981.
57. Aoki, M.; "Introduction to optimization techniques", McMillan, New York, 1971.
58. Hess, J.L.; "A fully automated potential-flow boundary-layer procedure for calculating viscous effects on the lifts and pressure distributions of arbitrary three-dimensional configurations", NSRDC Rept. No. MDC J7491, 1977.
59. Davis Jr., W.H.; "Technique for developing design tools from the analysis methods of computational aerodynamics", AIAA Paper No. 79-1529, 1979.
60. Jameson, A.; "Accelerated iteration schemes for transonic flow calculations using fast Poisson solvers", ERDA R&D Rept. COO-3077-82, Courant Inst. Math. Sci., N.Y. Univ., 1975.
61. Frey, J.M.J., Slooff, J.W., Boerstoel, J.W. and Kassies, A.; "Design of transonic airfoils with given pressure distribution, subject to geometric constraints", NLR, to be published.
62. Boerstoel, J.W.; "Numerical modelling and fast-solver calculation of approximately normal shocks", NLR MP 82026 U, 1982.
63. McFadden, G.B.; "An artificial viscosity method for the design of supercritical airfoils", Ph.D. Thesis, N.Y. University, 1979.

64. Garabedian, P., McFadden, G.; "Design of supercritical swept wings", proceedings of the 1980 Army Numerical Analysis and Computers Conference, ARO Report 80-3, 1980.
65. Garabedian, P. and McFadden, G.; "Computational fluid dynamics of airfoils and wings", proceedings of Symposium on Transonic, Shock and Multi-dimensional flows, University of Wisconsin, Madison (1981); Academic Press Inc. 1982, pp. 1-16.
66. Miranda, L.R.; "A perspective of computational aerodynamics from the viewpoint of airplane design applications", AIAA Paper 82-0018, January 1982.
67. Garabedian, P. and McFadden, G.; "Design of supercritical swept wings", to be published.
68. Bristow, D.R.; "A solution to the inverse problem for incompressible axisymmetric potential flow", AIAA Paper 74-520, June 1974.
69. Bristow, D.R.; "A new surface singularity method for multi-element airfoil analysis and design", AIAA Paper 76-20, January 1976.
70. Bristow, D.R.; "Development of panel methods for subsonic analysis and design", NASA CR 3234, 1980.
71. Kellogg, O.D.; "Foundations of potential theory", Dover Publications, Inc., 1953.
72. Labrujère, Th.E.; "Airfoil design by the method of singularities via parametric optimization of a geometrically constrained least squares object function", NLR MP 76139 U, 1976.
73. Labrujère, Th.E.; "Multi-element airfoil design by optimization", NLR MP 78023 U, 1978.
74. Labrujère, Th.E.; NLR Report to be published.
75. Oskam, B.; "A calculation method of the viscous flow around multi-component airfoils", NLR TR 79097 U, 1979.
76. Vanderplaats, G.N.; "CONMIN - A FORTRAN program for constrained function minimization", NASA TM X-62, 282, 1973.
77. Hicks, R.M., Murman, E.M. and Vanderplaats, G.N.; "An assessment of airfoil design by numerical optimization, NASA TM X-3092, 1974.
78. Hicks, R.M.; "Transonic wing design using potential flow codes - Successes and failures", SAE Paper 810565, 1981.
79. Vanderplaats, G.N.; "An efficient algorithm for numerical airfoil optimization, AIAA Paper No. 79-0079, 1979.
80. Hicks, R.M., Vanderplaats, G.N., Murman, E.M. and King, Rosa T.; "Airfoil section drag reduction at transonic speeds by numerical optimization, SAE Paper 760477, 1976.
81. Hicks, R.M. and Vanderplaats, G.N.; "Application of numerical optimization to the design of supercritical airfoils without drag-creep", SAE Paper 770440, 1977.
82. Hicks, R.M. and Henne, P.A.; "Wing design by numerical optimization", AIAA Paper No. 77-1247, 1977.
83. Haney, H.P., Johnson, R.R. and Hicks, R.M.; "Computational optimization and wind tunnel test of transonic wing designs", AIAA Paper No. 79-0080, 1979.
84. Lores, M.E., Smith, P.E. and Large, R.A.; "Numerical optimization: an assessment of its role in transport aircraft aerodynamic design through a case study", ICAS-80-1.2, 1980.
85. Hicks, R.M. and Vanderplaats, G.N.; "Design of low-speed airfoils by numerical optimization", SAE Paper 750524, 1975.
86. Nixon, D. (editor); "Transonic aerodynamics", Progress in Astronautics and Aeronautics, Vol. 81, AIAA, N.Y., 1982.
87. Lamar, J.E.; "Subsonic vortex-flow design study for slender wings", J. Aircraft, Vol. 15, No. 9, September 1978.
88. Polhamus, E.C.; "A concept of the vortex lift of sharp-edge delta wings based on a leading edge suction analogy, NASA TN D-3767, 1966.
89. Sobieczky, H.; "Related analytical, analog and numerical methods in transonic airfoil design", AIAA Paper No. 79-1556, 1979.
90. Sobieczky, H., Fung, K.Y. and Seebass, A.R.; "A new method for designing shock-free transonic configurations", AIAA Paper No. 78-1114, 1978.
91. Yu, N.J.; "Efficient transonic shock-free wing redesign procedure using a fictitious gas method", AIAA Paper No. 79-0075, 1979.
92. Eberle, A.; "Transonic flow computations by finite elements: Airfoil optimization and analysis", in: Recent developments in theoretical and experimental fluid mechanics, Springer Verlag, 1979.
93. Fung, K.Y., Sobieczky, H. and Seebass, R.; "Shock-free wing design", AIAA Paper No. 79-1557, 1979.
94. Rai, P., Miranda, L.R. and Seebass, A.R.; "A cost-effective method for shock-free supercritical wing design", AIAA Paper No. 81-0383, 1981.
95. Fung, K.Y., Seebass, A.R., Dickson, L.J. and Pearson, C.F.; "An effective algorithm for shock-free wing design", AIAA Paper No. 81-1236, 1981.
96. Nebeck, H.E., Seebass, A.R. and Sobieczky, H.; "Inviscid-viscous interaction in the nearly direct design of shock-free supercritical airfoils", AGARD CP-291, 1980.
97. Sobieczky, H.; "Die Berechnung lokaler räumlicher Ueberschallfelder", ZAMM 58T, 1978.
98. Subsonic/transonic configuration aerodynamics, Round Table Discussion, AGARD CP-285, 1980.
99. Van den Dam, R.F.; "SAMID, An interactive system for the analysis and constrained minimization of induced drag of aircraft configurations", AIAA Paper 83-0095, January 1983.
100. Narramore, J.C. and Yeary, R.D.; "Airfoil design and analysis using an information system approach", AIAA Paper No. 80-1444, 1980.

TABLE 1

Classification of aerodynamic design methods from the viewpoint of the aerodynamic designer

	2 D AIRFOIL		AXI-SYMMETRIC FLOW		3 D.WINGS	3 D ARBITP. BODIES
	single	multiple	solid bodies	engine nacelles		
SUBSONIC FLOW		Ormsbee & Chen, 1972, [37] Beatty & Narramore 1975, [49] Bristow+)(*) 1976/80, [69], [70] Labrujère+)*) 1976/78, [72], [73], [74]	Bristow 1974, [68]		Woodward I, 1967, [17], [18] Boeing A236, 1968, [8] NLR, 1974*) [22] Feifel, 1976, [23] Lamar, 1976, [24] 1978, [87] Fornasier, 1979, [52]	PANAIR, 1974+)? [35], [36] Malone, 1981+) [56]
TRANSONIC FLOW	ARA, 1973 [26] Tranen, 1974 [39] Carlson, 1975 [44] Shankar, 1978 [31] Davis, 1979 [59] McFadden, 1979 [63] Volpe, 1981 [12] NLR, 1982*) [61]	Volpe, 1978 [41] Arlinger, 1978+)? [42]			ARA, 1976 [28] Dornier/FFA, 1976 [30] Shankar 1979/80 [32], [34] Henne, 1980 [45] Garabedian & McFadden, 1980 [64], [65] Shankar, 1981 [47] Sobiecky, Fung, Seebass et al., 1978, [89]-[96] Hicks et al.+)*) [77]-[85]	

+) both full design and mixed analysis/design possible

*) geometry constraints possible

TABLE 2

Classification of aerodynamic design methods from the viewpoint of the theoretical/computational aerodynamicist

	INVERSE				INDIRECT (fictitious gas)	DIRECT (NUMERICAL) OPTIMIZATION
	linearization in b.c.			non-linear b.v. problem formulations		
	thin airfoil/ wing b.c.	iterative Dirichlet	iterative Neumann (residual/correction)			
linear flow model, PANEL methods (subsonic flow)	Woodward I, 1967,[17],[18] Boeing A236, 1968,[8]	Ormsbee & Chen 1972,[37] PANAIR, 1974 [35],[36]	Beatty & Narramore, 1975,[49]	Bristow, 1974/76/80 [68],[69],[70] Labrujère, 1976/78 [72],[73],[74]		
			NLR, 1974 [22]			
						Feifel, 1976,[23]
						Lamar, 1976,[24]
			Fornasier, 1979 [52]			Lamar, 1978,[87]
			Malone,[56], 1981			
non-linear flow model FD/FE/FV methods (transonic & subsonic flow)	ARA, 1973/76, [26],[28] Dornier, 1975 [29],[30] Shankar, 1978-80 [31]-[34]	Tranen, 1974 [39] Carlson, 1975 [44] Volpe, 1978/81 [41],[12] Arlinger, 1978 [42] Henne, 1980 [45] Shankar, 1981 [47]	Davis, 1979 [59] NLR INTRAFS, 1982 [61] McFadden, 1979 [63] Garabedian & McFadden, 1980 [64],[65]		Sobiezcky, Fung, Seebass et al. 1978,[89]-[96]	Hicks, VanderPlaats, et al. 1974,[77]-[8]
						Haney et al., 1979,[83]
						Lores et al., 1980,[84]

TABLE 3

Possibilities and limitations of various design approaches

		local or global (re) design?	direct control over geometry?	direct control over aerodynamics?					multi-point design?	computational effort	other aspects
				C_L, C_M	induced drag	wave drag	viscous drag	C_p-distr.			
Indirect (Fictitious gas)		local only	no	no	no	yes	no	no	no	acceptable	ill-posed problem in 3 D
Inverse		global	no*)	yes	yes	no°)	no°)	yes	no	acceptable	ill-posed problem in 3 D
		local		partially	partially			partially			
Direct numerical optimization	direct drag minimization	global and local	yes	yes	insufficient+)		no+)	no	yes	prohibitive	uniqueness problems?
	inverse mode			yes	yes	no°)		yes	no		
Inverse numerical optimization		global and local	yes	yes	yes	yes?	yes	yes	yes?	acceptable?	CONJECTURED

*) unless in the form of contraints

+) current situation, could be improved in future

°) indirect control through pressure distribution

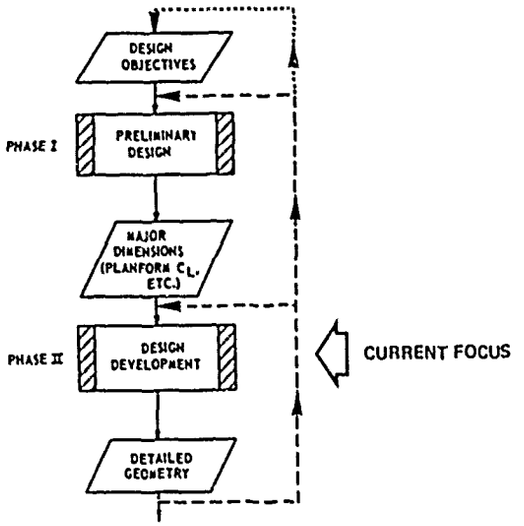

Fig. 1 Major phases of aerodynamic design process

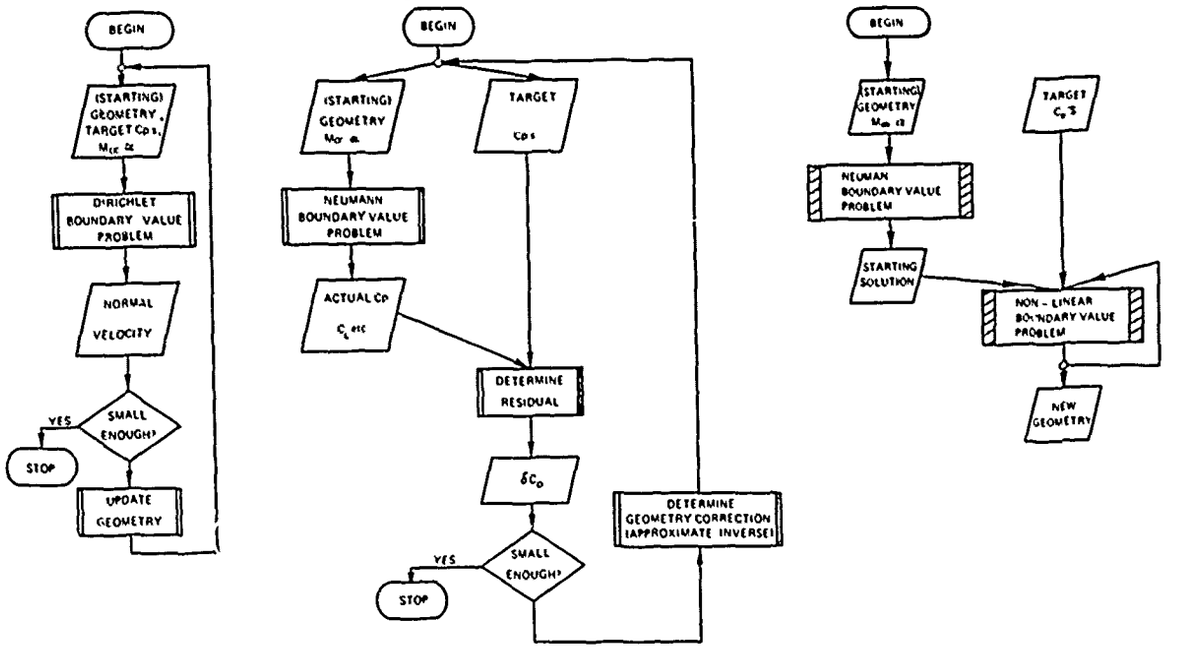

a) ITERATIVE DIRICHLET b) RESIDUAL CORRECTION (ITERATIVE NEUMANN) c) NONLINEAR BOUNDARY VALUE PROBLEM

Fig. 2 Flow charts of different formulations of inverse problem

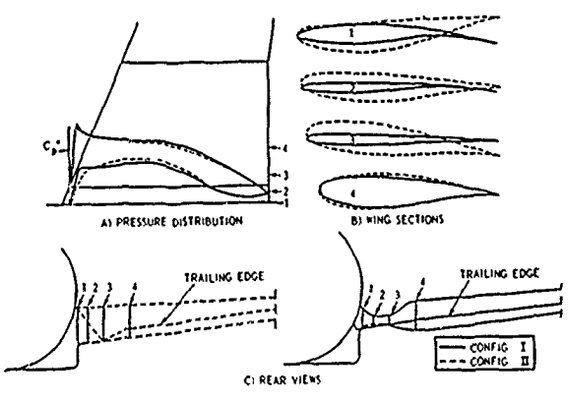

Fig. 3 Example illustrating ill-posed nature of 3-D inverse problem, [55]

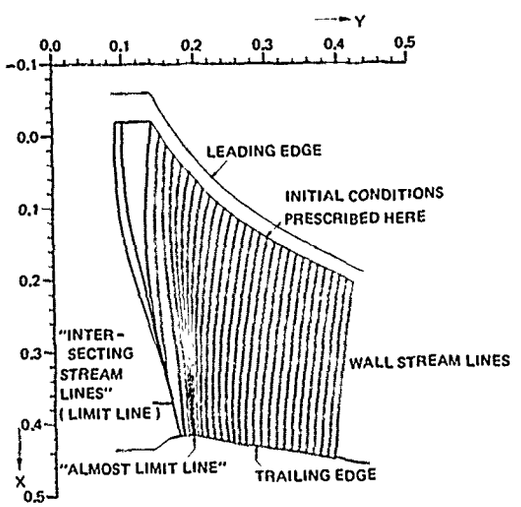

Fig. 4 Example illustrating the problem of "intersecting streamlines" (limit lines) in pressure specified surface flow (from NLR BOLA code, J.P.F. Lindhout)

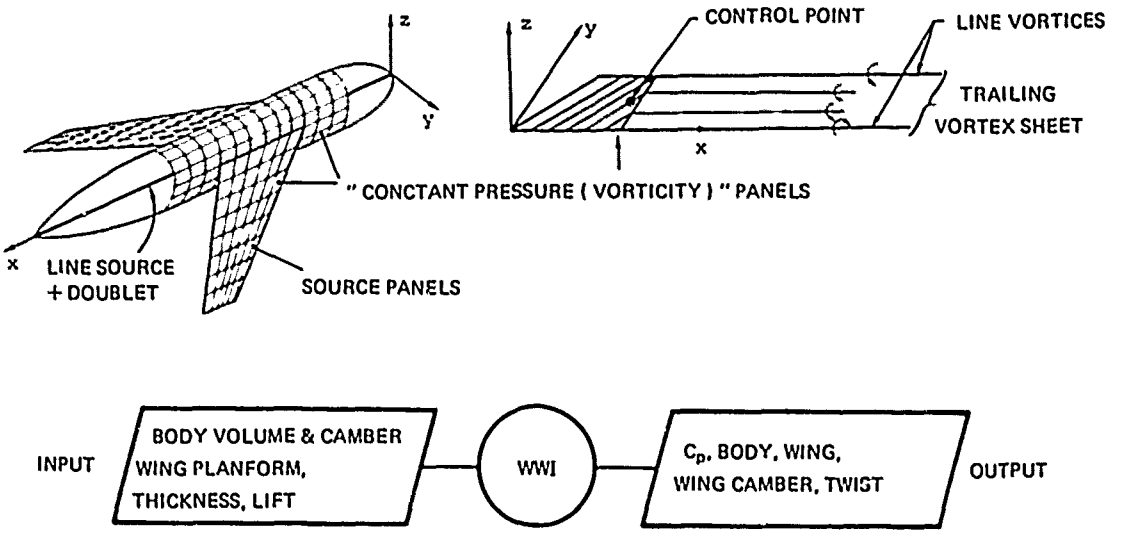

Fig. 5 Design option of Woodward I (1967) panel method, [16]

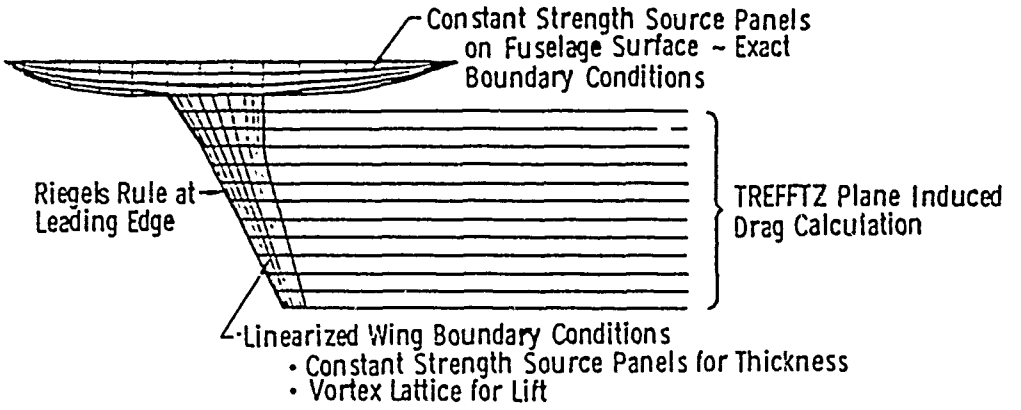

WING BOUNDARY CONDITIONS OPTIONS

Specify		Calculate	
Camber	Thickness	C_P^{upper}	C_P^{lower}
C_P^{upper}	C_P^{lower}	Camber	Thickness → UNSTABLE ?
C_P^{upper}	Thickness	C_P^{lower}	Camber
etc.	⋮	⋮	⋮ DESIGN OPTIONS
Airfoils	Span Loading	Twist Dist.	Pressure Dist.
Airfoils	Twist Dist.	C_P^{upper}	C_P^{lower}

Fig. 6 Design options of early Boeing subsonic wing/body code (A236, 1968)

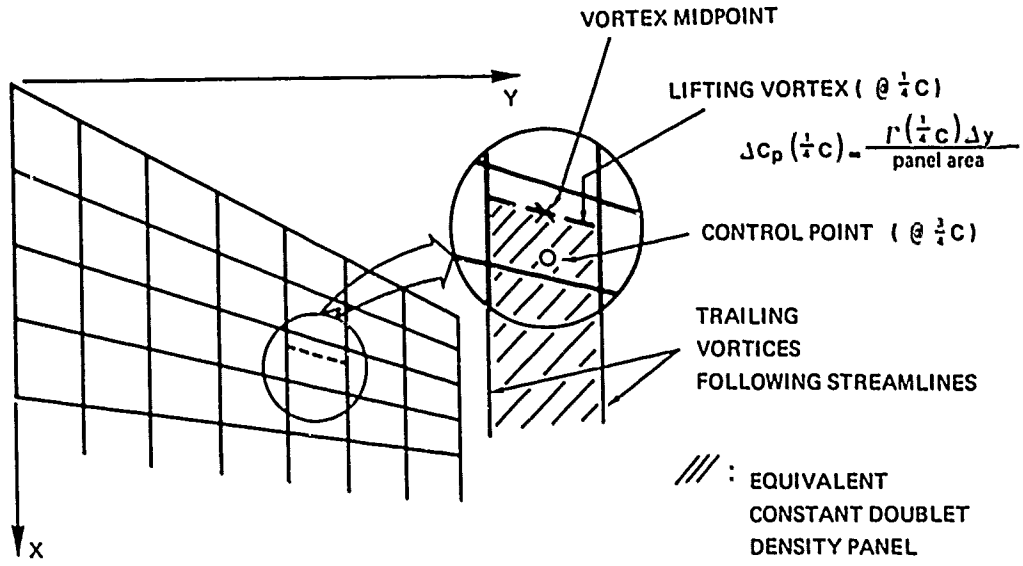

Fig. 7 Vortex lattice method

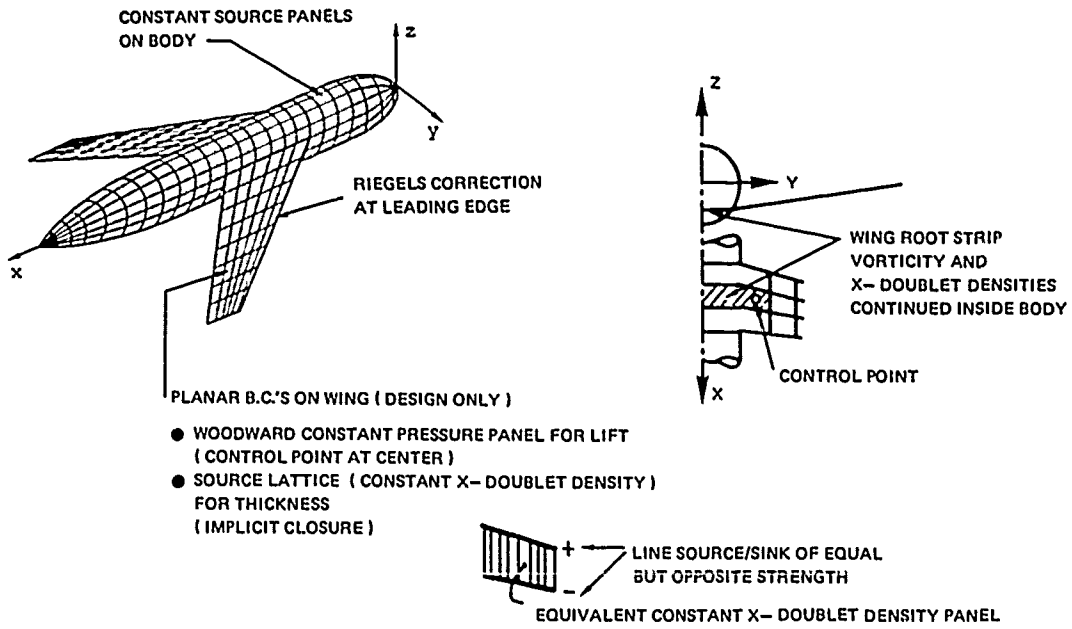

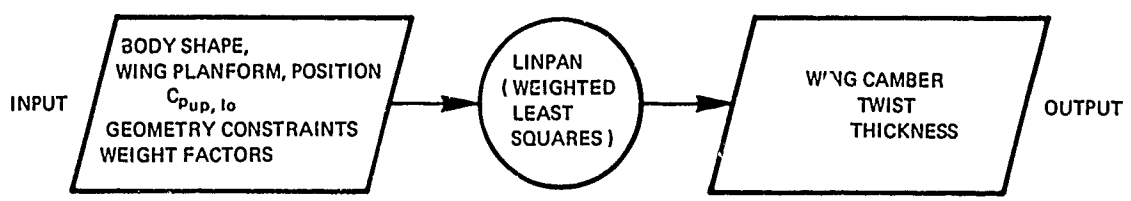

Fig. 8 NLR linear subsonic inverse code, [22]

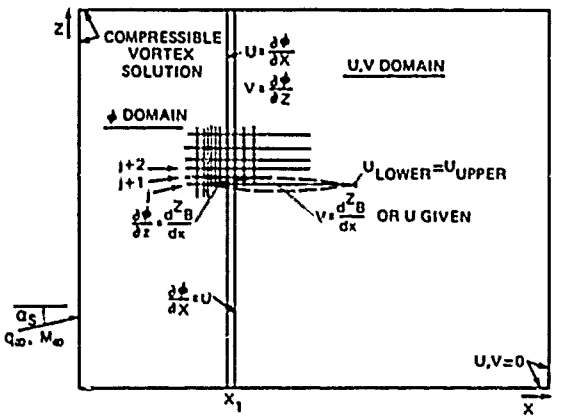

Fig. 9 Sketch of field subdivision in Steger/Klineberg[25] inverse method (2-D)

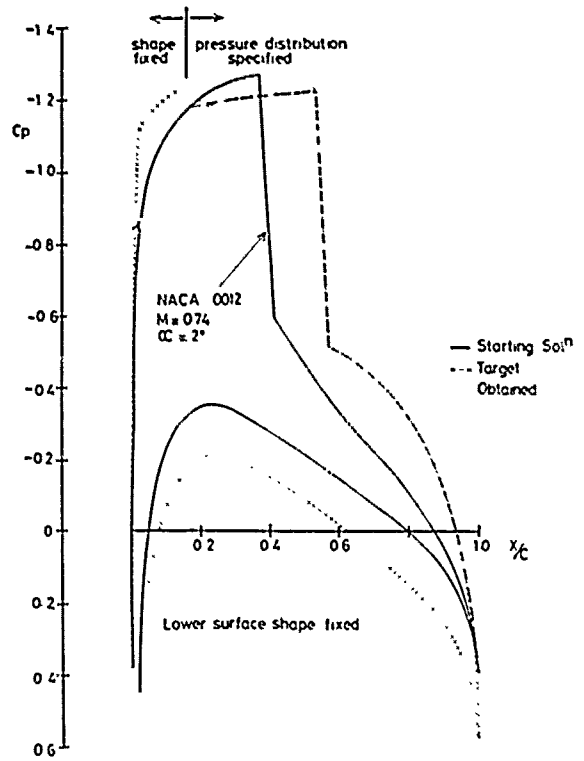

Fig. 10 Example of ARA inverse method (2-D), [26]

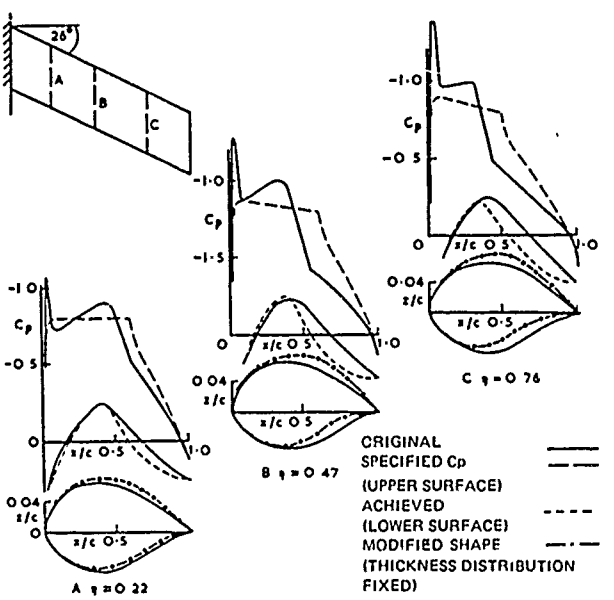

Fig. 11 Example of ARA TSP wing design method, [28]

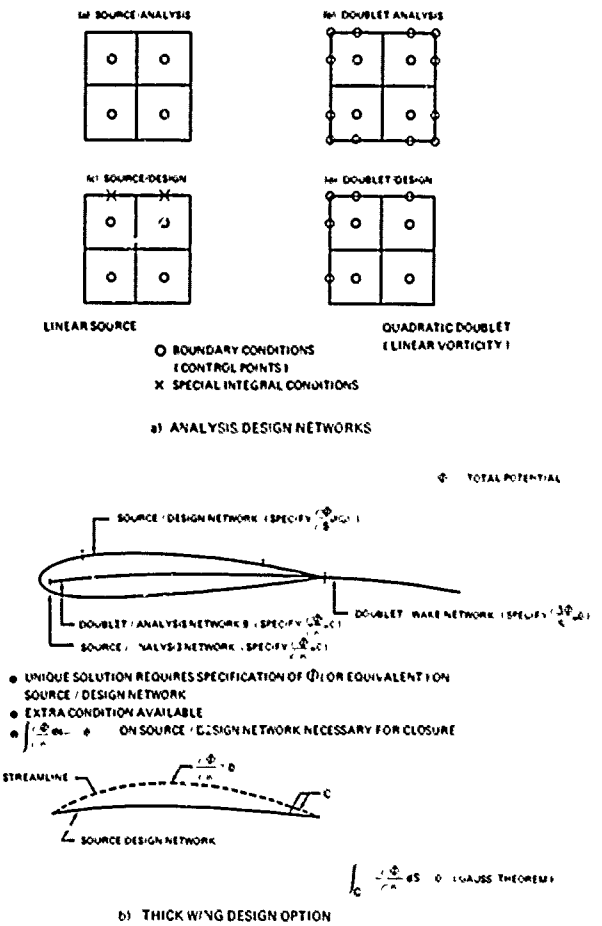

Fig. 12 PANAIR design options

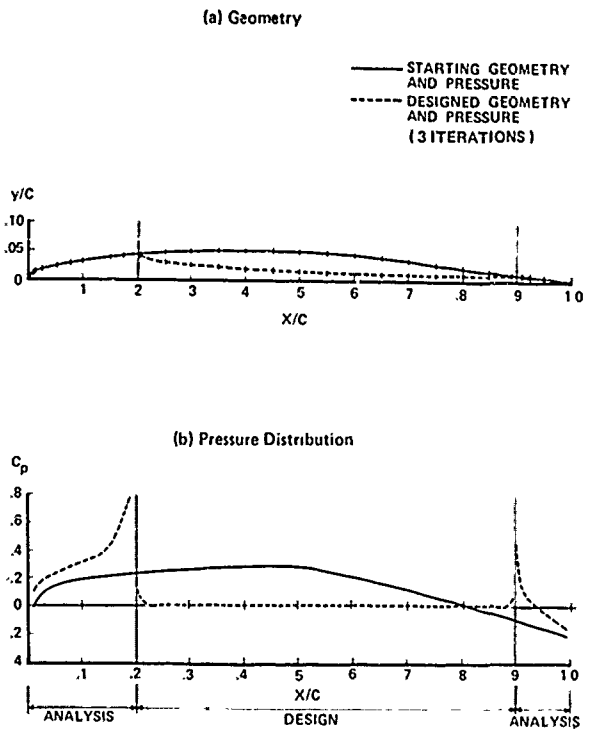

Fig. 13 PANAIR design example showing consequence of not satisfying the regularity condition, [36]

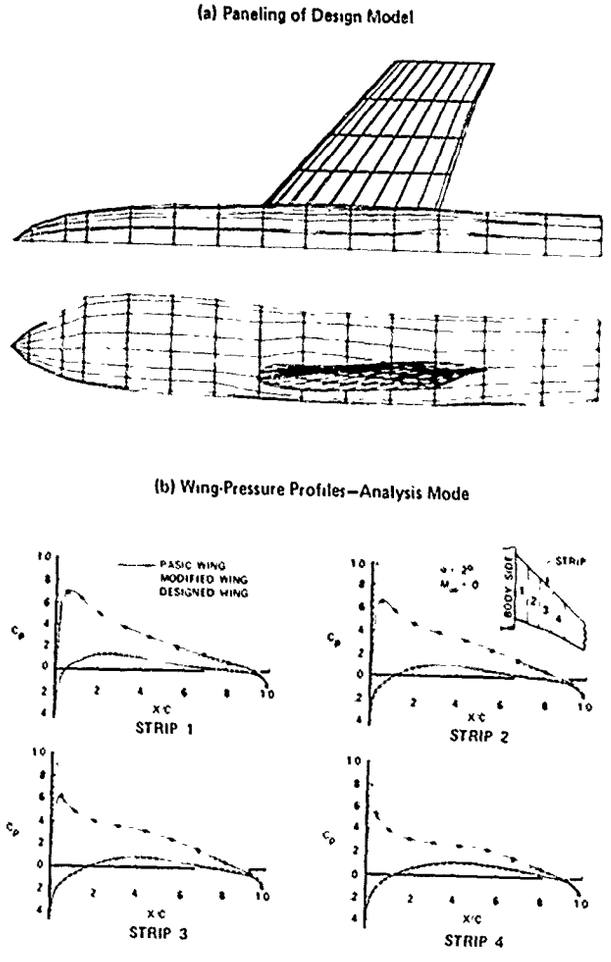

Fig. 14 PANAIR wing (re-)design, [36]

- STREAM FUNCTION FORMULATION (2-D)
- CONSTANT VORTICITY PANELS, CONTROL POINTS AT PANEL CENTERS
- NOT PROPERLY FORMULATED ?

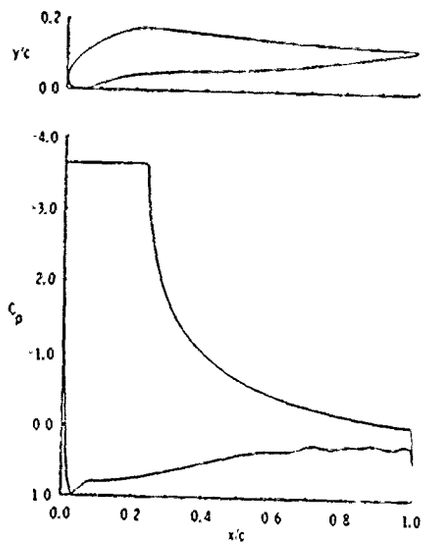

EXAMPLE OF SINGLE – ELEMENT HIGH LIFT AIRFOIL FOR $Re_0 = 5 \times 10^6, \alpha = 17.5°, C_L = 1.91$.

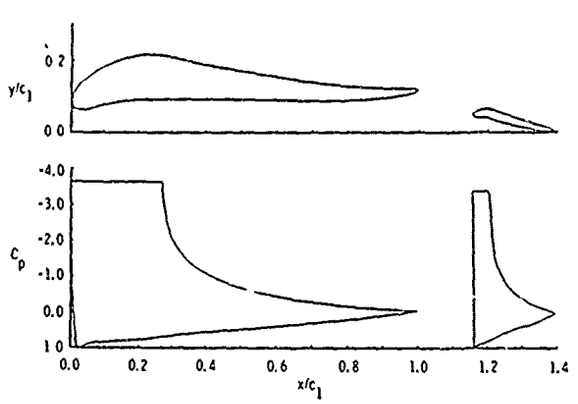

EXAMPLE OF TWO – ELEMENT HIGH LIFT AIRFOIL FOR $Re_{01} = 5 \times 10^6$ AND $Re_{02} = 10^6, \alpha = 11.25°, C_L = 2.32$.

Fig. 15 Stream function inverse method of Ormsbee and Chen, [37]

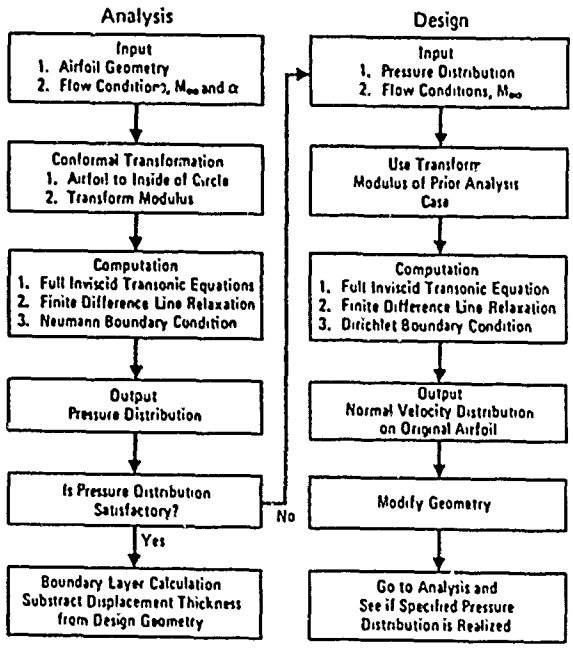

Fig. 16 Flow chart of Tranen's design procedure, [39]

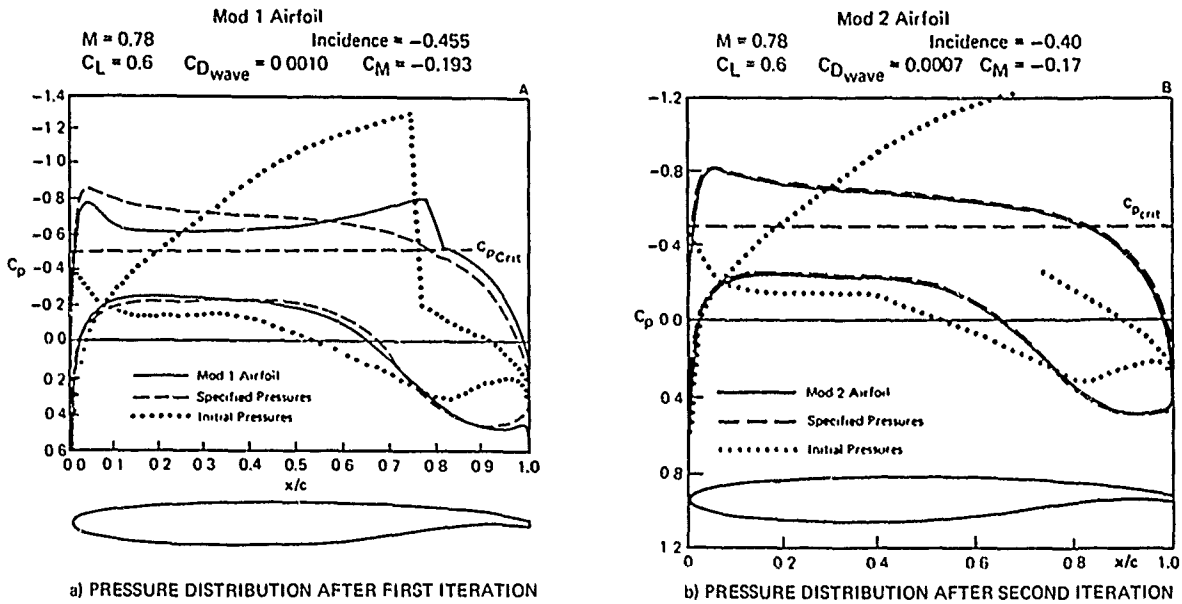

a) PRESSURE DISTRIBUTION AFTER FIRST ITERATION

b) PRESSURE DISTRIBUTION AFTER SECOND ITERATION

Fig. 17 Example of application of Tranen's[39] design procedure

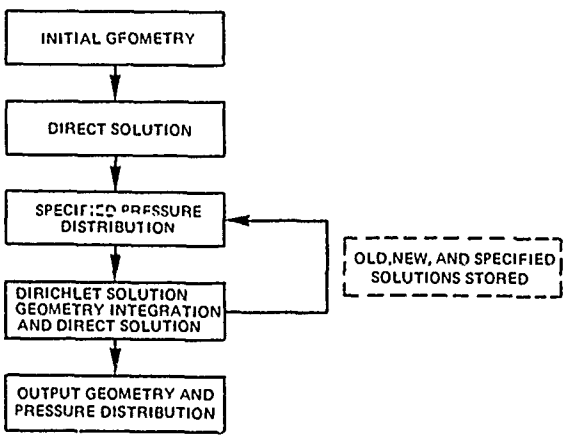

Fig. 18 Simplified flow diagram of Henne's method, [45]

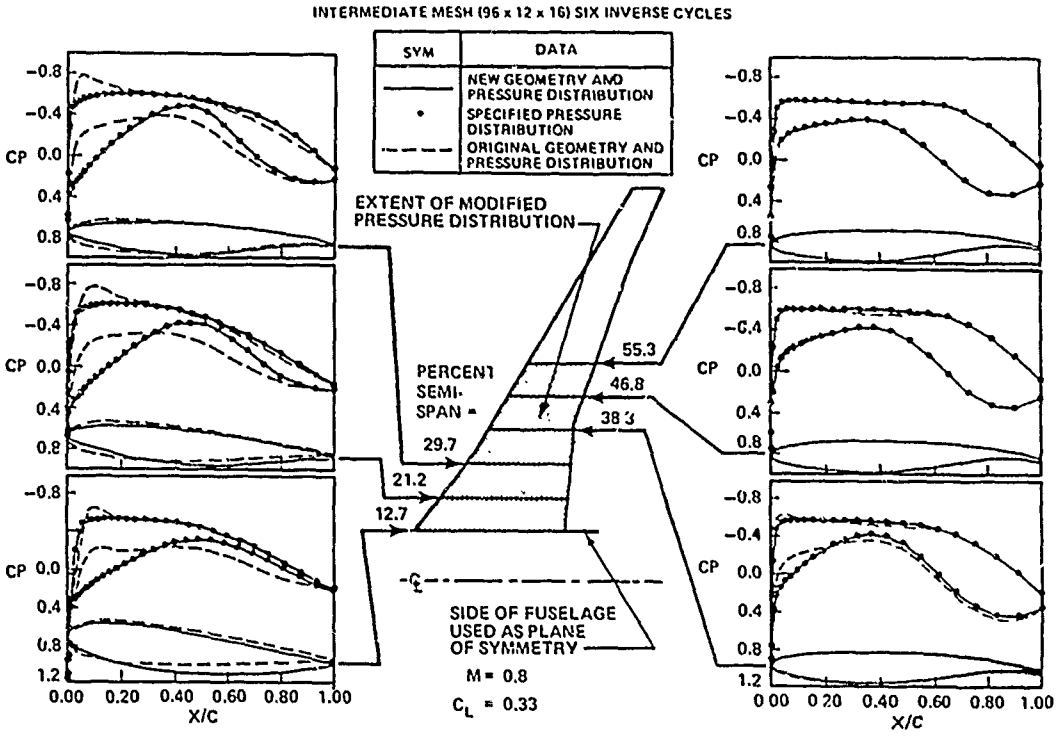

Fig. 19 Modification of supercritical swept wing inboard pressure distribution, Henne [45]

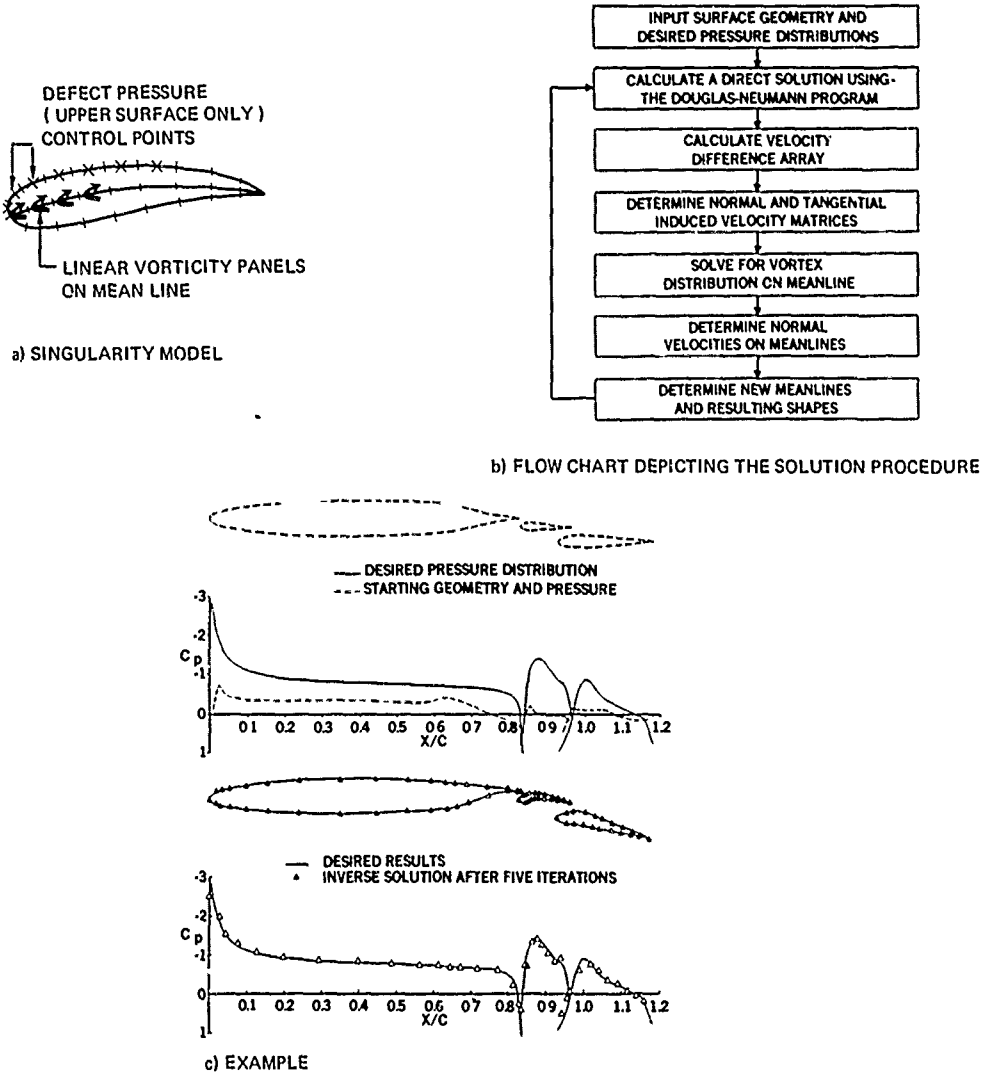

Fig. 20 Beatty & Narramore[49] (semi-)inverse (multi-element) airfoil method

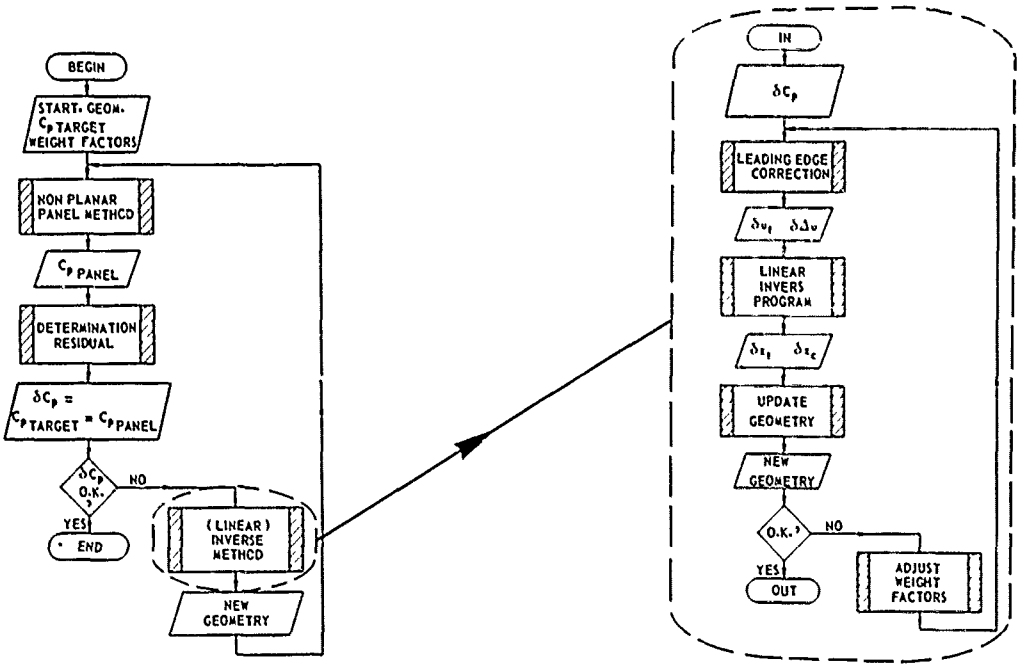

a) (OUTER) ITERATION PROCESS

b) LINEAR (THIN WING) INVERSE METHOD

Fig. 21 Flow diagrams of NLR 3-D subsonic inverse method, [22]

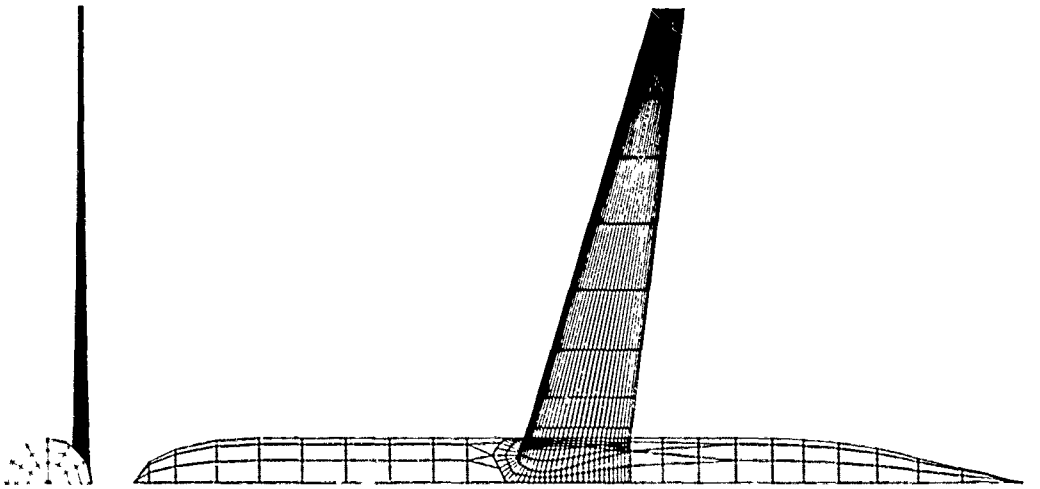

a) TOP AND FRONT VIEW AND PANEL ARRANGEMENT OF WING–BODY CONFIGURATION (BODY AT ZERO ANGLE OF ATTACK)

Fig. 22 Example of application of NLR 3-D subsonic inverse method

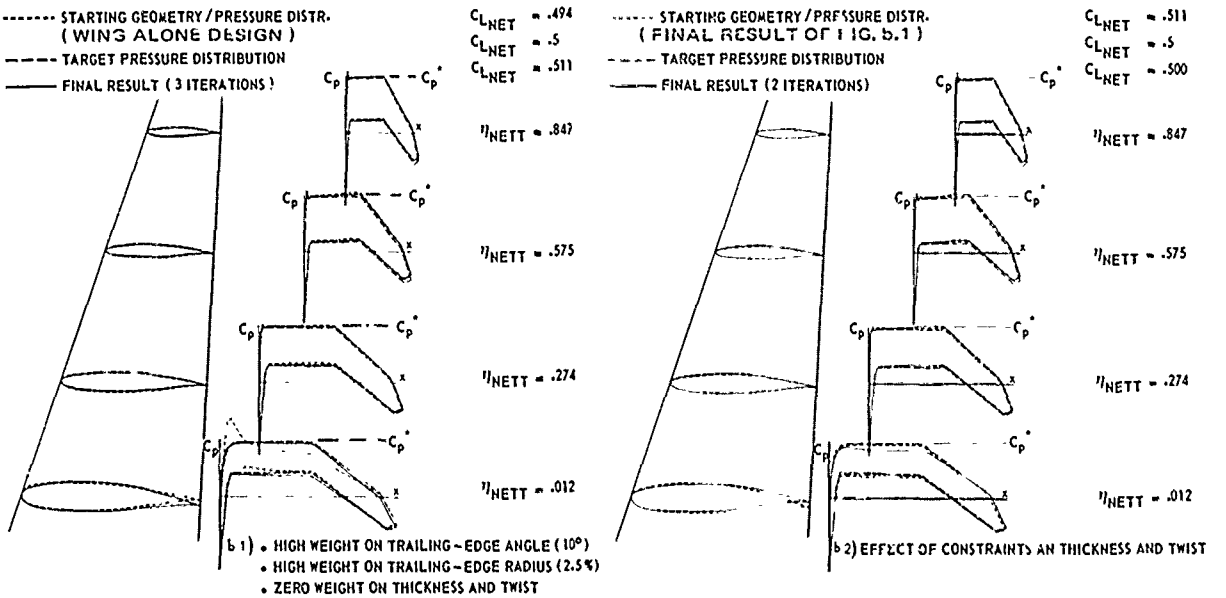

b 1) • HIGH WEIGHT ON TRAILING-EDGE ANGLE (10°)
• HIGH WEIGHT ON TRAILING-EDGE RADIUS (2.5%)
• ZERO WEIGHT ON THICKNESS AND TWIST

b 2) EFFECT OF CONSTRAINTS ON THICKNESS AND TWIST

b) RESULTS FOR WING–BODY CONFIGURATION (M_∞ = 0.7)

Fig. 22 Continued

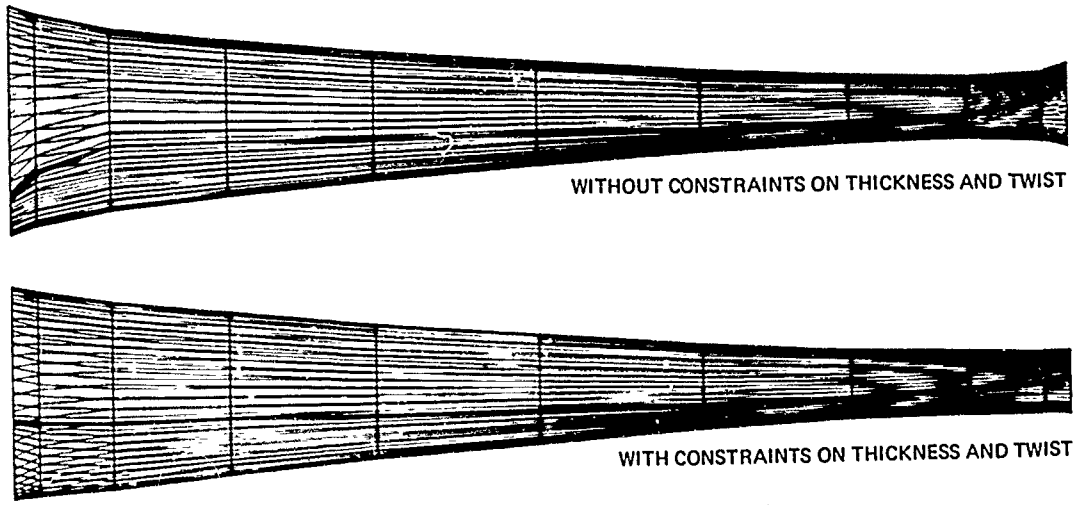

c) FRONT VIEW OF WINGS OF WING–BODY CONFIGURATIONS (Z–SCALE ENLARGED 5x)

Fig. 22 Continued

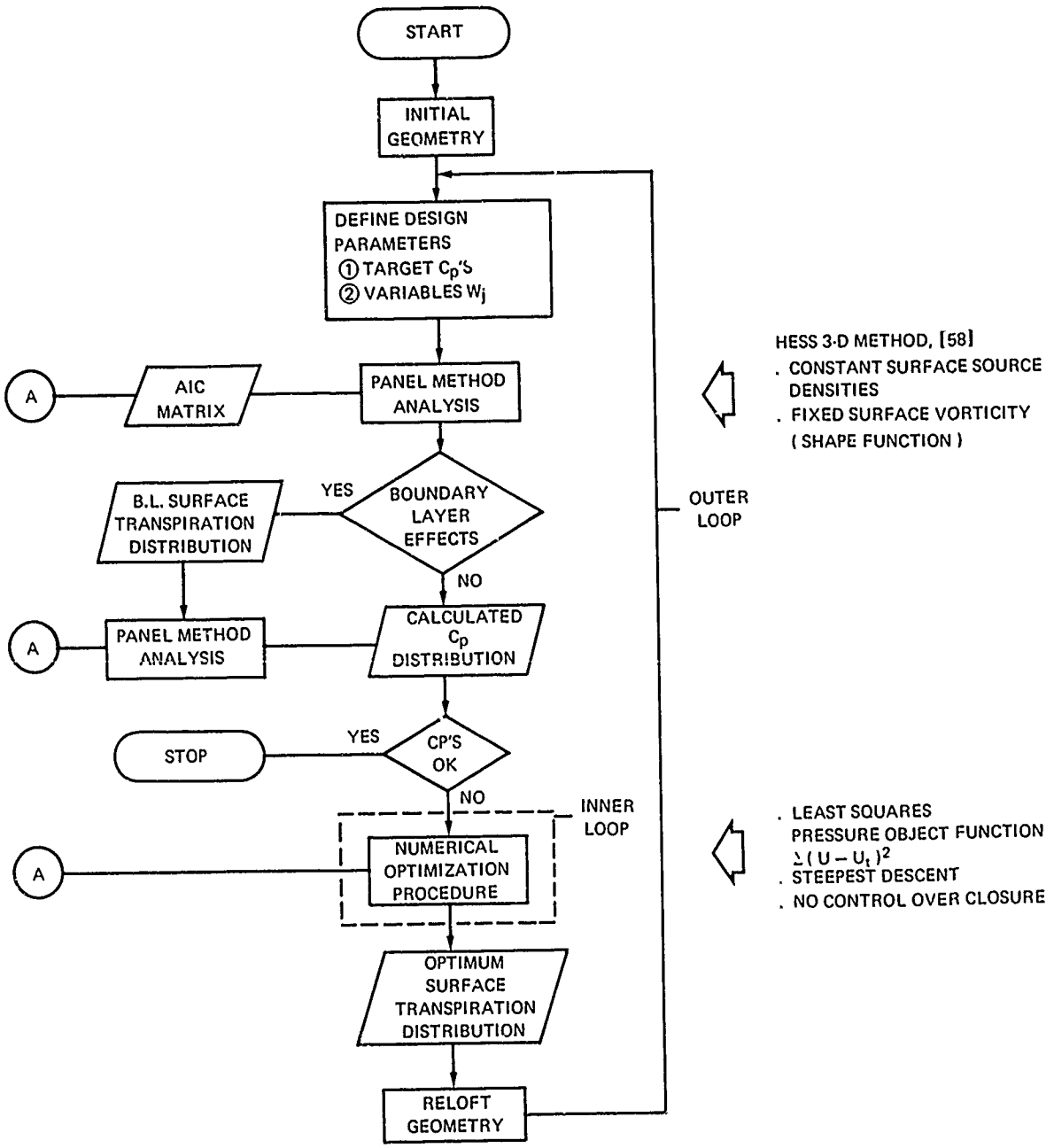

Fig. 23 Flow chart of Malone's[56] numerical optimization type inverse method

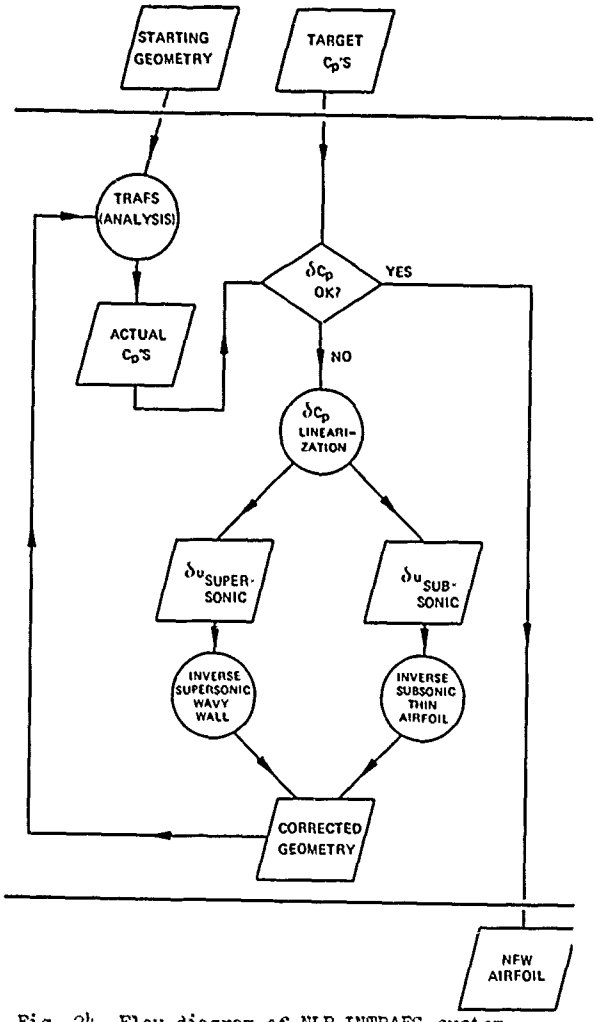

Fig. 24 Flow diagram of NLR INTRAFS system (2-D transonic airfoil design), [57]

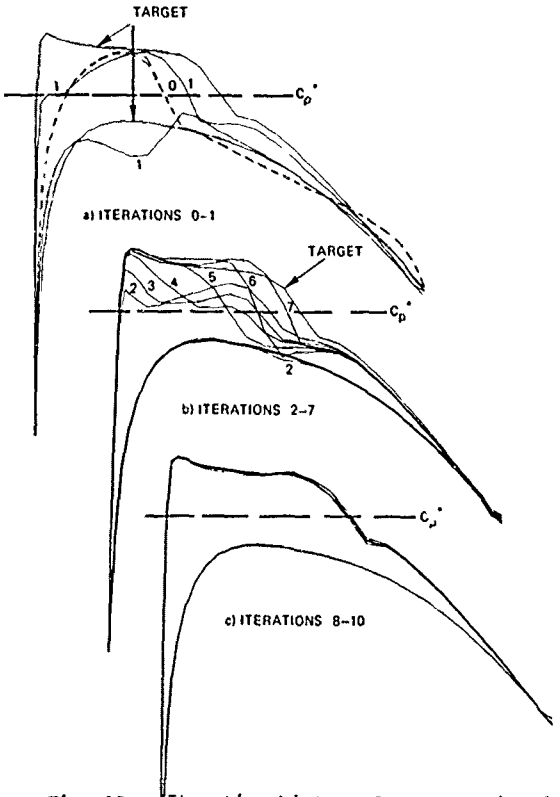

Fig. 25 Iteration history for transonic airfoil design (M = .77) with weak shock (NLR INTRAFS), [61]

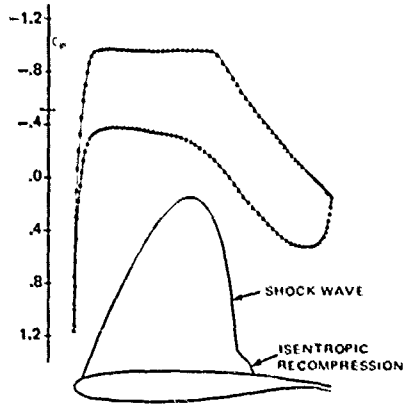

Fig. 26 Example of shock-free pressure distribution leading to shock wave in flow field with significant wave drag (McFadden[63])

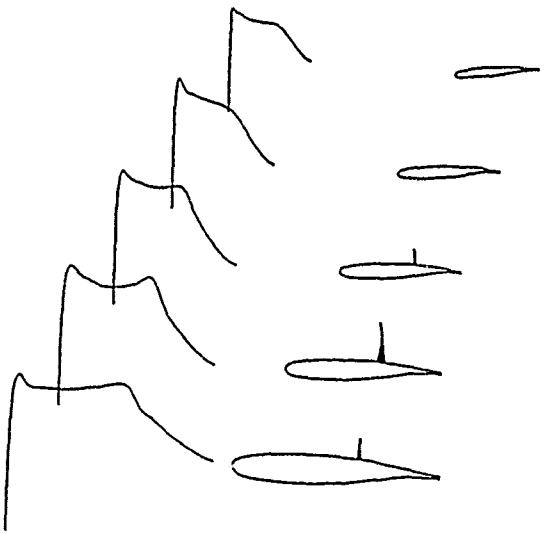

a) ORIGINAL WING

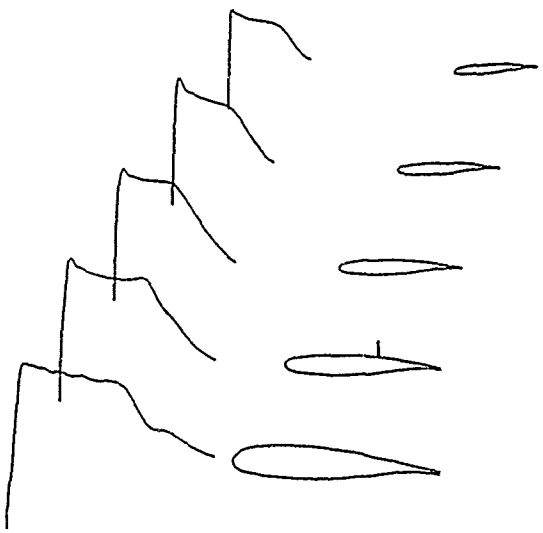

b) REDESIGNED WING

Fig. 27 Example of application of Garabedian/McFadden inverse redesign method, [65]

BRISTOWS METHOD (I)

- MINIMIZATION OF VELOCITY FUNCTIONAL (LEAST SQUARES)

$$E = \sum_i (U_i - U_t)^2$$

- CLOSURE THROUGH LAGRANGE MULTIPLIERS
- DERIVATIVES DETERMINED ANALYTICALLY
- DISCRETIZATION SCHEME (CONSTANT SOURCE DENSITY)

BASICALLY UNSTABLE; ELABORATE SMOOTHING OPERATION

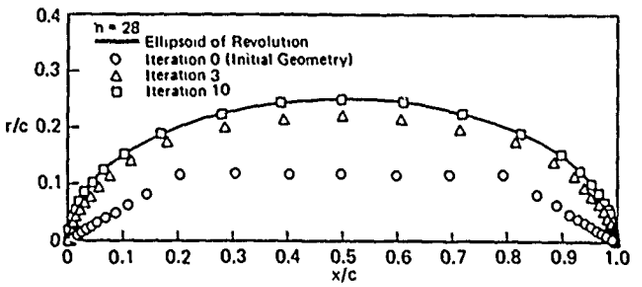

EXAMPLE: RECONSTRUCTION OF ELLIPSOID

Fig. 28 Characteristics of Bristow's[68] inverse method for bodies of revolution

BRISTOW II (MAAD PROGRAM)

- LEAST SQUARES FUNCTIONAL AS IN BRISTOW I (FIG. 28)
- CONSTANT/LINEAR SOURCE PLUS LINEAR VORTICITY ON FLAT PANELS (GREEN'S THIRD IDENTITY)
- MIXED ANALYSIS/DESIGN
- RELATIVE POSITION OF AIRFOIL ELEMENTS FIXED

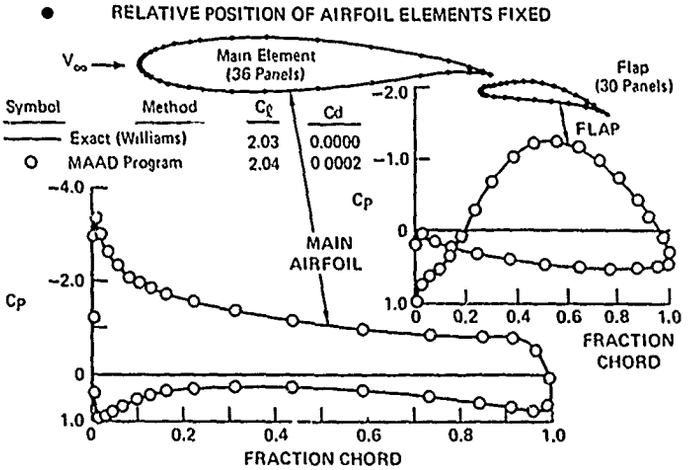

Two-Element Airfoil Analysis Solution

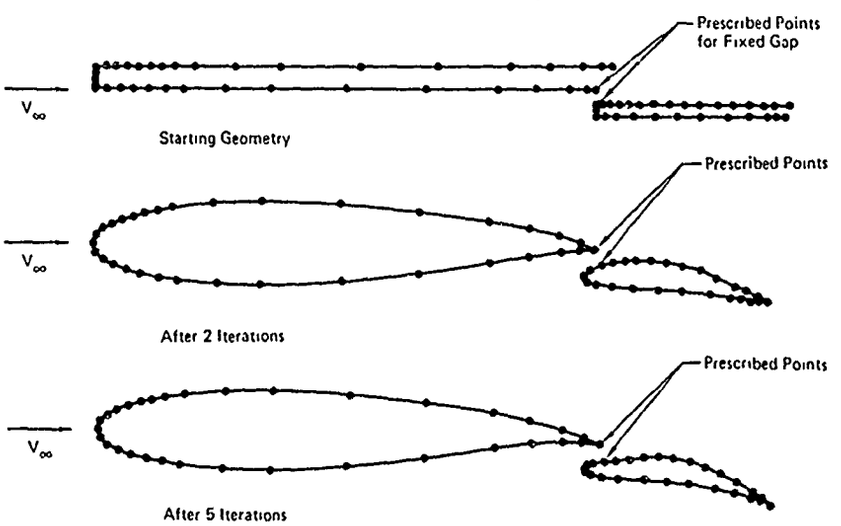

EXAMPLE: RECONSTRUCTION OF THE "WILLIAMS FLAP"

Fig. 29 Characteristics of the MAAD program system (Bristow[70])

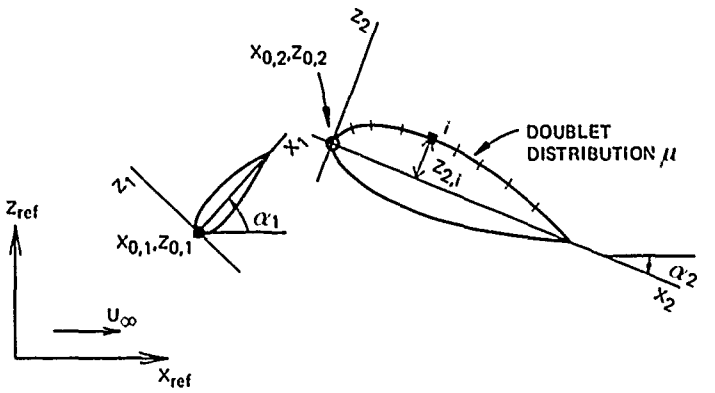

- MINIMIZATION OF FUNCTIONAL

$$E = \Sigma_p \oint \left\{ W_t \left(U - U_t \right)^2 + W_n V^2 + W_g \left(Z - Z^{(o)} \right)^2 \right\} ds$$

- QAUDRATIC REPRESENTATIONS FOR DOUBLET DISTRIBUTIONS AND GEOMETRY
- VARIABLES μ, Z, α, X_o, Z_o
- NEWTON LINEARIZATION

- MIXED ANALYSIS / DESIGN
  (THROUGH CHOICE OF LIMITING THE NUMBER OF VARIABLES Z, α, X_o, Z_o)
- FREE OR FIXED GAPS AND OVERLAPS
- REGULARITY AND GEOMETRY CONSTRAINTS THROUGH W_g

Fig. 30 Characteristics of NLR MAD system, (Labrujère[74])

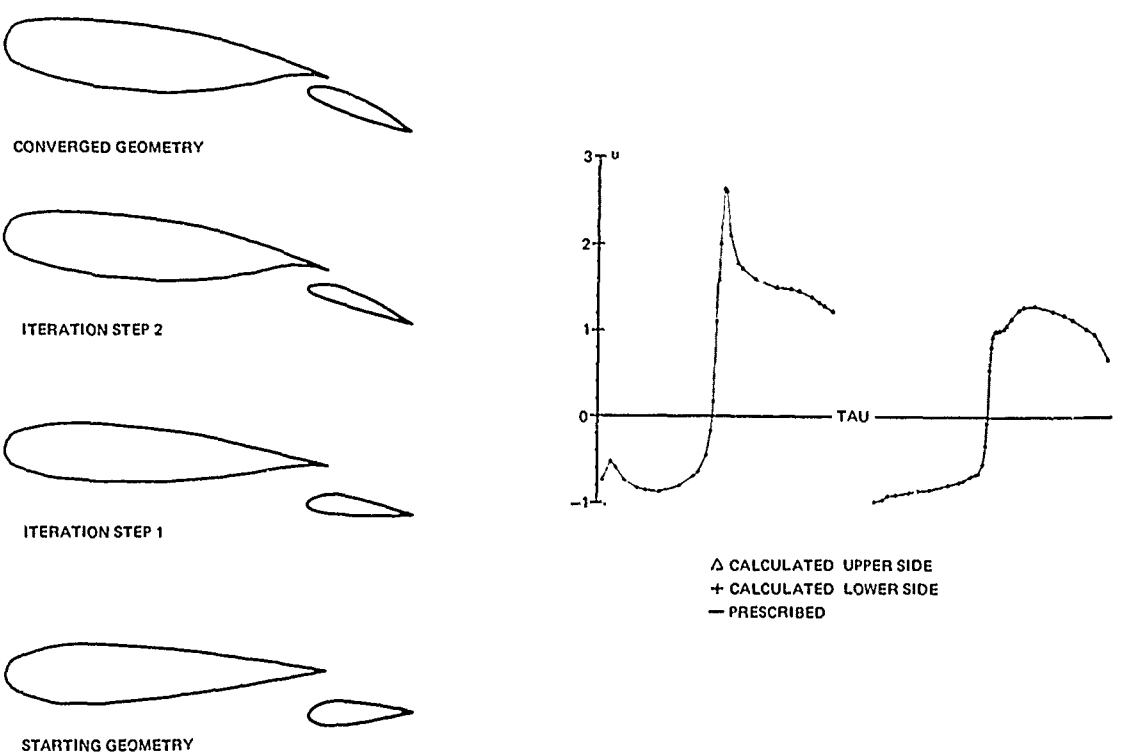

Fig. 31 Early (test) example of Labrujère's[73] method: reconstruction of an airfoil-flap configuration with fixed overlap

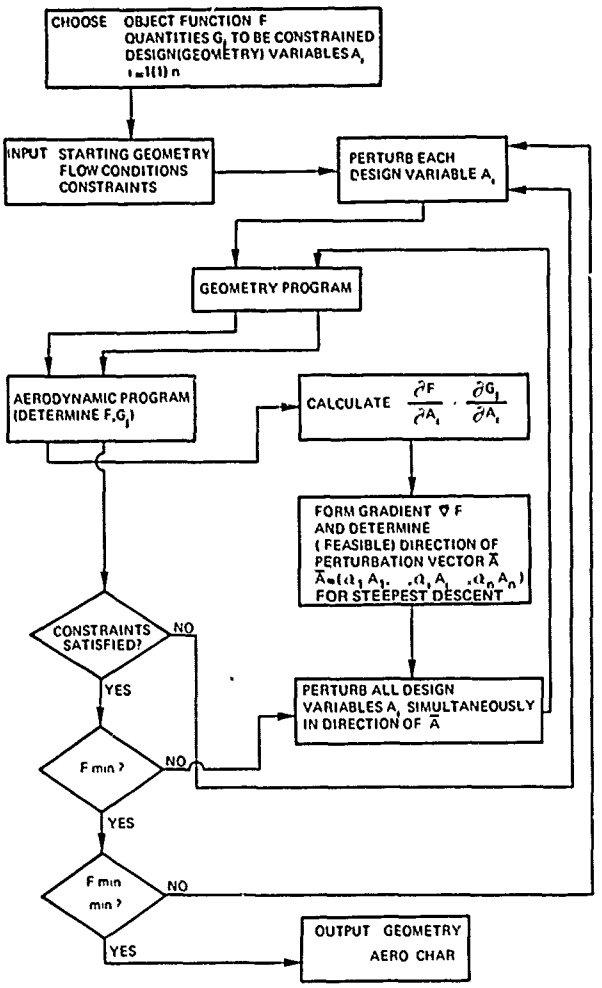

Fig. 32 Flow chart of design by direct numerical optimization

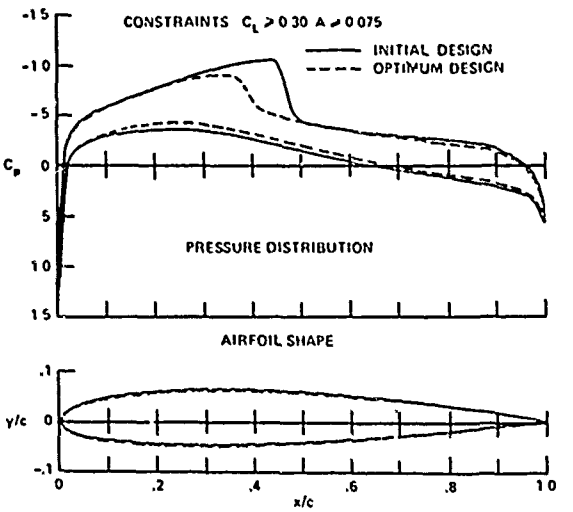

Example 3A—drag minimization, M = 0.75, α = 0°, beginning with analysis No. 27.

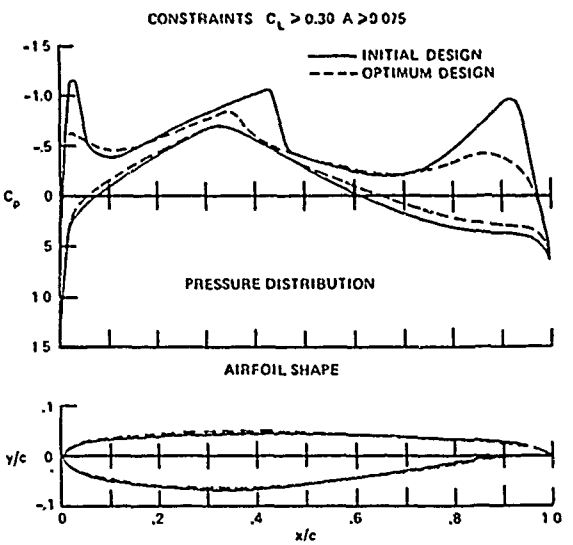

Example 3B—drag minimization, M = 0.75, α = 0°, beginning with analysis No. 48.

Fig. 33 Example of non-uniqueness of wave drag minimization problem, [79]

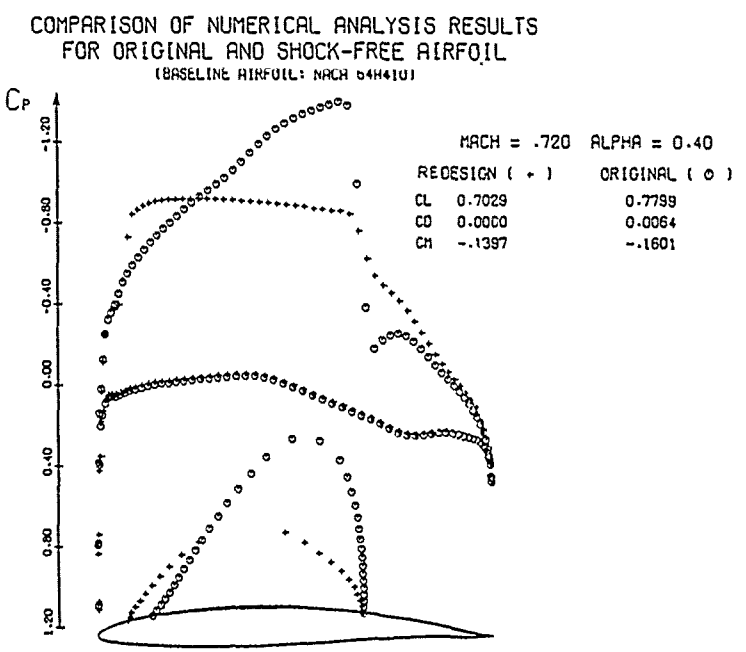

Fig. 34 Example of airfoil shock-free redesign by means of fictitious gas method, [88]

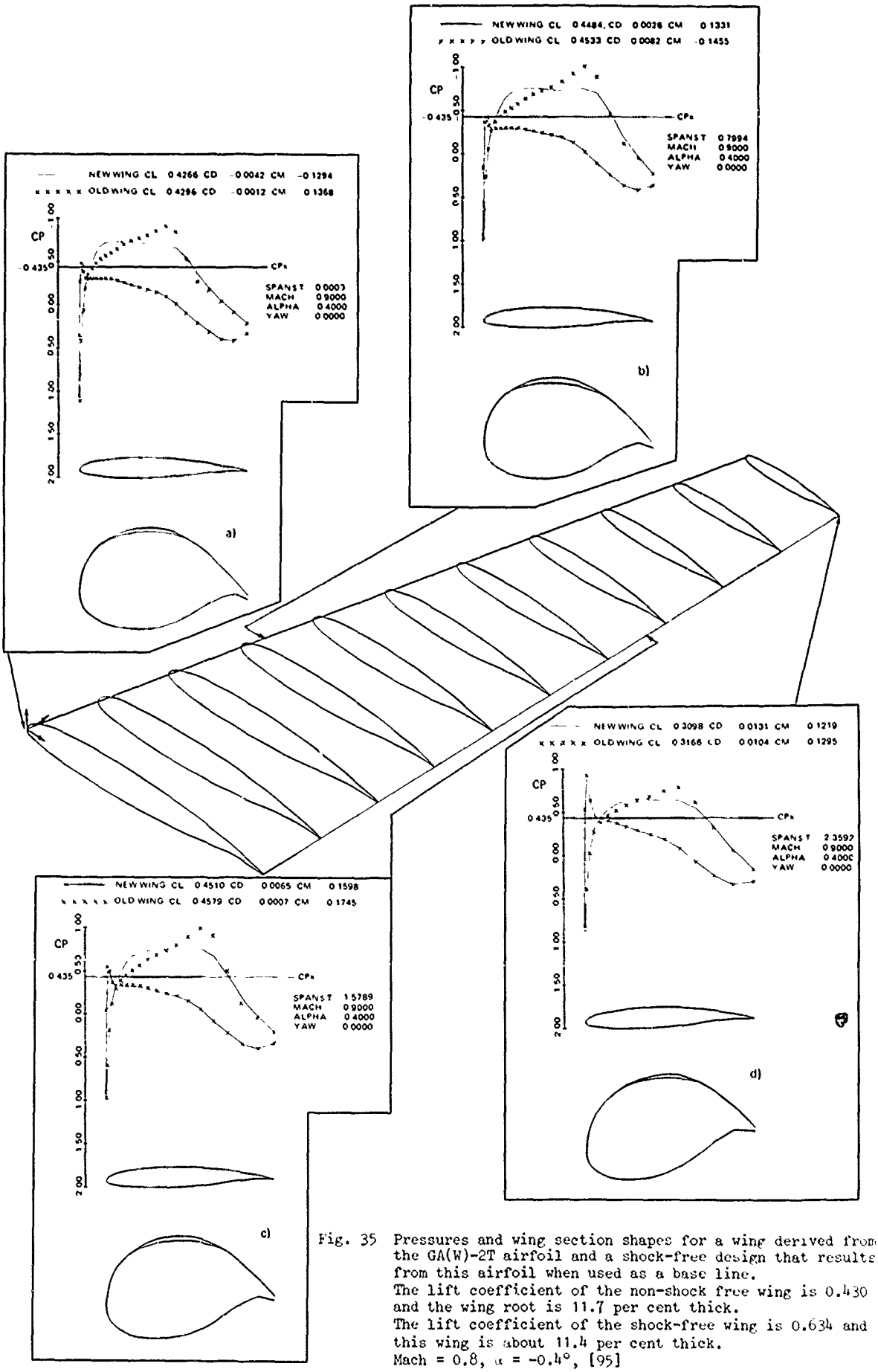

Fig. 35 Pressures and wing section shapes for a wing derived from the GA(W)-2T airfoil and a shock-free design that results from this airfoil when used as a base line.
The lift coefficient of the non-shock free wing is 0.430 and the wing root is 11.7 per cent thick.
The lift coefficient of the shock-free wing is 0.634 and this wing is about 11.4 per cent thick.
Mach = 0.8, α = -0.4°, [95]

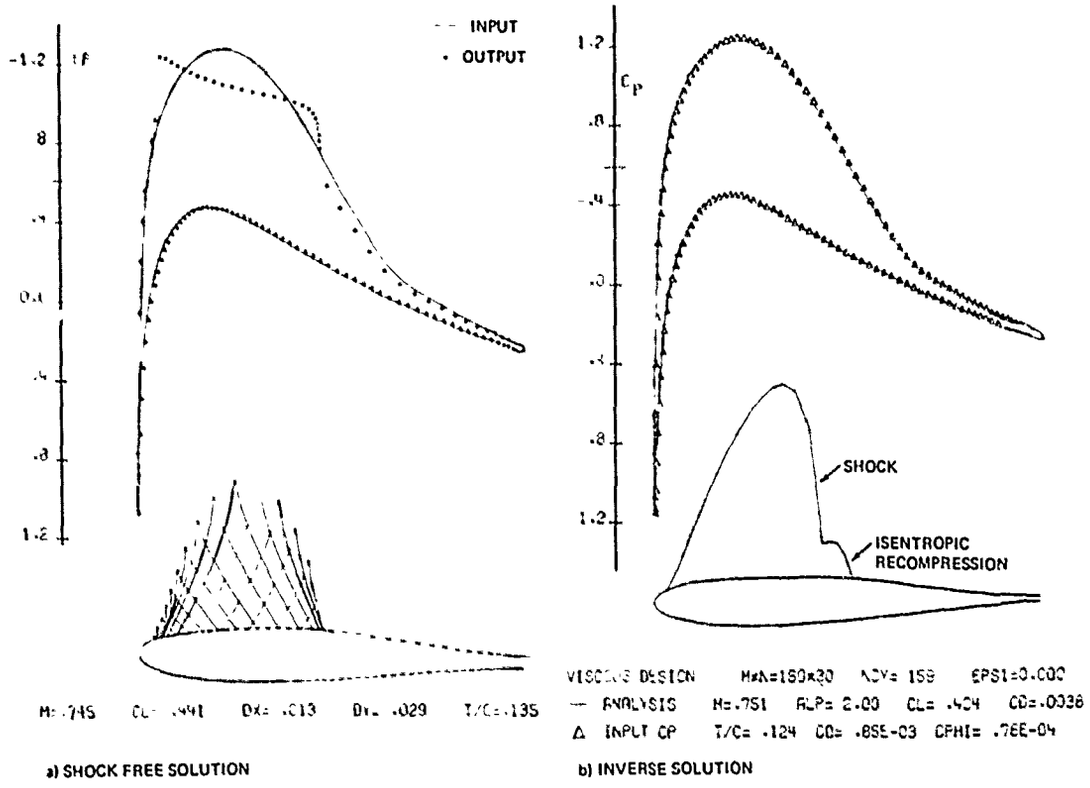

Fig. 36 Examples of design-to-pressure [64], illustrating the problem of specifying transonic pressure distributions with low wave drag

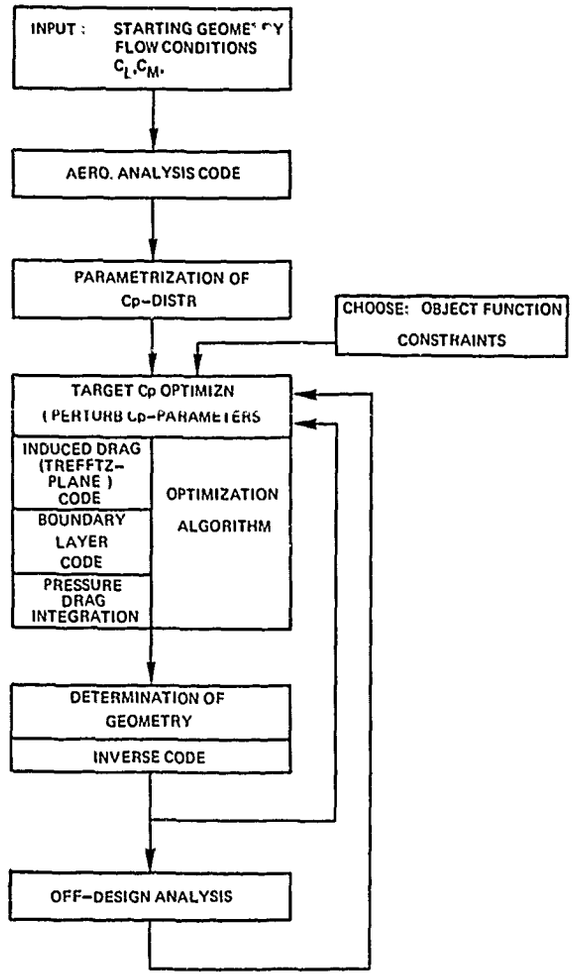

Fig. 37 Scheme for inverse numerical optimization (conjectural)

Subsonic/Transonic Viscous Interactions

by

H. Yoshihara
Boeing Company
Seattle, WA
98124 U.S.A.

SUMMARY

Significant viscous interactions arising at transonic cruise and maneuver conditions and low speed/high lift conditions are described for airfoils and swept wings. Consequences on the performance and stability of fighter and airlift aircraft are briefly sketched. Computational methods using the integral boundary layer/wake equations are then described in a narrative fashion.

1. INTRODUCTION

In transonic flow the forces and moments on an airfoil or wing cannot be predicted viably without incorporating the effects of viscosity. This is primarily due to the presence of shock waves on the configuration which interact with the boundary layer to distort the inviscid pressure distribution.

Important effects of viscosity also arise at low speed high lift conditions occurring for example during takeoff and landing. Of particular importance are the effects of viscosity on configurations with high lift devices where the maximum lift is limited by the appearance of severe separation.

Viscous interactions will accordingly play an essential role in the fluid dynamic interference mechanisms, key to the configuration optimization in both the transonic and subsonic flow regimes.

In the following we shall first describe the nature of the viscous interactions that arise for airfoils and swept wings as well as their consequences on the performance and stability of the aircraft. This is followed by a brief review of computational methods for two and three dimensional viscous flows where the viscous flow is modeled by the integral boundary layer/wake method which has received wide attention in the transonic case.

2. NATURE OF THE VISCOUS INTERACTIONS IN TRANSONIC FLOWS

Let us first consider the case of a typical aft-cambered airfoil at a high subsonic free stream Mach number at a cruise lift and a higher lift where the airfoil is in buffet. In Figure 1 are sketched side-by-side the flow patterns for the inviscid and viscous cases at the cruise lift together with a comparison of their pressure distributions. In the inviscid case it is seen that the shock wave is located at the trailing edge. The shock at lower free stream Mach numbers forms further upstream and displaces downstream as the Mach number is increased. When the shock reaches a point just upstream of the large convex surface curvature, a small further increase in the Mach number will displace the shock abruptly to the trailing edge. This behavior is typical of aft-cambered airfoils and is due to the fact that as the shock moves onto the aft camber region, the supersonic flow upstream of the shock is exposed to the high surface convexity. The result is a rapid expansion of the flow increasing the Mach numbers upstream of the shock. The resulting strengthened shock then displaces downstream further compounding the above effects until the shock reaches the trailing edge.

In Figure 1 the effects of viscosity are seen to modify significantly the above inviscid picture. Here as the shock displaces onto the aft camber region, the strengthened shock representing a severe adverse pressure gradient causes an abrupt thickening of the boundary layer. This wedging displacement at the base of the shock first impedes and finally halts the downstream movement of the shock thereby avoiding a strong shock. The shock/boundary layer interaction here has altered the normal shock in the inviscid case to an oblique shock with a greatly reduced pressure rise.

The viscous interactions as described above for the aft cambered airfoil are dramatic. The effects are less dramatic in the case of more conventional airfoils, but they are nevertheless still of significance.

Another significant effect of the viscous interaction is the reduction of the effective aft camber resulting from the difference of the boundary layer displacement on the upper and lower surfaces. This leads to the reduction of the plateau loading shown in Figure 1. Finally the effects of the near-wake modify the pressure distribution primarily in the trailing edge region.

For thick airfoils and for thinner airfoils at moderate lifts, an important synergistic viscous interaction can arise identified by Pearcey, Osborne, and Haines (Ref. 1). They labeled it as a Type B interaction, distinguishing it from the more familiar type A interaction where this synergism is absent. Such a case arises when the boundary layer encounters two successive adverse pressure gradients of sufficient strength, as for example the shock pressure rise followed by the trailing edge pressure recovery. After encountering a strong shock pressure rise, the boundary layer abruptly thickens, and its velocity profile loses its customary turbulent fullness. If the boundary layer then encounters the second adverse pressure gradient in this vulnerable state, it is less able to remain unseparated. The result is usually a sudden severe separation which extends from the shock to a point downstream of the trailing edge. The flow is especially susceptible to a severe Type B interaction if both a local shock-induced separation bubble and a trailing edge separation are present as shown in Figure 1.

A case with severe separation is sketched in Figure 2 where the airfoil is in buffet. Here buffet on the rigid airfoil is characterized by broad-band fluctuations of the lift and moment caused by the unsteadiness of the severely separated boundary layer. Here the unsteadiness produces fluctuations of both the aft pressures as well as the shock location. Buffet onset occurs when the shock-induced separation no longer reattaches on the airfoil but at some point downstream of the trailing edge as shown in Figure 2. It is characterized by a sudden drop in the trailing edge pressure.

Buffet as described above must not be confused with the flutter phenomena where the unsteady aerodynamic driving force is produced by the aeroelastic deformations of the wing.

For future reference it will be appropriate to comment here on the role of the Kutta condition at the airfoil trailing edge in establishing the circulation and hence the lift on the airfoil. Circulation is in general a global feature of the flow determined by the relative apportionment of the free stream into the portions passing above or below the airfoil. For sharp trailing edges this apportionment is established by postulating the flow to stream smoothly off the airfoil trailing edge, a model consistent with experimental observations. At a subsonic trailing edge, as the trailing edge is approached along the upper and lower surfaces of the airfoil and along the rear stagnation streamline, the pressure must then tend to a common value which in the case of a finite trailing edge angle must be the stagnation pressure. That is, the Kutta condition must be satisfied.

In the case of the high subsonic flow of Figure 2 with the terminating shocks at the trailing edge, the Kutta condition no longer plays a role in establishing the circulation. Here the match of the pressure and the flow direction just downstream of the trailing edge is achieved, independent of the circulation on the airfoil, by the adjustment of the obliqueness of the two trailing edge shocks. In this case the circulation is determined by the relative mass flux impedance (choking) of the space above (or below) the airfoil measured by the "throat" geometry at the shoulder of the airfoil.

At lower free stream Mach numbers than represented in Figure 2 where the shock wave is located upstream of the trailing edge, one must also expect a reduced role of the Kutta condition and a dominant role of the choking at the airfoil "throat" in establishing the circulation. That is, a relaxation of the Kutta condition in such a flow for example would affect the pressures near the trailing edge but not significantly distort the overall circulation.

Let us consider next the case of a swept wing of moderate sweep. In Figure 3 are shown the shock wave and separation patterns for two Mach numbers in the high subsonic range. In the upper sketch for the lower free stream Mach number the forward shock shown is the counterpart of the airfoil shock and is usually the first to appear as the flow becomes supercritical. The rear shock is formed at a higher Mach number by the coalescence of compression waves generated along the plane of symmetry of the wing. As the Mach number is further increased (the lower sketch), the rear shock strengthens and extends in the inboard direction. The forward shock assumes a greater sweep (at approximately the local Mach angle) eventually intersecting the rear shock. The shock outboard of the point of intersection, labeled the outboard shock, is usually the strongest of the shocks. Shock-induced separation first appears downstream of this shock. As the shock-induced separation worsens, it contaminates the trailing edge separation usually present, resulting in the compound (Type B) interaction described earlier. The separated region shown in Figure 3 then spreads to the tip and extends inward as the rear shock becomes stronger.

The part-span vortices shown in Figure 3 are the free trailing vortices that are the continuation of the bound vortices that terminate on the wing (see Küchemann, Ref. 2). They must be consistent with the corresponding span load distribution.

The separated region in Figure 3 has extended downstream of the trailing edge. The flow therefore is in buffet locally. Intensity of the overall wing buffet would then depend upon the extent of the wing span that is in buffet. In a wind tunnel test the output of the balance would indicate the expected broad band frequency spectrum, but it would also show discrete spikes. The latter are due to the unsteady loads generated by the excitation of the natural structural modes of the elastic wing by the buffet.

The swept wing considered above is characteristic of an airlift or commercial transport aircraft with wing sweeps of the order of 30° and aspect ratios of the order of eight. Fighter wings, on the other hand, are of considerably smaller aspect ratio of the order of four for swept wings with 40°-50° sweep and of even lower aspect ratio for delta or arrow wings with leading edge sweeps in excess of 60°. There is an essential maneuverability requirement for fighters to operate in the high subsonic region at lifts considerably beyond buffet onset. In such cases the viscous interactions become highly complex with the flow becoming unsteady.

Consider the case of a fighter swept wing shown in Figure 4 from Ref. 3. On the left side of the figure is shown the shock and separation patterns to be expected in the region between drag divergence and buffet onset. The flow configuration here is much the same as for the higher aspect ratio case of Figure 3. On the right side of the figure is a sketch of a "frozen" flow visualization picture prepared by Moss (Ref. 3) at a much higher angle of attack where not only buffet intensity is of serious concern but where catastrophic lateral instabilities can also arise. Here the strong outboard shock has unswept to an extent that it has reached the wing leading edge. The wing is stalled in the entire outboard region of the wing.

The second case is for a delta wing with a leading edge sweep in excess of 60° at a high subsonic Mach number. Here the wing has sufficient sweep that strong shocks, and therefore severe shock/boundary layer interactions, do not arise. Such wings, designed for high supersonic performance, have sharp leading edges. At large angles of attack, leading edge separation will arise as shown in Figure 5. Such a separation represents a free shear layer separation, a class of separations that is unique to three dimensional flows. Here the boundary layer air on both surfaces approaching the leading edge is convected away from the surface in a free vortex "sheet" which eventually spirals into a line vortex. Such a separation is in contrast to the bubble type separation shown earlier in Figure 3, where the low energy separated fluid is trapped in a bubble at the configuration surface. In the case of wings with sharp leading edges where the flow separates at the leading edge, the above free shear layer separation is essentially an inviscid phenomenon. The case of a blunt leading edge differs only in that the separation line on the leading edge along which the free shear layer leaves the surface must be determined from a viscous flow analysis.

Further examples of free shear layer separations as those arising in the case of lifting bodies are given in Ref. 4.

3. THE LOW SPEED/HIGH LIFT CASE

It is clear that an airfoil placed at large angles of attack at low speeds is susceptible, not only to leading and trailing edge separations, but to a Type B interaction between the two separations. It is also well known that leading and trailing edge devices significantly delay these difficulties. The case of the leading edge slat was described in an earlier lecture. Here it was found that the leading edge slat greatly reduced the leading edge suction peak on the main element while the latter induced a lower pressure at the trailing edge of the slat thereby greatly reducing the slat aft pressure recovery. These effects significantly delay leading edge separation on the main element and trailing edge separation on the slat.

A similar favorable interference with regard to alleviating the viscous effects for the case of an aft flap is shown in Figure 6 from Ref. 5. Here the favorable interference is shown at both a fixed lift and a fixed angle of attack.

In designing multi-element airfoils confluent boundary layers must be avoided where the low energy wake of an upstream element becomes entrained into the boundary layer of the following element to deteriorate the flow.

In a commercial transport configuration, leading edge slats or Kruger flaps are installed along essentially the entire span to protect the wing from leading edge separation. Spanwise gaps in the aft flap installations, however, are more difficult to avoid. Here an outboard gap is provided for low speed ailerons, while flaps are not deployed downstream of the engines to avoid jet impingement on the flap. In Figure 7 are shown an oil flow picture and a corresponding sketch pointing out the consequences of the above missing flap segments. Understandably trailing edge separation is present in the unprotected outboard span stations. Along the inboard gap the separation is significantly milder due to the unloading of this segment of the wing by the nacelle. Severe outboard separation is particularly undesirable since it will deteriorate the aileron effectiveness as well as contribute to pitchup.

2.3 PERFORMANCE CONSEQUENCES OF VISCOUS INTERACTIONS

In the present section the consequences of the transonic viscous interactions on the vehicle performance are briefly reviewed in order of increasing severity of the interaction. The discussion will be confined to the case of fighters or airlift aircraft with swept wings.

At the cruise condition the wing design is such that the shocks arising are sufficiently weak that their entropy losses are negligible. The shock/boundary layer interaction however, still modifies the shock location and thickens the post-shock boundary layer thus affecting the forces and moments on the wing. In the case of aft cambered airfoils the shock/boundary layer interaction had in fact a beneficial effect

in preventing a strengthening of the shock by halting its displacement onto the aft high convexity region.

At greater lifts both shock-induced and trailing edge separations worsen particularly downstream of the outboard shock, spreading first outboard to the tip and then inboard. Buffet will then occur, its intensity increasing with lift. Buffet is of concern for its effect on the fatigue life of the aircraft structure. Potentially more severe however is the possibility of tail flutter excited by the wake of the buffeting wing flow.

With the tip region of the swept wing severely separated, an undesirable longitudinal instability, pitchup, will arise. The responsible nose-up pitching moment is due in part to the inboard (and therefore an upstream) shift of the loading on the wing and to the resulting increased inboard wing downwash which induces an added download on the tail. Pitchup is an undesirable inherent feature of high aspect ratio sweep wings that must be avoided.

In fighter aircraft usable lift for transonic maneuverability is usually limited, not by buffet, but by the appearance of severe lateral instabilities. Such instabilities are caused by lateral differences of the wing separation or by the blanketing of the tail by the separated wing wake. Lateral rigid body divergences as wing drop and nose slice are of major concern.

The above examples by no means exhaust the important viscous interactions that impact performance. Omitted, for example, are viscous effects on the fuselage as the aft-fuselage drag, and other complex interactions of vortices and wakes generated by upstream configuration components with the downstream components.

3. FORMULATION OF THF VISCOUS FLOW PROBLEM

In the present section the problem of the viscous flow over wings in the transonic regime is formulated. The class of applicable flows is restricted here to those at large Reynolds numbers where the boundary layer is predominantly turbulent and attached with possible local regions of separation near the trailing edge or downstream of shocks. The scope of flows is thus restricted to only the simplest of viscous flows described in the previous section.

In Figure 8 is first shown the hierarchy of flow equations to treat real flows starting from the Boltzmann equation which gives a statistical accounting on a molecular scale. Averaging of this equation over the molecular velocities then results in the unsteady "Navier-Stokes" equations which in principle govern both laminar and turbulent flows. If such equations could be solved, they could handle all of the complex flows described in the previous section. If one now averages these equations in a suitable macroscopic fashion, the simpler steady Reynolds equations are obtained, but at the cost of having to provide an empirical modeling of the Reynolds stresses (the closure problem). An asymptotic expansion of these equations for large Reynolds numbers yields the thin layer viscous equations, which to first order simplify to Prandtl's boundary layer equations. "Averaging" of the boundary layer equations across the layer results finally in the integral boundary layer equations which we shall consider. The viscous equations in the thin layer approximation are valid only for the mildest viscous interactions described in the previous section, perhaps covering the region of drag divergence, but possibly stretched with additional empirical modeling to the buffet onset region.

At the level of the thin layer approximation, the problem is divided into two parts, that for the outer inviscid flow and the thin viscous layer adjacent to the configuration and in the downstream wake. A coupling of the two flows must then be devised. In the following we shall first comment only briefly on the inviscid flow methods, a detailed lecture having been given earlier by Dr. Jameson. Boundary layer/wake methods are then described followed by a description of the inviscid/viscous flow coupling procedures.

3.1 THE INVISCID FLOW PROBLEM

For most applied transonic problems th exact potential methods are best suited and most widely used. The potential approximation is valid so long as the total temperature is uniform, and the shock waves occurring within the flow are sufficiently weak. Here the shock strength is measured, for example, by the quantity $M_n - 1$ where M_n is the component of the Mach number normal to the shock upstream of the shock. The entropy change across the shock is then proportional to $(M_n - 1)^3$, a weak function of the shock strength. In a well-designed swept wing, the twist and camber are chosen such that at the design point the shock waves are adequately swept. At off-design conditions shock unsweeping can arise, for example at increased lift, but the resulting shock/boundary layer interaction as described earlier will incline the shock to an oblique shock. Both the sweep and obliqueness will weaken the shock sufficiently that the potential approximation will be valid.

Thus methods with the more complex Euler equations are not warranted with their increased computer costs and memory requirements. Small disturbance methods are inadequate, and they offer no reduction in computer costs.

3.2 BOUNDARY LAYER METHODS

Widely used viscous equations in the transonic problem are the integral boundary layer equations. Potentially more general formulations have been unable to treat any better the complexities arising in transonic flow due for example to shock waves. More complex differential equation methods for example have not only not yielded superior results but required more than an order of magnitude greater computing time than integral methods.

In the case of planar turbulent boundary layers, a representative integral method is that developed by Green (Ref. 6). It is composed of a set of three first order ordinary differential equations derived from the continuity equation, streamwise momentum equation, and the Bradshaw/Ferriss turbulent energy equation. Dependent variables arising in these equations are the momentum thickness θ, the form factor $H = \delta^*/\theta$ where δ^* is the displacement thickness, the entrainment function C_e measuring the rate at which the inviscid flow enters the boundary layer, and U_e the velocity at the edge of the boundary layer. The system of three equations with four unknowns is made determinate by considering one of the unknowns as a prescribed input function to be furnished from the inviscid flow, for example U_e in the case of attached flow (the direct problem). It will be seen later that for the separated case, the proper input function is the displacement thickness (the inverse problem).

In the three dimensional case, analogous integral boundary layer equations are those derived for example by Smith (Ref. 7). They form a set of four first order partial differential equations expressing the conservation of mass, streamwise and stream-normal momenta, and Green's lag entrainment equation in the streamwise direction. The unknowns are the streamwise momentum thickness θ_{11}, the streamwise form factor δ_1/θ_{11} where δ_1 is the streamwise displacement thickness, the entrainment function C_e, the angle β between the outer and limiting streamlines (the latter forming the skin friction lines), and U_e and α the magnitude and direction of the velocity vector at the edge of the boundary layer. Here again two of the six dependent variables must be taken as input functions, for example in the case of attached flow U_e and α.

In the case of attached flows with U_e and α as inputs, the above system of equations is fully hyperbolic where the characteristics are the outer inviscid flow streamlines (double family), the limiting streamlines, and a family lying between the above two. With the problem fully hyperbolic in the direct case, the formulation and solution of the problem are straightforward. Here the method of characteristics forms a reliable guide. Thus initial or starting conditions must be furnished along a space-like line near the wing leading edge where the values of the dependent variables must be prescribed. Additionally boundary conditions must be prescribed along time-like boundaries as along the wing centerline or the tip chord when the range of influence of these boundary points falls onto the wing. Here the number of data to be prescribed equals the number of characteristics pointing into the planform.

As in all hyperbolic systems, weak solutions containing flow discontinuities are possible. The physical nature of these discontinuities cannot be determined until the set of equations are expressed in proper conservation form so that jump conditions can be derived. It is to be noted that if other pairs of dependent variables are taken as input functions, the character of the equations will be different (see Ref. 8).

Both the two and three dimensional integral equations described above have also been applied to the wake by setting the skin friction equal to zero and adjusting the dissipation length scale parameter to be consistent with the asymptotic far-field wake.

A review of the three dimensional integral boundary layer/wake methods as well as differential equation methods was recently given by Smith (Ref. 9).

3.3 FORMULATION OF THE REAL FLOW PROBLEM - VISCID/INVISCID FLOW COUPLING

For the formulation of the real flow problem, we shall first introduce the concept of an equivalent inviscid flow. In such a flow the airfoil boundary condition is modified such that the flow outside the boundary layer in the real flow is reproduced. Within the thin layer approximation, this is accomplisned by displacing the airfoil surface by the boundary layer displacement thickness or alternatively by imposing a transpiration velocity at the surface of the airfoil (Ref. 10). Here, analogous to the relationship of the airfoil thickness to the source strength in thin airfoil theory, the transpiration velocity is related to suitable derivatives of the displacement thicknesses.

The formulation of the real flow problem follows directly from the introduction of the equivalent inviscid flow. The boundary layer equations, defining the necessary displacement thickness, constitute auxiliary relations that complete the definition of the airfoil viscous tangency condition for the equivalent inviscid flow. Since the pressure is assumed to be constant across the boundary layer, the surface pressures as determined in the equivalent inviscid flow will therefore yield the desired airfoil pressures in the real flow.

The highly implicit formulation of the real flow problem described above makes a direct numerical solution difficult. Iterative methods will be a necessity, and these are now described.

In the classical weak coupling procedure, for example in the case of an airfoil with an attached flow, both the inviscid and boundary layer/wake flows are posed in the direct form. First, the inviscid flow over the airfoil is computed yielding the (inviscid) pressure distribution. The latter is then inputted into the boundary layer/wake code, which in turn yields the displacement thickness or its equivalent the transpiration velocities. The latter forms an upgraded effective surface shape with which the above process is repeated. In the case of attached flow the above procedure has been found to be convergent even with shock waves present (see for example Refs. 11 and 12).

If the boundary layer is separated, Green's integral boundary layer equations in the direct form become "stiff"; that is, the coefficients of the equations become such that a small error in the pressure gradient input leads to a large error in the displacement thickness. The above classical coupling procedure then ceases to converge.

A coupling procedure to circumvent this difficulty has been proposed by Le Balleur (Ref. 13), that is, the semi-inverse method, where the inviscid flow is posed in the direct form, but the boundary layer flow is posed in the inverse form to avoid the above stiffness. With the displacement thickness inputted to both flows, each will result in a pressure distribution which in general will not match. An update scheme is then used which yields a correction to the input displacement thickness to reduce the pressure distribution mismatch. The above update scheme is based on the solution to a simplified boundary value problem where the small disturbance potential equation is used together with a linearized Green's equation (see Ref. 14).

The above semi-inverse procedure has yielded convergent solutions for the unseparated cases (Ref. 13), but as yet satisfactory results have not been achieved for the separated cases for which the method was developed. Posing the boundary layer problem in the inverse form has eliminated the stiff character of the equations, but it appears that the update procedure is inadequate in the shock region. Research is continuing in this area, but the scarcity of reliable experimental data for separated flows has impeded the progress.

Coupling of the inviscid and boundary layer/wake flows in the three dimensional case as for a swept wing are in the early stages of development. For the attached case both the classical weak interaction and the semi-inverse procedures can be used (Ref. 8).

In the semi-inverse procedure, the streamwise form factor and the inviscid flow angle α, for example, can be used as input functions for the boundary layer equations which will retain a fully hyperbolic character. Coupling procedures for the three dimensional separated cases are still in development.

3.4 HIGHER ORDER BOUNDARY LAYER EFFECTS

In the previous section the equivalent inviscid flow was defined. Here a modified airfoil tangency condition was used which yielded the real flow exterior to the boundary layer, in particular the pressure distribution at the edge of the boundary layer. Since the pressure was assumed to be invariant across the boundary layer, the airfoil surface pressures calculated in the equivalent inviscid flow would then yield the desired surface pressures for the real flow.

In the neighborhood of the shock and the trailing edge the invariance of the pressures across the boundary layer ceases to be valid. The surface pressures as calculated in the equivalent inviscid flow are no longer the desired surface pressures for the viscous flow in these regions. Fulfilling the Kutta condition in the equivalent inviscid flow for example would not satisfy the Kutta condition in the real flow leading to concern in the determination of the circulation.

In a subcritical flow a mismatch of the trailing edge pressures would clearly be of concern since the circulation is significantly affected by the Kutta condition. In the high subsonic region, however, it was pointed out earlier that the Kutta condition losses its significance in establishing the circulation with a greater role played by choking considerations. A mismatch of the trailing edge pressures caused by the failure of the first order boundary layer theory would therefore not affect significantly the overall circulation.

The real flow about the trailing edge is a strong interaction flow. That is, the presence of the boundary layer significantly alters the inviscid flow in these regions. The analysis of the boundary layer flow about the trailing edge therefore cannot be carried out by isolating it and imposing the inviscid flow conditions at its outer edge.

There have been a number of investigations deriving higher order boundary layer equations. Thus for example Nakayama, Patel and Landweber (Ref. 15) added a simplified transverse momentum equation in lieu of the transverse pressure invariance. The improved method added only minor complications to the first order theory. The importance of the remaining significant higher order effects not considered above however remains unresolved.

The strong interaction at the shock wave on the other hand is significantly more difficult. Usable theories cannot be expected in the near future. For the near-term one must use first order methods adjusting them phenomenologically to yield acceptable solutions in a consistent fashion.

4. EXAMPLES

In the present section computational examples are given which illustrate both recent advances as well as highlight significant shortcomings still unresolved.

In the case of airfoil flows with attached boundary layers, there have been notable contributions for example for the RAE 2822 airfoil for which test results are available (Ref. 16). In Figure 9 is shown the test/theory comparison of the pressure distribution and the displacement and momentum thickness obtained by Collyer and Lock (Ref. 11). Here an exact potential method was coupled to Green's lag entrainment integral method using the weak interaction procedure. A partially non-conservative shock capture was employed "to compensate" for the error in the entropy rise across the shock. A check of the normal Mach number upstream of the shock would show that such compensations are not needed in this case ($M_n = 1.15$, total pressure loss of 0.3%). A simple curvature effect was incorporated into the wake contact jump conditions. In the calculations the angle of attack was adjusted by $+0.55^\circ$ to match the measured lift.

Figure 10 shows the test/theory comparison for the pressure distribution obtained by Le Balleur (Ref. 13). An exact potential method is coupled to an integral boundary layer/wake code, developed by Le Balleur, using the semi-inverse procedure described earlier. Here the free stream Mach number was raised by 0.002 and the angle of attack decreased by 0.19°, both relative to the test values.

In Figure 11 is another set of test/theory comparisons, still for the RAE 2822 airfoil. One result is due to Longo, Schmidt, and Jameson (Ref. 12) who coupled the exact potential code with Horton's integral boundary layer/wake method in the weak coupling mode. The free stream Mach number in the calculation was increased by 0.004, while the angle of attack was decreased by 0.87° to match the measured lift. Another calculation shown in Figure 11 is due to Melnik (Ref. 17) who coupled the exact potential method with Green's lag entrainment method in the weak interaction mode. The Mach number here was increased by 0.003 while the angle of attack was decreased by 0.57° to match the measured lift. Finally the results with the Euler equations coupled with the integral boundary layer/wake method obtained by Schmidt, Jameson, and Whitfield (Ref. 18) are shown in Figure 11. Here only the Mach number was adjusted increasing it by 0.004. In the above case the normal Mach number upstream of the shock is approximately 1.16 corresponding to a total pressure loss across the shock of less than 0.4%. The entropy increase across the shock is therefore negligible removing any theoretical differences between the Euler and exact potential formulations.

The noteworthy feature of the above test/theory comparisons is the excellent agreement obtained in the pressure distributions and in the displacement and momentum thicknesses. The confusing aspect is that the merits of the refinements in the various methods have been masked by the widely varying adjustments of the free stream Mach number and angle of attack. Such adjustments, intended primarily to correct for the wind tunnel wall interference, have in some cases inadvertently compensated for shortcomings of the numerical solutions. This points to the need for reliable experimental results where the wall interference is suitably defined for example in terms of wall pressure measurements. Inputting the latter into the calculations would then preclude the need to adjust the free stream Mach number and angle of attack.

In the three dimensional case the development of real flow procedures understandably lags the planar case. Although there are ongoing activities in coupling the exact potential code with the three dimensional boundary layer/wake codes, no published accounts are presently available.

There are however interesting results published exercising the three dimensional integral boundary layer codes where the necessary input data are furnished from experiments. One case is the flow in the inboard region of a swept wing at low speeds tested by Lindhout, Elsenaar, and van den Berg (Ref. 19). A sketch of a flow visualization picture from Ref. 19 is shown in Figure 12 in which trailing edge separation is indicated.

In Figure 13 is shown the calculated limiting streamlines obtained by Cousteix and Houdeville (Ref. 20). Here the boundary layer problem was posed in the direct mode inputting the measured speed and flow direction of the outer inviscid flow. A marching in the streamwise direction was carried out using an explicit difference scheme, terminating the marching when the streamwise skin friction vanished. The envelope of limiting streamline characteristics suggested in Figure 13 would then correspond to a separation line. However with the boundary layer equations recast as a system of ordinary differential equations by the explicit marching procedure, a stiffness of the equations occurs in the vicinity of the envelope invalidating the solution in that neighborhood.

The above flow was calculated by a number of other investigators using integral as well as differential equation methods, and their results are summarized in Ref. 19. The results from most methods were found to be in reasonable agreement.

Another interesting set of calculations is for the case of the infinite yawed wing at low speeds tested by Elsenaar, van den Berg, and Lindhout (Ref. 21). This case was calculated by a number of investigators using both the integral and differential equation methods, and the results are reported in Ref. 22. One interesting calculation is due to Stock (Ref. 23). Since the experiments indicated trailing edge separation, an inverse formulation of the integral boundary layer method was used where the input function was the measured displacement thickness in the direction normal to the leading edge. In this formulation the explicit marching could be carried out through the separated region, yielding results that compare reasonably with experiments (see Figure 14). In the case of the infinite yawed wing where the spanwise derivatives are zero, the inverse formulation, behaves, perhaps not surprisingly, as in the planar case without stiffness difficulties. Such a behavior should not however be expected to carry over to the general three dimensional case formulated in a comparable inverse mode inputting the displacement thicknesses.

5. CONCLUDING REMARKS

Our primary objective has been to convey an appreciation of the significant effects of viscosity in transonic flows. Here key fluid dynamic mechanisms were described that make up the inviscid/viscous flow interactions. Performance consequences were also described ranging from the mild effects at cruise conditions, affecting the lift to drag ratio, to severe interactions leading to catastrophic flutter and rigid body instabilities.

Numerical methods were described to treat the real flow, but they were restricted to the mildest of strong interactions. Even within this limited scope, substantial further effort is needed to model the shock/boundary layer interaction in a reliable manner and to develop viscous equations and inviscid/viscous flow coupling procedures capable of treating three dimensional separated flows. Here it would be desirable to have a procedure capable of predicting buffet onset. Finally accurate and complete experimental data for transonic separated flows are needed for both airfoils and wings for the validation of computational methods.

REFERENCES

1. Pearcey, H., Osborn, J., and Haines, A. B., The Interaction between Local Effects at the Shock and Rear Separations, AGARD CP No. 35, 1968.

2. Küchemann, D., Types of Flow on Swept Wings, J. Roy. Aero. S., Vol. 57, November 1953.

3. Moss, G. F., Some UK Research of the use of Wing-Body Strakes on Combat Aircraft Configurations at High Angles of Attack, AGARD CP No. 247, 1978.

4. Peake, D. J., and Tobak, M., Three Dimensional Flows about Simple Components at Angle of Attack, NASA TM 84226, 1982.

5. Smith, A. M. O., Remarks on Fluid Mechanics of Stall, AGARD-LS-74, 1975.

6. Green, J., Weeks, D., and Brooman, J., Predictions of Turbulent Boundary Layers and Wakes in Compressible Flow by Lag-Entrainment Method, ARC R and M 3791, 1973.

7. Smith, P. D., An Integral Prediction Method for Three-Dimensional Compressible Turbulent Boundary Layers, ARC R and M 3739, 1972.

8. Wigton, L., and Yoshihara, H., Viscous-Inviscid Interactions with a Three-Dimensional Inverse Boundary Layer Code, Boeing Report D6-51713, 1982 (Also to be presented at the Second Symposium on Numerical and Physical Aspects of Aerodynamic Flows, 17-20 January 1983 at California State University (Long Beach)).

9. Smith, P. D., The Numerical Computation of Three-Dimensional Turbulent Boundary Layers, RAE TM (Aero) 1945, 1982.

10. Lighthill, M. J., On Displacement Thickness, J. Fluid Mech, Vol. 4, 1958.

11. Collyer, M. R., and Lock, R. C., Predictions of Viscous Effects in Steady Transonic Flow Past an Aerofoil, Aero Q. Vol. XXX, 1979.

12. Longo, J., Schmidt, W., and Jameson, A., Viscous Transonic Airfoil Flow Simulation, ICAS Proceedings, 1982.

13. Le Balleur, J. C., Strong Matching Methods for Computing Transonic Viscous Flows Including Wakes and Separations, La Recherche Aerospatiale, 1981.

14. Wigton, L., and Holt, M., Viscous-Inviscid Interaction in Transonic Flow, AIAA Paper 81-1003-CP, June 1981.

15. Nakayama, A., Patel, V. C., and Landweber, L., Flow Interaction near the Tail of a Body of Revolution, J. Fluid Eng. (ASME), September 1976.

16. Cook, P. H., McDonald, M. A., and Firmin, M. C. P., Aerofoil RAE 2822 - Pressure Distributions and Boundary Layer and Wake Measurements, AGARD-AR-138, 1979.

17. Melnik, R., Turbulent Interactions on Airfoils at Transonic Speeds - Recent Developments, AGARD CP 291, 1980.

18. Schmidt, W., Jameson, A., and Whitfield, D., Finite Volume Solution for the Euler Equations for Transonic Flow over Airfoils and Wings Including Viscous Effects, AIAA-81-1265, 1981.

19. Lindhout, J. P. F., Elsenaar, A., and van den Berg, B., Comparison of Boundary Layer Calculations for the Root Section of a Wing, NLR MP 80028, 1981.

20. Cousteix, J., and Houdeville, R., Singularities in Three-Dimensional Turbulent Boundary Layer Calculations and Separation Phenomena, ONERA CERT Report (Also AGARD CP 291, 1981).

21. Elsenaar, A., van den Berg, B., and Lindhout, J. P. F., Three-Dimensional Separation of an Incompressible Turbulent Boundary Layer on an Infinite Swept Wing, AGARD-CP-168, 1975.

22. Humphreys, D. A., Comparison of Boundary Layer Calculations for a Wing, FFA TN AE-1522, 1979.

23. Stock, H. W., Computation of the Boundary Layer and Separation Lines on Inclined Ellipsoids and of Separated Flows on Infinite Swept Wings, AIAA-80-1442, 1980.

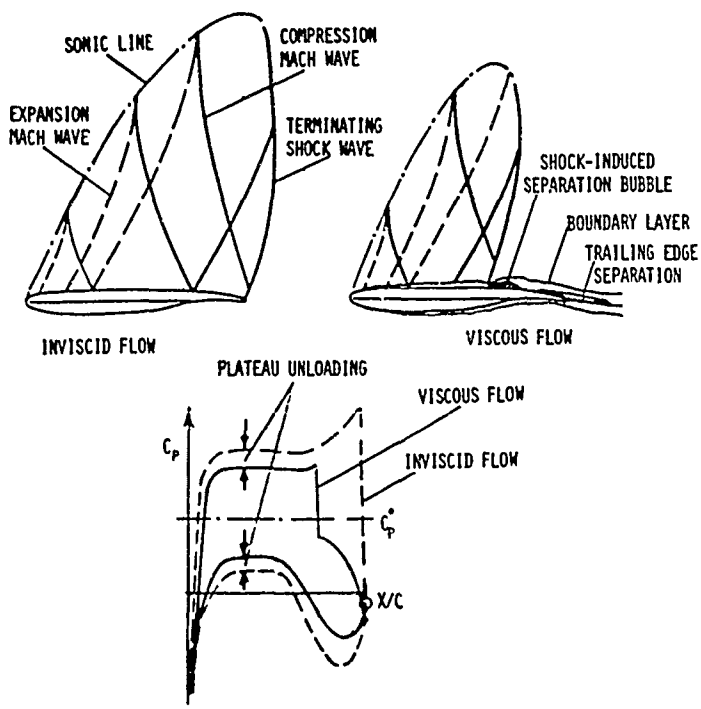

FIGURE 1. INVISCID/VISCOUS FLOW COMPARISON - CRUISE

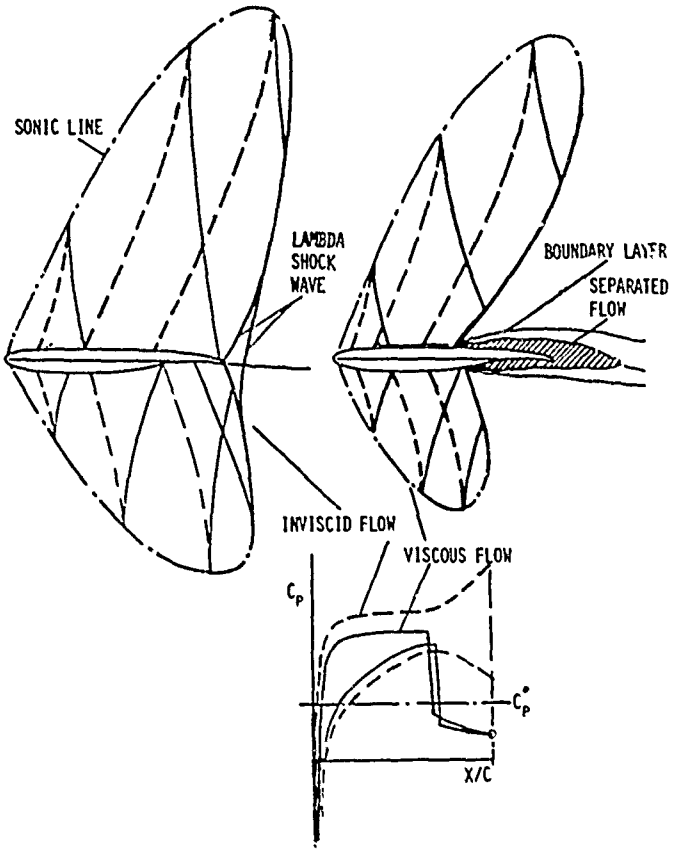

FIGURE 2. INVISCID/VISCOUS FLOW COMPARISON - BUFFET

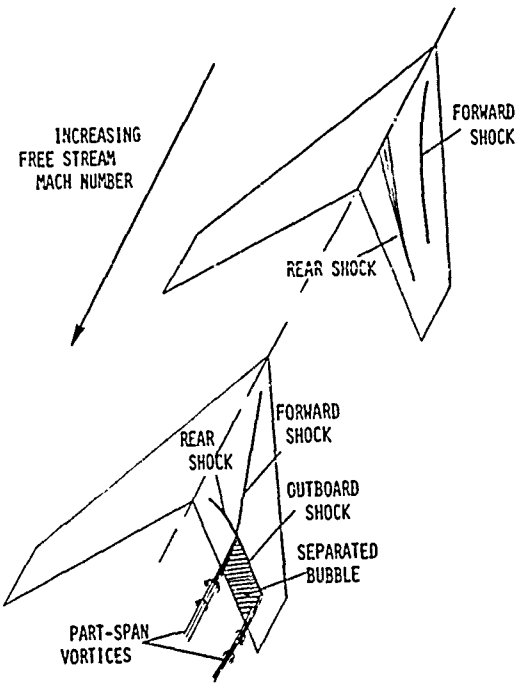

FIGURE 3. SHOCK WAVE AND SEPARATION PATTERN - SWEPT WING.

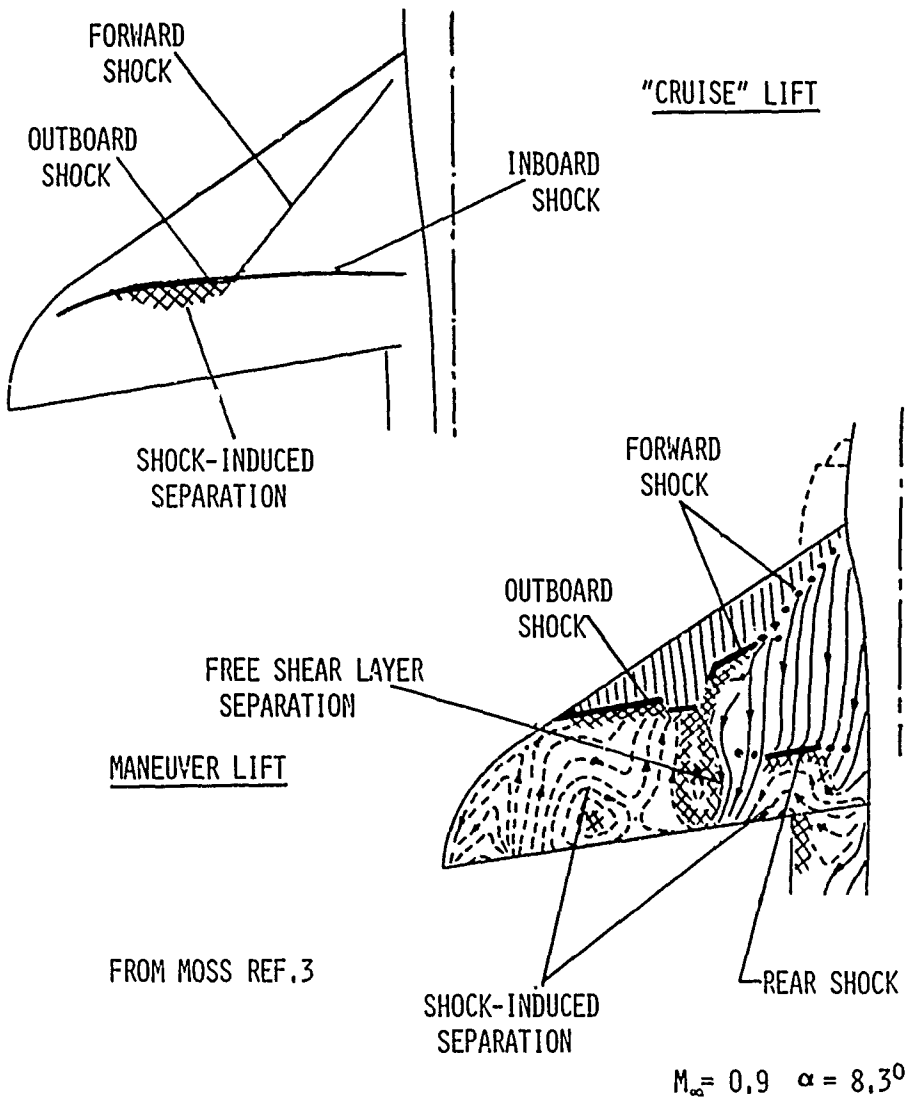

FIGURE 4. SHOCK WAVE AND SEPARATION PATTERN - FIGHTER WING.

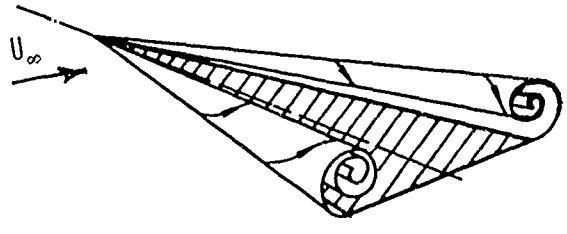

Figure 5. Leading Edge Separation Vortex.

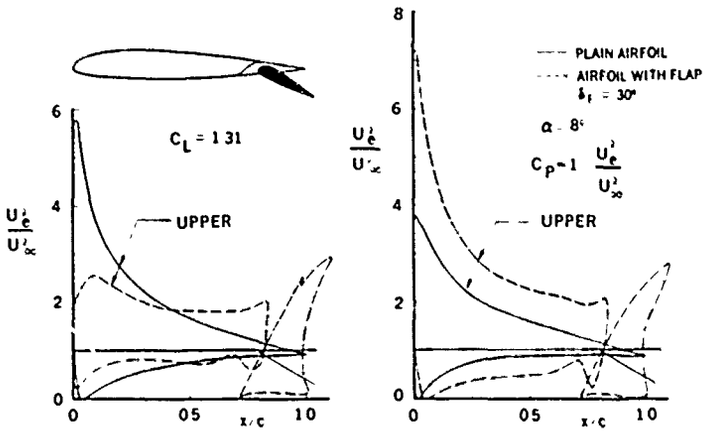

Figure 6. Aft Flap Favorable Viscous Interference (Smith Ref. 5).

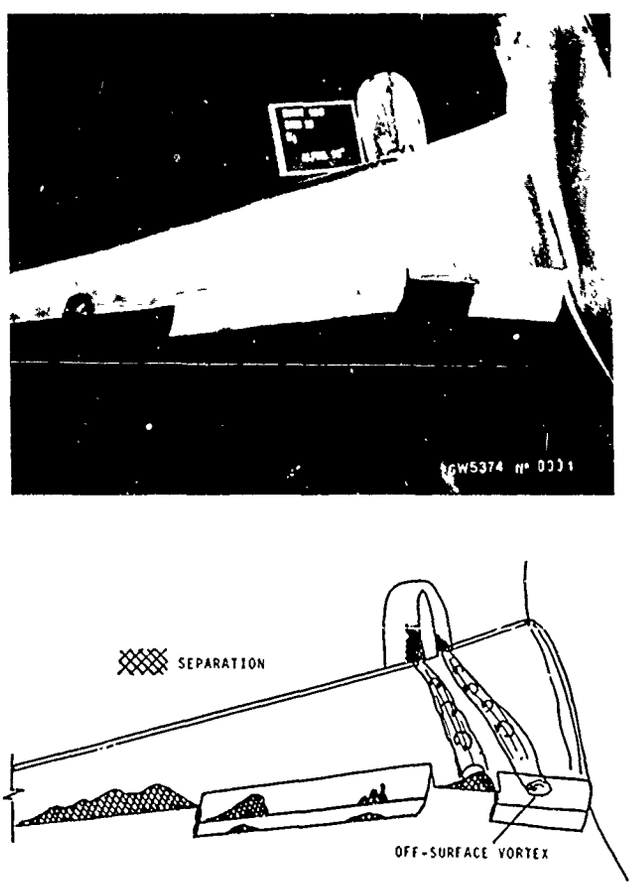

Figure 7. Flow Visualization Picture with High Lift Devices.
(Courtesy of Dr. J. McMasters, Boeing Co.)

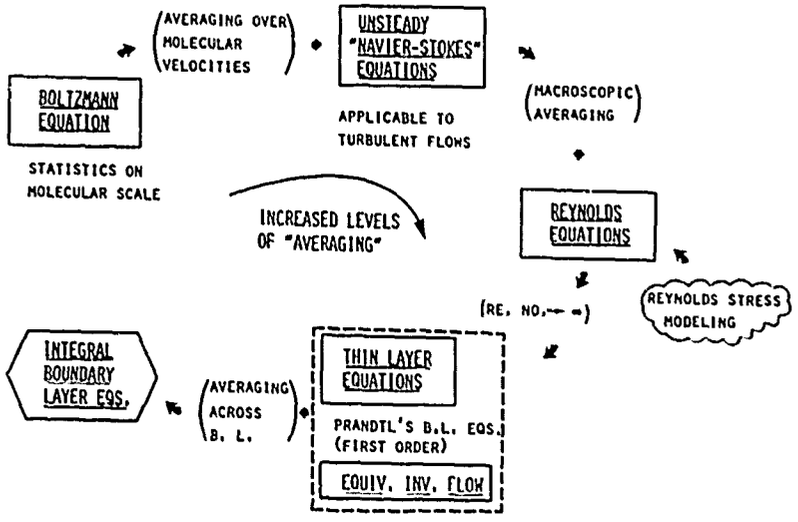

Figure 8. Hierarchy of Viscous Flow Equations.

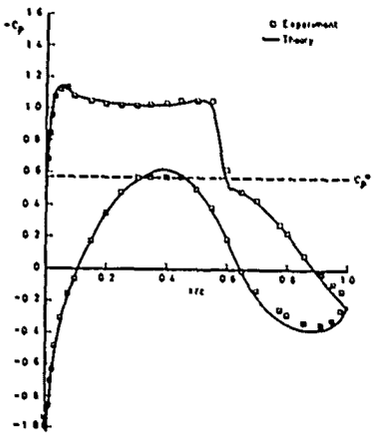

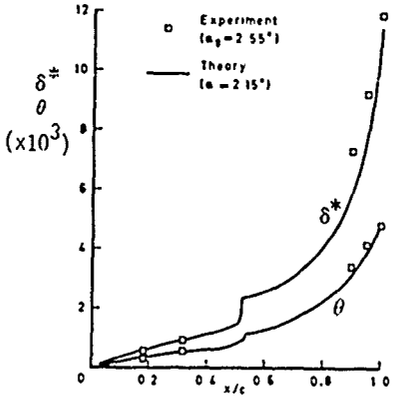

Figure 9. Test/Theory Comparison Collyer and Lock Ref.11.

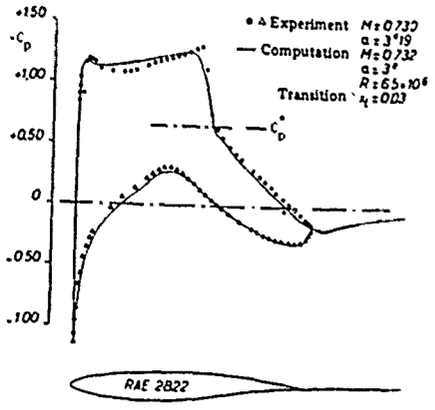

Figure 10. Test/Theory Comparison Le Balleur Ref.13.

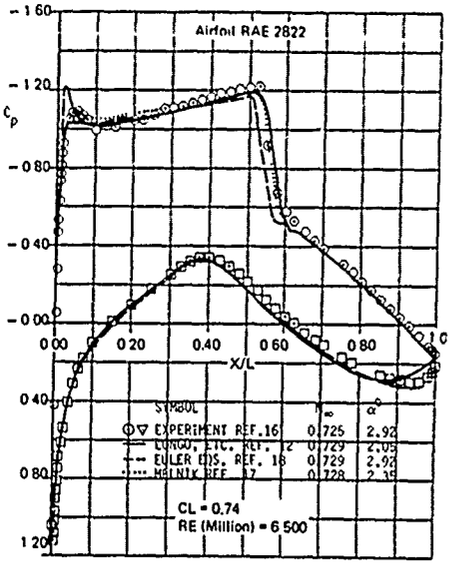

Figure 11. Test/Theory Comparison Ref.12.

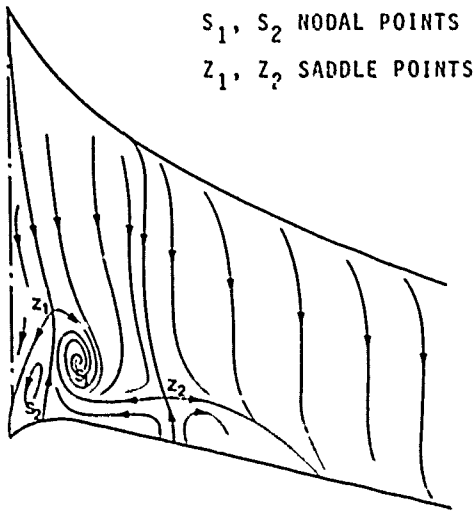

Figure 12. Limiting Streamlines (Experiments: Lindnout, Elsenaar, and van den Berg Ref. 19)

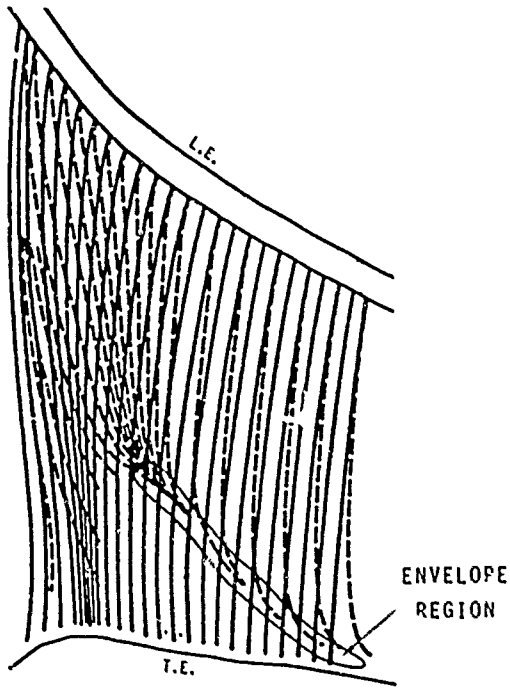

Figure 13. Limiting Streamlines (Calculated: Cousteix and Houdeville Ref. 20)

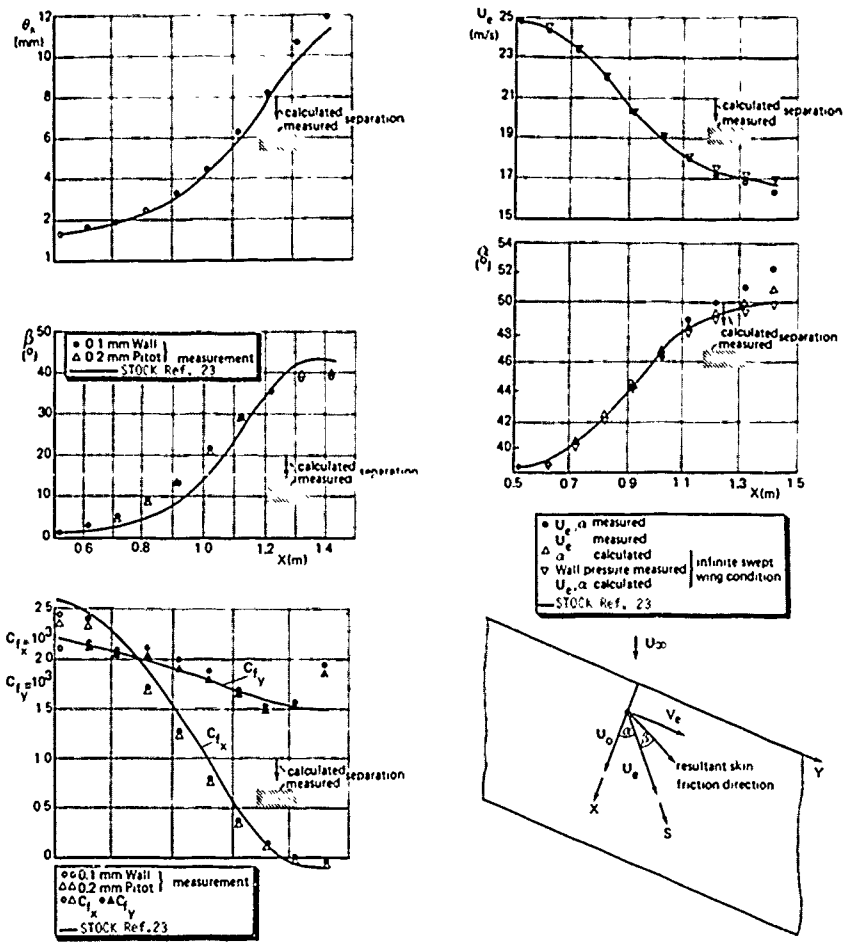

Figure 14. Test/Theory Comparison, Infinite Yawed Wing.

TRANSONIC AIRFOIL DEVELOPMENT

by Richard T. Whitcomb
Distinguished Research Associate
Langley Research Center, NASA
Hampton, Virginia 23665
U.S.A.

SUMMARY

This lecture consists of three parts, in which discussions are presented of the current state of development of transonic or supercritical airfoils designed for fully turbulent boundary layers on the surfaces, previous research on subcritical airfoils designed to achieve laminar boundary layers on all or parts of the surfaces, and current research on supercritical airfoils designed to achieve laminar boundary layers. In the first part the use of available two dimensional computer codes in the development of supercritical airfoils and the general trends in the design of such airfoils with turbulent boundary layers are discussed. The second part provides the necessary background on laminar boundary layer phenomena. The last part, which constitutes the major portion of the lecture, covers research by NASA on supercritical airfoils utilizing both decreasing pressure gradients and surface suction for stabilizing the laminar boundary layer. An investigation of the former has been recently conducted in flight using gloves on the wing panels of the U.S. Air Force F111 TACT airplane, research on the later is currently being conducted in a transonic wind tunnel which has been modified to greatly reduce the stream turbulence and noise levels in the test section.

SYMBOLS

C_D	drag coefficient, Drag/qS
C_L	lift coefficient, Lift/qS
C_p	pressure coefficient, $p_\ell - p_\infty/qS$
Hz	cycles per second
M	free stream Mach number
n	disturbance amplitude ratio
p_ℓ	local static pressure
p_∞	free stream static pressure
q	free stream dynamic pressure
R_n	Reynolds number
S	wing area
Λ	sweep angle

SUPERCRITICAL AIRFOILS DESIGNED FOR TUBULENT BOUNDARY LAYERS

The first airfoils designed specifically to delay drag rise by improving the transonic or supercritical flow above the upper surface were the "peaky" airfoils developed experimentally by by Pearcy (Ref. 1). They provide an isentropic recompression of the supercritical flow ahead of the shock wave located on the forward region of the airfoil. These airfoils provide approximately a .02 to .03 delay in the drag rise compared with NACA 6 series airfoils which had been used for many of the first generation of subsonic jet aircraft. These improved airfoils or their derivatives were used on many of the second generation of such aircraft. During the middle 1960's transonic airfoils with drag rise Mach numbers substantially higher than the "peaky" airfoils were developed experimentally at NASA Langley. These airfoils had supercritical flow over a major portion of the upper surface and therefore were named NASA supercritical airfoils. This work was classified until the early 1970's. An unclassified summary of this work is presented in reference 2. Following the work at NASA other organizations in the United States and Europe also developed similar supercritical airfoils (Ref. 3 for example).

The experimental development of such supercritical airfoils is extremely tedious, time consuming, and expensive. Therefore, theories and associated numerical codes to calculate the characteristics of supercritical airfoils were developed by several

organizations in the United States and Europe. One of the most successful of these efforts was that by the team at New York University under the direction of Garabedian. (Ref. 4.) Numerous comparisons between the pressure distributions and drag coefficient calculated using the NYU code and experimental results have indicated very good agreement. A typical example of the agreement for a pressure distribution is shown in figure 1. An example of the agreement for drag coefficient is shown in figure 2. The agreement for drag at higher lift coefficients is not as satisfactory. With the availability of such reliable computational methods the need for wind tunnel investigations of supercritical airfoils is greatly reduced. In fact, the differences between the calculated and experimental results are usually less than those between the measured two dimensional airfoils and three dimensional wing results. Therefore, during wing development at Langley the airfoils designed using the theory are applied directly to the three dimensional models.

Using the numerical codes, the various research and industrial organizations have designed many different supercritical airfoils, each to meet the specific requirements of various applications. However, most of these airfoils usually have certain common features which will now be discussed. A generalized design pressure distribution on a representative supercritical airfoil, together with the associated airfoil shape are presented in figure 3. Considering the upper surface first, numerous investigators have found a gradually decreasing velocity in the supercritical flow region usually results in the highest drag rise Mach number for a given design lift coefficient. Also, the highest usable drag rise or lift coefficient is generally obtained with a weak shock wave at the end of the supercritical region. Further, it is important that the final pressure recovery to trailing edge be sufficiently gradual to prevent local separation near the trailing. With respect to the lower surface, the design feature which is the most controversial and thus varies the most among the airfoils designed by various organizations is the concave region near the trailing edge together with the positive pressures associated with it. Both experimental and calculated results have indicated that these positive pressures are important in achieving a high drag rise Mach number for the usual design lift coefficient. However, the pressures result in an undesirable negative pitching moment and increased hinge moments, while the physical concavity reduces the structural depth of the flap or aileron. Therefore, the depth of the concavity must be a compromise based on a number of considerations. It is obvious when one compares the concavity of the supercritical airfoils designed by various groups that these groups have substantially different ideas as to the most satifactory compromise.

Generally, for the outboard region of a high aspect ratio wing the most satisfactory pressure distributions and airfoil shapes are similar to those determined using two dimensional calculations. However, because of the strong three dimension effects at supercritical Mach numbers the airfoil shape for the inboard sections of swept wings usual deviate substantially from the two dimensionally derived shapes. The shape developed for the inboard region a supercritical wing demonstrated in flight on a U.S. Navy F8 test bed will be discussed in my second lecture. The airfoil shapes developed for other configurations by other groups will probably be discussed by other lecturers.

PREVIOUS RESEARCH ON AIRFOILS DESIGNED FOR LAMINAR BOUNDARY LAYERS

Since the time of Prandl, at least, it has been recognized that the skin friction drag could be substantially reduced by achieving a laminar rather than a turbulent boundary layer on the surface of an aircraft component. However, results of early wind tunnel research on flat plates indicate that transition from a laminar to a turbulent condition occurred at relatively low critical Reynolds numbers, roughly 500,000. (Ref. 5). In the mid 1930's it was found that this value could be increased to about 1.5×10^6 by providing a decreasing pressure gradient on the surface (Ref. 6, for example). In 1938 B. M. Jones demonstrated that critical Reynolds numbers substantially higher than those determined in the wind tunnels could be achieved in flight (Ref. 7). The low wind tunnel values were associated with turbulence in the tunnel test sections. These flight results greatly encouraged world-wide research on configurations designed to achieve extensive regions of laminar flow at high Reynolds numbers. This work required the development of wind tunnels with turbulence levels much lower than those of previous tunnels.

Included among these new facilities was the Low Turbulence Pressure Tunnel at NACA Langley. Using this tunnel NACA developed a family of airfoils intended to have extensive regions of laminar flow at flight Reynolds numbers. These airfoils, known as 6 series, had decreasing pressures over the forward regions of the surfaces. The design pressure distribution for a typical airfoil of this family, is shown in figure 4. Investigation of these airfoils indicated that laminar flow could be maintained as far rearward as 60% of the chord on airfoils with reasonable thickness ratios for chord Reynolds numbers up to about 9.0×10^6 (Ref. 8). However, this was achieved only when the model surfaces were glass smooth. Flight tests of a wing incorporating such an airfoil and with extremely smooth surfaces indicated that extents of laminar flow similar to these measured in the wind tunnel could be achieved on an airplane (Ref. 9). However, for most production airplanes incorporating these airfoils little or no laminar flow was achieved, since the surfaces were not smooth enough. It should be noted, however, that these airfoils were used in the design of the first generation of United States jet aircraft since they had significantly higher critical Mach numbers than did the airfoils previously used.

In about 1940 it was proposed that the laminar boundary layer could be greatly stabilized and significant extents of laminar flow might be achieved by the removal of the lower part of the boundary layer by suction through slots or holes (Refs. 10 and 11). With this approach the extent of the laminar layer is not limited as with the use of favorable pressure gradients but can be extended to near the trailing edge. Pfenninger, in particular, (Ref. 12) and others conducted extensive wind tunnel and flight investigation on this approach over several decades. This research reached its culmination in the flight investigation of the X21 in the early 1960's (Figure 5). The results of this work indicated that laminar boundary layers could be maintained over most of this swept wing at very high Reynolds numbers. For the inboard sections a critical Reynolds number of 47.5×10^6 was achieved. However, because of the cost and complexities associated with providing and maintaining the systems and the surface smoothness required, work on laminar flow control in the United States was temporarily abandoned in the United States in 1966.

During the research on laminar flow control during the 1950's several important basic aerodynamic problems were uncovered. First, it was found that on swept wings instabilities in the laminar boundary develop due to the spanwise pressure gradients on such wings (Ref. 13). These effects, called cross flow instabilities, have been analyzed theoretically (Ref. 14, for example). Also, on wings with sufficient sweep turbulent flow which may develop on the leading edge of the inboard stations moves outboard in the stagnation region or attachment line at the leading edge and causes transition on the outer parts of the wing. This effect, called leading edge contamination, is discussed in reference 15. Further, it was found that the sensitivity to surface roughness is strongly dependent on the unit Reynolds number, that is, the Reynolds number per unit length (Ref. 16). Therefore, to maintain laminar flow for practical surfaces this unit value as well as the total Reynolds number must be limited. A summary of research on laminar boundary layer control to approximately 1958 is presented in reference 17 and a bibliography of reports on this subject to 1978 is presented in reference 18.

CURRENT NASA RESEARCH ON SUPERCRITICAL AIRFOILS DESIGNED FOR LAMINAR BOUNDARY LAYERS

With the recent large increase in the price of jet fuel, the economic value of reducing the skin friction has greatly increased and the complexities and costs associated with achieving laminar boundary layers might now be justified. Also new construction methods, such as composite materials, should greatly aid in the achievement of the required surface smoothness. Therefore, NASA, as part of a broad program called Aircraft Energy Efficiency (ACEE) undertook a reexamination of the technics for obtaining such boundary layers. This effort involves wind tunnel and flight investigations and extensive systems studies. One might ask why a new research program is needed since the subject had received so much attention in the past. The earlier work was all conducted at essentially subcritical conditions while the present research is involved primarily with supercritical conditions. Many of the phenomena associated with these new conditions are quite different than those studied in the past. In this effort both decreasing pressure gradients and suction as means for stabilizing the laminar boundary layer are being studied. In the present lecture the basic experimental research on transonic airfoils designed to exploit these two approaches will be discussed.

Stabilization by Decreasing Pressure Gradient

Since the stability of laminar flow is so strongly dependent on the Reynolds number any meaningful research must be conducted at near flight Reynolds numbers. Therefore, the initial exploratory research on a supercritical airfoil designed to obtain extensive laminar flow by decreasing pressure gradients was conducted in flight at the NASA Dryden Research Center. Partial span gloves were added to the wing panels of the United States Air Force TACT airplane (figure 6). This airplane is an F 111 retrofitted with a NASA supercritical wing. The use of theis airplane, with a variable sweep capability, allowed a systematic study of the crossflow instabilities described earlier. The shape of the new airfoil is substantially different from that on the TACT wing so that an extension of the glove forward and rearward of the original leading and trailing edge was required (fig. 7). In particular, the leading edge radius and the aft camber for the new airfoil are significantly less than those for TACT wing. The gloves, covered the middle regions of the panels. Because of the strong lateral spread of disturbances at supercritical speeds it was required that the shape of the upper surfaces of the panels inboard of the gloves be modified to achieve the desired pressure distributions on the gloves for such conditions. These changes were developed experimentally at the Langley 8-Foot Transonic Pressure Tunnel.

The airfoil for the flight investigation was developed at NASA Langley using the NYU code (Ref. 4) and an unpublished two dimensional laminar boundary layer stability code. The calculated pressure distribution for the supercritical design condition is shown in figure 8. The upper surface has a favorable pressure gradient from the leading edge to the 60% chord station followed by a weak shock and a gradual subsonic recovery. The lower surface has a favorable pressure gradient from the leading edge to the 50% chord followed by a recovery into a region of positive pressures characteristic of aft loaded supercritial airfoils. Obviously, the pressure distribution on the upper surface deviates substantially from that found to be most satisfactory when considering fully turbulent boundary layers, as discussed earlier. As a result, the drag rise Mach number for this airfoil is about 0.015 less than that for an airfoil designed for turbulent boundary layers with the same thickness ratio and design lift coefficient.

Laminar stability calculations for this airfoil, including the effects of compressibility and sweep were conducted for NASA at Boeing (Ref. 19). Representative results are presented in figure 9. Shown are variations of the growth of the Tollmien-Schlichting disturbances, that is those associated with longitudinal flow (Ref. 5), along the chord for a disturbance frequency of 2775 Hz for the design pressure distribution at a Reynolds number of 25×10^6. Of particular importance is the fact that the effects of compressibility for this condition reduces the growth of the disturbances by more than 50%. This effect greatly enhances the possibility of obtaining extensive regions of laminar flow at flight Reynolds numbers. The compressibility also reduces the crossflow instabilities, but to a much lesser degree. Predictions based on the compressible flow calculations (fig. 10) suggest that laminar flow should be achieved to the 60% chord station on the upper surface and 50% chord on the lower for 10° of sweep and a chord R_n of 35×10^6. For wing sweep angles greater than about 22° leading edge contamination, as described earlier, should cause transition near the leading edge. The instrumentation for this flight investigation was limited to wake survey probes. As a result relatively little information of a basic nature was obtained. However, the wake survey results indicate that substantial regions of laminar flow were achieved.

Stabilization by Suction

Because of the high cost of conducting flight research on advanced supercritical airfoils with the laminar boundary suction, the initial research on such airfoils is currently being carried out in a wind tunnel. Wind tunnel investigations of supercritical laminar flow airfoils require a large transonic tunnel with very low stream turbulence and noise levels. To provide such a facility the Langley 8-Foot Transonic Pressure Tunnel has been modified substantially (Ref. 20). To reduce stream turbulence five screens and honeycomb have been installed in the settling chamber of the tunnel. To eliminate the noise associated with mixing in the slots, the investigation is conducted with the slots closed. To greatly reduce the movement of noise from the diffuser into the test region variable choke plates have been installed between the test region and the diffuser. The stream turbulence and noise levels achieved are about .04% at a Mach number of 0.8.

To provide the required near full scale Reynolds numbers with acceptable unit Reynolds numbers, the chord of the model was made quite large, 2.15 meters. A large chord also facilitates the installation of the ducting in the model required for suction. With this large a model in a closed, unmodified test section the wall interference would be prohibitively large. To eliminate such interference the walls opposite the upper and lower surfaces have been contoured to the calculated streamlines of the flow about the model at the wall for the design condition. Further, to study the cross flow instabilities described earlier 23° of sweep was incorporated into the airfoil. To eliminate wall interference at the ends of the model these walls were contoured to the calculated cross flows due to this sweep. The model and contoured tunnel walls installed in the test region of the tunnel are shown in figures 11 and 12. The computational design of the shapes of the tunnel walls is described in reference 21.

The airfoil shape and associated pressure distributions for the model of this investigation were developed by W. Pfenninger using the NYU code of reference 4 and boundary layer stability analyses (Ref. 23). The chordwise pressure distributions and sonic lines for the design condition and an off-design condition together with the airfoil shape are shown in figure 13. The areas where various types of instabilities predominate are also indicated. In the supercritical flow region above the upper surface the pressure distributions have adverse gradients similar to that on most supercritical airfoils designed for turbulence boundary layers, as discussed earlier. The suction can readily maintain laminar flow through this gradual gradient since the instabilities are of the Tollmien-Schlichting type. The adverse gradients along the aft region of the airfoil are substantially greater than that used for most airfoils with turbulent boundary layers. The suction should maintain unseparated laminar boundary layers through these gradients even though the predominant disturbances are of the more critical cross flow type. However, substantially greater amounts of boundary layer removal are required than on the less critical region farther forward. Near the leading edge crossflow instabilities are particularly critical because of the pronounced pressure gradient.

The pressure distributions on the lower surface are markedly different from that on the usual supercritical airfoil with a turbulent boundary layer. The forward regions of positive, roughly uniform pressures, provides an area with reduced crossflow instability where a movable Kreuger flap type leading edge device could be incorporated. However, the concavity in the lower surface contour near the 15% chord associated with these pressure distributions leads to Taylor-Goertler instabilities (Ref. 5). The velocities along the middle region of the lower surface are nearly sonic. The recovery into the aft positive pressure region is significantly steeper than on airfoils with turbulence boundary layers. As for the upper surface the suction allows this steeper gradient. At the higher-lift off-design condition the pressure distributions are approximately the same as for design condition except for the development of a weak shock near the 65% chord station on the upper surface. This desired situation is achieved by providing the increased lift with the deflection of a 11% chord trailing edge flap (figure 14) rather than by increasing the angle of attack. Because of the steeper adverse gradients allowed with boundary layer suction the design Mach for this airfoil can be made

slightly greater than that for a comparable airfoil designed for a turbulent boundary layer. The suction system utilized to stabilize the laminar flow on the surfaces of the airfoil shown in figure 14. Very narrow slots are connected to a number of separate ducts in which the suction pressure can be varied individually. The spacing of the slots is closest where the boundary layer instabilities are the greatest.

Following the completion of the investigation other approaches to laminar flow control will be investigated in the modified Langley 8-Foot Transonic Pressure Tunnel using similar sized models and the contoured test section. Also, basic research at several United States aircraft companies on various methods for laminar flow control will continue. A large part of this research will be associated with airfoils incorporating hybrid boundary layer control systems, that is, systems utilizing both decreasing pressure gradients and limited suction. Much of this work will be experimental since the theoretical methods available ar_ still not definitive enough to exactly predict transition (Ref. 19). In addition to this basic work, research directed toward solutions of the practical problems associated with achieving laminar boundary layers, such as insect contamination on the leading edge, will continue. A bibliography of publications on laminar flow control work for the years 1976 to 1982 is presented in reference 22.

REFERENCES

1. Pearcey, H. H.: The Aerodynamic Design of Section Shapes for Swept Wings. Advances in Aeronautical Sciences, Vol. 3, P. 277, Pergamon Press, 1962.

2. Whitcomb, R. T.: Review of NASA Supercritical Airfoils. ICAS Paper No. 74-10, Aug. 1974.

3. Procedings of the Ninth Congress of the International Council of the Aeronautical Sciences. Haifa, Israel, Aug. 1974.

4. Bauer, F.; Garabedian, P.; Korn, D.; and Jameson, A.: Supercritical Wing Sections II. Volume 108 of Lecture Notes in Economics and Mathematical Systems, Springer-Verlag, 1975.

5. Schlichting, H.: Boundary Layer Theory, Sixth Edition, New York, McGraw Hill, 1968, Chapter 16.

6. Dryden, H. L.: Airflow in the Boundary Layer Near a Plate. NACA Rep. 562, 1936.

7. Jones, B. Melvill: Flight Experiments on the Boundary Layer. Journ. Aero. Sci., Vol. 5, No. 3, Jan. 1938, pp. 81-94.

8. Abbott, I; Von Doenhoff, A.; and Stivers, L.: Summary of Airfoil Data. NACA Rep. 824, 1945.

9. Gray, W. E.; and Fullam, P.: Comparison of Flight and Tunnel Measurements of Transition on a Highly Finished Wing (King Cobra). RAE TN Aero. 2383, 1950.

10. Holstein, H.: Messungen zur Laminarhaltung der Grenzchicht an einem Flugel. Lilenthal-Bericht S 10, 17-27, 1940.

11. Ackeret, J.; Ras M.; and Pfenninger, W.: Verhinderung des Turbulentwerdens einer Reibungsschicht durch Absaugung. Naturwissenschaften, 622. 1941.

12. Pfenninger, W.: Laminar Flow Control, Laminarization. AGARD-R-654. von Karman Institute, Belgium, 1977.

13. Gregory, N.; Stuart, J. T.; and Walker, W. S.: On the Stability of 3-Dimensional Boundary Layers with Application to the Flow Due to a Rotating Disc. Phil. Trans. Roy. Soc. London, Series A, No. 943, Vol. 248, 1955, pp. 155-199.

14. Brown, W. B.: A Stability Criterion for Three-Dimensional Laminar Boundary Layers. Boundary Layer and Flow Control, G. V. Lachmann, Editor, Vol. 2, 1961.

15. Gray, W. E.: The Effect of Wing Sweep on Laminar Flow. RAE TM Aero. 255, 1952.

16. von Doenhoff, A. E.; and Braslow, A. L.: The Effect of Distributed Surface Roughness on Laminar Flow. Boundary Layer and Flow Control, G. V. Lachmann, Editor, Vol. II, 1961, p. 657.

17. Lachmann, G. V. (Editor): Boundary Layer and Flow Control, Vol. 2, Pergamon Press, 1961.

18. Bushnell, Dennis M.; and Tuttle, Marie H.: Survey and Bibliography on Attainment of Laminar Flow Control in Air Using Pressure Gradient and Suction. Vol. I. NASA RP-1035, Sept. 1979.

19. Runyan, J. and Steers, L.: Boundary Layer Stability Analysis of a Natural Laminar Flow Glove on the F111 TACT Airplane. Viscous Flow Drag Reduction, H. G. Hough (Editor), AIAA C 1980, pp. 17-32.

20. Harvey, W. and Pride, J.: The NASA Langley Laminar Flow Control Airfoil Experiment. AIAA Paper No. 82-0567, 1982.

21. Newman, Perry A.; Anderson, E. Clay; and Peterson, John B., Jr.: Numerical Design of the Contoured Wind-Tunnel Liner for the NASA Swept-Wing LFC Test. AIAA Paper No. 82-0568, March 1982.

22. Pfenninger, W.; Reed, H. L.; and Dagenhart, J. R.: Design Considerations of Advanced Supercritical Low Drag Suction Airfoils. Viscous Flow Drag Reduction, G. R. Hough (Editor), AIAA C.1980, pp. 249-271.

23. Tuttle, M. and Maddalon, D.: Laminar Flow Control (1976-1982). NASA TM 84496, 1982.

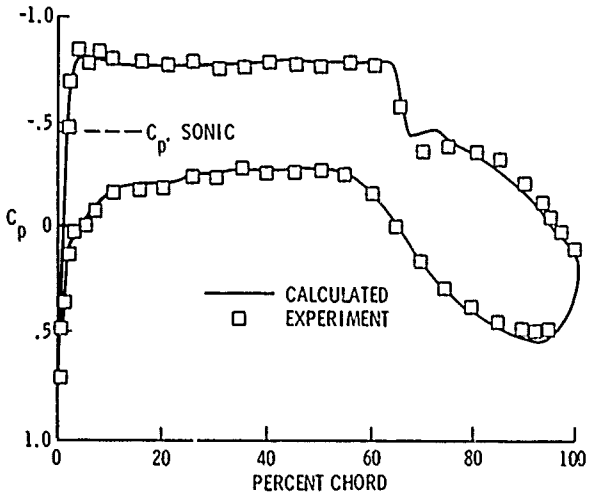

Figure 1.- Comparison of experimental and calculated pressure distributions for representative NASA supercritical airfoil.

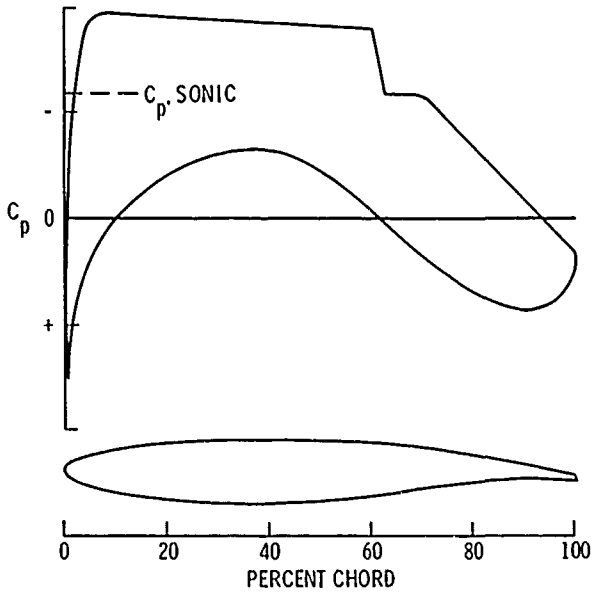

Figure 3.- Generalized pressure distribution and airfoil shape for supercritical airfoils.

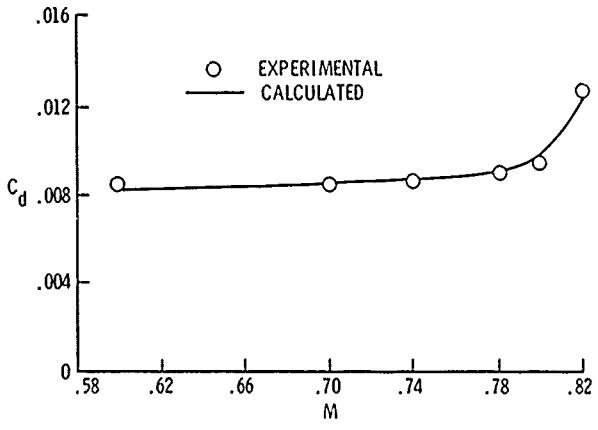

Figure 2.- Comparison of experimental and calculated drag characteristics for representative NASA supercritical airfoil at C_L = 0.50.

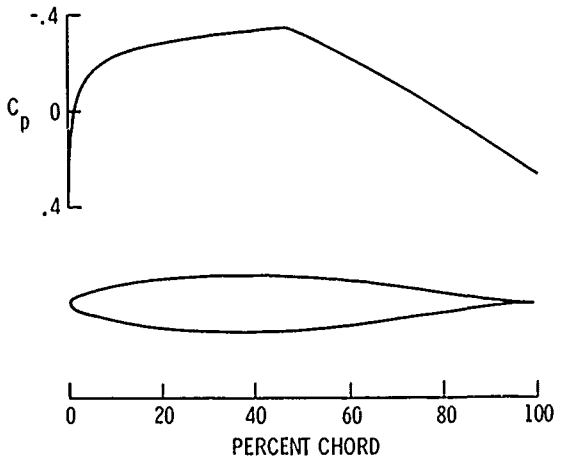

Figure 4.- Calculated pressure distribution and chordwise thickness distribution for representative NACA 65 series airfoil.

Figure 5.- U.S. Experimental X-21 airplane with suction slots to stabilize laminar boundary layer.

Figure 6.- U.S. Air Force F111 TACT with supercritical laminar flow airfoil gloves.

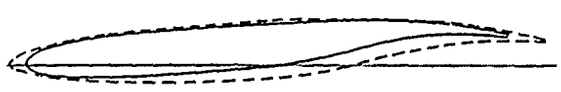

Figure 7.- Cross section of supercritical flow airfoil glove on U.S. Air Force F111 TACT airplane.

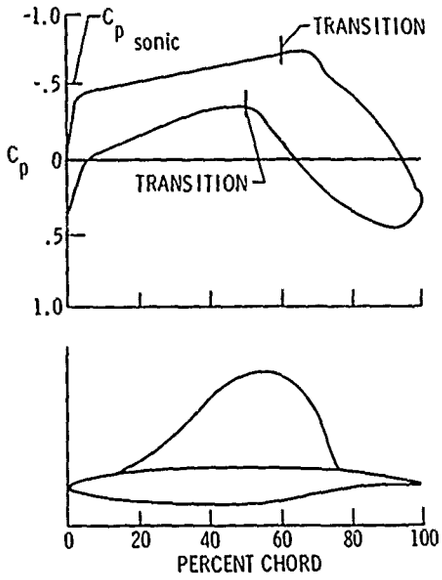

Figure 8.- Calculated pressure distribution and sonic line for supercritical laminar flow airfoil, M = 0.77, C_L = 0.50.

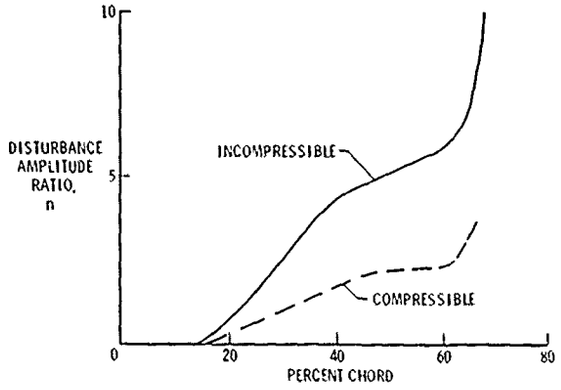

Figure 9.- Calculated growth of disturbance amplitude ratio for supercritical laminar flow airfoil, frequency - 2775 Hz

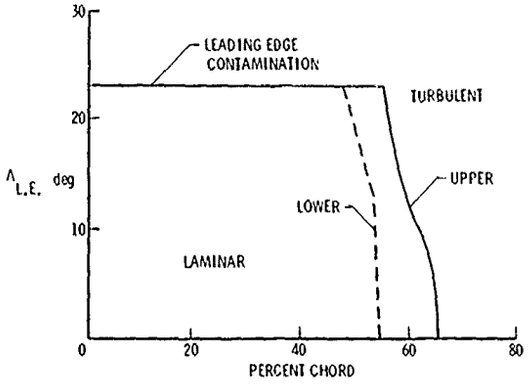

Figure 10.- Predicted location of fully turbulent flow for supercritical laminar flow airfoil, compressible stability, transition amplification factor = e12.

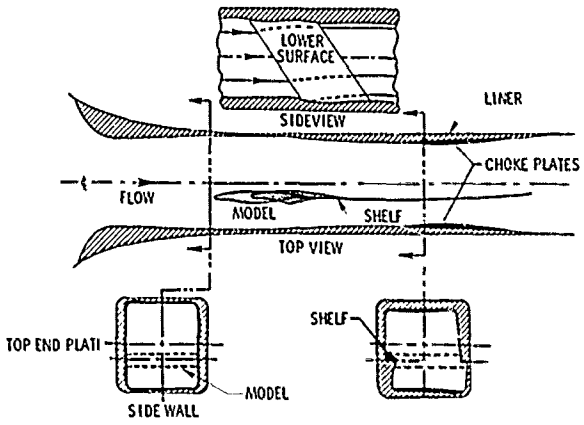

Figure 11.- Schematic drawing of contoured test section liner and airfoil model in NASA Langley 8-Foot Transonic Pressure Tunnel.

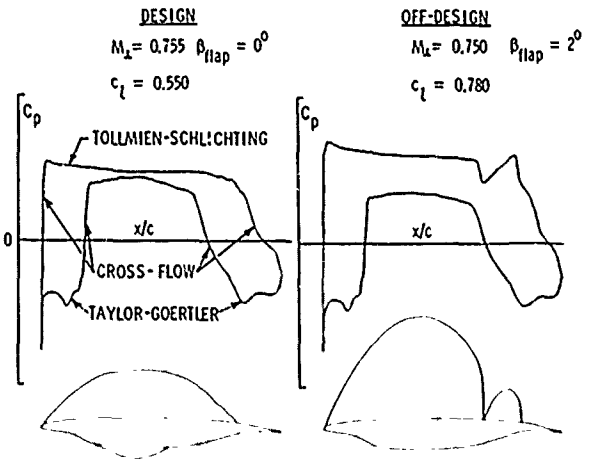

Figure 13.- Calculated pressure distributions and sonic lines for supercritical airfoil designed for laminar flow control by suction.

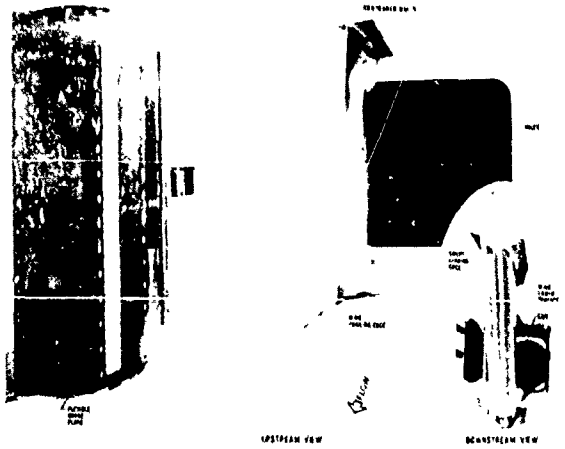

Figure 12.- Photograph of contoured test section and model.

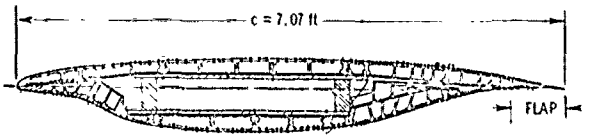

Figure 14.- Suction system for supercritical laminar flow control airfoil.

AERODYNAMIC DESIGN FOR OVERALL VEHICLE PERFORMANCE

I. H. Rettie
Unit Chief Aero Research and Development
The Boeing Commercial Airplane Company
P.O. Box 3707 M/S 79-93
Seattle, Washington, 98124 - U.S.A.

SUMMARY

The process by which a wing is designed and integrated into an aircraft configuration is examined in detail. The way in which the characteristics of the design are matched to the size of the aircraft and to the critical segments of typical missions is described with some examples. High-speed computers are used routinely today to determine optimum dimensions for the vehicle. Their growing use in Computational Fluid Dynamics for aerodynamic design prior to wind tunnel testing is examined particularly as regards the capability this offers to tailor a single component such as the wing leading edge to obtain improvements in more than one flight regime by one modification to the aircraft.

I INTRODUCTION

The integration of an airfoil shape into a three-dimensional wing matched to a specific vehicle and mission remains one of the most challenging tasks in aerodynamic design. Dr. Whitcomb in the previous lecture has described the development of airfoil theory and concepts over the past several years and I shall not repeat his excellent treatment of this topic. In this lecture I shall postulate that we have a requirement for an aircraft of specified size, range and speed for which we must provide a wing incorporating a suitable high lift system and accommodating the other major components of the aircraft such as landing gear, propulsion installation and horizontal stabilizer. Prime among the criteria for this wing design will be efficient structure, adequate fuel tankage, good overall handling qualities, low fuel comsumption and good field performance. These qualities will be traded to achieve the most attractive vehicle having regard, of course, to the paramount requirement for safety.

The process begins with a first cut at aircraft sizing, enabling the basic wing characteristics to be determined and a preliminary choice of airfoil and wing geometry to be made. Drag polars and lift curves are then predicted by empirical and theoretical methods; weights and fuel volumes are estimated; a parametric sizing study is carried out; and a specific design is determined which forms the basis for more detailed work. At this stage, a loft is prepared for wind tunnel models and the resulting test data are used as the basis for another cycle. The depth and accuracy of the sizing and design processes will be very important in reducing wind tunnel test time and hastening convergence. Also the skill and foresight of the designer will minimize interference problems in the configuration which might have to be solved in the wind tunnel before the expected performance of the model could be achieved.

This process is summarized in Figure 1 and is followed through in the discussion below.

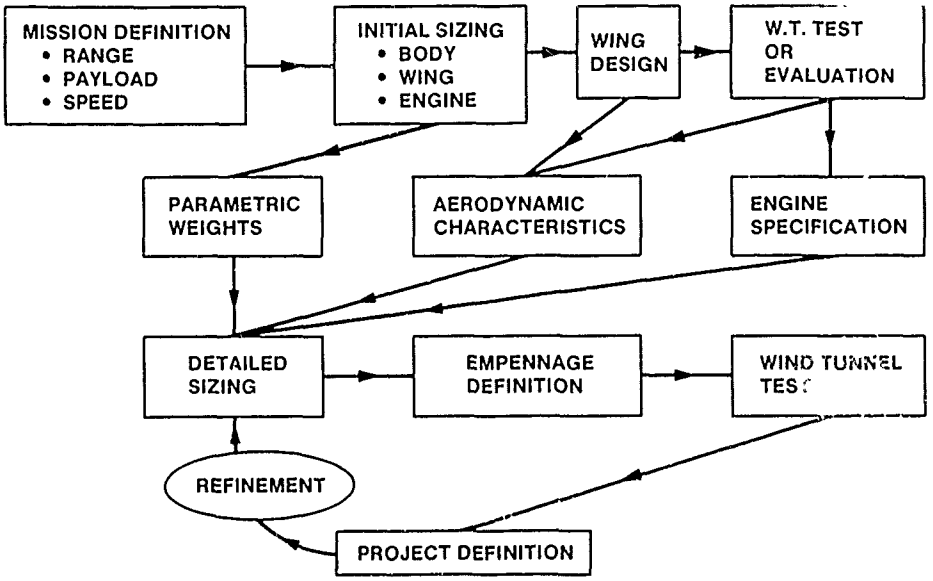

Figure 1. – Aircraft Design Cycle

II INITIAL SIZING

This will normally be accomplished either by direct reference to a previous study or by construction of simplified charts based upon existing configurations and guided by the Breguet range equation,

$$R = K \frac{V}{sfc} \frac{L}{D} \log_n \frac{W_1}{W_2}$$

$$\frac{V}{sfc} \frac{L}{D} = \text{Range Factor}$$

The factor K will depend on mission rules. Lift-to-drag ratio (L/D) can be related to span and total wetted area from the well known drag formula,

$$C_D = C_{DO} + \frac{C_L^2}{A}$$

$$A = \text{Aspect Ratio}$$

It can be verified by simple differentiation that maximum L/D occurs when the induced drag equals the zero-lift drag and the relationship shown in Figure 2 is easily derived. As a matter of fact, most current aircraft lie on a line corresponding to 85% of the theoretically achievable peformance. Such a "rule of thumb" can be used in the initial estimate of performance.

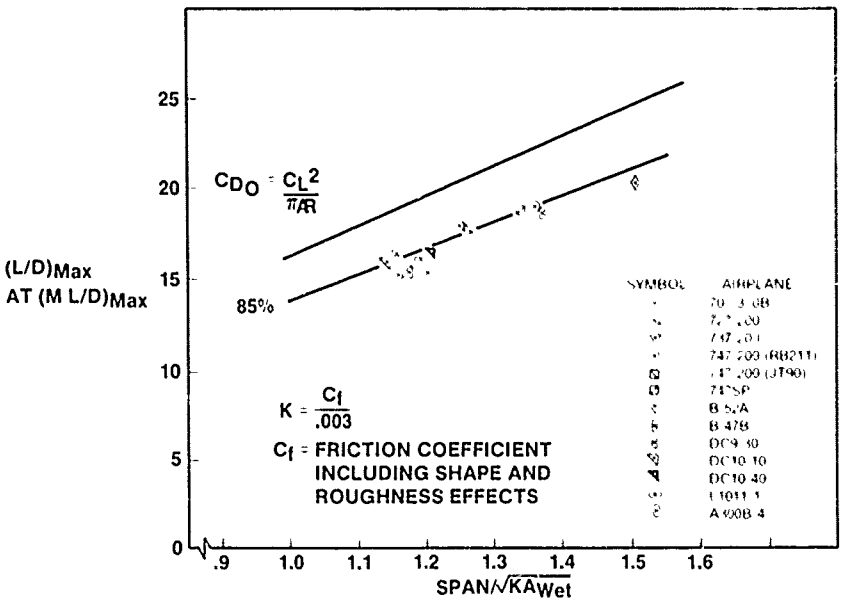

Figure 2. - Aerodynamic Efficiency at (M L/D) MAX

The first step in aircraft sizing is normally to construct a body appropriate to the desired payload and, from existing data, to determine the probable gross weight of the aircraft. An existing or proposed engine will be used and its weight and specific fuel comsumption will be known. From the Range Equation, a chart such as Figure 3 can be constructed relating Zero Fuel Weight (ZFW), Gross Weight and Range Factor. Also, from existing data, an estimate of ZFW can be made for several wing areas in the probable range. For each wing area, the total wetted area can be computed (allowing for the empennage, of course) and an L/D estimated. Combined with the known value of engine sfc, this provides a range factor for each value of ZFW. The most appropriate value of wing area must then be selected on the base of three considerations,

1) Packaging of wing structure, system and high lift devices
2) Cruise lift coefficient
3) Approach speed

The decision must be partly judgmental at this juncture. A typical high lift system (say, leading edge slats and double-slotted trailing edge flaps) will be chosen and an estimate of maximum lift capability on the approach to an airfield can be made assuming an approach speed in the range 125 kts (for a short range aircraft) to 135 kts (for a long range aircraft). From this a required wing area can be identified and an evaluation of packaging problems can be made which might result in change to the area the spanwise thickness grading or the taper ratio, for example. The groundwork done in creating

Figure 3 will then identify approximate weights for the aircraft. A check must be made of cruise lift coefficient and engine thrust match. If the lift coefficient in cruise is too high for a reasonable high speed design, the wing area must be increased accordingly. If the cruise thrust match is deficient, the engine size must be increased. At this point an initial sizing has been accomplished.

Such a procedure obviously involves a fair degree of experience and expertise. Existing data such as component weights of aircraft will be used throughout. The less experienced designer will have to repeat the cycle several times in order to obtain a balanced design. A layout drawing of the aircraft will now be created, fuel volume checked and the cycle repeated with improved weight estimating.

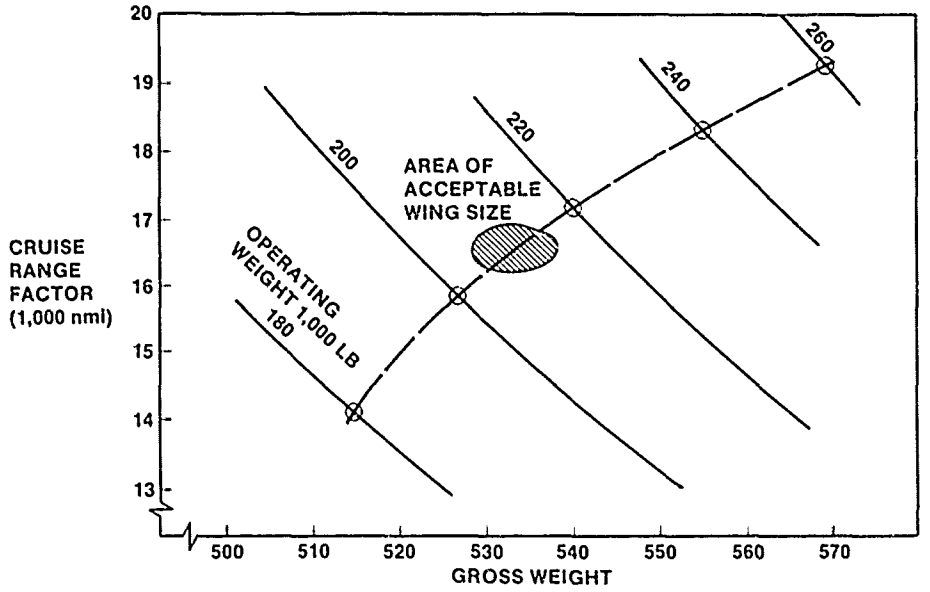

Figure 3. – Weight and Range Factor Relationships

III AIRFOIL SELECTION

Airfoil selection will be guided primarily by the requirements for cruise Mach number and fuel volume. These will enable a selection of sweep angle and maximum thickness to be made considering the outer wing as effectively a swept cylinder of unlimited span incorporating a section compatible with today's airfoil technology. The designer will choose as a basis a section defined by the available library of experimental and theoretical results. This will display the characteristics of supercritical flow, relatively aft, weak shock and aft loading described by Dr. Whitcomb. Two-dimensional computer codes are today so powerful and accurate that testing of airfoils is rarely required particularly if the modifications to an existing design are not too extensive. These modifications will be required to obtain a satisfactory supercritical pressure distribution of the type shown in Figure 4 at the thickness and lift coefficient indicated as in section II above. Care should be taken to avoid large adverse pressure gradients on the aft part of the airfoil and high maximum Mach numbers on the lower surface particularly if an underwing engine nacelle installation is intended.

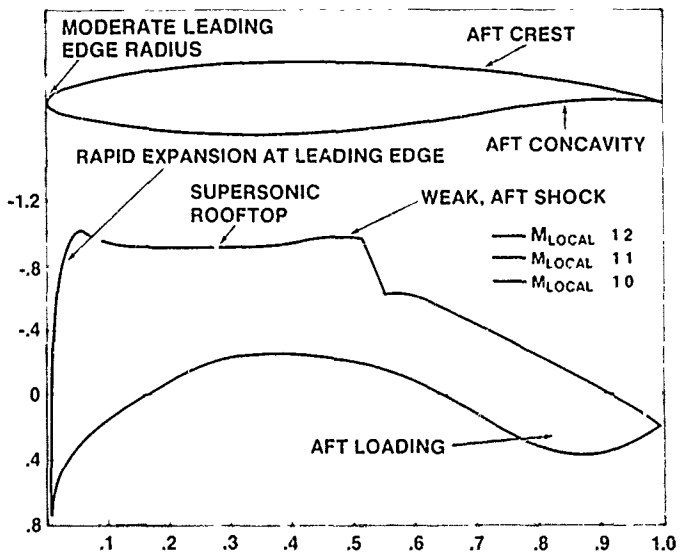

Figure 4. – Typical Supercritical Airfoil

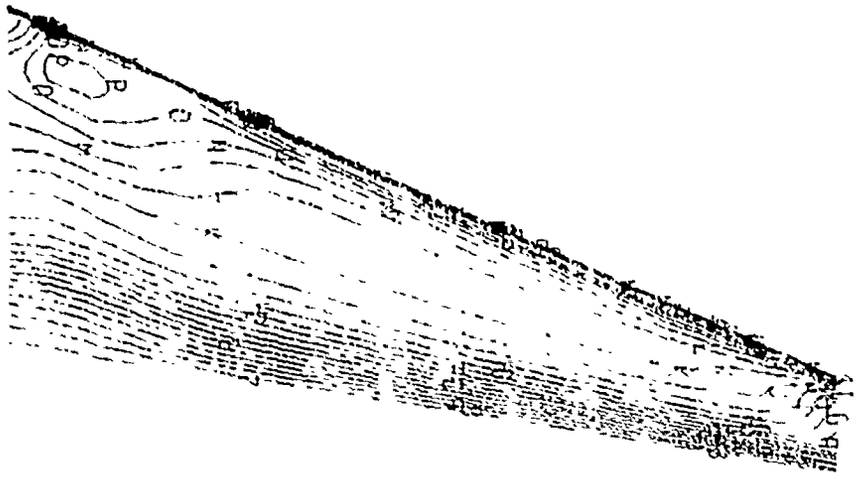

Figure 5. – Typical Wing Isobar Pattern

This basic airfoil section must then be blended across the span of the wing to obtain the chosen pressure distribution at every spanwise section in cruise. This is the condition known as "straight isobars" which will ensure a constant shock strength and position across the span. In fact, this condition is not an absolute requirement. In practice, the shock strength will decrease inboard towards the body side allowing some closure of the isobars there as shown in a typical successful isobar pattern in Figure 5. The outboard wing tends towards a peaky pressure distribution thereby gaining some additional lift. Inboard the pressure distribution is strictly roof-top. What is to be avoided is an unsweeping of the shock inboard which would result in a relatively strong shock normal to the flow fairly far aft on the body side section where the boundary layer would be prone to separation. Unsweeping of the shock can also occur near the wing tip, but here its effects are not severe. A useful way to avoid it is to round off the leading edge in plan view just inboard of the wing tip.

Some small modification to the section will be necessary to account for taper of the wing planform. The taper is usually incorporated to increase chord and thickness inboard where structural bending moments are high and requirements exist for stowage of landing gears and aircraft systems. The most significant challenge, however, is the section at the body side where the wing effectively "reflects" in the body providing conditions equivalent to those at the apex of a swept wing. As Figure 6 shows, the pressure distribution at this station is determined by systems of kinked source and vortex or source and doublet lines. A typical effect of the kink is shown in Figure 7 which is the result of a simple calculation of vortex lines. It is shown that the local lift curve slope is lower at the apex than on the outer wing. This is a result which will later be important in discussing the development of the wing pressure distribution at lift levels higher than the design point. Compared to conditions on the outer wing these kinked lines of singularities result in a pressure distribution at the apex with lower peak suctions situated farther back on the section. To correct for this we may take one or more of the following actions,

a) Increase section thickness,
b) Move section maximum thickness forward,
c) Increase section camber,
d) Move maximum camber point forward,
e) Introduce some negative camber.

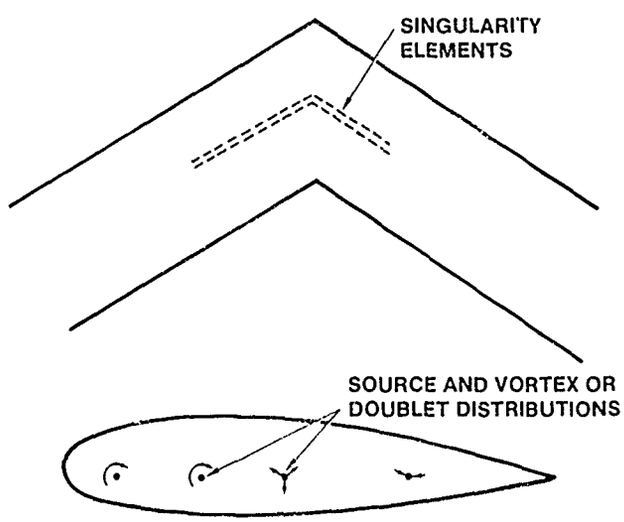

Figure 6. – Elementary Computation of Kink Effect

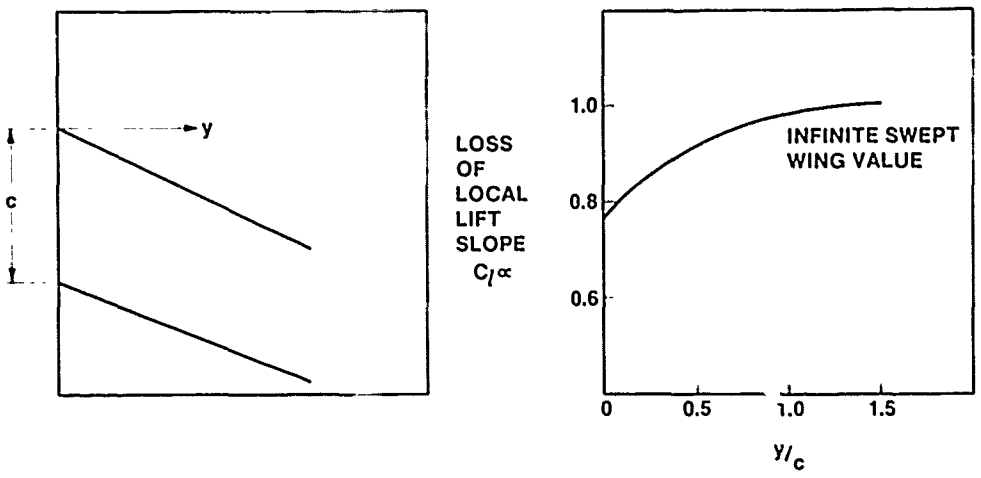

Figure 7. – Kink Effect on Lift

The determination of the root section and the blending of the section across the wing span is a problem well aided today by the three-dimensional flow calculation codes available for use with high-speed computers. At Boeing, we have developed a three-dimensional design code, A555, based upon the transonic full potential equations, which is capable of modifying the wing shape in response to a given perturbation of pressure distribution in a local or extended area. In this way, a wing loft can be created which will have good assurance of meeting its performance goals in the transonic wind tunnel.

IV DETAILED SIZING

At this stage a complete set of drag polars will be constructed representing the wing design. Today this can be done over a small range of conditions around the design point using computational methods. However, our ability to compute flows with moderately strong shock strength is limited and, depending on the resources and funding level of the project, a high speed wind tunnel test will be carried out to obtain sufficient data coverage.

Engine data, weight data and empennage sizing data are now required. These are best procured on a parametric basis, i.e. engine fuel flow and weight as a function of installed thrust, wing weight as a function of area and aircraft empty and gross weight, etc. One of the more difficult tasks is to estimate the variation of engine installation effects (weight and drag) with engine size and wing dimensions. Another important trade is the interplay between wing span loading and structure weight. Because of this, sizing studies usually follow each other at increasing levels of refinement as knowledge of the design becomes available. Generally a slightly under-elliptic span loading is chosen to reduce spanwise bending moments and structure weight.

Using the parametric data, a number of airplanes can be assembled by choosing different values of wing area and engine size. More complex, multi-dimensional studies can be accomplished but, remember, we postulated a given mission, payload and speed so that body size and wing sweep, thickness and planform were chosen a priori. A common and useful way of plotting the results of these computations is on a grid of wing loading and thrust-to-weight ratio as in Figure 8. Lines of constant fuel required can be constructed and it is apparent why the chart is sometimes referred to as a "Thumbprint". Lines of constant gross weight can be added and boundaries can be deduced corresponding for example to minimum acceptable levels of initial cruise altitude or engine out altitude.

The field performance of the aircraft must now be examined. The initial sizing of section 2 made a simple assumption of maximum lift obtainable in the approach. This is sufficient for us to be able to relate approach speed to wing area. We can then add lines of constant takeoff field length as an additional overlay on the chart of Figure 8. To avoid confusion Figure 8 does not contain all the information which will normally become available. A more complex version of the chart with color discrimination will be used during the presentation of this paper.

Several options will exist for achievement of high lift on the approach. These include (see Figure 9)

Leading edge variable camber flaps
Leading edge slats
Krueger flaps
Trailing edge flaps (single, double or triple slotted)
Trailing edge flaps (vane-main, main-vane) etc.

The ingenuity of the designer will be tested to find the most appropriate solution having regard to the field lengths envisaged, the take-off performance required and the drag and weight penalties involved.

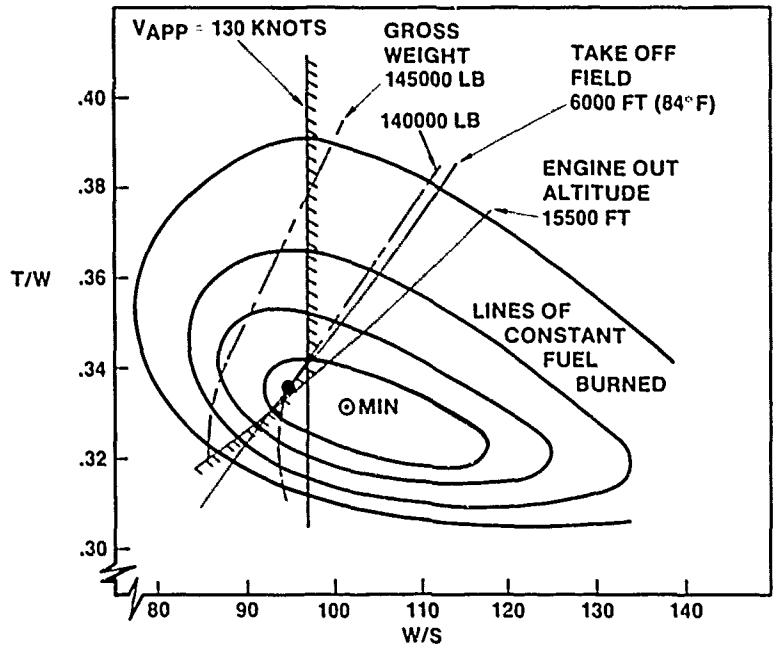

Figure 8. – Design Selection Chart

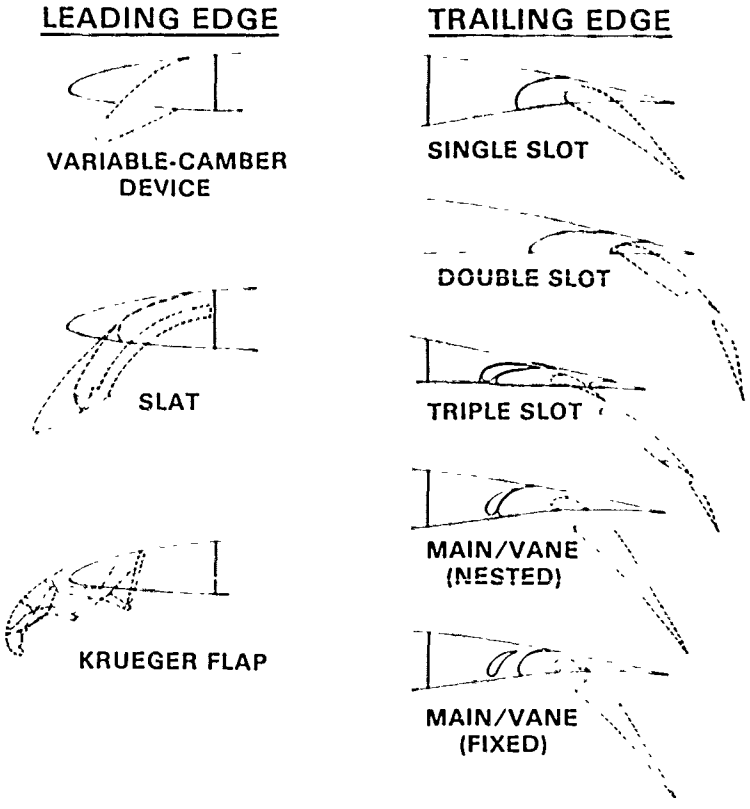

Figure 9. – High-Lift Options

It is not necessary here to discuss the options at length. However, a few comments on the trades involved will be useful. The variable camber leading edge flaps will not show as high maximum lift capabilities as the slats, but will provide better lift-to-drag ratios in climb out and may be valuable in achieving requirements for long ranges from hot, high airports. Another approach is to incorporate an intermediate extended position for the slat just before the gap is formed. This avoids the loss of energy involved in passing air from the lower to the upper surface. The vane-main or main-vane trailing edge flaps provide moderately high maximum lift and do not require large external fairings for the operating mechanisms.

At this point, a wing area and engine size can be selected which meets all mission requirements and which is close to optimum for the configuraton selected. Before a major new project is kicked off, the study just described would be repeated with different values of wing sweep and aspect ratio and probably also with different body lengths and diameter interior arrangements and passenger counts. The wing area selected will probably not be that corresponding to the "eye" of the Thumbprint. For short range designs this will probably be because of the need to keep approach speed within the desired range and to avoid heavy, drag-producing trailing edge flap systems. For long range aircraft, the need for adequate fuel volume may dictate the wing area. If the design shows a high aspect ratio wing, packaging of leading edge flap mechanisms may dictate chord lengths in the outer wing thus setting a lower limit to the wing area.

At this stage, it is instructive to look at the matching of the cruise lift coefficient with the chosen airfoil section and with the drag polar of the wing. Figure 10 shows typical sets of drag polars for low and high aspect ratio wings. At low aspect ratios (6 to 8), the cruise point of the aircraft may lie close to the maximum lift drag ratio, i.e. near the eye of the Thumbprint. The dashed line shows the effect of oversizing. In this case, there may be a small improvement in lift-to-drag ratio, offset by wing weight. The large wing, however, may be attractive on account of simplicity and its potential for growth. At high aspect ratios (9 to 11), it will be harder to achieve the lift levels and to solve the installation problems associated with the small wing area at the eye of the Thumbprint. It can be seen that the penalty for oversizing is now more severe. This puts pressure on the high lift system design and also on the airfoil selected for cruise to utilize high lift coefficients.

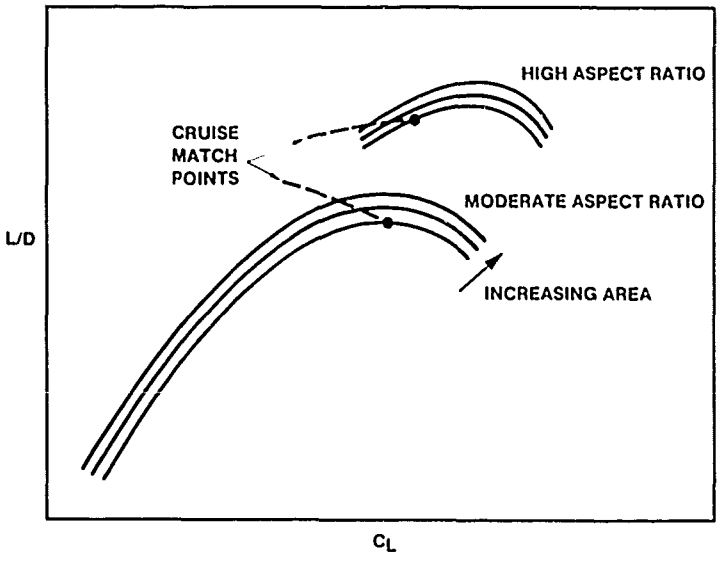

Figure 10. – Typical Wing Drag Polars

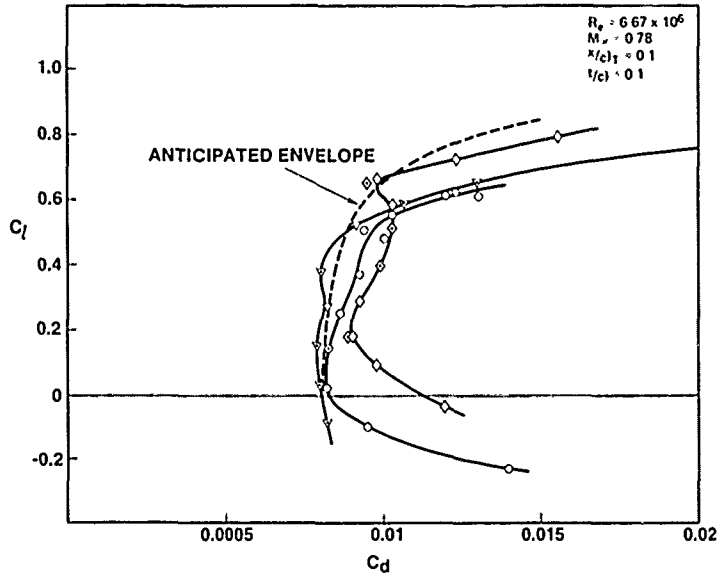

Figure 11. – Typical Section Characteristics

Figure 11 explains the options available for cruise airfoil sections. A family of section drag polars can be obtained from variation of section shape. From this an envelope of capability can be inferred in terms of section lift-to-drag ratio as a function of section lift coefficient. The higher aspect ratio wing being studied today require airfoil sections biased towards operation in cruise at relatively high lift coefficients. The current development towards more efficient structural materials such as composites will probably accentuate this trend.

V OFF-DESIGN CHARACTERISTICS

To be acceptable a design must not only achieve its performance goals, but it must also have good characteristics in upsets from normal flight conditions. We shall examine here some upset maneuvers from the cruise point. The problems at low speeds are similar, but more complex because of the various flap settings which have to be considered.

Figure 12 shows a typical variation of cruise lift coefficient with Mach number. From a given cruise point, we have to consider changes in altitude and speed. Both of these will cause lower pressures on the upper surface of the wing, strong shocks and possibly severe shock-boundary-layer interactions. The most common symptom of this is buffet, which usually arises from turbulent flow in the wing wake impinging on the horizontal stabilizer. A buffet boundary is established from wind tunnel test data, for example, by detecting the incidence at which the trailing edge pressures on the wing depart from linearity. A margin of at least 30% above the cruise lift coefficient to buffet is normally required. The margin in terms of speed is determined by calculation of upset maneuvers.

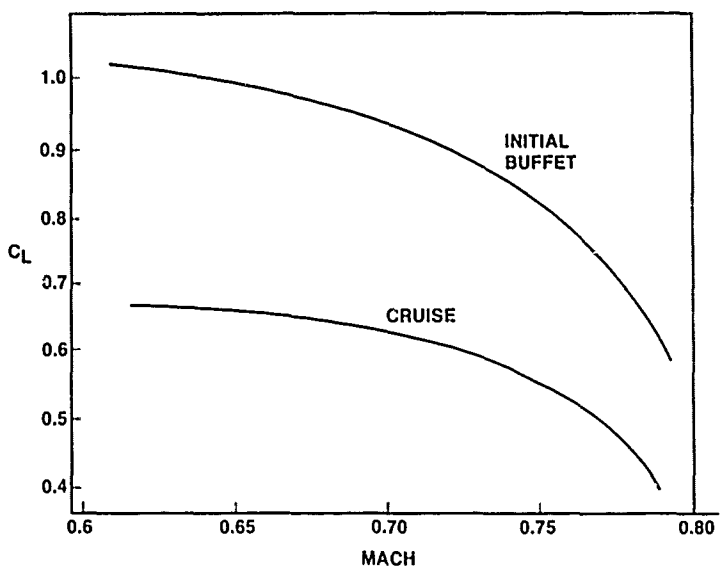

Figure 12. – Typical Buffet Margin

Another off-design requirement is for stability in terms of aircraft handling. In response to an increase in altitude, the aircraft should tend to nose-down rather than up. In response to an increase in speed the aircraft should tend to nose-up in order to increase drag and offset the speed increment. This requires an examination of how the wing flow develops beyond the design point, the way in which it breaks down and the effect of this on downwash at the horizontal stabilizer.

Consider first an increase in attitude. If the flow breaks down over the outer wing this will lead to a forward movement of the center-of-lift which is destabilizing. Futhermore, the concentration of lift over the inboard wing will increase downwash at the stabilizer and cause a part-span vortex from the wing which may interact with the tip of the stabilizer. The resultant loss of tail lift is a common cause of pitch-up.

In response to an increase in speed, a loss of lift on the outer wing is favorable since it will tend to push the aircraft into a high drag condition. On the other hand, a gradual breakdown all across the wing with an overall reduction in lift and downwash will cause the aircraft to tuck and tend to nose into a dive.

Figure 13 shows the ideal situation. The outer wing should be protected against flow breakdown in case of increased attitude. Breakdown should initially occur over as wide a section of span as practicable. On the other hand in the case of increased speed, the inboard wing should be tolerant and breakdown should initially occur outboard.

Returning to Figure 7 for a moment note the effect of sweep on the lift curve slope on the inboard wing. At high angles of sweep it is much reduced making the inboard wing tolerant of increases in altitude. If can be seen therefore that wings of high sweep will be prone to pitch-up and wings of low sweep to Mach tuck. This tendency is often exagerated by the spanwise drift in the boundary layer on the upper surface which can lead to lift loss on the outer wing.

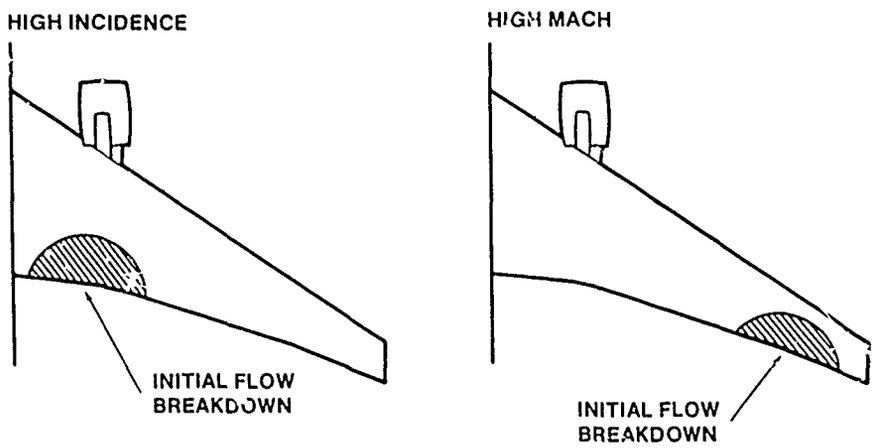

Figure 13. - Wing Design for High Speed Longitudinal Control

VI DESIGN BY CFD

Computational Fluid Dynamics (CFD) is today maturing as a powerful technology which can model reasonably complex flows and be of great value to the aerodynamic designers. Codes are available for subsonic, transonic and supersonic flows which, by means of iterative procedures, can take account of boundary layer effects. Some recent advances enable us to model shock-boundary-layer interactions at transonic speeds, at least for moderate shock strengths. Thus, off design conditions such as those described in the last section can be probed prior to wind tunnel testing and modifications made to improve the design, thereby reducing the number of cycles required in the wind tunnel.

The two most obvious advantages of CFD are therefore the ability to get closer to the optimum design and the reduction in total wind tunnel test hours. A third valuable feature is the ability to execute a design to operate well in more than one flight condition. The older approach to aerodynamic development involved a series of modifications to the design, say on a high-speed model in a transonic wind tunnel. The end result would then have to be checked on a low-speed model usually in another tunnel. Some additional cycling might then have to be accomplished. With CFD, however, the design can be developed for both conditions simultaneously with hopefully only confirmation testing in each wind tunnel.

A good example of the process is the design work done recently at Boeing on the 737 aircraft.

Figure 14 shows the 737-300 derivative aircraft where the existing JT8D engine is replaced by a high bypass ratio engine for greater fuel economy. The interaction between nacelle and wing was changed by this modification and the opportunity was taken to modify the leading edge of the wing to improve cruise Mach number. The changes to the leading edge are shown in Figure 15.

In this case, through the use of CFD, the new leading edge provided a more stable flow in high-speed upsets and, since the changed contours affected the slat design, maximum lift capabilities were improved with a useful reduction in approach speed and, consequently, improved landing field length.

Figure 14 - Boeing 737-300

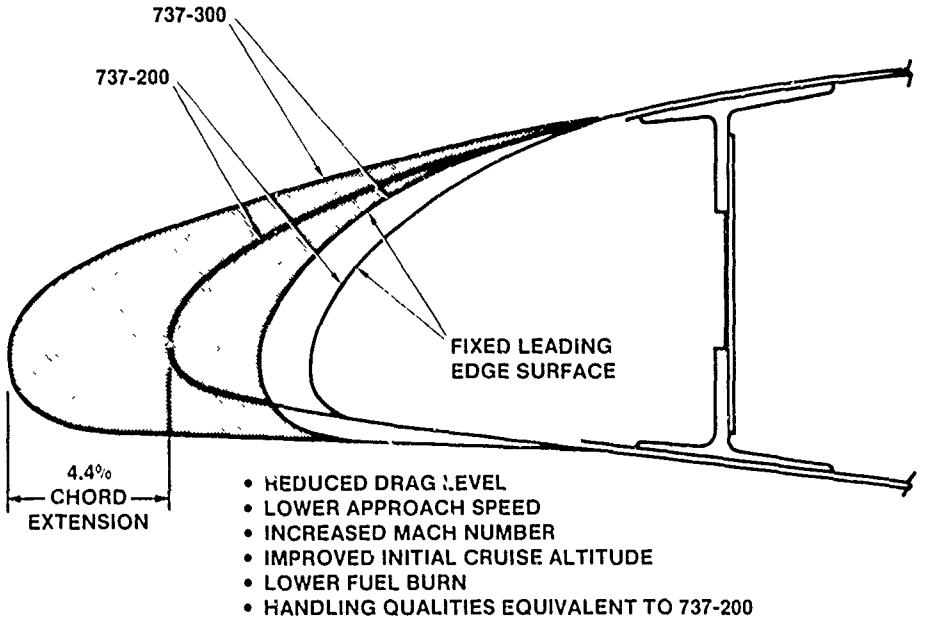

Figure 15. – Advanced Technology Slat for 737-300

VII CONCLUDING REMARKS

The process described in this paper is typical of the preliminary design activity aimed at overall integration of an air vehicle for optimum performance on a prescribed mission. The process is essentially iterative and is founded on previous experience with an available data base. Modern computing techniques enable design optimization to be accomplished with consideration of many variables and figures of merit. This means that the vehicle can be defined in great detail and that several aspects of its performance can be looked at simultaneously. Similarly, the use of computational techniques for flow analysis enable the components of the vehicle to be analyzed prior to wind tunnel tests. This is extremely valuable in accelerating the overall design cycle. It also makes it possible to foresee and avoid flow problems and adverse interference effects. Some of these will be the subject of my second talk later in the lecture series.

APPLICATION OF COMPUTATIONAL PROCEDURES IN AERODYNAMIC DESIGN

by

J.W. Slooff
National Aerospace Laboratory NLR
Amsterdam, The Netherlands

SUMMARY

Examples are discussed of the application of computational methods in aerodynamic design problems involving interference. Amongst these are: subsonic wing-body, sting support, pylon-nacelle and pylon-store interference, high-lift devices, induced drag minimization through constrained optimization in the Trefftz-plane and transonic wing-fuselage design and analysis. In addition a discussion is given on the problem of optimal usage of aerodynamic soft-ware in analyses and design, requiring an integrated systems approach.

CONTENTS

1. INTRODUCTION

In the preceeding lectures of this series [1], [2], [3], reviews were presented of the computational methods for aerodynamic analysis and design that are currently available to the aerodynamic designer. We have also seen how Computational Fluid Dynamics (CFD) is being used by the aircraft industry [4]. In this lecture a discussion will be presented on the use of CFD in aerodynamic design problems involving aerodynamic interference, as seen from the viewpoint and with the experience of the aeronautical research laboratory in its role as consultant to the aircraft industry.

First of all attention will be drawn to the point that, for optimal use of CFD, aerodynamic design procedures and the associated organizational structure of the design office must be adapted to the codes that are available and vice versa. The point will be stressed that with the continuously increasing number of codes that become available to the designer it is increasingly desirable to integrate the individual capabilities of these codes into Computer Program Systems. This, together with the increasing computer power available and increasing algorithm efficiencies, eventually, leads to the concept of Informatics Infra-Structure, [5].

The second part of this presentation will provide some examples of the use of CFD methods in a number of aerodynamic design and analysis problems involving aerodynamic interference. This survey is by no means intended to be complete and merely serves the purpose of illustrating some of the current possibilities of computational aerodynamics.

In conclusion some remarks will be presented on the key issues for future developments in computational aerodynamic analysis and design.

2. "OPTIMAL" USAGE OF AERODYNAMIC SOFTWARE: A SYSTEMS INTEGRATION PROBLEM

On the general time scale of the aeronautical sciences CFD is a young discipline. It's present state of evolution may, probably, be compared with moving from infancy into childhood, or into puberty at best. Such growing processes require adaptability from both the developing individual as well as the community. This applies also to CFD.

It is probably fair to say that the majority of CFD codes that are in use currently has never reached beyond the "pilot code" stage. That is, the codes were developed as mathematical model and algorithm demonstrators rather than as pieces of software that have to fit into a structured system for computer aided aerodynamic design. This is not necessarily to blame on the designers of these codes; in the early days of CFD code development firm ideas about software requirements, design and management probably hardly existed. Neither can it be blamed on the aerodynamic design office manager who was (and indeed could be) hardly aware of the possibilities, limitations and requirements of CFD as a (developing) tool for his

design work. Indeed, the emerging new discipline of INFORMATICS is required for optimal integration of the existing and evolving capabilities of CFD into structured systems for computer aided aerodynamic design. It is the responsability of both the informatics specialist and the aerodynamic designer that the contents and structure of the aerodynamics information system and the tasks and organizational structure of the aerodynamic design office are tuned to each other.

As an introduction to a sketch of what an information system for computer aided aerodynamic design could look like let us consider the design process depicted in figure 1. The process is thought to be representative of a situation in which methods for both aerodynamic design and analysis are available. Note the man-in-the-loop at decision points and the man(men)-beside-the-loop executing the (sub-)process(es).

Figure 2 shows a possible architecture (Loeve, [5]) for the information system that is necessary to execute the design process of figure 1 and to control the flow of information. An information system with this architecture is (partly) operational and being further developed at NLR. Key feature of the system is the NLR Engineering Data Interactive Presentation and Analysis System (EDIPAS, [6]) and in particular the Control Data IMF data base management part of it. Communication between the various process (sub-) systems is in the form of (data base) files whenever possible. In this way existing (and other) software can be coupled with the system, and through this, with other codes, with relatively little effort. If coupling of available codes on file basis is not possible or not desirable, (e.g. because the mathematical and/or numerical modeling require coupling on algorithm basis) the codes are integrated into bigger units prior to attachement to the overall information system.

It must be remarked that a significant number of the examples of application of computational aerodynamic software to be discussed in the following sections was produced before the system of figure 2 was in operation. This, ofcourse, does not affect the importance of the result in the aerodynamic sense. It means, however, that nowadays, the same result could be obtained at a fraction of the time and cost of the original effort.
It is also noted that some of the results were obtained with "isolated" codes while others were produced with integrated code systems. The latter will be described to some extent whenever this is relevant.

3. EXAMPLES OF APPLICATION OF COMPUTATIONAL METHODS IN AERODYNAMIC ANALYSIS AND DESIGN

3.1. Panel Methods; Work Horse for Computational Assessment of Aerodynamic Interference Effects.

During the past decade and a half panel methods have been in use almost everywhere in the aerospace community and an enormous amount of experience has been collected through applications to all kinds of subsonic (and supersonic) interference problems. The literature on the subject is abundant and we will not attempt to cover it here. Instead, we will discuss some of the, hopefully, more interesting applications from the immediate vicinity of the present author. Entry to the literature may, e.g., be obtained through references [7] - [9].

Computational assessment of wing-fuselage interference has probably been one of the major motives for panel method development. The "passive" assessment of the effect of the fuselage on, e.g., the wing pressure distribution is, ofcourse, one possibility. Another approach to the problem is the shaping of the wing-fuselage fairing with the objective of influencing the wing pressure distribution in a favourable sense. Conversely, the fairing shape can be used to influence the wing section geometry that would be required for a given wing pressure distribution.
Figure 3 provides an example of the utilization of the NLR Panel Method, [10], for the purpose just described. As illustrated by the figure an area-ruled fairing can be used to reduce the super-velocity over a significant part of the inner wing. For more details on this kind of application, see Voogt and Van der Kolk, [11]. We will return to the subject of (transonic) wing-fuselage design and analysis in section 3.4.

A second subject where panel methods have, gratefully, been used is interference involving engine nacelles. A simple example, taken from [8], concerning rear-mounted nacelle-wing interference, is presented in figure 4. Shown is the effect of the presence of the nacelle (modeled as a coarsely paneled ring-wing) on the spanwise distribution of the wing lift and pitching moment of a small commercial transport at cruise condition. Note that in spite of the extremely simple modeling, involving a "dummy" plane of symmetry at the side of the body, the agreement between calculated and measured effect of the nacelle is quite good. The discrepancy in the level of the section pitching moment on the inner wing is caused by the fact that the fuselage has not been modeled in these calculations.
Figure 5 shows the result of a similar study for a take-off configuration with deflected flap, [12]. The particular effect studied in this case is that of engine mass flow ratio on the wing lift. As indicated by the figure the effect is appreciable.
A final example involving rear-mounted nacelle interference is depicted in figure 6,[13a]. Shown are the results of adverse interference minimization studies for a high-bypass ratio nacelle + stubwing. The example illustrates the usefullness of the panel method in (re)shaping nacelle, stubwing and rear fuselage with the objective of minimizing supervelocities (and, through that, of avoiding shock waves) in the passage between nacelle and fuselage. As indicated by figure 6c the predicted results were fully confirmed by wind-tunnel tests.

An example of an application to the underwing pylon/nacelle/jet interference problem,[13b] is covered by figure 7. In the particular case considered the greater part of the calculations was done for the configuration labeled "FLIGHT" in figure 7a. Wind-tunnel test were performed on a half model configuration of the type depicted in the lower picture of figure 7a. Note the faired inlet and the strut/support containing the compressed air supply for blown jet simulation. Figures 7b-d present comparisons of calculated and measured pressure distributions on the wing lower surface, pylon and nacelle cowl. Note that the calculated results were obtained for the "FLIGHT" configuration.
It can be noticed, that although the agreement between theory and experiment is generally fair, a distinct local discrepancy can be noticed on the outboard facing side of the pylon and in the adjacent wing lower surface pressure distribution. The reason for this could not be traced, although it could be explained partly, but by no means completely, by the effect of the strut and inlet fairing in the experiment and by

improper modeling of compressibility effects in the calculations.

A further subject for which the application of panels methods can be very useful is windtunnel wall and model support interference. Figure 8 presents an example taken from a study, [14], on the interference caused by various types of sting support. A comparison of calculated and measured interference, in terms of errors in lift and pitching moment is given in figure 8b. Note that the experimental results were obtained with and without dummy stings while the model was supported by a third, vertical strut (Fig. 8c).

As a final example we consider airplane-store interference for a fighter-type configuration, [15]. In the particular example (Fig. 9) the panel method was used to calculated the part due to interference of the forces and moments on the store for several positions and attitudes below the wing. These data, together with windtunnel data for the isolated store were fed into a store trajectory prediction program. Figure 9b presents a comparison of the predicted store depth and attitude, as a function of time-since-release, with flight test data. Applications such as this serve to improve safety in weapon certification.

3.2. Where Interference is Crucially Important: Slat and Flap Design

As described so illustratively by A.M.O. Smith in his famous lecture on high-lift aerodynamics, [16], aerodynamic interference is probably nowhere as important as in the design of high-lift devices. In the following we will consider an example of the application of computational methods to the problem of leading edge slat design for low speed. The particular application formed part of a program of validation of the NLR MAD computer program system [17], for the aerodynamic design of multi-element airfoil . The methodology underlying the MAD system was briefly discussed in [2].

The design problem is illustrated by figure 10. The objective [18] was to (re) design the slat of a conventional airfoil-slat configuration with the purpose of reducing the drag, without affecting the maximum lift, at conditions representative for take-off. The design parameters in such a problem are the shape of the intersection separating the slat and the main airfoil (for a given slat chord), gap and overlap of the slat and the incidence of both slat and main airfoil.

Starting point for the design study was the conventional slat configuration of figure 10a. Figure 10b shows measured and potential flow pressure distributions for this configuration. Note that the upper surface boundary layer on the main airfoil separates at about 70 % chord.

The potential flow pressure distribution, generated by the analysis mode of the MAD System, was used as a basis for specifying a new "target" pressure distribution. Note that this potential flow pressure distribution was obtained for a slat geometry incorporating a simulation of the separation bubble on the lower surface. The shape of this bubble had been determined through an earlier mixed analysis/design mode application of the MAD System with the experimental "bubble" pressure as input. The incidence for the calculation was chosen to lead to, approximately, the same suction peaks as in the experiment. We may call this potential flow pressure distribution on "equivalent inviscid" pressure distribution.

With the objective of reducing the drag, without effecting maximum lift, the equivalent inviscid pressure distribution was modified in the sense indicated in figure 10b, implying

I - reduced suction peak level of the main airfoil
II - more rapid expansion of the flow around the leading edge of the main airfoil, allowing
III- a higher "dumping" velocity at the slat trailing edge
IV - high "bubble pressure" level on the slat lower surface. (Whether this will be realized in the real flow is, ofcourse, highly questionable, since the real level will be determined by viscous rather than potential flow phenomena.

The potential flow pressure distribution, modified as described above was used as input for the MAD System. In the design calculations only the intersection between slat and main airfoil, the slat angle, gap and overlap and the incidence were allowed to vary. In addition a lower bound was imposed on the slat trailing edge angle. Figure 10c presents a comparison of "target" and obtained pressure distributions as a function of arc length. The resulting slat geometry is given in figure 10d.

Experimental results for the new slat are present in figure 11, in comparison with those of the conventional (starting) configuration. Pressure distributions at a condition representative for take-off are compared in figure 11a. It can be noticed that the objectives I-III have, indeed, been realized. Not surprisingly, a higher level of the slat lower surface "bubble pressure" has not been achieved. Note further that there is a significant rearward shift of the separation point on the upper surface of the main airfoil.

The consequences of the new slat shape in terms of lift and drag are evident from figure 11b. It can be observed that the design objective of reduced drag at conditions ($0.9\ C_{\ell_{max}}$) representative for take-off, without effecting $C_{\ell_{max}}$, has been achieved indeed.

The example discussed above is somewhat academic in the sense that in real design practice trailing-edge flap deflection would be an additional design variable to consider. Nevertheless, in the author's opinion, it illustrates that potential flow inverse methods can even be helpful in situations with complex viscous interference.

3.3. Configuration Induced Drag Minimization Utilizing Constrained Optimization Techniques in the Trefftz-plane

It has been (and perhaps still generally is) common practice in aircraft analysis and design to decompose the airplane drag in components like zero lift drag, lift dependent drag and compressibility drag. While this has been a useful, and perhaps the only viable way for drag breakdown in a situation that only the total drag could be determined from windtunnel tests, computational fluid dynamics have created possibilities for drag breakdown and analysis that are based on physical rather than phenomenological principles (see also section 3.4). In such a breakdown it is convenient to distinguish between viscous (boundary layer) drag, induced (or vortex) drag and wave drag. This latter drag breakdown offers a framework that may be used for drag minimization studies. It places induced drag minimization in a useful perspective.

Induced drag is an inevitable phenomenon associated with lifting configurations of finite dimension .

However, the precise level of the induced drag is governed by interference between the lifting parts of the configuration.

According to Munk's theorem[19], the induced drag of an aircraft configuration is only a function of it's spanwise loading and independent of it's chordwise loading. This allows the induced drag to be determined from the downwash (and sidewash) in the so-called Trefftz-plane, infinitely far downstream of the configuration. In the Trefftz-plane the downwash is a function of the spanwise loading only.

At NLR a computer program has been developed for determining the optimal spanwise loadings of the various interfering lifting parts of multiple, non-planar configurations, [20]. The program utilizes constrained optimization techniques and panel method "technology" in the Trefftz-plane. It is capable of dealing with pitching moment (trimmed situation) and bending moment constraints.

The input required by the program is summarized in figure 12. It comprises general geometric configuration data, position of the center of gravity, required (trimmed) lift coefficient, wing, body and tail pitching moment and drag data.

A typical example of the capabilities of the program is presented in figure 13. Figure 13a illustrates the type of configuration considered, with various vertical positions of the horizontal tail.

Optimum spanwise load distributions for a high and a low positioned horizontal tail for a given wing-body pitching moment and 30 % MAC c.g. location are compared in figure 13b. It illustrates the point that optimal wing design cannot be achieved without taking account of the tail configuration.

Minimum induced drag span loads for two different levels of wing-body pitching moment for a low tail configuration are compared in figure 13c. Figs 13d en e illustrate the point that the minimum trimmed induced drag of high tail configurations is much more sensitive to variations in wing-body pitching moment and c.g. positions than that of low tail configurations. This, however, does not necessarily imply that a low tail configuration is to be preferred; there may be other design criteria that dominate this choice.

In conclusion, figure 13f presents the optimum span load for a configuration which utilizes "active" loading of nacelle/pylon and flap rail fairings. In the particular example a 1.5 % reduction of the minimum trimmed induced drag can be realized by "active" rather than "passive" (streamline) shaping of pylons and flap rail fairings.

Programs such as just described can be very helpful in the conceptual and preliminary design of aircraft. They are also used for creating the starting point for the specification of "target" pressure distributions in the detailed aerodynamic design of wings by means of inverse methods of the type described in [2].

3.4. Transonic Wing Design and Analysis

In this section some experiences will be communicated in the use of methods and program systems for sub/transonic wing design and analyses for transport type configurations. In terms of the scheme of figure 1 we will discuss examples of application of the processes labelled I and II.

3.4.1. Design of transonic wings by means of 2D transonic and 2D subsonic theory

As may have become clear from the preceeding lectures in this series, [2] in particular, "design" methods for three-dimensional transonic flow are not (yet) generally available. At NLR as well as, presumably, in many other places, we have learned to live with this situation. With "design" (inverse) methods available for two-dimensional transonic and three-dimensional subsonic flow, the following procedure was found to be effective, [21].

The first step is the design (or selection) of one, or several, basic airfoils, for selected span stations, by means of transonic theory for two-dimensional flow. Originally the hodograph method of Boerstoel[22] was used for this purpose. More recently, the more flexible constrained inverse method of [23], (see also section 3.4 of [2]), has become available. The basic airfoils may also be selected from a suitable transonic airfoil data base, if available.

When the basic 2D airfoils have been obtained the next step is to construct an "equivalent subsonic target pressure distribution" (ESPD) for the 3D wing. For this purpose analyses calculations are performed for each of the basic 2D airfoils at their transonic (or subsonic) "design" conditions*) by means of a subsonic panel method, [10]. While these equivalent subsonic pressure distributions are of no physical significance they may serve to construct a target pressure distribution for 3D subsonic inverse calculations (Fig. 14). For this purpose the 2D equivalent subsonic pressure distributions for the selected span stations are transformed into pressure distributions for the 3D wing by means of an extended form, due to Lock[24], of simple sweep theory. Construction of the "target ESPD" for the 3D wing is completed by spanwise interpolation and extension towards the root and tip. In this process the lower surface pressure level is adjusted so as to conform to the required spanwise load distribution. Further details of the process may be found in [21] and [11].

With the (equivalent subsonic) target pressure distribution established, the final step is to find the sectional geometry of the wing that will generate this pressure distribution in the presence of the fuselage (and, if necessary, of other parts of fixed geometry). This is accomplished by means of the subsonic inverse method, with geometry constraints, of [25], (see also section 3.4 of [2]).

While a situation of having to design for transonic flow by means of subsonic methods is far from ideal, the procedure described above has nevertheless proved successful. An example, in the form of a comparison between "expected"**)(inviscid, shock-free) and measured pressure distributions for an aspect ratio 11 wing is given in figure 14. Further examples may be found in [21], [11], [26].

It is worth mentioning that efforts are underway to extend the capabilities of the constrained

---

*) The "design" condition, in this context, is not necessarily a transonic "shock-free" condition. Here it is, rather, the (local) condition at which the airfoil is required to operate at the specific span station of the 3D wing. Off-design considerations may require that this local condition represents a C_ℓ and Mach number below that for "optimal" supercritical (shock-free) flow of the basic airfoil section.

**) The "expected" pressure distribution was obtained by correcting the equivalent subsonic pressure distribution of the 3D wing for the difference between the exact transonic and equivalent subsonic pressure distributions of the basic 2D airfoils.

residual-correction type of inverse method of [25] to transonic flow. It is expected that, similar as in 2D, [23], (see also section 3.4 of [2]), this can be realized by replacing the subsonic panel method [10], which forms part of the system, by a 3D transonic code and by adding a supersonic (local) geometry correction module.

3.4.2. Wing-Fuselage transonic aerodynamic analysis

A typical example of the integrated use of aerodynamic software, in the sense of the discussion of section 2, is formed by the NLR XFL022 (program) SYSTEM for the aerodynamic analysis of wing-fuselage configurations in transonic flow, [27]. The system comprises an extended version of the Jameson-Caughey FL022 wing alone code, [28], the NLR subsonic PANEL METHOD, [10] and the 3D turbulent boundary layer code BOLA, [29], as well as several auxiliary modules (Fig. 16). The modifications and extensions to the FL022 code include a modified boundary condition in the plane (of symmetry) at the wing root, allowing the modeling of wing-fuselage interference through the prescription of a non-zero spanwise velocity component. The magnitude of the latter is obtained from a panel method calculation for the complete configuration.

The XFL022 SYSTEM is used to check the design of wings obtained through the "equivalent subsonic" approach described in section 3.4.1, and for estimating the transonic off-design characteristics of these (and other) wings. For such purposes it is necessary to perform computations for 20 to 25 angle-of-attack Mach-number combinations within, preferably, one, or at most two successive overnight batch mode runs (pre- and post-processing being executed interactively). In the absence of access to a class VI computer such as the CRAY 1 or Cyber 205 this requires a fast transonic code.
Computational speed was the main motive for choosing the (X)FL022 code. In it's present NLR version it is almost 3.5 times faster than FL027 and almost 10 times faster than the more sophisticated FL028 and FL030 finite volume codes. The system has, nevertheless, been constructed such that the XFL022 code can be replaced by a faster and/or geometrically more versatile one when it becomes available.

Some of the possibilities of the system are illustrated by figs 17, 18, 19. Figure 17 presents examples of standard graphics output; pressure distributions and isobar patterns, boundary layer surface streamlines and momentum thickness. Figure 18 illustrates the improved pressure prediction capability of the system relative to the original FL022. The improvement is particularly noticeable near the wing root.

The drag prediction capability of the system is illustrated by figure 19. Figure 19a presents a comparison of calculated and measured drag polars for a narrow-body type subsonic transport at a sub-critical and a supercritical Mach number. The drag at constant lift is presented in figure 19b. Further examples may be found in [27].

Examples such as those given above serve to illustrate the point that the capabilities of a suitably integrated aerodynamic software system far exceed the sum of the capabilities of the individual components. As far as the XFL022 SYSTEM is concerned this is particularly true for the drag prediction capabilities. The diagnostic means provided by the latter have proven to be extremely valuable in drag minimization studies.

4. CONCLUDING REMARKS

In the preceeding sections examples have been discussed of the application of computational methods in aerodynamic design and analyses. Also some general remarks have been given with respect to requirements for "optimal" usage of computational aerodynamic software in the research/design support environment of the aeronautical research laboratory in it's role as consultant to the aircraft industry.

While the examples show that much has been achieved in the field of prediction of aerodynamic interference effects and the computational design of configurations with the allowance for or the active utilization of interference, there remains far more to be done. This is particularly true for interference dominated by viscous effects, and, perhaps to a lesser extent, for transonic interference involving complicated geometrical configurations. With the former, even the modelling of the physics (turbulence!) still poses formidable problems. For the latter, spatial grid generation is, ofcourse, the pacing item. Depending, to some extent, on the computer power available, the development of "robust" fast solvers is another subject of importance.

Regardless of the "progress-in-depth" in computational fluid dynamics, "progress-in-breadth", in the form of integrated software systems, is equally desirable in order to be able to make optimal usage of developments in CFD. The same is true, ofcourse, for the other disciplines in aircraft design, not to mention the "ultimate" integration problem of multi-disciplinary design!.

5. REFERENCES

1. Jameson, A.; "Review: Inviscid Computational Methods", Lecture presented at AGARD-FDP-VKI Special course on "Subsonic/Transonic Aerodynamic Interference for Aircraft", May 1983.
2. Slooff, J.W.; "Computational Methods for Subsonic and Transonic Aerodynamic Design", idem.
3. Yoshihara, H; "Review: Viscous Interactions", idem.
4. Rettie, I; "Aerodynamic Design for Overall Vehicle Performance", idem.
5. Loeve, W.; "An Infrastructure for Computational Fluid Dynamics to Serve Computer Aided Design", Invited paper (in Dutch) presented at symposium for users of finite element methods, Delft University of Technology, Sept. 3, 1982 (NLR MP 82046).
6. Heerema, F.J., and Van Hedel, H.; "An Engineering Data Management System for Computer Aided Design", NLR MP 82050 U, 1982.
7. Rubbert, P.E., and Saaris, G.R.; "Review and Evaluation of a Three-Dimensional Lifting Potential Flow Analysis Method for Arbitrary Configurations", AIAA Paper No. 73-188, Jan. 1972.
8. Labrujere, Th. E., and Sytsma, H.A.; "Aerodynamic Interference Between Aircraft Components: Illustration of the Possibility for Prediction", ICAS Paper, 1972, also NLR MP 72020 U.
9. Tinoco, E.N., and Rubbert, P.E.; "Panel Methods: PAN AIR", Paper presented at International Center for Transportation Studies (ICTS) Short Course on "Computational Methods in Potential Aerodynamics", Amalfi, Italy, May/June 1982.
10. Labrujere, Th. E., Loeve, W., and Slooff, J.W.; "An Approximate Method for the Calculation of the Pressure Distribution on Wing-Body Combinations at Sub-critical Speeds", AGARD CP. No. 71, Paper 11, 1970.

11. Voogt, N., and van der Kolk, J. Th.; "Design Study for the Inner Wing of a Transonic Wing-Body Combination of Aspect Ratio 8", AGARD CP. No. 285, Paper 25, 1980.
12. Joosen, C.J.J., and Sytsma, H.A.; "Calculation of Some Aerodynamic Aspects of Rear-Mounted High-By-Pass-Ratio Engines", Unpublished NLR Report, 1977.
13a. Voogt, N., van Hengst, J., van der Kolk, J.Th; "Aerodynamic Aspects of a High By-pass Ratio Engine Installation on a Fuselage Afterbody", AGARD CP. No. 301, paper 29, 1981
13b. Sytsma, H.A.; Unpublished NLR Report.
14. Rip, C.H.; NLR unpublished work
15. Sytsma, H.A., Slooff, J.W., Janssen, Th., and Nijhuis, G.H.; "Theoretical Determination of Aerodynamic Aircraft-Store Interference for a Fighter Aircraft with Underwing Store", NLR TR 77026 U, 1977.
16. Smith, A.M.O.; "High-Lift Aerodynamics"; J. Aircraft, Vol. 12, No. 6, June 1975.
17. Labrujere, Th. E.; NLR Report to be published.
18. Van Egmond, J.E., v.d. Berg, B., and Labrujere, Th. E.; NLR Report to be published.
19. Munk, M.M.; "The Minimum Induced drag of Airfoils", NACA Report 121, 1921.
20. van den Dam, R.F.; "SAMID, An Interactive System for the Analysis and Constrained Minimization of Induced Drag of Aircraft Configuration", AIAA Paper 83-0095, Jan. 1983.
21. Slooff, J.W., and Voogt, N.; "Aerodynamic Design of Thick, Supercritical Wings through the Concept of Equivalent Subsonic Pressure Distribution", NLR MP 78001 U, June 1978.
22. Boerstoel, J.W.; "Design and Analyses of a Hodograph Method for the Calculation of Supercritical Shock-Free Aerofoils", NLR TR 77046 U, 1977.
23. Fray, J.M.J., Slooff, J.W., Boerstoel, J.W., and Kassies, A.; "Design of Transonic Airfoils With Given Pressure Distribution, Subject to Geometric Constraints", NLR Report, to be published.
24. Lock, R.C.; "An Equivalence Law Relating Three- and Two-dimensional Pressure Distributions", ARC R&M 3346, 1962.
25. Fray, J.M.J., and Slooff, J.W., "A Constrained Inverse Method for the Aerodynamic Design of Thick Wings with Given Pressure Distribution in Subsonic Flow", AGARD CP. No. 285, paper 16, 1980.
26. Voogt, N., and Slooff, J.W., "Advanced Aerodynamic Wing Design for Commercial Transports-Review of a Technology Program in the Netherlands", ICAS Paper 82-5.6.1, 1982.
27. van der Vooren, J., van der Kolk, J. Th., and Slooff, J.W.; "A System for the Numerical Simulation of Sub- and Transonic Viscous Attached Flows Around Wing-Body Configurations", AIAA Paper 81-0[illegible], 1981.
28. Jameson, A., and Caughey, D.A.; "Numerical Calculation of Transonic Flow Past a Swept Wing", ERDA Report C00-3077-140, Courant Institute of Mathematical Sciences, N.Y. University, 1977.
29. Lindhout, J.P.F., Moek, G., de Boer, E. and van den Berg, B; "A method for the Calculation of 3-D Boundary Layers on Practical Wing Configurations", Transaction of the ASME, March 1981. Also NLR MP 79003 U, 1979.

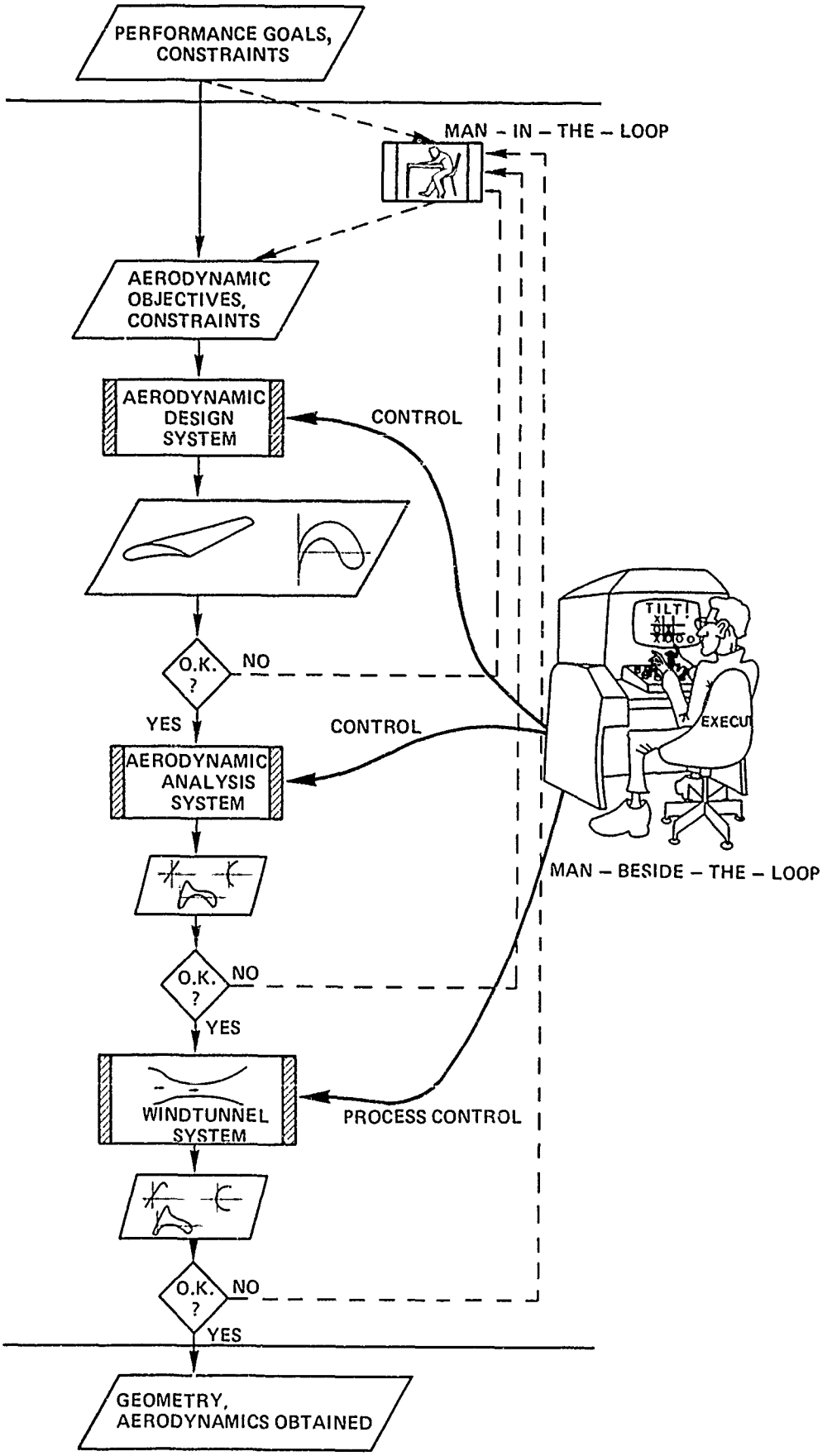

Fig. 1 Typical flow chart for aerodynamic design process

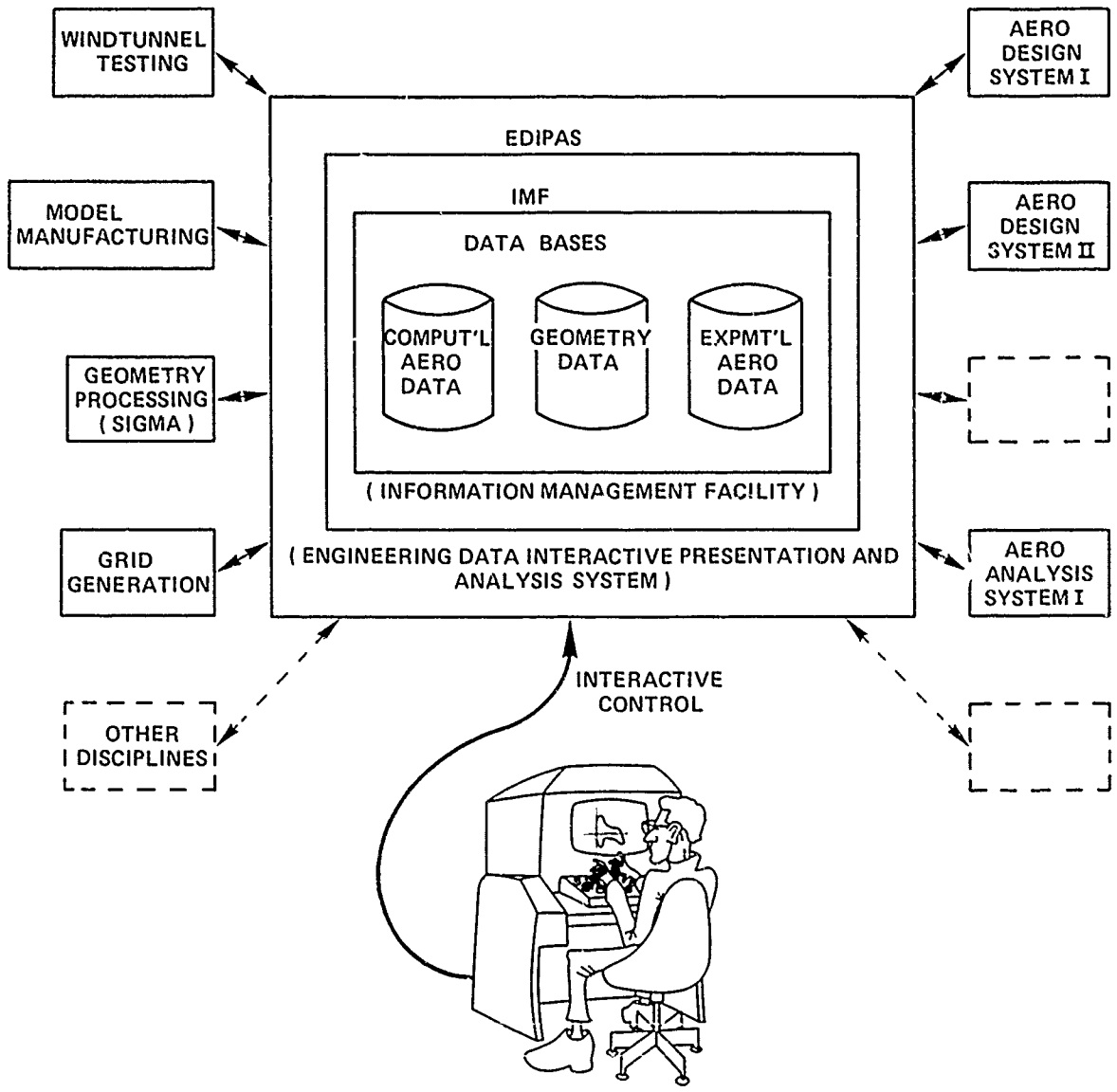

Fig. 2 Architecture for an aerodynamic information system

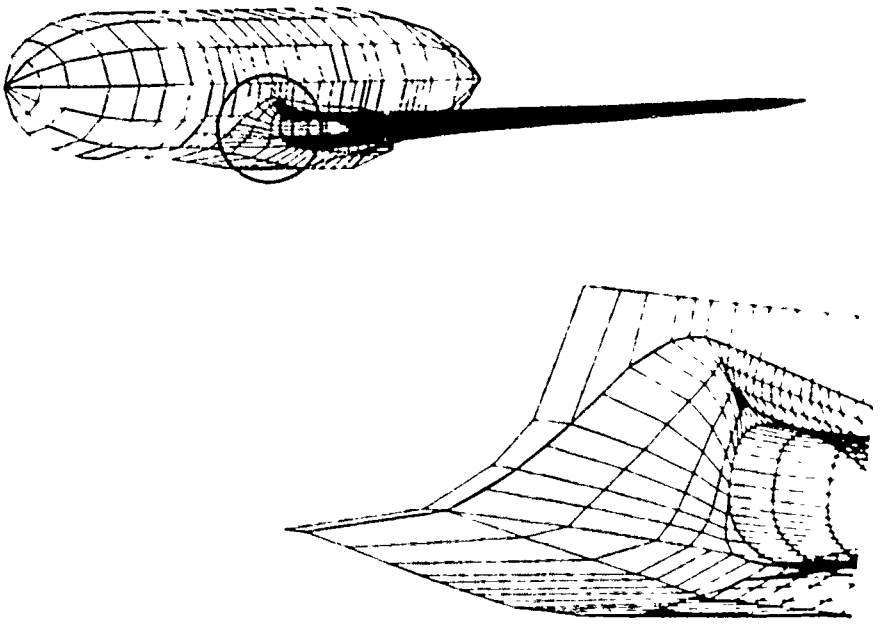

a) GEOMETRY OF " ACTIVE " WING – BODY FAIRING

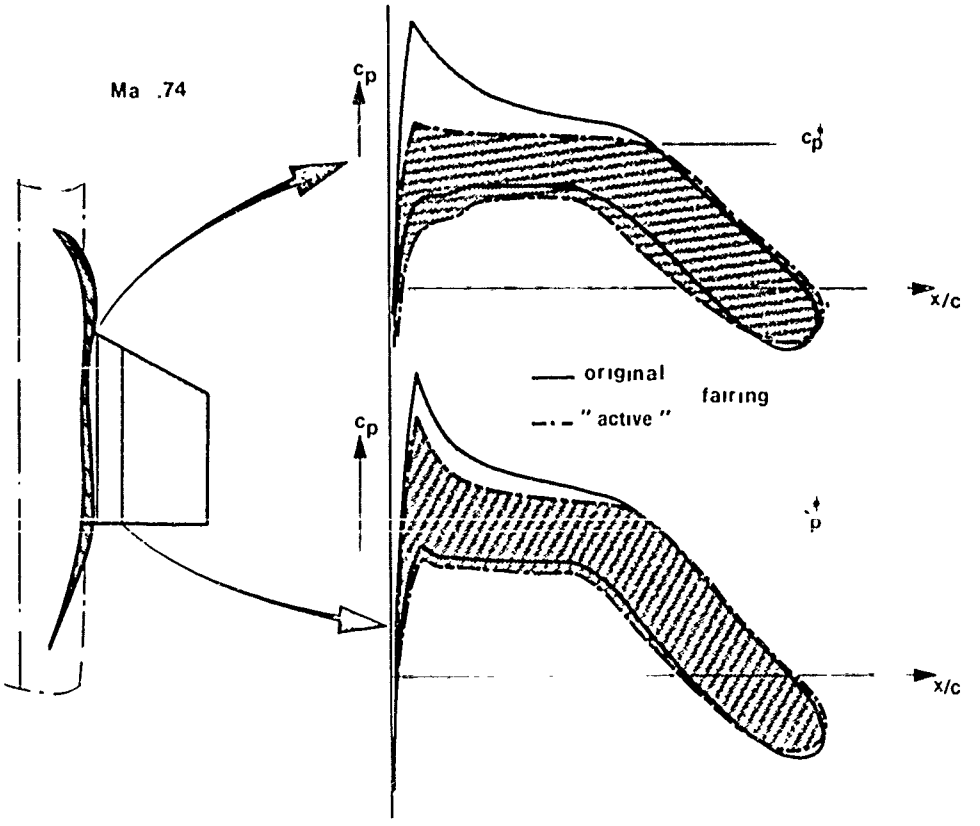

b) EFFECT OF " ACTIVE " FAIRING ON INNER WING PRESSURE DISTRIBUTION

Fig. 3 "ACTIVE" shaping of wing-fuselage fairing by means of panel method, [11]

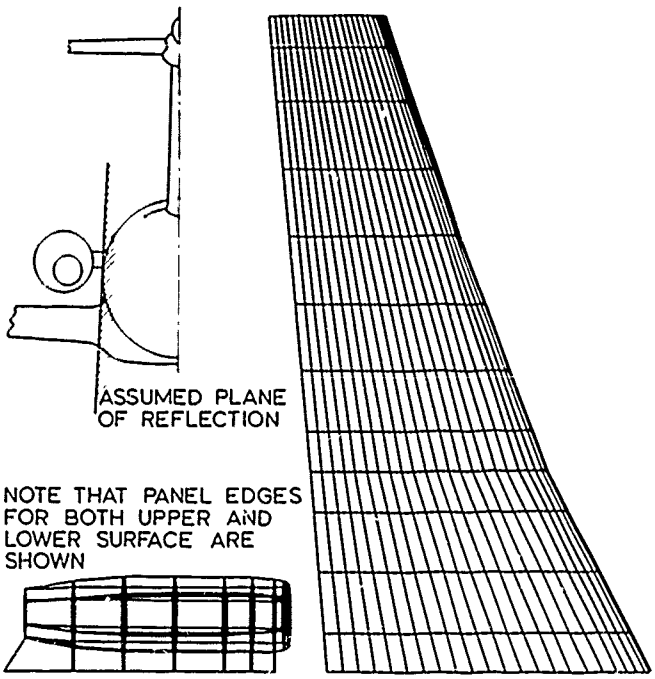

a) PANEL ARRANGEMENT AND SCHEMATIC REAR VIEW OF WING – NACELLE CONFIGURATION.

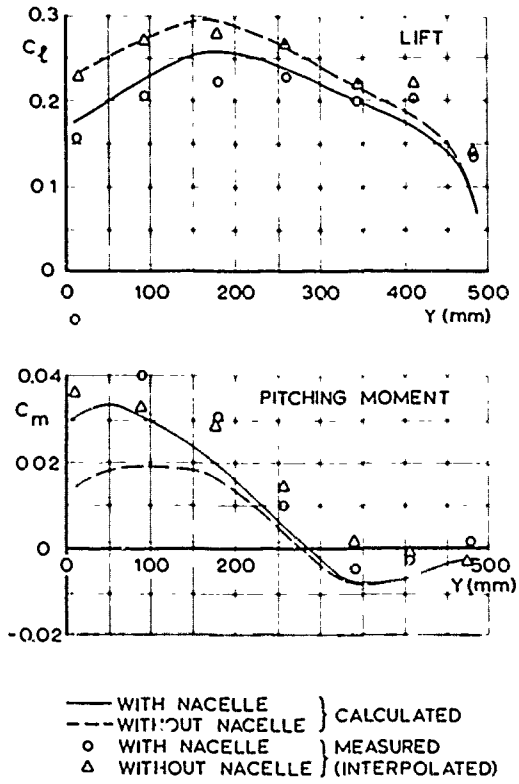

b) COMPARISON OF MEASURED AND CALCULATED SECTION AERODYNAMIC COEFFICIENTS OF WING – NACELLE CONFIGURATON

Fig. 4 Effect of (close-coupled) rear-mounted nacelle on wing lift and pitching moment (cruise configuration), [8]

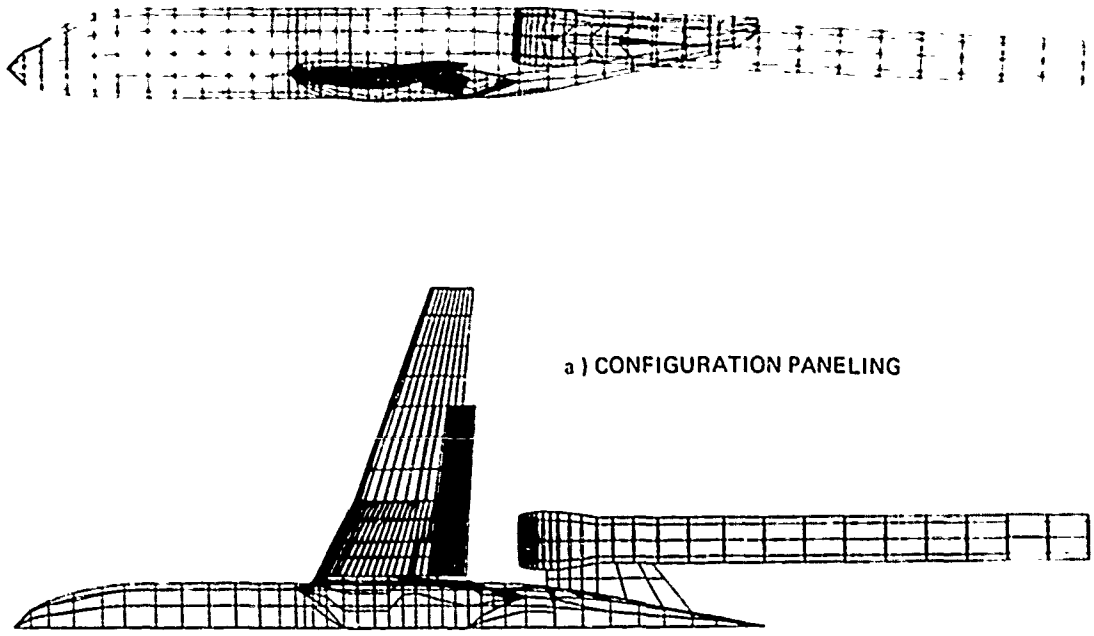

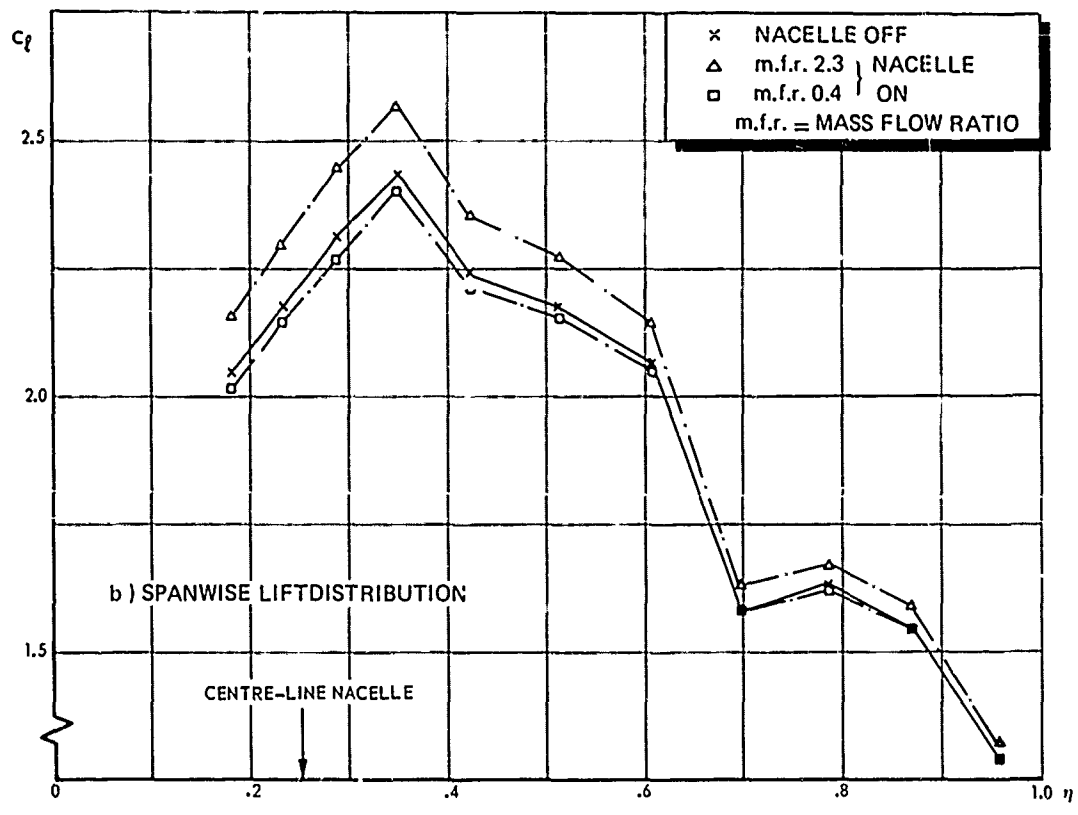

Fig. 5 Effect of nacelle flow on lift (take-off configuration, $\alpha = 18^{o}$), [12]

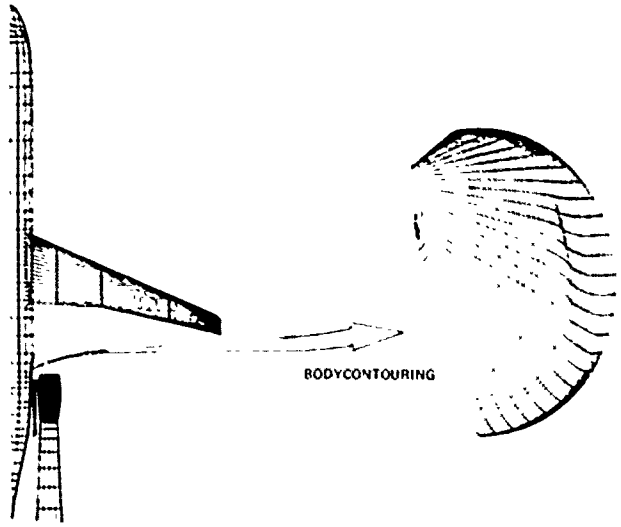

a) GEOMETRICS OF CONFIGURATION

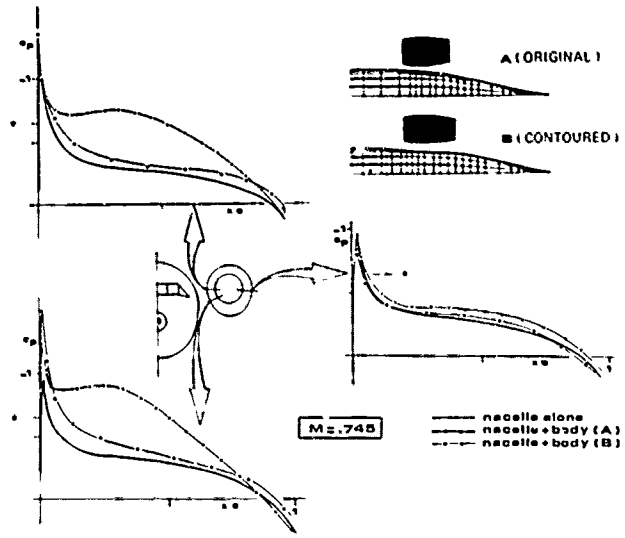

b) EFFECT OF BODY CONTOURING ON PRESSURE DISTRIBUTION

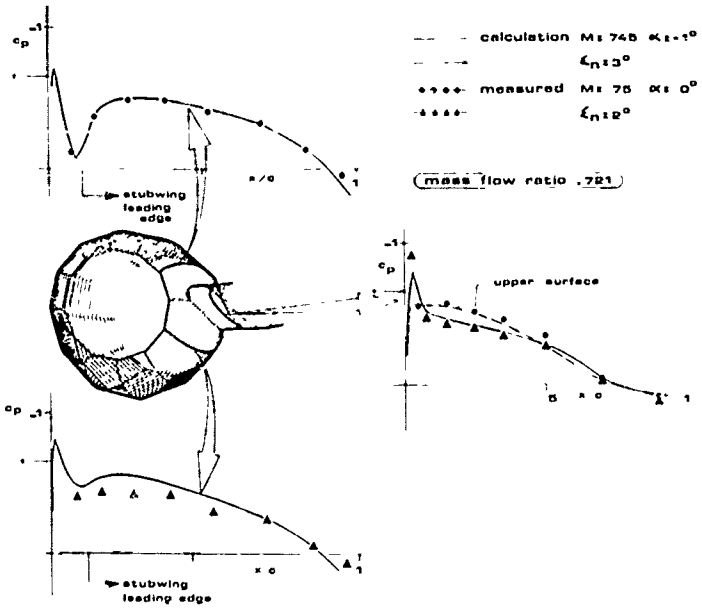

c) COMPARISON OF MEASURED AND CALCULATED PRESSURES

Fig. 6 Rear-mounted high-bypass ratio nacelles; a local interference problem

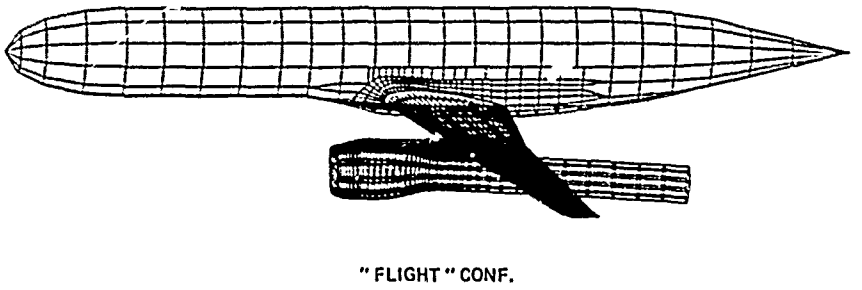

" FLIGHT " CONF.

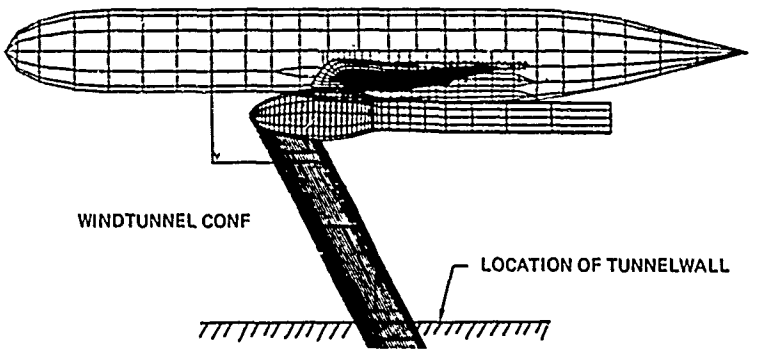

a) CONFIGURATION PANELING

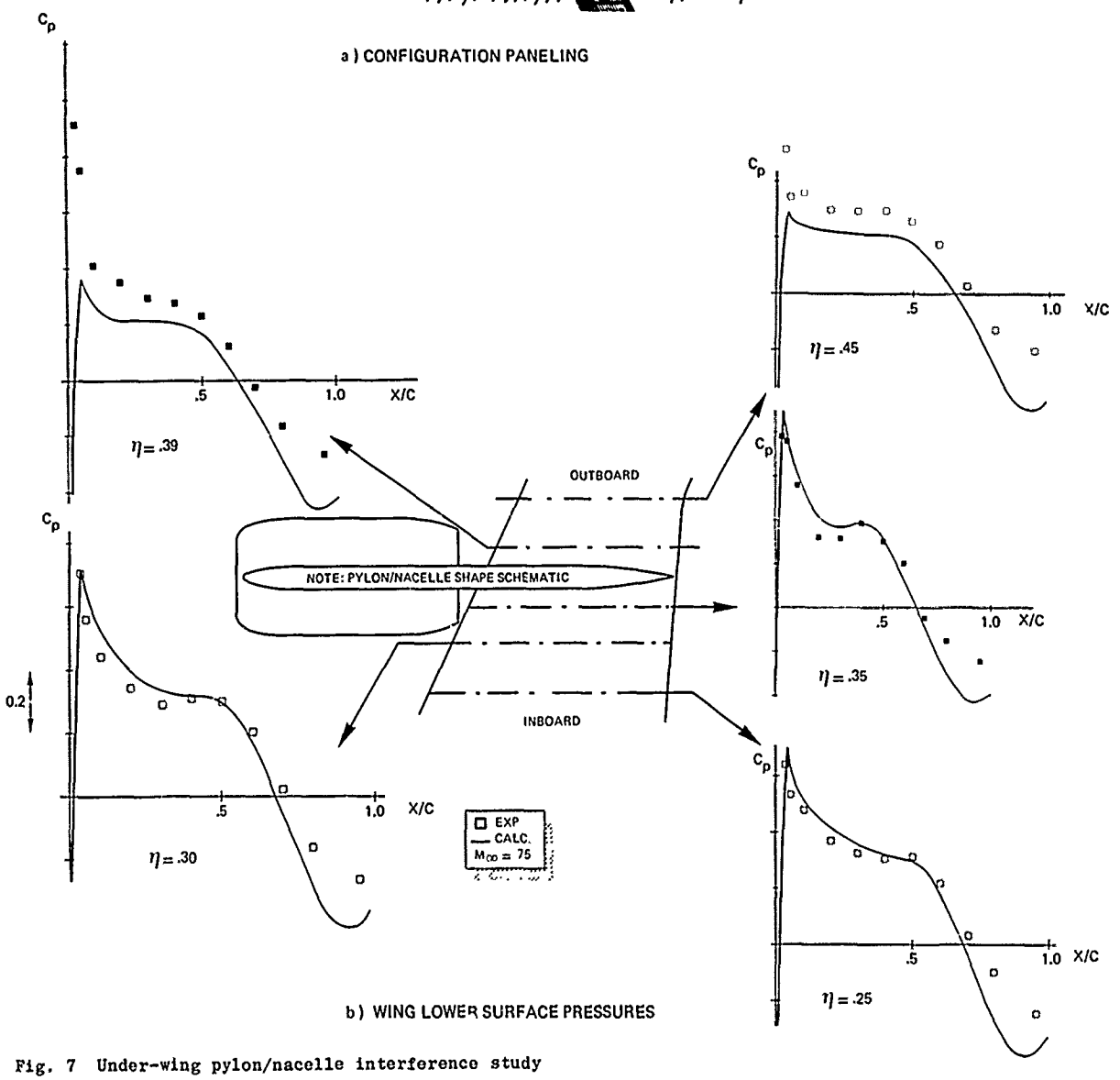

b) WING LOWER SURFACE PRESSURES

Fig. 7 Under-wing pylon/nacelle interference study

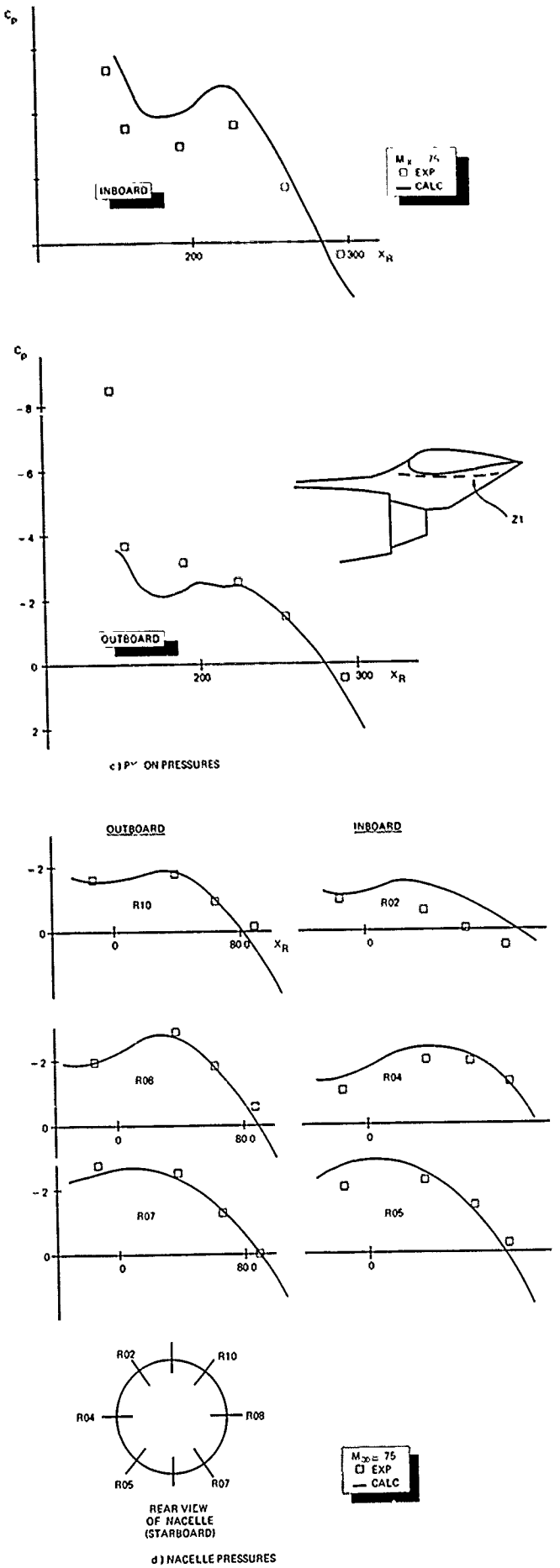

c) PYLON PRESSURES

d) NACELLE PRESSURES

Fig. 7 Continued

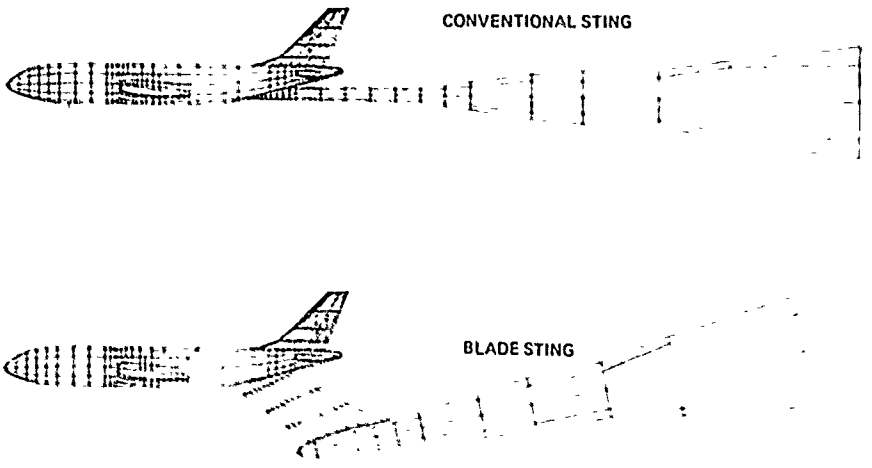

a) PANEL ARRANGEMENTS

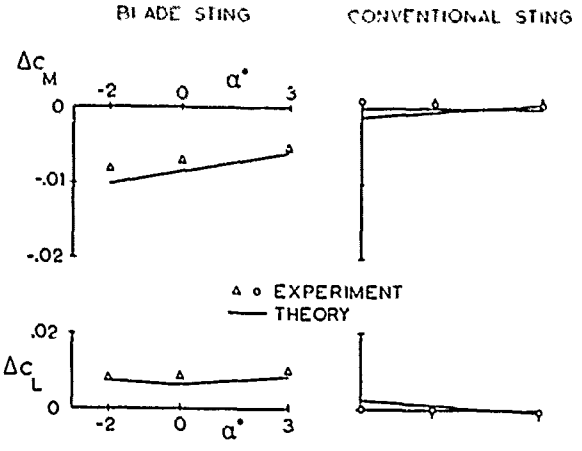

b) COMPARISON OF MEASURED AND CALCULATED MODEL SUPPORT INTERFERENCE

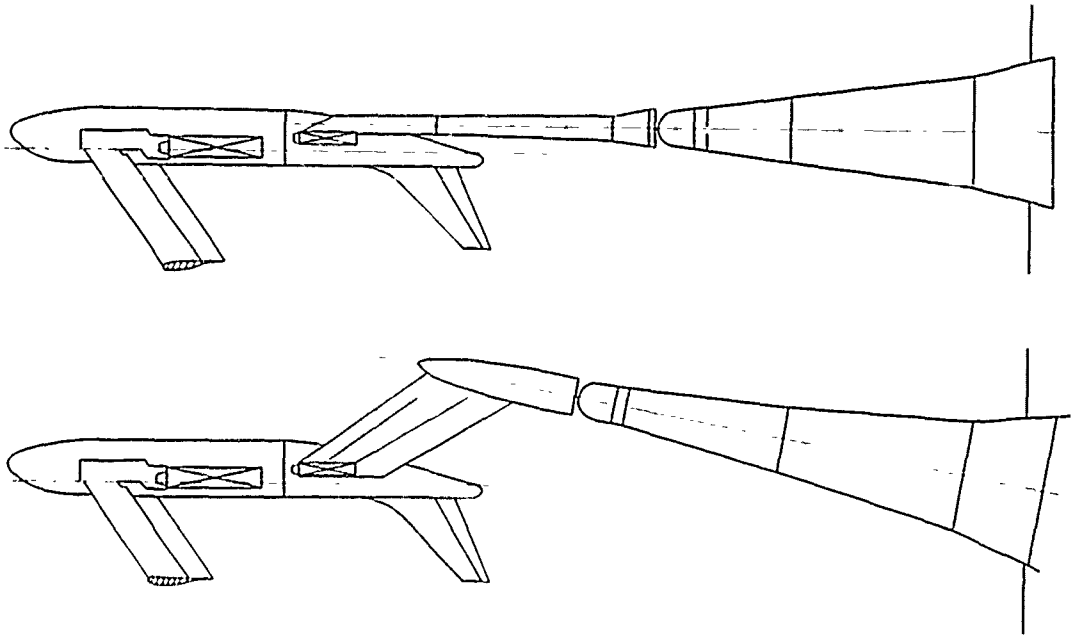

c) WINDTUNNEL MODEL SUPPORTED BY VERTICAL STRUT WITH DUMMY STINGS

Fig. 8 Assessment of sting support interference

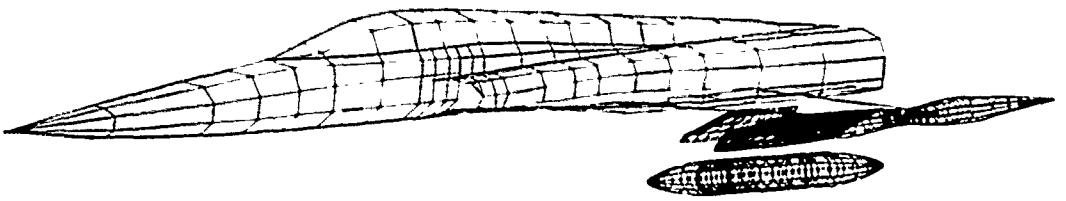

a) PANEL ARRANGEMENT

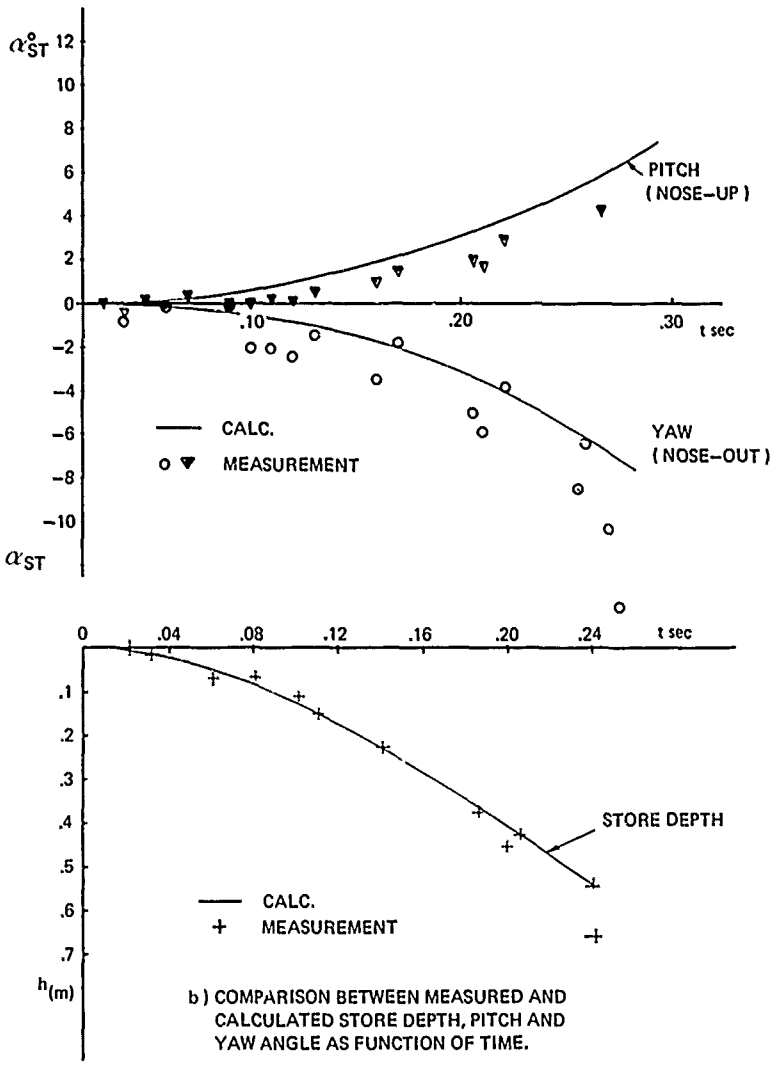

b) COMPARISON BETWEEN MEASURED AND CALCULATED STORE DEPTH, PITCH AND YAW ANGLE AS FUNCTION OF TIME.

Fig. 9 Use of panel method in predicting interference forces for store trajectory prediction

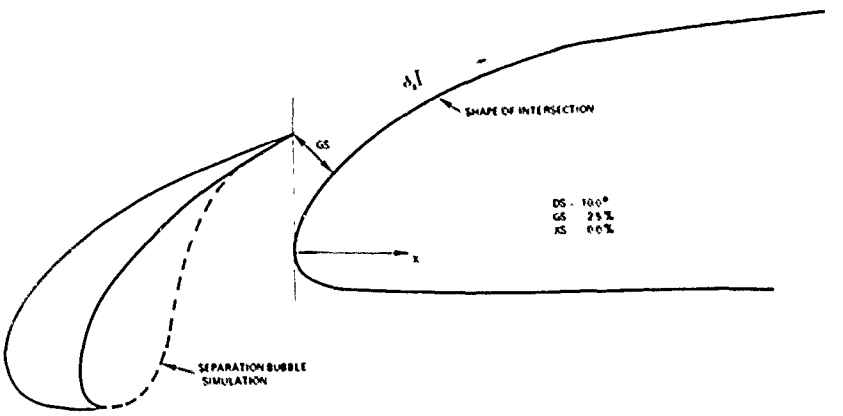

a) DESIGN VARIABLES AND STARTING GEOMETRY IN LEADING EDGE SLAT DESIGN STUDY

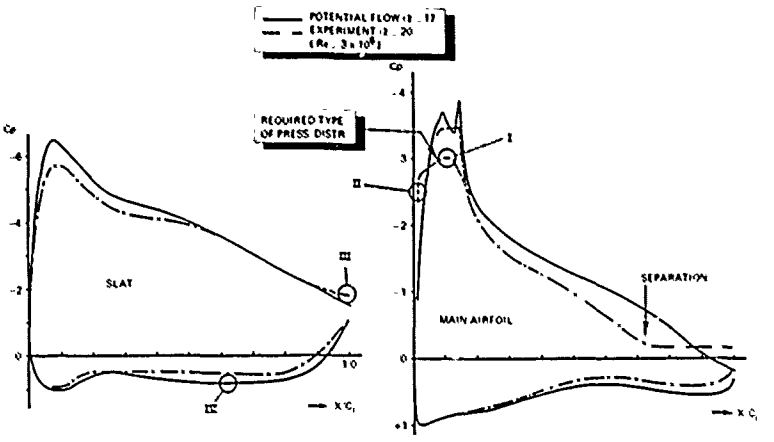

b) PRESSURE DISTRIBUTION ON STARTING CONFIGURATION AND REQUIRED MODIFICATION

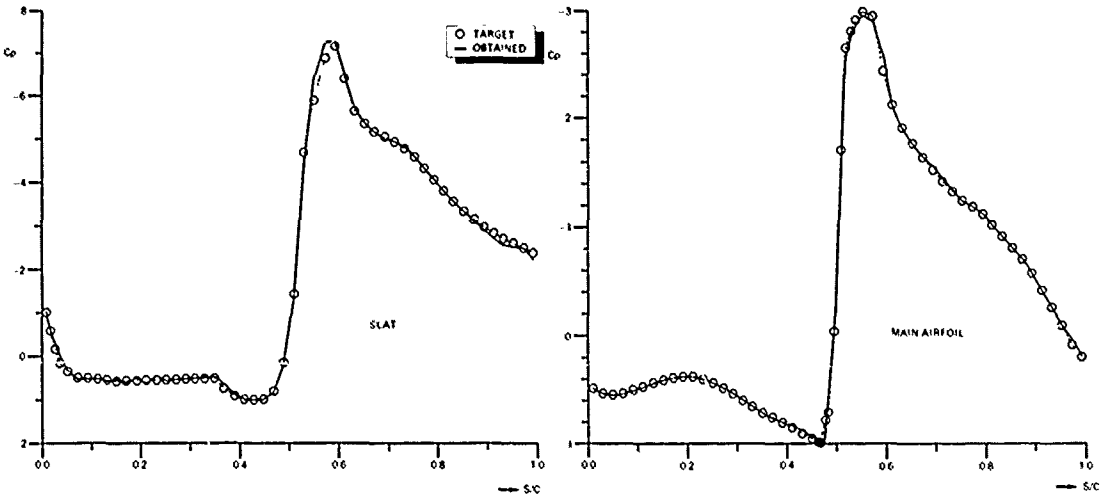

c) RESULT OF DESIGN CALCULATIONS

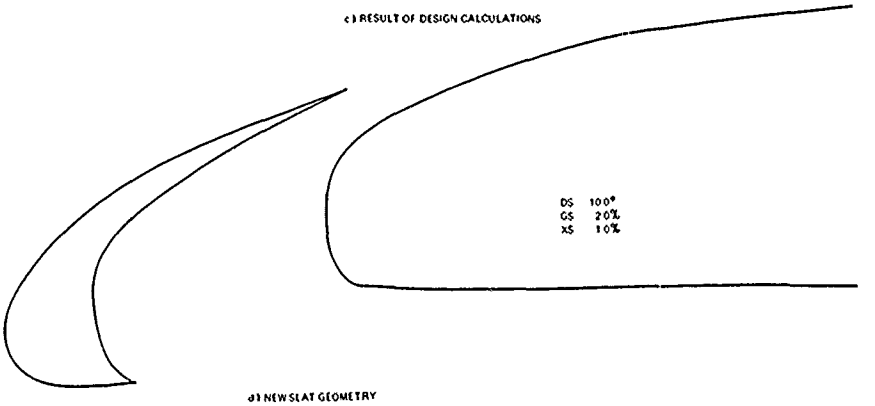

d) NEW SLAT GEOMETRY

Fig. 10 Example of computational slat (ro) design

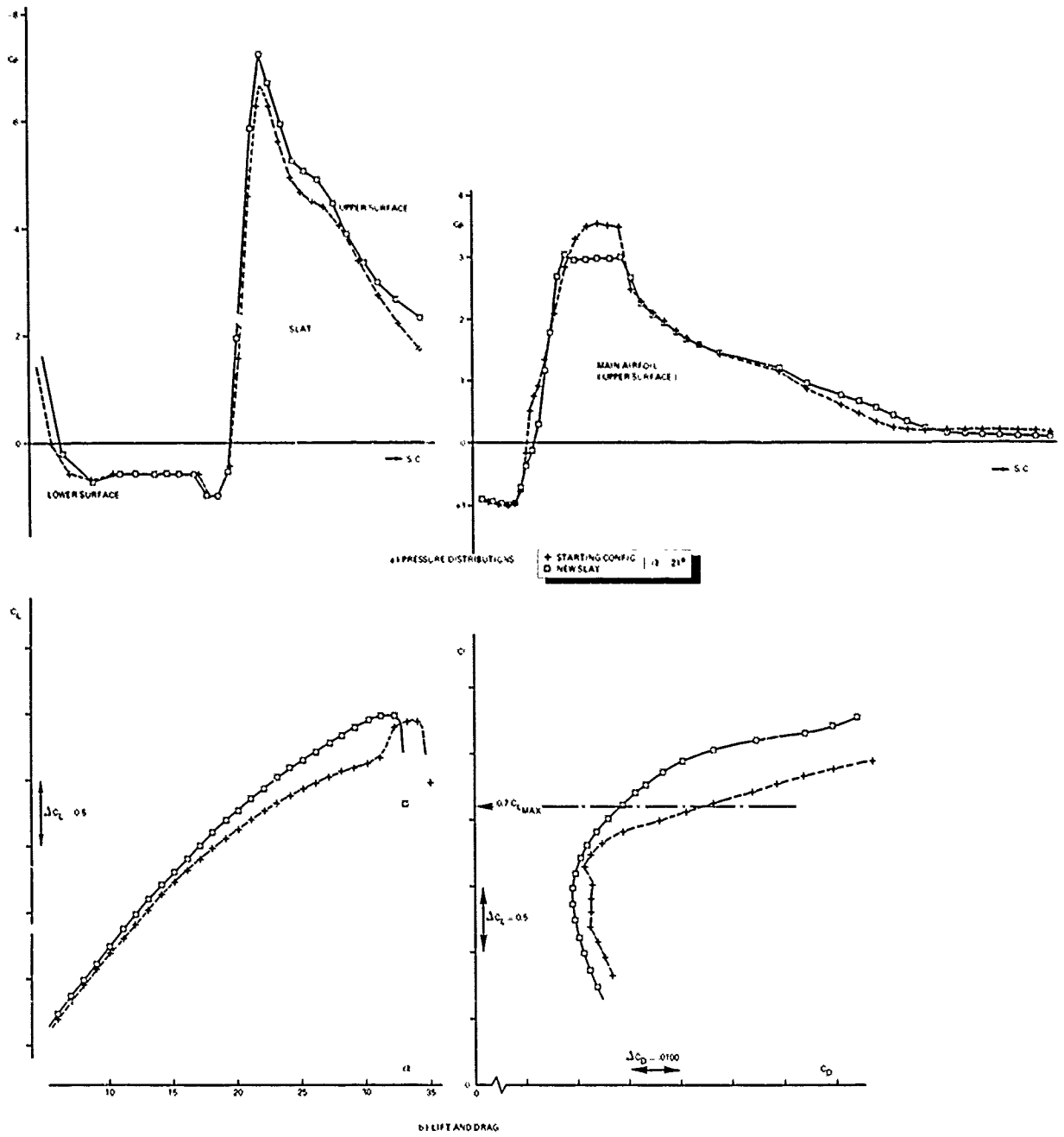

Fig. 11 Experimental results for computationally designed slat of figure 10 (Re = 3×10^6)

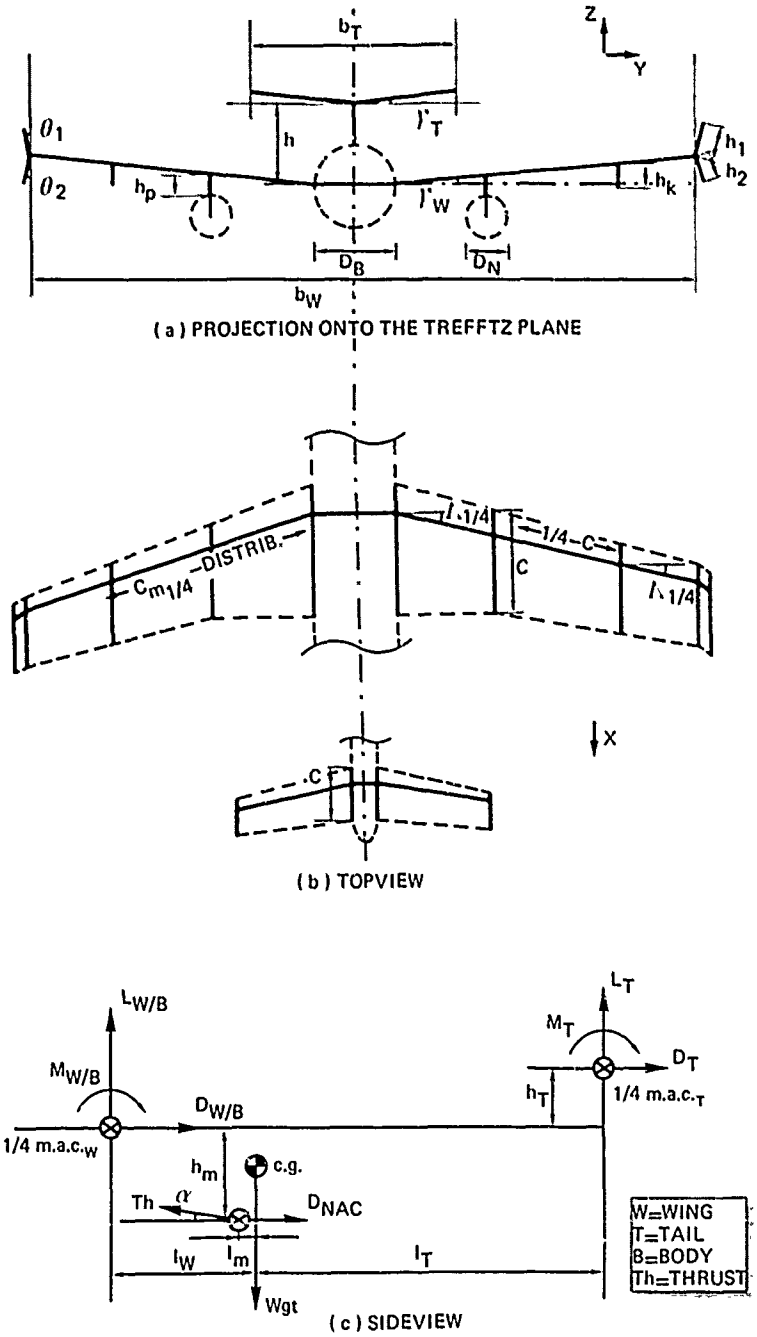

Fig. 12 Summary of input parameters for trimmed induced drag minimization

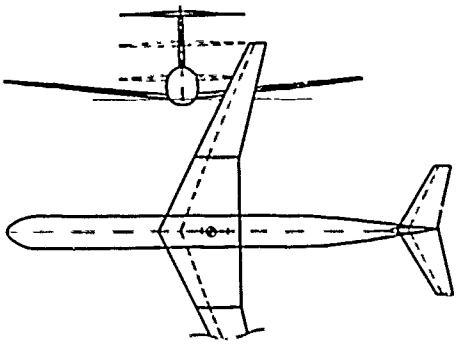

a) SKETCH OF AIRCRAFT CONFIGURATION

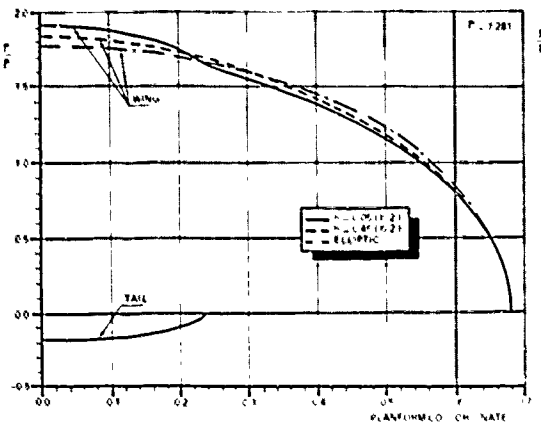

b) BOUND-CIRCULATION FOR C.G. AT 30%MAC ($C_{M_{W/B}} = -0.09$)

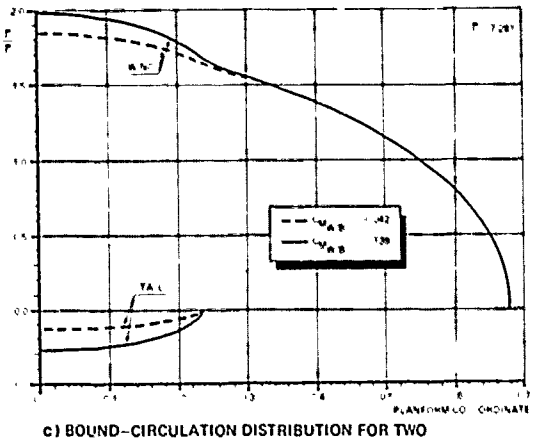

c) BOUND-CIRCULATION DISTRIBUTION FOR TWO DIFFERENT VALUES OF THE WING-PITCHING MOMENT COEFFICIENT (LOW-TAIL CONFIGURATION, C.G. AT 25%MAC)

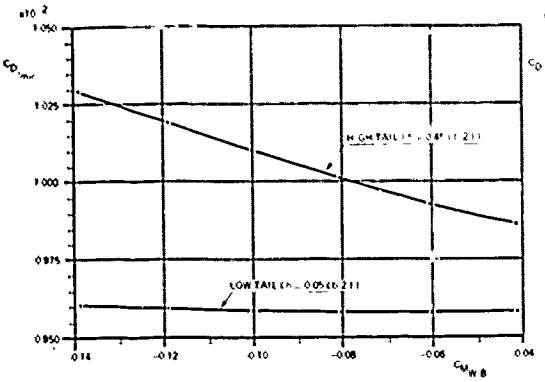

d) INFLUENCE OF THE WING/BODY PITCHING MOMENT COEFFICIENT $C_{M_{W/B}}$ ON THE MINIMUM TRIMMED INDUCED-DRAG ($C_{M_B} = 0.007$; C.G. AT 25%MAC)

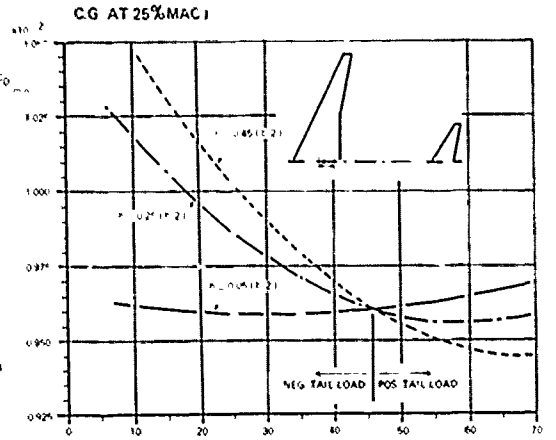

e) EFFECTS OF THE LOCATION OF CENTER OF GRAVITY AND THE TAIL HEIGHT RELATIVE TO THE WING ON THE MINIMUM TRIMMED INDUCED-DRAG ($C_{M_{W/B}} = -0.09$)

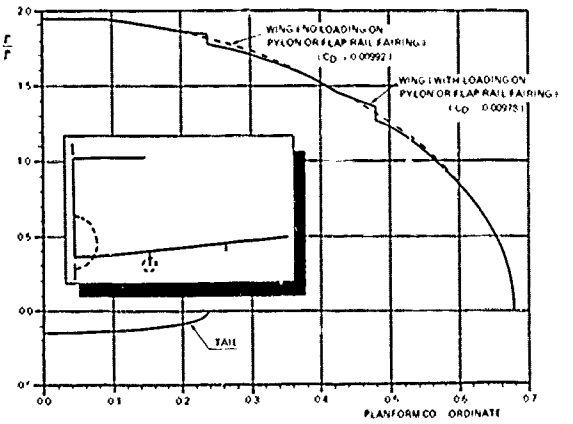

f) THE AIRCRAFT CONFIGURATION WITH PYLON/NACELLE AND FLAP-RAIL FAIRINGS, DESIGNED FOR MINIMUM TRIMMED INDUCED DRAG (C.G. AT 32%MAC)

Fig. 13 Examples of trimmed induced drag minimization studies

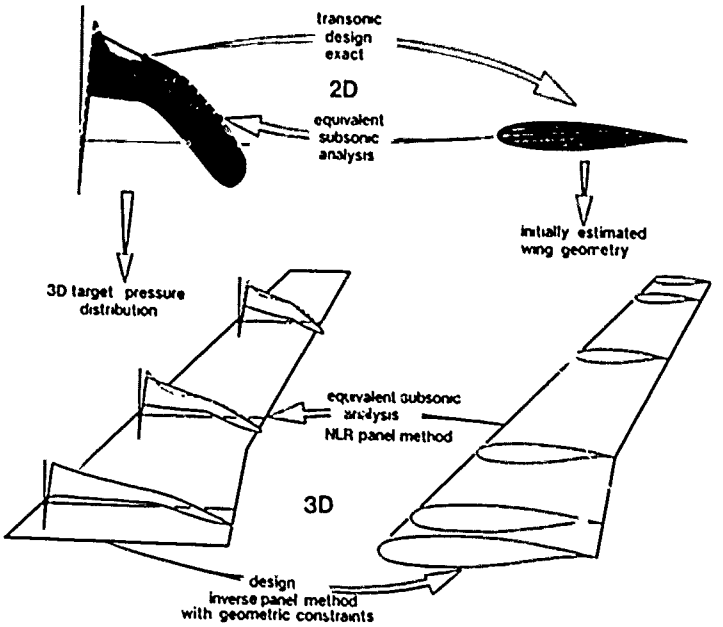

Fig. 14 Transonic wing design through equivalent subsonic pressure distribution

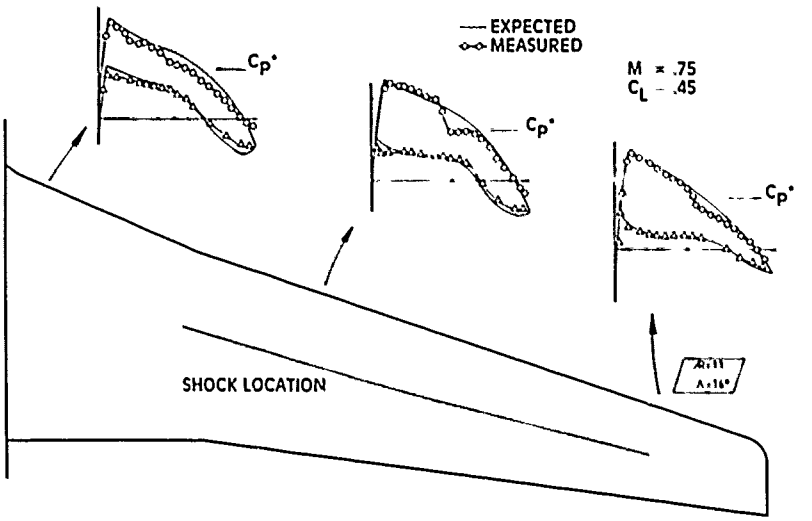

Fig. 15 Comparison of expected and measured pressure distribution in transonic flow for wing designed by means of 2D transonic and 3D subsonic theory

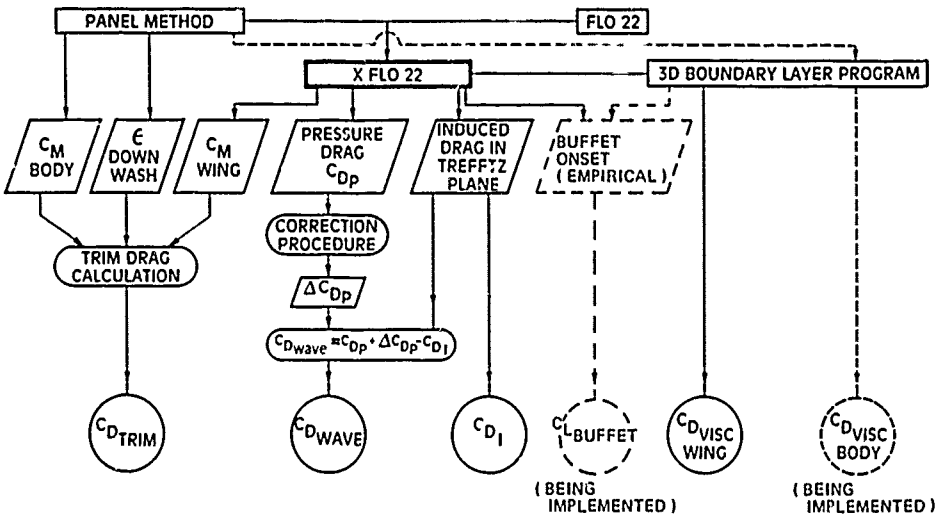

Fig. 16 Schematic of NLR XFLO22 system for the analysis of wing-fuselage configurations in transonic flow

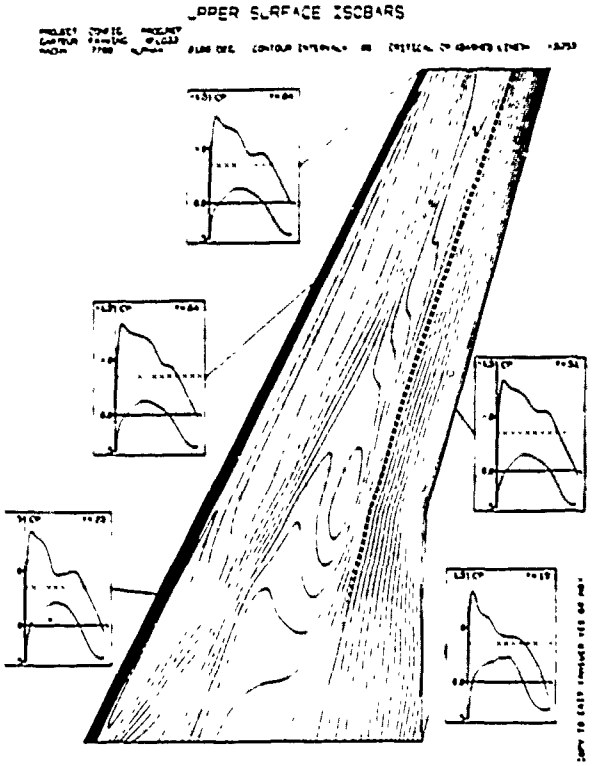

a) ISOBAR PATTERN AND SECTION PRESSURE DISTRIBUTIONS

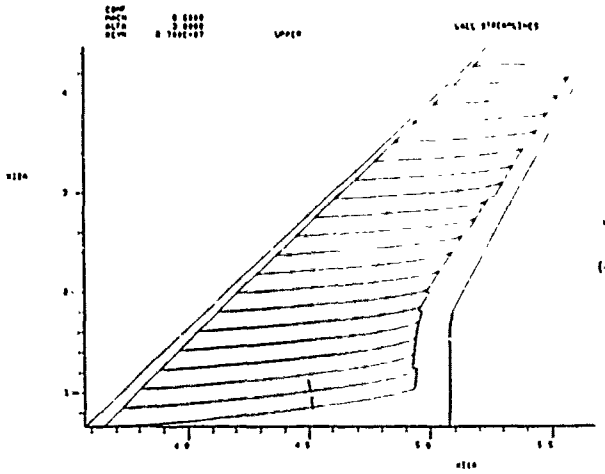

b) "NUMERICAL SURFACE OIL FLOW PICTURE"

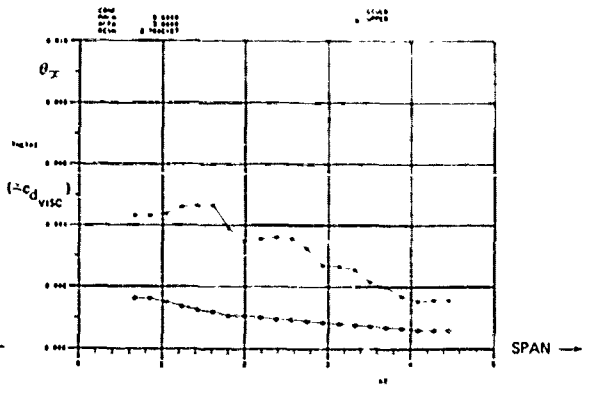

c) "NUMERICAL WAKE RAKE DATA"

Fig. 17 NLR XFL022 wing-fuselage transonic analysis system: examples of standard graphics output

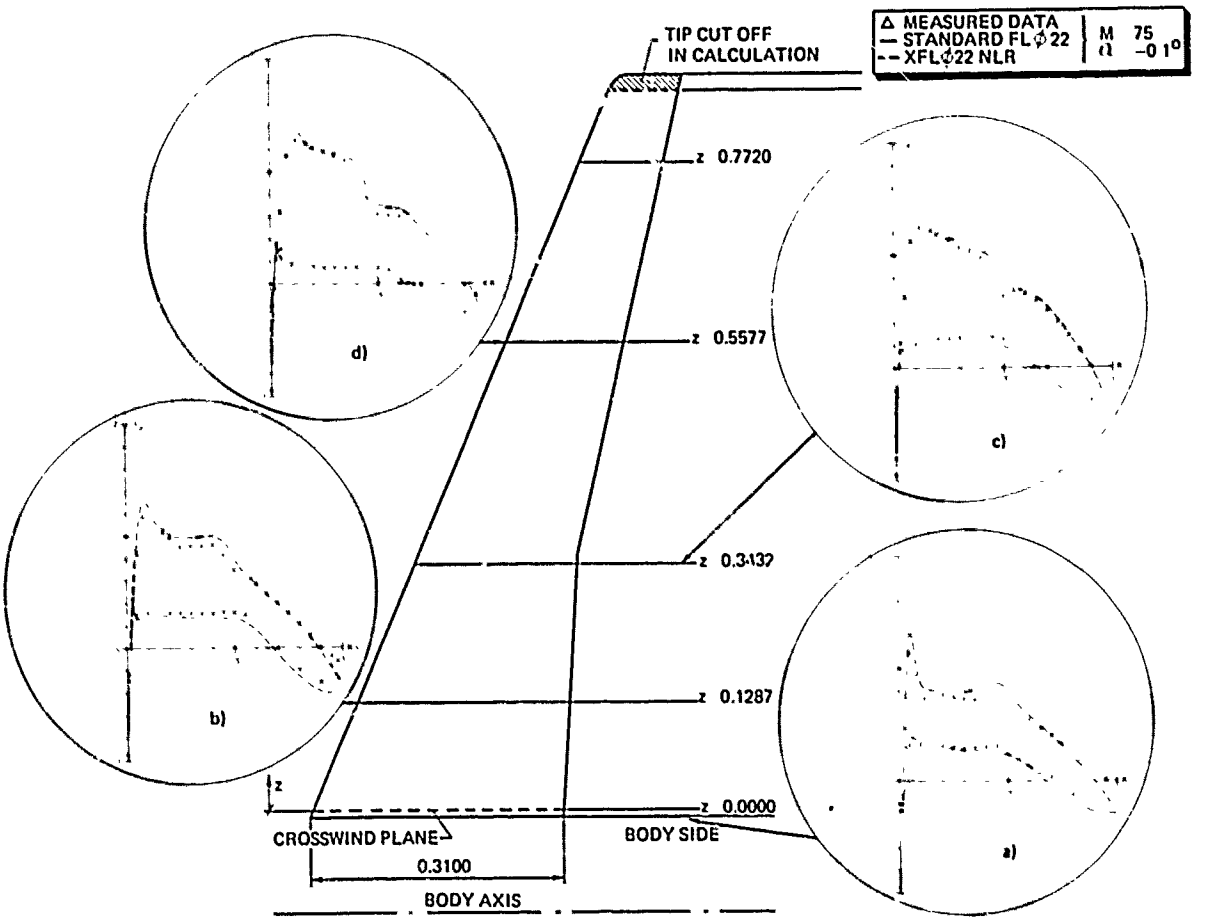

Fig. 18 Example of pressure prediction capability of NLR XFLO22 system

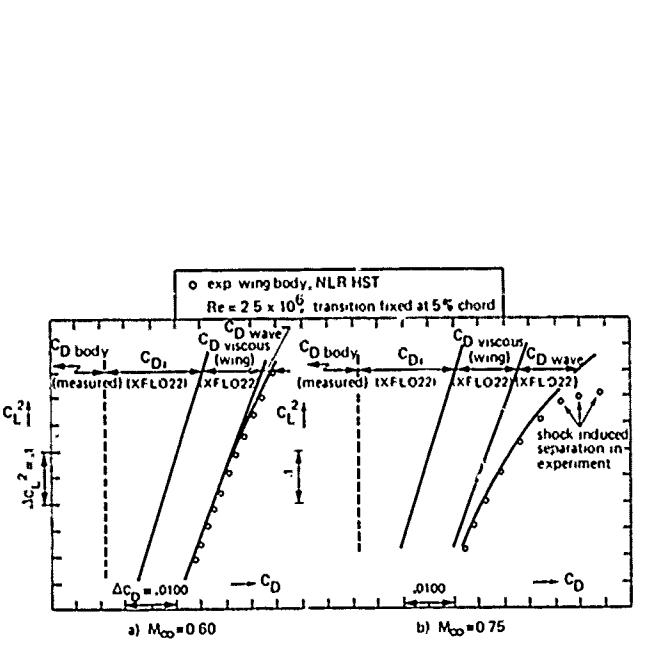

a) DRAG CORRELATION AT CONSTANT MACH NUMBER

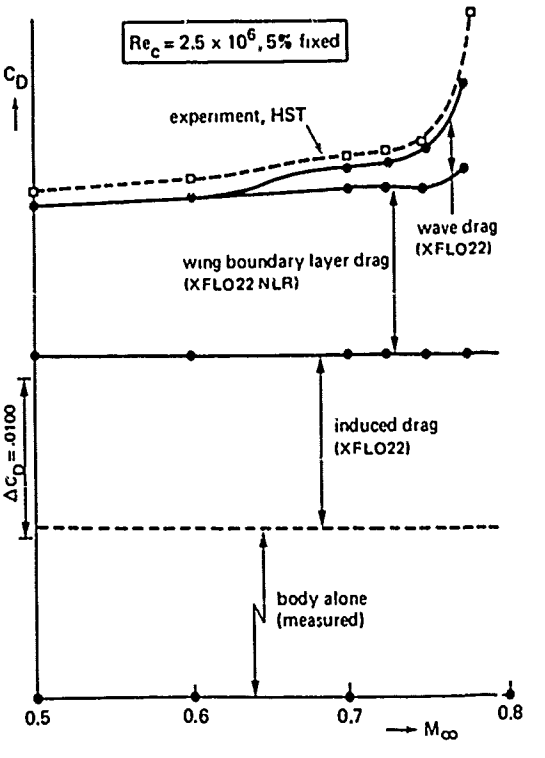

b) DRAG CORRELATION AT CONSTANT LIFT

Fig. 19 NLR XFLO22 drag analyses for narrow-body transport configuration

TRANSONIC EMPERICAL CONFIGUPATION DESIGN PROCESS

by Richard T. Whitcomb
Distinguished Research Associate
Langley Research Center, NASA
Hampton, Virginia 23665
U.S.A.

SUMMARY

This lecture describes some of the experimental research pertaining to transonic configuration development conducted by the Transonic Aerodynamics Branch of the NASA Langley Research Center. Discussions are presented of the following: use of florescent oil films for the study of surface boundary layer flows; the severe effect of wind tunnel wall interference on the measured configuration drag rise near the speed of sound as determined by a comparison between wind tunnel and free air results; the development of a near sonic transport configuration incorporating a supercritical wing and an indented fuselage, designed on the basis of the area rule with a modification to account for the presence of local supersonic flow above the wing; a device for improving the transonic pitch up of swept wings with very little added drag at the cruise condition; a means for reducing the large transonic aerodynamic interference between the wing, fuselage, nacelle and pylon for a fuselage mounted nacelle having the inlet above the wing; and methods for reducing the transonic interference between flows over a winglet and the wing.

SYMBOLS

$\bar{c}$	mean aerodynamic chord
C_D	drag coefficient, Drag/qS
C_L	lift coefficient, Lift/qS
C_M	pitching moment coefficient, pitching moment/$qS\bar{c}$
C_p	pressure coefficient, $p_\ell - p_\infty/qS$
M	Mach number
p_ℓ	local static pressure
p_∞	free stream static pressure
q	free stream dynamic pressure

INTRODUCTION

Before the recent development of numerical codes for three dimensional transonic flow, such as these described in several preceding lectures, the development of configurations intended for operation at transonic speeds was primarily an emperical process. Most of the designs were based on extensive wind tunnel data from systematic investigations and tests of specific configurations. These new analysis methods have greatly improved the design process. The transonic characteristics of lifting wing-fuselage combinations, including the effects of unseparated boundary layers can now be calculated quite well. However, the theoretical methods generally available still cannot handle conditions with separated boundary layers or complex configurations such as these with nacelle-pylon arrangements or external stores. Resort must still be made to the wind tunnel to develop the most satisfactory overall configuration for the complete operating envelope of an airplane. In other lectures presented here, results of a number of experimental programs in Europe and the United States will be presented. In this lecture the discussion will be limited to experimental research carried out at the Transonic Branch of the NASA - Langley Research Center. Consideration will be given to the technics used to guide configurations development, a wind tunnel wall interference problem, some of the configuration design problems encountered and selected solutions to these problems.

EXPERIMENTAL TECHNICS

The experimental development of transonic configurations need not be blind cut- and try. Various experimental technics have been developed over the years which greatly aid in the determination of the actual flow over a configuration and thus provide the basis for the rational development of the configuration. The most used and probably the most valuable technic is the measurement of pressure distributions. Also, at condition for which extensive shock waves are present schlieren pictures can be quite helpful. Since most aerodynamicists are familiar with these technics no further discussion is needed.

A very important tool for locating some of the sources of aerodynamic problems is a means for indicating visually the airflow in the boundary layer. Several methods are available. Tufts have been used for years to indicate boundary layer flow for subsonic type configurations. However, for transonic configurations the tufts available until recently caused unacceptable interference effects on the flow being observed. Recently, however, very fine florescent tufts have become available (Ref. 1) which provide good indication of the boundary layer flow without interfering with it. These tufts, which are being used by several organizations in the United States, are especially useful for indicating massive separation. The method used extensively by the author and others to visualize the boundary layer is the florescent oil film technic (Ref. 2). In this method, a lubricating oil with a florescent power added is coated on the model surface and illuminated with ultraviolent light. With airflow over the model the oil moves to conform with boundary layer flow at the surface of the model. Numerous experiments have indicated that the presence of the oil has no measurable effect on the aerodynamic characteristic of the model. This technic, while inferior to the fine florescent tufts for indicating massive separation, can indicate laminar boundary layer transition, incepient separation, boundary layer thickening before separation, shock boundary layer interaction and separation bubbles which the tufts cannot. For moderate separation the two methods are arguable of equal usefulness.

To illustrate the indications provided by this oil film technic several typical photographs will be discussed. The oil film on a high aspect ratio NASA supercritical wing at the design Mach number and lift coefficient is presented in figure 1. To simulate full scale Reynolds numbers the transition trip is located at the 35% chord on the outer panel (Ref. 3). It is angled forward inboard so as to be ahead of the oblique shock eminating from near the leading edge of the wing-fuselage juncture. The transition at the trip is indicated by the fine lines of oil behind the trip. The shock wave is indicated by the spanwise line at about the 70% chord line. The boundary layer deceleration as it moves through adverse pressure gradient aft of the 90% chord line is shown by the thickening of oil in this region. A small region of separation near the trailing edge just outboard of the planform trailing edge break is indicated by the accumation of oil in this region. The oil film on the same wing at a higher lift coefficient is shown in figure 2. The oil film indicates a significant region of boundary layer separation on the aft part of the wing outboard the trailing edge planform break. The outward flow of the boundary layer in the separated region also can be seen.

WIND TUNNEL WALL INTERFERENCE NEAR MACH NUMBER OF 1.0

Transonic wind tunnel wall interference effects has been studied extensively over the years. Reasonably reliable methods for calculating these effects at primarily subsonic or supersonic conditions have been available for some time. However, for conditions where the flow field in the tunnel is primarily supercritical, that is with a large region of supersonic flow immersed in a subsonic field, methods for the calculation of the wall interference effect have only recently become available (Ref. 4 for example).

As part of the overall development program of a near-sonic transport configurations, to be discussed in the next section, the problem of supercritical wall interference near a Mach number of 1.0 was explored experimentally. The free air drag rise for a supercritical body of revolution, as developed in a wind tunnel, was determined using a freely falling body (Ref. 5). The test configuration is shown in figure 3. The results of this investigation were much more accurate than those of a much earlier investigation (Ref. 6). The drag rise characteristics for the same finned configuration was also measured in the Langley 8' and 16' transonic tunnels. A comparison of the results of these investigations is presented in figure 3. At Mach numbers below the drag rise the drag creep for the body in the 16' tunnel is roughly the same as that mesaured in free air. However, that for the body in the 8' tunnel is substantially greater due to larger conventional wall blockage in this tunnel. The drag rise Mach number measured in the two wind tunnels is approximately the same, 0.99. However, the drag rise measured in free air is only 0.98. At higher Mach numbers the drag rise for the body in the 8' tunnel is substantially less than that in the 16' tunnel. Obviously these blockage effects measured near the speed of sound are opposite to those usually measured or calculated at lower Mach numbers. Pressure distributions measured on the tunnel wall indicate that they are associated with an expansion of the supercritical flow region to the tunnel wall.

To evaluate the magnitude of this blockage problem a series of supercritical bodies of different size were investigated in the Langley 8' and 16' tunnels (Ref. 7). Some of the results are presented in figure 4. Drag rise characteristics which approximated those for free air were not achieved until the blockage rate was reduced to .00017. However, a reasonable indication of the drag rise Mach number was achieved for a blockage ratio of .00034. These blockage values are associated with much smaller models than those generally utilized in transonic investigations. Results for models with such low blockage ratios would be severely distorted by Reynolds number effects. Also, they would generally be too small to incorporate pressure tubing. Therefore, it would not be reasonable to make models this small. Since these effects are associated primarily with flow phenomena at a significant lateral distance from the model it is probable that they are primarily a function of the longitudinal area development for the model. Thus

a reasonable procedure for investigations in this Mach number range should be to use models of rational size to investigate the details of a configuration and then correct the drag rise characteristics by the drag increments between those measured for two equivalent bodies of the configurations. One body would have the blockage area of the actual model and another an area of roughly .0002. This is the procedure which was used in the development of near sonic transport configuration to oe discussed in the next section.

DEVELOPMENT OF A NEAR SONIC TRANSPORT CONFIGURATION

Following the initial development of the NASA supercritical airfoil several United States government agencies undertook an extensive research and development program to exploit the various applications of this concept. As part of this program Langley initiated the development of a transport configuration with substantially higher cruise Mach numbers than those for the then current designs since the historic trend had been to continually higher speeds for each newer generations of such vehicles. Specifically the configuration was designed to achieve a cruise speed as close to the speed of sound as possible utilizing both the new airfoil and an uncompromised application of the area rule. This research involved the solution of a number of challenging interference problems and a summary of this work should be pertinent to the subject of this conference.

The wing developed for this configuration is shown in figure 5. The NASA supercritical airfoil would provide a major part of the desired increase in the design speed of the wing, however, not all of it. Therefore, the quarter chord sweep of the wing was increased to 42° from the 35° to 37° of the then current configurations. The aspect ratio was made similar to the then current practice, 7.0. Wing section thickness ratios somewhat greater than those for the then current configurations were incorporated to eliminate the structural weight penalty associated with the increased sweep. The thick forward glove provided an extension of the longitudinal area development for the wing, which would allow a more gradual indentation of the fuselage as defined by the Area Rule. The airfoil shapes shown were developed emperically. The airfoils for the outboard region are quite similar to those developed earlier in a two dimensionally investigation (Ref. 9). However, at the wing fuselage juncture the airfoil deviated substantially from sections developed two dimensionally. Pressure distribution measurements, oil film studies and wake surveys indicated that a drag rise Mach of 0.99 was achieved for the wing.

Even with the most ideal functioning of the area rule the drag rise Mach number for a total configuration cannot be greater than that for the equivalent body. Therefore, to achieve a total configuration with the best possible drag rise Mach number the equivalent body must also have a superior drag rise. Using the principles arrived at during the development of the NASA supercritical airfoil a supercritical body of revolution was developed (figure 6). The area development for this body is also shown, For the forward part of this body the second derivation of the area variation is inversely proportional to the area. For the aft part the second derivative of the area variation is constant. A fineness ratio of 9.0 was selected to provide a reasonable fineness ratio for the fuselage when the cross sectional area equivalent to that for the wing is removed. The pressure coefficients pressure measured on this body at a Mach number of 0.98 are approximately constant from 10% to 80% of the length. As discussed in the previous section the free air drag rise Mach number is 0.98. A numerical code is now available for calculating the supercritical flow on a body of revolution near the speed of sound (Ref. 10).

The total configuration is shown in figure 8. It incorporated two nacelles mounted on the sides of the fuselage and one in the vertical tail. The horizontal tail was located at the top of vertical surface. The fuselage was initially shaped on the basis of the simple linear area rule to provide the overall area development of the supercritical body of revolution described previously. The initial investigations of the configuration without nacelles or tail surfaces indicated that for the cruise lift coefficient the drag rise occurred earlier than for an equivalent body wth the same wind tunnel blockage. The flow surveys obtained for the wing, as mentioned earlier, had indicated that this premature drag rise was not associated with local flow conditions on the wing. Schlieren photographs indicated that this excessive drag was associated with extensive normal shock waves located longitudinally near the leading edge of the root of the wing and near the wing tip. At the zero lift condition the shock waves disappeared and the drag rise for total configuration was much closer to that for the equivalent body. These results indicated that the effective cross sectional area for a wing increases with the addition of lift at least for supercritical wings near the speed of sound. This increase is associated with stream tube expansion in the local region of supersonic flow just above the wing for these lifting conditions. For the flow fields at greater distances from wing this expansion is equivalent to a greater physical cross sectional area.

On the basis of two dimensional calculations of local supersonic flow field expansion and wind tunnel experiments the fuselage cross sectional area was modified as shown in figure 7. The extraneous shock waves at lifting conditions disappeared and the drag rise approached that for the equivalent body (Ref. 11). Since the experimental work just described analytic procedures have been developed which provide at least an approximation of the modifications required in the area equivalent for the wing at lift

conditions (see Ref. 12, for example). However, the extreme sensitivity of the flow over the wing to detail in the fuselage shaping will probably still require that the modification be refined on the basis of wind tunnel investigations.

Following the development of this near sonic transport configuration, three United States transport manufacturers made design studies of actual transports based on this design. However, follwing of the abrupt increase in fuel prices in 1974 all work on a near sonic transport configuration was stopped. At that time the airlines became far more interested in increasing fuel efficiency than in greater speed.

A MEANS FOR PITCH-UP IMPROVEMENT

The supercritical wing used for the near sonic transport described in the preceding section was demonstrated in flight using the U.S. Navy F8 as a test bed. The initial development of the wing was done on the wind tunnel model of this flight configuration (Ref. 13). Initial results from this investigation indicated a severe pitch up problem associated with the increased sweep of the wing. This is illustrated by the results for M = 0.95 presented in figure 9. The slope of the pitching moment curve breaks upward at a lift coefficient of 0.8. To achieve an acceptable wing configuration and, more importantly, to assure pilot safety during the flight program it was required that this pitch up be eliminated. An oil film study of the boundary layer flow on the upper surface of the wing for a Mach number of 0.95 and a lift coefficient of 0.92 (fig. 10) indicates that the outboard region is completely stalled. In addition there is strong outward flow of the boundary in the midspan part of the wing toward the separated region, as has been noted during many previous flow studies on swept wing for similar conditions. As has been noted by previous investigators, this outward flow greatly thickens the boundary layer on the outboard region which severely aggravates the separation problem there.

In the past, various devices such as large fences and leading edge notches have been investigated as means to reduce the spanwise flow. However, these usually caused substantial increases in drag at high subsonic speed cruise conditions. To greatly reduce the pitch up without a signficant drag increase we turned to a device invented at the Douglas Aircraft Company which they called a vortelon. It consists of a wing like surface which extends downward below the leading edge of the wing at about the 30% semispan station. It significantly improved the deep stall problem for the DC9, but had little effect on pitch up. For the F8 pitch up problem a surface simlar to the vortelon was placed below the leading edge at the 60% semispan station (figure 11). It is cambered with curvature outward. With this surface installed the pitch up was greatly reduced for all Mach numbers (figure 9, for example). Also the pilot experienced no pitch up problems during the flight tests.

An oil film study of the boundary layer flow on the upper surface of the F8 wing with this surface installed for the same conditions as those of figure 10 is presented in figure 12. A distinct line in the oilflow eminates rearward from the position of auxiliary surface. At the line, the spanwise flow of the boundary layer is stopped and the outboard separation is greatly reduced. The surface produces a discontinuity of circulation around the swept leading edge which results in a vortex above the upper surface. The rotation of this vortex is such that at the surface the flow is inward. This inward flow of higher energy air drawn from outside boundary layer by the vortex stops the outward flow of the lower energy air in the boundary layer. The action is quite similar to that produced by a notch of the leading edge as has been used on previous wings. However, the present surface, called a lower surface vortex generator, caused an increase in the drag coefficient at the cruise condition of only .0003.

A substantial delay in the break of the lift coefficient versus angle-of-attack and a large reduction in the high lift drag were also associated with addition of the auxiliary surface. It would be expected that it also reduces buffet at high lift coefficients. More complete results from the wind tunnel investigation are presented in references 14 and 15. Similar surfaces can also be used to improve the high lift characteristics of wings with lower sweep but with higher aspect ratios. Also they can be used to improve the characteristics of swept fighter wings. However, they must be developed emperically using the observed boundary layer flow phenomena as a guide. Since the surface produces the favorable effect by reducing the spanwise flow in the boundary layer it is important that it be placed at the spanwise station where this flow is greatest, not where the separation is greatest.

FUSELAGE MOUNTED NACELLE INTERFERENCE

Among the areas of transonic aerodynamics that still cannot be handled adequately by generally available numerical methods is the flow interference between engine nacelles and wings. The interference for underwind mounted nacelles is considered in other lectures. The interference between fuselage mounted nacelles and the wing-fuselage combination will be discussed here. For larger transport type airplane with fuselage mounted nacelles, the nacelles are usually located sufficiently far behind the wing so that the flow interference between the two components is insignificant. However, for smaller business jet size aircraft the balancing of the airplane usually requires that the nacelle be placed close to the wing. Wind tunnel information has been obtained for a number of such aircraft. While much of this information is proprietary, a number of business jets have been investigated in NASA facilities during cooperative programs so that the results are generally available. Some of these will be discussed.

Generally, it has been found that the most important factor determining the interference between the nacelle wing and fuselage is the longitudinal location of the nacelle with respect to the wing. For configurations with swept wings and the inlet of the nacelle at or just aft of the inboard wing trailing the transonic interference can be favorable, the drag rise for the wing fuselage nacelle combination being higher than that for the wing-fuselage. The nacelle, operating at the normal cruise mass flow ratio, produces a significant postive pressure field ahead of it. This pressure field moves the shock location on the inbord region of the wing forward of that for the wing-fuselage along. As a result the sweep of shock on the critical middle region of the wing is increased and the drag rise for that region is improved.

For configurations with the forward region of the nacelle overlapping the aft portion of the wing, the interference can be very adverse. This arrangement, which is usually required to balance configurations with unswept wings, is illustrated in figure 13. To indicate the causes of this adverse interference for such arrangements and to illustrate how it can be substantially reduced, the results of a wind tunnel investigation of this configuration (Ref. 16) will be discussed. The configuration incorporated a replacement NASA supercritical wing which had the same planform and was located longitudinally at the same location as the original wing. The supercritical wing as first tested was designed by the sponsoring company with very little consideration of the effects of the nacelle. The pressure distribution on the side of the fuselage of the configuration as first tested for the near design condition is shown in figure 14. An extreme negative pressure peak corresponding to a local Mach number of 1.4 occurs at a longitudinal location just forward of the wing trailing edge. The peak results in a strong local shock wave which caused local boundary layer separation on the side of the fuselage and on the pylon. As indicated in figure 15 these effects resulted in a severe drag creep for the configuration

To reduce the pressure peak the upper surface of the wing and the pylon were modified as shown in figure 16. In particular the wing surface was made concave at the location of the negative pressure peak. The added wing depth and length of the nacelle was required to achieve the desired concavity without cutting into the rear spar of the wing. (It also resulted in a desired increase of the fuel volume.) The concavity greatly improved the local longitudinal area development for the channel defined by the upper surface of the wing, the fuselage, the lower surface of the pylon, and the lower, inner quarter of the nacelle. The change reduced the local pressure peak (figure 14) with a resulting reduction of the local shock strength and the associated boundary layer separation. The drag coefficient at a Mach number of 0.80 was reduced by .0080 (figure 15). This channel area rule concept was used intially to overcome a very severe wing-nacelle-pylon interference problem for the Convair 990 and has been used over the years to solve the problem on other configurations. However, this may be the first case in which the wing was modified rather than the nacelle or pylon as has been done for previous problems.

WINGLETS

Winglets, small approximately vertical wing like surfaces placed at the tips of wings, have now been applied to a number of aircraft. They are incorporated on production versions of several business jets for example and have been flight tested on the U.S. Air Force KC 135, and Douglas DC 10 (figure 17). In most cases they were designed following the procedures described in reference 17. While a reasonable close approximation of the most satisfactory configuration can be achieved without resort to wind tunnel tests, the tuning of the final still requires some experiments. In particular, the optimum toe in must be determined by a systematic test. Also for applications intended for high speeds the problems associated with the interference between supercritical flow fields over the inner surface of the winglet and the upper surface of the wing must be solved experimentally. This interference can cause a strong shock wave at the juncture of the winglet and wing whcih results in boundary layer separation in the juncture region. In several cases this problem has been eliminated by indenting the upper surface of the wing in the vicinity of the winglet. As for the case of the fuselage mounted nacelle described earlier, this is essentially a local application of the area rule. This special shaping is particularly important for applications to configurations with supercritical airfoils since the use of such airfoils results in supercritical flow velocities above the wing farther aft on the chord.

REFERENCES

1. Crowder, J. P.: Florescent Mini Tufts for Non-Intrusive Flow Visualization. MDC-J7374, McDonald Douglas Company, 1977.

2. Loving, Donald; and Katzoff, S.: The Florescent-Oil Film Method and Other Techniques for Boundary-Layer Flow Visualization. NASA MEMO 3-17-59L, 1959.

3. Blackwell, James A.: Preliminary Study of Effects of Reynolds Number and Boundary-Layer Transition Location on Shock-Induced Separation. NASA TN D-5003, 1968.

4. AGARD Fluid Dynamics Panel Specialists' Meeting on Wall Interference in Wind Tunnels. AGARD CP 335, 1982.

5. Thompson, Jim Rogers: Measurements of the Drag and Pressure Distribution on a Body of Revolution Throughout Transition From Subsonic to Supersonic Speeds. NACA RM L9J27, 1950.

6. Usry, J. W.; and Wallace, John W.: Drag of a Supercritical Body of Revolution in Free Flight at Transonic Speeds and Comparison with Wind-Tunnel Data. NASA TN D-6580, 1971.

7. Couch, Lana M.; and Brooks, Cuyler W., Jr.: Effect of Blockage Ratio on Drag and Pressure Distributions for Bodies of Revolutions at Transonic Speeds. NASA TN D-7331, 1973.

8. Whitcomb, Richard T.: A Study of the Zero-Lift Drag-Rise Characteristics of Wing-Body Combinations Near the Speed of Sound. NACA Rep. 1273, 1956.

9. Whitcomb, R. T.: Review of NASA Supercritical Airfoils. The Ninth Congress of the International Council of the Aeronautical Sciences, Haifa, Israel, Paper No. 74-10, 1974.

10. South, J. C., Jr.; and Jameson, A.: Relaxation Solutions for Inviscid Axisymmetric Transonic Flow over Blunt or Pointed Bodies. Proceedings of AIAA Computational Fluid Dynamics Conference, July 19-20, 1973, pp. 8-17.

11. Langhans, Richard A.; and Flechner, Stuart G.: Wind-Tunnel Investigation at Mach Numbers from 0.25 to 1.01 of a Transport Configuration Designed to Cruise at Near-Sonic Speeds. NASA TM X-2622, 1972. (Declassified)

12. Barnwell, Richard W.: Approximate Method for Calculating Transonic Flow about Lifting Wing-Body Configurations. NASA TR R-452, 1976.

13. Bartlett, Dennis W.; and Re, Richard J.: Wind-Tunnel Investigation of Basic Aerodynamic Characteristics of a Supercritical-Wing Research Airplane Configuration. NASA TM X-2470, 1972. (Declassified)

14. Harris, Charles D.; and Bartlett, Dennis W.: Wind-Tunnel Investigation of Effects of Underwing Leading-Edge Vortex Generators on a Supercritical-Wing Research Airplane Configuration. NASA TM X-2471, 1972. (Declassified)

15. Bartlett, Dennis W.; Harris, Charles D.; and Kelly, Thomas C.: Wind-Tunnel Development of Underwing Leading-Edge Vortex Generators on a NASA Supercritical-Wing Research Airplane Configuration. NASA TM X-2808, 1973. (Declassified)

16. Bartlett, Dennis W.: Application of a Supercritical Wing to an Executive-Type Jet Transport Configuration. NASA TM X-3251, 1975. (Declassified)

17. Whitcomb, Richard T.: A Design Approach and Selected Wind Tunnel Results at High Subsonic Speeds for Wing-Tip Mounted Winglets. NASA TN D-8260, 1976.

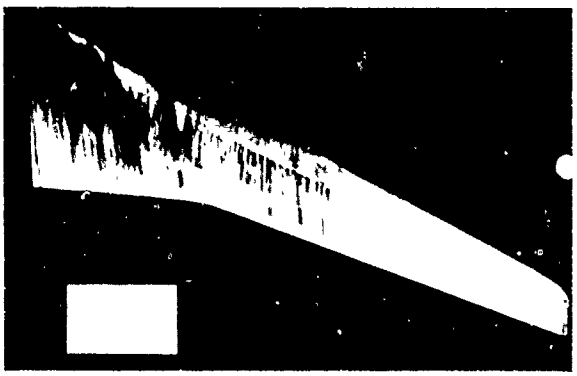

Figure 1.- Oil film study on high aspect ratio NASA supercritical wing at near cruise condition.

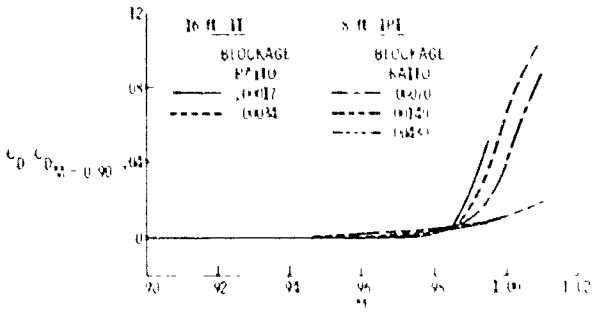

Figure 4.- Comparison of drag rise characteristics for supercritical bodies of revolution with various wind tunnel blockage ratios.

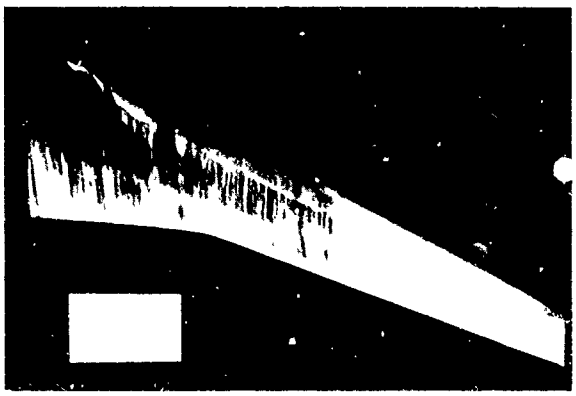

Figure 2.- Oil film study on high aspect ratio NASA supercritical wing at lift coefficient above cruise value.

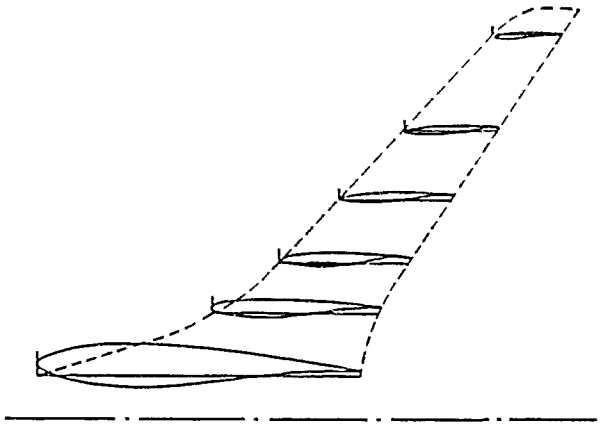

Figure 5.- Airfoil shapes for supercritical wing on near sonic transport.

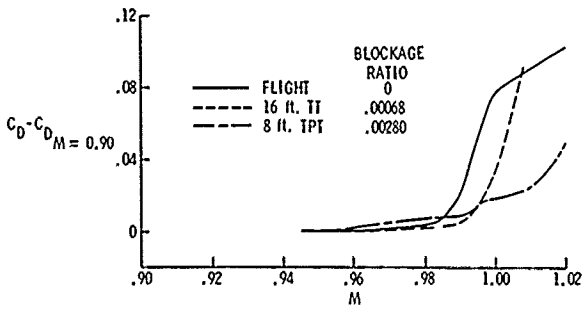

Figure 3.- Comparison of drag rise characteristics for supercritical body of revolution as measured in free flight and in wind tunnels.

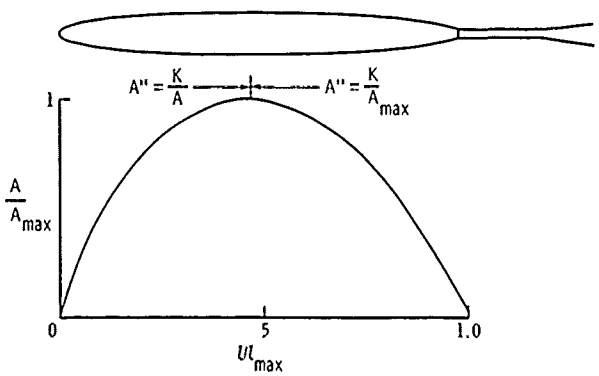

Figure 6.- Supercritical body of revolution.

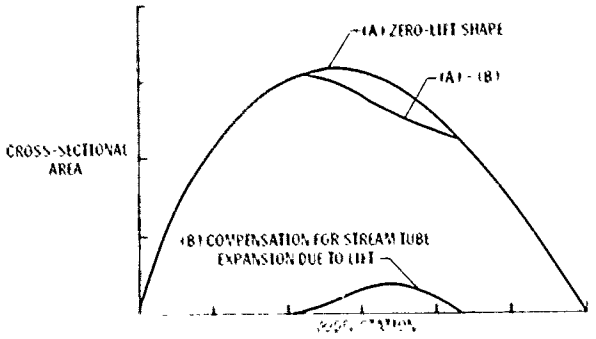

Figure 7.- Second order area-rule considerations.

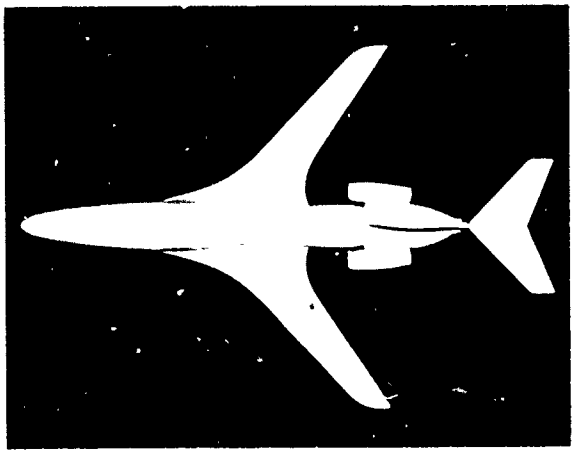

Figure 8.- Near sonic transport configuration.

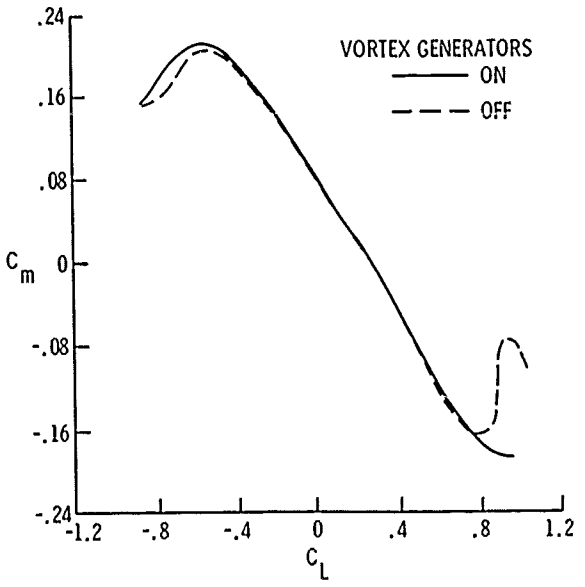

Figure 9.- Effect of leading edge vortex generators on pitching moment characteristics of supercritical wing at M = 0.95.

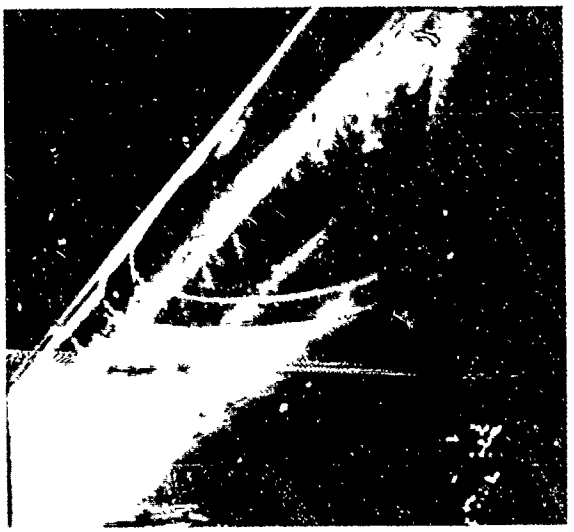

Figure 10.- Oil film study on wing upper surface without leading edge vortex generators at M = 0.95.

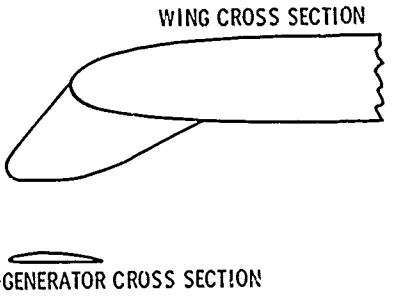

Figure 11.- Sketch of leading-edge vortex generator.

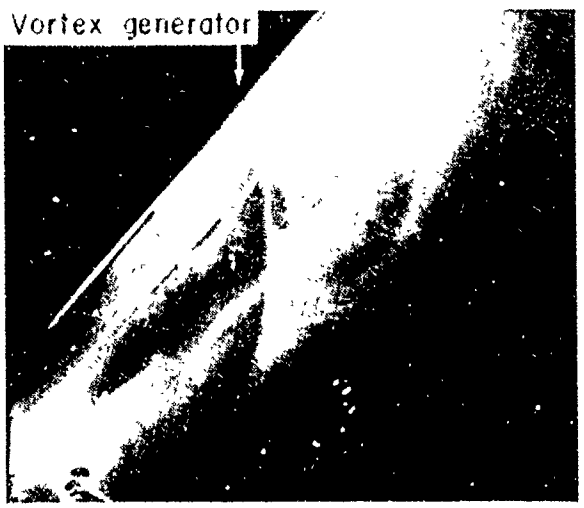

Figure 12.- Oil film study on wing upper surface with leading edge vortex generator at M = 0.95.

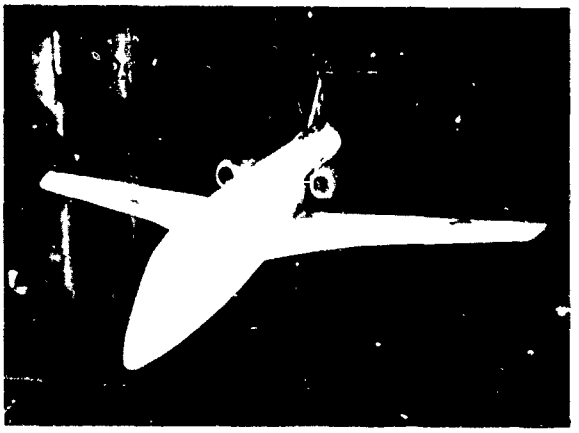

Figure 13.- Model of business jet with supercritical wing.

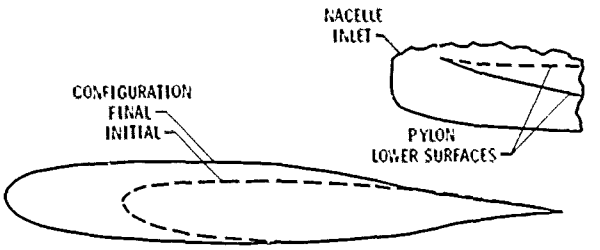

Figure 16.- Wing-root airfoil and pylon modifications for business jet.

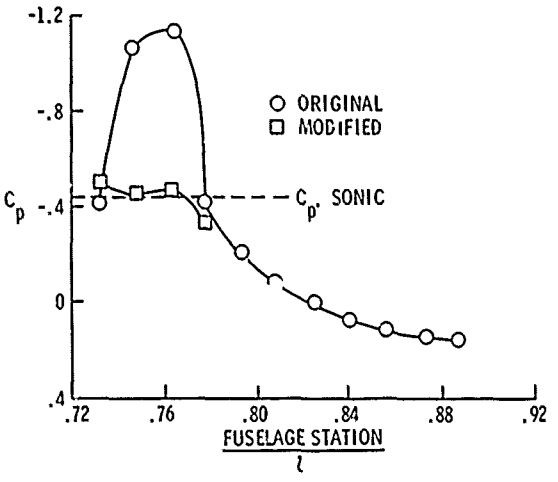

Figure 14.- Pressure distributions on side of fuselage of business jet, M = 0.80.

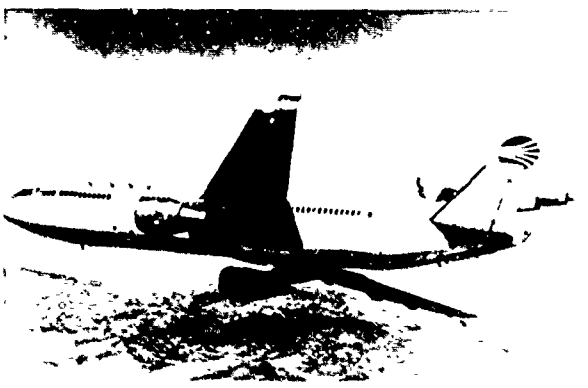

Figure 17.- McDonnell Douglas DC-10 with winglets.

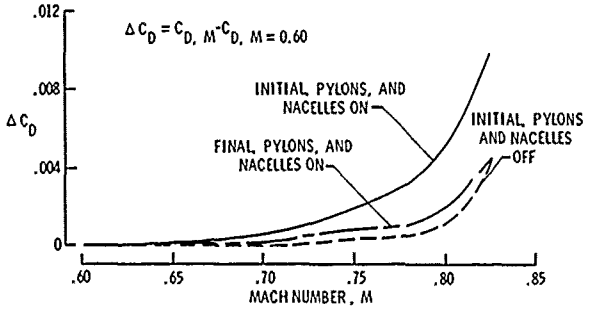

Figure 15.- Effects of wing-root and pylon modifications on drag rise characteristics for business jet, C_L = 0.25.

AERODYNAMIC INTERFERENCE - A GENERAL OVERVIEW

A B Haines
Chief Executive
Aircraft Research Association Ltd
Manton Lane, Bedford, UK

SUMMARY

This lecture contains a general survey of the sources of aerodynamic interference and shows how adverse interference can be avoided and favourable interference exploited in the optimisation of the design of complete configurations for modern civil transport and military combat aircraft. The survey is wide ranging, many concepts are introduced with suitable examples in the expectation that these will be discussed in more detail in subsequent lectures. The basic nature of wing-body interference is however discussed at some length since these effects are at the root of much of what is to follow. Naturally, there is considerable emphasis on means to reduce profile, vortex and transonic wave drag but it is also stressed that favourable interference concepts can be employed to improve usable lift for manoeuvre and to optimise stability and control characteristics at high incidence.

1 INTRODUCTION

The previous lectures in this course have reviewed the present state-of-the-art in advanced theoretical methods for the design of aircraft for high subsonic and transonic speeds, and have shown how to design two-dimensional wing sections and three-dimensional wings in isolation. We now turn however to the more complex task of optimising the design of a complete aircraft configuration with full regard for the aerodynamic interference between the flow over different components of the aircraft. This lecture contains a general survey of how interference can arise, the emphasis being on the physical nature of the interference rather than on the methods for calculating the flow. It is hoped that in this way, the lecture will serve to focus attention on ideas and concepts that will enable the designer to avoid adverse interference and to exploit favourable interference.

The lecture starts by considering the simplest case - the interference between a wing and fuselage in inviscid, incompressible flow. Viscous effects are then introduced and then, the effects in transonic, supercritical flow when the interference is no longer confined to the immediate vicinity of the wing-fuselage junction. Examples are included to show how, at high subsonic and transonic speeds, the flow over the entire wing can be affected significantly by interference from the fuselage. Adverse interference can be avoided or at least alleviated by appropriate shaping of the fuselage, by applying area rule principles, and by the use of suitable fairings in the wing-fuselage junction.

The lecture then considers other examples of aerodynamic interference in a complete aircraft configuration, eg

(i) between the wing and pylon-mounted nacelles or external stores,
(ii) between the wing and nacelles mounted on the rear fuselage,
(iii) between bodies in close proximity as for example, in an array of external stores,
(iv) in non-planar configurations such as a wing fitted with winglets or sails,
(v) between the flow over the wing and the flow field of a forward surface such as a canard or strake.

The lecture emphasises that for flight at high subsonic and transonic speeds, favourable interference is a real possibility. In other words, the interference between different flow fields can be exploited to produce

(a) a more highly swept isobar pattern over a given planform,
(b) more lift in regions where there is little risk that this will lead to more profile drag or wave drag,
(c) less lift-dependent drag
(d) less wave drag
(e) a more acceptable flow breakdown at high C_L and more usable lift

than would be achieved with the best possible wing design in isolation.

Many of the examples are drawn from the author's own experience. This is consistent with the aims of the lecture series; the author is well aware that similar examples could have been drawn from other sources, as will be evident in later lectures.

2 WING-BODY INTERFERENCE: INVISCID, INCOMPRESSIBLE

In the classical concept of aircraft design, the wings provide lift and the fuselage provides volume. Originally, it was believed that these functions could be discharged independently. This principle was first enunciated by Sir George Cayley [1] in 1810 and apparently confirmed in papers by Lennertz [2] and Vandrey [3] in 1927 and 1937 who claimed that the lift on an unswept wing mounted centrally on a simple fuselage treated as a sphere would be the same as on the wing without the fuselage. However, it has now been known for more than 30 years, that these early analyses are oversimplified and indeed, misleading. Interference effects are in fact present even in the simplest case. incompressible, inviscid flow past a wing mounted centrally on a fuselage of circular cross-section. Clearly, the effects are largest in the actual wing-fuselage junction and they decay rapidly with distance out along the span. They have been described in depth by Küchemann [4,5] but for the sake of completeness, some of his quoted results are reproduced here in Figs 1-4.

Let us consider first displacement effects at zero lift ignoring for simplicity the flow around the fuselage nose. For an unswept wing of finite thickness t mounted in a mid position on a fuselage of radius R, assuming that R is not dramatically greater than t, the wing-fuselage intersection will be waisted and as a result, even in inviscid flow, the velocities in the junction will be reduced relative to the values further out on the span. These interference effects could now be calculated for any specific case by means of

computer programs based on one of the several available panel methods but the calculated results presented by Küchemann [5] were obtained by the earlier method [7] of Weber in which sources were placed inside the body (and wing) and correcting sources were then introduced on the surface of the body in order to ensure zero velocity normal to the body surface. Approximate second-order numerical solutions of the resulting integrals were developed and results for two wing-fuselage configurations are shown by curves 1 in Fig 1. These predicted results for inviscid flow cannot be compared directly with the experimental measurements of Körner. [6] However, by adding the predicted inviscid interference to Körner's measured results for the wing mounted on a flat plate (curves 2), one obtains curves 3 which, as can be seen, are in reasonable agreement with the measured results for the wing-fuselage. This serves to confirm the predictions for the interference on the reasonable assumption that at zero lift, the viscous effects are similar for the two cases (wing-plate and wing-fuselage). As would be expected from the association with the curved intersection lines in the wing-fuselage junctions, the reduction in velocity in the junction is greater for the case with the smaller fuselage. Two important conclusions for wing-fuselage design can already be drawn from these simple examples:

(i) it is likely that this form of wing-body interference will permit an increase in wing thickness/chord ratio in the junction,
(ii) the velocities on the wing upper surface will tend to be lower for high wing than for low wing layouts.

Similar calculations [7] showed that this interference velocity increment (strictly, decrement) in the junction varies with wing sweep as shown in Fig 2a, ie in a manner broadly similar to the effect of sweepback on the velocity distribution at zero lift at the centre section of a symmetrical three-dimensional wing. Fig 2b contrasts these two effects for an example where calculations [8,9] and experimental measurements [10] were made for a tapered wing of 30° midchord sweepback, aspect ratio 6 and a 9% thick RAE section, tested either as a wing-alone or mounted on a fuselage with R/c = 2/9. The chordwise pressure distribution at 0.4 x semi-span is little affected by the wing-body interference but in the junction, as with the unswept wing of Fig 1, the velocities are again reduced. However, in this simple case with a sweptback wing, of constant section shape across the span, mounted on a fuselage with no change in cross-sectional radius opposite the wing, the wing-body interference accentuates the distortion in shape of the chordwise pressure distribution in the junction. In passing, it is worth noting that Fig 2b contains a comparison between results calculated by an early version of the RAE standard method subsequently published [9] by ESDU and by the panel method of Hess and A M O Smith. [10] Better results would probably be achieved by modern panel and transonic methods particularly at M = 0.8 bearing in mind that only approximate allowance for compressibility effects was included in these early calculations.

Küchemann [5] pointed out that it was convenient to think of the velocity in the junction being expressed in the form

$$V_J(x) = V_O + v_B + v_J + v_S + v_C \qquad (1)$$

where
V_O = freestream velocity
v_B = contributions from forebody and afterbody
v_J = wing-body interference contribution being discussed here
v_S = velocity increment over infinite sheared wing
v_C = velocity increment due to centre effect.

As we have seen, v_J is negative for a body with no special shaping but equation (1) is an easy way of demonstrating how shaping of the body and thus, modifying the interference effects can be turned to positive advantage. For example, choosing the fuselage to give $v_J = -v_C$ will restore the pressure distribution to be the same as on the infinite sheared wing in the presence of the forebody and afterbody. Since v_J is generally negative and v_B positive, one might achieve $v_J + v_B + v_C \leq 0$ and thus, a flow near the junction that has more effective sweep than on the corresponding infinite sheared wing of constant section. These remarks serve as a simple introduction to the concepts of favourable wing-body interference developed in more detail later in the lecture.

Turning now to the lifting effects in inviscid, compressible flow, Weber [11] was one of the first to give an explanation for the mistaken concept of zero interference referred to earlier. The wing flow is modified by the velocity field of the sources representing the fuselage, this field induces zero downwash at any given line vortex but (and this is the essential point) the downwash distribution does not approach zero as the line vortex is approached from either side. Therefore, representing the wing loading by a chordwise distribution of bound line vortices leads to a non-zero change in the chordwise and spanwise loading due to the wing-body interference. The effects on the spanwise loading for an unswept rectangular wing mounted on a cylindrical fuselage are shown in Fig 3; it is clear that the interference effects as calculated by Weber [11] are in close agreement with the measured results of Körner. [6] The interference can be termed 'adverse' in the sense that if no change is made to the wing or body design, the region of the wing near the junction will not carry its fair share of the total lift; allowance for the effects should be made when choosing the camber and twist for the wing design or to put the conclusion in the language of modern transonic theory, wings should be designed by wing-body programs or at least, wing-alone programs with boundary conditions at the root representing the flow past the fuselage.

3 WING-BODY INTERFERENCE: VISCOUS EFFECTS

It is likely that most newcomers to the subject of aerodynamic interference think first of the adverse viscous effects which are frequently observed when a wing is mounted on a body. All readers will have seen pictures showing the flow over an inner wing disturbed by interference from a relatively thick boundary layer on the side of the fuselage, and vortices forming ahead of the wing root leading edge and trailing along the side of the fuselage above or below the wing. Such pictures emphasise the need for fairings to eliminate these potential sources of interference drag.

To begin with a simple example, let us return to Fig 1 which presents some measured results (curve 2) for a wing mounted on a flat plate. In the junction, the pressure coefficients are only about 80% of the values on the wing well away from the junction. This reduction must be related to a viscous effect that is more complex than just a local thickening of the wing boundary layer. Secondary flows can develop [12] in

the corner and may tend to promote separation near the trailing edge. Such separations are observed in aerofoil tests in two-dimensional tunnels and this is why suction through the side walls of the tunnel is employed to obtain reliable values of $C_{L_{max}}$ in an allegedly two-dimensional test.

The spacing of the points along curve 2 in Fig 1 is however not sufficiently close to reveal all the interference effects. The variation in C_D as the junction is approached on either the wing or the plate is not necessarily as regular as suggested by Fig 1. This is illustrated in Fig 4 which presents some results by East and Hoxey [13] from tests in which the model was large enough and the pressure points close enough to pick up the suction peaks induced by the concentrated vorticity of the vortex sheets shed ahead of the wing leading edge. The physical explanation of the origin of these vortices lies in the fact that the boundary layer on the plate ahead of the round wing leading edge cannot negotiate the pressure rise to the stagnation point on the wing without separating. There is therefore a three-dimensional separation, from a separation line on the plate, which trails as a vortex sheet or rolled-up vortex along the junction. In the results in Fig 4, the centre of the vortex is within the plate boundary layer which can no longer be regarded as a simple boundary layer but in other examples to be considered later, the size and strength of these vortices are evidently much greater.

These viscous flows in a wing-plate junction have been extensively studied at Queen Mary College at London University and some leading results and flow photographs from these experiments were discussed by Young in his 20th Ludwig Prandtl Memorial Lecture [14] in 1977. A study of the flow in a right angled streamwise corner with fully turbulent boundary layers confirmed earlier studies by Prandtl and others that there was a secondary flow pattern in the corner with an inward flow towards the corner in the plane of symmetry in the boundary layer and outward flows close to the walls. As a result, the streamwise growth of the boundary layer thickness on the horizontal wall close to the corner was less than further outboard. However, in the present context, the interference effects due to the vortices which form ahead of the wing leading edge in a wing-plate or wing-fuselage junction are potentially more serious. The research [14] at QMC included tests on a simple wing-body, traverses immediately behind the wing trailing edge showed that the fuselage boundary layer and wing wake were merging smoothly but a traverse further aft indicated a much more confused picture with a considerable region having low total head pressure. Extra downwash destroyed the expected lift contribution from the rear fuselage; as a result, the wing incidence would have to be increased to achieve a given total lift; a good example of how adverse interference drag can arise.

A more recent experiment [16] at a larger scale has been undertaken at RAE on a model of the configuration shown in Fig 5a. An untapered, 25° sweptback wing of aspect ratio 6 was mounted in a mid position on a fuselage of circular cross-section with dimensions representative of a wide-bodied transport design. Leaving aside the flow field of the model support arrangement, the comprehensive pressure and flow angle traverses in the wake of this configuration showed that there were as many as 3 vortex pairs in the wake downstream of the fuselage/wing root. Typical streamwise vorticity contours in this region are presented in Fig 5b. The three relevant vortex pairs are identified by A, A'; B, B' and C, C'; D, D' should be ignored. All these vortex pairs lie within the $\Delta H/q_0 = 0.025$ total head deficit contour but in the centre of the vortices in the strongest pair, A, A', $\Delta H/q_0 > 0.70$. A and B evidently originated in the upper and lower wing root junctions while C appeared to spring from the top shoulder of the forward fuselage. Limited traverses further forward suggested that the strongest pair A, A' remained highly concentrated along the parallel part of the fuselage but then diffused rapidly under the influence of the adverse pressure gradient on the rear fuselage, migrating upwards to the positions shown in Fig 5b.

Intuitively, one would expect that these vortices would be responsible for significant interference drag. In many cases such as those to be discussed below, this is true. However, this is not always the case and indeed, the lift-dependent drag derived from the traverses for the configuration in Fig 5 was about the same as that obtained from earlier traverses for the same wing tested as a wing-alone without fuselage. Priest et al in their detailed analysis [16] of these results, concluded that the vortex lift-dependent drag was higher for the wing-body configuration but that this increase was offset by a reduction in the profile drag-due-to-lift. They suggested that this reduction was associated with the strong inwash flows generated by the wing-root vortices (and the flow convergence over the rear fuselage).

Despite this reassuring result, there can be little doubt that the use of fairings to weaken or eliminate these wing-body junction vortices will be beneficial in many cases. The issue to be decided in practice is whether the ability of a fairing to reduce the adverse interference drag is worth more than the penalty of the extra weight. A thick wing mounted on the top of the fuselage as in Fig 6a is a particularly good example of where large adverse interference drag is present if no fairing is employed. Tests were made [17] in the ARA transonic tunnel in 1964 on this configuration with no fairing and with a number of different fairing designs. For the without-fairing case, the wing was simply added to the top of the body with merely a small 0.03" radius in the underwing junction. Fairing A was designed as an envelope of local wing flow streamlines except that for practical reasons, the full waisting could not be adopted below the rear of the wing. Fig 6b shows that this streamline fairing A although small was successful in reducing C_D, by as much as 0.0010 under certain conditions. Oil flow patterns showed however that the flow was still separating on top of the fuselage just ahead of the wing leading edge and as a result, a relatively strong pair of vortices trailed back along the side of the fuselage as shown in the upper photograph in Fig 6c. Larger fairings were then developed, culminating in fairing B, Fig 6a, which virtually converts the configuration into a shoulder wing layout and eliminates the re-entrant corners in the junctions below the wing. The oil flow pattern in the lower photograph in Fig 6c indicates that the flow along the side of the fuselage is still dominated by the wing interference but the nature of the interference is significantly different from that in the upper picture. The dividing streamline between the flow from the forward fuselage and the flow around the immediate wing leading edge can be clearly seen but there is no sign of the herring-bone pattern under a vortex. The improved flow is reflected in the sizeable reductions in drag evident in Fig 6b: typically $\Delta C_D = -0.0010$ at $C_L = 0.2$ or -0.0025 at $C_L = 0.5$, relative to the values for the original wing-body without fairing. The actual reductions in interference drag must be even greater since the configuration with fairing B clearly has a larger surface area. Comparisons of the results for fairing B with estimates suggested that the remaining interference drag was trivial.

This thick high-wing configuration considered in Fig 6 should not be dismissed as an isolated, extreme example. The lessons are still relevant to the design of modern transport aircraft. Jupp [18] in 1980

emphasised that the present trend towards exploiting advanced wing technology in terms of greater wing thickness/chord ratio particularly at the wing root, has accentuated the need for, and value of, wing root fillets. Jupp contrasted t . .perience with the A300 and A310. Fig 7a shows the wing root section of the A310 with the outlines of the root fillets incorporated on the A300 and A310. Developing a leading edge fillet completely to suppres, the vortex pair ahead of the root leading edge gave a reduction of 1.5 in the cruise drag of the A310 with its relatively thick root section compared with only 0.5 for the A300 and the reductions in drag achieved on the A310 with the larger A310 fillets compared with those for the A300 are quoted on Fig 7a. The smooth flow on the A310 leading edge fillet is shown in Fig 7b.

Other examples could doubtless be adduced and clearly, for transport aircraft in particular, the art of fillet design should not be forgotten as a means of eliminating adverse interference drag. The word 'art' is used advisedly. ·id generation techniques and methods for allowing for viscous effects, eg Euler solutions, will have to advance much further before the design of fillets and fairings can be handled solely by a theoretical approach. At present, the best results are still obtained by the experienced experimental aerodynamicist who has a feel for what constitutes a 'good shape' and a 'smooth flow'. His aim will be to

Eliminate flow separations including those that lead to stand-off vortices,
Alleviate strong cross-flows in the boundary layer,
Merge different airstreams as smoothly as possible,
Avoid gross thickening of different boundary layers and wakes.

Much can be achieved in a low speed tunnel or even in a water tunnel. [19] A good general rule is that although in a poor junction or on an unsatisfactory fairing, flow separations are often observed at the rear, the trouble spot to be tackled by the designer will be at the front.

It should be noted that fairings and fillets can be - and often are - used not merely to eliminate adverse interference as above but also as a means of introducing favourable interference. The flow field round them can serve to induce extra lift on the wing in regions where otherwise, the local velocities are low. As a result, the critical section of the wing can be unloaded for a given overall C_L, and drag-rise and buffet boundaries improved. Flap track fairings are a good illustration. These are also discussed by Jupp [18] who showed that for both the A300 and A310, it was possible to design flap track fairings that were successful in delaying the wing drag-rise with Mach number to an extent that within the cruise flight envelope, addition of the fairings actually reduced the total aircraft drag. In both cases, the successful fairings increased C_L at a given incidence and Jupp concludes [17] that this favourable effect is critically dependent on the size and shape of the fairings near the wing trailing edge. It is intriguing that an optimised configuration is not necessarily the one that succeeds in hiding its flap supports within the wing!

4 WING-BODY INTERFERENCE: EFFECTS AT TRANSONIC SPEEDS

4.1 Influence of Body on Wing Flow

The general aims of many high speed wing designs can be summarised as follows:

(i) for a transport aircraft, to carry the required lift in the cruise with as little wave, viscous and vortex-induced drag as possible, with an adequate margin to buffet while meeting all practical constraints,

(ii) for a military combat aircraft, to carry as much lift as possible on the sustained manoeuvre boundary as defined by a certain level of wave drag, and on the instantaneous manoeuvre boundary beyond which the flying qualities create problems, or in other words, high C_L for both a certain level of wave drag and separation onset and a reasonable stall development beyond separation onset.

The wing-body interference effects already discussed remain relevant. In principle, the effects were present even in low speed flow but their consequences can be far greater at high speeds. Any reduction in lift or effective sweepback due to an interference effect near the wing-body junction, if uncorrected in the design process, would tend to degrade the wing design performance as described above but the changes with Mach number are not just a question of degree. When the flow is transonic, effects which were confined near the junction at subcritical speeds, can propagate laterally and affect the flow over the complete wing - even a high aspect ratio wing of a typical transport layout. The presence of the body clearly modifies the flow over the wing near the root and as appreciated rapidly by every theoretical designer of a sweptback wing, conditions near the root rapidly modify the flow over the rest of the wing. It is now generally accepted that advanced wings should be designed whenever possible by wing-body programs and it has been an urgent need in recent years to develop programs capable of handling complex body shapes and arbitrary wing-body settings and positions.

Many examples could be quoted at this point but two should suffice: first, a simple case shown in Fig 8 and second, a more realistic combat aircraft design in Fig 9. To consider Fig 8 first, tests were made in the ARA 9ft x 8ft transonic tunnel on a half-wing model, 25° sweptback, untapered, the same section shape throughout and mounted on a parallel half-fuselage with the nose section sufficiently far ahead that its influence on the wing flow can be safely ignored. Calculations of the pressure distribution for the station marked $\eta = 0.37$ at $M = 0.86$, $\alpha = 4.2°$ were made by the Forsey wing-alone [20] and wing-body [21] full potential programs and compared with experimental data. Good agreement is shown in Fig 8 with the wing-body calculations, both calculation and experiment showing forward and rear shocks but the supercritical development is quite different in the wing-alone calculations irrespective of whether the wing is treated as a nett wing or a gross wing. Arguably, the gross wing results can be dismissed simply on the grounds that the wing root is clearly not at the model centre line but the change to the nett wing assumption was found to make little difference. One is left with the conclusion that the experimental data are significantly affected by wing-body interference, viz a lack of full reflection effect at the wing root. Whether the interference in this case should be regarded as adverse or favourable is not obvious.

The second example in Fig 9 is a clearer illustration of the possible influence of the fuselage on the wing flow at transonic speeds. Tests were made in the ARA transonic tunnel on a model of a combat aircraft research wing mounted on two alternative bodies of about the same width but different cross-section shape, length and streamwise curvature. These results were first presented by Treadgold and Wilson [22]. For simplicity, one is described as the square body and the other as the elliptic; as shown in Fig 9a, the latter is fitted with some fairings designed to suppress some locally undesirable flow features in the wing-body junction. In both cases, the wing was mounted in a high position. The elliptic body configuration was designed first and served as the basic model for the fairing experiment to be described later in §4.3. The longer square body followed later specifically as a vehicle for obtaining test data to compare with, and validate theoretical methods. Viewed as an aerodynamic shape for a real aircraft, the configuration with the square body appears unattractive. it has greater volume and surface area and indeed, at C_L = 0.45, C_D at low Mach numbers is about 0.0070 higher than for the configuration with the elliptic body. However, in the context of the present lecture, the significant point in the measured wing pressure distributions in Fig 9b is that the shock strengths at either a given incidence or given C_L (by interpolation) were much weaker with the square body. The shorter length and continuous streamwise curvature of the elliptic body may play a large part in this comparison as they would both tend to increase the oncoming stream Mach number ahead of the inner wing leading edge. The effect of the fuselage design is still evident as far out as 0.83 x gross semi-span. It clearly affects the spanwise position of the intersection point of the 3-shock pattern and as a result, the buffet characteristics and stall development at this Mach number (M = 0.87) could be very different. The difference in C_D at C_L = 0.45 quoted above as being 0.0070 at low Mach number is only 0.0054 at M = 0.87 and less than 0.0030 at M = 0.90. This relative improvement of the square body with Mach number should be ascribed to the lower shock strength evident in Fig 9b offset partly by the fact that the local velocities on the wing lower surface at a given incidence would be higher with the square body with its extra volume, thus tending to reduce the lift at a given incidence.

Examples such as those discussed above show not only that wings should be designed by wing-body programs but that these methods should allow realistically for the detailed size and shape of the body. Simplified representations of the body may yield misleading results in shock strength and position and their variation across the span. Naturally, these remarks relate more to combat aircraft wings of moderate aspect ratio than to subsonic transport aircraft where the design Mach number is likely to be lower and the fuselages are of simpler shape with the forebody and afterbody further from the wing. Nevertheless, the Transonic Symposium conference proceedings [23] contain several examples where, even for transport aircraft, weaknesses in theoretical calculations can be ascribed to lack of proper representation of the body interference.

4.2 Area Rule

No overview of aerodynamic interference and in particular, of means to exploit favourable interference would be complete without a reminder and tribute to what area rule theory has achieved and what it can achieve. The original references [24-27] on the subject date from the 1950s but in the last 10 years, there has been renewed interest both in extending the theoretical formulations [28,29] and in highlighting the benefits of applying area rule principles not merely to the design of complete configurations but also to local arrangements of components such as arrays of external stores. [30]

The basic concept is so well known that it hardly needs any recapitulation. Put briefly, the transonic drag rise is related to the longitudinal distribution of the cross-sectional area of the aircraft. In the far field at M = 1.0, the flow field of the aircraft is the same (to the first order) as that of the equivalent axisymmetric body with the same cross-sectional area distribution, S(x). To minimise the drag, $S(x)_{max}$ should be as small as possible and the changes in S(x) with x, as gradual and smooth as possible. In other words, the fuselage of the aircraft should be waisted opposite the wing, tailplane/canard and other components. The resulting shapes of the wing-body junctions are not unlike those that would have been derived from the methods discussed in §2 and applied to conditions at transonic speeds. In the 1960s, the advocates of these two approaches did not always realise that both were in fact needed. Area rule can provide a guide to the required shapes but the objectives would not be achieved if the shapes were so severe and the adverse pressure gradients so great that a flow separation occurred. Even with the help of area rule, therefore, calculations of the pressure distributions and boundary layer growth are still needed and the shapes will need refinement in the light of these calculations. The effects of finite thickness, high design lift coefficients (particularly for combat aircraft), complex shapes, the need to optimise for a range of design conditions: all these are factors which must affect the choice of a final optimum shape. Theoretical methods for transonic flow, if developed to deal with bodies of arbitrary shape, will offer the opportunity for a genuine understanding of why one shape is better than another.

One of the best experimental demonstrations in the published literature of how area rule is effective is still that presented by Kane and Middleton at an AGARD meeting in 1971. Relevant pictures from this paper are reproduced in Figs 10a,b. Admittedly, the design Mach number for the area-ruled body in this case is M = 1.4 rather than M = 1.0 but this does not in principle affect the inclusion of the example in this lecture. The favourable reduction in wave drag from the change from the Sears-Haack to the area rule body is shown in Fig 10a and then, Fig 10b provides the understanding. The pressure field of the area ruled body propagates across the wing inducing negative pressures on forward facing surfaces and positive pressures on rearward facing surfaces. Integration of the measured pressure distributions gives results consistent with the overall drag data and shows how the body shaping has created the favourable interference.

Area rule as originally specified strictly applied to the zero-lift condition. At lift, the transonic flow past the wing gives a further expansion of the streamtube and additional area should therefore be incorporated in the equivalent axisymmetric body. Theoretical studies of these lifting effects have been made by both Cheng and Hafez [32] and Barnwell [28,29] and recently, an experimental programme to compare with these theoretical predictions has been undertaken [33] at NAE Ottawa. Tests were made on models of the configurations shown in Fig 11a. The wings of WB1 and WB2 have the same longitudinal distribution of cross-sectional area, ie the greater span of the wing of WB2 is compensated by extra thickness in WB1. Body B1 is equivalent to WB1 and WB2 according to classical area rule, ie at zero lift, and B2 with its larger bulge is equivalent to WB1 and WB2 at C_L = 0.37, M_∞ = 0.975 according to the formulae developed by Hafez [32] and reproduced by Chan. [33] These formulae dictate that a design Mach number has to be chosen

but the change in body shape with design Mach number is small, the variation in S_{max} with a change from M = 0.8 to M = 1.1 being only 10 .

Comparisons of the measured drag from these tests are presented in Figs 11b,c. They are encouraging. At zero lift in the upper picture, the variation of the wave drag coefficient, ΔC_{D_0} with M_∞ for WB2 with its 4.4 thick wing is almost identical with that of the equivalent body B1; for WB1 with its 8 thick wing, the transonic drag rise is about 10 greater, presumably because of the stronger shock on the thicker wing. The corresponding comparison for C_L = 0.37 in the lower picture is broadly similar although numerically, not as good because the wave drag of B2 is less than that of WB2 as well as WB1. Chan concludes however that these results do not invalidate the formulae for the lifting effects; rather, he ascribes the lower wave drag of B2 to the observed presence of a flow separation on the rear of the larger bulge which has served to weaken the shock on B2 relative to WB1 and WB2.

The results of these basic research experiments therefore provide experimental support for area rule but even for the simple configurations in Fig 11, viscous effects are already intruding into the comparisons. The next section, §4.3, extends the discussion to the effects of body shaping for configurations closer to a real aircraft.

4.3 Favourable Interference from Body Waisting

Only limited opportunities for exploiting favourable interference through body shaping can be found in subsonic transport aircraft design. First, the design cruise Mach numbers have rarely exceeded M = 0.80 and second, the requirements for a pressurised cabin obviously rule out any idea of an indented fuselage. To add bulges to the fuselage opposite the wing leading and trailing edges will only give a nett benefit if the favourable interference outweighs the extra profile drag associated with the increased surface area. Nevertheless, the fillets and fairings discussed earlier as a means of alleviating adverse viscous effects and inducing extra lift on 'safe areas of the wing surface' frequently improve the aircraft area distribution and thus, weaken the shock on the inner wing. If, however, design cruise Mach numbers had increased to nearer M = 1.0 - as was expected in the early 1970s ahead of the first fuel crisis - a shaped fuselage would probably have been an essential element of any viable transport design. Results [34] for such a configuration are presented in Fig 12.

The plan geometry of this near-sonic transport design is shown in Fig 12a. A complete model was first tested in the ARA transonic tunnel with a simple parallel fuselage and the C_D - M curve in Fig 12b falls well short of the design target of cruising efficiently at M = 0.95. If the three-dimensional wing design had been successful in achieving the performance of the equivalent two-dimensional section converted merely on the basis of the mid-chord sweepback, a cruise Mach number of more than M = 0.96 would have been possible. A shortfall of this magnitude would not necessarily occur if this design exercise were repeated in 1983. This particular three-dimensional wing was designed in 1972 before any of the present methods for transonic flow calculations became available. The model with the parallel fuselage was tested in 1974 and by then, the first transonic small perturbation (TSP) method had been developed at RAE. [35] This provided an opportunity to improve the configuration. It was still felt that any revised wing design would be in difficulty meeting the ambitious design target. It was feared that extreme and unacceptable changes in geometry would be needed if all the treatment was confined to the wing. The more attractive option was to study what could be achieved with a shaped fuselage - described in Fig 12 as a 'waisted fuselage' but in reality, including bulges fore and aft of the wing with a concave region in between as shown in Fig 12a. The longitudinal distribution of the cross-sectional area of the configuration with the waisted fuselage is not smooth in a detailed sense but is clearly more uniform than the distribution for the original wing + fuselage. On area rule principles, it should have less wave drag near M = 1.0 than the original, despite the increase in S_{max}. The measured drag results plotted in Fig 12b confirmed these hopes: the M = 0.95 target was achieved at the expense of an increase in drag at lower Mach numbers such as M = 0.90 (accentuated at higher C_L, not shown in Fig 12b).

Despite present lack of interest in a near-sonic transport, it is worth discussing this example in more detail as it illustrates some useful general points. First, some comments on the design of the fuselage bulges. Calculations were first made of the flow field around the isolated body and the local stream directions from this calculation were specified as boundary conditions at grid points used by the TSP program for calculation of the flow over the wing treated as a nett wing alone: a useful expedient particularly in 1974 when there were no wing-body programs and even now, perhaps useful in gaining an appreciation of the effects of small changes in body shape. Comparison of these results with those calculated with zero slope boundary conditions in the root reflection plane, ie for the low wing on the parallel fuselage, suggested that the waisted fuselage would succeed in its main design aims to weaken and move forward the aft shock on the inner wing. The measured results for M = 0.95 presented in Fig 12c confirm that these aims have been achieved. At M = 0.90, however, the corresponding results in Fig 12d show that the strength of the shock wave on the forward inner wing has been increased by the flow field induced by the forward bulge - hence, the somewhat greater wave drag in this condition. Several flow field calculations and iterations of shape had to be performed for the body alone, primarily to obtain a satisfactory flow over the rear bulge.

The general lessons from this exercise include the following:

1) Area rule can provide a general guide to the shape of body that will give favourable interference - substantial in this particular case but calculations of the transonic flow over both the body alone and the wing-body combination are needed to refine the shape.

2) When the flow is supercritical, the body flow field propagates much further out (and rearward when the wing is sweptback) than would be expected simply from the body-alone calculations.

3) Even with a wing of high aspect ratio, the body effects can therefore extend out to near the wing tip: in the present case, a forward movement of the shock from about 0.65c to about 0.55c was observed at 0.9 x semi-span at M = 0.95.

4) The benefits of the fuselage shaping can vary with M (and C_L) and the benefits and indeed, possible penalties in different conditions have to be assessed against the aircraft requirements. The

interference design problem thus is complex and unlikely to be soluble with any simple numerical optimisation routine.

5) Body shaping offers an extra design freedom and favourable interference is possible relative to the best possible three-dimensional wing mounted on the basic unshaped fuselage with the same forebody and afterbody. For the reasons given earlier, it may not be possible to exploit this conclusion to any major extent with the fuselage of a civil transport cruising near M = 0.80 but as will be seen later, the propulsion installation offers real possibilities. The words 'favourable (or adverse) interference' have to be used carefully. The overall effect of the fuselage is still likely to be adverse because the wing has to operate in a stream where the Mach number has been increased by the expansion of the flow round the forebody and afterbody. Jupp [18] points out that for an aircraft such as the A310, this effect can amount to about 0.015 in Mach number. Some favourable interference from fillets, fairings etc and a good propulsion installation are needed to keep the adverse interference in the complete aircraft drag-rise boundary relative to that for the wing alone to no more than 0.02 ~ 0.025 in Mach number.

Turning to a second example taken from tests in the ARA transonic tunnel on the combat aircraft research model discussed earlier, the configuration with the elliptic fuselage was tested with the alternative fairings on the body above the wing shown in Fig 13a. The results of these tests have been discussed in detail by Treadgold and Wilson [22] but the salient points of their analysis are repeated below with supporting evidence in Figs 13b-e.

The two fairings have roughly similar cross-sectional area distributions. Neither fairing has any serious pretension to being an optimum shape from a drag standpoint and in fact, the measured drag values differ significantly. Fairing A was designed to conform mostly to a stream surface of the gross wing flow field while fairing B attempted to preserve a junction with the wing that resembled the streamline over the wing at 0.4 x semi-span at the design condition at M = 0.87. Fig 13a shows that fairing B had a slightly greater cross-sectional area than A but estimates suggested that this difference would only give ΔC_D = 0.0003 at M = 1.0 and can therefore be ignored.

Fig 13b shows that the measured values of C_D are much lower (by as much as 0.0020 under certain conditions) with fairing A; the lower pictures show that these lower values of C_D can be related to a weaker strength of the rear shock over much of the span. The differences are greater on the inner wing and can be seen more clearly in the comparisons in Fig 13c for the wing upper surface pressure distributions at 0.24 x semi-span for a range of C_L at M = 0.87. In terms of local C_L, weaker suctions ahead of the rear shock with A are compensated by higher suctions further forward and these beneficial effects propagate further outboard to give the higher sweepback on the isobars shown in Fig 13d for fairing A. Courageously, Treadgold [22] integrated the differences between the pressure distributions for A and B and confirmed that the better overall drag with A could be related to these changes in wing pressure distributions. Fig 13e reproduces one of Treadgold's comparisons showing how well the analysis supports this conclusion. Fig 13e also illustrates how the effects of the fairing design spread over more of the wing span as the Mach number is increased from M = 0.825 to M = 0.925. One could sum up this comparison by saying that fairing A has produced favourable interference relative to a design (fairing B) that attempted to produce the flow over an infinite sheared wing.

This is a good example on which to end this discussion of wing-body interference. It has shown the extreme sensitivity of the wave drag at high subsonic speeds and moderate C_L to the precise details of the wing-body fairing and the need for calculation methods that will model the complex geometry and viscous effects near the junctions if there is to be any hope of obtaining a truly optimised design.

5 EXPLOITATION OF FAVOURABLE INTERFERENCE IN CONFIGURATION AERODYNAMICS: DRAG

5.1 Pylon-Mounted Underwing Nacelles

Many experimental studies have been undertaken to optimise the design of pylon-mounted underwing nacelle installations. It is an extremely complex subject and as yet, not fully amenable to theoretical treatment, further, because of the very large number of variables it does not readily lend itself to rigorous experimental optimisation. A later lecture in this series is being specifically devoted to this topic but it is such an outstanding example of aerodynamic interference in a practical situation that this overview would not be complete without also including some detailed discussion of the subject.

There are many sources of interference drag in an underwing nacelle installation and most of them are interrelated. Some clearly contribute only to adverse interference and indeed, the modest aim of many of the studies has been merely to find an installation that avoids any serious adverse interference. However, it is now clear that for several reasons, favourable interference is a real possibility with a well designed installation under appropriate operating conditions. favourable not merely relative to the clean wing without nacelles but also relative to the best clean wing of the same planform.

Fig 14 lists some of the main features of the wing/pylon/nacelle flow field in a case with some adverse interference components. The most obvious source of aerodynamic interference is the flow through the channel formed by the wing lower surface, the pylon, and the nacelle or nacelle efflux. It would however be simplistic and misleading to imagine that all interference drag is a direct result of changes of viscous or wave drag in the flow through this channel; a comprehensive list of the important features of the interference would include:

A) changes in development of intake cowl spillage flow in the presence of the upwash, sidewash and velocity field due to the lifting wing,

B) the flow development over the rear of the fan cowl as affected by the adverse gradients imposed by the wing stagnation field,

C) pylon leading edge flow as affected by the wing upwash and sidewash in the region of the wing leading edge.

8

D) channel flow regions inboard and outboard where the flow can be supercritical with a strong shock wave and where mixing, entrainment and possible separation effects can be present,

E) non-planar lifting surface effects on drag as influenced by nacelle 'lift', pylon 'side lift' and wing lift,

F) local lift pocket at nacelle station and its influence on lift-induced drag and the wave drag and viscous drag from the upper surface,

G) changes in the supercritical flow development and viscous effects on the wing upper surface as a result of lift shedding and/or volume effects arising from the gross presence of the nacelle/pylon,

H) possible regions of over-expanded fan jet flow over the conical or curved afterbody with associated increased 'friction' drag and 'strong' terminal shock leading to wave and form drag increases in cowl/pylon base region.

Design structural weight considerations are, as always, present in the selection of suitable cases for aerodynamic study; also the important relationship between the aeroelastic behaviour of the wing/pylon/nacelle and the relative location of the wing and engine nacelle. Furthermore, the optimisation of nacelle installation design clearly includes study of the structural weights of all components necessary to cowl the bare engine as well as pylon and wing weight variations due to the presence of contending nacelle/pylon designs as well as of nacelle performance variations.

It is particularly important to recognise that, aerodynamically, the presence of the nacelle/pylon has significant effects on the overall wing flow field and lift development since the pylon/nacelle 'end plate' effect is propagated laterally across both the wing upper and lower surfaces with flow consequences that depend on the wing planform, section design, nacelle size and fuselage proximity as well as on the local wing/pylon/nacelle channel region. Before discussing some of the aerodynamic features in more detail, it must be noted that the changes in the flow over the wing arising directly from the presence of the pylon/nacelle should not, as in some earlier reports on this subject, be dismissed as trivial; these changes can be important, as will be seen below, and may be adverse or favourable.

To explain the nature of the interference due to the presence of a nacelle in more detail, let us consider some results presented in Figs 15a-c. These are taken from some research tests in the ARA transonic tunnel using a single-body through-flow nacelle. Although the simulation did not include the important jet flow features it is considered that many of the results are reasonably representative of physical pylon/nacelle body effects on modern transport aircraft designs. The following comments relate to an unpowered pylon/nacelle simulation; the additional jet flow effects of interference will be discussed later.

Fig 15a shows the two fore-and-aft positions of the nacelle relative to the wing (A and B); nacelle-to-wing vertical spacing was fixed at a level non-dimensionally similar to some modern designs. Fig 15b indicates how the nacelle installation drag increment for these two positions varies with Mach number at a typical cruise C_L and how it varies with C_L at a typical cruise Mach number, and also, shows how the drag-rise C_L - M boundaries compare with the boundary for the clean wing-body without nacelles. Finally, Fig 15c compares the wing pressure distributions, with and without the pylon/nacelle in the further aft position B at three stations on the wing at the two values of C_L marked on the boundaries. The nacelle is mounted at $\eta = 0.285$, ie at 0.285 x nett semi-span and so, the pressure distributions are given for two stations inboard and outboard of the pylon ($\eta = 0.265$ and 0.30) and one further out station ($\eta = 0.45$). It is also worth noting that the wing has a crank in the planform at $\eta = 0.319$ (no crank in the leading edge but an unswept trailing edge inboard of this station).

The direct effect of the flow through the channel can be seen most clearly in the pressure distributions for the lower C_L at $\eta = 0.265$ with the nacelle in the aft position B. The nacelle exit plane is then at 0.25 x local wing chord and Fig 15c shows that at $\eta = 0.265$, the suctions on the wing lower surface are increased ahead of 0.2c by the addition of the nacelle installation. In the manner suggested by Yoshihara [37,38], these effects can be accentuated when the local flow is supersonic - the expansion waves in the forward channel are not reflected as compression waves from a sonic line but as expansion waves from the opposite solid surface. As a result, a shock wave is present inboard of the nacelle - near 0.2c at $\eta = 0.265$ and in results not shown, at about 0.25c at $\eta = 0.18$. Outboard of the nacelle, because of the wing sweepback, the flow field is propagated laterally to a region further forward on the chord: at $\eta = 0.30$, the extra suctions due to the channel flow, when added to the low suctions near the leading edge of the clean wing, are not sufficient to create a local supersonic flow. Aft of the nacelle, the suctions are reduced by the addition of the nacelle; this effect can be observed aft of 0.2c at $\eta = 0.265$ and over most of the chord at $\eta = 0.3$; it is still evident at $\eta = 0.45$.

The adverse effects in the forward channel are most pronounced at low C_L. Fig 15c shows that the local supersonic region has disappeared at the higher C_L but the increase in suctions followed further aft by a decrease can still be observed. At the higher C_L, the flow is supercritical over the wing upper surface and the addition of the nacelle installation has an effect, similar in nature but smaller in magnitude to that over the wing lower surface. The suctions and shock strength on the wing upper surface are increased inboard of $\eta = 0.2$ where the shock is ahead of 0.25c but for the stations shown in Fig 15c, the strength of the wing upper surface shock situated downstream of the nacelle is reduced, this effect being particularly pronounced outboard of the nacelle, ie near the wing crank station.

Having now drawn attention to some of the main features of the pressure distributions, let us turn to a discussion and interpretation of the drag data in Fig 15b. In this summary, it is not possible to refer to all aspects of the interference but the main features are as follows:

(i) the high drag increment implying considerable adverse interference at low C_L particularly with the nacelle in the aft position B which is related to the extra wave drag on the wing, pylon and nacelle afterbody associated primarily with the shock wave in the flow field inboard of the nacelle,

(ii) the rapid decrease in ΔC_D with C_L at low and moderate C_L which relates primarily to the disappearance of this local supercritical region,

(iii) the more gradual decrease in ΔC_D with C_L at higher C_L, and for the further forward nacelle position which can be interpreted in various ways, eg

a) reduced viscous drag on the wing and pylon due to the disappearance of the high suction region and succeeding adverse pressure gradient in the forward part of the channel,
b) reduced flow velocities and local Mach numbers over the nacelle, thus leading to a decrease in the nacelle form drag and possibly, nacelle wave drag,
c) an endplate effect from the pylon on the wing, thus reducing the vortex-induced drag [39] associated with
d) an increased side load on the pylon having a component relative to the free stream flow, in the thrust direction [40], or
e) a change in the nacelle drag also induced by the change in sidewash with incidence below the sweptback wing.

(iv) ultimately, at high C_L and particularly at high Mach number, a more rapid decrease in ΔC_D with either C_L or M which can be related to the favourable effects on the flow over the wing upper surface,

(v) an increase in ΔC_D with M at a given C_L which can be largely associated with the development of a supercritical flow in the channel, and

(vi) a reduction in ΔC_D with M at high Mach number which occurs for all except the worst installations and which can be due to favourable effects on both the wing upper and lower surfaces. With some arrangements, the favourable effects on the upper surface at high Mach number are due to the fact that a single strong shock wave has been replaced outboard of the pylon by a weak, highly swept forward shock originating at the wing-pylon junction followed by a relatively weak rear shock. Favourable effects on the lower surface can arise when the increased pressures aft of the nacelle are effective in restraining the rearward movement of the main lower surface shock wave. This interference can be very beneficial in minimising reductions in longitudinal stability at high Mach number and low C_L which are generally caused, if they occur, by relative shock movements on wing upper and lower surfaces with the shock on the lower surface showing a strong tendency to move rapidly far aft with increasing Mach number.

Clearly, the adverse effects can be relieved by a forward movement of the nacelle as shown in Fig 15b. Changes in the shape of the pylon and nacelle can also be introduced [41] to improve the area distribution of the channel viewed as a channel or to improve the cross-sectional area distribution of a limited region of local wing, pylon and nacelle. These ideas were first used to advantage on the Convair 990 by Kutney [41]. It is possible that the shape of the resulting area distribution is in fact better than for the clean wing. This is therefore one method of obtaining favourable interference, other methods include the following:

1) the increase in pressure on the wing lower surface aft of the nacelle, particularly outboard of the nacelle can be exploited to advantage as a means of offsetting the high peak suctions which tend to occur near 0.6c on the lower surface with modern advanced wing sections. In practical terms, this could mean that the wing sections could be thickened near the rear spar,

2) the effects on the wing upper surface can be exploited to advantage by relieving conditions at, for example, a crank station outboard of the nacelle where wing designers often have difficulty in reducing the suctions and shock strengths to an acceptable level,

3) the favourable effects from the pylon described under (c,d) above.

The values of interference drag can depend on many detailed points, eg

(i) whether the forecowl can cope with the asymmetric flow field ahead of the wing leading edge,

(ii) whether the boundary layer over the rear of the fan cowl can accept the extra adverse pressure gradient induced by this flow field,

(iii) whether the leading edge shape of the pylon can cope with the sidewash of this flow field,

(iv) whether the pylon is cambered and whether it is the mean line or the inboard surface of the pylon that follows the streamlines of the wing flow field or whether some other philosophy is adopted to exploit the side load on the pylon.

No clear general rules can be tabled because the design of an optimum nacelle installation cannot be divorced from that of the parent wing. For example, the question of whether and how the pylon should be wrapped round the wing leading edge will depend on the type of wing design pressure distribution that has been chosen. One general rule can however be given: if the nacelle drag increment is increasing with Mach number at the design cruise Mach number, the package has not been optimised successfully. either the wing design has not recognised the need to accommodate the nacelle or there is some weakness in the nacelle installation.

The results discussed above were obtained with free-flow nacelles and therefore did not include any effects of the pressurised jet. These can be very significant, particularly for the fan jet. All civil aircraft designers now appreciate the paramount importance of testing with either blown nacelles, ejector nacelles, or turbine powered simulators (TPS units). In the UK great strides [42,43,44] have been made in the past decade in the ability to obtain very accurate and repeatable interference drag data through the use of TPS units. All of the results are subject to commercial constraints; however, we may draw on some published evidence.

The level of interference drag may be dominated by the presence of the thrust-producing fan jet/nacelle afterbody. For example, it is possible that experiments undertaken with free-flow nacelles such as that described above may provide totally misleading answers. In particular, the mutual development of the flows in the channel and in the fan jet may prove decisive for certain installations. Bagley [45] has shown that the jet will produce an increase in the wing lower surface suction peak in the channel; this is typical, but the incremental increase is clearly a function of local geometric features as well as free stream and jet conditions.

The interaction between the in-jet and in-channel flows is subtle and complex; as discussed by Yoshihara [37,38] and above, the sonic line, or surface, in the channel flow is followed by a series of expansion waves, including those from the curved wing lower surface. As illustrated by the flow photograph in Fig 16, many complex three-dimensional flow fields can develop, eg

a) the reductions of channel flow pressure are 'read' at the fan jet boundary leading to further expansion within the fan jet; this expansion further throttles the channel flow leading to a set of compression waves or more likely a shock,

b) on the other hand, reductions of channel flow pressure and consequent over-expansion of the fan jet may, due to the wing and fan stream relative inclination, lead to an extension of the channel flow supercritical region causing further fan jet over-expansion, higher channel flow Mach numbers and, in both streams, stronger terminal shocks. These shocks may result in additional viscous and wave drag and since they may well lie in the all important thrust producing fan stream, could be vital to the thrust/drag balance.

In the presence of the curved wing, pylon and nacelle physical components, it is not difficult to see that such flow characteristics as those discussed above may also result in substantial interference lift. Hence, at a given lift, changes in lift-induced drag (viscous and wave) could be present. It is also clear that the thrust performance of the nacelle afterbody components may be appreciably modified in the installed case and these thrust changes are accounted as interference drag changes in most studies. Control of these flow mechanisms is an obvious target for further study; exploitation seems to be further away but a full appreciation of these flow features could lead to avoidance of significant adverse drag effects.

If the nacelle is mounted well forward, early NASA results [40] showed that the jet could contribute substantial favourable interference. Patterson [40] interpreted this in terms of an increased side load on the pylon, thus strengthening the favourable interference effects (c,d) in the list above. Measured pressure distributions on the pylon showed that when the jet was unpressurised some of the pressure field on the inboard side of the pylon leaked forward through the subsonic fan jet round to the outboard side whereas when the jet was pressurised, this leakage was inhibited by the choked jet stream. These favourable effects are more apparent at high values of cruise lift coefficient, ie they give a reduction in the drag-due-to-lift. Patterson's explanation for these results is not universally accepted and it is perhaps notable that there has been no consistent trend in transport aircraft design to mount the nacelles on longer (ie deeper) pylons, which at first sight would be a means of further strengthening effects (c,d). Naturally, even if longer pylons genuinely contribute favourable aerodynamic interference, the benefits would have to be assessed against the likely weight penalties which could well be more important. Also, tests of military stores suggest [49] that at high subsonic and transonic speeds, increasing the depth of the store below the wing does not necessarily reduce the aerodynamic interference as would be expected at low speeds. There is a fair amount of evidence indicating that when the flow is supercritical, the adverse interference first increases with store depth before starting to decrease. Oil flow tests and pressure plotting measurements with military stores have shown that with a longer pylon, the flow separations in the wing-pylon junctions can be more severe. In a tightly constrained channel, the flow does not expand to such a high local Mach number, the shock across the channel is therefore both shorter in extent and weaker. Reverting to engine nacelles, the vertical depth of the nacelle below the wing is therefore a major parameter but it is difficult to quote any general rule; the interference will depend on detailed features of the nacelle and wing design as well as on the fore-and-aft position of the nacelle.

The development of a reliable theoretical method [38,47] for calculating the transonic flow over a wing-fuselage-pylon-nacelle with full allowance for intake and pressurised jet effects, must be considered a priority task. Even then, however, there will still be a continuing need for careful experiments since it is already clear that the interference drag can be sensitive to small changes in shape of nacelle and pylon - changes that may be difficult to model in any refined theory. One last comment - in a practical aircraft design, the best nacelle installation may not be the layout that gives optimum aerodynamic interference; the best layout will always be a compromise between the aerodynamics in various conditions, and between aerodynamic drag and structure weight.

5.2 Overwing Nacelles

On present knowledge, it seems unlikely that a nacelle installation could be mounted above a wing and obtain any favourable interference at high subsonic speeds. However, the results presented [38] by Wai, Sun and Yoshihara show that by contouring the nacelle, the large adverse interference obtained with a symmetric nacelle can be substantially reduced. Fig 17a shows the configuration tested and the nature of the interference with the symmetric nacelle; a very strong shock wave was observed inboard of the nacelle which is positioned at $\eta = 0.31$. Fig 17b contrasts the pressure distributions measured at $\eta = 0.15$ on the wing upper surface in the presence of the symmetric and contoured nacelles. The value of $(-C_p)$ ahead of the shock was reduced from about 1.14 to 1.02; assuming no sweepback of the shock front, this corresponds to a reduction of the shock upstream Mach number from about 1.4 to 1.3. This improvement inboard of the contoured nacelle is partially offset by a deterioration outboard but as shown in Fig 17a, there is a dramatic reduction in the nacelle installation drag increment from $\Delta C_D = 0.0140$ to $\Delta C_D = 0.0090$ at the cruise C_L. The shape of the drag polars suggests however that even with the contoured nacelle, there is still considerable adverse interference.

5.3 Nacelles mounted on the Rear Fuselage

The interpretation of measured drag increments due to nacelles mounted on the rear fuselage can be even more difficult than for wing-mounted nacelles. There is plenty of scope for aerodynamic interference on the rear fuselage and nacelle assembly itself but as with wing-mounted nacelles, the effects on the flow over the wing are likely to be the dominant factor, particularly at transonic speeds.

Early UK experience with the VC10 and BAe 1-11 was reviewed [49] by Williams and Stewart at the AGARD 1971 conference on interference. They identified various sources of interference, eg

(i) extra profile drag on the rear fuselage and nacelle. Clearly, the afterbody-pylon junction and the channel between rear fuselage and nacelle are regions where one would expect to find the viscous interference effects discussed in §3. Fairings are likely to be needed [50] to weaken or eliminate stand-off vortices originating ahead of the pylon leading edge, to reduce the expansion and subsequent compression in the con-di channel and to prevent strong cross-flows or flow separations on the boattailed afterbody immediately behind the pylon trailing edge. With a 4-nacelle (ie 2 per side) installation, there may be further problems in the gully between the two nacelles: on the VC10, these were relieved by the introduction of a 'Beaver tail' fairing,

(ii) extra wave drag on the rear fuselage and nacelle assembly. This can be alleviated by the application of area-rule principles to this local region. The fairings mentioned under (i) should be designed with this in mind,

(iii) changes in the lift-dependent drag on the wing and tailplane as a result of lift changes on the wing and tailplane in order to maintain a given trimmed overall C_L in the presence of a non-zero (in general) lift contribution from the nacelle. This interference can be adverse or favourable depending on the nacelle setting and the relative efficiency of the wing and nacelle assembly as a producer of lift with low drag. General rules may be dangerous but it is probable that when the flow over the wing is subcritical, it will be better to carry the lift on the wing than on the low aspect ratio nacelle assembly but at typical cruise conditions, it may be preferable to carry some positive lift on the nacelle assembly where the flow is likely to be subcritical, thus reducing the wing C_L for a given overall C_L and easing the task of the wing designer,

(iv) reduction of the drag of the inner wing sections as a result of the buoyancy effect of the forward pressure field of the nacelles. In inviscid, subcritical flow, this would be cancelled by an equal and opposite effect on the rear of the aircraft but in the real flow, this could lead to significant changes in profile drag, wave drag and vortex-induced drag which would not be cancelled at the rear. These effects can be adverse or favourable depending on the wing design and will be discussed in more detail below,

(v) reduction of the wing drag through a rotation of the lift vector. This applies when the nacelles are contributing positive lift and thus, there is an induced upwash over the wing, and

(vi) exit jet interference on the empennage and rear fuselage.

Many of the above effects will also change the pitching moment for a given lift. Untrimmed drag data can therefore be misleading.

In the development of a new aircraft with engines mounted on the rear fuselage, extensive wind tunnel test programmes have generally been undertaken to choose the optimum nacelle settings in pitch and yaw, and to refine the installation to avoid adverse interference but the main lesson from the data bank is that to exploit favourable interference, the wing-fuselage-nacelle installation should be designed as an entity. This was graphically illustrated in the paper [51] presented by Laugher at the AGARD 1981 conference on the aerodynamics of power plant installation. Laugher noted that in all cases, whatever the wing design, the addition of a rear nacelle assembly reduces the suctions on the aft surfaces of the inner wing and when the nacelles are mounted above the wing chord plane (as is usual with a subsonic transport), the loss of lift on the inner wing has to be recovered by an increase in wing incidence. The wing design and in particular, the variation of shock strength across the span and the nature of the pressure distribution ahead of the shock determines whether the nett interference is adverse or favourable. For the interference to be favourable, the shock on the inner wing in the absence of the nacelle has to be relatively strong; this ensures that the reduction in wave or profile drag from the direct effect of the nacelles on the flow over the inner wing more than offsets any increase in drag due to the increase in incidence.

Figs 18a,b reproduced from Laugher's paper [51] contrast two cases where the interference is adverse (Fig 18a) or favourable (Fig 18b). In the first case, the nacelle intake plane is coincident with the wing local trailing edge. The effect of the nacelle in destroying lift on the inner wing is clearly substantial and has to be offset by an increase in incidence of 1.4°. As a result, the comparison at a given C_L indicates that when the nacelles are present, there is a major increase in shock strength at all stations across the wing. Admittedly, this adverse interference could probably have been relieved by an increase in the pitch setting of the nacelles but it seems unlikely that this would be sufficient to change the sign of the interference. The advanced wing design that appeared so attractive in the absence of the nacelle (eg an extensive supersonic region terminated by a relatively weak shock, a near-isentropic recompression on the inner wing, suctions decreasing progressively towards the root giving highly swept isobars aft of the peak suction line) is clearly an unsuitable design if an aft nacelle has to be mounted at this position. With the nacelle present, not only is there a strong shock across the span, the position of this shock is much further forward than on the clean wing - by about 0.4c on the inner wing and 0.3c out at $\eta = 0.534$ x semi-span.

It follows that the design aim should be to obtain a favourable supercritical development on the wing in the presence of the nacelles, ie to adopt a geometry that would probably be unacceptable as a clean wing. This was the aim of a design exercise undertaken by BAe in 1978 and Fig 18b presents some pressure distributions from tests in the ARA transonic tunnel on a model of this design. The nacelle in this case is mounted somewhat further aft than for the example in Fig 18a and so the nacelle interference on the wing flow would have been less adverse even if the same wing design as in Fig 18a had been used. However, the main reason for the favourable interference shown in Fig 18b lies in the new wing design. Measured pressure distributions are shown for a wing station just outboard of the nacelles. A near-isentropic recompression is achieved on the wing in the presence of the nacelles whereas on the clean wing, the pressure distributions in the two cruise conditions expand again at the rear of the supersonic region leading to a strong shock at respectively, 0.6c and 0.7c in the two conditions, and a rear separation in the high speed cruise. Fig 18b certainly implies favourable interference relative to the wing without nacelles (less wave drag and viscous drag) but the important point to note is that the wing design and wing flow for such a configuration are possibly better than could be achieved for any wing of this planform, nacelles-off. Laugher noted [51] that the wing geometry that gave the pressure distributions in Fig 18b, nacelles-on

would have 2.5% more fuel volume compared with the wing that would give similar pressure distributions, nacelles-off.

The results quoted by Laugher therefore validate the concept of obtaining favourable interference with the aid of a rear nacelle installation. They were obtained by a technique in which the nacelle effect on the supercritical flow development over the wing was simulated by means of an 'equivalent interfering body'. This proved very cost-effective but in future, better results should be possible when methods for calculating the transonic flow over a complete configuration are available.

5.4 Interference between Adjacent Bodies

The interaction between the flow fields of adjacent bodies in close proximity is another source of adverse aerodynamic interference on some aircraft, notably combat aircraft carrying many external stores. The adverse interference is not inevitable; with the right shape and relative position for the bodies, favourable interference can be obtained when the bodies are staggered or are in tandem or when the bodies are used to improve the longitudinal distribution of aircraft cross-sectional area.

The first example of this type of interference is not taken from a test on a model of a combat aircraft but from results for the high wing transport [17] whose wing-fuselage interference was discussed in §3 and illustrated in Fig 6. Fig 19a shows two versions of the complete layout (without empennage). It is a 4-engined aircraft with 2 engine nacelles pylon-mounted below each inner wing and the test data revealed that the proximity of the inner nacelle to the protruding undercarriage fairing on the fuselage was a major potential source of interference. Adding the undercarriage blister with the nacelles already fitted to the poorer configuration A gave a drag increment an order greater than the predicted profile drag of the fairing. Configuration B is less prone to adverse interference than A because

(a) the pylon is more swept and longer, thus placing the nacelle significantly further forward relative to the undercarriage fairing, and

(b) the width of the undercarriage fairing is less at a depth opposite the nacelle and more of the volume of the fairing is concentrated below the fuselage. The plan view in Fig 19a in particular shows how the change from A to B relieves the passage between the fairing and the inner nacelle but one would expect that the interference drag has been reduced at the expense of extra profile drag on account of the greater surface area of the pylons and fairing in B. The measured differences in C_D between A and B are plotted as a function of Mach number and C_L in Fig 19b. The differences are very large being always greater than $\Delta C_D = 0.0020$ and being about $\Delta C_D = 0.0050$ at a likely cruise condition, $M = 0.71$, $C_L = 0.5$ or 14% of the total C_D for the better layout B in this condition. The extra interference drag increases significantly with C_L and this trend can be related to a reduction in C_L at a given incidence of about 0.07 for A relative to B near $M = 0.71$, $C_L = 0.5$. The increase in ΔC_D with C_L and M can be interpreted as follows: high suctions in the passage between the undercarriage blister and the inner nacelle destroys considerable lift on the inner wing and thus: extra incidence for a given C_L and extra wave drag from the wing upper surface - probably on the outer wing well away from the source of the effect.

The layout in Fig 19, particularly with its external undercarriage blister, may be thought somewhat unusual but plenty of evidence of this type of interference can be found in test data [48,52,53,54,55] for external store installations. These will be discussed in detail in a later lecture but it is appropriate to include some examples in this overview lecture. Fig 20a contrasts the adverse interference observed at low C_L when several stores are carried on separate pylons under a 40° sweptback wing and the favourable interference possible when a number of stores are mounted in an array below a fuselage. If expressed as an installation drag factor, the drag increment for the 3 pylon-mounted underwing stores reaches about 5 at $M = 0.90$ but it is more sensible to relate such results to the drag characteristics of the clean aircraft. In other words, the increase in ΔC_D with M for the single underwing store can be interpreted simply as a reduction of the drag-rise Mach number of the wing-pylon-store relative to the clean wing whereas the multiple arrangement with 3 pylon-mounted stores introduces a significant drag creep ahead of the steep drag-rise because it has completely modified the nature of the flow over the wing lower surface. The oil flow pictures included in the later lecture show that with 3 pylon-mounted underwing stores disposed in a standard sensible arrangement related to the aircraft centre of gravity, a strong unswept shock tends to appear prematurely in the passages between the pylons. The resulting wave drag and local shock-induced separations account for the drag creep and the potential benefits of wing sweepback have been partly lost on the wing lower surface.

Turning to the right hand side of Fig 20a, the upper picture has been used in several previous papers; it is repeated here because it is such a dramatic example of favourable interference. It shows the results of tests in which 4 rows of 5 small stores with flat bases were mounted on a pallet below a flat-bottomed fuselage. Above about $M = 0.92$, the total drag increment for the 20 stores is smaller than the increment for a single row of 5 stores: to reiterate, the total drag increment and not just the drag per store. It may be argued that this very favourable result is simply due to the fact that they are small stores mounted tangentially and mostly immersed in the fuselage boundary layer. However, the stores in the lower picture are comparable with those for the underwing installation on the left. Tests were made in the RAE 8ft x 6ft tunnel on an array of 6 large boattailed stores again mounted tangentially on a pallet below an aircraft fuselage. It will be seen that even in this case where the stores are much larger in relation to the size of the aircraft, the drag increment for the array consisting of 3 rows of 2 stores is generally, particularly at high subsonic speeds, less than the sum of the free-air drag of the stores in isolation. This implies that the favourable effects of tandem carriage have more than offset the adverse effects in side-by-side carriage.

Fig 20b has been included to show the potential favourable effects of store stagger and tandem carriage more explicitly. These results were obtained [56] in tests in the 2ft x 1½ft tunnel at RAE Farnborough in which drag measurements were made on various arrays of stores mounted just clear of the tunnel roof boundary layer; in effect, the stores were being tested close to a reflection plane simulating the surface of a wing with zero thickness. Results are shown for two types of store, one with a pointed nose and one with a bluff nose. It will be seen that at say, $M = 0.9$, staggering 2 stores fore-and-aft by six calibres reduces the

drag by about 10% relative to 2 x the drag of a store in isolation whereas positioning the stores directly opposite each other at the same lateral spacing increases the drag by 40-60%. The more detailed information in the later lecture shows that even staggering the stores by one calibre, ie sufficient to displace the peak suctions on the stores but not sufficient to introduce any significant tandem effect, gives about half this improvement, ie $K_{st} \simeq 1.2$. Finally, the results in Fig 20b show that carrying stores in tandem is a very powerful method of obtaining favourable interference, particularly with bluff-nose stores. If the stores are virtually nose-to-tail, ie $X_T = 0.005$ calibres, the reduction in overall drag for a column of 2 stores amounts to about 30% near M = 1.0 for the bluff nose and 20% for pointed nose stores; even at a separation of 3 calibres, the same test series showed that the figures were 20% and 15% respectively. The mechanisms by which tandem carriage achieves such large favourable effects are listed in detail in the later lecture.

5.5 Non-Planar Configurations

To quote from papers [39,57] by Whitcomb, it has been recognised for many years that a nonplanar lifting system should have less induced drag than a planar wing. Theoretical studies suggested and experimental tests confirmed that reductions in induced drag could be obtained by mounting vertical surfaces or endplates at the wing tips but the overall benefits were generally small as the reductions in induced drag were only marginally greater than the profile drag of the endplates. It is only within the past decade that the real potential of tip devices has been fully realised. Whitcomb was the first to emphasise that to be effective, the vertical surfaces at the tip must be designed to produce a significant side force. The vertical surface or winglet should be designed as a lifting wing required to perform efficiently over a wide range of operating conditions. Flow surveys [58] behind a wing tip with and without a winglet fitted showed that the basic physical effect of a winglet can be interpreted as a vertical diffusion of the tip vortex flow immediately downstream of the wing tip; this is the source of the reduced vortex-induced drag. Another interpretation is that the inward side force on the winglet normal to the local flow direction (inflow above the wing tip) when resolved in the free-stream direction yields a significant thrust component.

The pioneering research [57,58] of Whitcomb et al established some guidelines for the design of a successful winglet. The primary winglet should be mounted above the rear, say 60% of the wing-tip upper surface and

(i) should have a height roughly equal to the wing tip chord,
(ii) should be canted out at an angle of about 20° to the vertical,
(iii) should be toed-out but cambered and possibly twisted to produce an inward side force in the cruise which, when expressed as a coefficient based on winglet area, is comparable with the wing lift coefficient.

Theoretical analyses suggested [59] that winglets should be more effective when fitted to wing designs that are relatively highly loaded on the outer wing sections. Some aerodynamicists have therefore argued they are only likely to be effective when fitted retrospectively on early wing designs such as the KC-135 (the subject of the first tests) or on the relatively simple wings that have been used on commuter or small executive jet aircraft (for which winglets have already been used in practice). However, the test data for both the first generation [57] and second generation [58] US transport wings showed that in both cases, an effective winglet gave a larger drag reduction for a given wing root bending moment than the corresponding span extension. Looking to the future, it is arguable that for a new transport aircraft, one should design a wing-winglet combination with the wing geometry deliberately chosen to suit the addition of a winglet - just as on combat aircraft, it is becoming standard practice to carry weapons at the wing tip to obtain, in principle at least, similar beneficial effects [48,52]. Such wing-winglet combinations could have a better performance than the best corresponding wing-alone even when due allowance is made for the winglet weight and added engineering complexity.

Various aspects of winglet design can be described as either exploiting favourable or minimising adverse interference. For example,

(i) mounting the winglet above the rear of the wing-tip upper surface ensures that there is no adverse interference with the development of the supercritical region over the forward upper surface,

(ii) mounting an additional winglet below the forward lower surface controls the angle of flow ahead of the leading edge of the upper winglet at high incidence: an example of favourable interference between two surfaces,

(iii) the winglet derives some of its benefit from the loading it induces on the extreme outer wing. This extra lift will serve to reduce the maximum local lift on the wing for a given overall lift and there is thus, the possibility that at high Mach number, there will be a reduction of wing wave drag as well as vortex-induced drag: again, favourable interference,

(iv) the essential art in designing an effective winglet lies in the blending of the junction between wing and winglet to avoid adverse viscous interference effects.

The list could doubtless be extended but as an illustration of the last point (iv), Fig 21 compares two views of the winglet (A) used in the US tunnel tests [58] on the second-generation transport with a more recent layout (B) developed in UK research on a relatively advanced wing design. In this case, great efforts were made to blend the region from 0.985 x basic wing semi-span up to about 0.2 x winglet height. When 'unwrapped', the winglet in both plan and section shape development was blended neatly into the start of a basic wing tip design involving a curved leading edge as advocated many years ago by Küchemann. It will be noted that winglet B is smaller than winglet A; the winglet area for B was in fact only about 1.5% of the half-wing area but even so, the reduction in drag-due-to-lift amounted to about 12.5% and possibly more at high Mach number. Such reductions would clearly more than offset the profile drag of such a small winglet.

Further improvements in winglet design may be possible when the transonic theoretical methods are fully developed [60] to be used as a design tool for wing-winglet design. The present author feels that much of the evidence in the published literature could give a pessimistic idea of the effectiveness of a good

winglet design - either because the test Reynolds numbers were not high enough to avoid boundary layer thickening or separation in the junction or on the winglet lifting surface or because the winglet section shape was chosen without regard to the requirements that the section should have high drag-rise Mach number at a typical cruise C_L and good $C_{L_{max}}$ at lower Mach numbers.

Two winglets, one above and one below the wing tip may not represent the ultimate development of this theme. Spillman of CIT has proposed [61,62] the use of a number of small surfaces or 'sails' arranged around the wing tip in a way such that no surface is ever in the wake of another. Fig 21 shows an arrangement of 3 sails mounted on a body at the wing tip; flight tests at Cranfield suggested that 3 sails would be more effective than a single sail in reducing the drag-due-to-lift. There is no intrinsic reason for the sails to be mounted on a tip tank, they could be attached directly to the wing tip. Spillman has noted the analogy between these 'sails' and not only the sails on a yacht but also the primary feathers of many birds of prey. For the best results, one really needs to imitate the birds even further - the sails should be flexible and Spillman suggests, driven mechanically by a vane sensing the local flow directions.

6 EXPLOITATION OF FAVOURABLE INTERFERENCE IN CONFIGURATION AERODYNAMICS: USABLE LIFT

Favourable interference can be exploited not only to reduce the drag but also to improve usable lift boundaries, ie to improve the development of the aerodynamic characteristics beyond separation- or buffet-onset. Many devices are used for this purpose, eg vortex generators, small fences around the wing leading edge, strakes at the wing root leading edge, canards, jets blowing over flaps etc but when anlaysed, one can see that all derive their effectiveness from a favourable interference between different flow fields. Before discussing some of these effects, however, let us consider the effects of pylon-mounted underwing stores as an interesting follow-up to the discussion in §5. As already noted, the carriage of such stores can give rise to serious adverse interference with the flow over the wing lower surface at low C_L but it is interesting and somewhat unexpected that the interference with the flow over the wing upper surface at high C_L can be favourable. This has now become a very important point in the light of trends in modern advanced wing design.

When sweptback wings were first introduced, much effort had to be devoted to the control of their inherent tip stalling tendencies which led to both pitch-up and lateral stability problems. These early wings had little twist or camber, their basic geometry was generally designed to give good performance at one particular operating condition. Now, however, the designer no longer has to act under past constraints. he can employ variable leading edge and trailing edge devices and he can optimise the twist for various operating conditions by means of aeroelastic tailoring. More lift is carried on the inner wing with modern designs and the present tendency is for the wing flow to separate first somewhere near mid-semi-span rather than at the tip. Routine theoretical design calculations can only be made for attached-flow conditions and the common design aim is to carry as much lift as possible at separation-onset. If this aim is pursued to the exclusion of all other considerations, the subsequent flow breakdown may well be unacceptable. In other words, immediately beyond separation-onset, the separation spreads rapidly forward to the leading edge and across the span with only a small increase in incidence. In a wind tunnel test, this can lead to severe model bounce which may make it unsafe to continue with the incidence traverse, in flight, there may be an unacceptable deterioration in flying qualities, the flow being too sensitive to small changes in incidence, sideslip and other variables. This is the type of situation that can be improved by the addition of a set of pylon-mounted underwing stores.

At first sight, one might have expected that the pylon-mounted stores would have an adverse effect. In general, they will reduce the lift at a given incidence and also, there may be a premature flow separation inboard of each pylon. These effects have, indeed, been observed in many model tests and as a result, the first break in the lift versus incidence curve often occurs at a lower C_L when the pylon/stores are fitted. However, the subsequent flow breakdown tends to be more progressive and so, the usable lift may still be higher with the stores fitted than for the clean wing.

Fig 5 of the subsequent lecture [48] presents an illustration of favourable interference of this type; the measured pressure distributions confirm the more progressive flow breakdown. Fig 22 in the present lecture gives another example. In this case, tests were made on a research model with an advanced wing with 38.7 leading edge sweepback, aspect ratio 4.03, taper ratio 0.3, with and without 3 underwing stores mounted at 0.59, 0.70 and 0.87 x gross semi-span. Fig 22 contains $C_{L_{trim}}$ - α curves for 4 test Mach numbers for the model with and without the pylon mounted stores. The prominent symbols on each curve indicate predicted values of usable C_L assessed on the basis of the behaviour of the model (bounce or oscillation in pitch) and/or the mean level and amplitude of oscillation of the rolling moment signal as a guide to wing drop and wing rock tendencies in flight. This comparison shows

(i) at low Mach number, M = 0.6, the addition of the pylons/stores improves both the break C_L (or buffet-onset) and the usable lift by about $\Delta C_L = 0.05$. The primary physical reason for these improvements is that the changes in flow direction ahead of the wing leading edge inboard and outboard of each pylon serve to break up the spanwise spread of the flow separation which, at this Mach number is occurring close to the wing leading edge,

(ii) at higher Mach numbers, the pylons/stores reduce the break C_L, ie degrade the buffet-onset boundary by an amount increasing with Mach number by about 0.03 at M = 0.75 to more than 0.10 at M = 0.885,

(iii) on the other hand, the addition of the pylons/stores results in a smoother variation of C_L with α beyond the break and it should be noted that the predicted values of usable C_L are still at least as high as for the clean wing; indeed, at M = 0.75, the value is 0.1 higher than for the clean wing,

(iv) the curves for the clean wing at M = 0.80 and 0.885 are terminated at an incidence where the model bounce became so severe that it was judged unsafe to continue the traverse; with the pylons/stores, the traverses were extended successfully.

With wings designed 20 years ago, the addition of the pylons/stores might well have degraded usable lift boundaries assessed on any basis but it should be emphasised that Fig 22 is not an isolated example of the type of results obtained with modern wing designs. The dominant feature of the flow over the upper surface

of such wings at high subsonic speeds prior to buffet-onset is the well known 3-shock pattern, viz a highly swept forward inboard shock, an inboard rear shock and a single outboard shock. Separation tends to occur first just outboard of the point of intersection of these 3 shocks and it then spreads rapidly over the entire outer wing: this is the explanation for the abrupt stall on the clean wing. When the pylon-mounted stores are fitted, the flow pattern prior to separation onset can be more complex, eg additional highly swept forward shocks may originate from each pylon-wing leading edge junction. Put crudely, the flow breakdown no longer occurs suddenly over a large part of the span; instead, there are successive flow breakdowns over 4 segments of smaller spanwise extent. This is a likely but not necessarily the only explanation of the more progressive flow breakdown. The results certainly suggest that a viable design approach for a combat aircraft wing at the present time is to design a clean wing that gives the best possible C_L for separation-onset and then to assume that the underwing pylons will ease the buffet penetration at the expense of some acceptable worsening of the buffet-onset boundary. Hopefully, in the future, it will be possible to design the wing/pylons as an entity and then, one could obtain good buffet penetration with less reduction of the buffet-onset boundary.

One possible explanation for the beneficial effects of the pylons/stores at the lower Mach numbers such as $M = 0.6$ is that the pylons are acting in the same manner as small fences wrapped around the wing leading edge. Such fences have been used with great effect on some aircraft, eg the Harrier. Some research was undertaken in the ARA transonic tunnel to establish the underlying physical mechanism for their effectiveness. The flow patterns induced by the fences were very complex but some discussion of these results is worthwhile because they provide a good illustration of favourable interference between different flow fields.

Some features of the model geometry and test results are presented in Figs 23a,b. A large half-wing model of a sweptback wing-fuselage was tested in the ARA transonic tunnel with and without various alternative designs of small leading edge fence mounted at 81.5% semi-span, two of the fences are shown in Fig 23a. In addition to overall force and moment measurements, the wing was extensively pressure plotted and Figs 23a,b include some results for the four stations A-D, A being just inboard and B,C,D outboard of the fence.

The results presented in Fig 23 were obtained at a test Mach number of $M = 0.6$. Two types of flow separation were observed on the clean wing as the incidence was increased. first, a leading edge separation initiated near the tip at about $\alpha = 6°$ and extending in to about 75% semi-span at $\alpha = 10°$ and second, a rear separation appearing first at $\alpha = 4°$ near the trailing edge at about 75% semi-span and then spreading forward and inward, the two separations merging above about $\alpha = 10°$. The overall $C_L - \alpha$ curve in Fig 23a suggested that the fences had little effect on the overall characteristics until about $\alpha = 13°$ but the measured pressures showed that local effects close to the fence were present even at $\alpha = 4°$. At low incidence, the peak suctions close to the leading edge is reduced outboard of, and increased inboard of the fence: the expected result in subcritical, inviscid flow at effectively the root and tip of a sweptback wing. This leads to a premature separation inboard of the fence but as with the basic leading edge separation spreading in from the tip, this rolls up to form a part-span vortex. There is no significant loss in lift from this separation and indeed, at $\alpha = 9.75°$, as shown by the pressure distributions for station A in Fig 23b, the region close to the leading edge inboard of the fence carries more lift at this incidence when the fence is fitted. There is therefore no serious adverse interference inboard of the fence.

Turning now to the flow outboard of the fence which creates the favourable interference above $\alpha = 13°$, this is a complicated story. The trigger for the flow development is the fact that with the large fence 1, the fence interrupts the spanwise flow along the attachment line and even with the smaller fence 2, it interrupts the flow just ahead of this line, ie the flow that is about to stream over the upper surface. The fences therefore cause this flow to separate and in the case of the large fence 1, two primary stand-off vortices (see § 3) form, one rotating in an anti-clockwise sense looked at from upstream and streaming over the lower surface, and the other rotating in a clockwise sense and streaming over the upper surface; with the smaller fence 2, only the upper vortex was observed in the flow patterns. At moderate incidences, when the flow close to the leading edge immediately outboard of this vortex is attached, the vortex streams back over the upper surface crossing station C (see Fig 23a) aft of the short line of pressure tappings which does not extend beyond 10% chord. This flow pattern is illustrated in sketch (i) in Fig 23b. At higher incidences, when the separation close to the leading edge initiated near the tip has spread to the vicinity of the fence and primary vortex, the air in this three-dimensional separation is drawn into a secondary anti-clockwise vortex lying forward and outboard of the primary vortex: see sketch (ii) in Fig 23b. As soon as this secondary vortex is established, its origin appears to move forward almost to the source of the primary vortex, ie almost to the leading edge attachment line. This allows the secondary vortex to be fed by high energy air and then, with increasing incidence, the vortex grows in strength. The high suction region under this secondary vortex can be seen in the measured pressure distributions for $\alpha \simeq 13.2°$ at stations B,C,D in Fig 23b and in the variation of C_p at 1% chord with α for these stations in Fig 23a. Clearly, the contribution from the secondary vortex is the main factor responsible for the reasonable overall lift-curve slope above $\alpha = 13°$, fence on and hence for the increase due to the fence in the predicted usable lift. Fig 23a shows that the smaller fence 2 gives a slightly better result than fence 1 suggesting that it is preferable for the fence not to intersect the attachment line. Other tests in this series showed that a certain minimum fence height (smaller than for fence 2) was required to maintain the vortices in a stable state close to the wing surface at high incidence.

The effect of these fences has been described in some detail as an example of where a form of wing-body interference has been exploited to produce a favourable result. The significant point is that the favourable result would not have been obtained if there had not been an interaction between the fence stand-off vortices and the leading edge separation of the stall of the clean wing. This interpretation of the results was further confirmed in tests on a related model which showed that when the fence was moved in to 71% semi-span, it was completely ineffective, the significant point being that at this station, on the clean wing, the flow no longer separated from near the leading edge. (As noted at the beginning of this discussion, the stall inboard of 75% semi-span was dictated by a rear separation spreading forward from near the trailing edge).

It is now well known that much larger benefits in usable lift can be obtained through the use of sharp-edged strakes ahead of the wing leading edge at the wing root. Fig 24 presents some results showing the

effect of such strakes on the wing buffeting and unsteady rolling moment characteristics for a model of the Harrier aircraft. This figure is taken from a paper [62] by Moss which gives various examples of the benefits of wing-root strakes. Moss notes that the strakes were designed to be compatible with the aircraft structure and basic stability requirements in flight. The results in Fig 24 show that in the model tests, the strakes gave dramatic improvements in lift at high incidence, the rolling moment behaviour at zero sideslip and in the steadiness of wing-root bending moment at high incidence. In explanation of the rolling moment plots, a large mean value of C_{ℓ} in the model tests has been found to correlate reasonably with wing dropping in flight and the spread between the upper and lower bounds of the signal in the model tests is a guide to whether 'wing rock' is likely to occur in flight. The improvements shown in Fig 24 were subsequently confirmed in flight tests.

Various factors contribute to the beneficial effects of the strakes. Clearly, as on a slender wing, a vortex is shed from the leading edge of the strake. Direct effects of this vortex include an extra non-linear lift contribution, and improved flow and a thinner boundary layer over the rear upper surface of the inner wing. However, the indirect effects are perhaps more important; the benefits at high incidence can be traced at least partly to the ability of a strake and its vortex flow to control the flow breakdown on the outer wing panel. At low and moderate subsonic speeds, the feature of the flow that exercises this control is a second strake-induced vortex that springs from the strake-wing leading edge intersection. This vortex is present because, as shown in numerous oil flow patterns on many sweptback wings, the strake reduces the angle of incidence at which a flow separation occurs near the leading edge of the outer panel just outboard of the strake-wing leading edge junction. Fiddes and Smith have explained [63] this observation in terms of two consequences of the presence of the main strake vortex viz

(i) an increase in the effective angle of sweep of the leading edge of the outer panel near the strake-wing intersection, and
(ii) an increase in the effective incidence of the outer panel.

The outflow under this second vortex reduces the boundary layer thickness on the rear upper surface near mid-semi-span, thus reducing any tendency to a rear separation and also serves to limit the rearward extension of any separation bubble near the leading edge of the outer wing. The last effect is often the most important and it is frequently noted in low speed tests that a separation on the forward outer wing which, in the absence of the strake, would develop to cause a complete flow breakdown over the upper surface, starts to extend rearward with increasing incidence but then retreats forward under the influence of the strengthening of the strake-induced vortices.

At higher subsonic speeds when the flow over the wing upper surface is supercritical, the addition of the strake results in the inner forward shock of the 3-shock pattern originating from the strake-wing leading edge junction rather than from the wing-body junction. It follows that the outboard shock which usually induces the flow breakdown is shorter in spanwise extent and the supercritical region ahead of the forward shock is shorter in chordwise extent at a given incidence. These two effects tend to offset each other: the first reduces the extent of any shock-induced separation if present and hence is beneficial; the second reduces C_L at a given incidence and so could be adverse although it may be more than compensated by the extra lift from the vortex off the strake. No general conclusion can therefore be drawn as to whether the overall effect will be favourable or adverse. It is however likely that the benefits from adding a strake will tend to decrease with Mach number above say, $M = 0.80 \sim 0.85$ for a 40° sweptback wing.

The flow field from a forward canard surface can have a similar effect to that of a strake at high subsonic speeds and high incidence. This is illustrated by the flow patterns* in Fig 25. The canard at 0° deflection clearly unloads the inner wing and the supercritical region on the outer wing is reduced in the same manner as described above for a strake. The forward shock originates from near the intersection of the edge of the canard wake and the wing leading edge. It is interesting to note that the overall C_L at this incidence was only 0.015 less when the canard was fitted, ie the lift on the canard almost compensates for the lift deficit on the wing. The interference in this case can therefore be classed as favourable; for other positions and deflections of the canard, it could be adverse or non-existent either for example because the wake from a stalled canard disturbs the flow on the inner wing or because the canard wake passes well above or below the wing: again, this is a case where the configuration has to be carefully designed to exploit the favourable interference.

The limited results with pylons/stores, fences, strakes and a canard surface have been included to illustrate that interference between components and between different flow fields can improve the usable lift at both low and high subsonic speeds. Another possibility that will undoubtedly be exploited to a greater extent in the future is to obtain extra lift from favourable jet-wing interference. This will be discussed in a later lecture in this series but an early idea of what this might achieve for a combat aircraft was given by Vint [64] in a paper at the AGARD FDP 1980 conference. Vint described the development of a theoretical prediction technique which suggested that a conventional propulsive jet at the wing trailing edge could give a significant improvement in the high lift characteristics of the wing if jet deflections up to 30° could be used. The research indicated that the best results in practice would be obtained if these ideas were applied to a configuration with a canard surface. A propulsive jet at the trailing edge would avoid the complexity of a blown flap which has of course been used for many years on some aircraft, eg the Buccaneer. This whole subject deserves however a full lecture in its own right and it will not be considered further here.

7 CONCLUDING REMARKS

This lecture has reviewed the main sources of aerodynamic interference at high subsonic and transonic speeds. Examples have been given of when favourable interference between different aircraft components and different flow fields have been exploited

(i) to reduce wave drag, profile drag and/or vortex-induced drag,
(ii) to improve the flow development beyond separation-onset and hence, the usable lift.

*The white streaks ahead of the shock are due to the fact that in this particular test, transition was fixed by strips round the leading edge.

Wing-body interference and also the interference due to nacelle installations mounted either on the wing or on the rear fuselage, and wing-tip devices have been treated in some detail. In other areas, ideas have been introduced with some illustrative examples; they will be developed further in later lectures.

Jet-wing interference is an important area that has not been discussed except in the context of underwing nacelle installations.

8 ACKNOWLEDGEMENTS

The author gratefully acknowledges the help from colleagues at the Aircraft Research Association Ltd in preparing this lecture and for permission by MOD (Procurement Executive) to use some of the material in the lecture, mostly from tests in the ARA tunnel undertaken under MOD(PE) research contracts.

REFERENCES

1 Cayley, Sir G, On aerial navigation 1809-10, 1962, Reprinted in Sir George Cayley's Aeronautics 1796-1855, HMSO London, C H Gibbs-Smith.
2 Lennertz, J, Beitrag zur theoretischen Behandlung des gegenseitigen Einflusses von Tragfläche und Rumpf, 1927, ZAMM 7, 249.
3 Vandrey, F, Zur theoretischen Behandlung des gegenseitigen Einflusses von Tragflügel und Rumpf, 1937, LF 14, 347.
4 Küchemann, D, The aerodynamic design of aircraft, 1978, Pergamon Press.
5 Küchemann, D, Some remarks on the interference between a swept wing and a fuselage, 1971, Paper no 1, AGARD CP-71-71.
6 Körner, H, Untersuchungen zur Bestimmung der Druckverteilung an Flügel-Rumpfcombinationen, Teil 1 Messergebnisse für Mitteldeckeranordnung aus dem 1,3 m Windkanal, 1969, DFVLR Bericht Nr 0562.
7 Küchemann, D, Weber, J, The subsonic flow past swept wings at zero lift, without and with body, 1956, ARC R&M 2908.
8 Hess, J L, Smith, A M O, Calculation of potential flow about arbitrary bodies, 1967, Prog in Aeronautical Sciences 8, 1.
9 Method for predicting the pressure distribution on swept wings with subsonic attached flow, 1973, ESDU TDM 73012.
10 Treadgold, D A, Jones, A F, RAE unpublished work.
11 Weber, J, Interference problems on wing-fuselage combinations, Part 1, Lifting unswept wing attached to a cylindrical fuselage at zero incidence in mid wing position, 1969, RAE TR 69150.
12 Young, A D, Zamir, M, Experimental investigation of the boundary layer in a streamwise corner, 1970, A Qu 21, 313.
13 East, L F, Hoxey, R P, Boundary layer effects in an idealised wing-body junction at low speed, 1968, RAE TR 68161.
14 Young, A D, Some special boundary layer problems, 1977, Zeitschrift fur Flugwissenschaften und Weltraumforschung 1, Heft 6, 401-414.
15 Mojola, O O, Young, A D, An experimental investigation of the turbulent boundary layer along a streamwise corner, 1971, AGARD Conf Proc 93, Turbulent Shear Flows, Paper no 12.
16 Priest, A J, Dobney, D G, Hill, R P, Measurements in the near-wake of a transport model, to determine the lift, drag and drag components using Maskell's analysis, 1981, RAE TR 8012.
17 Hutton, P G, Lift, drag and pitching moment results from a 1/20 scale model of the AW 681 in the ARA 9ft x 8ft transonic tunnel: body alone and wing + body with and without wing-body fairings and undercarriage blisters, 1964, ARA Model Test Note H14/1.
18 Jupp, J A, Interference aspects of the A310 high speed wing configuration, 1980, Paper no 11, AGARD-CP-285.
19 Bowes, G M, Aircraft lift and drag prediction and measurement, 1974, Paper no 4, AGARD Lecture Series No 67, 36,37.
20 Forsey, C R, Carr, M P, The calculation of transonic flow over three-dimensional swept wings using the exact potential equation, 1978, DGLR Symposium Transonic Configurations, Bad Harzburg.
21 Baker, T J, Forsey, C R, A fast algorithm for the calculation of transonic flow over wing-body combinations, 1981, AIAA Paper 81-1015.
22 Treadgold, D A, Wilson, K H, Some aerodynamic interference effects that influence the transonic performance of combat aircraft, 1980, Paper no 24, AGARD-CP-285.
23 Transonic Aerodynamics, 1982, Vol 81, Progress in Astronautics & Aeronautics, AIAA, ed D Nixon.
24 Whitcomb, R T, A study of the zero lift drag rise characteristics of wing-body combinations near the speed of sound. 1956, NACA Report 1273.
25 Heaslet, M A, Lomax, H, Spreiter, J R, Linearised compressible flow theory for sonic flight speeds, 1950, NACA Report 956.
26 Sheppard, L M, Methods for determining the wave drag of non-lifting wing body combination, 1958, ARC R&M 3077.
27 Lomax, H, The wave drag of arbitrary configurations in linearised flow as determined by areas and forces in oblique planes, 1955, NACA RMA55A18.
28 Barnwell, R W, Analyses of transonic flow about lifting wing-body configurations, 1975, NASA TR R-440.
29 Barnwell, R W, Approximate method for calculating transonic flow about lifting wing-body configurations, 1976, NASA TR R-4[illegible].
30 Drag and other aerodynamic effects of external stores, 1977, AGARD-AR-107.
31 Kane, E J, Middleton, W D, Consideration of aerodynamic interference in supersonic airplane design, 1971, Paper no 3, AGARD-CP-71-71.
32 Cheng, H K, Hafez, H M, Transonic equivalence rule: a nonlinear problem involving lift, 1975, Vol 72, Part 1, J Fluid Mech, 161-187.
33 Chan, Y Y, An experimental study of the transonic equivalence rule with lift, 1982, NRC Aeronautical Report LR-609.
34 Bocci, A J, Aerodynamic research on near-sonic transports: experimental results and analysis, ARA report to be published.
35 Albone, C M, Hall, M G, Joyce, Gaynor, Numerical solutiosn for transonic flows past wing-body combinations, 1975, IUTAM Symposium Transsonicum II, Göttingen.

36 Baker, T J, Ogle, Mrs F A, A computer program to compute transonic flow over an axisymmetric solid body, 1977, ARA Memo 197.
37 Yoshihara, H, Introductory lecture to AGARD/VKI course in Subsonic/Transonic Aerodynamic Interference for Aircraft, 1983, AGARD-FDP-VKI Special Course.
38 Wai, J C, Sun, C C, Yoshihara, H, Transonic perturbation analysis of wing-fuselage-nacelle-pylon configurations with powered jet exhausts, 1982, NASA CR 165852.
39 Whitcomb, R T, Methods for reducing subsonic drag due to lift, 1977, AGARD/VKI Special Course on Concepts for Drag Reduction.
40 Patterson, J C Jr, A wind tunnel investigation of a high bypass engine on wing-nacelle interference drag of a subsonic transport, 1968, NASA TN D-4693.
41 Kutney, J T, Piszkin, S T, Reduction of drag rise on the Convair 990, 1963, AIAA 63-276, 1964, Vol 1, J Aircraft No 1.
42 Harris, A E, Pauley, G I, Simulation techniques for pylon-mounted turbofan engines, 1975, ARA Report 36.
43 Harris, A E, Carter, E C, Wind tunnel test and anslysis techniques using powered simulators for civil nacelle installation drag assessment, 1981, Paper no 24, AGARD-CP-301, Aerodynamics of Power Plant Installation.
44 Pugh, G, Harris, A E, Establishment of an experimental technique to provide accurate measurement of the installed drag of close coupled civil nacelle/airframe configurations, using a full span model with turbine powered engine simulators, 1981, Paper no 25, AGARD-CP-301, Aerodynamics of Power Plant Installation.
45 Bagley, J A, Wind tunnel experiments on the interference between a jet and a wing at subsonic speeds, 1968, Paper no 22, AGARD-CP-35.
46 Yu, N J, Transonic flow simulations for complex configurations with surface-fitted grids, 1981, AIAA Paper 81-1258.
47 Forsey, C R, An extension of the transonic wind-body code to include underwing pylon nacelle effects, ARA paper to be published.
48 Haines, A B, Prospects of exploiting favourable and minimising adverse aerodynamic interference in external store installations, 1980, Paper no 5, AGARD-CP-285, 1983, AGARD Lecture Series.
49 Williams, P R G, Stewart, D J, The complex aerodynamic interference pattern due to rear fuselage mounted power plants, 1971, Paper no 24, AGARD-CP-71-71.
50 Haines, A B, Wingfield, J G, Results of a test programme designed to exploit the favourable, and alleviate the unfavourable interference effects of an aft-fuselage nacelle installation (including wing-mounted bodies and changes to the fuselage cross-sectional shape), 1970, ARA Report 13.
51 Laugher, R D, The influence of close-coupled rer fuselage mounted nacelles on the design of an advanced high speed wing, 1981, Paper no 28, AGARD-CP-301.
52 Drag and other aerodynamic effects of external stores, 1977, AGARD-AR-107.
53 Haines, A B, Drag of external stores: present standards and possibilities for reduction, 1975, ARA Report 40.
54 Haines, A B, The reduction of the installed drag of multiple store carriers, 1975, Paper no 7, JTCG Aircraft/Stores Compatibility Symposium Proceedings, Arlington.
55 Evaluation of the conformal carriage concept on the performance and basic static longitudinal stability of the F-4E aircraft, 1971, AFATL-TR-71-76.
56 Lee, P, Drag measurements at transonic speeds of individual stores within multiple store arrangements, Unpublished RAE memo.
57 Whitcomb, R T, A design approach and selected wind tunnel results at high subsonic speeds for wing-tip mounted winglets, 1976, NASA TN D-8260.
58 Flechner, S G, Jacobs, P F, Whitcomb, R T, A high subsonic speed wind-tunnel investigation of winglets on a representative second-generation jet transport wing, 1976, NASA TN D-8264.
59 Lundry, J L, A numerical solution for the minimum induced drag and the corresponding loading of non-planar wings, NASA CR 1218.
60 Boppe, C W, Aidala, P V, Complex configuration analysis at transonic speeds, 1980, Paper no 26, AGARD-CP-285.
61 Spillman, J, Riding on air, 1982, C of A Note 8113, Inaugural Professorial Lecture, Cranfield College of Aeronautics.
62 Spillman, J, The use of wing-tip sails to reduce vortex drag, 1978, JRAeS.
63 Moss, G F, Some UK research studies of the use of wing-body strakes on combat aircraft configurations at high angles of attack, 1978, Paper no 4, AGARD-CP-247.
64 Fiddes, S P, Smith, J H B, Strake-induced separation at moderately swept leading edges, 1977, RAE TR 77128.
65 Vint, A, Jet-wing interaction to give improved combat aircraft performance, 1980, Paper no 17, AGARD-CP-285.

FIG. 1

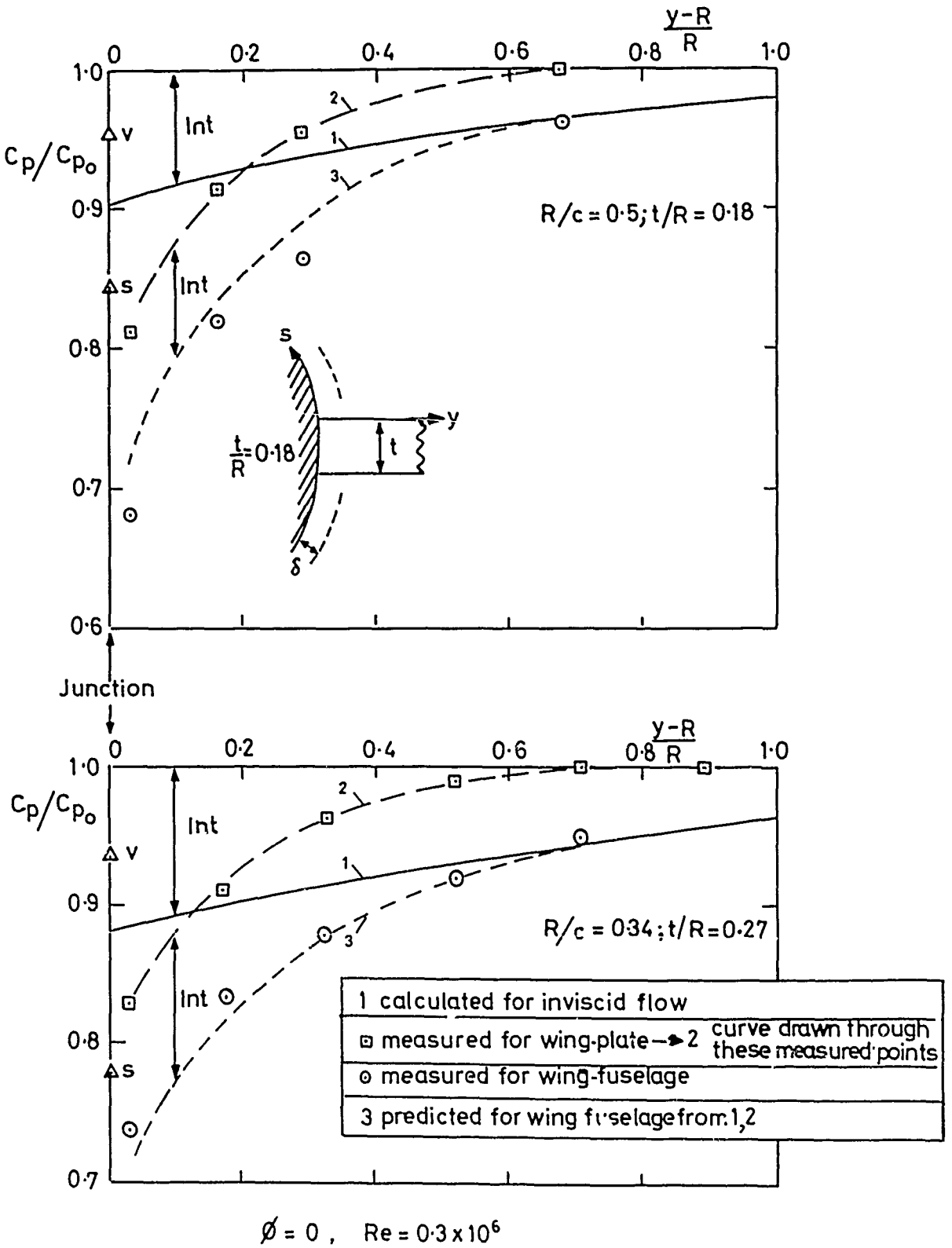

FIG. 1 PRESSURE DISTRIBUTIONS ALONG THE SPAN OF A RECTANGULAR WING AT ZERO LIFT. TESTS BY KÖRNER[6]

FIG. 2(a,b)

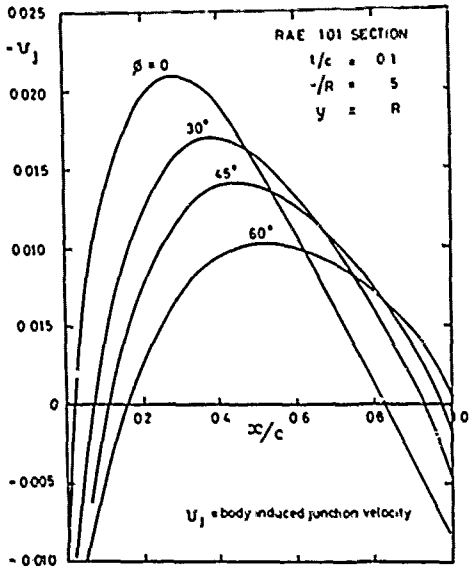

FIG 2(a) EFFECT OF SWEEPBACK ON BODY-INDUCED JUNCTION VELOCITIES AT ZERO LIFT

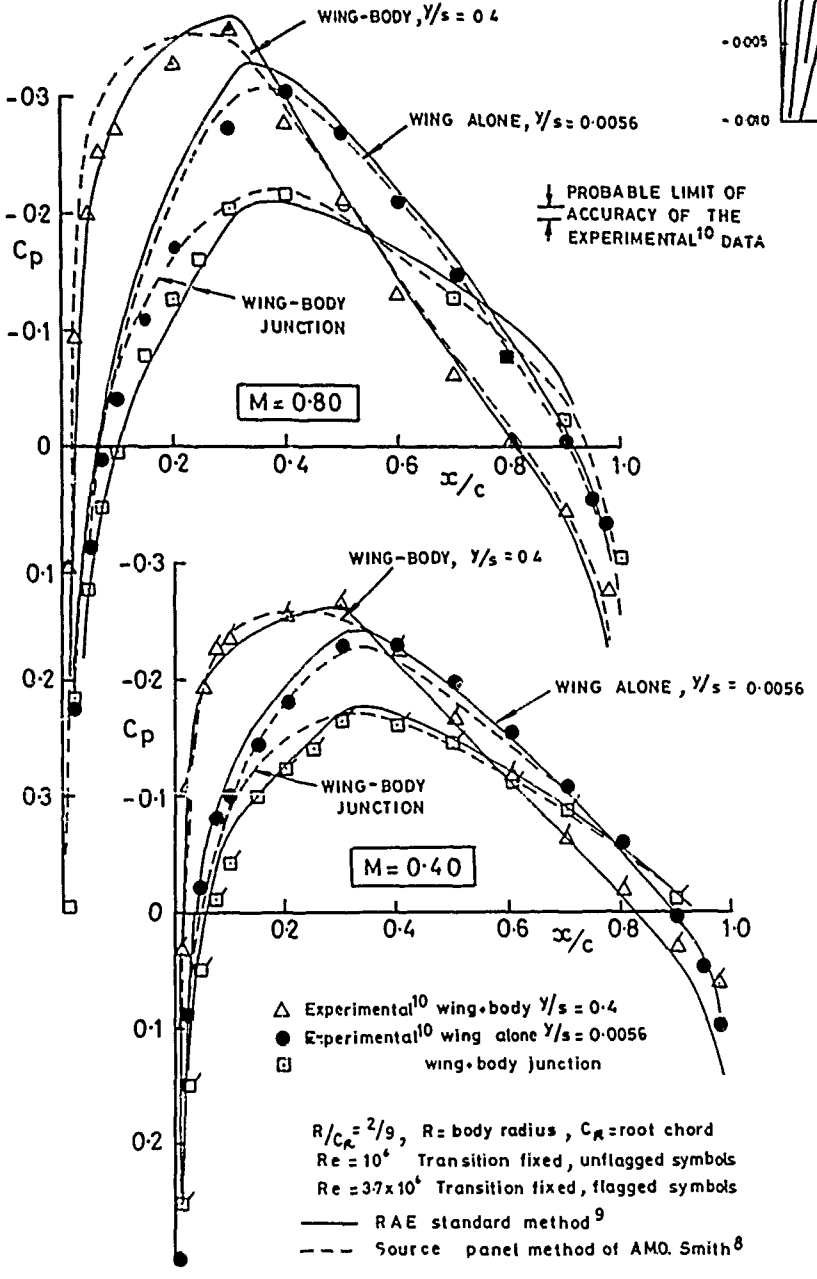

FIG. 2(b) CHORDWISE PRESSURE DISTRIBUTIONS ON A SWEPT WING AT ZERO LIFT

FIG. 3, 4.

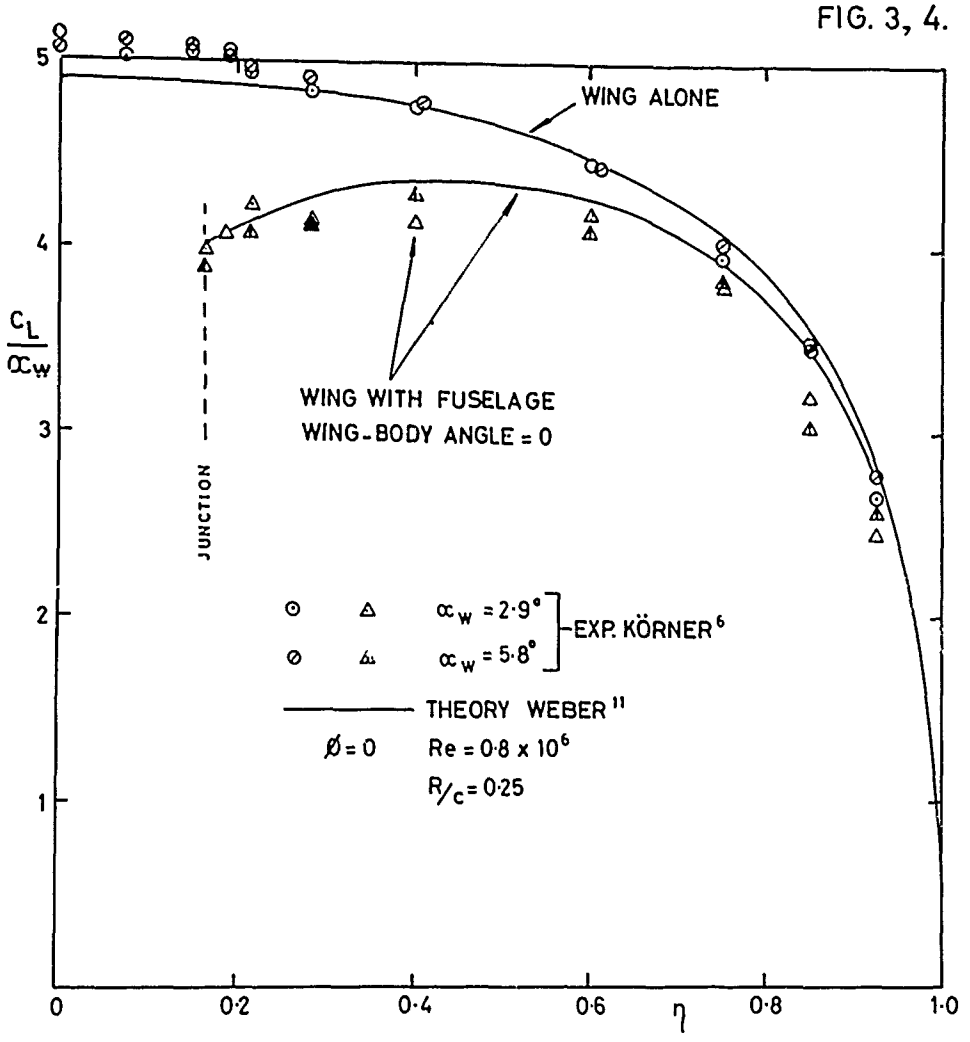

FIG.3 SPANWISE LOADINGS OVER A RECTANGULAR WING WITH AND WITHOUT FUSELAGE

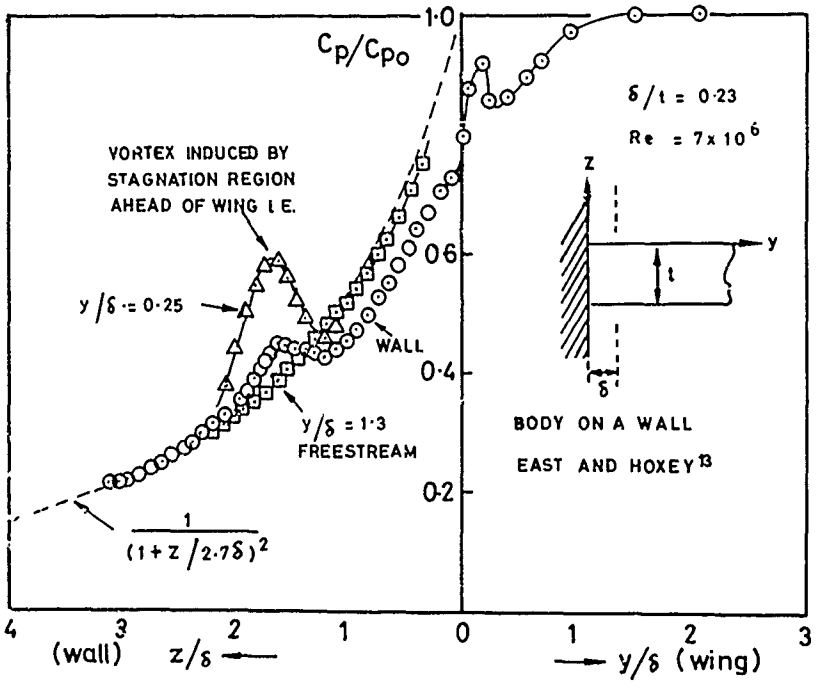

FIG.4 VISCOUS EFFECTS IN RIGHT-ANGLE JUNCTIONS

FIG. 5 (a,b)

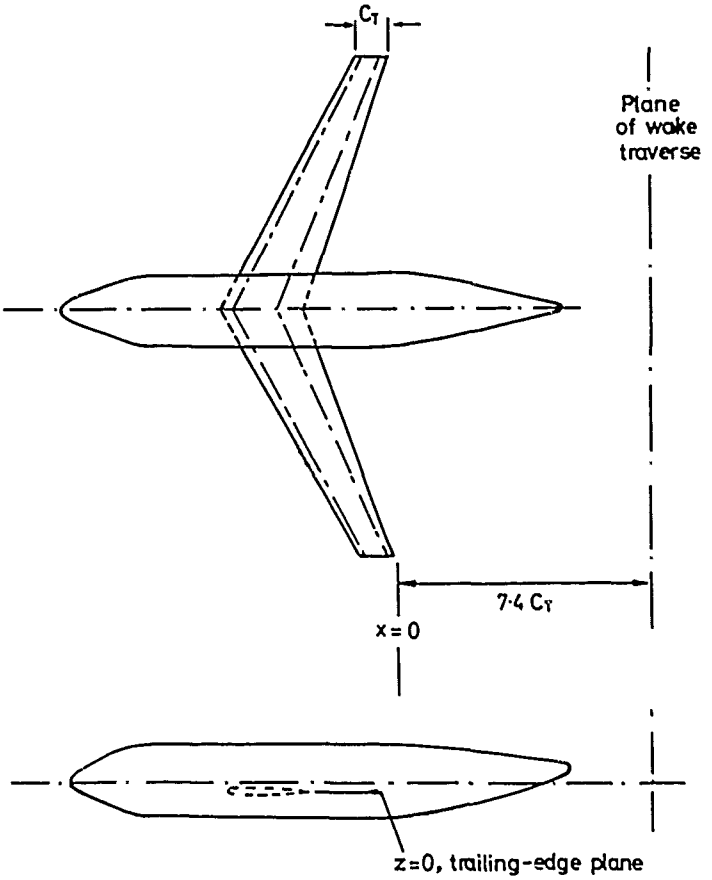

WING HAS NO DIHEDRAL OR TWIST

(a) G.A. of model and wake traverse plane

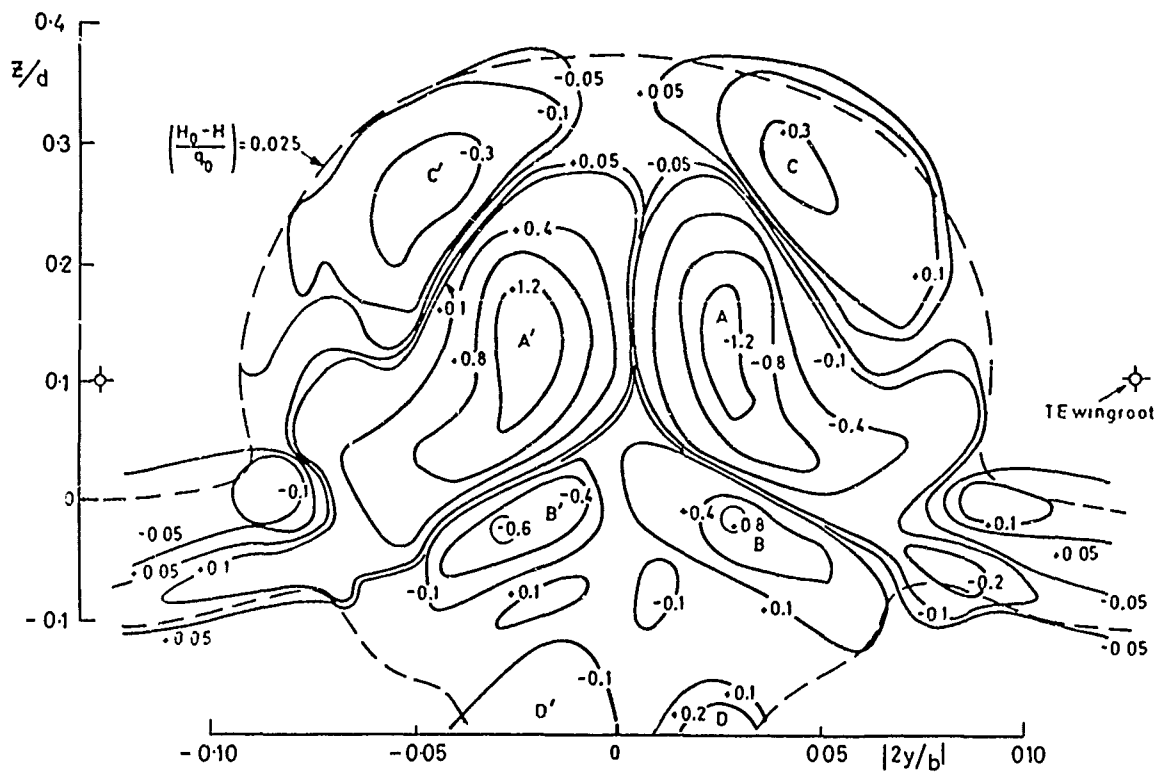

(b) Iso-vorticity contours (constant $\zeta\bar{c}/U_0$) in plane of wake traverse downstream of fuselage

FIG. 5 3D WAKE TRAVERSE TESTS IN RAE LOW SPEED TUNNEL

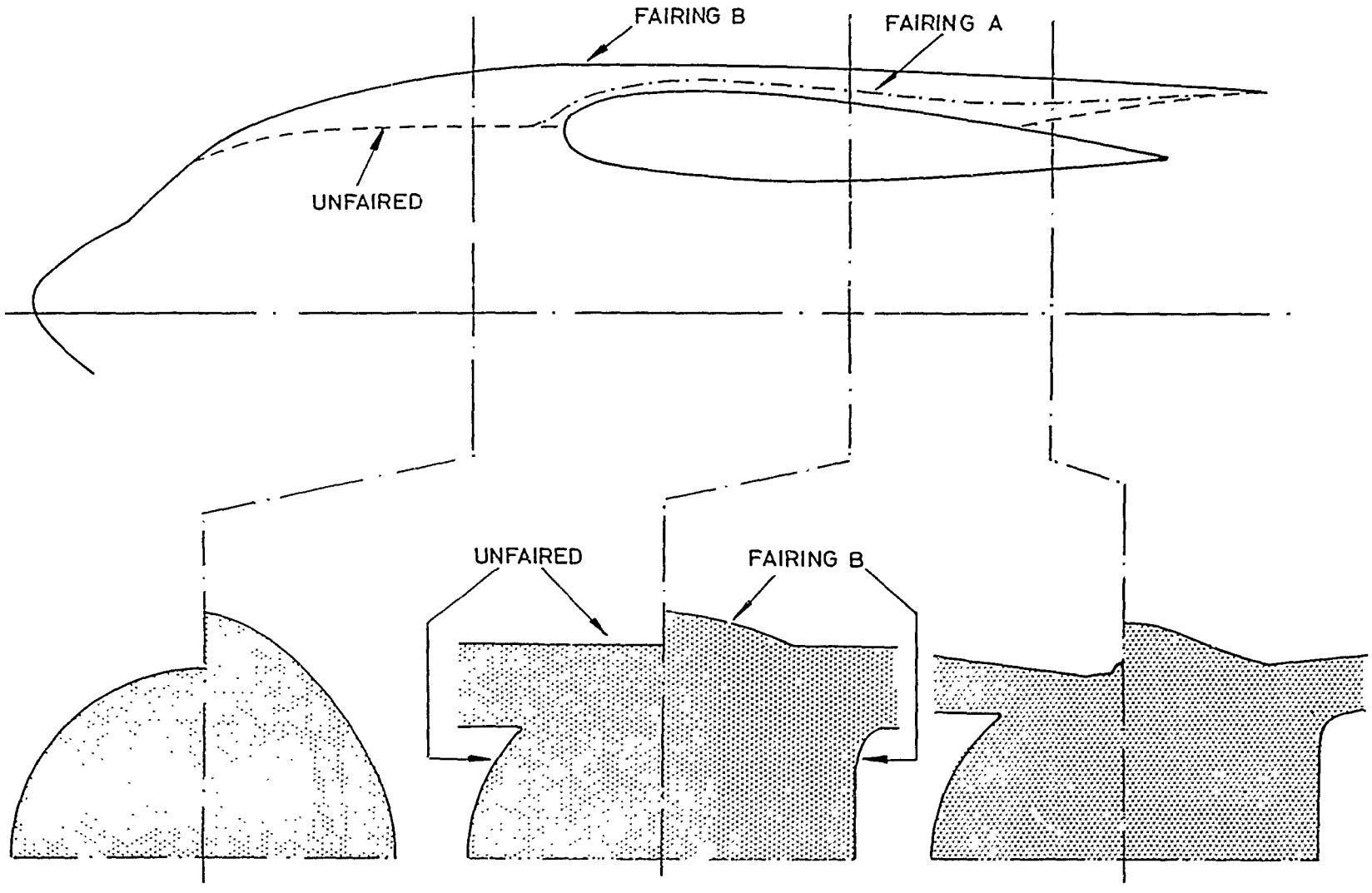

(a) Geometry of fairings

FIG. 6. WING–BODY FAIRING RESEARCH : HIGH WING SUBSONIC TRANSPORT

FIG. 6(a)

FIG. 6(b,c)

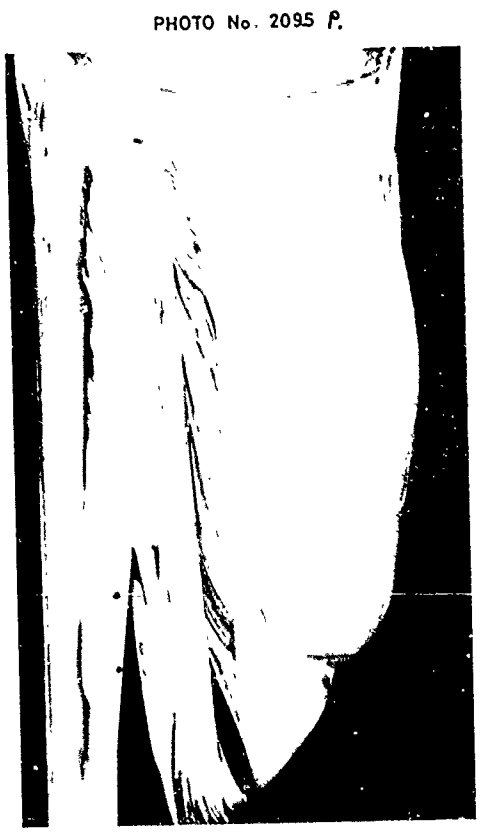

(c) Oil flow at design condition, $M=0.71$, $C_L=0.5$.

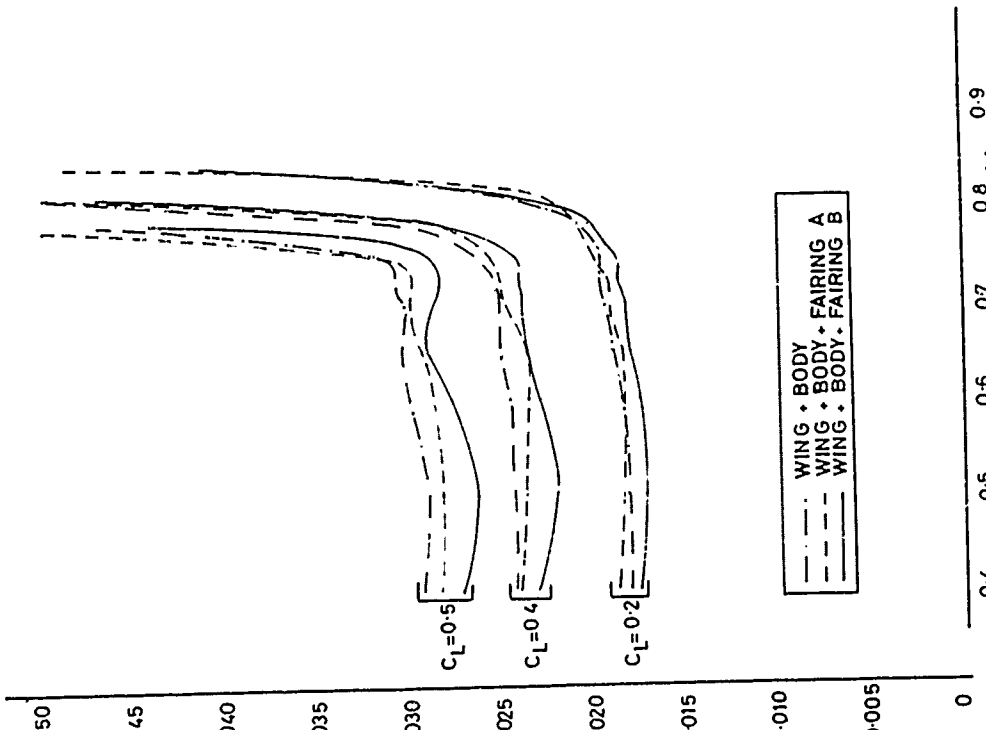

(b) Comparative drag data.

FIG. 6. WING BODY FAIRING RESEARCH: HIGH WING SUBSONIC TRANSPORT

FIG. 7(a,b)

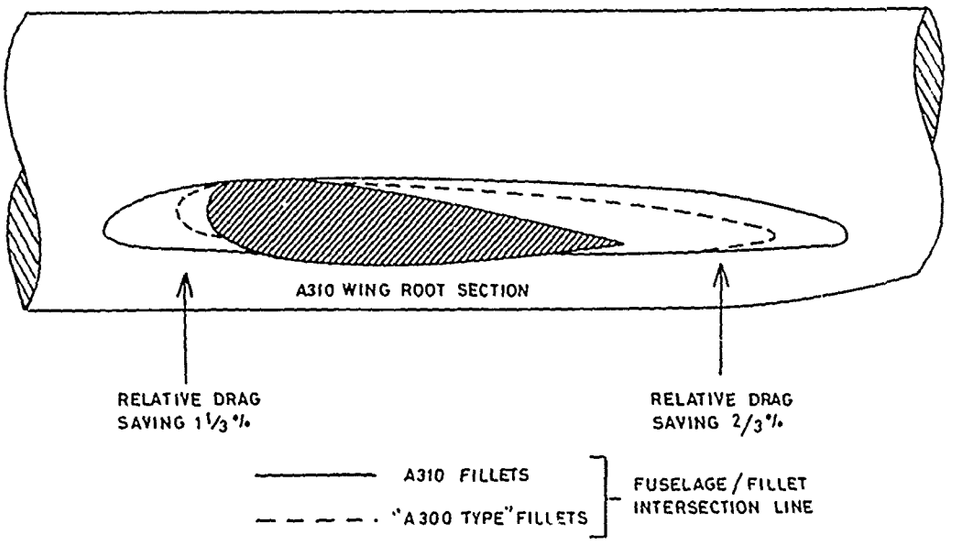

(a)Drag improvements relative to "A300 type" fillets

(b) Surface flow over leading edge fillet

FIG.7 WING-BODY FILLET ACHIEVEMENTS: A 310

FIG. 8

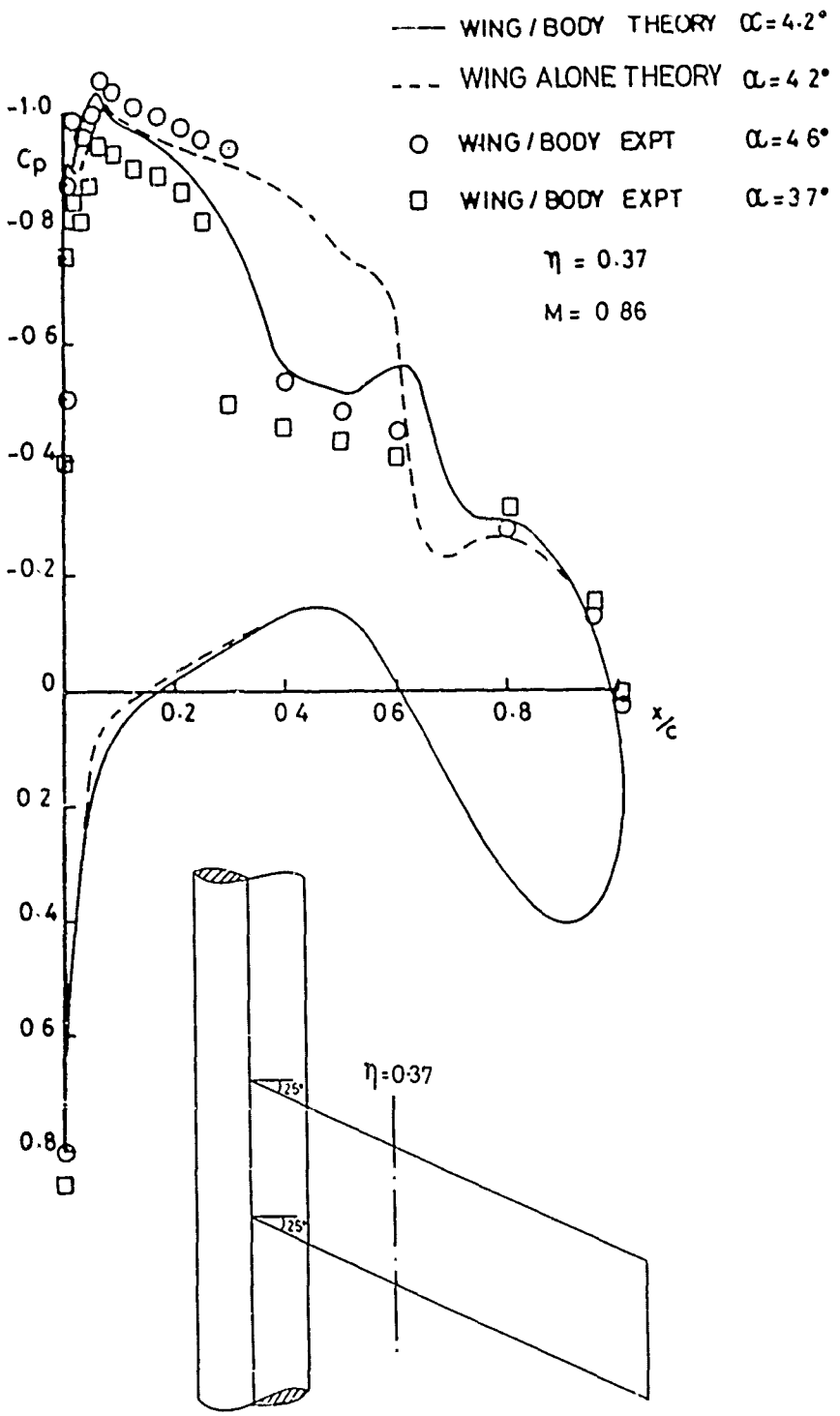

FIG. 8 INFLUENCE OF BODY ON FLOW OVER SIMPLE SWEPT-BACK WING

FIG. 9(a,b)

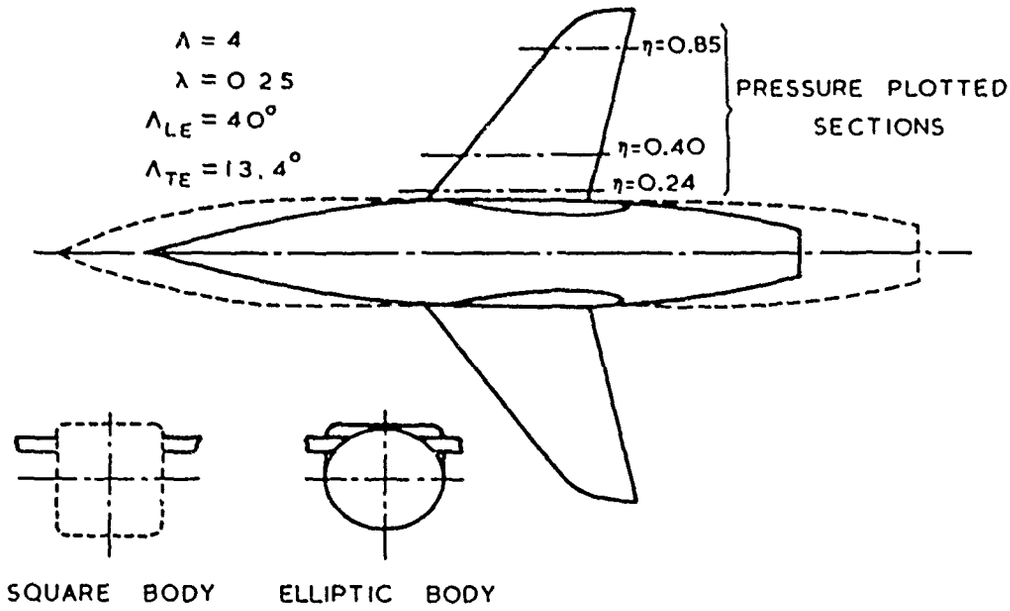

(a) Model geometry

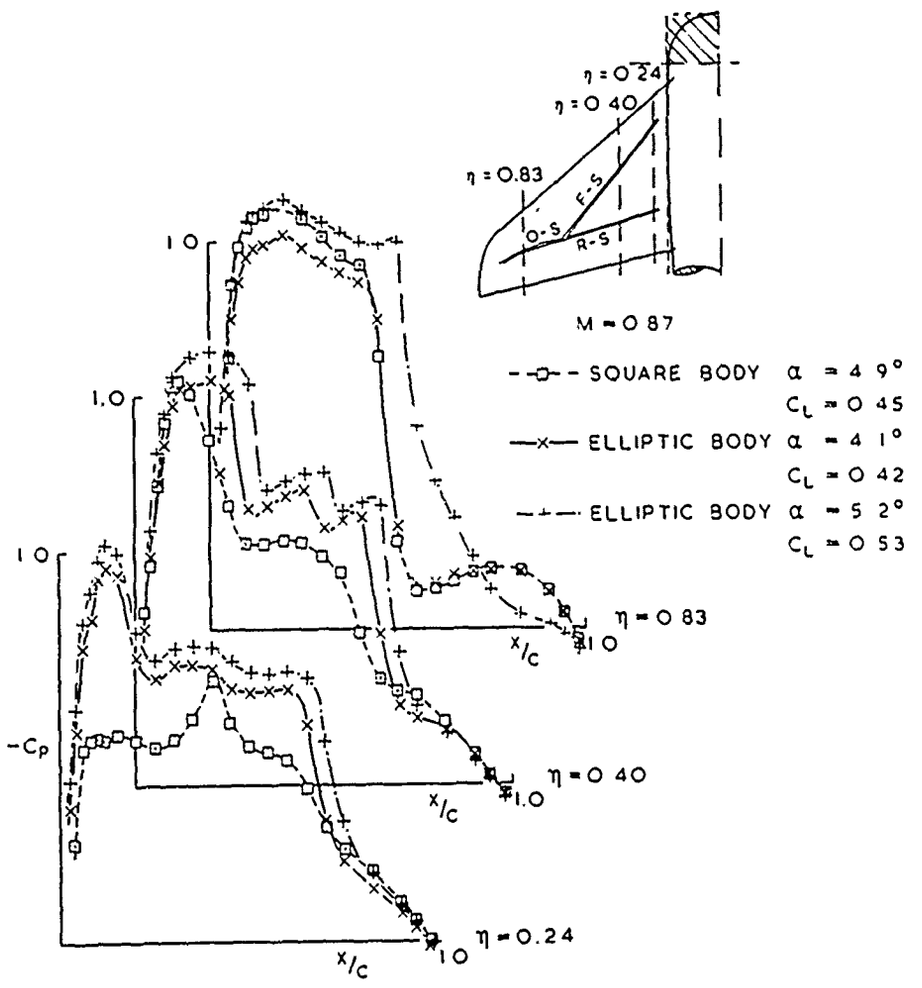

(b) Pressures at design Mach number, M= 0·87

FIG. 9 EFFECT OF BODY DESIGN ON WING PRESSURES: COMBAT AIRCRAFT RESEARCH MODEL

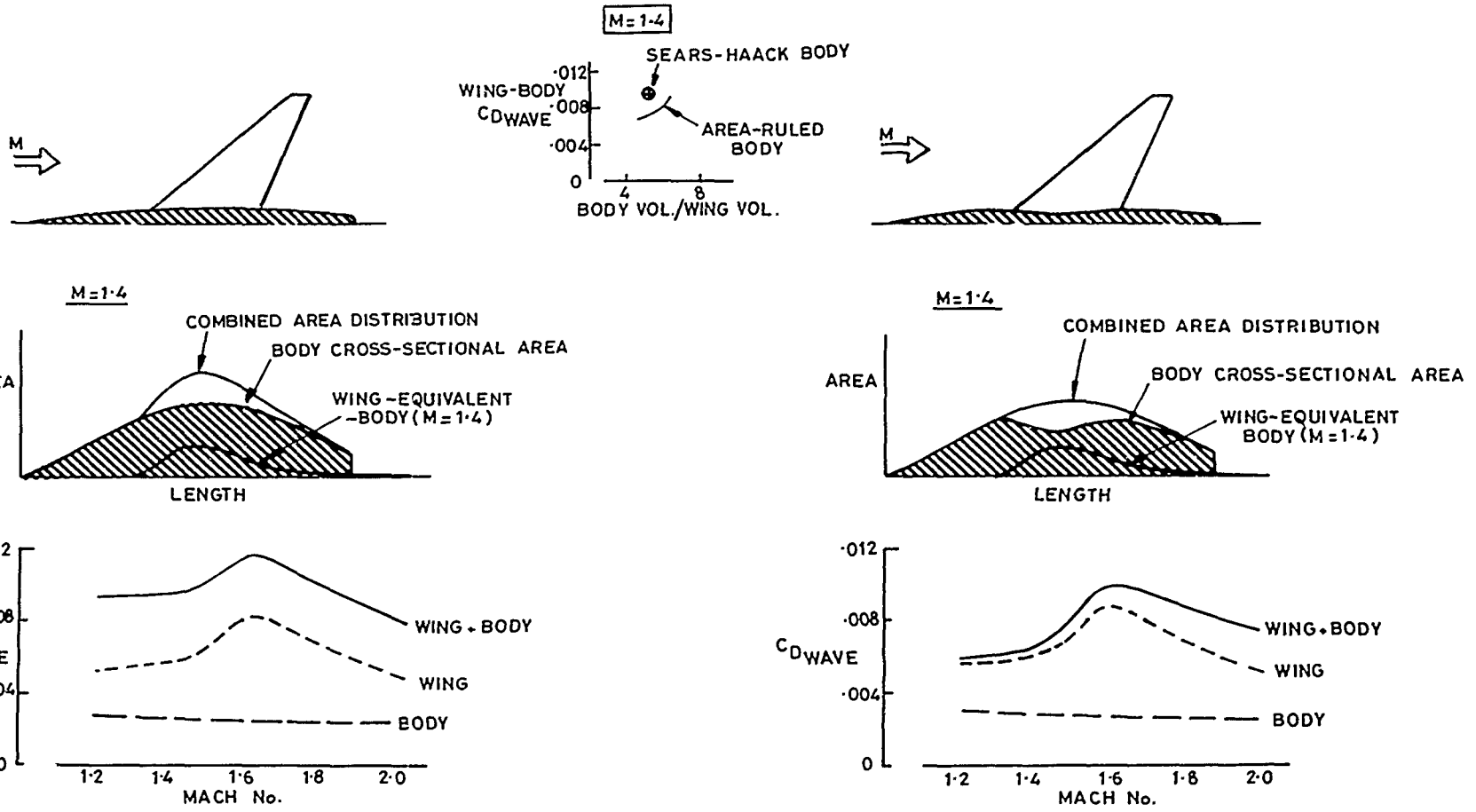

(a) SEARS-HAACK BODY

(b) AREA-RULED BODY

(a) Geometry and wave drag reduction

FIG. 10 EFFECT OF AREA-RULING FOR M = 1·4

FIG. 10 (a)

FIG. 10 (b)

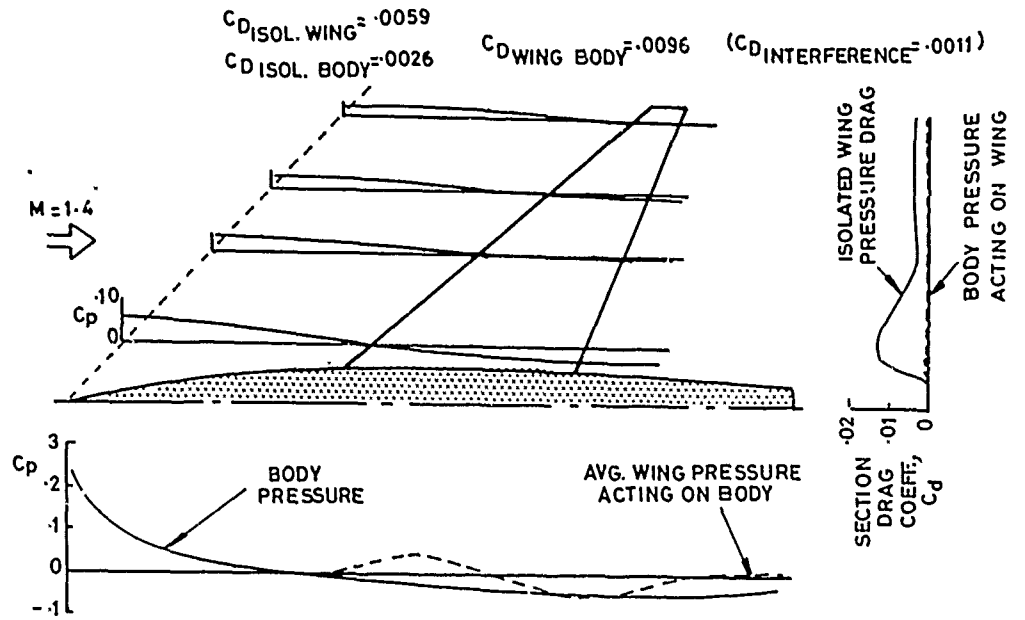

(a) SEARS HAACK BODY

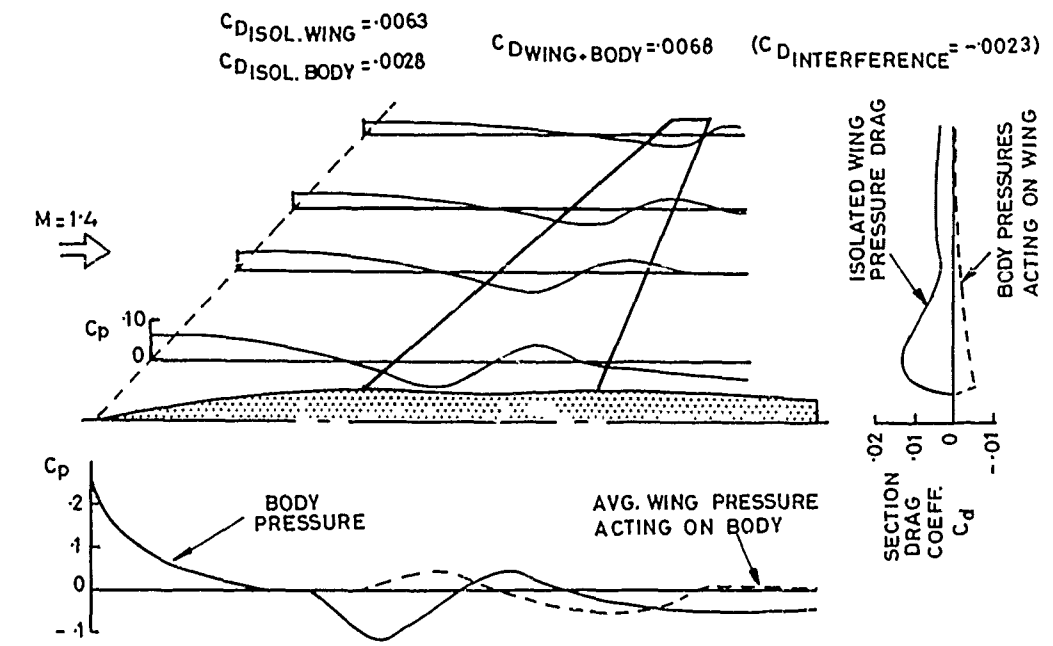

(b) AREA RULED BODY

(b) Interference pressure fields

FIG. 10 EFFECT OF AREA-RULING FOR M = 1·4

FIG. 11(a)

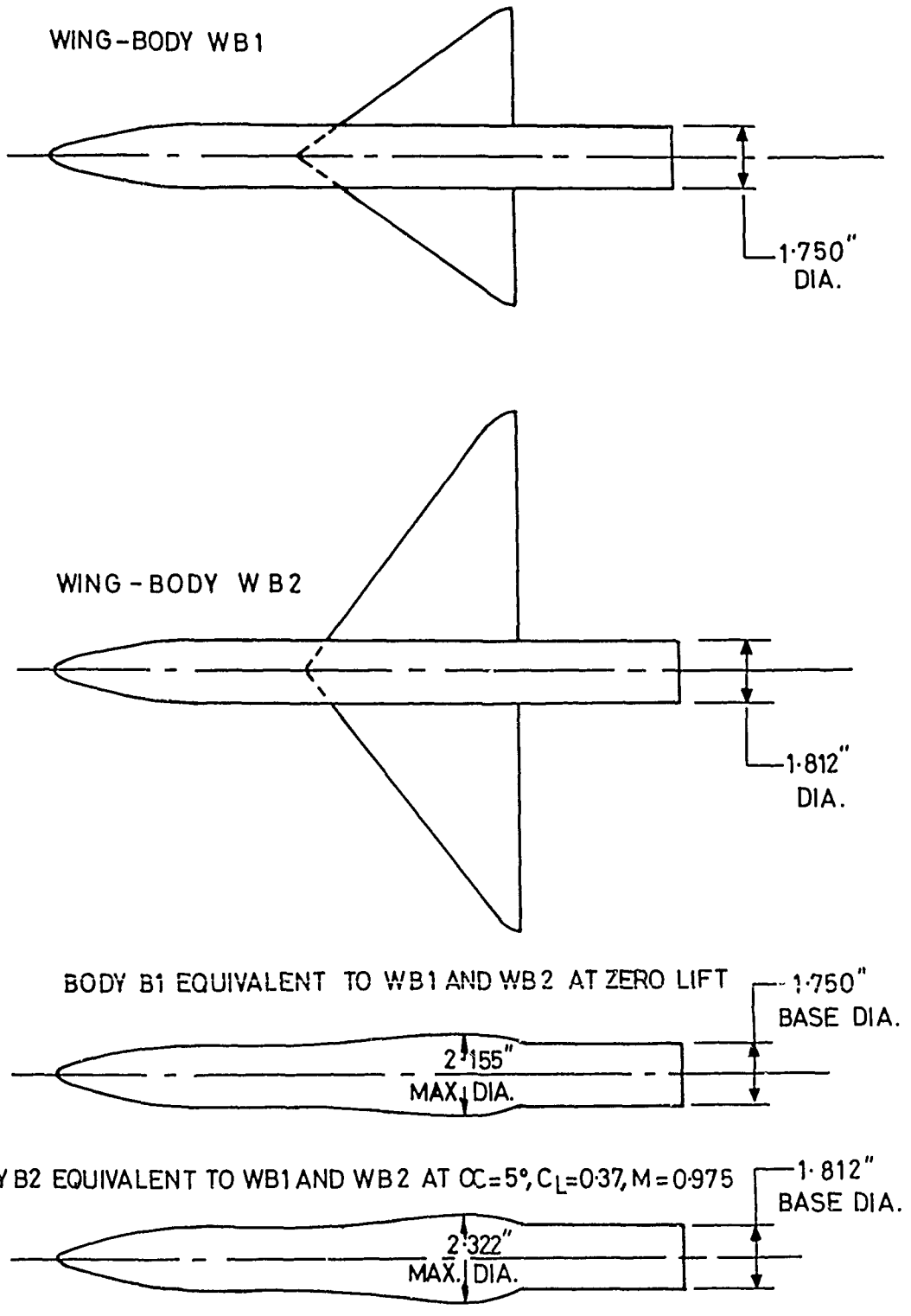

(a) Geometry of model tested at NAE, Ottawa

FIG. 11 EXTENSION OF AREA-RULE TO A LIFTING CONDITION

FIG. 11(b,c)

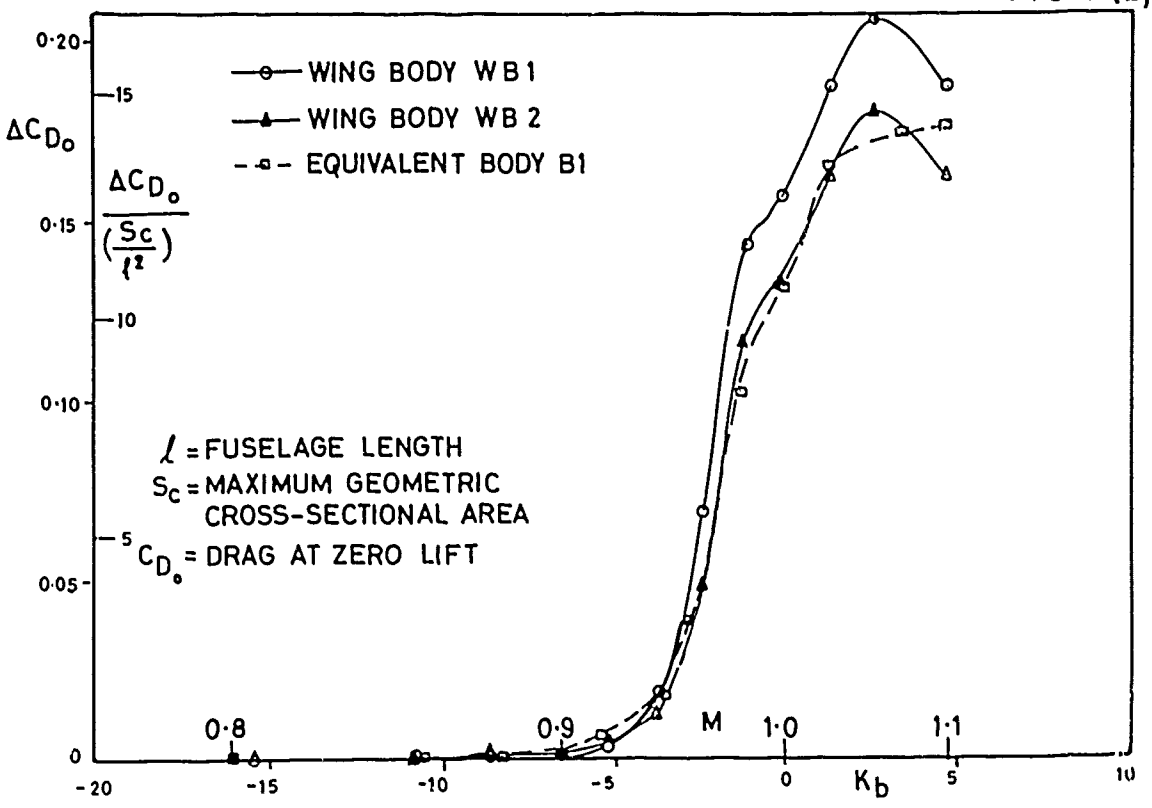

(b) Drag comparison: zero lift

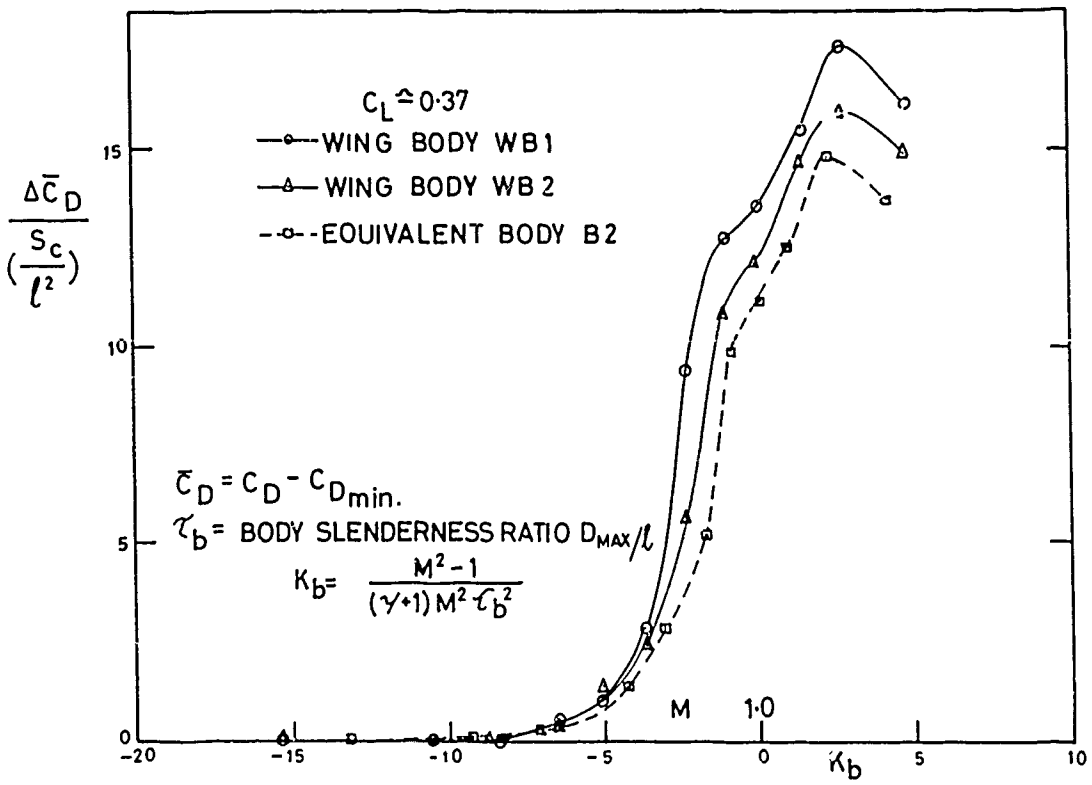

(c) Drag comparison: design lifting condition

FIG 11 EXTENSION OF AREA-RULE TO A LIFTING CONDITION

FIG.12(a,b)

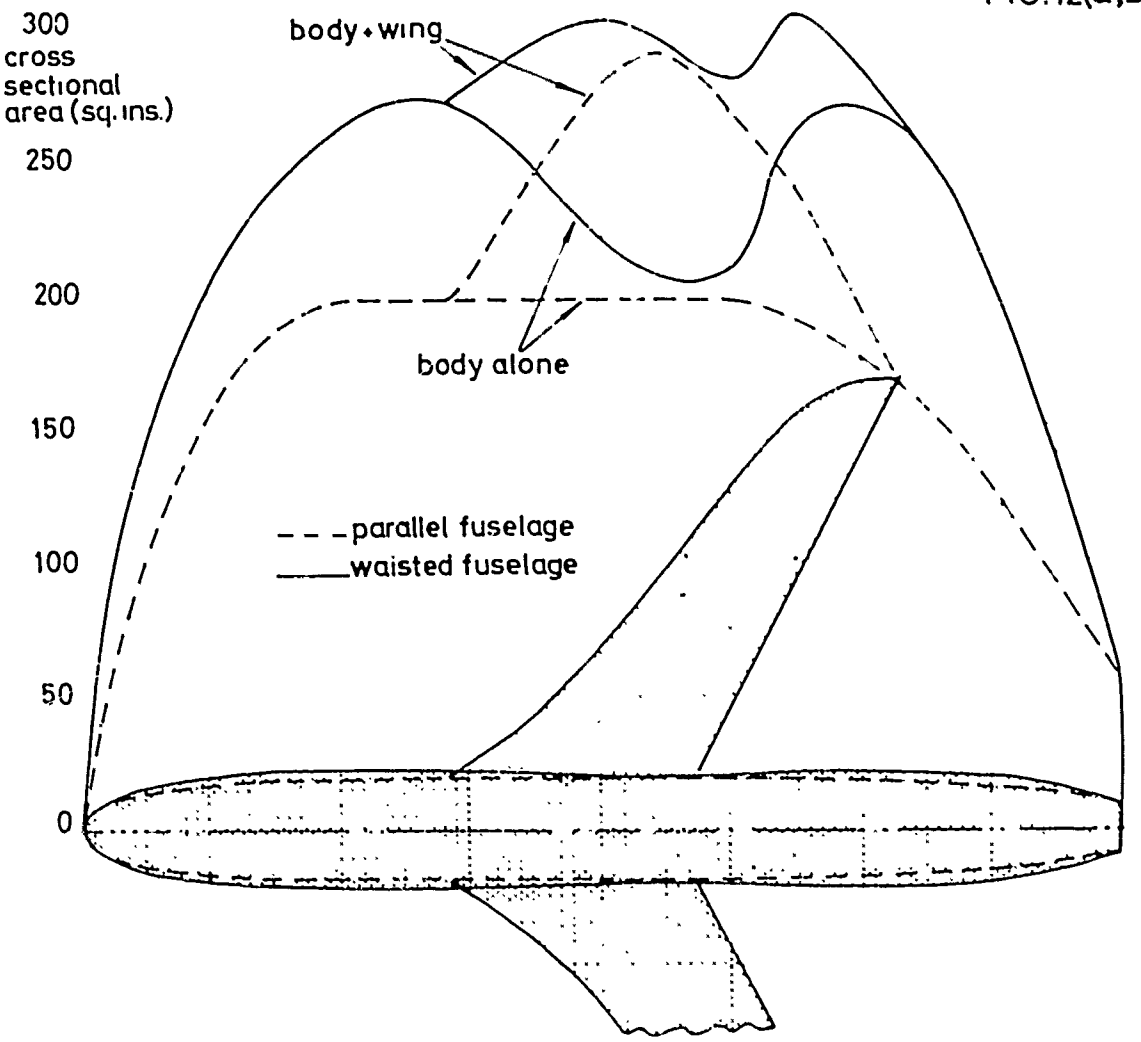

(a) Model geometry

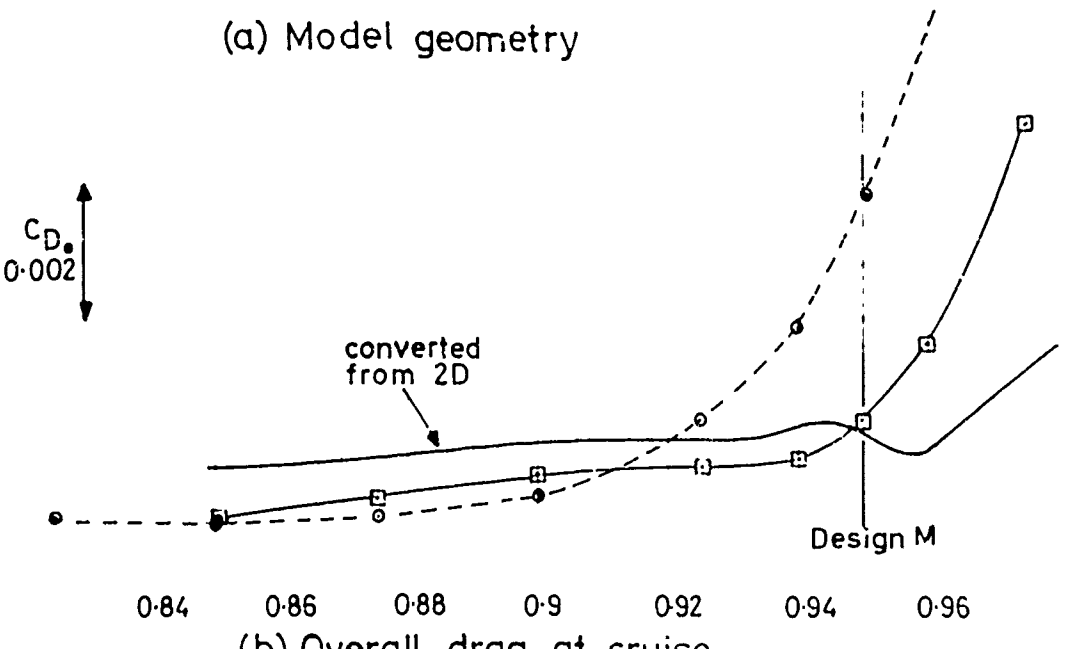

(b) Overall drag at cruise

FIG.12 NEAR-SONIC TRANSPORT: EFFECT OF WAISTED FUSELAGE

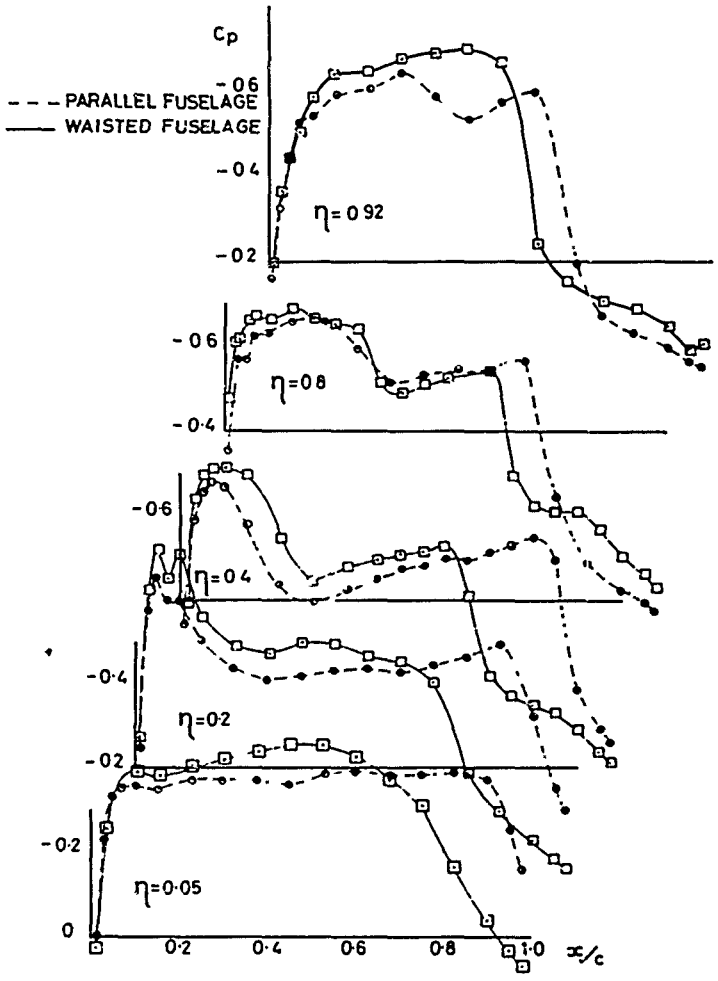

(c)Wing pressures at M=0·95, design C_L

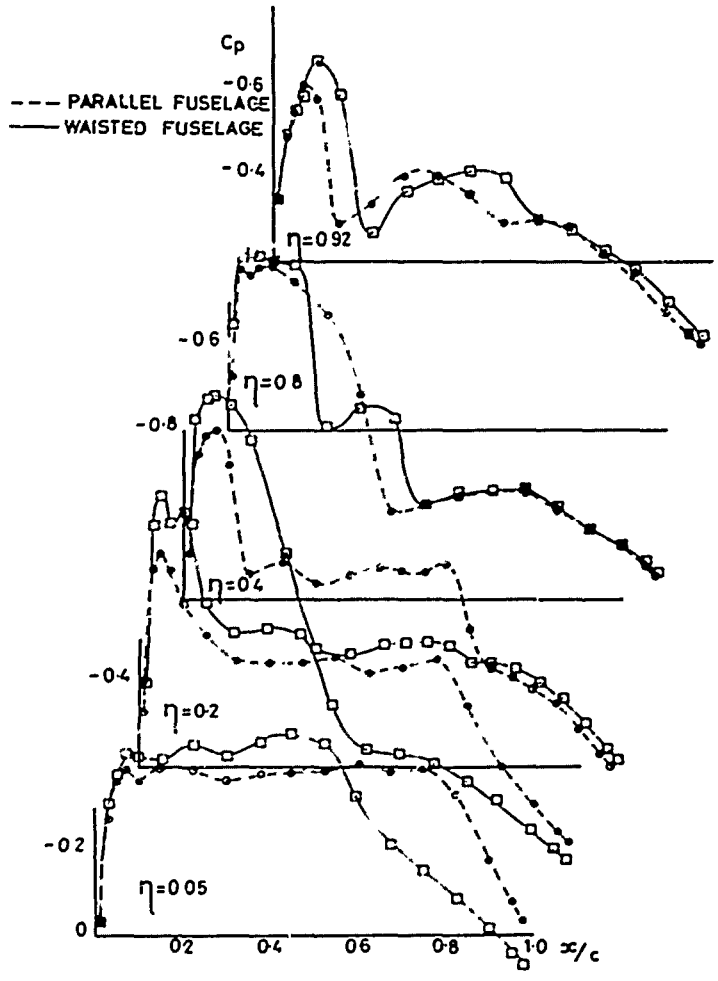

(d)Wing pressures at M=0·90, design C_L

FIG.12 NEAR-SONIC TRANSPORT: EFFECT OF WAISTED FUSELAGE

FIG.12(c,d)

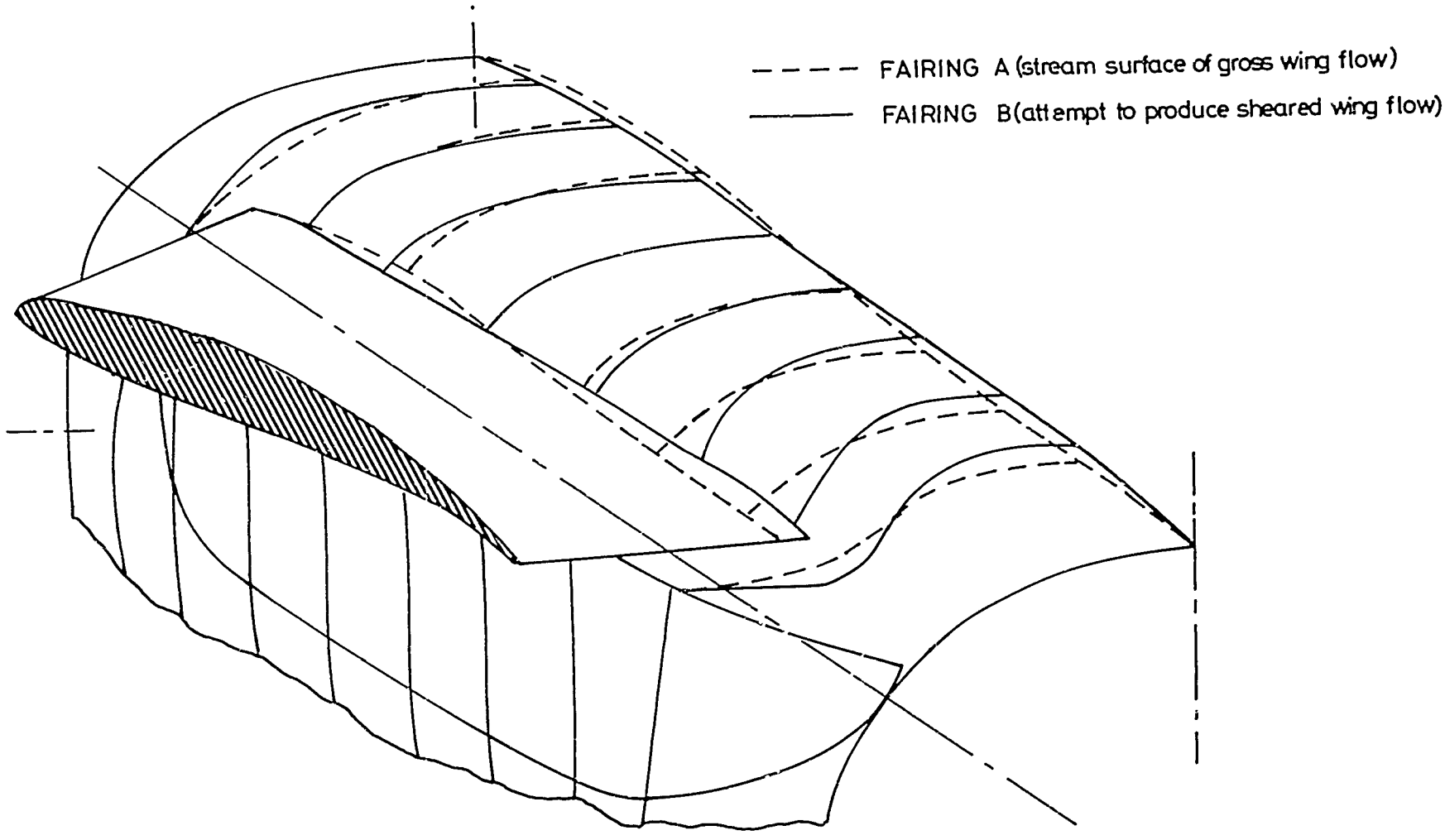

(a) Geometry of top-cap fairings

FIG. 13 EFFECT OF WING-BODY FAIRINGS: COMBAT AIRCRAFT RESEARCH MODEL

FIG. 13(a)

FIG. 13 (b)

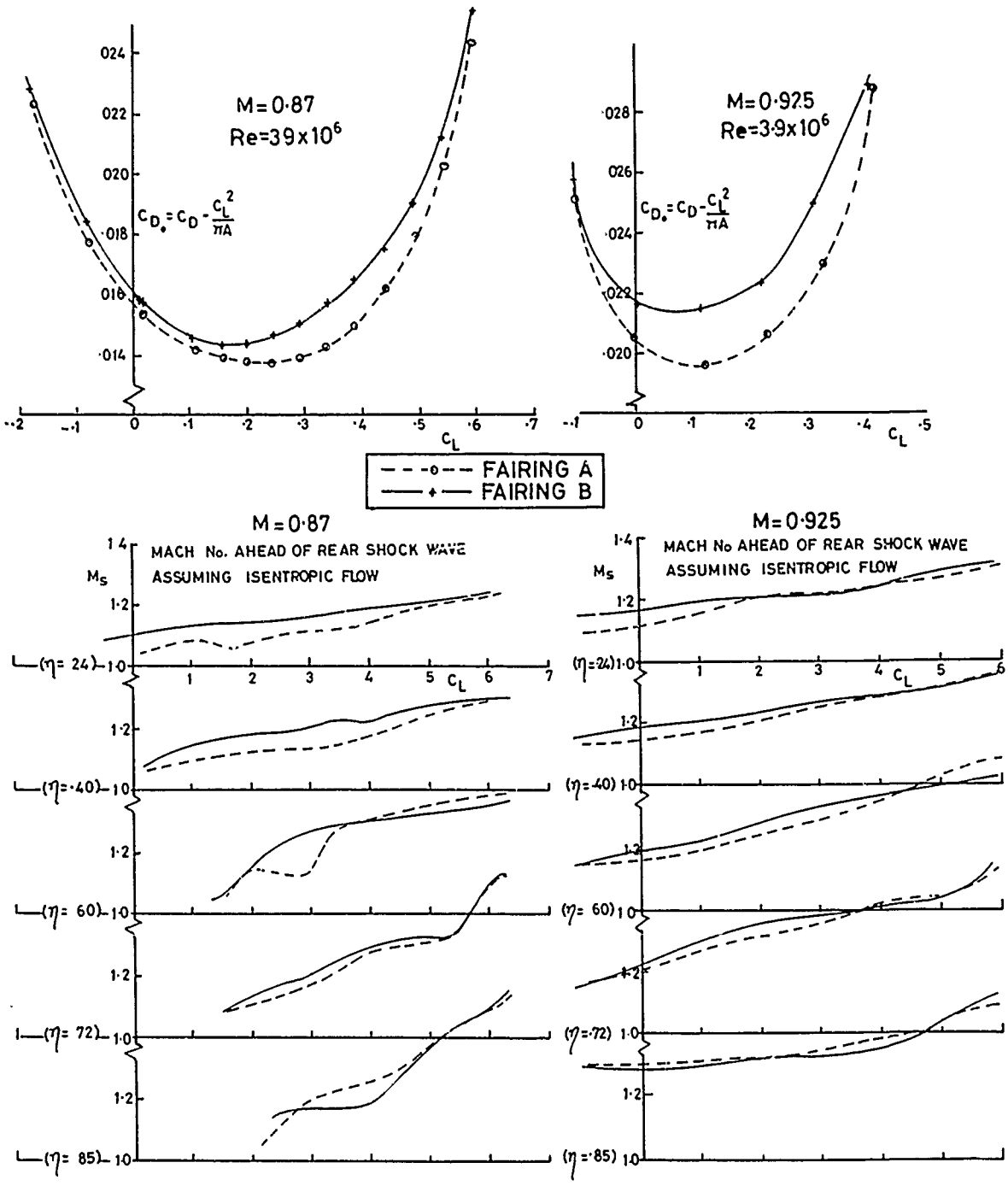

(b) Overall drag and rear shock strength

FIG.13 EFFECT OF WING–BODY FAIRINGS: COMBAT AIRCRAFT RESEARCH MODEL

FIG. 13(c, d)

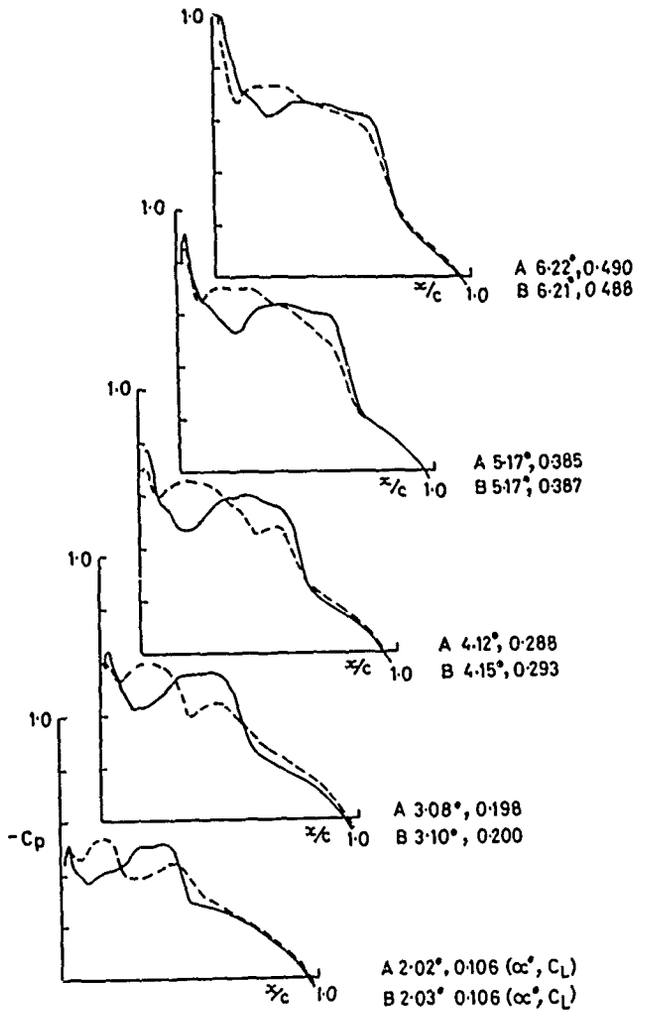

(c) Upper surface pressures, 0·24 x semi-span

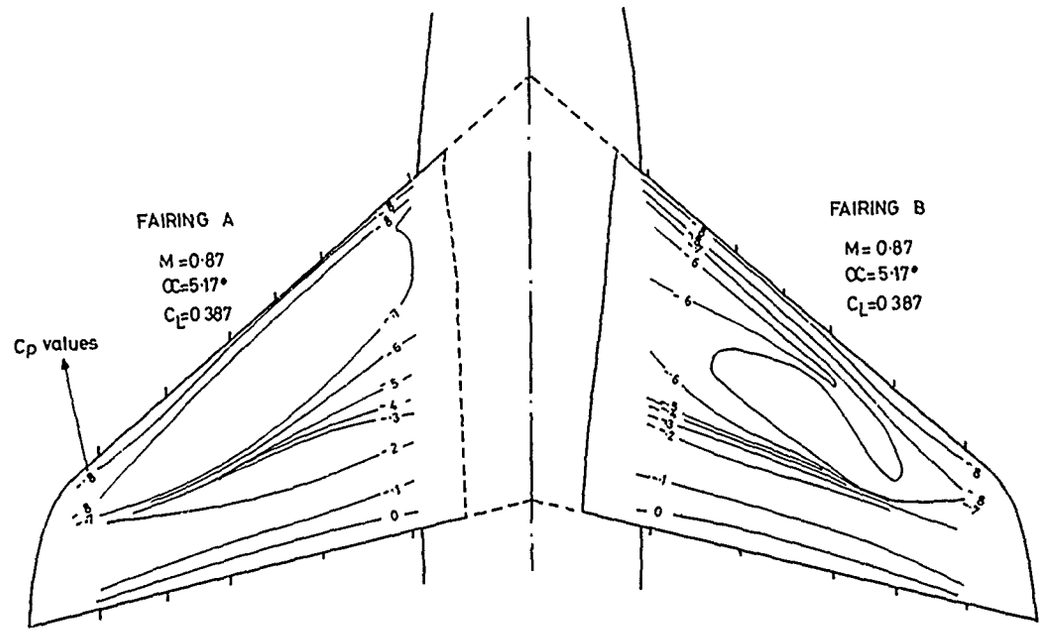

(d) Upper surface isobar patterns

FIG. 13 EFFECT OF WING - BODY FAIRINGS: COMBAT AIRCRAFT RESEARCH MODEL

LOCAL DRAG INCREMENTS GIVEN BY SURFACE PRESSURE INTEGRATION

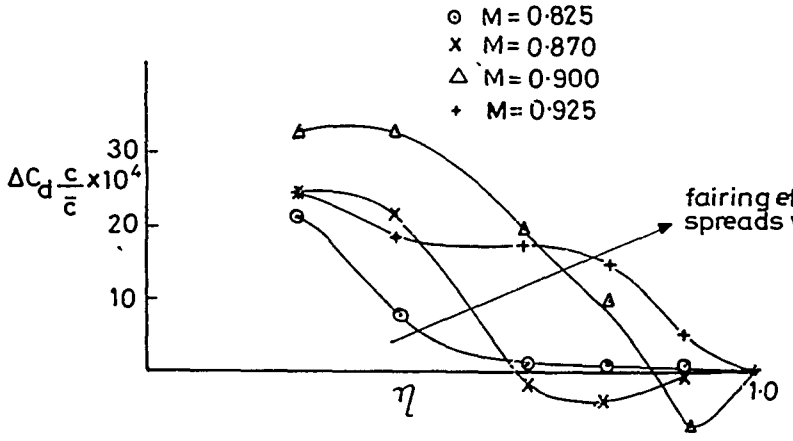

COMPARISON OF DRAG INCREMENTS FROM BALANCE AND PRESSURE MEASUREMENTS

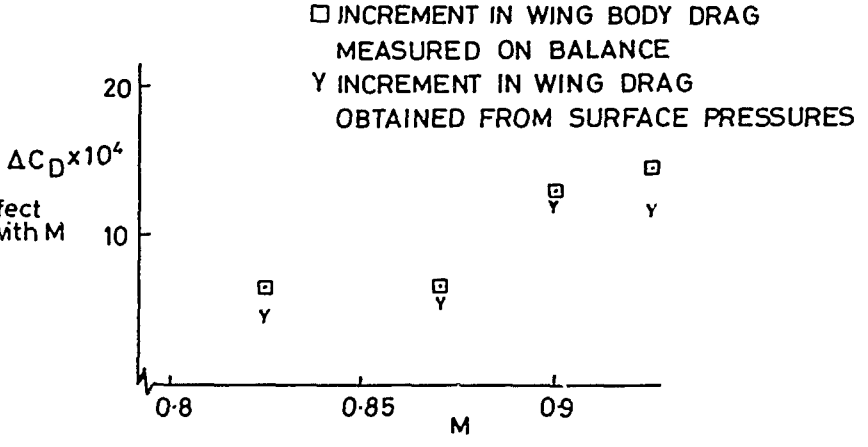

$\alpha = 3{\cdot}1°$

Δ : FAIRING B — FAIRING A

(e) Drag differences: overall vs. pressure integrations

FIG. 13 EFFECT OF WING–BODY FAIRINGS: COMBAT AIRCRAFT RESEARCH MODEL

FIG 13(e)

FIG. 14.

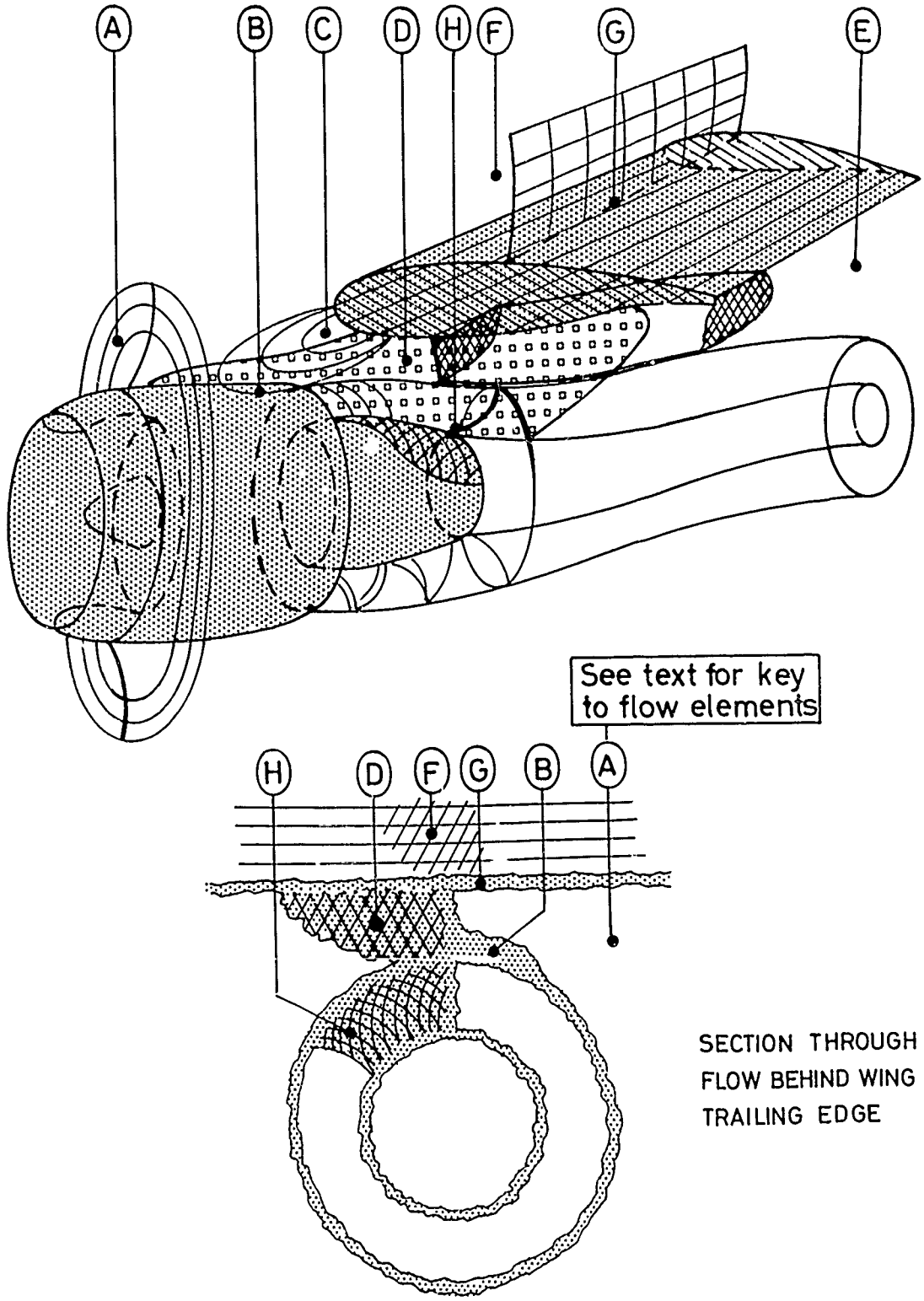

FIG. 14. MAJOR ELEMENTS OF THE WING PYLON NACELLE INTERFERENCE FLOW FIELD

FIG. 15(a,b)

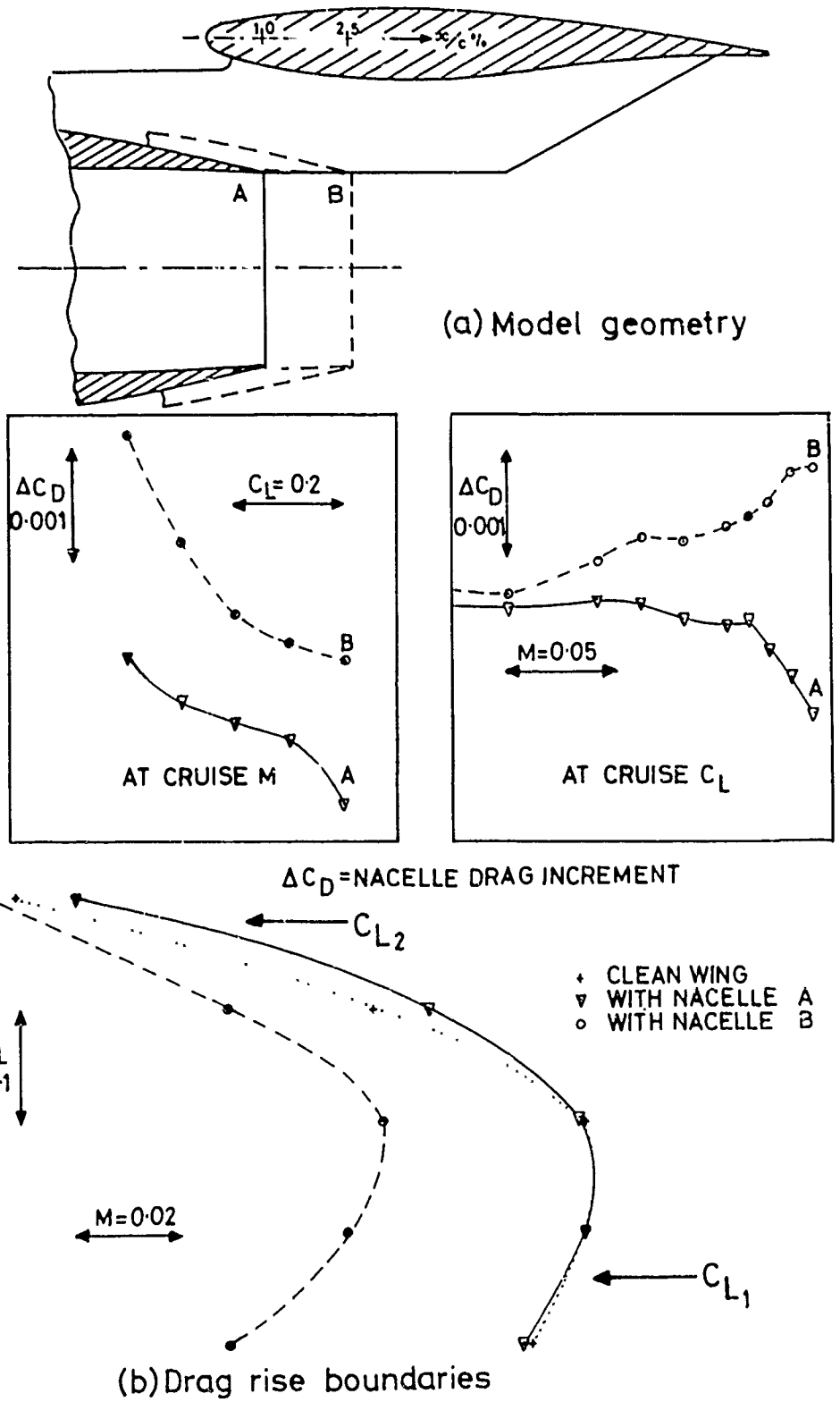

FIG.15. EFFECT OF UNDERWING NACELLE POSITION ON INTERFERENCE

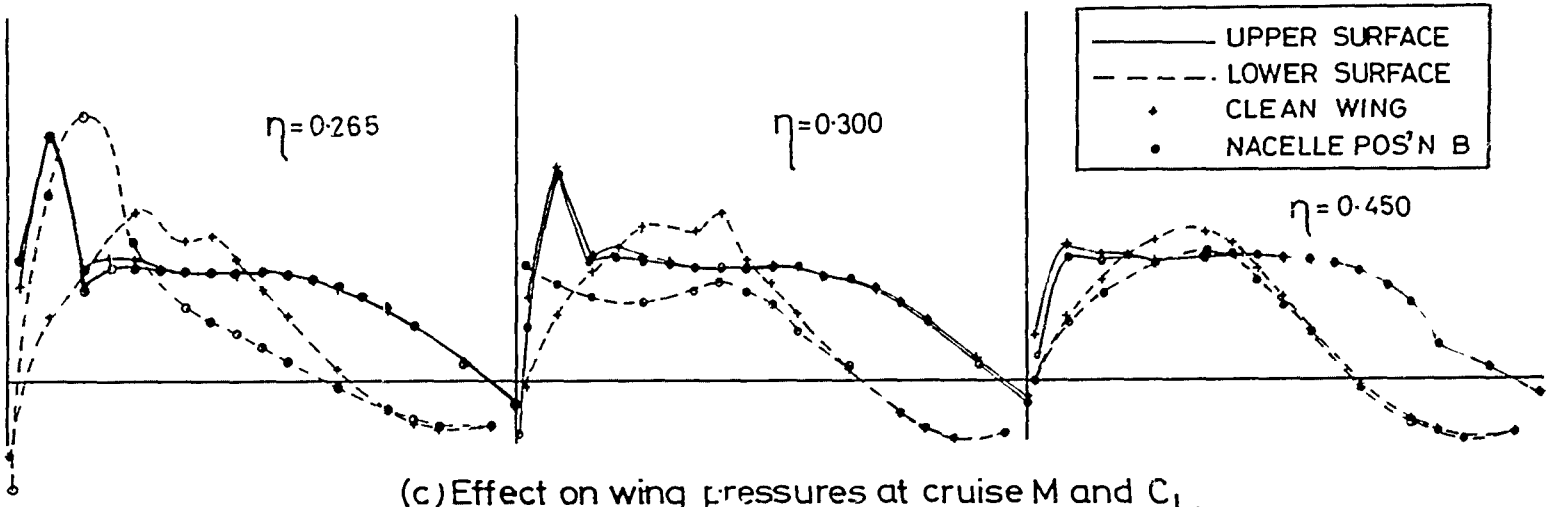

(c) Effect on wing pressures at cruise M and C_{L_1}

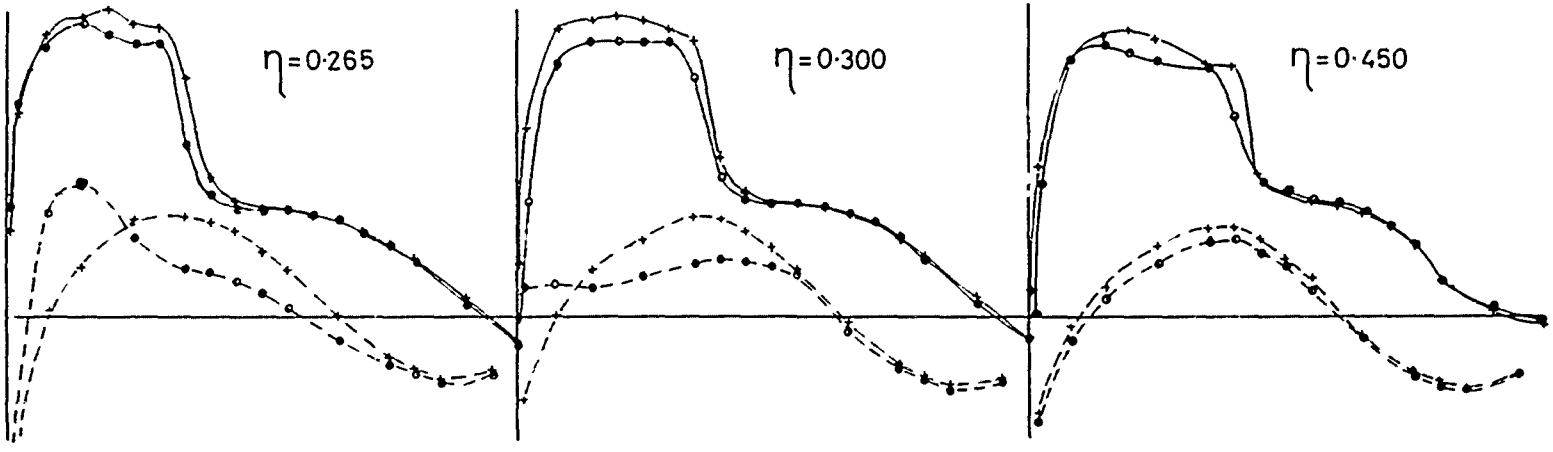

(d) Effect on wing pressures at cruise M and C_{L_2}

FIG 15 EFFECT OF UNDERWING NACELLE POSITION ON INTERFERENCE

FIG. 15(c,d)

PHOTO No 2415/62

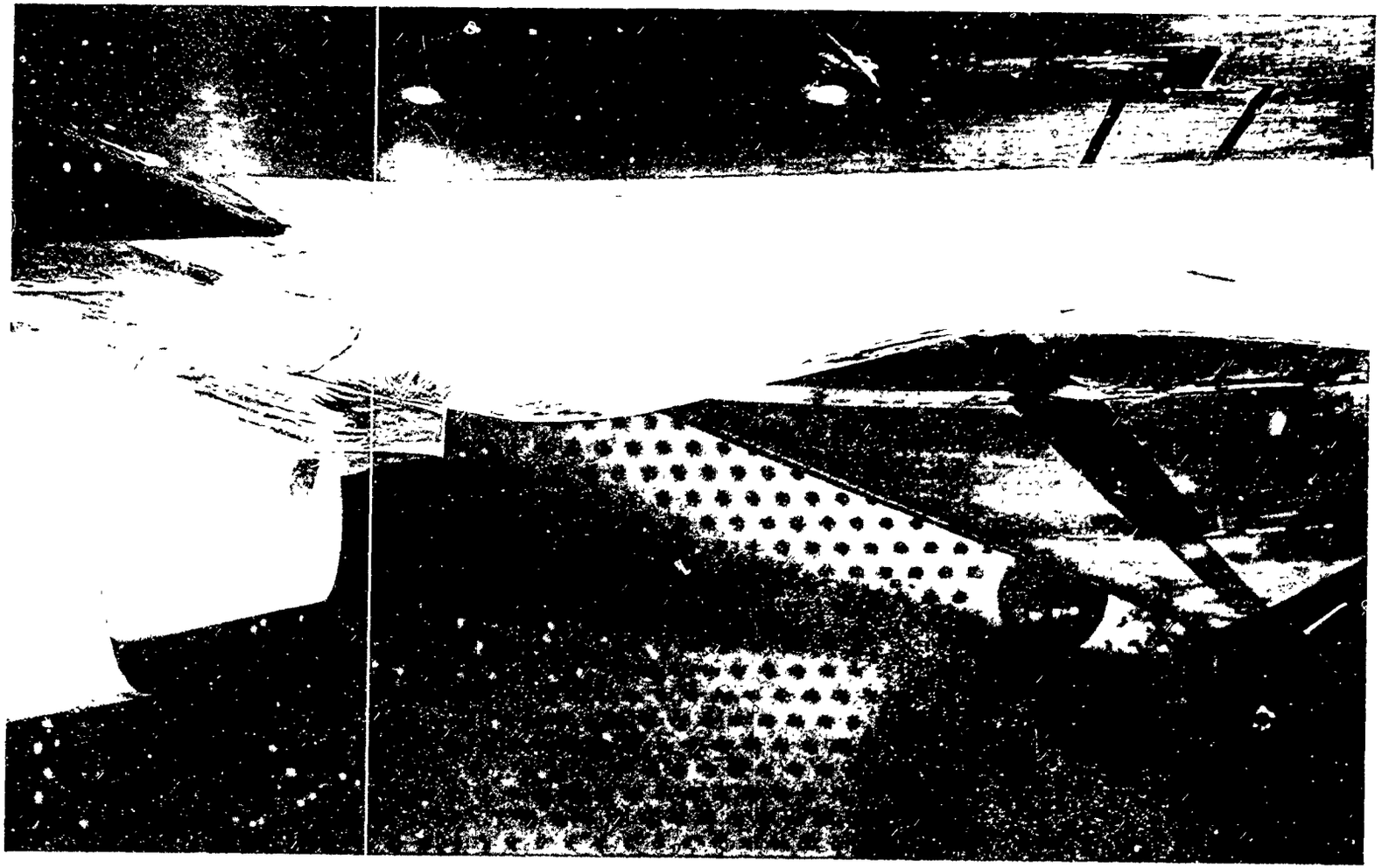

FIG. 16 OIL FLOW OF TYPICAL OFF-DESIGN ADVERSE INTERFERENCE CONDITION

FIG. 16

FIG. 17(a,b,c)

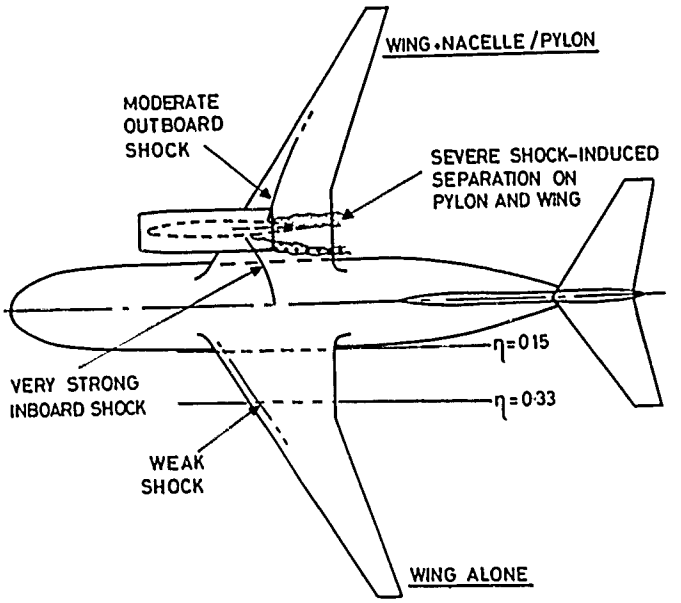

(a) Flow pattern with symmetric nacelle.

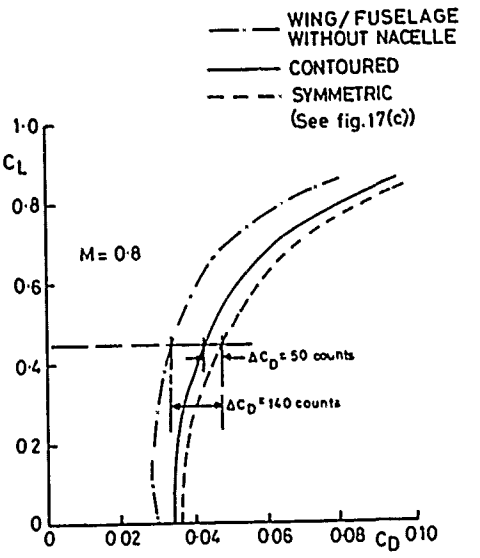

(b) Drag comparison: symmetric versus contoured nacelle.

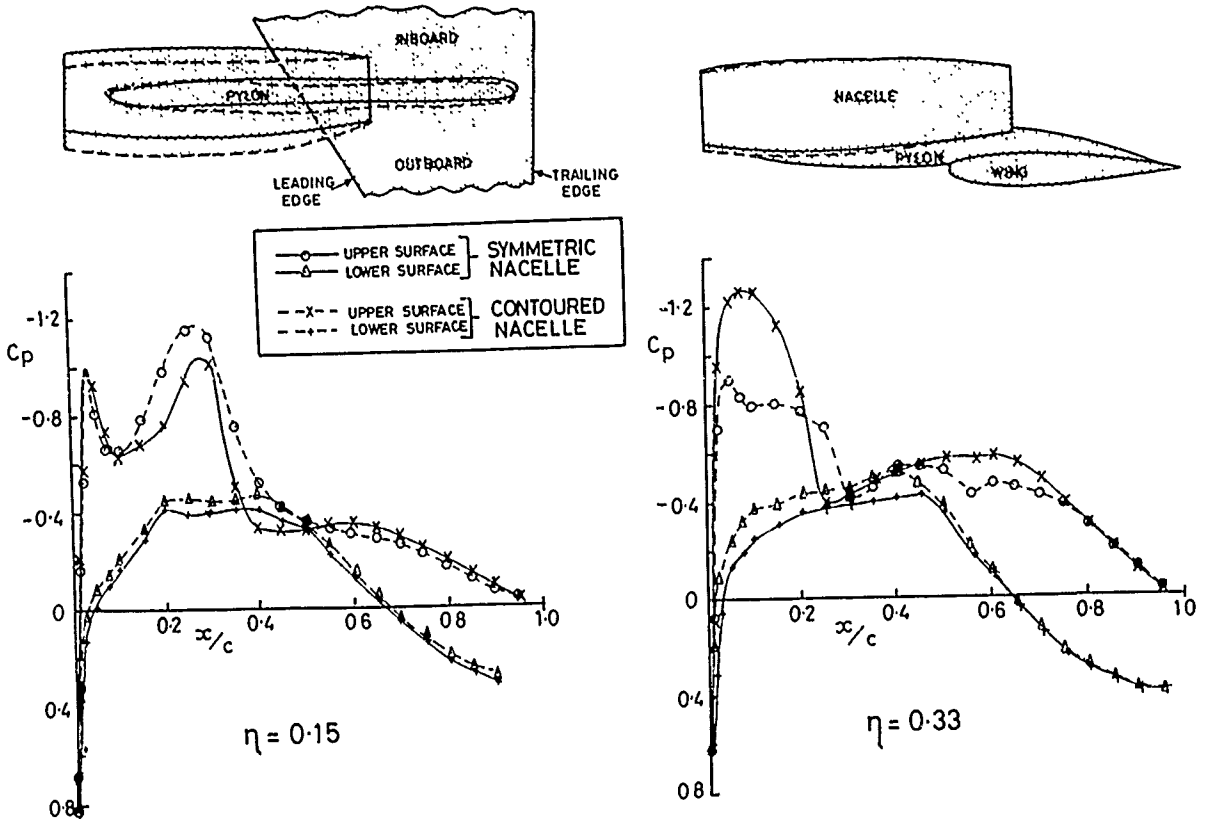

(c) Pressure distribution comparison: contoured versus symmetric

FIG. 17 INTERFERENCE FOR OVERWING NACELLE INSTALLATION

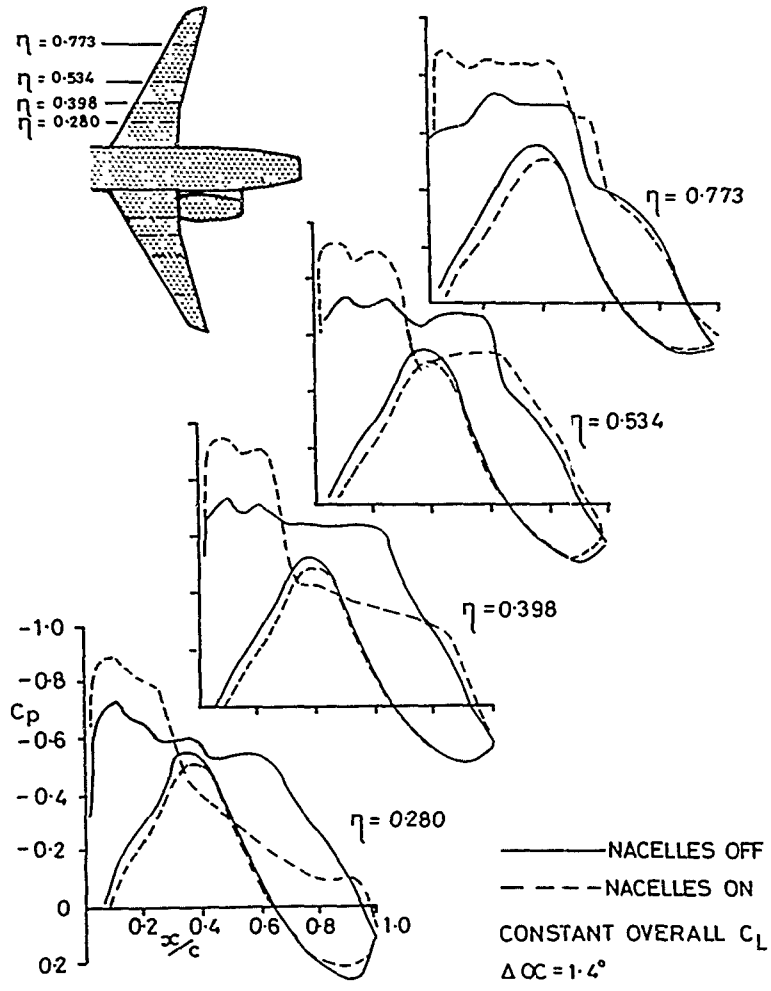

(a)Wing designed with no allowance for nacelle

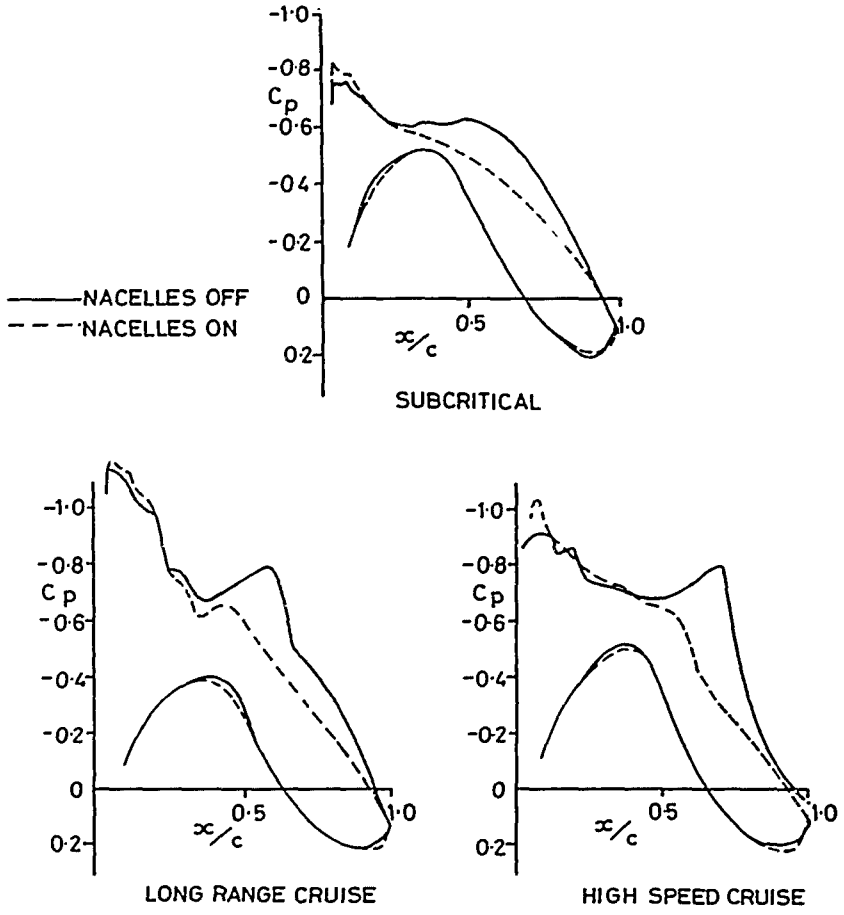

(b)Wing designed allowing for presence of nacelle

FIG. 18(a, b)

FIG.18 INTERFERENCE FOR AFT-FUSELAGE NACELLE INSTALLATIONS

FIG. 19 (a,b)

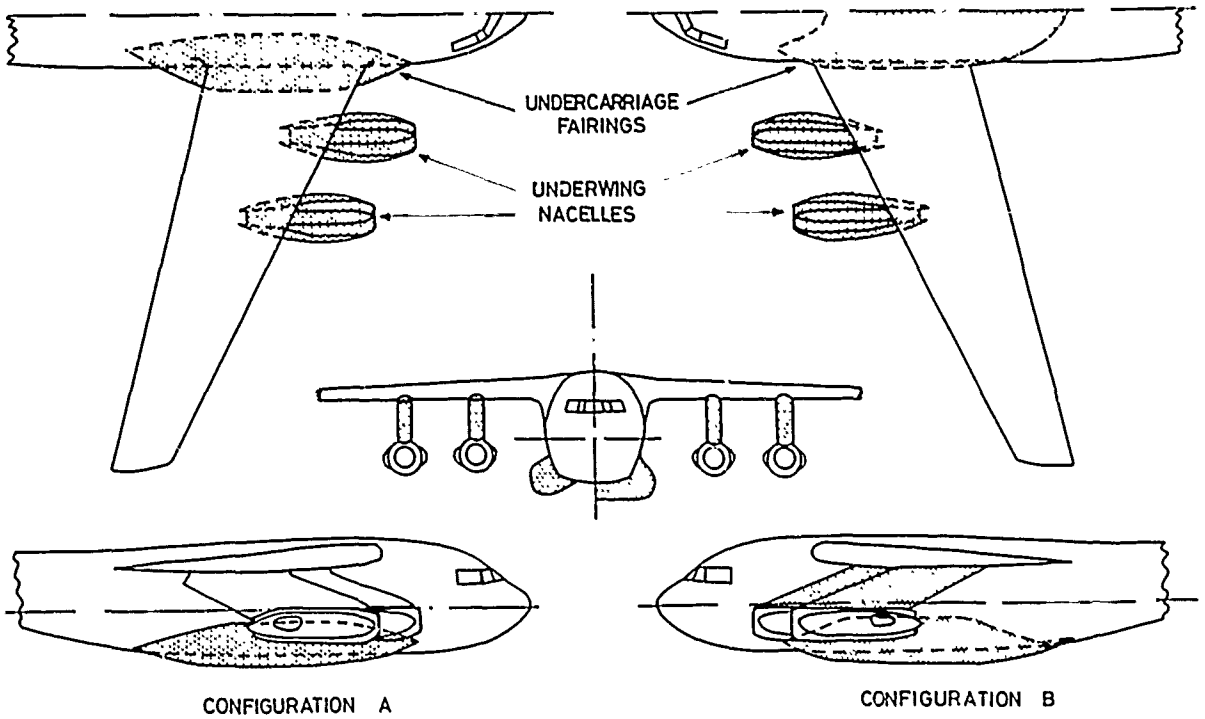

(a) Aircraft geometry

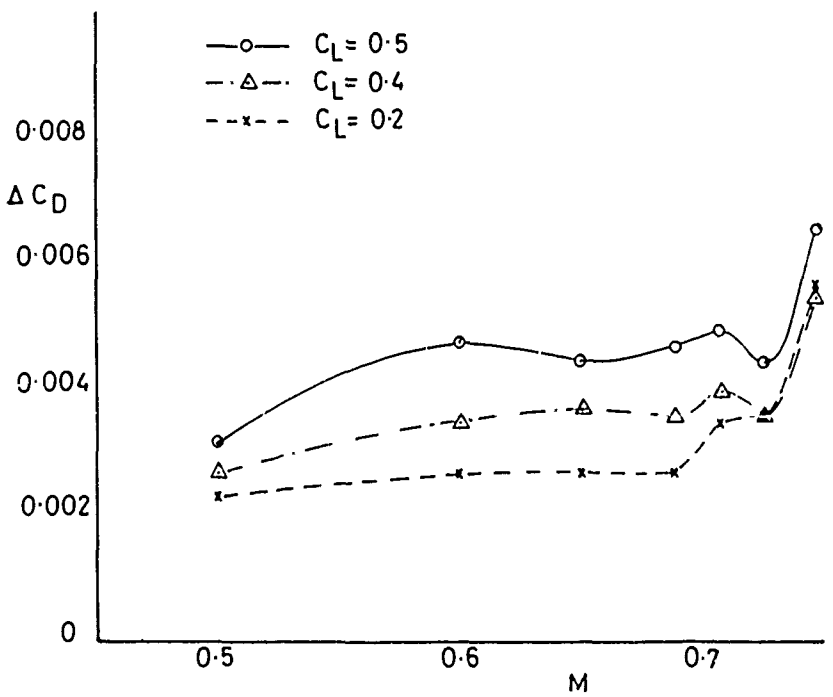

$\Delta C_D = (C_D \text{ for A}) - (C_D \text{ for B})$

(b) Comparison showing extra interference drag with configuration A (see fig. 19(a))

FIG. 19. EXAMPLE OF INTERFERENCE BETWEEN AIRCRAFT COMPONENTS

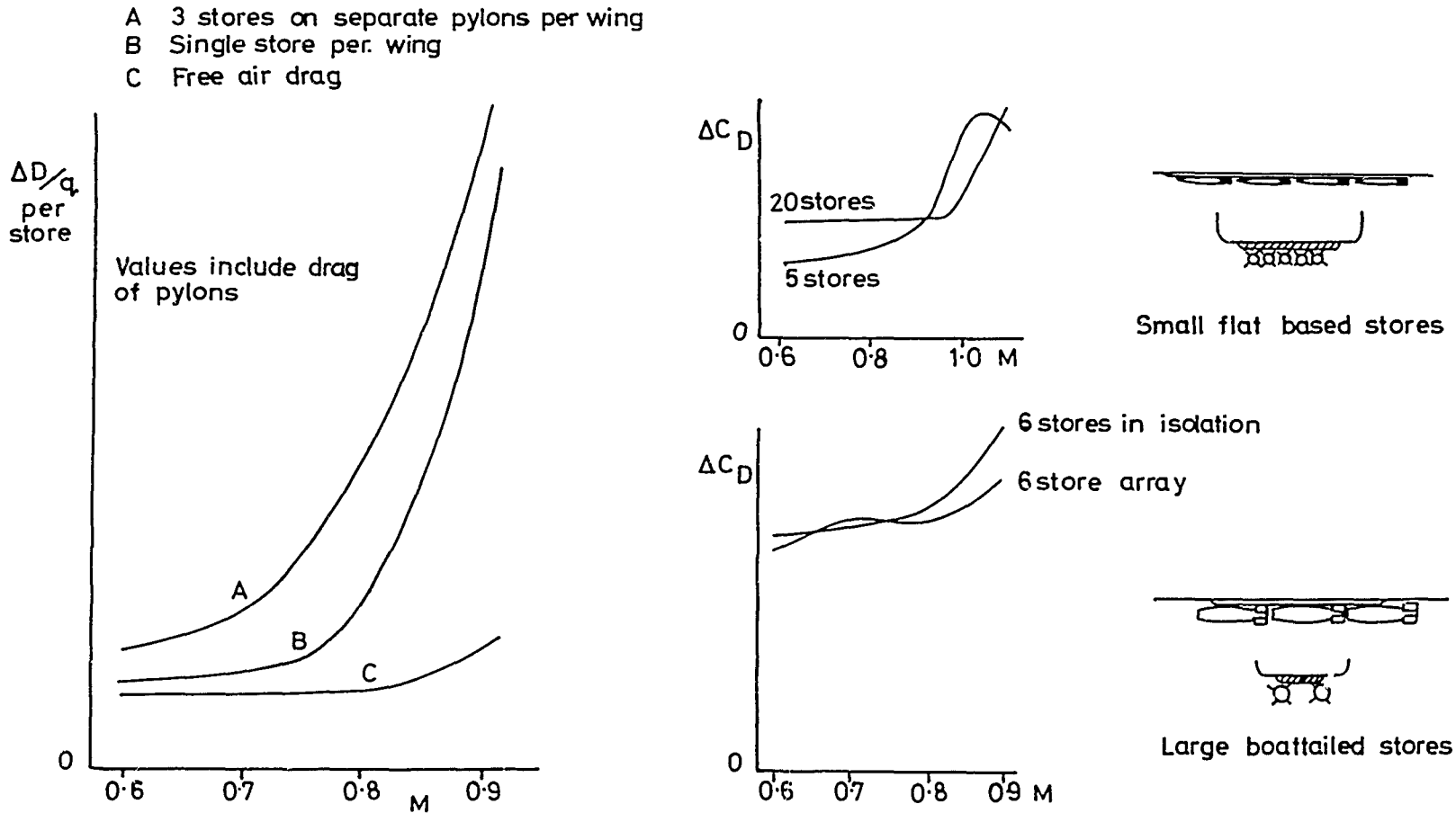

(a) Adverse interference underwing

(b) Favourable interference underfuselage

FIG. 20 EXAMPLES OF FAVOURABLE AND ADVERSE INTERFERENCE FOR MULTIPLE STORE CARRIAGE

FIG. 20(a,b)

FIG.20 (c)

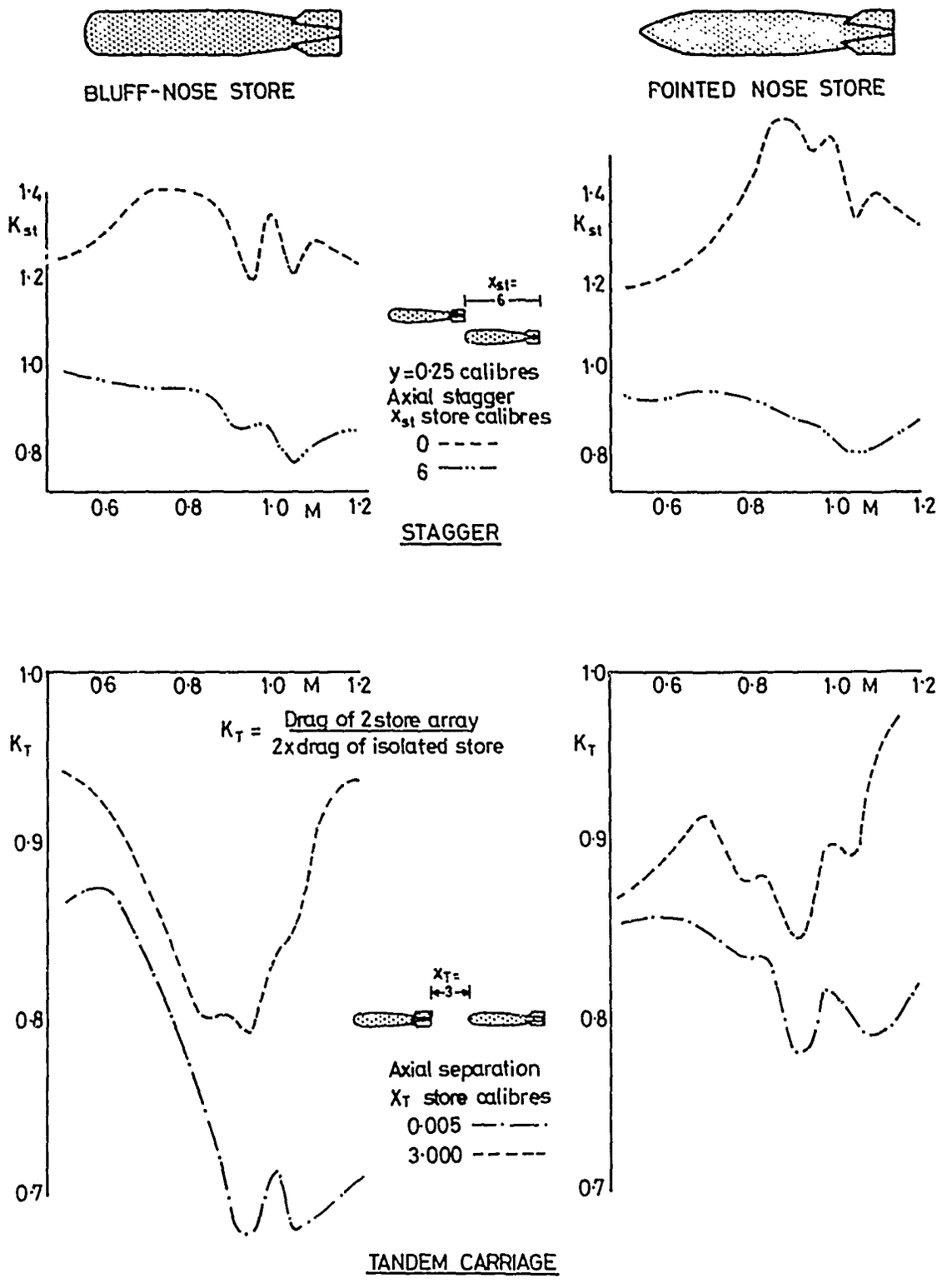

(c) Favourable interference concepts : multiple store arrays

FIG.20 EXAMPLES OF FAVOURABLE AND ADVERSE INTERFERENCE FOR MULTIPLE STORE CARRIAGE

FIG.21

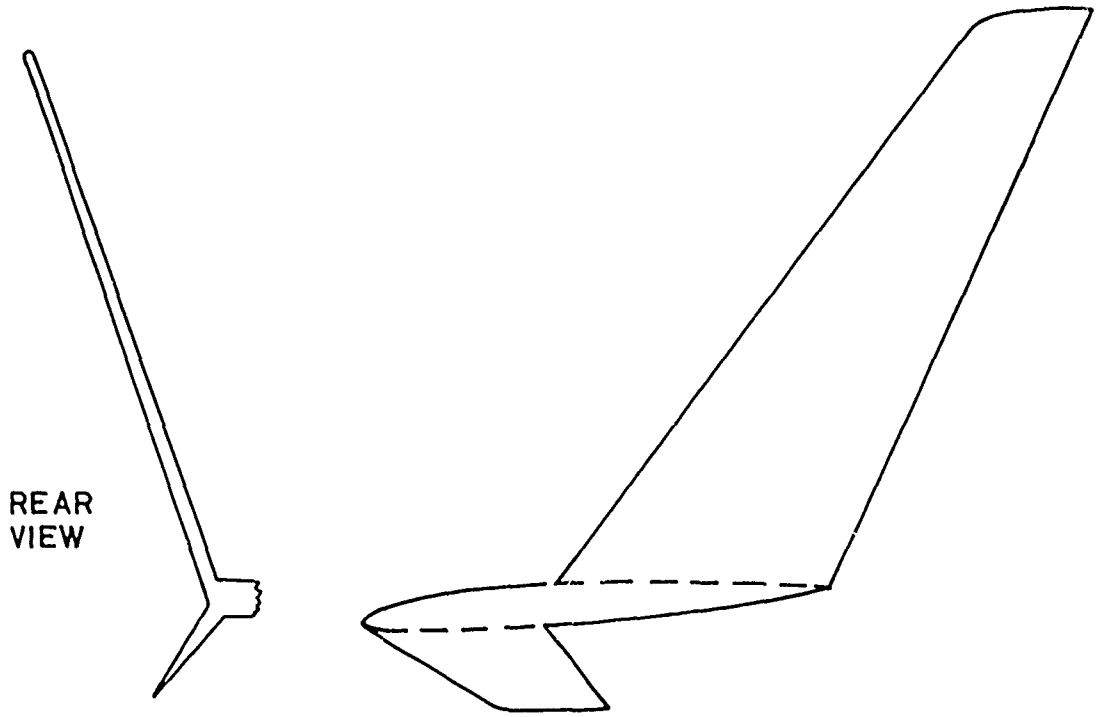

WINGLET A

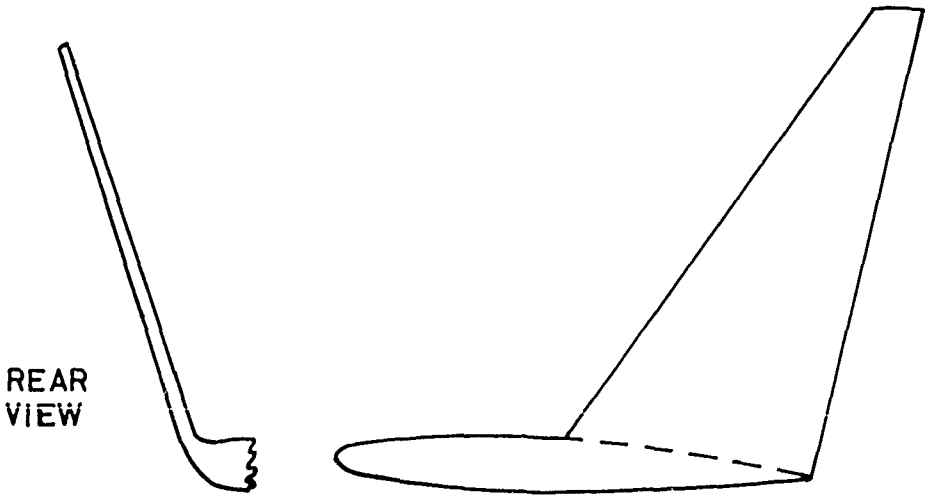

WINGLET B

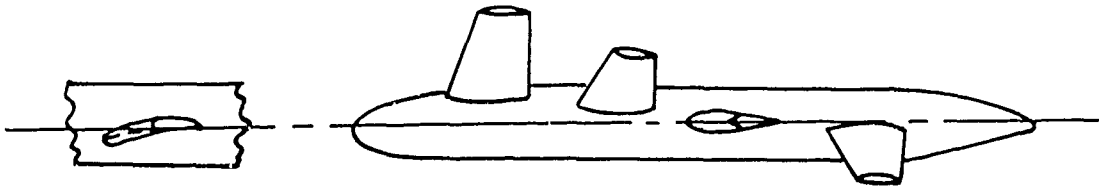

SAILS MOUNTED ON WING-TIP BODY

FIG.21 WING-TIP DEVICES

FIG.22.

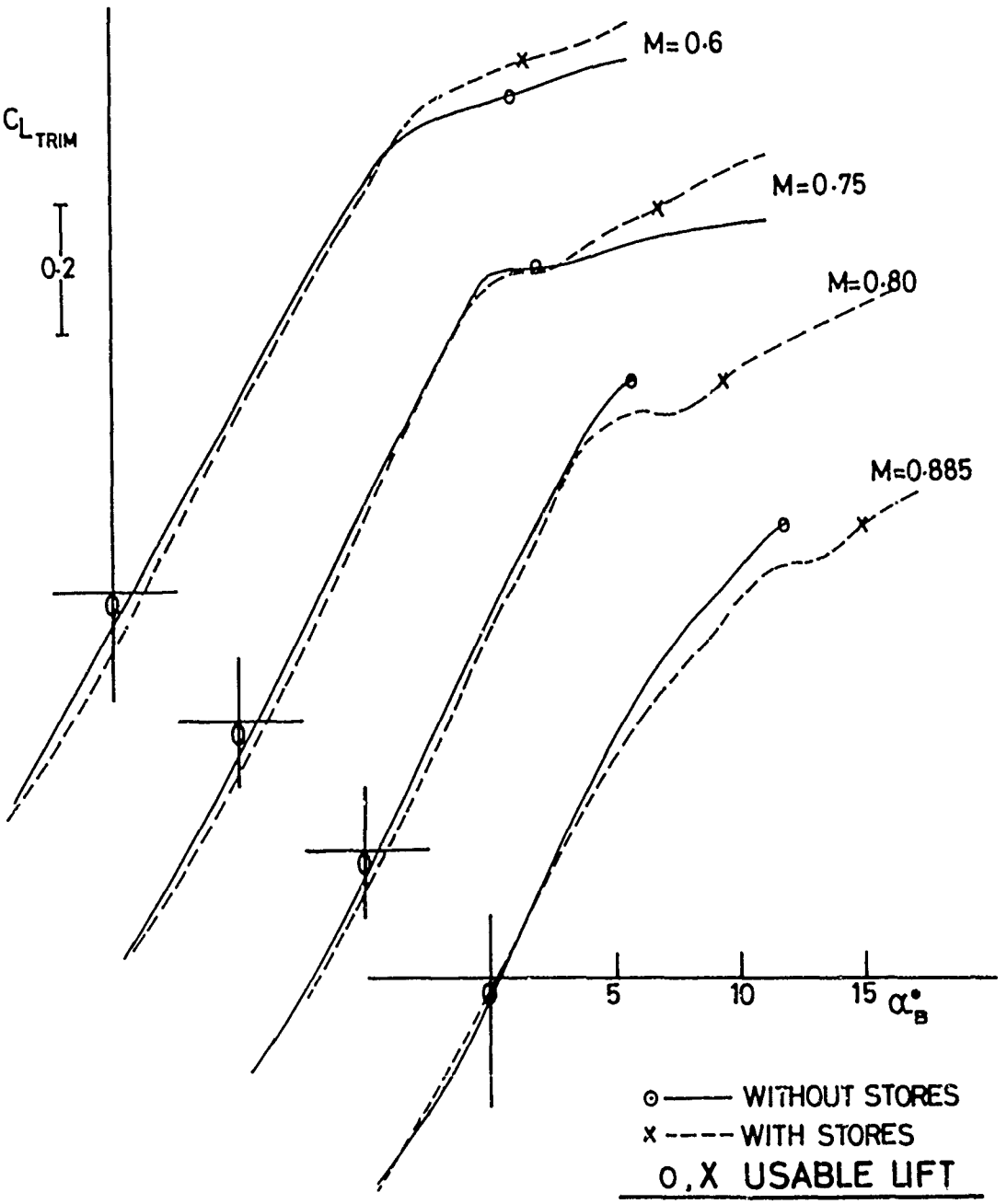

WING L.E. SWEEP 38·7°
ASPECT RATIO 4·03
TAPER RATIO 0·3
STORES MOUNTED UNDERWING AT 0·59, 0·70, 0·87 SEMI-SPAN

FIG.22. EFFECTS OF UNDERWING PYLONS/STORES ON USABLE LIFT

FIG 23(a)

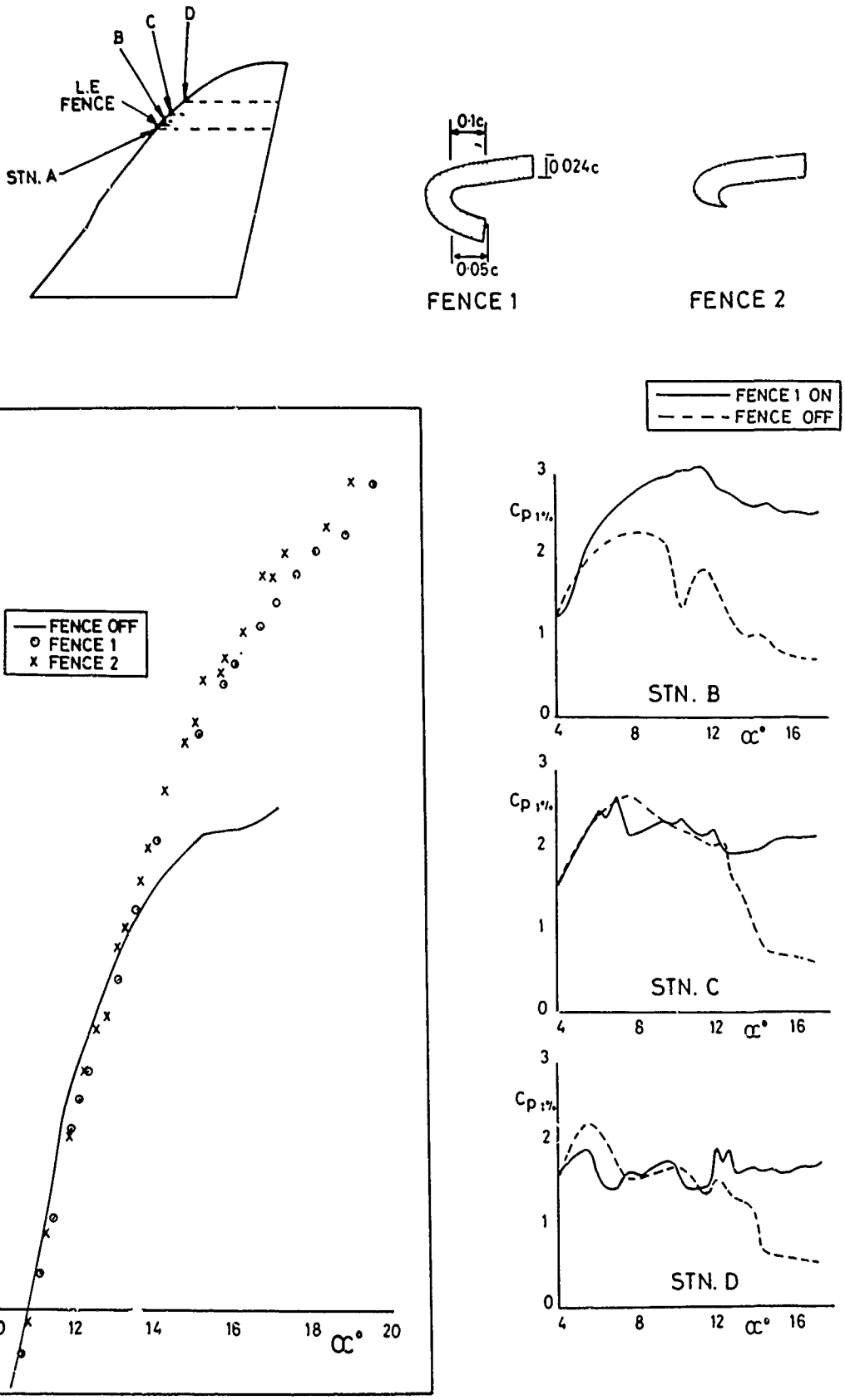

(a) Overall C_L - α and pressures near leading edge.

FIG. 23. EFFECT OF LEADING EDGE FENCES ON USABLE LIFT

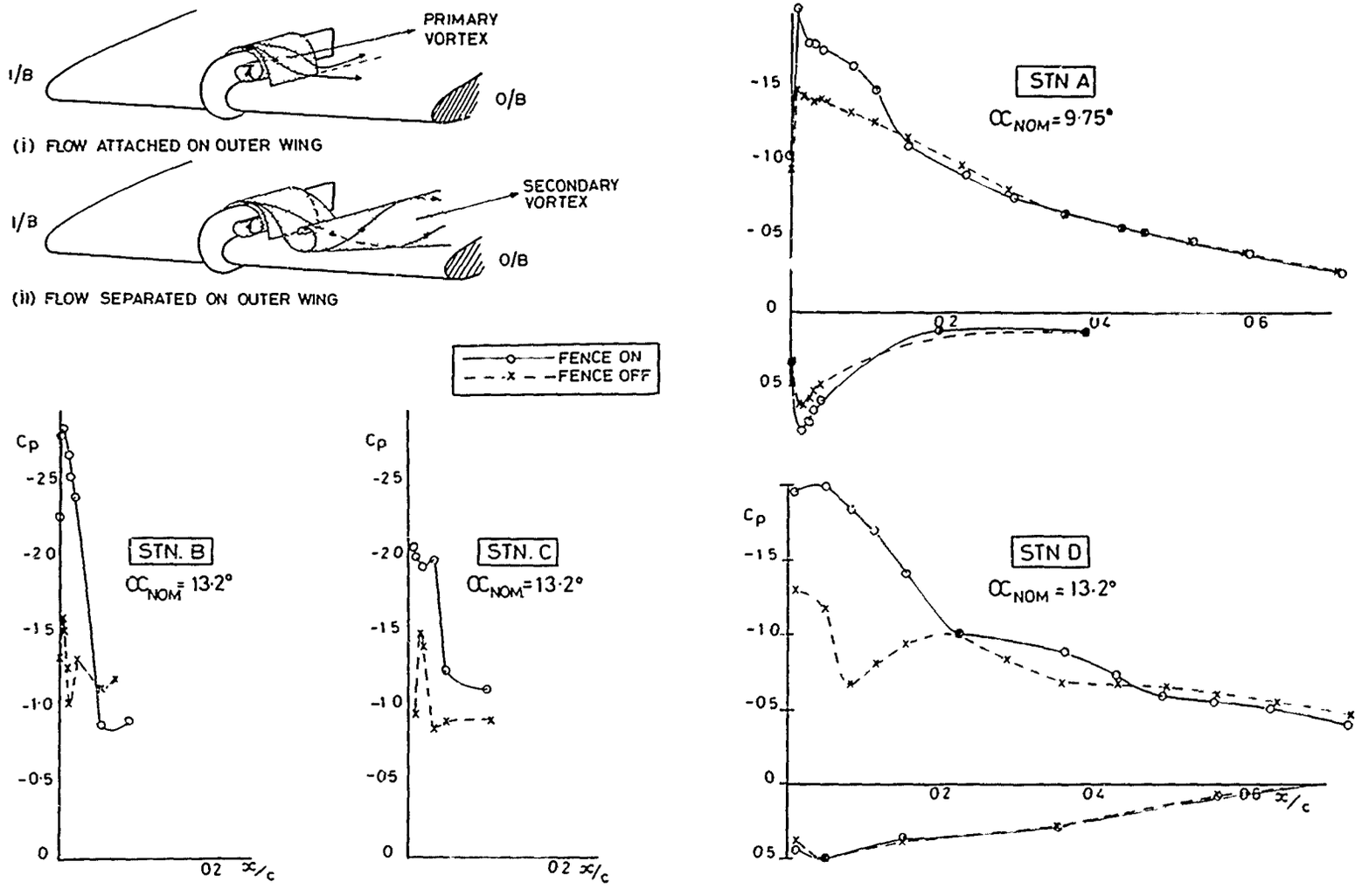

(b) Fence-induced vortices (see page 15)

FIG. 23 EFFECT OF L.E. FENCES ON USABLE LIFT

FIG 23(b)

FIG 24

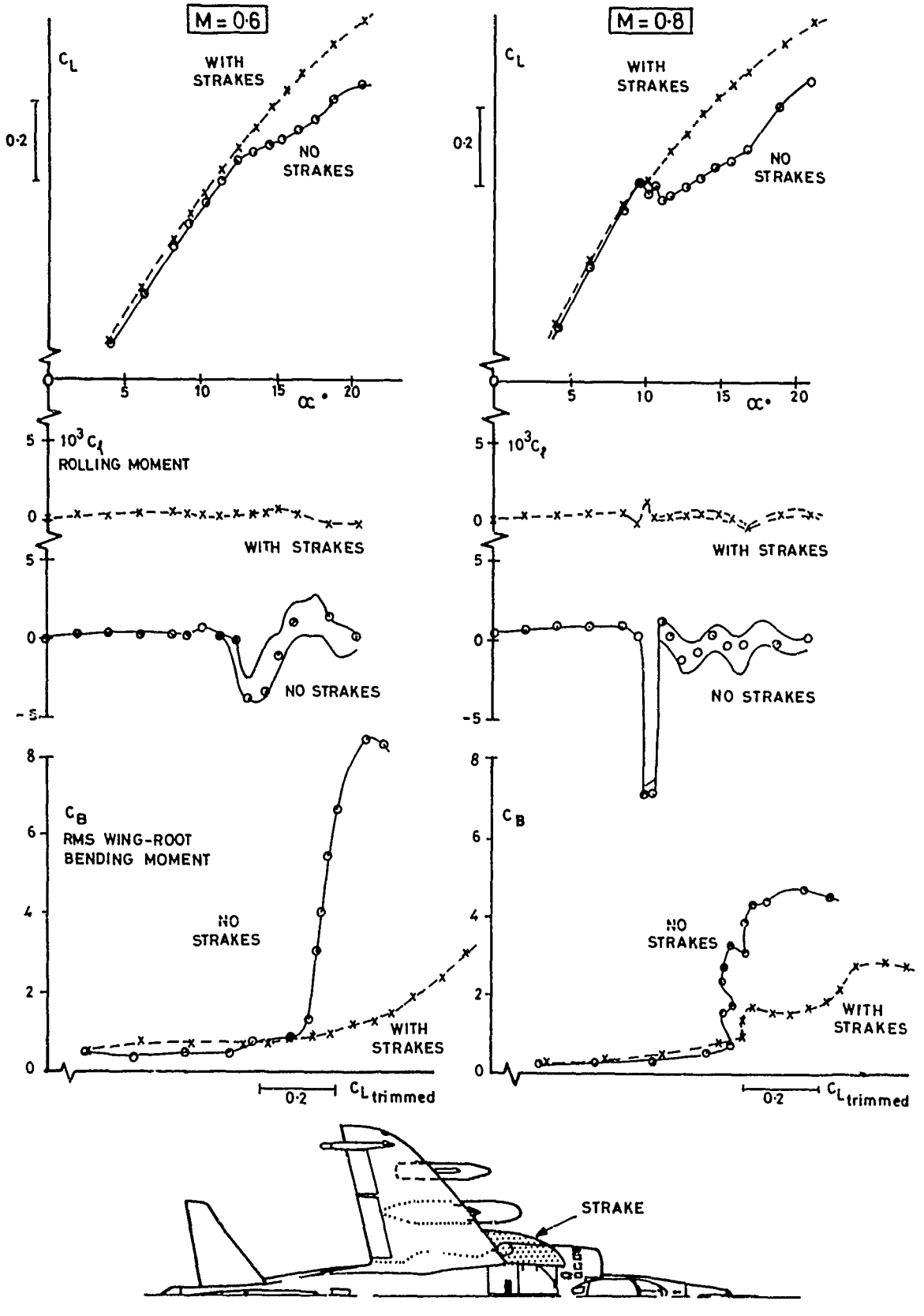

FIG 24 EFFECT OF STRAKES ON WING BUFFETING AND UNSTEADY ROLLING

FIG. 25

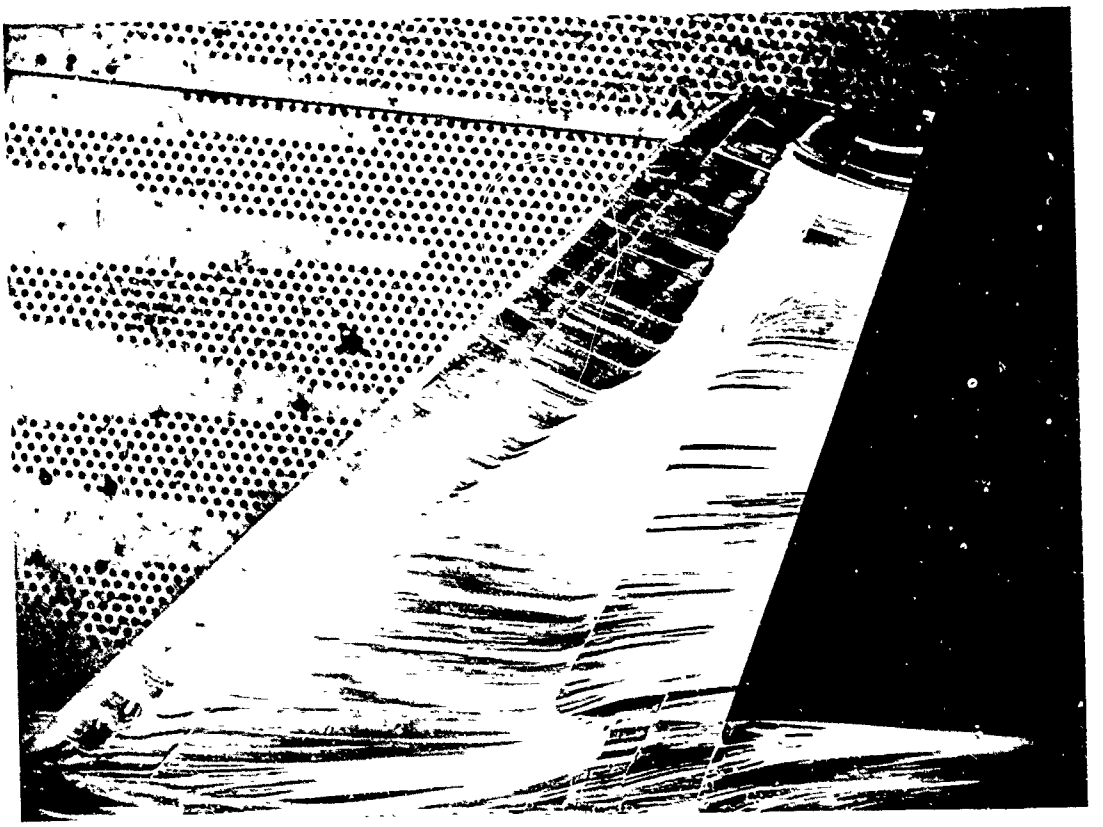

PHOTO No 3898/0

DATUM (CANARD OFF)

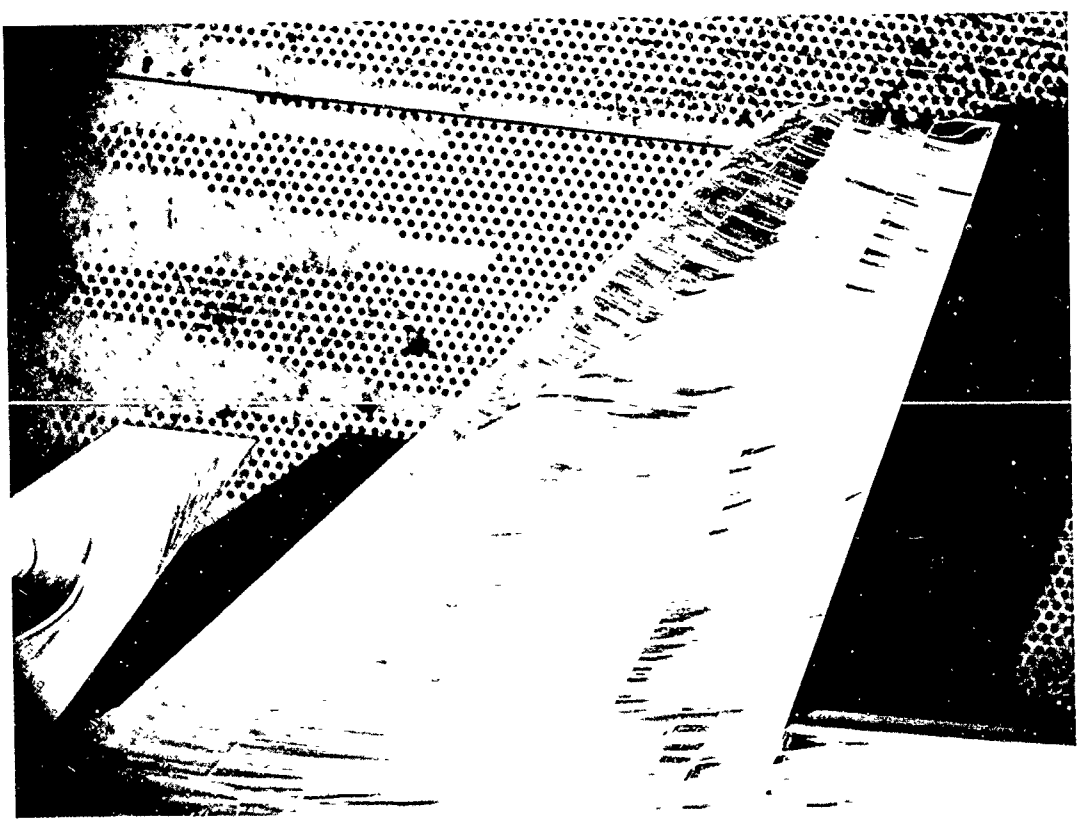

PHOTO No 3903/20

CANARD AT 0° DEFLECTION

FIG. 25 EXAMPLE OF INTERFERENCE FROM CANARD FLOW FIELD AT M=0·88 α=7·5°

TRANSONIC CONFIGURATION DESIGN

by

G. Krenz

MBB / Vereinigte Flugtechnische Werke GmbH
D 2800 Bremen
Germany

SUMMARY

The progress in aerodynamics during the last decade has immensely improved fuel efficiency of commercial transport aircraft, one major part being the transonic configuration design. The wing contributes in the order of two-thirds to the total aircraft drag in cruise flight and hence is the main objective of the present paper. General design aspects as well as specific criteria for a transonic wing lay-out are described and some special problems inherent in any transonic wing design are discussed on the basis of wind-tunnel measurements. Aerodynamic wing concepts are considered, following two different design strategies by model tests in the transonic wind-tunnel. - It was found that the shock development on the upper wing surface has a strong effect on both the design and off-design performance of the wing in terms of L/D.

The progress in transonic configuration design is partially based on the tremendous efforts made in computational aerodynamics and basic theories are being discussed during the current VKI-Lecture Series. Two simpler potential flow methods used in actual transonic wing designs at MBB/VFW are presented in this paper. Major obstacles for proper wing design and aircraft performance predictions in the transonic flight regime by either calculations or wind-tunnel measurements are shock-boundary layer interaction and viscid-inviscid flow interference at the trailing edge. For several years our work in the field of calculating and testing boundary layers is therefore concentrated on these two subjects, and the present paper contains main results we received with modern transonic aerofoils.

The lack of knowledge which still exists in these areas of viscid-inviscid flow interference is limiting the acuracy of performance predictions for modern transonic wing with a large amount of rear loading.- One concept followed at MBB/VFW to improve the predictions of full scale aircraft data is discussed in the present paper.

LIST OF SYMBOLS

AR	aspect ratio	SFC	specific fuel consumption
c	chord		nondimensional streamwise coordinate
$\bar{c}$	mean aerodynamic chord	t/c	thickness chord ratio
C_D	drag coefficient	u	boundary layer velocity
c_f	friction coefficient	v	velocity
C_p	pressure coefficient	w	weight
C_p^*	critical pressure coefficient for M = 1.0	x/c	relative chord position
C_L	lift coefficient		
cts	counts; 1 ct = 0.0001 C_D	GREEK SYMBOLS	
D	drag	α	angle of attack
L	lift	δ	boundary layer thickness
L/D	lift/drag ratio	δ_1	displacement thickness
M	Mach number	δ_μ	viscous sublayer thickness
M x L/D	performance parameter	ΔC_{D_M}	drag rise due to compressibility $\Delta C_{D_M} = C_D - C_{D_{M=0.6}}$
n	normal coordinate		
R_N, R_e	Reynolds number	η	relative wing span
s	streamwise coordinate	Λ_{25}	wing sweep at 25 % chord

1. INTRODUCTION

Tremendous efforts were made during the last years in aerodynamic design to increase cruise performance efficiency, and qualified teams at different places of the world are working and competing for further improvements in aerodynamics.

The basic technologies contributing to future improvements of fuel efficient transport aircraft are shown in FIG. 1. The main disciplines are aerodynamics, materials & structures and systems, the latter being strongly dependent on the efforts of the system manufacturers. The main technological progress is to be expected where the disciplines are connected. As an example, the further increase of aspect ratio for better L/D is eased by materials with higher stiffness and improved fatigue behavior than aluminium alloys as carbon fibre structures. Also, the aerodynamic impact of unsteady movable wing parts like flaps, spoilers or ailerons on the load alleviation effects is a typical result of combined efforts of a combination of aerodynamics with systems technology. Considerable fuel reduction can be expected from the engine manufacturers, their progress partially being associated with improved transonic design of the compressor blades of the advanced engines.

What are the sources and reasons for the dramatic progress in aerodynamic design? - One, of course, is the rapid progress in computer technology and its use in computational aerodynamics. The progress in experimental research and methods is less spectacular, because here we are waiting for the new facilities at NTF in the USA and ETW in Europe in opposition to the big computers.

Another source of substantial progress in aerodynamics is the development of new concepts and configurations and the men standing behind them with their ideas and their toughness to realise them. - Advanced transonic wing technology, now being introduced in the new airplanes of Europe and the USA, and propulsion-airframe concepts, investigated in the AMST-programme with the YC 14 and YC 15 aircraft, are examples.

A further motive for the tremendous progress in aerodynamics is the economic necessity for a reduction in fuel consumption, especially as far as commercial transport aircraft are concerned. FIG. 2 presents the increase of fuel price valid for the USA and taken from Boeing [1] . The dotted line gives the real price increase up to the end of 1982. After a strong increase we see a stagnation and even a small decrease during the last 1 1/2 years, but until today the price is rather within the predicted area. The rapid fuel price increase considerably effects the direct operating costs D.O.C. directly and contributes to the disproportionate increase of the fuel costs in the D.O.C. FIG. 3 shows the cost development as estimated by Airbus Industry in 1979 [2] . From the different methods used in this forecast only the results from Boeing are shown because of its simplicity (4 parameters), and it strongly reflects the fuel costs within the D.O.C. In the EURAC method however, the fuel costs represent about 2/3 of the Boeing estimate. The fuel cost price development corresponding to FIG. 3 is based on the lower broken curve in FIG. 2.

A proportionate change within the cost items of the D.O.C., as shown in FIG. 3, has a considerable effect on aircraft design. To elaborate this, the fuel consumption as determined by the main aircraft and engine parameters have to be analysed. FIG. 4 contains a simplified basic formula for mission fuel efficiency, defined as trip fuel burned per distance. The first term, the ratio of specific fuel consumption to cruise speed is defined as propulsive efficiency, and the second term is the airframe efficiency with aircraft weight to lift/drag ratio. Considering the latter, L/D to weight ratio must be as large as possible for fuel efficient flight.

2. AIRCRAFT DESIGN FOR CRUISE FLIGHT AT TRANSONIC SPEED

2.1 Overall design aspects

One dominant design goal for commercial transport aircraft at cruise is low fuel consumption, as shown in the formula for the trip fuel given by the performance parameter M x L/D. FIG. 5 shows the characteristics of commercial transport airplanes of technology level achievable today. The M x $L/_L$ increases to an optimum up to a Mach number where the drag rise due to wave drag is equal to the Mach number increase. The optimal cruise Mach number is in the range of $0.75 \lesssim M \lesssim 0.82$ depending on the design and is very close to the Mach number for maximum M x $L/_{D_{max}}$. This derives from trade-off studies for the main parameters determining the D.O.C. as fuel consumption, maintenance crew costs and aircraft price. The fuel consumption part reduces the optimum Mach number, because of the improved engine efficiency in cruise flight at lower Mach number, the other parts decrease with increasing Mach number as typical time-dependent costs. Thus the overall optimum is often about 99-percent of the maximum value. The amount of maximum M x L/D and the shape of the curve is dependent on the quality of the aerodynamic design and on the specific design requirements. Fuselage and above all the wing geometry with their basic parameters: area, span, sweep and relative thickness determine the M x L/D characteristics to a certain degree, as given by the overall project design, however, the aerodynamic lay-out based on the same project wing design can infuence the M x L/D curves considerably. Our experience is that different design teams arrive at different M x L/D characteristics and standards even in case they work on comparable technology standards. Therefore it is extremely desirable to lower the development and production risk to perform the design - and here especially the wing design - in a strong and serious competition.

The wing contribution to the drag is the main part, and thus aircraft design above all means wing design. This is demonstrated in FIG. 6 with the breakdown for a typical commercial transport aircraft at

cruise flight conditions. We see that about two-thirds of the total aircraft drag is contributed by the wing; but even this convincing figure does not sufficiently explain the major importance the wing has in an aerodynamic design. Two more factors among others must be mentioned:

1. The compressibility drag of about five percent is a rather low figure and, in comparison with the other drag parts, mainly the parasitic and lift dependent drag, seems to be less important. The drag breakdown here gives a wrong impression about the importance of the compressibility drag component, which is connected with the wing flow, because in a commercial airplane design it sets the boundary up to where fuel efficient flight can be performed. FIG. 7 shows the boundaries defined as drag-rise in the well known C_L-M-diagram. Due to the supercritical aerofoils with their increased lift capability as sketched in the picture the drag-rise boundaries are shifted to considerably higher lift coefficients for a modern transonic wing design. As the benefits of the advanced aerofoils are mostly used to increase the wing thickness without changing the design Mach number, a reduction of the drag-rise boundary at low C_L-values outside the design range occurs. The improvements at higher lift coefficients are equivalent to a performance advantage for the aerodynamic design as well as for the fuel consumption when the aircraft can be operated at higher altitudes.

2. The other dominating aerodynamic performance parameter next to M x L/D is the buffet boundary which is more or less completely associated with the wing design. Buffet arises as structural response to flow separation on the wing, and FIG. 8 shows how the buffet boundary is limiting the maximum cruise lift coefficient. A 1.3 g margin during flight to the buffet onset boundary is required to enable a pilot to fly a 35° bank angle and have sufficient margin against flow separation occuring in a heavy gust. A too low limitation of the desired cruise lift coefficient leads to reduced fuel efficiency, because the specific fuel consumption of the engine increases with lower altitude flight.

Thus the large emphasis to be made on the aerodynamic wing design at transonic speeds for a commercial transport airplane is obvious: Two-thirds of the total cruise drag and the whole compressibility drag limiting the fuel efficient flight of the airplane are attributed to the wing, and furthermore the buffet boundary determined by the wing lay-out limits the maximum cruise lift coefficient and thereby fuel efficient operating of the engines. The following chapters will mainly cover wing design aspects.

2.2 Design targets for cruise flight at transonic speeds

In general a research institute places other design objectives than an industrial company that has to sell commercial airplanes. In pure research main emphasis is put to better pysical mathematical understanding and to elaborate fundamental theoretical and experimental methods as powerfull tools for wing design. A large number of wind-tunnel models with different wing shapes is tested therefore and the comparison of measurements and theory leads to improved theoretical and experimental methods. The main work is concentrated at low Reynolds numbers, roughly 1/10 of the full scale Reynolds number as can be reached in the present wind-tunnels. An industrial team has to design a wing for specific economic criteria with penalising restrictions. The design must be made for full-scale Reynolds numbers and aircraft performance and load data predictions are dominant compared to the methods used to achieve them. The reliable data basis for a wing lay-out and aircraft performance predictions until today are the knowledge of former aircraft configurations as well as wind-tunnel tests of the the new wing to be designed. The theoretical work is primarily done to limit the number of wing shapes to be tested up to the desired performance data and to estimate the Reynolds number effects in case they are different due to changes in aerodynamic characteristics of the new design compared to the flying airplane. In the following presentation the industrial aspects during a wing design will dominate.

Some general design criteria to be fulfilled in a transonic wing design are:

- high M x L/D_{max} with good M x L/D characteristic for the entire design range; for short/medium range aircraft $0.7 \lesssim M \lesssim 0.8$; $0.3 \lesssim C_L \lesssim 0.6$
- high buffet boundary to allow for high cruise design lift coefficients
- no pitch-up near stall and buffet onset
- sufficient space (wing thickness) to house the undercarriage, the required fuel volume and movable parts of the wing
- sufficient thickness in areas like fuselage junction, planform crank, outboard aileron to keep the structural weight low, increase flutter speed and maintain control effectiveness.

One overall design aspect is that the wing geometry should be as simple as possible to keep production and maintenance costs low. FIG. 9 shows the wing planform of a typical transport configuration, which was tested in a research programme. The dashed lines indicate areas of double curvature on the wings upper and lower surface. The criterion of 30 m curvature radius for shotpeening the panels without difficulties and extra manufacturing costs led to small areas of double curvature as shown here. The other part of the wing was designed by linear lofting and thus gave a quite simple geometry. The aerodynamic characteristics as presented by the pressure distribution in FIG. 10 were encouraging. The flow is rather shock free at the design point and increasing C_L and Mach number leads to nearly constant chord shock positions maintaining straight isobar lines following the wing sweep.

Another point of interest and often of controversial discussion regarding the wing planform is the crank at the trailing edge, which is designed to increase the chord of the inner wing to receive space for the undercarriage housing, see FIG. 11. An elliptical lift distribution for low induced drag is hardly to realize because the large wing chord of the inner wing section does not coincide with the requirement for acceptable stall characteristics. Designs we made and tested for different trailing edges as shown in the figure - the aim was a more elliptical load distribution by softer cranks - gave no improvements in the total drag at cruise. It must be considered that the lift dependent drag in transonic flow does not only depend on the lift distribution along the wing span and hence on the vortex drag but is influenced by the development of viscous and wave drag in the transonic flow at the individual aerofoil sections.

Regarding the wing section as a further overall and fundamental design aspect as we did for the planform and wing geometry above, the wing root profile is of major importance, see FIG. 12. For design purposes structural and manufacturing aspects must be taken into account. Besides this, fuel tank volume of the inner wing and the centre fuselage as well as the accomodation of the main landing gear influence the design. Root profiles of the same maximum thickness as shown in the picture derived from different design concepts satisfy to very different extents the non-aerodynamic requirements. It is evident that aerofoil B has a greater fuel volume and provides more space for the undercarriadge behind the rear spar when given the same nominal thickness ratio as aerofoil A. Besides that, the greater height of the rear spar of aerofoil B reduces the structural weight of the wing. - For the aerodynamic performance of the wing the careful design of the root section with a dominant effect on the inner wing flow and the fuselage-wing interference is of major importance. Some aspects will therefore be discussed in more detail.

One critical part of the wing root section design is the shape of the nose. 2-D section tests show that the leading edge radius influences the drag creep over the Mach number. FIG. 13 contains data taken from F.T. Lynch [17] comparing the effect of leading edge radius on drag measured for 2-D aerofoils. The drag creep over Mach number for the thicker nose is demonstrated, though not quantified. We have to be cautious with the interpretation of the leading edge radius effect, because changes at that part can considerably change the pressure distribution on the upper profile side and thereby can have strong effects on drag creep, as indicated in the next diagram. FIG. 14 shows the drag characteristics and the pressure distribution at two significant points of the drag curve for a 12 % thick transonic aerofoil tested at the ARA in Bedford. We notice a pronounced drag creep with Mach number below the design point and the corresponding pressure distribution at $C_{D_{max}}$ explains the drag creep of 30 counts mainly by the occurence of a double shock at about 35 % and 65 % of the chord resulting in strong wave drag. At the design point the drag is nearly 10 counts less and the explanation is once more given by the pressure distribution. The shocks are considerably weakened and the wave drag is decreased. To overcome the drag creep the aerofoil was redesigned by increasing the upper side curvature by a very small decrease of the leading edge radius. The effects of the modification are presented in FIG. 15. The drag development of both sections is compared for three lift coefficients. The tests again were performed at the ARA at $6 \cdot 10^6$ Reynolds number and transition fixed at 7 % chord on both upper and lower section sides. The drag creep is strongly decreased the more the lift coefficient is raised. It was not checked and it is not known to what amount the smaller leading edge radius on one side and the improved upper surface pressure type with less wave drag on the other side are contributing to the decreased drag creep. We can suggest that the bigger part comes from the lower wave drag of the improved aerofoil. - In any case the tests show the complexity of the drag build-up due to changes of the leading edge radius in case of practical aerofoil design, because the designer seeks a certain type of pressure distribution at the design point associated with low drag also in the neighborhood of the design point and high buffet boundaries. He does not design for a specific leading edge radius. Even if he keeps the upper surface pressure distribution constant and changes the lower pressure distribution by modification of the leading edge radius at the design lift coefficient, the comparison of the drag is of little practical importance, as both sections have quite different drag characteristics at off-design, different buffet boundaries, pitching moments and low speed characteristics with and without leading edge devices.

Another effect of the leading edge radius is on the interference with the fuselage. A too blunt nose results in drag increase due to boundary layer separation in the wing-fuselage corner in the neighborhood of the attachment line. A large wing root fillet is often needed to prevent the separation and reduce the root section velocities for drag reduction. The size of the fillet as shown in FIG.16 can be quite different depending on relative root thickness and setting angle, leading edge radius and wing height position at the fuselage. It depends on the aerodynamic lay-out of the entire inner wing, where the root section is one dominant part. The picture simplifies the correlation of wing root pressure distribution and fillet size. The higher the velocity over the root section upper side and the suction peak at the leading edge, the larger the fillet needed for drag reduction. This drag reduction is normally of the order of 1 % up to 2 % of the total aircraft drag and hence quite important with respect to the aircraft performance. FIG. 17 contains drag polars for a research wing of modern transport type we tested in the NLR-HST. The wing was of the type shown on the right hand side of FIG. 16, i.e. without high velocity at the front of the inner wing leading edge area. FIG. 17 presents drag measurements at a typical cruise Mach number for two wing-fuselage fillet sizes compared to the configuration without fillet showing, a 5 counts improvement by adding a rather small fairing while the larger fillet does not further improve the drag. FIG. 18 shows influence of the fillet on the drag creep over the Mach number. It is comparable to a wave drag reduction as in FIG. 14 and FIG. 15, when the shock on the upper surface of the aerofoil section is weakened. Regarding the test procedure for testing the wing root fillet effects the transition fixing must be handled carefully. Due to changes of the leading edge pressure gradients caused by different fillets the boundary layer reacts sensitive to transition band. It has to be made sure by accenaphten pictures or other techniques that transition occurs at the strip, and the strip location must allow firm conclusions about the fillet effect on drag comparing the wind-tunnel results with and without fillet.

Another critical part of the wing root section design is the trailing edge, FIG. 19. Any modern transport aircraft design with a rather thick root section $15\ \% \leq t/c \leq 18\ \%$ has to prevent separation occuring in the cavity of the wing-fuselage junction at the rear wing part by a more or less large fillet. Besides that, the camber affecting the load in the aft section and the downwash behind the trailing edge can have a strong influence on drag as well as on lift. FIG. 20 gives the planform of a research wing, where the trailing edge angle was changed at the root section. The wing was designed and the wind-tunnel model manufactured with linear lofting between three stations at the root, kink and tip. For modification the trailing edge at the root was set 3 mm downward corresponding to an angle of 3 degrees. The new trailing edge was again a straight line between the downward t.e point at the root and the unchanged t.e. point at the kink. FIG. 21 presents the modified root section. The changes were within the aft 20 % chordwise position at the upper side and 35 % at the lower side. The effect of the modification on lift and drag is shown in FIG. 22 with test results from the NLR-HST. We see improved lift and buffet onset characteristics and a change in the shape of the drag polar, which is rotated around the design point. Because of the increased nose-down pitching moments the crossover point of the trimmed drag polars is shifted to lower C_L, however. There is a large drag increase at low C_L and a decrease in lift dependent drag. No separation at the wing or fuselage was detected by flow visualization tests. Our experience from these and further tests with other wing lay-outs was, that the trailing edge design and the corresponding flow

in this area sensitively effects the drag and lift development in the transonic flight regime of a transonic aircraft wing, and as a consequence we found that only limited loads on the rear part of the root section can be allowed in a high performance transport aircraft wing design.

Besides the root section, the basic aerofoil profile, designed for the major part of the wing, undisturbed by the fuselage and tip, is dominant for the transonic wing performance, FIG. 23. A large effort in transonic aerofoil design was made during the last ten to fifteen years and the theoretical methods for flow calculations around such aerofoils are well advanced today. The 2-D wind-tunnels in the USA and Canada allow for tests up to $30 \cdot 10^6 \leq R_N \leq 40 \cdot 10^6$ per meter and this improves the experimental basis for a transonic wing, to be designed for a full-scale Reynolds number of 40 million based on mean aerodynamic chord in case of a transport aircraft like the Airbus. There is still a scatter in the test data of comparable wind-tunnels - more or less pronounced - but testing a new aerofoil for a new wing design in comparison with well known basic 2-D sections of existing aircraft tested in the same tunnel gives a sound design basis.

Important aerodynamic goals for the basic aerofoil design are:

- high C_{Lmax} and Buffet Onset Limits for the whole flight regime
- delayed Drag Rise over the Mach number without a pronounced "Drag Creep" at the lowest possible drag level
- smallest possible Zero Pitching Moment
- good Off-Design Characteristics.

These objectives characterize the type of design pressure distribution, e.g. with respect to

- extent and strenght of supersonic region and recompression gradient
- quasi shockfree conditions for the design point
- stable shock development as far as possible under off-design conditions
- separation beginning at the trailing edge
- strength of "Rear Loading".

The aerodynamic realization of these objectives must consider requirements from other fields such as structures, engineering design and production:

- the forward part of the profile up to the wing-box should allow a favourable shape for the leading edge flaps - a flattening of the aerofoil lower side in this region which is sometimes introduced in order to increase the load at the nose part may be detrimental to the design of high C_{Lmax} and favourable leading edge devices.
- The aerofoil part behind the wing box must have the space and the shape for accomodating effective trailing edge flaps - too thin rear aerofoil regions lead to structural difficulties, especially in the region of the spoilers.
- The middle part of the aerofoil must be as thick as possible, in order to allow the use of a big box. A high rear spar reduces the structural weight of the wing box.

2.3 Considerations about the wing design concept

Referring to the general wing planform of today's transonic transport aircraft as shown in FIG. 20, the importance of the basic aerofoil section characteristics is much greater than for older conventional aircraft designs. This results from the increased wing aspect ratio leading to a larger wing portion where the flow is not influenced by the tip or the root of the wing, respectively. On the other hand the section itself is much more advanced and to a higher degree imposes its characteristics on the wing.

Concerning the 3-D wing design, the flow development at the inner wing portion determines the span region over which mainly one type of flow appears on the wing, see FIG. 24. At design conditions the flow must be shockless as far as possible, but when C_L or Mach number increases different types of shock configurations can develop depending on the design concept as shown in the picture. A shock e.g. extending in the region outside the wing planform crank changes position and strength with variations in flow conditions and thus the characteristics of the wing aerodynamics. Fully developed twin-shock configurations often arise under off-design conditions associated with strong drag creep when the design point is shockfree. Such a low-loss pressure distribution can also be achieved at the design point if the double shock development at off-design is restricted to the inner wing portion and in addition is of weak intensity. In this case the wing has one dominant flow type, with the character of a quasi 2-D section flow changing rather continuously with Mach number and incidence. Hence the governing impact of the aerofoil characteristics on the wing is evident and the 3-D effects including the 3-D boundary layer influence are less pronounced. - For computational treatment of the wing and specific wing sections this type of transonic flow concept is a simplification, as will be described in the chapter "theoretical methods".

Following those two design concepts mentioned above a transonic wing design with the aid of wind-tunnel tests at the NLR-HST will be considered. FIG. 25 and FIG. 26 present the pressure distributions tested at $R_N = 2.5 \cdot 10^6$ with fixed transition at 7 % chord on the upper and lower wing side. In FIG. 25 a the double-shock wing is shown at the design point, the shocks already appearing rather strong. In FIG. 25 b, for increased angle of attack, the forward shock is stronger and extends outboard the planform crank which is at 40 % semispan. The second wing lay-out was aimed at decreasing the forward shock strength, without loosing suction in the forward region of the wing up to the crest. In FIG. 26 a only a weak forward shock up to 25 % halfspan is recognized. At design conditions we can see that a somewhat stronger shock only occurs near the kink position of the wing at the pressure measurement phase $\eta = 0.415$. Increasing the angle of attack in FIG. 26 b the forward shock has disappeared almost completely. Thus we have reached a similar flow development over about 80 % wing half span as in case of the exposed wing. At the outboard section the extension and the strength of the supersonic flow was decreased to prevent this wing part to initiate the high speed stall and to maintain outboard aileron effectiveness.

A comparison of the drag characteristics of both wings at the design lift coefficient is demonstrated in FIG. 27. The decrease in drag is about 5 counts at the design Mach number for wing 2, however, there is an even higher improvement at off-design Mach numbers. The rather strong drag creep for the first wing is associated with compressibility drag as far as can be concluded from the corresponding pressure distribution. The twin shock of this wing strongly influences the wave drag leading at $M = 0.75$ to about 8 counts drag increase. Near the design Mach number, at $M = 0.78$ the drag rise is softer and the difference between both wings decreases to 5 counts due to the improved pressure distribution with weaker shocks. The design lift coefficient for the wings studied at an early stage of our ZKP research programme was $C_L = 0.5$ at $M = 0.78$. We then found the best characteristics with respect to pressure distribution, and buffet onset to be at $C_L = 0.47$. This was taken as the actual design lift coefficient for the wings. Further designs for $C_L = 0.5$ were performed on the basis of slightly decreased wing thickness at the planform crank station and at the outer wing portion.

The drag creep occuring for a transonic wing is one feature, where the designer has to work with great emphasis and care. The reason is, that sometimes a large part of this drag can worsen the wing design considerably. Not only that the design is no longer competive, but also a serious estimation of the expected drag creep for the full scale aircraft is extremely difficult. In chapter 2.2 describing some aerofoil characteristics we did recognize already the complexity of this drag feature being dependent on the leading- and trailing-edge shape of the aerofoil as well as on the shock development over the upper surface. From our experience, mistakes can be made when all efforts are directed towards the minimum wave drag. This is often done, because one main task of transonic aerodynamics for any designer is to produce a favourable pressure distribution - shockless if possible - at the design point to keep the wave drag low. We made promising lay-outs regarding the upper and lower surface pressure distribution and the drag creep was still 15 counts and more. Hence we had to conclude that designing for a favourable pressure type is not sufficient for a high performance transonic wing design. - It is one fundamental condition and design aid, but no prove, that the drag characteristics are adequate. Another remarkable part contributing to the drag creep can be caused by the viscous flow due to boundary layer thickening without or with separation.

The above described drag development is most uncertain already in two dimensional flow, as discussed previously, and therefore is the most risky component in a transonic wing design. The reason is a limitation by the low maximum Reynolds numbers which can be tested in the wind-tunnels ($Re_{\bar{c}max} \approx 8 \cdot 10^6$ compared to $Re_{\bar{c}} \approx 40 \cdot 10^6$ for the Airbus) and the lack of theoretical methods.

Two features are predominant for properly calculating and testing the transonic flow: The shock-boundary layer interaction and the viscid-inviscid flow interaction at and behind the trailing edge. These phenomena are basically two-dimensional and nearly all our work at MBB/VFW concerning boundary layer calculation and testing is concentrated since several years on these problems. - In chapter 3.2.3 theoretical and experimental results are presented.

As is generally known, the real effects are of three-dimensional character as indicated by transonic wind-tunnel tests showing severe cross-flow at the trailing edge of the models. The flow over a swept wing fitted to a fuselage is furthermore complicated by crossflow effects at the leading edge, due to fuselage contamination, but these stability effects are connected with low Reynolds number tests we are limited to in the current wind-tunnels. FIG. 28 represents a characteristic picture of the problems enhanced with the crossflow instability at the wing leading edge. This picture we derived from a transonic research wing at cruise conditions of modern transport aircraft. Re_θ is the Reynolds number for the boundary layer along the attachment line calculated with the momentum thickness, incorporating the leading edge sweep angle. The critical Reynolds number, where turbulent flow starts from the attachment line, is found to exist at two different boundaries, one $240 \lesssim Re_{\theta_\infty} \lesssim 280$ for natural transition on a clean edge, the other $100 \lesssim Re_{\theta_\infty} \lesssim 120$ when contamination by the fuselage boundary layer ahead of the wing leading edge exists [3]. The diagram shows that, we have to expect laminar boundary layer flow at the attachment line over the full wing span at low Reynolds numbers, however, substantially mixed laminar-turbulent flow at so called high Reynolds number tests regarding the measurements in the European wind-tunnels. From this we can conclude that, testing in the lower Reynolds number range $2.5 \cdot 10^6 < Re_{\bar{c}} < 3 \cdot 10^6$, is most reliable. It keeps the leading edge flow laminar up to the transition band and, when by means of acenaphthene pictures the flow behind the band is observed to be turbulent, one has distinct areas of laminar and turbulent flow on the wing surface. This may be related to the aircraft in flight, where the entire flow is turbulent downstream from the attachment line. - However, there are other flow phenomena changing at higher Reynolds number, either improving or sometimes deteriorating the wing design. Trailing edge separation due to excessive adverse pressure gradients often is cured by increasing the Reynolds number. When interpreting the test results in the available range $2.5 \cdot 10^6 < Re_{\bar{c}} < 6.5 \cdot 10^6$ for complete models in our wind-tunnels, and, making predictions for the aircraft in flight, we have to be cautious. Surface irregularities, sometimes much stronger on the aircraft wing surface than on the wind-tunnel model can overrule the benefits of increasing Reynolds number taken from model tests. Furthermore, the trailing edge flow of transonic wings with a high degree of rear loading is more difficult to predict for full-scale Reynolds number, because the flow over the lower surface of the wing can influence the trailing ege separation considerably. So far the development of viscid-inviscid flow interaction at the trailing edge and in the wake is not fully understood.

For these reasons one can follow a simple rule in a transonic wing design to avoid any risk for the aircraft with flow separation at the trailing edge. To avoid any separation at any model tested in the appropriate transonic wind-tunnels, in the whole design range of cruise flight, and, in the whole range of Reynolds numbers, typical for tests at cruise conditions. In Europe the range is $2.5 \cdot 10^6 \leq Re_c \leq 6.5 \cdot 10^6$ with respect to Airbus scale.

3. DESIGN PROCEDURE FOR TRANSONIC WINGS

3.1 Objectives for theoretical and experimental work

Wing design in industry is very closely connected with the experience of previous wing development for aircraft built and flight tested by the company. The predecessor, for example the A 310 following the A 300 B, has in most cases a significant influence on the new design efforts. The experience with existing designs of flying aircraft and the risk involved with the next technological step determine the approach in industry.

With respect to the aerodynamic design, wind-tunnel testing in a reliable tunnel is still the fundamental working basis. - Intensive transonic tests were conducted e.g. in the tunnels of ARA and RAE in England and also in the NLR-HST in Amsterdam during the A 300 development, FIG. 29. The analysis of the measurements and the correlation with flight-tests, also repetitions and intensifications of these test series have formed the basis of new developments, as was done earlier in the same tunnels in case of new design like the A 310. Then the question arises concerning specific differences between wind-tunnel and flight test results of flying aircraft on one side and the results of the new design measured in the same tunnels on the other side. Due to retaining the flight Mach number of the new aircraft generation this question in mainly reduced to the influence of the Reynolds number, FIG. 30. Since new transonic wind-tunnels for three-dimensional measurements have not been built in Europe since the development of the Airbus and the Reynolds numbers have remained unchanged in existing tunnels, the evaluation of new designs and characteristics at higher Reynolds numbers is limited to two-dimensional testing. Reynolds numbers per meter up to $15 \cdot 10^6$ in Europe and $30 \cdot 10^6$ up to $40 \cdot 10^6$ in the USA and Canada are possible. ($Re_c \approx 40 \cdot 10^6$ for the A 310). Because of the higher impact of the aerofoil characteristics on a modern transonic wing design described in chapter 2.3, the 2-D tests at high Reynolds numbers are helpful to support the prediction of the aerodynamic characteristics of the new aircraft design.

As the prediction of the aircraft performance - as far as the aerodynamic part is concerned - is based on wind-tunnel data, the theoretical work in industry is concentrated on some main objectives:

a) The first approach in transonic wing design must meet the desired aerodynamic efficiency as closely as possible. This alone is a difficult task, because in a first step several parameters have to be weighed in trade studies leading to a basic wing design. As a minimum we have as

Main Parameters for Basic Wing Design

- area	- thickness
- planform	- design Mach number
- aspect ratio	- design lift coefficient
- sweep angle	- weight
- taper ratio	- low speed performance

The design method must be powerfull, allowing the designer to evaluate the best basic design in an optimization study. As a number of additional parameters are included in the trade studies, in most practical cases we arrive at more than one basic wing design, all competing against each other. However, the advances in transonic computational techniques have considerably improved the design method and reduced the cycles for an optimized basic design.

The second step is to optimize the aerodynamic efficiency of the basic wing design given by planform, area, aspect- and taper-ratio, sweep angle and relative thickness at some spanwise station like root crank, and tip. The design variables for this task are for

Optimization of Aerodynamic Efficiency

- aerofoil shapes	- load distribution v_s span
- thickness distribution	- L/D (C_L, Mach number)
- twist distribution	- buffet boundary (M)
- wing setting angle	- pitching moment
- dihedral v_s span	- stall characteristics
- space for fuel, systems main landing gear	- aileron effectiveness

The quality of the design method to a large extent contributes to the aerodynamic efficiency of the wing design.

b) A further objective of the theoretical work is to limit the number of wind-tunnel models, needed for testing up to the final wing design stage. Model tests are time and money consuming and the design process can be laborious and inefficient if the theoretical methods are not powerful enough. It must be realized, that several features like fillets, fairings and local shape changes can only be optimized in the experiment and require extensive wind-tunnel testing. Thus the design of the clean wing has to be established in a limited number of improving steps. Today the model shop needs six weeks for the manufacture of a high speed wing and three months for a wing with pressure orifices. Hence no more than two up to three design steps can be tested per year, including the design process and analysis of wind-tunnel test results. Following different design concepts simultaneously the number of tests can be increased. The theoretical methods used should be capable of improving the wing performance in only a few steps up to the design target.

c) Another objective of the theoretical work is to estimate the Reynolds number influence on the aerodynamic performance in the range between model tests and aircraft flight. One part of this work is the understanding of wind-tunnel test results and the definition of test procedures as will be discussed in chapter 4.

The objectives have to be fulfilled with suitable theoretical methods which will be discussed in the next chapters.

3.2 Wing design methods

The evaluation of the optimum basic wing geometry, for which the main optimization parameters are described in the previous section, is considerably improved by the assistance of appropriate transonic computational methods. Voogt and Slooff, ICAS paper 82-5.6.1, have shown that the drag characteristics versus Mach number can be very well calculated by the NLR-method. The shape of the drag curve versus Mach number is excellent and the drag level seems good enough for optimization of basic wing geometry.

Moreover, as Voogt and Slooff have shown, the method is well applicable for design purposes and calculations of target pressure distributions of wing-body configurations in transonic flow. The central part of the computer programme system consists of Jameson's FLO 22. Hence it is a reliable tool to optimize the aerodynamic efficiency of a transonic wing in connection with W/T-measurements. There are several other methods, discussed at the present VKI Lecture Series and described in the literature, which are based one 3-D full potential transonic flow calculation combined with 3-D or 2-D boundary layer codes. - In industrial wing design we have good experience with simpler methods, which will be described in the following chapter.

3.2.1 Analogy method for transonic wing design

A well tested procedure which we call "analogy method" to design a transonic wing for transport aircraft is shown in FIG. 31. It is used to calculate the transonic pressure distribution over a wing including wing/body interferences. The calculation starts with subsonic pressure distributions at different spanwise stations of the wing taken from experiment or 3-D panel calculations. Thus it takes advantage of the cheaper, more exact and easier handling of theory and experiments in the subsonic flow regime, together with the greater experience compared to the transonic flow regime. In the second step analogous profiles, Mach numbers and angles of attack are determined for the desired wing sections. This is done by starting from the 3-D pressure distribution at one station and applying an inverse 2-D method to obtain an equivalent section profile generating the 3-D pressure distribution. This "analogous profile" is now handled with an accurate 2-D transonic method including boundary layer effects. FIG. 32 contains results for a research wing. In this method of approach the differences between subsonic and transonic 3-D effects are neglected for the investigated wing section. However, this method delivers adequate results for the desired spanwise pressure distribution and its transonic development. FIG. 33 shows a comparison of calculated and tested pressure distributions near the fuselage.

3.2.2 A hybrid method for transonic wing design

A special combination of a panel method and a finite difference method was developed for transonic wing design. This hybrid method, in contrast to the analogy method, requires

no analogous profile

no analogous Mach number

no analogous angle of attack.

The first point is of great practical importance, because in many cases it is laborious even for a skilled designer to determine an analogous profile. The second point is substantially significant, because the analogy method is by definition not able to calculate the correct shock strength due to the low analogous Mach number. The last point will become important as soon as 3-D boundary layer effects can be included in a satisfactory manner. At present the local lift coefficient must be adjusted according to the analogy method. Summing up, a designer using the hybrid method instead of the analogy method needs less experience in practical wing design.

When using the hybrid method the transonic wing flow is solved in spanwise sections, similar to the analogy method. However, in contrast to the latter, 3-D flow effects are taken into account by calculating the cross flow using a 3-D panel method for each wing section. This procedure is based on the assumption

that even in transonic flow the significant 3-D effects are linear in a first approximation. Then succeeding non-linear 2-D calculations with linear cross-flow are only corrections of the linear calculation.

The transonic full potential equation is the basis of the hybrid method:

$$\phi_{xx}\left(C^2-\phi_x^2\right)+\phi_{yy}\left(C^2-\phi_y^2\right)+\phi_{zz}\left(C^2-\phi_z^2\right)-2\phi_x\phi_y\phi_{xy}$$
$$-2\phi_x\phi_z\phi_{xz}-2\phi_z\phi_y\phi_{yz}=0$$

where ϕ is the velocity potential and C is the local speed of sound. When y denotes the spanwise direction all terms with derivatives of y are shifted to the right side and one gets the equation

$$\phi_{xx}\left(C^2-\phi_x^2\right)+\phi_{zz}\left(C^2-\phi_z^2\right)-2\phi_x\phi_z\phi_{xz} = \qquad (*)$$
$$= -\phi_{yy}\left(C^2-\phi_y^2\right)+2\phi_x\phi_y\phi_{xy}+2\phi_y\phi_z\phi_{yz}$$

When the derivatives ϕ_{yy}, ϕ_y, ϕ_{xy} and ϕ_{zy} are known in the entire plane of a wing section $y=\eta$ then (*) is an inhomgeneous 2-D transonic potential equation which can be solved by a finite difference method for the original wing section.

ϕ_{yy}, ϕ_y, ϕ_{xy} and ϕ_{zy} can be calculated by a panel method and this is how 3-D flow effects are taken into account by the hybrid method. For demonstrating the difference between this method and the analogy method one should remember:

The basic equation of the analogy method is the homogeneous 2-D full potential equation

$$\phi_{xx}\left(C^2-\phi_x^2\right)+\phi_{zz}\left(C^2-\phi_z^2\right)-2\phi_x\phi_z\phi_{xz}=0$$

This equation is solved by a finite difference method for an analogous profile for simulation of 3-D flow effects.

When applying the hybrid method to wing analysis there are four necessary steps in the calculation:

a) 3-D panel calculation for the actual Mach number using a compressibility rule (such as Göthert's rule).

b) Grid generation of 2-D streamline coordinates at the actual wing section. In many cases it is not necessary to compute the grid for the entire plane. Only a small region containing the supersonic flow field bounded by Γ_0, Γ_1, Γ_2 and Γ_3 is considered (see FIG. 34)

c) Computation of the cross flow at all mesh points of the grid and calculation of the boundary values at Γ_1, Γ_2, Γ_3 by means of the 3-D panel method.

d) Finite difference calculation solving the inhomogeneous full potential equation (*). The result is a transonic pressure distribution around the actual wing section.

The hybrid method is an analysis method. When using it for design or modification of a wing the same steps as described in the preceeding chapter are necessary. The block diagram, in FIG. 35 shows a practical way of modifying the spanwise sections of a wing. Calculations were performed for several configurations including propulsion interaction. Results are presented in the Lecture "Engine/Airframe Interference" during the present VKI course.

3.2.3 Computation of shock-boundary layer interaction and trailing edge flow

The importance of these flow phenomena for theoretical and experimental design of a wing at transonic speeds was discussed in chapter 2.3. Therefore the main work performed at VFW, partially in cooperation with the DFVLR, is presented in this section.

3.2.3.1 Shock-turbulent boundary layer interaction

The interaction between a normal shock wave and a turbulent boundary layer produces both local and global effects on the aerofoil flow:

- The local interaction effect is a smearing of the discontinuous pressure rise across the shock over several boundary layer thicknesses, which has only a small influence on the aerofoil characteristics.

- An important global effect arises from the substantial thickening of the boundary layer by the shock, FIG. 36 , which significantly increases the boundary layer thickness at the trailing egde, directly affecting the Kutta condition responsible for the aerofoil circulation and consequently also for the shock strength and position.

The influence of a normal shock wave on the turbulent boundary layer characteristics is evident from the measurements of Stanewsky [4] at DFVLR on a CAST 10-2 supercritical aerofoil at various angles of attack, FIG. 37.

The diffraction of the shock wave by the nonuniform flow within the boundary layer leads to significant normal pressure gradients and to a breakdown of the boundary layer approximations. Nevertheless, in the available viscid-inviscid weak interaction aerofoil flow prediction methods, the boundary layer characteristics across the shock wave are calculated by first order boundary layer methods, ignoring the strong interaction feature of the shock region. The main problem of this approach is the inability of the inviscid transonic flow methods to smear the pressure rise of the shock over a much greater chordwise distance than actually occurs (depending on the computational mesh used). This spread can easily rise up to 20 local boundary layer thicknesses instead of 5 to 6 thicknesses experimentally observed.

FIG. 38 shows the effect of the shock pressure gradient smearing on the calculated boundary layer characteristics at the rear part of a VFW supercritical aerofoil, calculated by the VFW 2-D finite-difference method [5] . The Mach number just ahead of the shock M_S = 1.288 is close to the value for which a shock-induced separation bubble will occur at the foot of the shock. Prescribing the experimental pressure distribution but with the shock smeared over about 20 boundary layer thicknesses, the predicted skin friction coefficient indicates attached flow at the end of the shock and the predicted boundary layer thickening through the shock is only 70 percent of that measured in the experiments. With a realistic shock smearing over 6 boundary layer thicknesses, the predicted boundary layer is just approaching separation behind the shock as expected, and the predicted displacement thickness behind the shock is in good agreement with the experimental data. This difference in the calculated boundary layer characteristics behind the shock influences the boundary layer behaviour at the trailing edge especially when the flow is close to separation.

To overcome the drawbacks of the first order boundary layer approach we will use the shock-turbulent boundary layer interaction model of Bohning and Zierep [6] in the future. This analytical strong interaction model is based on a triple deck solution, FIG. 39 , first introduced by Lighthill and consisting of

- a viscous sublayer formulation
- an inviscid but rotational shear layer solution
- and an outer inviscid transonic flow solution.

With closed form solutions in the 3 regions coupled iteractively, the velocity and pressure field is obtained in the strong interaction region, taking into account also the aerofoil wall curvature in this area.

As a typical example, FIG. 40 shows some details of the shock-boundary layer interactive solution of Bohning and Zierep. The calculated flow field structure given on top is represented by the lines of constant Mach number. The influence of the snock extends over 2 - 3 boundary layer thicknesses upstream of the shock, resulting in a lifting of the isolines. In consequence of both the flow field curvature and the boundary layer thickening in the shock region the interaction model predicts a post-shock expansion at the boundary layer edge just behind the shock as observed in the actual flow. The total length of the interaction region is about 6 boundary layer thicknesses. On the bottom, predicted pressure distributions within the interaction region are plotted for various wall distances. The pressure distribution at the boundary layer edge shows the typical singular behaviour at $x \longrightarrow 0$ and the following post-shock expansion. In contrast, the wall pressure distribution is smoothed across the shock, and the difference of both demonstrates the strong normal pressure gradient in the shock region. Corresponding to the wall pressure rise the wall shear stress decreases in the shock region. Ahead of the shock at higher Mach numbers than considered in FIG. 40 , shock-induced separation can occur. With the condition of vanishing wall shear stress, a criterion for the beginning of the shock induced separation is included in the interaction model.

FIG. 41 shows a comparison between results obtained with the interaction model and experimental data by Stanewsky [7] of a CAST 10-2 supercritical aerofoil. Both the predicted wall pressure and the displacement thickness distribution in the shock region are in excellent agreement with the measurements.

In order to incorparate the interaction model of Bohning and Zierep into a global iterative prediction method for transonic aerofoil flows the wall curvature, which has to be prescribed, can serve as an adaptive parameter.

3.2.3.2 Trailing edge flow

The flow near the trailing edge also involves a strong viscid-inviscid interaction problem. The highly curved streamlines at the trailing edge and in the near wake generate large static pressure variations across the boundary layer and the wake that are at least of the same order than those induced by displacement effects, FIG. 42 . As in the shock region, the strong interaction and the large normal pressure gradients lead to a failure of the boundary layer approximations in the trailing edge region, which directly effects the Kutta condition, largely responsible for the aerofoil characteristics.

In case of a supercritical aerofoil, FIG. 43, demonstrates, that the viscous lift loss is significantly underpredicted by the standard first order boundary layer approach. In particular, the measured pressure distribution on the upper surface shows considerable deviations from an inviscid calculation, wherein the measured boundary layer displacement thickness is superimposed to the aerofoil contour.

Therefore, it is apparent that for a completely satisfactory description of viscous effects on aerofoils at transonic speeds with a higher order boundary layer type method we have to account for:

- displacement effects on the aerofoil and in the wake,
- normal pressure gradient effects in the trailing edge region (aerofoil and near wake),
- strong interaction at shocks and at the trailin edge.

The appropriate viscous flow model is shown in FIG.44 . For simulation of viscous effects the equivalent surface mass flow concept is used. In case of aerofoil flow calculations with an iterative global procedure, this concept is most effective, using only modified boundary conditions but with an unmodified aerofoil shape during the iteration. The boundary conditions, which simulate the viscous effects, are

- a normal velocity distribution prescribed on the aerofoil contour
- and normal and tangential velocity jump distributions prescribed at the wake centerline.

To complete the viscous solution, the static pressure variations across the boundary layer and the wake must be added to the inviscid solution. This concept forms the basis for the incorporation of the strong trailing edge interaction into the viscous aerofoil solution.

For iterative coupling of both the boundary layer solution and the inviscid flow solution, the direct matching technique is normally adopted for aerofoil flow predictions, which converges fast as long as the inviscid flow dominates over the boundary layer flow. However, approaching the trailing edge, convergency difficulties arise due to the increasing interaction between the boundary layer and the inviscid flow. In order to avoid these difficulties, the semi-inverse matching technique, coupling iteratively an inverse boundary layer solution with a direct potential flow solution, may be applied in the trailing edge region. Here, the inverse boundary layer approach (prescribing the displacement thickness and treating the pressure as dependend variable) removes the Goldstein singularities at the separation and reattachment point, so that separated flow regions can be included.

FIG. 45 shows the flow chart of the semi inverse matching procedure. Here, from a given displacement thickness the boundary layer edge velocity is computed simultaneously by the direct potential flow method, modified to incorporate the appropriate viscous boundary conditions, and by the inverse boundary layer method. The resulting edge velocities of both solutions are used to adjust the displacement thickness for the next iteration cycle by the matching condition of Carter [8] . Using a relaxation factor control the solution has a high convergency rate.

The inverse boundary layer method, developed at MBB/VFW [9] , solves the moment and the moment of momentum integral equations for steady 2-D compressible flows. The relations for laminar velocity profiles are deduced from similar solutions of Stewartson including the lower-branch solutions for reverse flow velocity profiles. In the turbulent case the relations of the Walz method are incorporated in the attached flow regime, while for separated flow similar solutions of Alber are taken as a basis. In the near wake the profiles of Reeves and Lees are used, whereas the far wake profiles are approximated by the cosinus-profile. Deviations from the equilibrium condition are considered by an empirical dissipation law. With these relations, the integral equations are solved with a prescribed displacement thickness by a standard Runge-Kutta integration.

The semi-inverse matching technique, which provides a highly efficient computation of strong viscid-inviscid interactions, was applied to attached and separated trailing edge flows of rear-loaded aerofoils including the wake, and presents a substantial improvement of aerofoil flow prediction methods. First a global method for subsonic aerofoil flows was developed [10] , switching from a conventional weak interaction analysis to the present approach for strong trailing edge interaction. In this case, the inviscid flow is solved by the MBB/VFW panel method [11] modified to incorporate the viscous boundary conditions.

FIG. 46 shows viscid-inviscid flow predictions over a VFW rear-loaded aerofoil at high incidence. For comparision with the experiments [12] three different calculations have been performend:

- inviscid mode
- viscous mode (with boundary layer and wake thickness terms only)
- full viscous mode (including curvature terms).

An excellent agreement between the predicted and measured pressure distribution is achieved with the full viscous solution. For the different calculation modes the convergence of the lift coefficient is also shown in FIG. 46 . The viscous lift loss is significantly underpredicted, when curvature terms are not taken into consideration.

As a detail of this solution, FIG.47 shows the streamline slope of the full viscous solution within the trailing edge region in comparison to the inviscid result. The discontinuity at the trailing edge obtained in the inviscid flow simulation is completely removed by the full viscous solution.

In FIG. 48 predicted lift, moment and drag polars of a NLR rear-loaded aerofoil are compared with experimental data [13] . Beyond 6 degrees incidence the flow on the upper surface separates near the trailing edge. With exception of the drag coefficient at high incidence, where also large spanwise scatter was measured, the full viscous predictions agree remarkably well with the measurements for both attached and separated flow cases.

In FIG. 49 compressible flow quantities (pressure distribution and boundary layer data) over a RAE rear loaded aerofoil are presented. Also this compressible test case shows generally good agreement between the predicted results and the experimental data of Cook et al [14] .

The results obtained for subsonic aerofoil flow cases show significant improvements in the trailing edge region, leading to an improved global prediction of the wing section characteristics compared to

standard methods. Therefore, the application of the strong trailing edge interaction mode for transonic aerofoil flow predictions is under development at MBB/VFW.

4. PREDICTION OF AIRCRAFT PERFORMANCE

In chapter 3.1 it was explained that the estimation of aircraft performance as far as aerodynamics is concerned relies on proper wind-tunnel testing and from there objectives for the evaluation of theoretical methods and their application were derived. The process of transforming wind-tunnel test results to full scale aircraft performance data in the transonic flight regime is one of the main and most difficult tasks of the designer in industry. Errors in the prediction of cruise drag can have serious consequences for the manufacturer, because of the stringent performance data he must guarantee to be competitive. In the following we concentrate on performance estimates, but in addition the most accurate determination of the aerodynamic loadings has large effects on the structural weight and hence on the fuel consumption. Because of the compensating effect of intertia and aerodynamic loads, a relatively small error in aerodynamics can become a major structural design problem. Conservatism in load prediction leads to unnecessary structural weight, while optimism can request structural redesign and perhaps catastrophic failures. Today's use of more exotic materials, higher stress levels, and elaborate manufacturing techniques to achieve highly efficient, light weight structures has magnified the degree of accuracy needed in predicting full-scale aerodynamic loads.

The aerodynamic problem is focused on the Reynolds number influence. As the modern transonic wing sections excessively stress the boundary layer flow with a large amount of rear loading, strong boundary layer-shock interaction and high pressure gradients at the upper and lower side of the trailing edge, the full-scale estimates are considerably complicated. - Here is another reason why at MBB/VFW we concentrate on the two subjects discussed in the previous section namely the shock-turbulent boundary layer interaction and the viscid-inviscid interaction including separation at the aerofoil trailing edge.

For full-scale aircraft performance predictions deduced from wind-tunnel measurements we work with basically two approaches, the direct scaling method and the reference method.

4.1 The direct scaling method

The wind-tunnel data are used to establish the absolute drag level of a model, and with an understanding of Reynolds number effects the full-scale drag level can be predicted.

The drag components which together comprise the total cruise drag are

$$C_D = C_{Dp} + C_{Di} + C_{DC} + C_{DTrim}$$

A typical drag break-down was shown in FIG. 6 . Besides friction and pressure drag the parasitic drag then contains

- interference drag = influence of supervelocities on various components
- intersection drag = interference in junctions
- excrescences = steps, gaps, rivests, base areas
- protuberances = antennas, canopy, lights, vents
- ventilation drag = air conditioning, cooling
- fuselage up sweep drag

All of these drag increments may be subject to Reynolds number effects, however, only the skin friction drag is adequately documented. But even in this area, there are a number of empirically derived equations for smooth turbulent flat plate skin friction coefficients and their variation with Reynolds number. This is shown in FIG. 50 for three established skin friction laws in the Reynolds number range from 10^6 to 10^9. The c_f is varying about 4 % at 10^6, 5 % at 10^8 and 7 % at 10^9. For typical current jet transports with a range $30 \cdot 10^6 \leq R_e \leq 60 \cdot 10^6$ an error of 5 % in the profile drag estimate possibly leads to about 2.5 % total drag error. Correcting wind-tunnel data to full scale Reynolds number by deducting from the wind-tunnel measured model drag the difference between the estimated profile drags at full and model scale Reynolds number then, the errors can be 1 % on full-scale profile drag or 0.5 % on full-scale total drag. The factors available in Hoerner and R.Ae.S data sheets were empirically derived from wind-tunnel tests with conventional aerofoil sections of varying thickness. They are less accurate for transonic aerofoils with rear loading.

The effect of Reynolds number on all other drag components is even less known. For this reason, in addition to the direct scaling method, we base the prediction for the aerodynamic characteristics of a new design on the so called reference method. A detailed description of the direct scaling method is given in [15] which is quite similar to the method we use at MBB/VFW.

4.2 The reference scaling method

This method utilizes all the experience inside a company obtained in wind-tunnel and flight tests. Best use can be made mainly in case when the new aircraft configuration is in many aspects similar to an earlier one, built and tested in the whole range of Reynolds numbers up to flight conditions. The fuselage for example often keeps quite a similar shape in an aircraft family concept as with the Airbus. This is a great advantage during wind-tunnel tests, because the same model supports and force balances can be employed with the same model connection. Hence the relative accuracy of wind-tunnel corrections is extremly

high, in contrary to the direct scaling where the absolute accuracy of the tunnel corrections needed is normally of comparable low standard.

The basic concept of the reference scaling method is simple and sketched in FIG. 51. The changes of aerodynamic characteristics between wind-tunnel and flight test of a known aircraft are transfered to the new design. The model tests for the reference aircraft and for the new design have to be performed for the same configuration, i.e. wing-fuselage - vertical tail at the same test conditions as sting support, transition fixing etc. A detailed description of the method is not the task here, because it has been already discussed earlier by Pelagatti, Pilon, Bardaud [16] , but there is one major problem inherent. If the wing section characteristics are changed - as in case from conventional to supercritical aerofoils - the method is not accurate. This will be discussed in the following section.

FIG. 52 contains the pressure distribution of two aerofoil sections, where mainly the shock position and rear loading at higher Mach numbers above the design point are different. For these sections the b.l. displacement thickness on the upper surface was calculated at model and full-scale Reynolds numbers below and above the design Mach number and is presented in FIG. 53. Transition from laminar to turbulent boundary layer was assumed at the leading edge and at 15 % chord for full-scale and model Reynolds number respectively. All changes in b.l. thickness at lower Mach numbers are smooth and not very different for model and full-scale Reynolds numbers though at the trailing edge the boundary layer as expected is thinner for the high Reynolds number. This changes with increasing Mach number due to the appearence of shocks and higher adverse pressure gradients and the Reynolds number effect is more pronounced for the projected aircraft with more aft shock positions and steeper pressure gradients towards the trailing edge. The b.l. thickness at model scale Reynolds number increases so strongly that an overestimation must be expected with respect to main aerodynamic characteristics like separation leading to buffet onset and lift/drag ratio during the low Reynolds number wind-tunnel tests.

Employing the reference method for scaling wind-tunnel data to full-scale results the predictions for advanced wings based on conventional aircraft data lead to pessimistic performances when the model tests were conducted applying the same transition fixing position.

An improvement of the reference method is outlined in FIG. 54 . In addition to the test data transformation, calculations have to be performed for the reference and projected aircraft at model as well as full-scale Reynolds numbers. The theoretical corrections for the reference aircraft are soundly based on the correlation of wind-tunnel and flight test data which improves the corrections for the projected aircraft. The main advantage of the higher order corrections is the allowance for more realistic test conditions. In the example discussed above, a more aft transition fixing at high Mach numbers for the projected aircraft results in the effect, that the boundary layer thickness is less increased not only across the shock but also by the adverse pressure gradient. Thus, an improved numerical simulation of the viscous effects mainly in the shock and trailing edge regions allows for the future both

- a more consolidated transition fixing on the wing in wind-tunnel measurements
- and a more reliable scaling of the wind-tunnel data to full-scale conditions in the case of different aerofoil types of the references and the projected aircraft.

Therefore, at MBB/VFW an improved viscous supercritical aerofoil flow prediction code is under development, taking into account the strong shock-boundary layer and trailing edge interactions especially.

REFERENCES

1	J.W. Swihart J.I. Minick	A fresh look at aviation fuel prices . AIAA, March 1980
2	J. Thomas	Future technology to comply with changing design requirements. AI/TD-160/79, ATA 1979, Engineering and Maintenance Forum, Oct. 31-Nov.11,1979
3	D.I.A. Poll	Transition in the infinite swept attachment line boundary layer. College of Aeronautics, Cranfield Institute of Technology, March 1979
4	E. Stanewsky	Wechselwirkung zwischen Außenströmung und Grenzschicht an transsonischen Profilen. Dissertation TU Berlin, 1981
5	E. Elsholz	Non-equilibrium boundary layer flow prediction. 4. Int. Symp. on "Turbulent Shear Flows", Karlsruhe, Sept. 1983
6.	R. Bohning, J. Zierep	Normal shock-turbulent boundary layer interaction at a curved wall. AGARD-CP-291, Febr. 1981
7.	E. Stanewsky, M. Nandanan, G.R. Inger	The coupling of a shock-boundary layer interaction module with a viscous-inviscid computation method. AGARD-CP-291, Febr. 1981
8.	J.E. Carter	A new boundary-layer inviscid interaction technique for separated flow. AIAA-Paper 79-1450, 1979
9.	P. Thiede	Ein inverses Integralverfahren zur Berechnung abgelöster turbulenter Grenzschichten. DLR-FB 77-16, 1977

10	P. Thiede, G. Dargel, E. Elsholz	Viscid-inviscid interaction analysis on aerofoils with an inverse boundary layer approach. In "Recent Contributions to Fluid Mechanics", ed. by W. Haase, Springer-Verlag, 1982
11.	H. Jakob	Erweiterung eines 2-D Panelverfahrens auf Profile mit dicken Hinterkanten und Kopplung des Verfahrens mit einem Grenzschichtverfahren. VFW-Report Ef 612, 1976, not published
12	R.D. Boehe	Ergebnisse der Windkanalmessungen WX 77-1. VFW-Report Ef 2-12/77, 1977, not published
13	C.J.J. Joosen, C.G. Kho	2-D low-speed wind-tunnel investigation on a NLR 73-108-10 aerofoil with fowler type flap, part 1. NLR TR 74058 C, 1975
14	P.H. Cook, M.A. Mc Donald, M.C.P. Firmin	Aerofoil RAE 2822-pressure distributions, boundary layer, and wake measurements. AGARD-AR-138, 1979
15	J.H. Paterson, D.G. Mc Wilkinson, W.T. Blackerby	A survey of drag prediction techniques applicable to subsonic and transonic aircraft design. AGARD-CP-124, April 1973
16	C. Pelagatti, J.C. Pilon, J. Bardaud	Analysis critique des comparaisons des resultats de vol aux previsions de soufflerie pour des avions de transport subsonique et supersonique. AGARD-CP-No. 187, June 1975
17	F.T. Lynch	Commercial transports-aerodynamic design for cruise performance efficiency. Transonic Perspective Symposium, NASA Ames Res. Ctr. Feb. 1981, also Douglas Paper 7026
18	G. Krenz	Transonic wing design for transport aircraft. AIAA Atlantic Aeron. Conf. "Advancing Technology", Williamsburg, Virginia, March 1979
19	G. Krenz, R. Hilbig	Aerodynamic concepts for fuel-efficient transport aircraft. ICAS proceedings, Seattle, Aug. 1982
20	G. Krenz, B. Ewald	Transonic wing technology for transport aircraft. AGARD-CP-285, Munich, May 1980
21	R.Hilbig	Transsonischer Profilentwurf Va 2. ZKP-FB-W80-023. Sept. 1980
22	R. Hilbig	Transsonischer Flügelentwurf. ZKP-FB W80-021, Sept. 1980
23	G. Redecker	Aerodynamischer Entwurf von subsonischen Transportflugzeugen. Carl Cranz Gesellschaft Lecture Series: "Aerodynamik des Flugzeugentwurfs" F6.01, Braunschweig, Sept. 1981
24	S. Rohlfs	Transsonisches Profil Va 2-4, Entwurf und Ergebnisanalyse. Ergebnisbericht ZKP "IFAS" Nr. 3, VFW, Bremen, April 1980
25	Whitcomb, R.T.	Review of NASA supercritical aerofoils. ICAS Paper 74-10, 1974
26	Pfenninger, W., Reed, H.L. Degenhardt, J.R.	Design considerations of advanced supercritical low drag suction aerofoils. Symp. on Viscous Drag Reduction, Dallas, Tex., 1979 ,
27	Kessler, K.	Aerodynamische Entwurfsmerkmale der transsonischen Tragflügel in Tief- und Hochdeckeranordnung. ZTL 1-Abschlußbericht:"Konzeptuntersuchungen zu einem MR-Transporter VFW-Fokker, 1.26-3, 1979
28	N. Voogt, J.W. Slooff	Advanced aerodynamic wing design for commercial transports - review of a technology program in the Netherlands. ICAS Paper 82-5.6.1

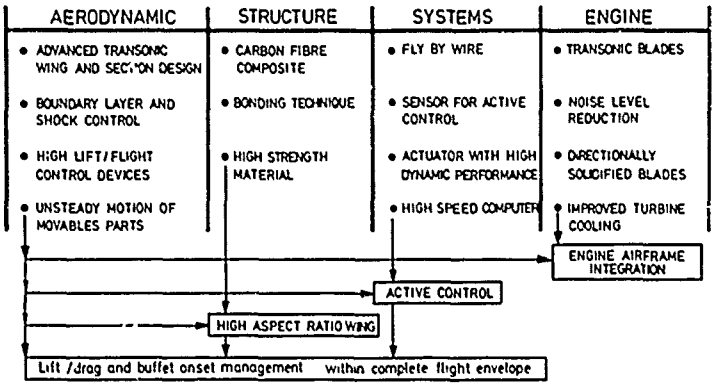

FIG. 1: Advanced technologies of commercial transport aircraft
— engagement of aerodynamics —

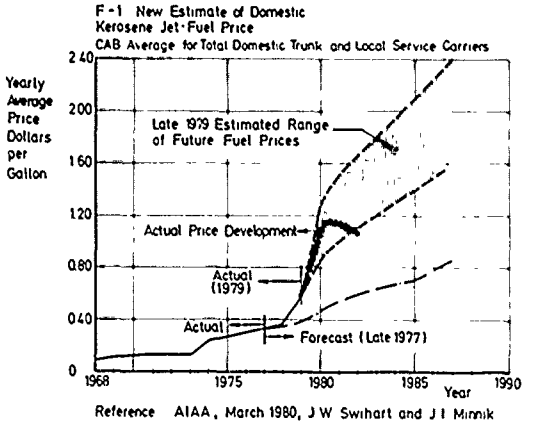

Reference AIAA, March 1980, J W Swihart and J I Minnik

FIG. 2 Increase of fuel price

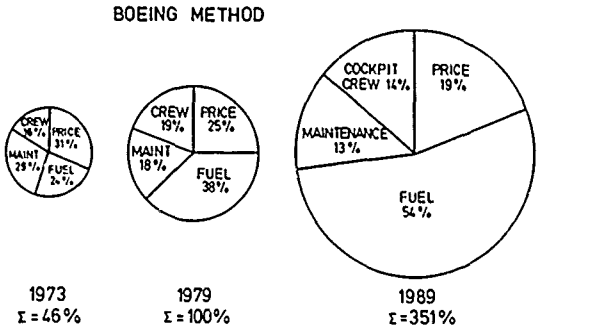

Reference 1979 ATA Engineering and Maintenance Forum, J Thomas

FIG 3 Increase of operating expenses with time and change of distribution

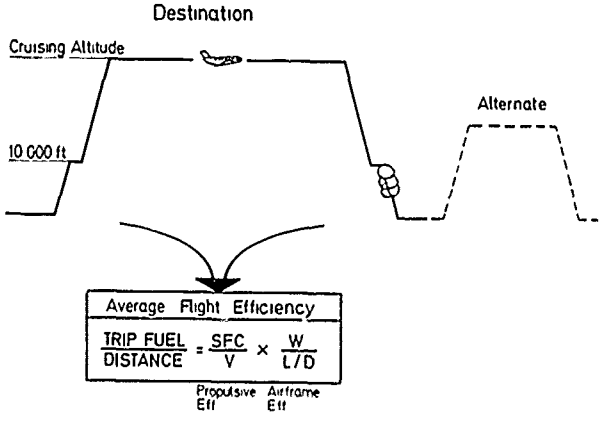

FIG.4 Mission fuel efficiency

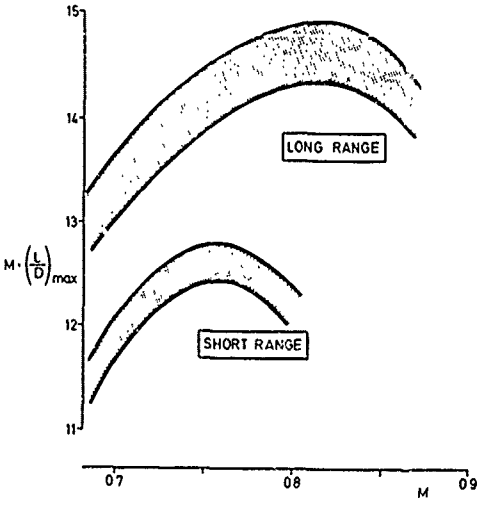

FIG 5 Performance parameter of commercial transport aircraft

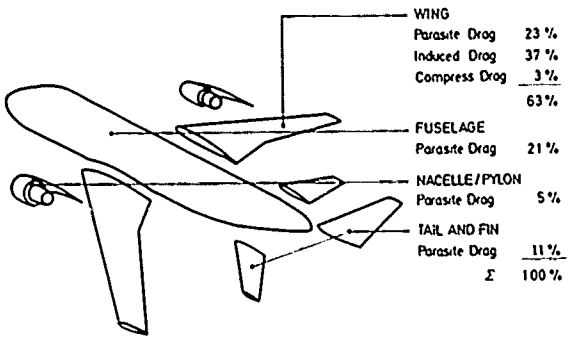

FIG. 6 Drag breakdown at cruise condition of typical commercial transport aircraft

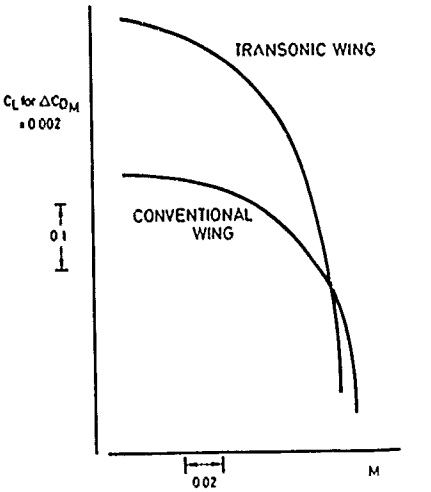

FIG 7 Drag rise boundaries at cruise Mach numbers

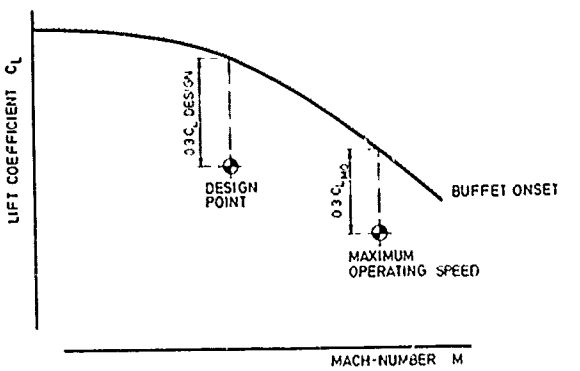

FIG 8. Design points and buffet boundary

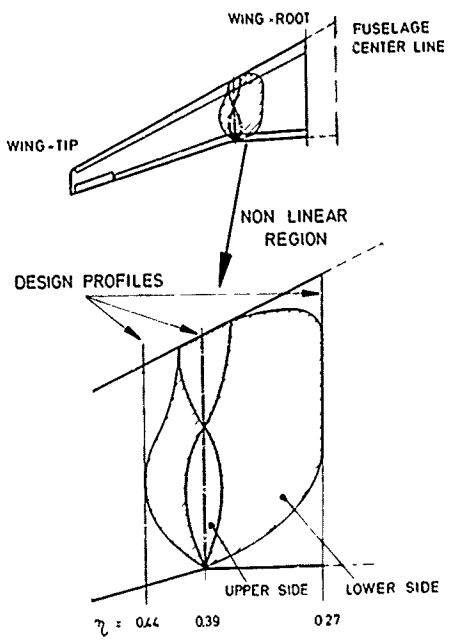

FIG 9 Non linear lofting regions

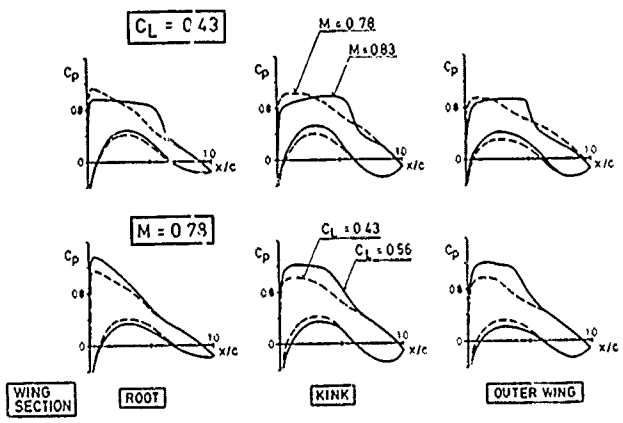

FIG 10 · Wing section pressure distribution

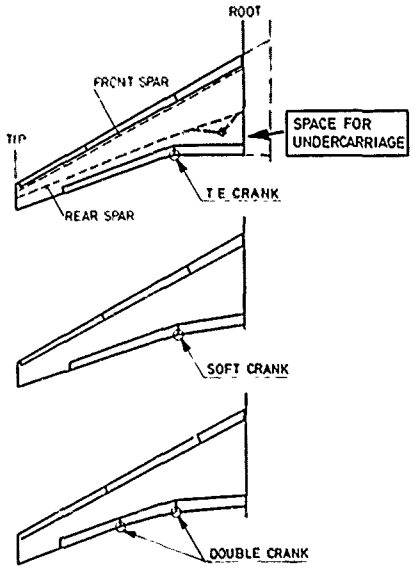

FIG 11: Trailing edge crank to increase space for undercarriage housing

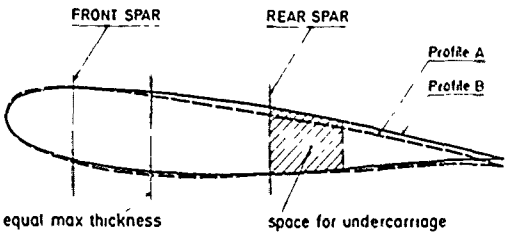

FIG. 12 Root section comparison

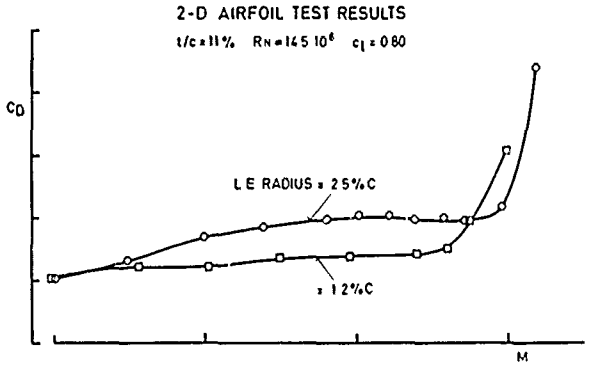

FIG. 13 Leading-edge radius effects on drag characteristics of supercritical airfoil (F.T. LYNCH, [17])

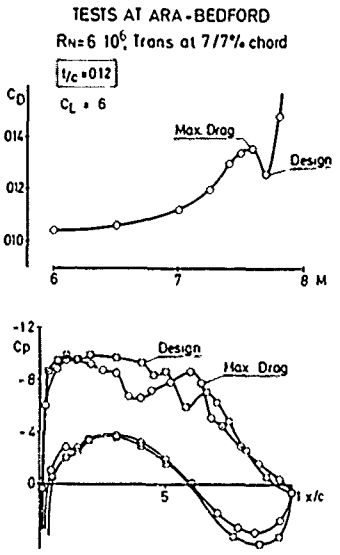

FIG 14 Aerofoil characteristics

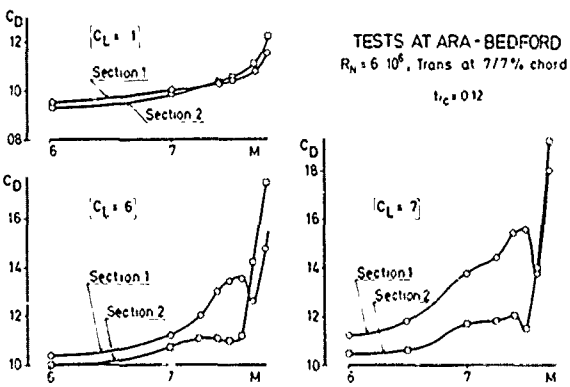

FIG 15 Drag comparison for two aerofoils

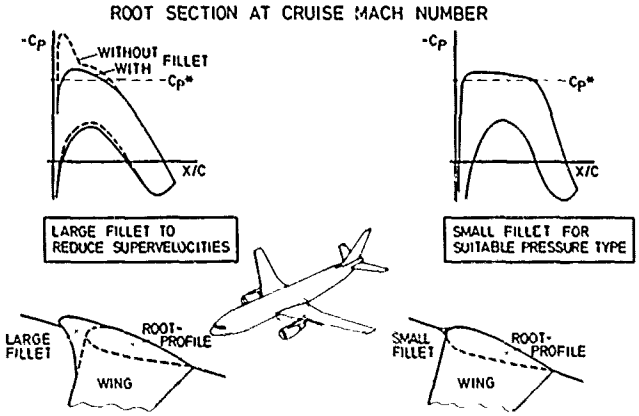

FIG 16 Correlation of fillet size and pressure distribution

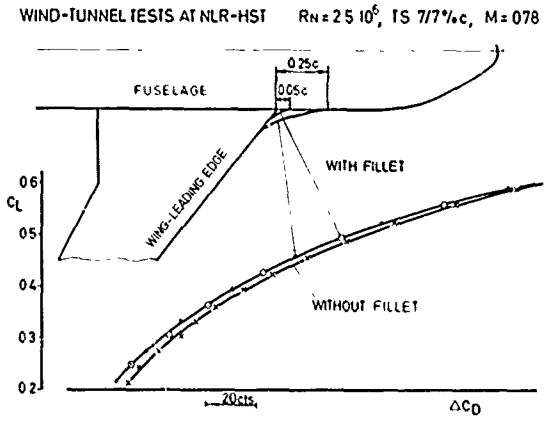

FIG. 17 Effect of wing-fuselage fillet on drag for a research wing of Airbus-type

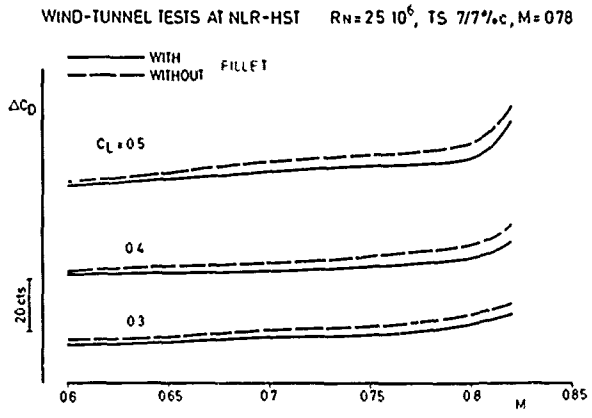

FIG. 18 Effect of wing-fuselage fillet on drag

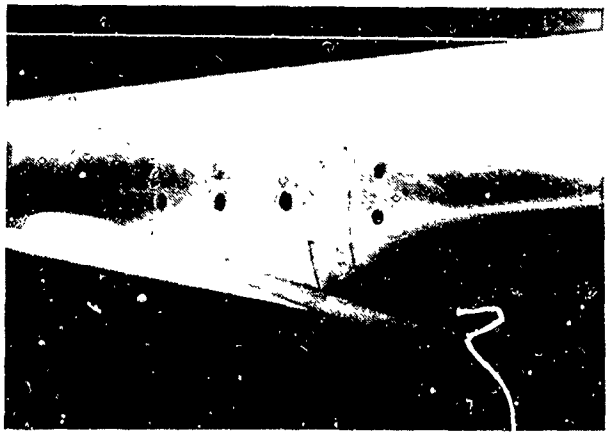

FIG 19 Large wing root fillet

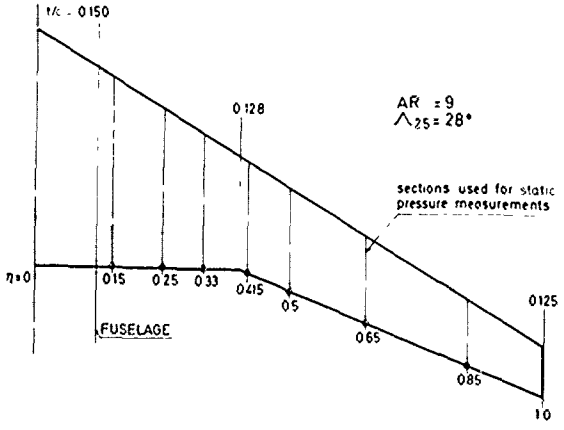

FIG 20 Typical planform and thickness distribution of transport aircraft

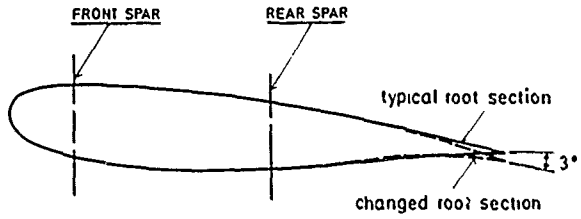

FIG. 21 Root section change

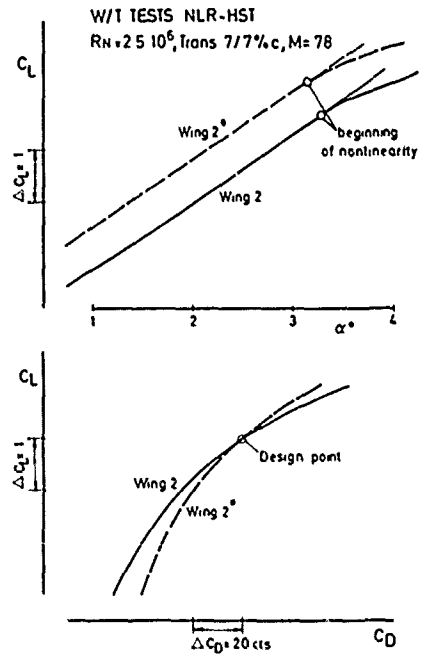

FIG.22 Effect of root trailing edge camber

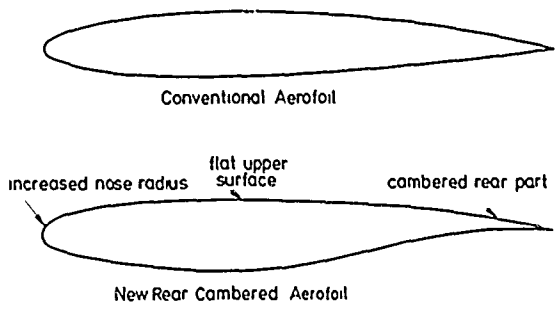

FIG 23 Changes of aerofoil geometry

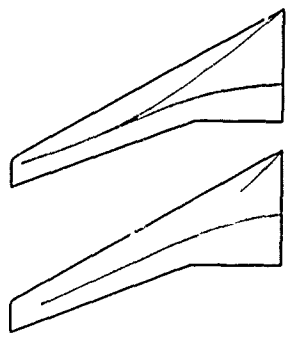

FIG 24 Wing shock systems at off-design conditions

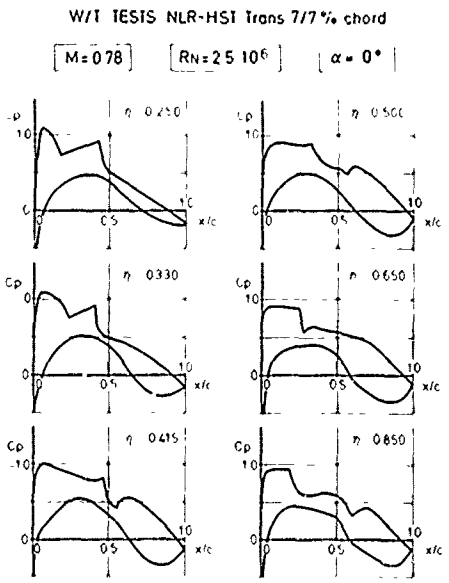

FIG 25a Development of pressure distribution at wing 1

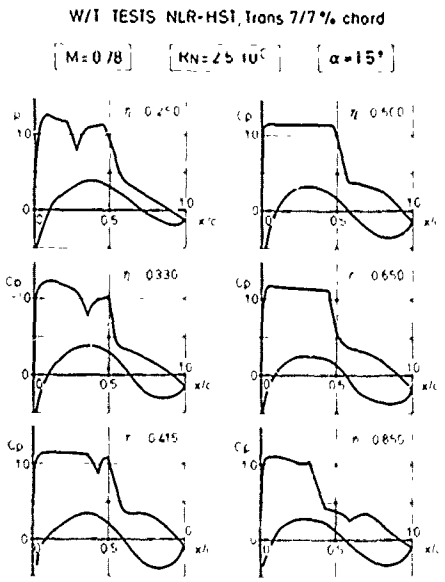

FIG 25b Development of pressure distribution at wing 1

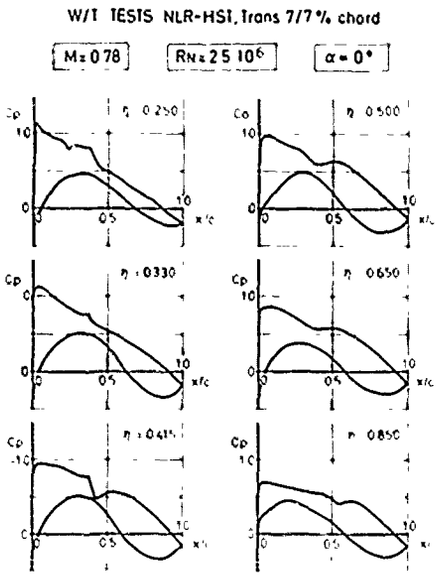

FIG. 26a Development of pressure distribution at wing 2

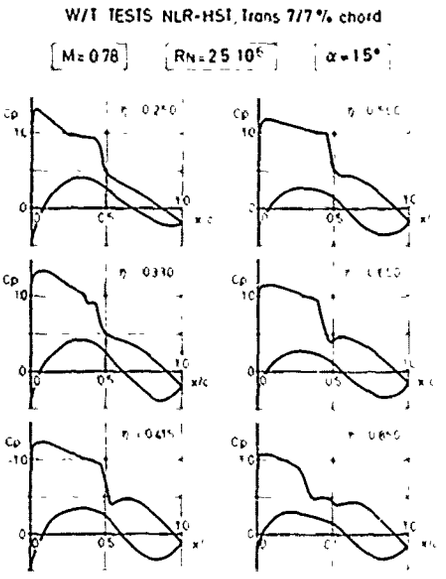

FIG. 26b Development of pressure distribution at wing 2

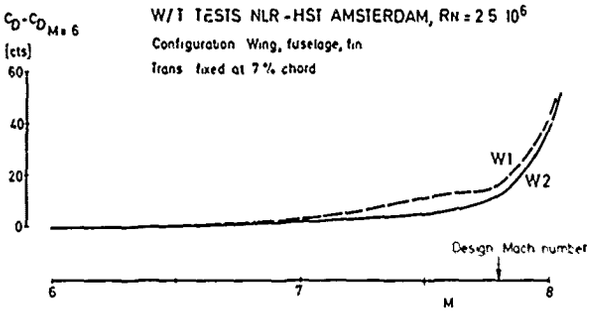

FIG 27 Drag comparison wing1 vs wing2 at design $C_L = 0.47$

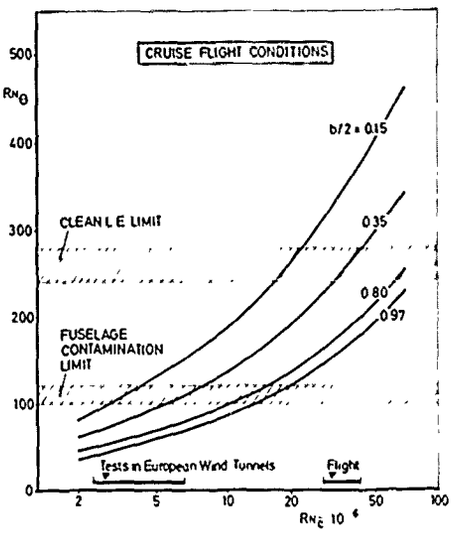

FIG 28 Attachment line Reynolds number for a research wing of Airbus-type

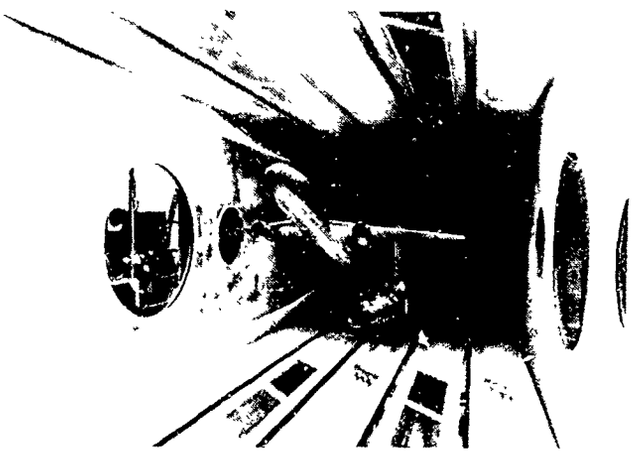

FIG 29 Airbus model in the transonic wind-tunnel of NLR

TRANSONIC 3D-WIND-TUNNELS

FACILITY	SIZE OF TEST SECTION (m^2)	MACH NUMBER	RN-NUMBER ** x 10^6
ONERA/S1 MA	8 ø	0.1 ÷ 1.03	8.0
ONERA/S2 MA	1.8 x 1.8	0.5 ÷ 2.9	3.0
NLR/Amsterdam	2.0 x 1.6	0.2 ÷ 1.4	3.0
RAE/Bedford	2.4 x 2.4	0.1 – 2.8	6.5
ARA/Bedford	2.7 x 2.4	0.3 – 1.4	3.5

TRANSONIC 2D-WIND-TUNNELS

TWB/Braunschweig	0.34 x 0.6	0.4 ÷ 1	3 *
TWG/Göttingen	1.0 x 1.0	0.4 ÷ 2.2	1.5
NLR/Amsterdam	0.55 x 0.42	0.1 – 1.0	1.0
ARA/Bedford	0.2 x 0.46	0.4 ÷ 0.85	1.5

REMARKS

* with $\varepsilon = 0.1 \sqrt{\text{TEST SIZE SECTION}}$

** related to MAC of typical Airbus models at cruise conditions

FIG. 30 Transonic wind-tunnels suitable for Airbus tests in Europe

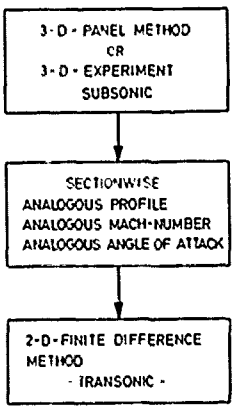

FIG. 31 VFW Analogy method

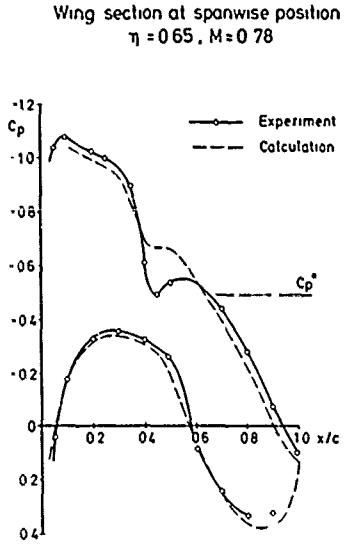

FIG 32 : Comparison calculation - experiment

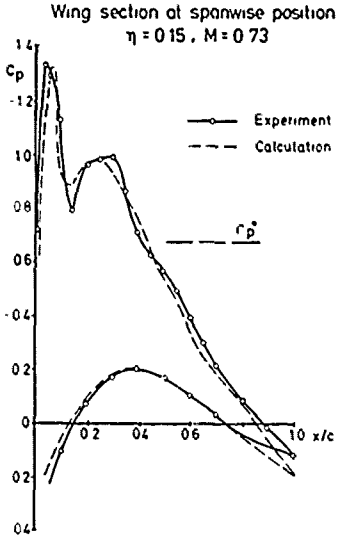

FIG 33 : Comparison calculation - experiment

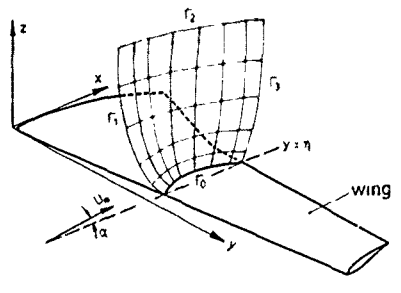

FIG 34 Coordinate system and grid scheme for hybrid method

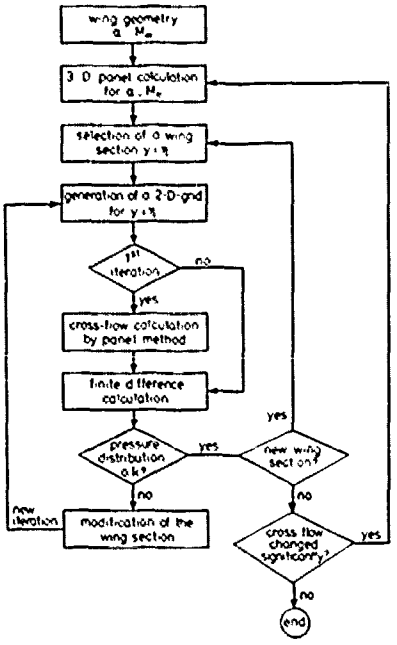

FIG 35 Wing modification concept

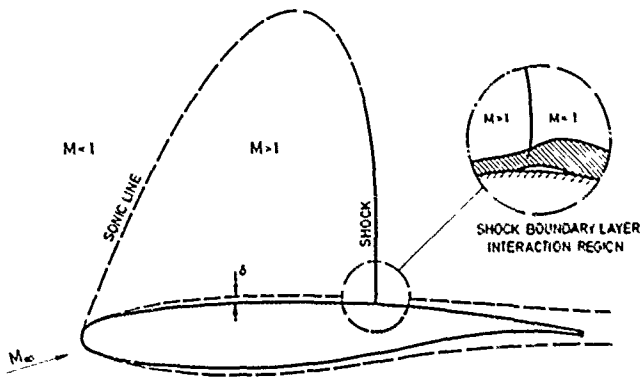

FIG.36 Shock-turbulent boundary layer interaction on a supercritical airfoil in transonic flow

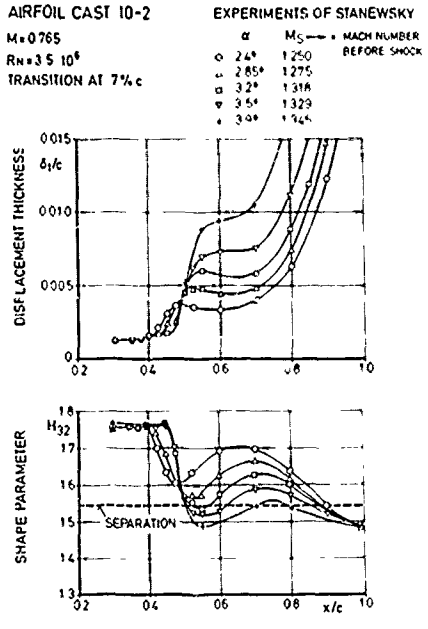

FIG. 37 Measured boundary layer characteristics in the shock region at different angles of attack

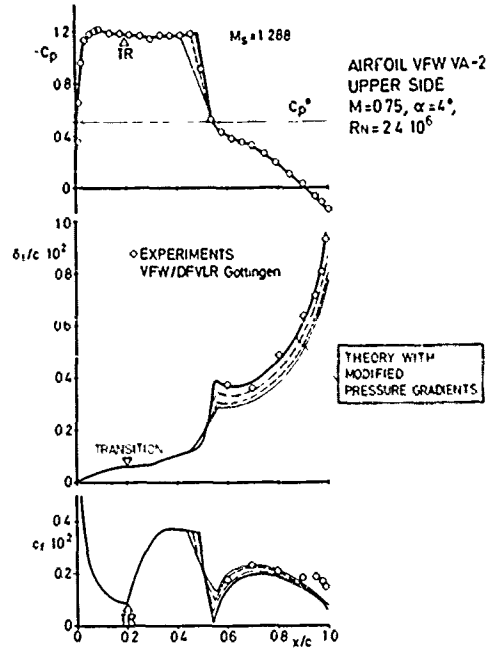

FIG. 38 Effect of shock pressure gradient smearing on calculated boundary layer characteristics

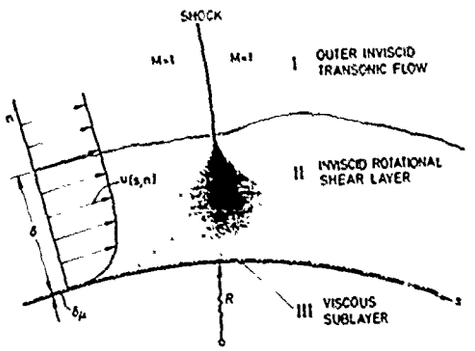

FIG. 39 Triple deck shock-turbulent boundary layer interaction model of Bohning/Zierep

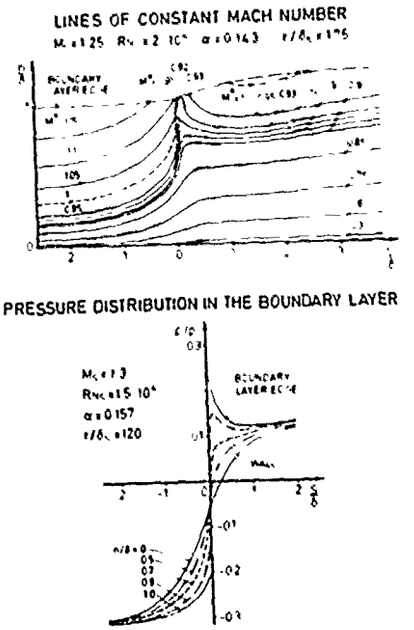

FIG. 40 Details of the shock-turbulent boundary layer interaction model of Bohning/Zierep

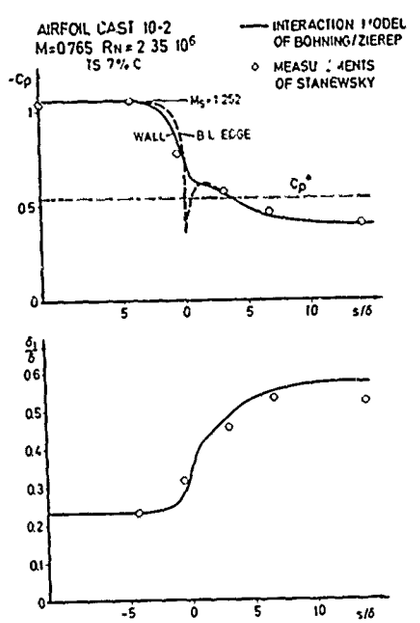

FIG. 41 Comparison of the shock-boundary layer interaction model with measurements

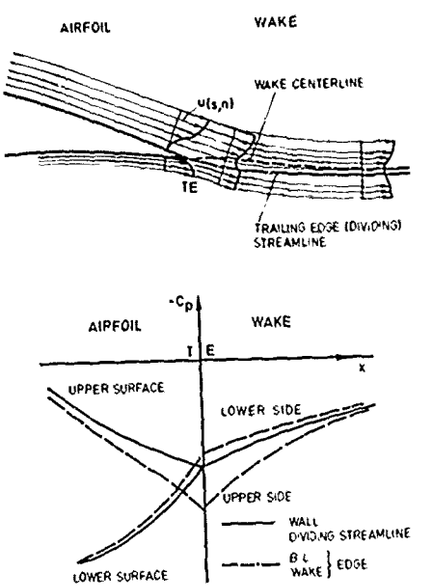

FIG. 42 Trailing edge flow

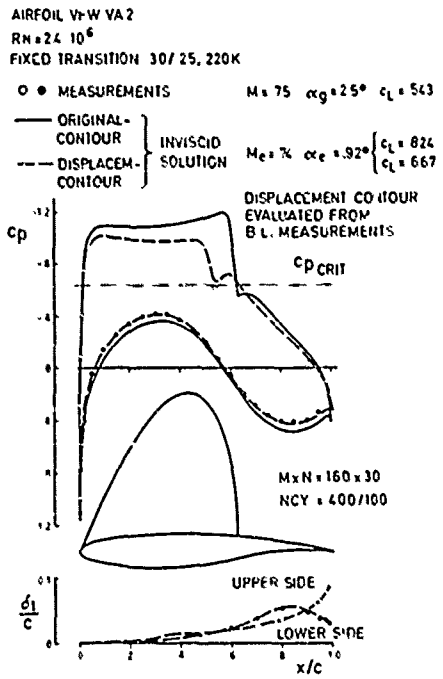

FIG. 43 Comparison of the boundary layer displacement concept with measurement

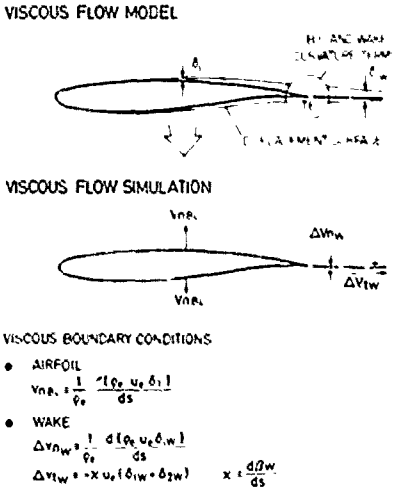

FIG 44 Simulation of viscous effects for airfoil flows by surface mass flow concept

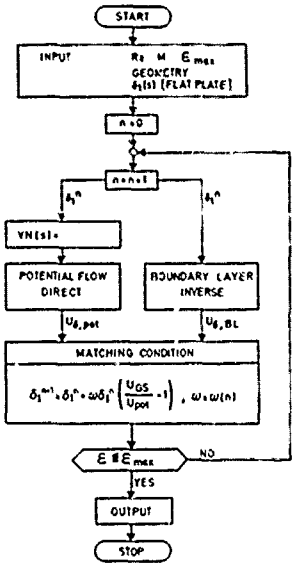

FIG 45 Semi-inverse matching procedure

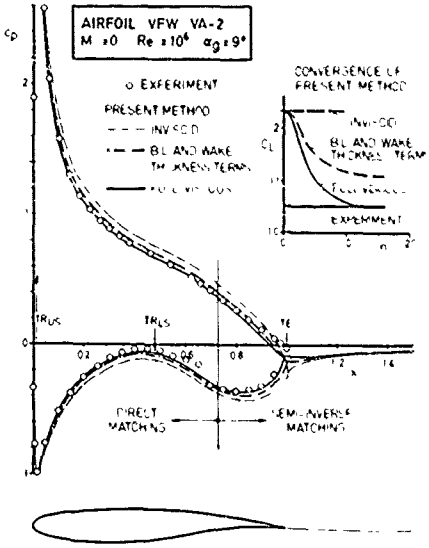

FIG 46 Viscous/inviscid flow prediction over a rear-loaded airfoil

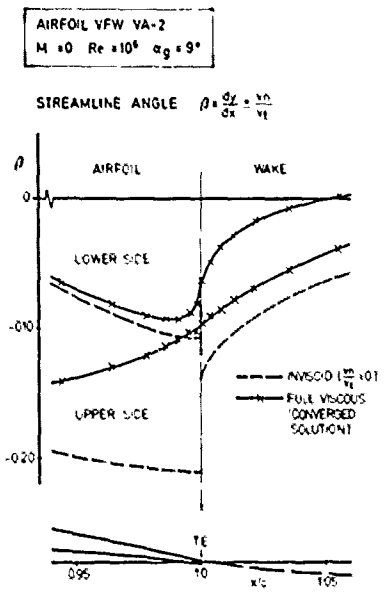

FIG.47 Predicted streamline slope in the trailing edge region of a rear-loaded airfoil

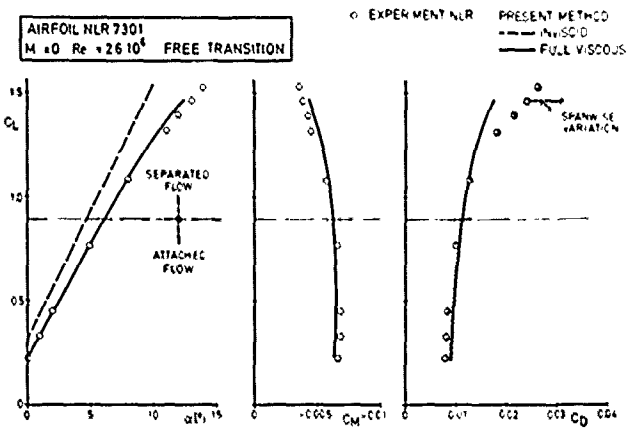

FIG. 48 Lift, moment and drag prediction of a rear-loaded airfoil

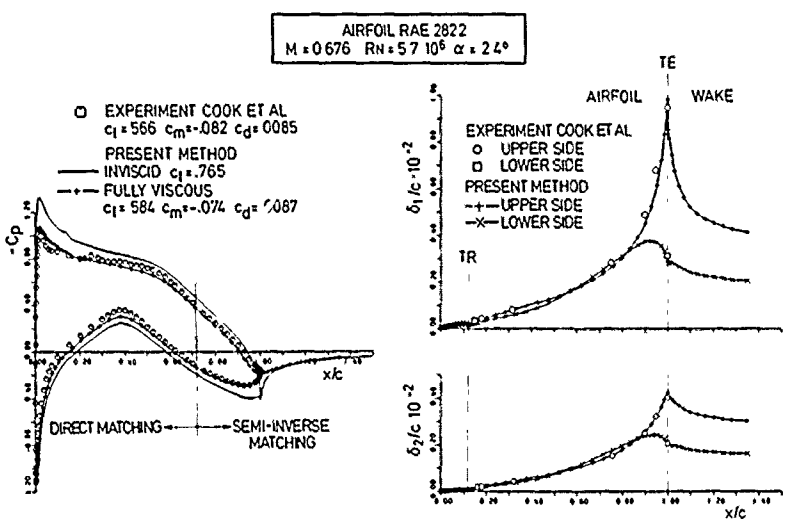

FIG.49 Viscous/inviscid flow prediction over a rear-loaded airfoil

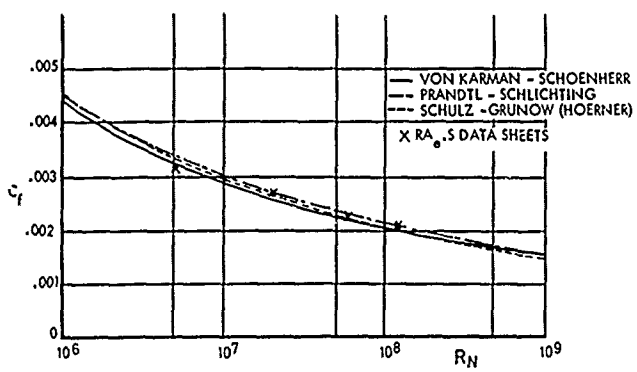

FIG. 50 Flat plate skin friction - fully turbulent -

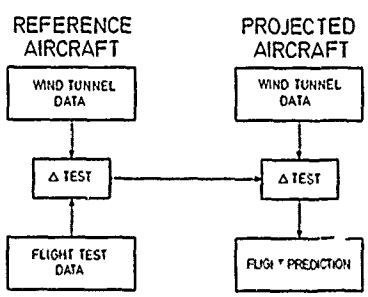

FIG. 51 Reference scaling method

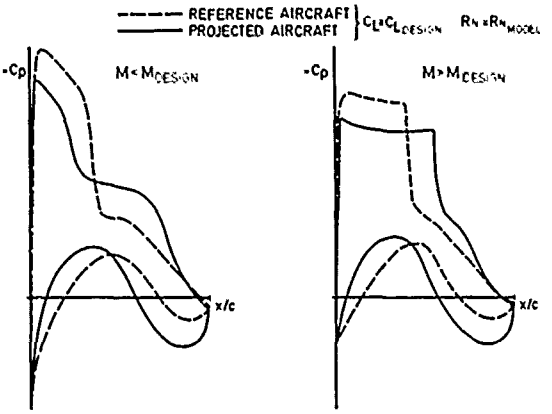

FIG.52 Representative wing section pressure distribution below and above design Mach number

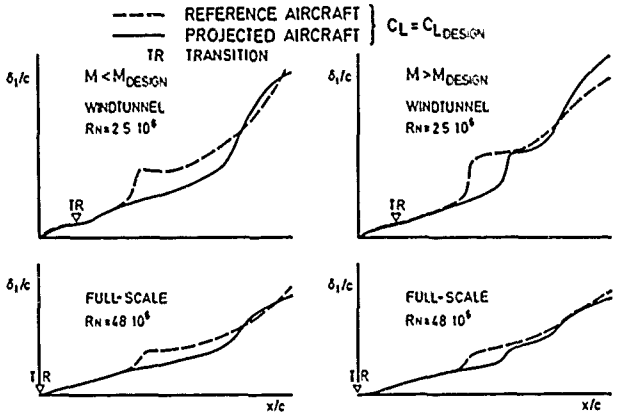

FIG. 53 Representative boundary layer displacement thickness on upper wing surface

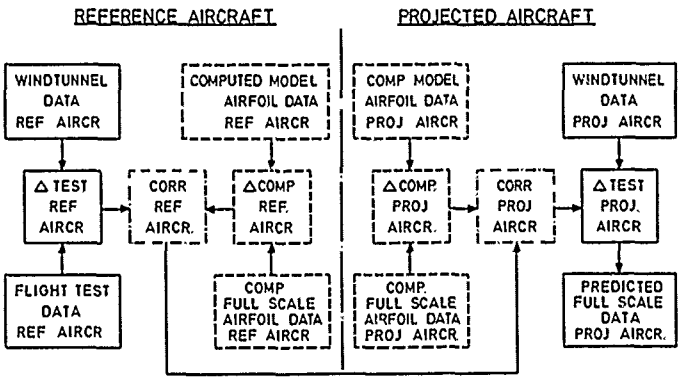

FIG. 54 Higher order reference method

Transonic Configuration Design (Fighter)

by: Mr. D. E. Shaw

Assistant Chief Aerodynamicist
British Aerospace PLC
Aircraft Group
Warton Division
Warton Aerodrome
Preston Lancashire PR4 1AX

SUMMARY

The lecture covers the current design procedures with special reference to aerodynamic interference and the associated use of computational fluid dynamics. It also gives a number of illustrations of various interference phenomena that play a major part in the optimisation of a new design

Specifically, the examples which will be given are:

* The detailed effects of twin fins versus single fin
* Flap/Taileron effects on laterals
* Wing/Store - will be touched on, though Mr. Haines' lecture will cover this point in much more detail
* Effects of vortices
* Wind Tunnel effects with vortices included.

INTRODUCTION

To start with, I will attempt to cover in general terms the task which faces the aerodynamic designer when establishing a new fighter aircraft design. I will also illustrate the use of at least some of the recently developed computational fluid mechanic methods and suggest how they have influenced current design philosophies.

Finally, I will show specific examples of aerodynamic interference which could play a major part in configuration optimisation.

Most of this lecture will attempt to follow the defined scope of the Lecture Series, that is subsonic/transonic aerodynamics. However a lecture which is aimed at a description of Fighter Design would be incomplete without reference to Mach numbers where the flow is (almost) everywhere supersonic.

TOTAL DESIGN TASK

The Aerodynamic Design task is to work as part of a multi discipline team covering all aspects of aeronautical engineering but perhaps more specifically with the engine manufacturers and the structural engineers. The former aspect (which covers engine - aircraft integration including intake, duct and nozzle design) will be discussed later in the series.

The total design task is to design a vehicle which meets specific requirements. Possibly the most important are (Fig. 1):

* SAFETY - even with combat aircraft - which constrains aerodynamics through handling requirements, e.g. if fin/rudder is sized for cross-wind landing, and structural requirements: an example of this is the rear fuselage frame which the aerodynamicist would prefer as thin as possible to ease afterbody boattailing requirements; in fact the frame may need to be very thick to take fin and/or tailplane mounting loads.
* PERFORMANCE - aimed at establishing optimum relative to the requirements.
* COST, which has to include development, production and in service.
* AVAILABILITY which leads to specific design and production timescales which can easily interfere with obtaining optimum in other areas.
* MAINTAINABILITY which can dictate other than aerodynamically optimum positions for equipment, and
* RELIABILITY: which again could dictate other than aerodynamically optimum equipment and systems.

Let us consider two of these aspects in more detail. First safety - obviously vital. Here there are 4 interconnecting aspects (Fig. 2):

- Vehicle stability and control must be acceptable
- Structural strength must be adequate
- Aeroelastic characteristics, that is static stiffness must be acceptable
- Flutter free, that is structural dynamics must be stable.

All these criteria must be satisfied throughout the total required flight envelope.

Performance however warrants a more detailed study.

Performance parameters result from a blend of aircraft requirements and weapon load carrying capabilities within a required flight envelope of speed and altitude. The simplest approach is to regard these as various mission range and agility requirements. These in turn can be further simplified into (Fig. 3):

- Cruise Range: Airmile per lb of fuel used
- Specific excess power or the ability to accelerate or climb
- Manoeuvrability or the ability to turn without losing speed (sustained turn rate) or allowing a transient drop of speed (attained turn rate), and also
- Field Performance - take off and landing distances - note military aircraft in general have very high T/W ratios though coupled with relatively high wing loadings - as a result, meeting T/O requirements is normally much easier than meeting landing requirements.

These would be specified at various critical points within the flight envelope for the aircraft carrying specific weapon loads. These points, along with total list of weapons which the aircraft has to carry and any specific manoeuvre requirements, allow the design to settle down to a fixed initial freeze.

The objective of designing a configuration so that a number of (frequently conflicting) design points are met requires a careful selection of the design parameters involved. Take the wing for example. Here is shown the very basic steps in wing design (Fig. 4) - these will be dealt with in slightly more detail later. First we have to examine requirements in detail:

* Is the A/C to be supersonic as well as subsonic
* What is the mix of low/high altitude flying
* What about manoeuvrability - is the aircraft to be a bomb truck or a fighter - though note that the tendency is to go for a high performance in all areas though biassed to a primary role
* Special requirements - short field or V/STOL

Having examined these requirements the basic design can begin to take shape:

- First the wing loading and hence area coupled with span loading and hence span and aspect ratio.
- Fixed or variable sweep - variable sweep offers a lot of aerodynamic advantages for a multi-role A/C, Example is Tornado shown here with wings forward for low speed manoeuvrability (Fig. 5).
- Taper ratio must be selected.
- Would any overall benefit be obtained from strakes or LE?
- Need to define sections to meet the required wing performance including:

  * Thickness to chord
  * Twist
  * Camber

  Do we need to use camber changing , that is high lift, devices on the L.E.:

  * Slat
  * Droop - Plain L.E Flap
    - Varicam

On the trailing edge:

Flaps:

- Plain
- Varicam
- Fowler
- Slotted
- Special (split etc)

Also, need to consider controls:

- Ailerons and flaps
- Flaperons
- Spoilers
- Special (rotating wing tips, spoilered slat etc).

Finally, there is aeroelastic tailoring increasing the options open to the Aerodynamic designer as he seeks for a wing design which will meet all the various specific requirements within the required flight envelope. This leads to the expression "envelope design" as opposed to the "point design" where the wing shape is optimised for what is seen as the most critical design point within the envelope. A good example of this latter philosophy is a transport aircraft aimed at a narrow band of potential cruise speeds and altitudes. But let us consider wing design in much more detail. Fig. 6 shows a typical set of design points covering the flight envelope required. In particular: point A represents a sustained manoeuvre point; point B a low level 'dash' point; point C a high altitude cruise and point D the landing and/or take-off requirement. Fig. 7 shows a simplistic design procedure which must be applied to all the critical 'corner points' of the envelope until a balanced design is obtained giving the best compromise between the various critical features.

At each point we get design point geometry and loading - calculate the aeroelastic effects on twist and camber - note that we can in fact design into the wing desirable aeroelastic effects to some extent - and identify the 0g wing shape. This is then productionised involving some change in shape - this needs to be shown to be satisfactory - if not the design has to be looped back until an acceptable design is obtained.

With respect to this looping the wing geometry must be simplified as much as possible to ease manufacture and hence reduce build costs. Fig. 8A illustrates this latter point at different spanwise positions by identifying the pressure distribution at a key design point with no constraints on curvature of skin surfaces etc. Compared with this is the pressure distribution for an equivalent wing with three control stations and the surfaces between these control stations generated by straight lines. Fig. 8B shows the final comparison between this latter wing and an even simpler wing where the surface has only two control stations. Considerable debate often occurs amongst aerodynamicists about the importance of establishing the required geometry with its very complex variation of twist and camber. Frequently it is claimed that it is essential . This is probably true for point designs. It may be true for envelope designs but in this case it was not. The small differences in performance which could be evaluated from the differences in pressure distribution were not sufficient to force the project designer to the complex shape. Subsequent wind tunnel testing also showed the performance differences to be small and indeed some of the differences at "off design" points made the performance better.

Now let us consider again the aeroelastic distortion which plays an important part in both performance estimation and in the overall design. For a swept back wing, the natural tendency as the wing bends upwards under load is for the local incidence to decrease at the tip (or wash out) and this is a favourable effect. Long before aeroelastic tailoring became a fashionable design feature, many conventional metal structure wings must have exhibited a marked amount of this phenomena. Simple calculations based on bending beam theory and lifting surface theory shows (Fig. 9) that a reasonable match is possible for wings with leading edge sweeps of approximately 40° if taper is suitably selected, i.e. about 0.35. Aeroelastic tailoring (Fig. 10) by using (say) composite materials gives a further degree of freedom in that the wing twist caused by loading can be amplified or attenuated to give the right amount for the selected planform. However care must be exercised such that the high altitude cruise point (which will only have the built in (or jig) twist plus the twist due to 1g and yet be at high C_L) is not compromisd by defining the jig twist at too low a value.

Finally, consider design camber. Fig. 11 shows the pressure distribution used as an objective for the sustained manoeuvre point. In this position it also shows the resultant type of pressure distribution and the pronounced reduction in drag rise Mach number which occurs at low lift. Obviously if a reasonable Mach number is required for the low level dash, some form of device to modify the pressure distribution is required. This could take the form of simple leading edge and trailing edge hinged flaps or (Fig. 12) sophisticated devices which give smooth variations of camber across the wing span, i.e. VARICAM.

For further details on wing design attention is drawn to Ref. 1.

If we leave the wing here and return to the overall design process - everything, and SAFETY and PERFORMANCE in particular, is affected by interference and it seems almost axiomatic that the next basic layout selected will be more prone to potential problems which - if not identified and allowed for at any early stage of the configuration selection - could cause serious problems to the aicraft development.

I hope some of the illustrations used later in the paper will give ample evidence of some of the phenomena.

However, the description of the aerodynamic designers task implies two types of "Aerodynamic Interference". There is the aerodynamic interference of part of the airframe on another and the mutual interference of the various conflicting requirements of one design parameter on another. For example (Fig. 1):

Basic Performance v Cost

Weapon System Performance v Airframe Performance

Fuel Volume v Supersonic Drag

Technical Sophistication v Short Time Scale

The remainder of this lecture will be restricted to the former "aerodynamic interference" even though both are equally interesting and some may regard the latter, i.e. the mutual interference of various conflicting requirements, as more important.

As previous papers have indicated, over recent years the advances in computational fluid mechanics have had a considerable effect on design procedures. I would therefore like to set the scene from the point of view of a design aerodynamicist.

Until the advent of modern computational methods the only reliable way of establishing most interference effects was to tunnel test. This was an expensive and time consuming activity, and is increasingly so. Nevertheless until the full range of fluid dynamic phenomena have been modelled on the computer, and these models evaluated, the aerodynamic designer will still have to depend to a very large extent on wind tunnel test techniques. However, theoretical fluid dynamics has always played an important part in predicting and/or explaining some intereference phenomena and it will always be the Aerodynamicists' task to use the most effective combination of experience, theory (computational fluid dynamics) and experimental data obtained by wind tunnel testing to arrive at efficient trouble free designs.

Whilst discussing Computational Fluid Dynamics, I would like to use as a starting point what I still regard as a very important AGARD Conference held in 1970 at the U.S. Naval Ordnance Laboratory, Silver Spring, Maryland (Refs. 2 and 3).

I left this conference with four major predictions foremost in my mind:-

- Subsonic panel programs were here to stay and would be joined by practical supersonic method (using linearised flow approximations). These would be regarded as standard methods by industry within a very few years.

- Experimental techniques including water tunnel tests are and will remain invaluable for a long time yet.

- Transonic methods for other than simple shapes would not be available for a considerable time.

- With the amount of interest and effort concentrated on viscous flows in three dimensions and including separation, industry should have design and prediction methods within 5 to 6 years.

Looking at the methods that are available to us as aerodynamic designers - firstly subsonic:

The subsonic panel programmes pioneered by A.M.O. Smith and J. Hess at Douglas and subsequently developed by P. E. Rubbert and G. R. Saaris at Boeing and also W. Loeve and J. W. Slooff at NLR received considerable attention at many design and research centres. Subsequent work was also carried out by of our partner company in the Tornado programme at MBB by W. Kraus and others and also at B.Ae. Brough by J. Petrie and also B.Ae. Weybridge by A. Roberts.

We at Warton are in debt to all this work which helped us set up and sustain a significant and dedicated effort over a period of some ten years aimed at establishing easy to use, accurate and cost effective methods. These methods are now used for a wide range of applications associated with subsonic (subcritical) flow where the boundary layer is essentially attached but where the so called Kutta-Joukowski condition is included on most relevant sharp edges or indeed on smooth surfaces along prescribed 'separation' lines (Refs. 4, 5, 6 and 7).

Work at Warton is now aimed at extending the range of applications and on the associated evaluation. Two examples of applications are wind tunnel wall constraint effects (ref. 8) and airframe - store interference (ref. 9).

Turning to the international scene. Although an initial attempt to compare results from what were then (in the mid 70's) the most commonly used methods was sponsored by AGARD and completed (Ref. 10), the test cases were relatively simple and did not even include a wing-body. This is frustrating in the light of D. J. Peakes' main recommendation, and I quote (this already alluded to in a previous lecture) "If there was one recommendation, it was to the effect that a calibration model of a wing-body combination be chosen, against which to check the various computation schemes available" (Ref. 3).

Turning now to the state of the art of the linearised supersonic flow models. Considerable developments have taken place. F. A. Woodward's work is well known in Europe and many firms are familiar with his methods. We are all very much in debt to this pioneering work and many programmes currently in use are direct developments. For example B.Ae. Warton still use one of his later programs with only limited development and linked with the structural stiffness model for early project aeroelastic evaluations. However, as with the subsonic methodology, many organisations have developed second or third generation methods to replace Woodward's original work. Warton is no exception and I hope we will have the opportunity of presenting our new developments to an international audience in the near future (Reference 11).

To summarise - BAe and, I assume, most other companies not only have both subsonic and supersonic "panel" methods but use them as standard every day design and prediction tools.

Turning to the transonic theoretical methods. The situation is reviewed in Ref. 13 and is much further advanced than I thought possible in 1970. The computer programs developed by such workers as Charles Boppe in the States (Ref. 14) and Clive Albone in the U.K. (Ref. 15) using the small perturbation equations which approximate the shape and the flow to an accuracy which gives very useful results for quite complex shapes has already given significant improvements in design capabilities. The more accurate representation of the shape offered by full potential flow solutions of Tony Jameson in the States (Ref. 16) and Malcolm Carr of ARA (Ref. 17) are as yet limited to wing body combinations. These, along with the possibility of usable Euler solutions with the associated advantage of proper shock modelling, indicate that, even in the transonic regime, computational fluid mechanics should assist in the art of design and prediction.

However all is not solved yet - by a long way taking the more pessimistic view of what has been said in the previous lectures - the more major outstanding items are boundary layer and separated flow prediction methods. I accept there are three dimensional boundary layer methods available. However I suspect we have not got things right at the trailing edge - or indeed any edge with separation. In addition have we got a reliable method to cope with junction flow? From the previous papers it would appear not. Obviously more attention is required to produce methods to deal with these regions.

Moving on to experimental techniques. Looking back to the hopes of ten and more years ago, it now seems that, for all the theoretical method development that has occurred, the configurations we are now creating are of such a type that the gap between what theory can model and what the aerodynamic designer is interested in is actually greater. it is certainly true that we seem to spend more time testing in the water tunnel or using flow visualisation techniques in the air tunnels now than we did ten years ago. D. Küchemann would possibly approve. He was only half joking when he suggested that perhaps a water tunnel should be delivered with every large computer "so that a reliable physical flow model could be developed on which to finally base a computer program" (Ref. 3).

Even if the gap closes - we will remain very dependent on wind tunnels to allow us to do just what Küchemann proposed. It seems even more relevant when one hears the problems associated with Navier Stokes solutions and Turbulence Modelling etc. (reference 12). Obviously the need to establish a "reliable physical flow model" before a mathematical model can be developed is self evident.

To summarise:

We continue to depend on Wind Tunnel facilities for a large range of design and prediction tasks. However the computational fluid mechanic methods are now so powerful that (for at least the situation of attached flow) we can undertake a considerable part of the design procedure and many production tasks on the computer in a very much shorter time scale than was possible (say) 13 years ago in 1970. These advances in inviscid modelling would be considerably enhanced if the three dimensional viscous effects could be coupled in: this is an important point as many interference phenomena are caused by viscous effects.

These developments of inviscid computational fluid mechanics have allowed advances in design where range and/or manoeuvrability have been improved considerably by judicious use of the methods available and by careful selection of target pressure distributions at various points of the flight envelope (see for example Ref. 1).

However the methods have allowed a more scientific approach to be used for many phenomena complicated by interference effects.

The remainder of the paper will illustrate this point with a number of examples. The first of these will be concerning the choice between twin fins and single fins. This dilemma has been on our minds significantly at Warton recently and I would like to show you some of the results of the investigations.

The basic phenomena have been known for a number of years. Indeed there are NACA reports by Nielsen at al written in the mid to late 50's which used the basic approach still given in DATCOM. (See for example Ref. 18). With the advent of the supersonic panel program it is now possible to estimate quickly and cheaply the tailplane to fin interference or, in the case of twin fins, the mutual interference. Both theory and experiment show that the mutual interference has a significant effect on fin efficiency giving a marked reduction at low supersonic Mach numbers (Fig. 14). It is not unusual for fins to be sized at the aircraft maximum Mach number - this is generally where the fin contribution to directional stability and as a result, total aircraft directional stability are a minimum. With twin fins this may not be the case and the total supersonic range must be checked - including the effects of aeroelastics.

One important aspect which is not adequately covered by either subsonic or supersonic theory is the effect of front fuselage configuration and canopy layout in particular. High canopies are required for modern fighter designs to give good all round pilot view. The increased fin contribution to offset the increased instability introduced by the canopy height is relatively easy to estimate (Fig. 15). What is difficult to estimate is the effect of the canopy on fin effectiveness. For a modern fighter canopy the effect could be negligible at subsonic speeds for both single and twin fins and ma y vary from small to up to 10% for twin fins and 15% for single fins across the supersonic speed range (Fig. 16). In addition incidence effects which have vortical flow and/or separations etc are not amenable to calculation.

Fig. 17 shows directional stability as a function of incidence at M = 1.4 and 2.0. clearly showing that both single and twin configurations are adversely affected, the single more so than the twin.

The selection of fin configuration is not of course limited to consideration of supersonics - low speed rudder and fin effectiveness especially over the high incidence range must also be considered. Fig. 18 shows at the top a comparison of rudder effectiveness for the single and twin fins highlighting the marked reduction for twin fins as incidence increases to higher values whereas the rudder on the single fin maintains its effectiveness throughout.

The lower figure compares single and twin fin effectiveness as a function of incidence. Here it can be seen that at low incidence the single fin is slightly better - at high incidence however we get a cross-over such that the twin fin is now better though still at a very low value.

The loss at high incidence for the single fin can be explained by examination of the effects of vortices generated upstream for instance by strakes or highly swept foreplanes.

Fig. 19 shows the effect of the high incidence assymetric vortex pattern to be a destabilising pressure field giving the reduction in C_n for the single relative to the twin.

But there is a further effect - this time on performance - due to the effect of the vortices on the twin fin configuration. If we examine the lower part of Fig. 19 we can see that the vortex gives a suction on the "lower side" of the outwardly inclined fins coupled with an increased pressure between the fins - the result, as can be seen from the graph, is a significant reduction in $C_{L_{max}}$ of about 10%. This phenomenon was studied in some depth at Warton using: existing computational methods; water tunnel testing in the small Warton facility (for an excellent paper reviewing water tunnel techniques etc. I recommend M. Werle paper which describes work undertaken at ONERA in a similar facility see reference 20); and also using pressure plot results and smoke flow visualisation in the Warton 18' L.S.T. A fundamental understanding was obtained - but only by a good deal of detective work and by cross checking experimental and theoretical evidence.

Thus it can be seen that the selection of the fin configuration requires considerable work before an optimum selection can be made. Computational fluid mechanics assist in selecting cant and toe angle as well as planform if twin fins are shown to offer an advantage over a single fin configuration. The basic lesson is - there is no evidence to support a simplistic conclusion that one fin is right (or wrong) whereas twin fins are wrong (or right). It is equally evident that fashion should not prejudice the designers choice. This, as will be seen, is true of almost all aspects illustrated.

To continue however:

Roll Control:

The strong supersonic aerodynamic interference discussed earlier is evident in many phenomena. I will restrict this paper to one other example.

When supersonic roll control is obtained from either inboard ailerons or flaps or from moving the total surfaces (eg. differential tailplane) then the pressure field generated impinges on adjacent vertical surfaces (eg. fins or the side of the fuselage) (Fig. 20).

The results of this for a specific example taken from the same configuration as the previous case with twin fins and inboard ailerons that are almost inline with these fins shows that the inteference mechanism produces a reduction in the rolling power (Fig. 21) along with an associated (proverse) yawing moment (Fig.22).

Wave Drag:

As an aside these supersonic interference effects are very important when optimising for supersonic drag. The well known (far field methods) which use equivalent axisymetric bodies (e.g. supersonic area rule) are not capable of allowing for the interference effects in anything like a rigorous manner. How could they as the local details of the geometry and their associated local pressure distributions and the resultant interference are not modelled. For complex shapes where the interferences are equally complex the total interference predicted by the far field methods can be of the wrong sign. This situation again emphasises the importance of the supersonic panel programs. Although even these have to be used with caution due to the use of the linearised flow approximations.

Subsonic Interference:

To return to subsonic flow. The interference effects that can occur are many and varied. Obviously there is no direct equivalent to the strong interference effects that can appear at supersonic speeds where there is little attenuation of the pressure jump through a shock with distance from its source. In subsonic flow the effect of a pressure perturbation decays at something like the inverse square of the distance BUT (at least for incompressible flow) - the pressure spreads in all directions. Hence the aerodynamic interference between two bodies or lifting surfaces is always mutual, whilst for supersonics the interference is limited to within the down stream Mach cone.

Nevertheless the interference effects can be appreciable. Consider a store mounted under a wing (Fig. 23), the case illustrated being reasonably typical. Fig.24 compares the experimental and theoretical chordwise pressure increments due to the pylon and store over the lower surface at spanwise stations inboard and outboard of the pylon (via a first generation panel programme with lift modelled by vortex lattice). Fig.25 gives the same data but this time plotted against spanwise position at 13% and 40% chordwise position.

Over the last few years the modelling of this type of phenomena has been extended to the high subsonic flow regime where strong shocks occur. Although there are a number of workers in this particular area I would like to mention in particular Clive Albone of the RAE and Charles Boppe of Grumman as I am familiar with their work. We are indebted to Grumman & RAE for supplying the theoretical results and ARA the experimental results illustrated in the next example (Fig.26) in Fig.27 where a comparison of theory v experiment , on selected wing pressures store "on and off", is given.

The planform of the wing, store spanwise position and store approximate configuration relative to the wing are shown here. It can be seen (Fig.27) that the characteristics are everywhere as expected and similar to the subcritical results shown previously except where the regions of high suctions are not terminated by normal shocks. Note that the methods used here are the TSP type methods. It is possible that use of a modified full potential theory could give a better representation of the effects. Results for a subcritical case of the same geometry for which the Albone/Boppe calcs were made from a code under development at ARA by Mr. C. Forsey shows very good agreement with expt. and this would give rise to some optimism in this respect.

Moving on to store release.

Consider the arrangement of bombs mounted on a twin carrier underwing (Fig.28). The requirement is to predict the trajectory of the inboard store following release, with and without the outboard one being present.

Using the subsonic panel methods can give very good results as shown in Fig. 29, showing the normal force on a store as it moves away from its installed position. The store trajectory is simplistic in that (relative to its installed position) the store fore and aft, lateral and angular position remain constant. It can be seen that as the store moves further away, the lift approaches a constant value - equivalent to that corresponding to the store in free air. In the installed position the lift is considerably greater.

Where does this increase in lift in the installed position come from? First, wind tunnel tests (at the ARA) were undertaken to establish the local flow conditions in the volume swept by the store, but excluding the store (Fig. 28). From this data, the force on the store due to this flow field was predicted. Second, the primary effect missed by this procedure was judged to be the mutual interference between the store and the wing. We assumed that for the store this could be represented by considering the wing as an infinite reflection plane. The mutual interference of the store and its image was predicted and added to the first contribution. Agreement was better than expected (not only for lift but pitching moment as well) for both the very difficult case with the outboard bomb present (Fig. 30) as well as for the single store case. This investigation not only lead to a better understanding of the phenomena but also to a very simple and easy to apply improvement to a method used by many organisations which essentially only included the first step in the procedure described.

One interesting point to notice is that the full panel method results show good agreement for the single store lift even in the installed position. This is not the case for the twin stores which are mounted very close together. This illustrates that mutual interference effects can often be predicted using inviscid (and in this case shock free) flow models but if the configuration is such that strong viscous effects or shocks occur obviously inviscid theory will only illustrate part of the situation. It is still hoped that the time will come when these viscous effects can be modelled within a method which can be used by industry on a day to day basis.

Flutter:

Before leaving store related interference effects I would like to make brief reference to an important development made by NLR now almost 10 years ago. This is the development of an 'unsteady' aerodynamic subsonic panel programme which is capable of modelling wing store combinations (Fig.31) (see Refs. 21 and 22).

The configuration is for a tip mounted missile. Fig.31 shows the importance of including the missile aerodynamics and the associated missile wing mutual interference as well as the inertia effects: the more realistic aerodynamic model predicts a 30% reduction in the flutter speed compared with the prediction where the aerodynamics are modelled for the wing alone .

Vortex flow.

Possibly the type of subsonic aerodynamic interference which influences the design of modern combat and fighter aircraft is that associated with vortex flow. Unlike the mutual interference effects discussed above there is a strong down-stream influence. One example has already been used in the discussion on fin configuration choice where the effect on the fin or fins of the vortex system which is usually created on fighter aircraft was described.

The next examples give more details of this type of interference.

After developing the vortex flow methods it was considered essential to compare theory with experiment for a simple configuration. This was done by pressure plotting a body and then a wing body combination in a tunnel (Warton 9' x 7' low speed tunnel) on their own and in the presence of an externally created vortex of known (measured) strength and position. Differencing the results then would give the effect of the vortex on the body (or wing body).

Fig.32 shows the configuration used for these tests.

The body only is shown - the main wing (with 25° leading edge sweep) is omitted for clarity. Note the auxiliary wing used to generate a vortex of known strength. An illustration of the change in pressure coefficient measured on the body is shown in Fig. 33. The externally generated vortex strength was typical of the strengths of vortices created on modern fighter aircraft from say front fuselage separation, side mounted intakes or foreplanes. The pressure changes are not insignificant. On a more realistic body shape (for a fighter aircraft) these changes could (and often do) change the characteristics significantly from acceptable to unacceptable or indeed the reverse.

The pressure increments on the wing are also very significant near the vortex but fade out rapidly away from the vortex (Fig. 34). This simplistic statement needs some qualification. The velocity perturbation follows an inverse square law against distance and this is clearly seen at the outboard station (3). However at the inboard station (1) the situation is complex. It can be argued that the fuselage acts as a partial reflection plane constraining and modifying both the basic flow and the effects of the vortex. Thus, stations inboard of the vortex and hence nearer the fuselage are by implication nearer the vortex image. Thus the interference effects can be amplified between the vortex and fuselage side. Again this can lead to favourable and unfavourable effects and will largely depend on the state of the boundary layer in the wing fuselage junction as well as the free stream Mach number.

Also note that the change in pressure distribution on the wing has a centre of pressure forward of that due to incidence - thus the assumption that the upwash/downwash can be regarded as a change in effective twist along the wing is only an approximation. This can have serious implications to the formation of the wing root shock system where the vortex system from (say) a foreplane can unload the root such that the shock system is much weaker.

Whilst investigating vortex phenomena and their associated interference effects, it is worth considering the problems associated with the tools of the trade: firstly wind tunnels and especially the effects of wall constraints. The schematic of the model used to investigate these effects - showing the vortex paths and tunnel walls - is shown in Fig.35. Fig.36 shows the tunnel wall has a significant effect on the lift but not on the lift induced by the vortex. However this should not be taken as evidence that there are NO problems. Two additional phenomena complicate the situation.

1. The vortex path is constrained by the tunnel walls so that the natural downward drift for a lifting vortex system is inhibited and,

2. The vortex is of the wrong strength when the tunnel walls are present due to the classical wall constraint which increases the lift on a surface at a given incidence.

These facts would seem to give some doubt with regard to wind tunnel data on measured stability and control characteristics of, for instance, the foreplane of a canard configuration.

Theory can help sort out this problem, but only if care is used. Take the following illustration (Fig. 37).

The model in this case is a cranked delta canard configuration.

The results of theoretical predictions (Fig. 38) show the predicted spanwise loading and illustrates the improvement obtained for relaxing the vortex path. In fact four models of the foreplane wake were used (Fig. 39):

1. Full wake allowed to take its own predicted position.

2. Full wake defined with a predetermined (guessed) position.

3. Single trailing vortex of strength and an initial spanwise extent to approximate the same total foreplane lift as above and allowed to take its own predicted position.

4. Single vortex as above but defined with a predetermined (again guessed) position.

If the strength of the equivalent vortex is known and that implies knowing the foreplane lift in the presence of the wing upwash (another interesting interference phenomena that can affect the stress loading cases on foreplane by a significant amount) - then the single vortex with a relaxed path looks very good compared with the nominally exact solution with the relaxed wake. With the predetermined position both the full wake and single vortex models are poor giving misleading resuls.

So now to conclude:

The illustrations shown and examples given have attempted to give some indication of the scope of "aerodynamic interference". Obviously only a very narrow spectrum has been covered. There are many other types of interference than those described and some could be regarded as of primary importance.

For example (Fig. 40):

- separated boundary layer phenomena where control surfaces are "buried" in low energy air and hence lose their effectivness.
- air data sensors used to measure pitot-static pressures, incidence, etc. influenced by spurious effects such as the movement of a nearby control surface or change in engine mass flows.
- distortion of the flow entering the intake by upstream parts of the aircraft.
- the interference effects of fins, tailplanes etc. on the rear fuselage.
- the interference effects of secondary flow outlets for intake boundary bleed systems, and air coolers etc. and for the latter, inlets as well.

The list seems endless. There are few aspects of aerodynamic design where interference effects are not of primary importance. This is especially true of modern fighter aircraft. As avionic systems become more compact and as engine fuel consumption and also thrust/engine size improve the basic airframe becomes smaller and more compact. On the other hand size of stores to carry seem to get bigger as do cockpits with the requirements for all round vision. The result tends to be very compact airframes with the various components very close together. The days of design which were considered as a collection of separate parts are long gone. Now aerodynamic interference is an essential if not the essential design consideration.

REFERENCES

1) D. R. HOLT & B. PROBERT, BAe Warton
Some particular configuration effects on a thin supercritical variable camber wing.
Paper 15 of AGARD F.D. Panel Symposium on Subsonic/Transonic Configuration Aerodynamics.
AGARD CP 285.

2) Aerodynamic Interference
AGARD CP 71-71, September 1970.

3) D. J. PEAKE
Technical evaluation report on AGARD specialist meeting on "Aerodynamic Interference"
AGARD-AR-34-71.

4) B. HUNT, BAe Warton
The panel method for subsonic flows: a survey of mathematical formulations and numerical methods and an outline of the new British Aerospace Scheme.
Von Karman Institute for Fluid Dynamics, Lecture Series 1978-4
(Computational Fluid Dynamics, March 1978).

5) S. A. JEPPS, BAe Warton
The computation of vortex flow by panel methods.
Von Karman Institute for Fluid Dynamics Lecture Series 1978-4
(Computational Fluid Dynamics, March 1978).

6) B. HUNT, BAe Warton
Recent and anticipated advances in the panel method, the key to generalised field calculations.
Von Karman Institute for Fluid Dynamics Lecture Series 1980-5
(Computational Fluid Dynamics, March 1980).
Including an appendix by D. J. Butter (BAe Manchester) on "viscous flow modelling in panel methods".

7) W. G. SEMPLE, BAe Warton
An economic and versatile panel method for aircraft and aircraft/store configurations. An outline of the principal features of the mathematical modelling and numerical implementation of the British Aerospace (Warton) Mk.II panel method.
Von Karman Institute for Fluid Dynamics Lecture Series 1980-5
(Computational Fluid Dynamics, March 1980).

8) B. HUNT and D. R. HOLT, BAe
The use of panel methods for the evaluation of subsonic wall interference.
Paper 2 Wall Interference in Wind Tunnels AGARD Conference 335, May '82.

9a) B. HUNT, BAe Warton
The prediction of external store characteristics by means of the panel method.
BAe Warton Report Ae/372, January 1977.

9b) Airload prediction by C. B. Mathews (Editor), R. Deslandes, R. A. Grow, B. Hunt. F. W. Martin and J. N. Nielson.
Paper 4 "Drag and other aerodynamic effects of external stores" Unclassified paper.
AGARD Advisory Report No. 107 (NATO Restricted), November 1977.

10) H. S. SYTSMA (NLR), B. L. HEWITT (BAe), P E RUBBERT (Boeing)
A comparison of panel methods for subsonic flow computation.
February 1978, AGARD AG 241.

11) W. R. MARCHBANK, J. A. CROWLEY, B. L. HEWITT - BAe Warton
Development of a supersonic panel program at BAe Warton.
Company Confidential report, November 1980.

12) A. B. HAINES
Turbulence Modelling.
Report of a working party edited by the Chairman, A. B. Haines
The Aeronautical Journal of the Royal Aeronautical Society, August/September 1982.

13) M. G. HALL
Advances and shortcomings in the calculation of inviscid flows with shock waves.
Paper presented at the IMA conference on numerical methods in Aeronautical Fluid Dynamics, March and April, Reading.
RAE Tech Memo Aero 1913, October 1981.

14) C. W. BOPPE and M. A. STERN
Simulated transonic flows for aicraft with nacelles, pylons and winglets.
AIAA 80-0130, Pasadena, California, 1980.

15) C. M. ALBONE, M. G. HALL & JOYCE GAYNOR
Numerical solutions for transonic flows past wing-body configurations.
Symposium Transsonicum II, Gottingen
Springer and Verlay (1976)
(and subsequent developments).

16) A. JAMESON
Iterative solution of transonic flows over airfoils and wings, including flows at Mach 1.
Comm. Pure Appl. Math, Vol. 27, 283 - 309 (1974).

17) C. R. FORSEY and M. P. CARR
The calculation of transonic flow over three-dimensional swept wings using the exact potential equation
DGLR Symposium Transonic Configurations, Bad Harzburg (1978).

18) B. R. A. BURNS & K. CARR, BAe Warton
Transonic/Supersonic lateral aerodynamic derivatives
Von Karman Institute for Fluid Dynamics Lecture Series 76-77 No.8
Aerodynamic inputs for problems in aircraft dynamics.

19) B. HUNT, BAe Warton
The role of computational fluid dynamics in high angle-of-attack aerodynamics.
Paper 6, AGARD Lecture Series No. 121
High Angle of Attack Aerodynamics, March 1982.

20) H. WERLE, ONERA
Flow visualisation techniques for the study of high incidence aerodynamics.
Paper 3, AGARD Lecture Series No. 121
High Angle of Attack Aerodynamics
March 1982.

21) R. ROSS, B. BENNEKERS and R. J. ZWAAN (NLR)
A calculation method for unsteady subsonic flow about harmonically oscillating wing-body configurations.
AIAA Paper 75-864.

22) B. BENNEKERS, R. ROSS and R. J. ZWAAN (NLR)
Calculations of aerodynamic loads on oscillating wing/store combinations in subsonic flow.
NLR MP 74028 (1974)
or AGARD-CP-162 Lecture No. 4 (1974).

23) J. FLETCHER
Forward swept wings at British Aerospace, Warton - an overview.
Bristol International Conference on Forward Swept Wing Aircraft
March 1982, To be published.

24) D. E. SHAW
Experimental investigations into forward swept wings.
Bristol International conference on Forward Swept Wing Aircraft
March 1982, To be published.

- SAFETY: CONSTRAINS AERODYNAMICS THROUGH HANDLING REQUIREMENTS, STRUCTURAL REQUIREMENTS.
- PERFORMANCE: AIMED AT ESTABLISHING OPTIMUM, RELATIVE TO REQUIREMENTS.
- COST: INCLUDES DEVELOPMENT, PRODUCTION AND IN-SERVICE.
- AVAILABILITY: LEADING TO SPECIFIC DESIGN AND PRODUCTION TIME-SCALES.
- MAINTAINABILITY: DICTATING OTHER THAN AERODYNAMICALLY OPTIMUM POSITIONS FOR EQUIPMENT
- RELIABILITY: DICTATING OTHER THAN AERODYNAMICALLY OPTIMUM EQUIPMENT.

FIGURE 1. TOTAL DESIGN TASK

- VEHICLE STABILITY AND CONTROL MUST BE ACCEPTABLE
- STRUCTURAL STRENGTH MUST BE ADEQUATE
- AEROELASTIC CHARACTERISTICS - THAT IS, STATIC DEFLECTIONS - MUST BE ACCEPTABLE
- FLUTTER FREE - THAT IS, STRUCTURAL DYNAMICS MUST BE STABLE

Figure 2 SAFETY REQUIREMENTS

- CRUISE RANGE: AIRMILES PER KILOGRAM OF FUEL
- SPECIFIC EXCESS POWER: ABILITY TO ACCELERATE OR CLIMB
- MANOEUVRABILITY: SUSTAINED TURN RATE: ABILITY TO TURN WITHOUT LOSING SPEED.
  ATTAINED TURN RATE: MAXIMUM ACHIEVABLE TURN RATE, WITH TRANSIENT DROP IN SPEED.
- FIELD PERFORMANCE: TAKE-OFF AND LANDING DISTANCES

Figure 3. BASIC PERFORMANCE REQUIREMENTS

- ANALYSE REQUIREMENTS: SUBSONIC/SUPERSONIC
  LOW ALTITUDE/HIGH ALTITUDE
  MANOEUVRABILITY
- PLANFORM: FIXED OR VARIABLE SWEEP
  HIGH ASPECT RATIO/LOW ASPECT RATIO
- SIZING: AREA
  SPAN
- SECTION: THICKNESS/CHORD RATIO
  CAMBER : F.C.S REQUIREMENTS
  CAMBER CHANGING DEVICES, LEADING EDGE: SLAT
  DROOP: PLAIN
  VARICAM
  TRAILING EDGE: FLAPS : PLAIN
  VARICAM
  FOWLER
  SLOTTED
  SPECIAL
- CONTROLS: AILERONS
  FLAPERONS
  SPOILERS
  SPECIAL

Figure 4. BASIC STEPS IN WING DESIGN

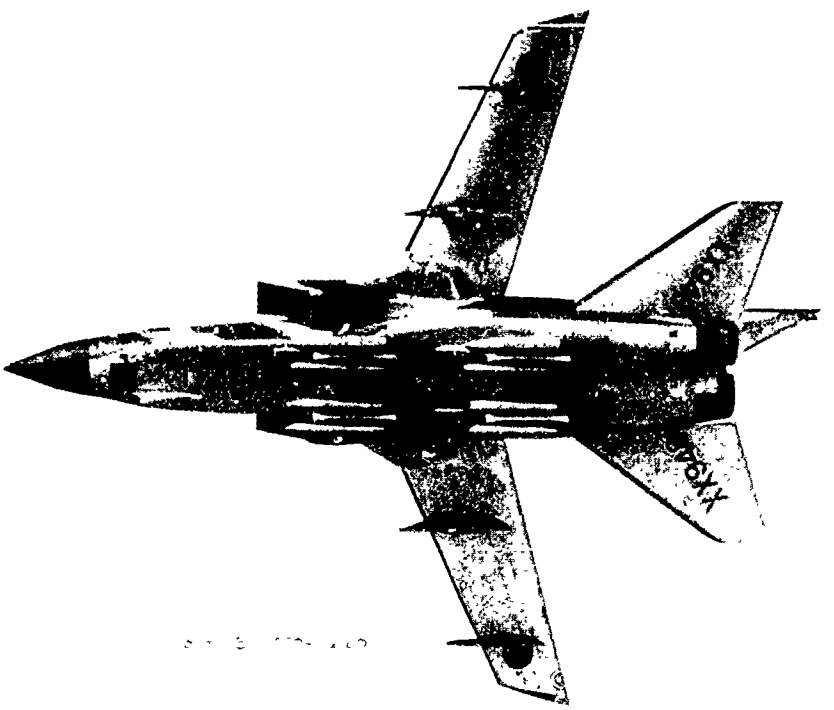

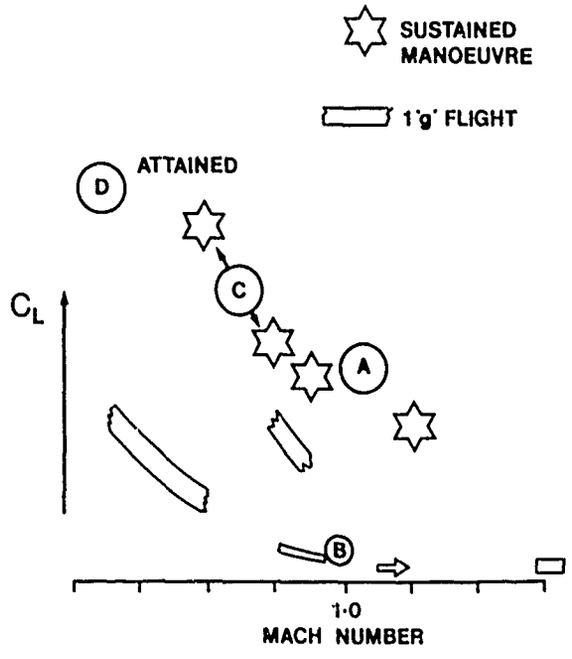

Fig. 6

Typical Design Requirements

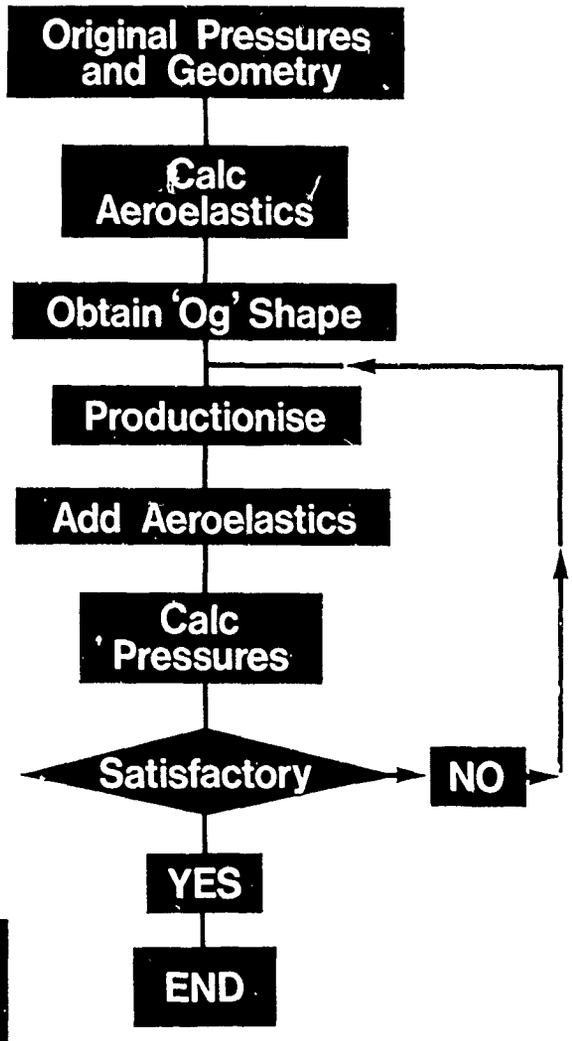

Fig. 7 Design Procedure

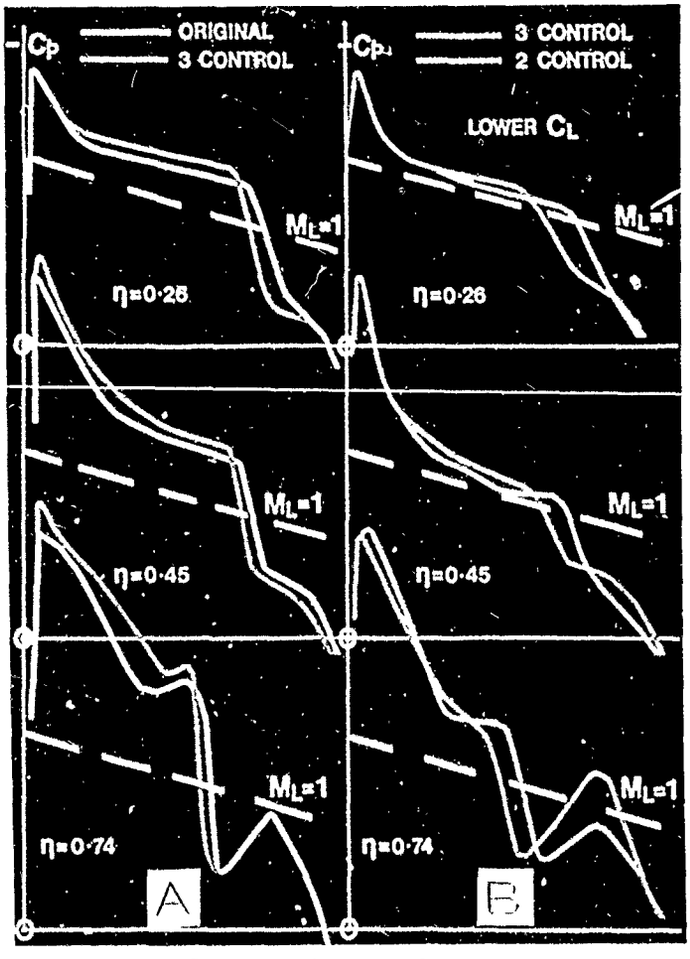

Fig. 8 **Comparison of Pressures**

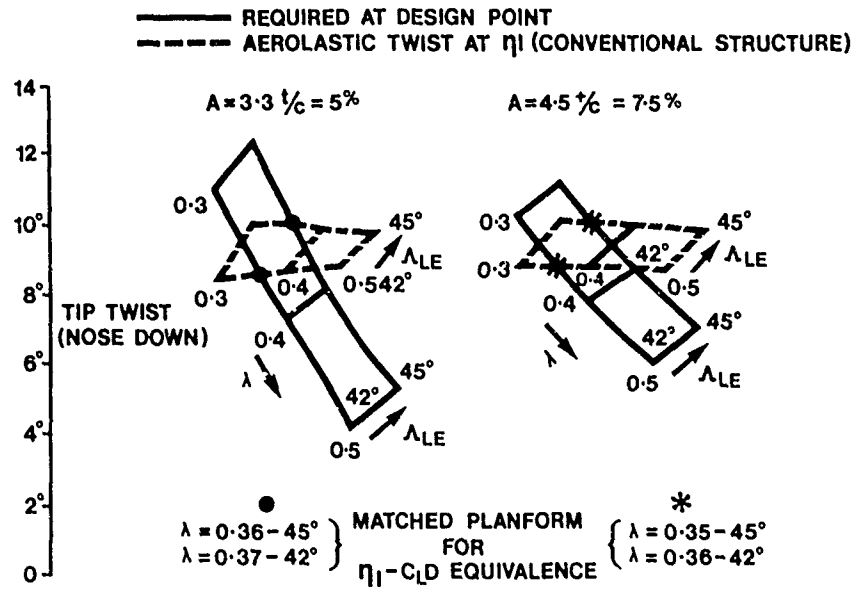

Fig. 9 **Comparison of Required Twist and Aeroelastic Due to Bending**

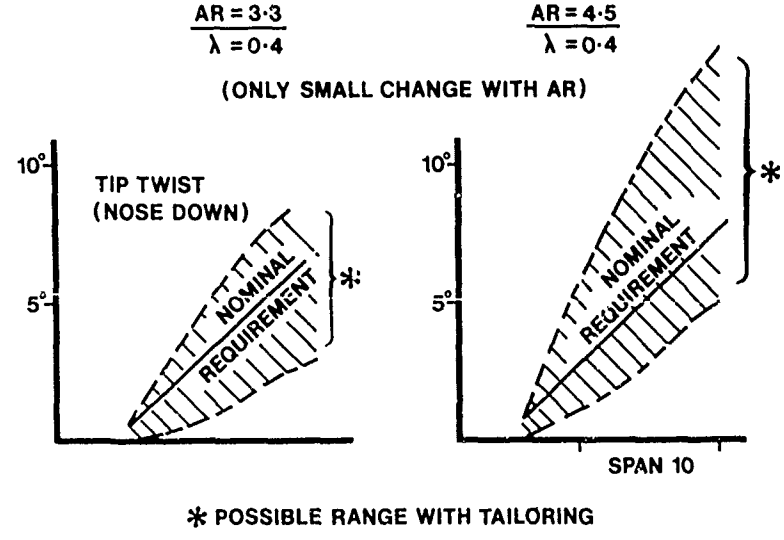

Fig. 10 **Effect of Aspect Ratio on Aerolastic Tailoring Boundaries**

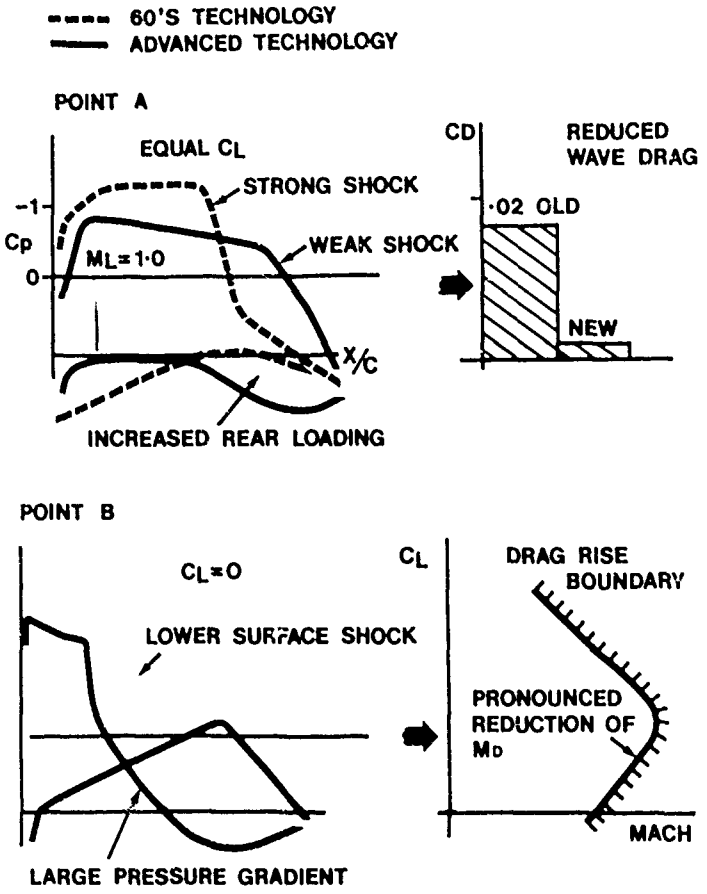

Fig. 11 **Main Flow Features**

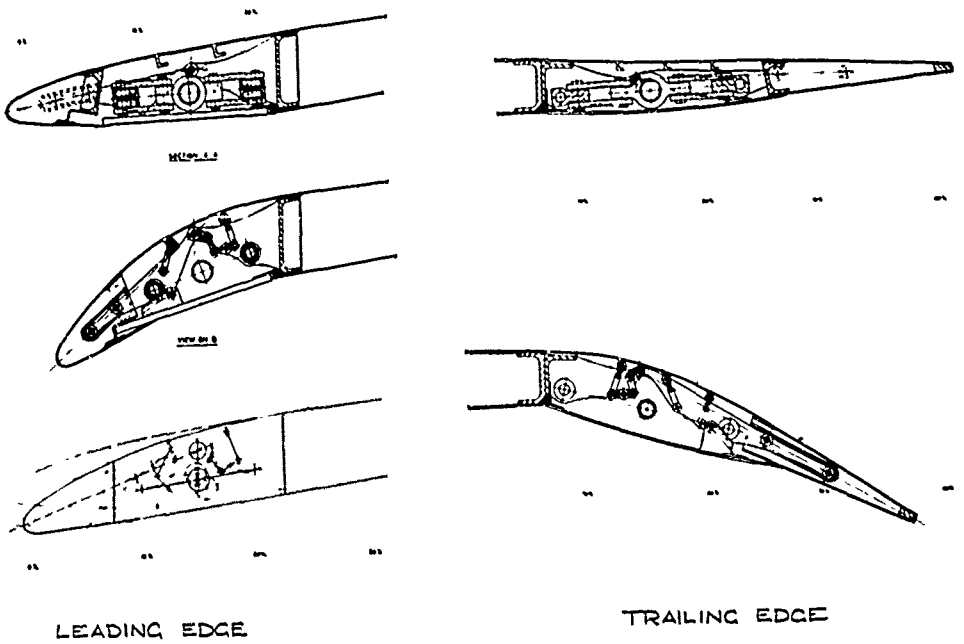

Fig. 12 Variable Camber Devices

- BASIC PERFORMANCE VERSUS COST
- WEAPONS SYSTEM PERFORMANCE VERSUS AIRFRAME PERFORMANCE
- FUEL VOLUME VERSUS SUPERSONIC DRAG
- TECHNICAL SOPHISTICATION VERSUS SHORT TIME SCALE

FIGURE 13. EXAMPLES OF "INTERFERENCE"

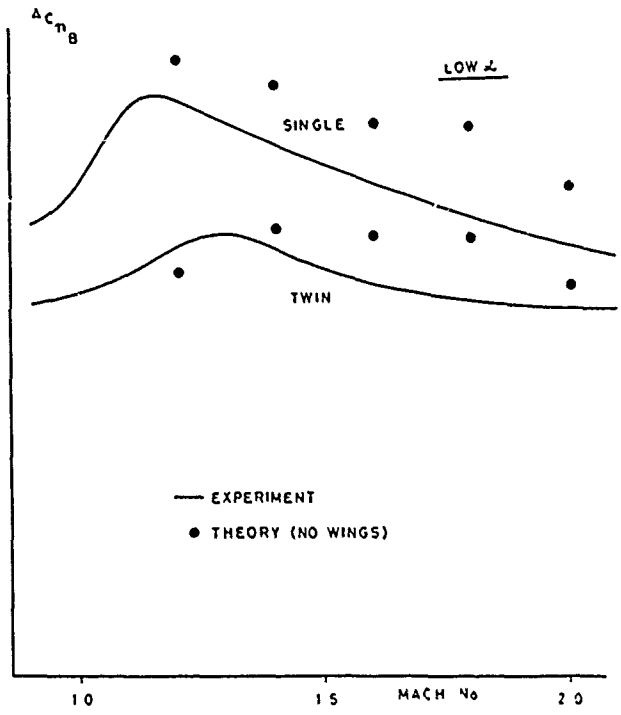

FIG 14 EFFECT OF MUTUAL INTERFERENCE WITH TWIN FINS

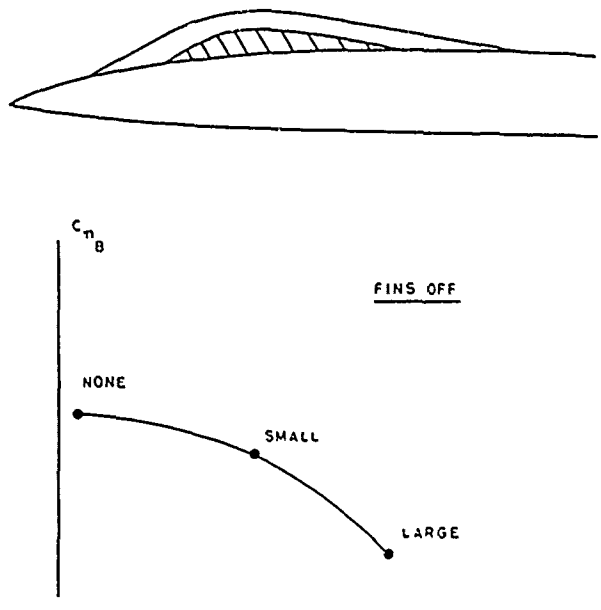

FIG 15 VARIATION OF CnB WITH CANOPY SIZE (EXPERIMENT)

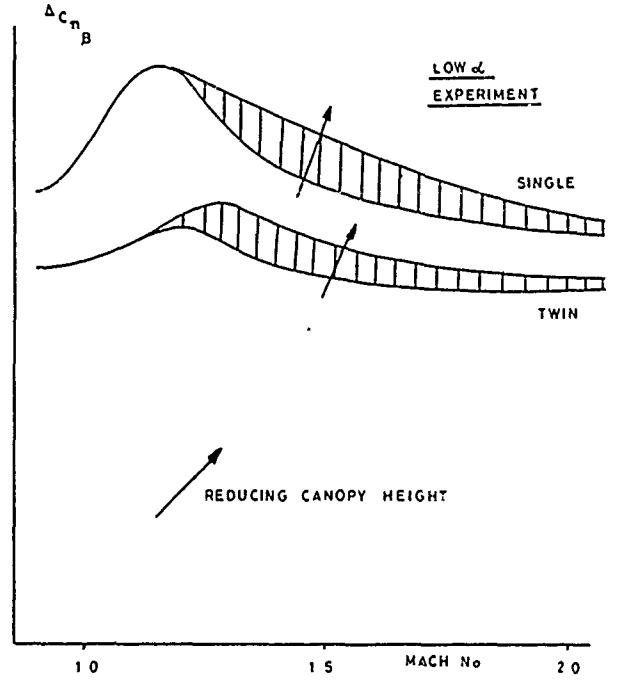

FIG 16 EFFECT OF CANOPY SIZE ON FIN CONTRIBUTION TO Cnβ

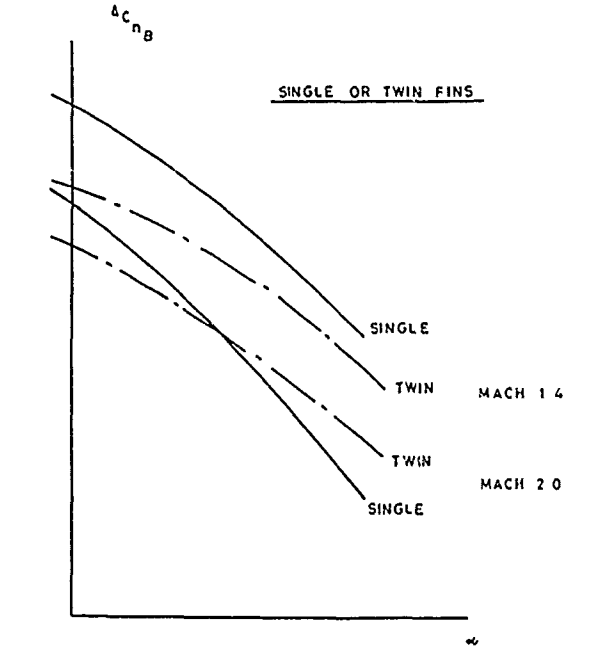

FIG 17 INCIDENCE EFFECTS ON FIN CONTRIBUTION TO CnB (EXPERIMENT)

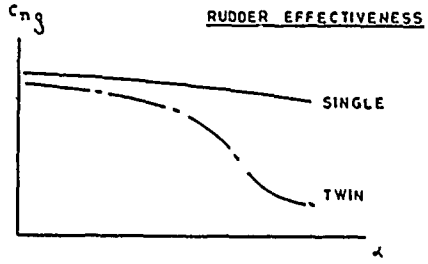

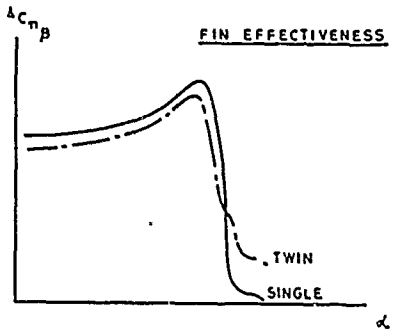

FIG 18 INCIDENCE EFFECTS ON FIN AND RUDDER (LOW SPEED EXPERIMENT)

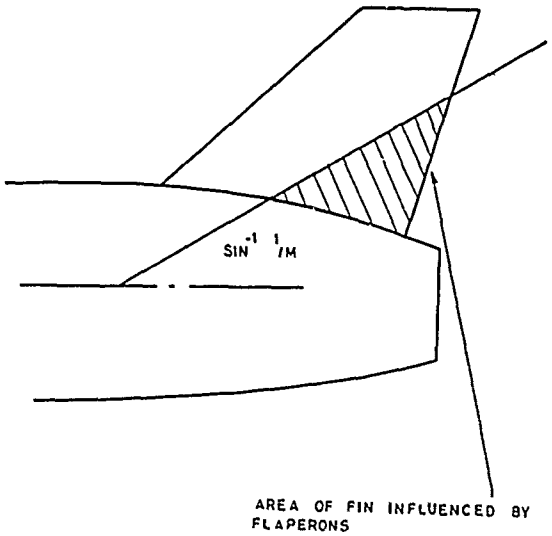

FIG.20 SUPERSONIC INTERFERENCE

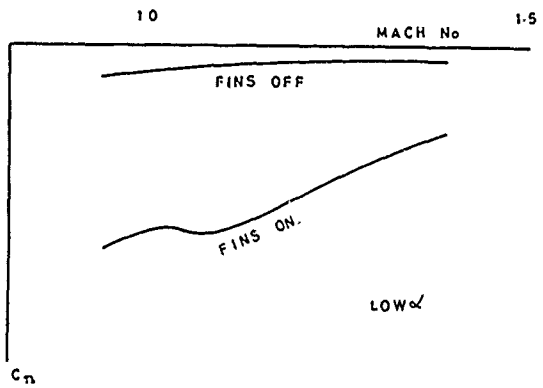

FIG. 22 AILERON YAW MOMENTS (EXPERIMENT)

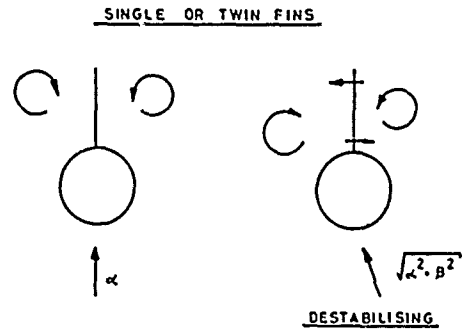

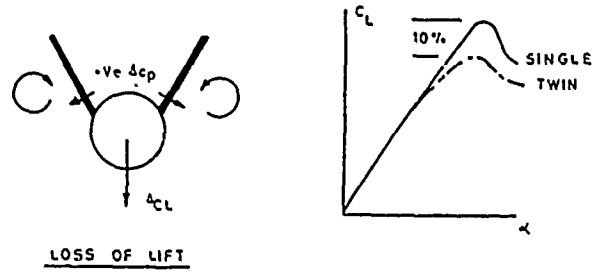

FIG 19 VORTEX INTERFERENCE @ HIGH α

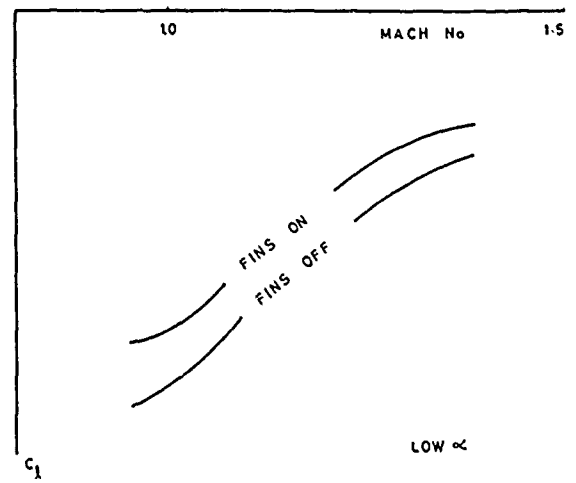

FIG. 21 AILERON ROLL CONTROL POWER (EXPERIMENT)

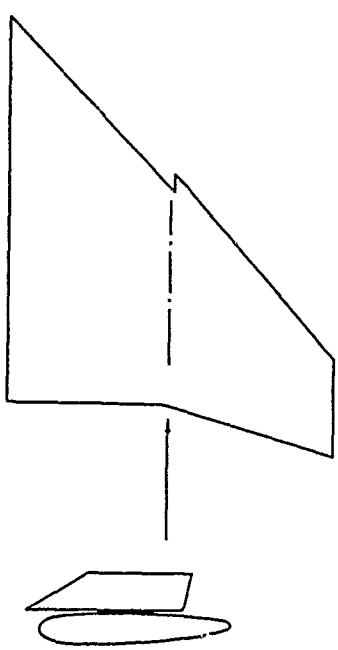

FIG. 23 GROSSWING + STORE

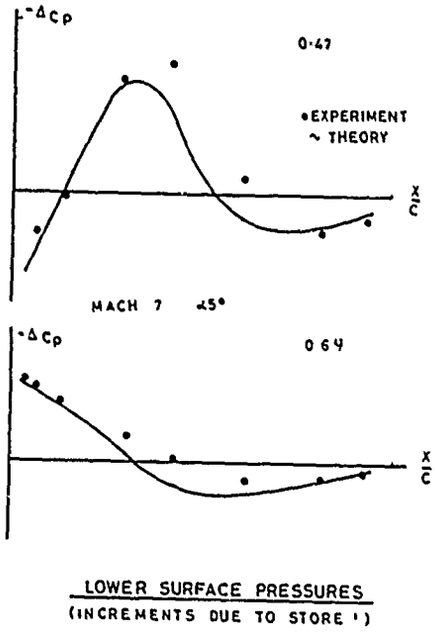

LOWER SURFACE PRESSURES
(INCREMENTS DUE TO STORE 1)

FIG 24 THEORY VS EXPERIMENT

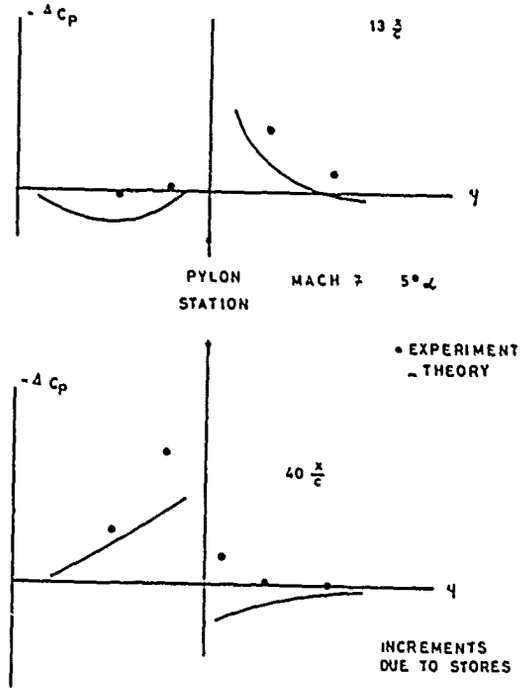

FIG 25 LOWER SURFACE PRESSURE

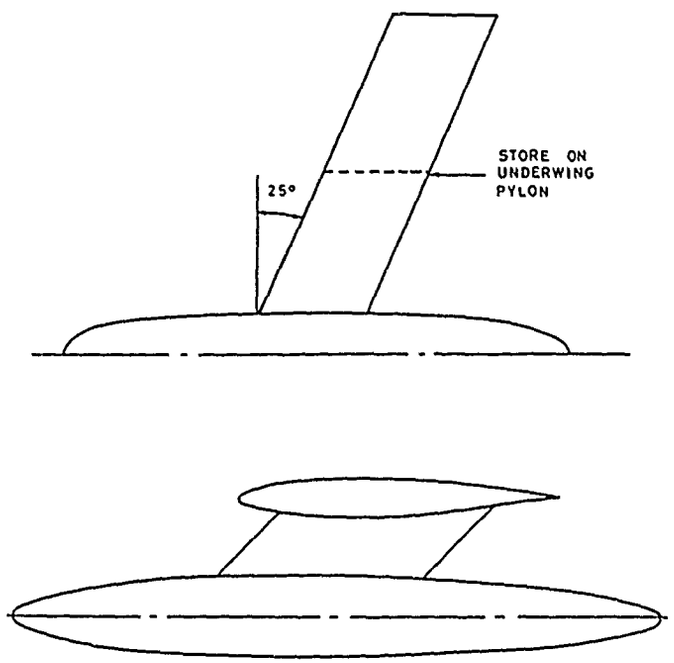

FIG. 26 SWEPT WING MODEL + UNDERWING STORE

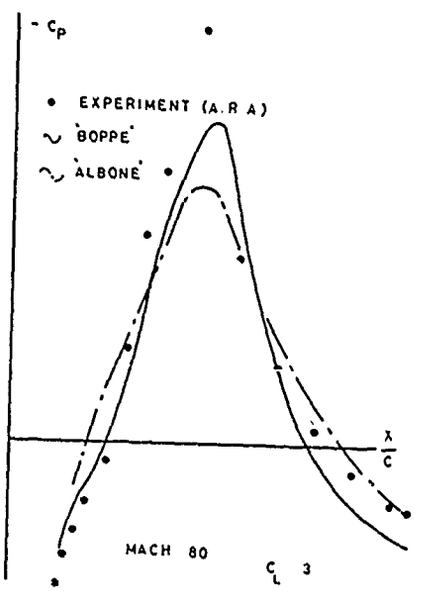

FIG. 27 LOWER SURFACE PRESSURES-
INBOARD OF PYLON

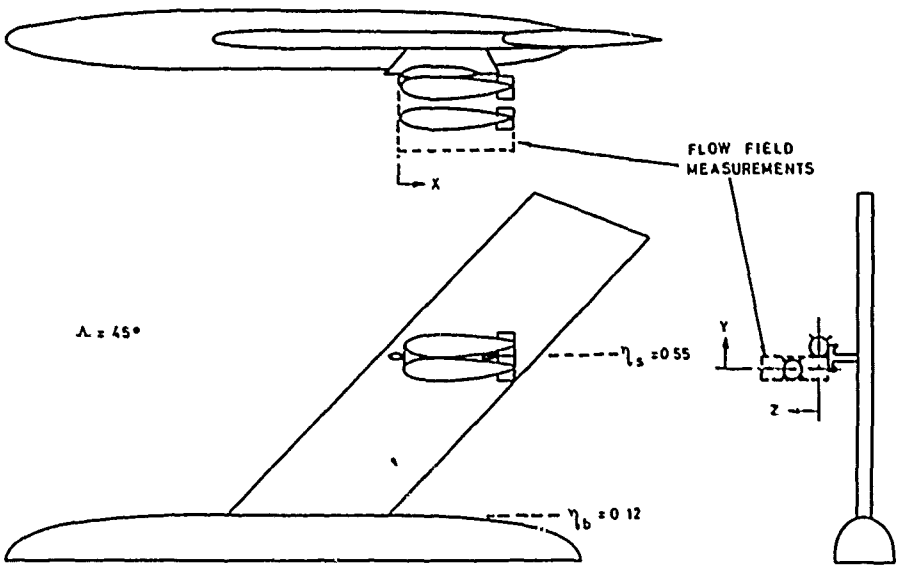

FIG. 28 GENERAL ARRANGEMENT

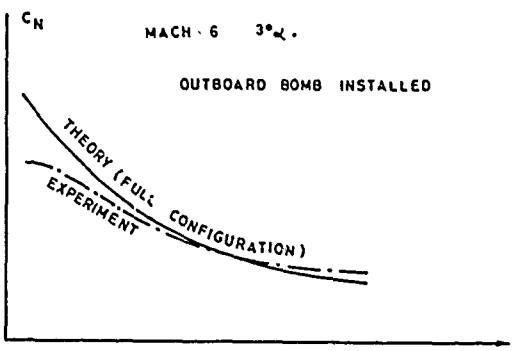

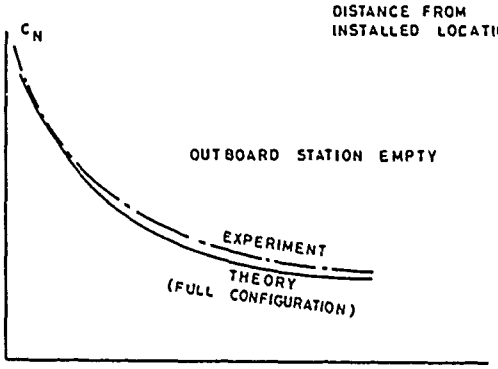

FIG 29 NORMAL FORCE ON RELEASED BOMB

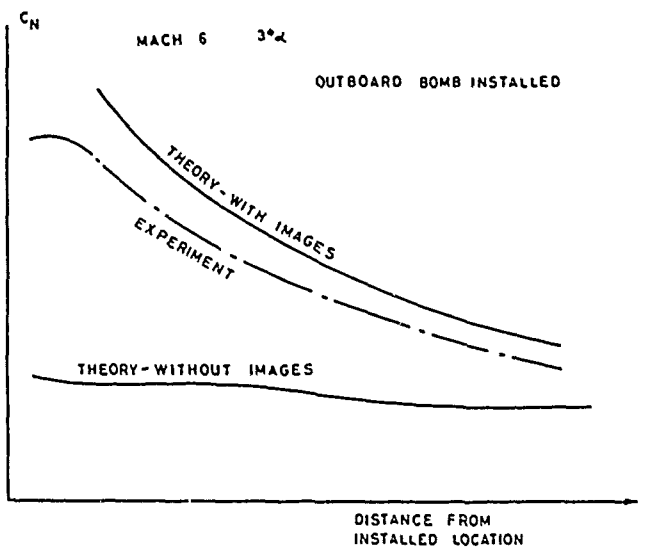

FIG. 30 NORMAL FORCE ON RELEASED BOMB (EFFECT OF INCLUDING IMAGES) USING FLOW ANGULARITY DATA

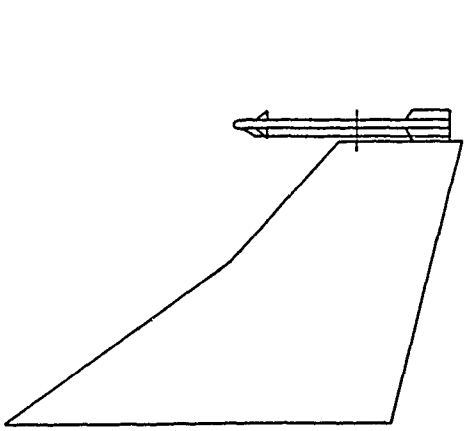

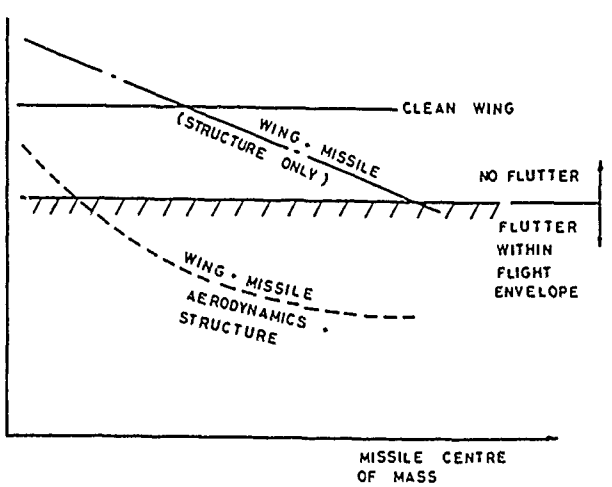

FIG. 31 EFFECT OF TIP MISSILE ON WING FLUTTER

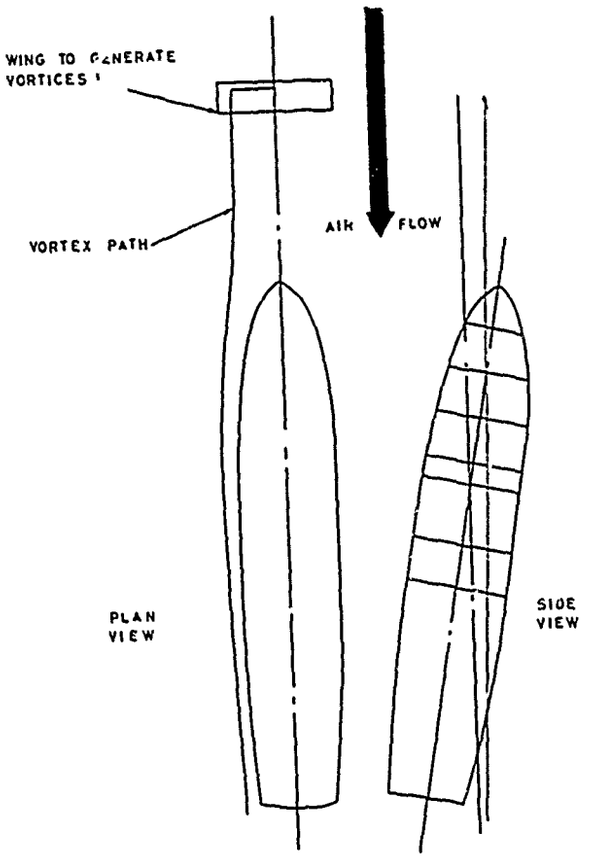

FIG. 32 SCHEME OF MODEL

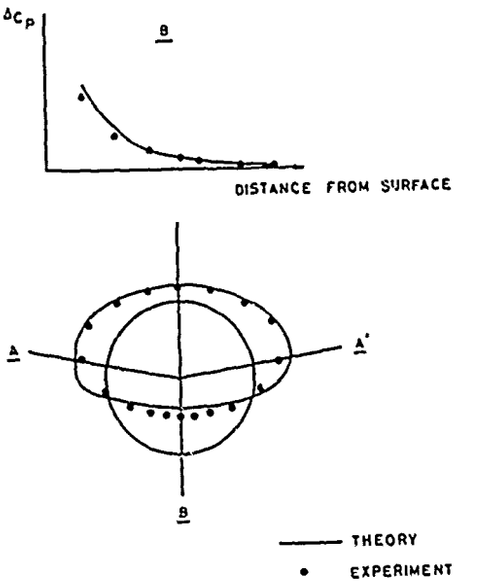

FIG 33 EXPERIMENT VS THEORY

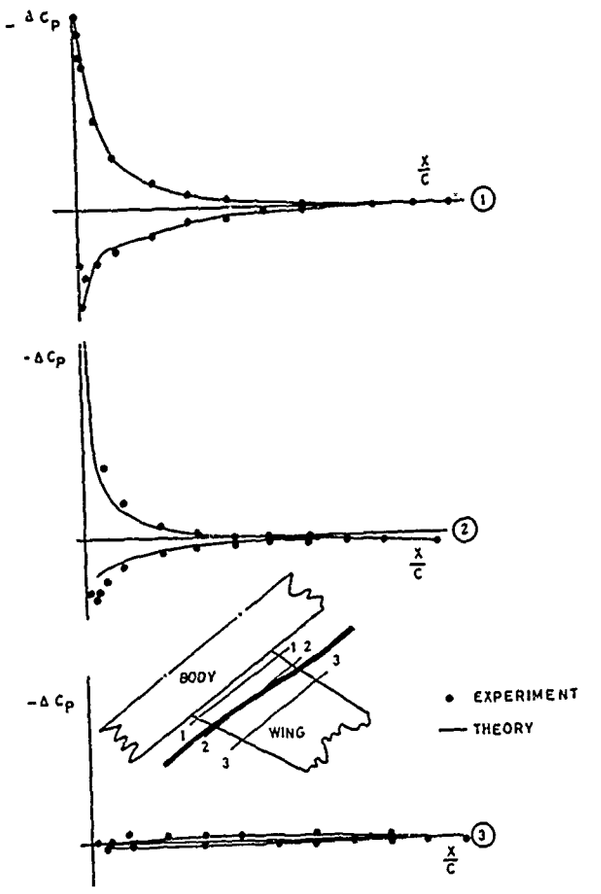

FIG 34 INCREMENTAL WING SURFACE PRESSURES DUE TO VORTEX

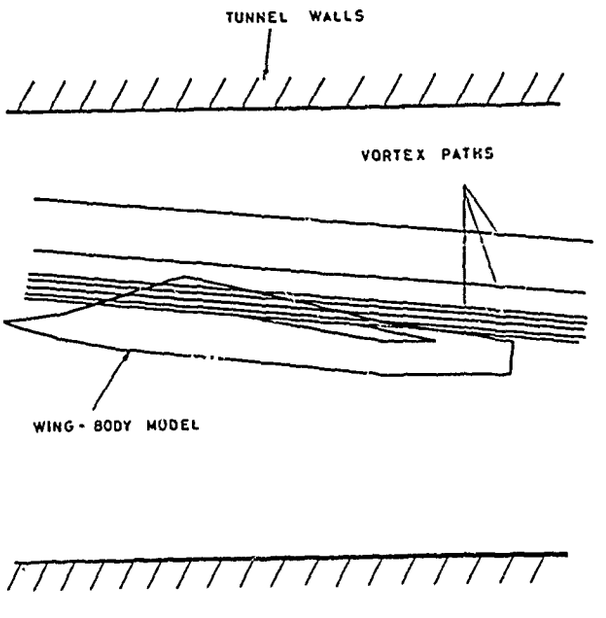

FIG 35 WING-BODY MODEL IN WIND-TUNNEL + VORTICES

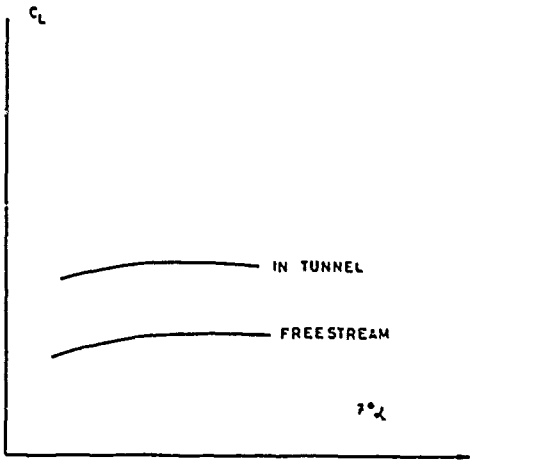

FIG 36 EFFECT OF TUNNEL WALL CONSTRAINT

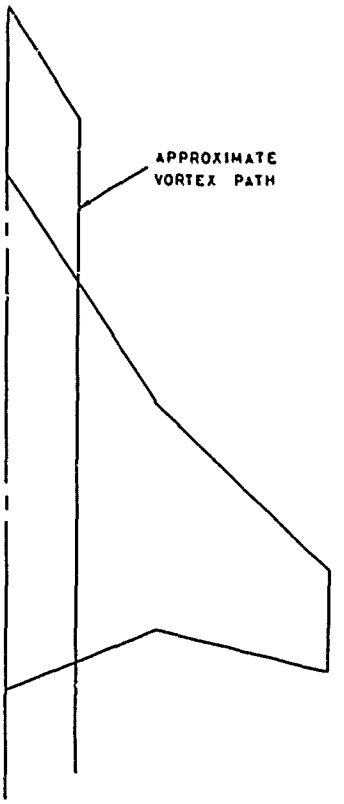

FIG 37 PLANFORM VIEW OF WING

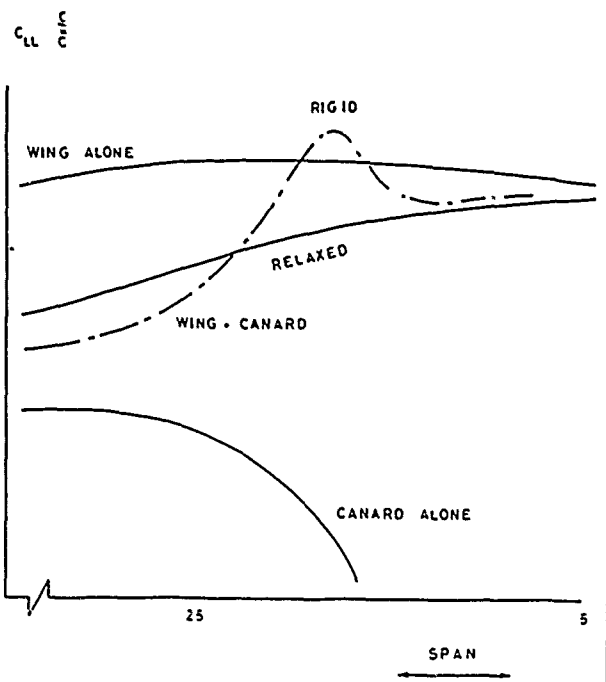

FIG 38 EFFECT OF RELAXING VORTEX

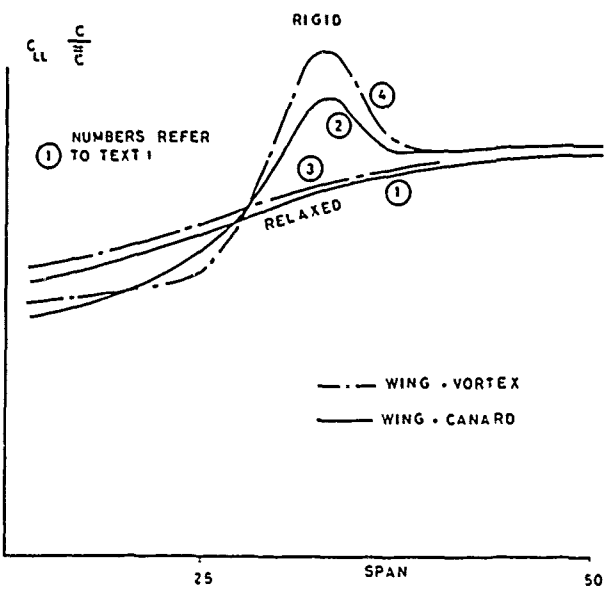

FIG 39 DIFFERENT VORTEX MODELS

- SEPARATED BOUNDARY LAYER PHENOMENA, WHERE CONTROL SURFACES ARE "BURIED" IN LOW ENERGY AIR, AND HENCE LOSE THEIR EFFECTIVENESS.
- AIR DATA SENSORS, USED TO MEASURE PITO-STATIC PRESSURES, INCIDENCE, ETC., INFLUENCED BY SPURIOUS EFFECTS SUCH AS THE MOVEMENT OF NEARBY CONTROL SURFACES, OR CHANGES IN ENGINE MASS FLOW.
- DEFLECTION OF THE FLOW ENTERING THE INTAKE BY UPSTREAM PARTS OF THE AIRCRAFT.
- INTERFERENCE EFFECTS OF FINS, TAILPLANES, ETC., ON THE REAR FUSELAGE.
- INTERFERENCE EFFECTS OF SECONDARY FLOW INLETS AND OUTLETS, SUCH AS INTAKE BOUNDARY LAYER SYSTEMS, OR HEAT EXCHANGER SYSTEMS.

Figure 40. FURTHER EXAMPLES OF AERODYNAMIC INTERFERENCE

EXTERNAL STORES INTERFERENCE

A B Haines
Chief Executive
Aircraft Research Association Ltd
Manton Lane, Bedford, UK

SUMMARY

External store installations are frequently a source of considerable adverse aerodynamic interference giving large increases in drag, reductions in usable lift and poor store release characteristics. Research has however shown how this adverse interference can be greatly alleviated or even transformed into favourable interference. This lecture reviews some of the available evidence for a wide variety of arrangements. The nature of the interference, both adverse and favourable, is described, particular emphasis being placed on the major adverse interference in standard multiple carriers and in some underwing installations. The possible benefits of wing tip carriage and carefully arranged underfuselage arrays are noted. Throughout, stress is laid on the fact that dramatic improvements might be possible by adopting a radical approach to store carriage.

1 INTRODUCTION

The main theme of this lecture series is optimisation. how should we optimise a configuration to minimise adverse aerodynamic interference and exploit favourable interference. Nowhere is this more important than in the design and mounting of external store installations. The traditional approach followed for many years was to mount the stores either separately on underwing pylons or on standard multiple (triple or twin) carriers. Many papers [1,2,3] in the mid-1970s stressed that this was a recipe for serious adverse interference. One could design a highly efficient clean airframe and then lose all the benefits of advanced design when the stores were added. Examples were quoted where the installed drag increment due to carrying say, six stores was greater than the drag of the clean aircraft. Noting this situation, the AGARD FD Panel in 1974 set up a Working Party to consider 'Drag and Other Aerodynamic Effects of External Stores'. This group reported [4] in late 1977 and some of the evidence and their conclusions were included and updated in a paper [5] presented at the AGARD 1980 conference on 'Configuration Aerodynamics at Transonic Speeds'. These papers did more than just identify the sources of the interference; they showed that adverse interference was not inevitable, favourable interference was a real possibility and the performance gains relative to standard practice could be substantial. Various recommendations were put forward as to how these improvements might be achieved, eg

(i) carry as many stores as possible in conformal arrays below the fuselage, these arrays being arranged to exploit the benefits of store stagger and tandem carriage,

(ii) for aircraft where stores have to be carried under the wing, design the wing with due allowance for the presence of the stores or at least, treat the design of the wing and underwing pylons as a single operation,

(iii) apply area-rule principles both to the complete configuration and to the local store assemblies,

(iv) exploit the benefits of wing-tip carriage for missiles,

(v) for cases where multiple carriers have to be used, develop carriers of improved aerodynamic cleanliness and if possible, including the benefits of store stagger, tandem carriage and optimum lateral spacing of the stores,

(vi) wherever possible, adopt a radical approach.

It must be admitted that some of these recommendations are difficult to implement retrospectively on past aircraft designs. There is also the natural reluctance to abandon the stocks of standard equipment. It has therefore been difficult for research workers to advance their arguments for radical change. Progress has been slow and there have been many disappointments where promising ideas have been rejected in practice on non-technical grounds. Nevertheless, there have been some notable advances particularly in France and it is to be hoped that new aircraft designs will take advantage of what has been learnt in extensive research testing. One cannot emphasise too strongly that the possible advances relative to the interference implicit in the installations of the 1970s are very great - not only in terms of reduced drag and better performance but also as less buffet, smaller installed loads and better release characteristics.

This lecture is an abbreviated and slightly modified version of the paper [5] presented at the 1980 conference. Some of the earlier examples have been omitted on the grounds that they have already been published in several documents [1,2,3,4,5]. The emphasis throughout is on the understanding of the adverse or favourable interference.

2 UNDERWING FUEL TANKS AT LOW C_L

It seems appropriate to start the detailed discussion by considering the interference effects due to the carriage of external fuel tanks. A fuel tank is the simplest and probably the cleanest type of store. Fuel tanks are generally carried on pylons below the wing or fuselage. It is far more efficient to carry them under the fuselage. For example, in model tests [6] at AEDC for the F-4C, it was found that carrying fuel in a 2264 litre (600 gal) tank under the fuselage was more than 4 times as efficient at $M = 0.7$ and almost 3 times as efficient at $M = 0.9$ as carrying fuel in 1396 litre (370 gal) tanks under the wing, efficiency being defined as the ratio of fuel capacity divided by the installed drag. Nevertheless, on many aircraft there are practical reasons why the fuel tanks have to be carried underwing and Fig 1a presents results for 15 different aircraft/fuel tank combinations. In all cases the tanks were pylon-mounted under the wing near mid-semi-span; except for the curves marked A and B, this figure was included in the Working Party report [4] . The graph shows the variation with Mach number at $C_L = 0$ of a 'figure-of-merit' or inverse efficiency,

$$\lambda_I = \frac{\text{Measured installed drag increment (or drag in isolation)}}{\text{Estimated profile drag for tank/pylon at low Mach number}}$$

ie assuming the estimate in the denominator is correct, $\lambda_I = 1.0$ implies zero net drag contributions from flow separations, base drag, bluffness drag, excrescence drag, wave drag and interference within the assembly and between the assembly and the aircraft.

The results for a typical fuel tank in isolation are included for comparison. The figure clearly illustrates that most of the drag increment is related to the installation interference effects. For the tank in isolation, λ_I is less than 1.1 up to $M = 0.94$ but for the installed tank assemblies, values of λ_I ranging from 1.2 to 3.5 are obtained even at $M = 0.6$; rapid increases in λ_I with Mach number are already occurring at $M = 0.6$ in the worst case but not to beyond $M = 0.86$ in the best case. At first sight, it may appear an impossible task to predict or interpret this figure but certain trends can be deduced. First and foremost, as shown in Fig 1b, there is a trend for both λ_I at $M = 0.6$ and M_{D_S}, the Mach number for the start of the rapid increase in λ_I, to improve in sympathy with the drag-rise Mach number M_D of the clean wing. This is only to be expected. an increase in M_D will generally imply a reduction in wing thickness/chord ratio and/or an increase in wing sweepback and thus, a reduction in the suctions below the wing lower surface and a later appearance of a shock wave in the channel between the wing and tank. Research has shown that the appearance of this shock wave generally collates with M_{D_S}. With tanks of a standard shape, therefore, it may be difficult to obtain notably better results than those implied by the dashed lines in Fig 1b but the significant point is that there are a fair number of installations where the interference is such that the results do not approach this norm.

Let us consider two of these examples. First, Fig 1c compares [3] configurations 6 and 11. For both cases, the installed drag values for $C_L = 0$ lie above the norm, Figs 1a,b, but the excess is far greater for case 6; even at $C_L = 0.4$ where one would expect some improvement, the results are still poor. Looking at the geometry, it will be seen that in case 6, the tank is larger relative to the aircraft. Partly because the pylon is relatively thin (7% thick comapred with 13% thick for case 11), the crutch arms are exposed and unfaired. A simple estimate suggests that the drag of these crutch arms treated as isolated excrescences would be about the same as the extra drag of the thicker pylon in case 11 but it has generally been found that such excrescences can induce serious interference if the flow downstream of the excrescences encounters a region of high adverse pressure gradient. This would be true in the present case. The major weakness however with configuration 6, is the rapidly diverging channel at the rear. All three surfaces, ie wing, pylon and tank contribute to this divergence. One could say that the installation could not have been tailored better to produce a shock across the channel at a relatively low Mach number, or to produce a flow separation on one or all of the rear surfaces! Extra viscous drag and early wave drag are therefore only to be expected. Fig 1c shows a revised configuration for which the interference would be expected to be less; the λ_I curve for this revised configuration is a speculative estimate. no tests have been made on this layout.

Second, Fig 1d presents a comparison between cases A and B. These results are for the same tank mounted on the same pylon at the same spanwise position on two wings A and B of the same planform but which differ in section shape. The section of wing B is thicker and is designed to give more rear loading. Strictly, the results for A and B are not comparable with the other cases in Fig 1a because two additional bare pylons were present on the inner and outer wing and thus it is probable that the values of λ_I have been increased by the aerodynamic interference between the tank/pylon and these other pylons. However, it is still fair to compare A and B and Figs 1a,b show that the values of λ_I and M_{D_S} are much poorer for wing B. These differences can be explained qualitatively in terms of the measured pressure distributions over the wing lower surface. These are shown in Fig 1d for $M = 0.80$ for a station at 0.4 x semi-span, ie inboard of the tank. These distributions can be described as follows:

	A	B
Clean wing	Subcritical	Subcritical
Wing with 3 pylons	Subcritical	Strong shock, no separation
Wing with 3 pylons and tank	Strong shock, no separation	Shock-induced separation*

*Indicated by the lower pressures downstream of the shock relative to the other cases and by the partial collapse of the supersonic region ahead of the shock.

One can therefore forecast from the pressure distributions that both the wave drag and the viscous drag will be higher with the tank mounted on wing B. The greater interference for a given Mach number and C_L is a consequence of the different pressure distributions over the clean wings. The significant features are that near 0.35c the suctions are about 70% higher on wing B than on wing A and that the subsequent adverse pressure gradient is about twice as great.

It would be wrong to conclude however that the greater interference with wing B is an inevitable consequence of attempting to carry the tank on a more advanced, thicker wing. For example, as with configuration 6 in Fig 1c, one could either

(i) move the tank forward or aft in an attempt to separate longitudinally the peak suctions on the wing and the tank,

or (ii) change the shape of the tank to one with a parallel centre section opposite the peak suction on the wing,

or (iii) reshape the rear of the tank with either a longer, less tapered boattail or a raised upper line, ie a banana-shaped tank,

or (iv) modify the pylon design,

or (v) change the wing camberline to produce a more suitable shape of lower surface pressure distribution.

It is worth noting that concept (ii) was introduced more than 30 years ago on an early jet fighter to eliminate flow separation and buffeting problems that had resulted from the underwing carriage of a tank having a continuous longitudinal variation in cross-sectional area. The problem was solved by changing the tank shape to one with a forward, parallel mid and tapered aft section mounted in such a position that

the peak suctions at the junctions between the three sections were displaced fore and aft of the peak suction in the clean wing flow field. Now, when the need for care in eliminating adverse interference is even greater with modern wing designs, the concept is rarely used. This is not true of configuration 6 discussed above but in this case, for practical reasons, the concept was misapplied as will be realised from the sketch in Fig 1c. Logistically, it may be unattractive to think in terms of a different tank shape for different aircraft and to some extent, one could argue that (i-iv) should be regarded as palliatives for a situation that should not have arisen. The real lesson - and this will become even clearer in section 4 below - is that wings should be designed with store carriage in mind from the outset. At the very least, one should design a wing/pylon combination rather than a clean wing.

3 UNDERWING STORES: FACTORS AFFECTING INTERFERENCE DRAG AT LOW C_L

3.1 Store Shape

It should be apparent from the discussion of the fuel tank examples in Fig 1 that the aerodynamic interference with underwing mounted stores is likely to be proportionately more serious for clean streamlined stores than for parallel or dirty stores. Even relatively small changes to the shape of the store can have a significant effect on the interference. This is shown by the comparison in Fig 2a. Two alternative stores X and Y were mounted [8] on wing A, Fig 2d, on the same underwing pylon at 0.55 x semi-span. The two stores have about the same overall dimensions but a somewhat different shape, store Y having a bluffer nose, a longer parallel centre section and a shorter boattail. The free air drag and indeed, the installed drag increment was much greater for store Y but as shown in Fig 2a, the interference contribution ΔC_{D_i} to the drag increment,

$$\text{ie} \quad \Delta C_{D_i} = C_{D_{installed}} - C_{D_{isolated}}$$

is generally somewhat less for store Y, particularly in the range M = 0.80-0.85. There are two possible qualitative interpretations of this result. Either it is an example of a general trend that when the store shape is such that there is poor flow over the store afterbody even under free-air conditions, there is less chance that the interference with the wing flow field will further degrade the flow over the afterbody. Or the shape and position of store D are such that the interference increases the wing wave and/or viscous drag. Oil flow patterns for M = 0.85, C_L = 0 suggested that the second interpretation is more likely in this case. The main features of these flow patterns are reproduced in the sketch in Fig 2a:

(i) with store Y, the shock is further aft - consistent with the position of the start of the afterbody,

(ii) with store X, the sweepback of the shock both outboard and inboard of the store is somewhat less than with store Y, and

(iii) with store X, the change in flow direction through the shock is notably more acute, thus implying a stronger shock.

It is thought that (iii) is the dominant factor.

This comparison has been included to act as a warning against naive use of interference drag factors and to encourage the hope that by attention to detail and with the benefit of the theoretical calculations that will be possible in the future, adverse interference can be alleviated.

3.2 Store Depth below the Wing

Various investigations, eg Refs 3,9,10,11 have specifically considered the effects of the vertical position of a store below the wing. All have confirmed that this can be an important parameter but it is difficult to draw simple generalised conclusions. When the flow is entirely subcritical, an increase in the length and hence, surface area of the pylon will increase the pylon profile drag but will generally tend to reduce the interference drag. There is however a fair amount of evidence indicating that when the flow is supercritical the adverse interference first increases with store depth before it starts to decrease. Oil flow tests and pressure plotting measurements have shown that with a longer pylon, the flow separations in the wing-pylon junctions can be less severe. The channel between wing and pylon is therefore less constricted and the flow can expand to a higher local Mach number. The shock as well as being longer in extent, is stronger and there are therefore two reasons why the wave drag is increased.

An example of the effect of store depth is shown by the drag results in Fig 2b. A missile-type store was mounted at two vertical positions below the wing of a 25° sweptback wing research model in the ARA transonic tunnel [11]. At low Mach number, at both C_L = 0 and 0.3, the drag increment was higher with H/D = 0.88 than with H/D = 1.23, thus showing that in this particular case, the reduction in interference as the store and wing were moved apart more than offset the extra pylon profile drag. Above M = 0.75, however, the drag increment increased with Mach number more rapidly with H/D = 1.25, thus supporting the hypothesis of extra wave drag when the wing and store are further apart.

Quantitatively, the results could well be different with other stores on other wings and the correct choice of pylon length will depend on the aircraft requirements. It seems possible that in many cases, a compromise will have to be made between a short pylon to improve the dash capability with bare pylons and a long pylon to minimise the drag and usable lift penalties at high C_L (a point not illustrated in this lecture).

3.3 Spacing of Pylons across the Span

In §§2, 3.1, 3.2, we have been concerned with the carriage of a single store per wing panel. In practice, however, it is likely that current and future aircraft will be designed to carry a heavy store load requiring 2, 3 or even as many as 5 pylons per side. Tests have been made [8] to show whether the drag increments for a 3-pylon load of 3 stores on wing A of the previous example are sensitive to the spanwise spacing of the pylons. Three alternative spacings were compared, the widest and narrowest spacings being indicated by the photographs of Fig 2c. The graph shows the variation with Mach number of $\Delta(\Delta C_{D_i})$

where $\Delta(\Delta C_{D_i}) = (\Delta C_{D_i})_{narrow} - (\Delta C_{D_i})_{wide}$

and ΔC_{D_i} is defined as in the example in §3.1.

The figure shows that as might have been expected, bringing the stores closer together increases the interference drag at low and moderate Mach numbers, the maximum changes being as much as $\Delta(\Delta C_{D_1}) = 0.0030$ or perhaps 15% of the drag of the clean aircraft. At high subsonic speeds, the trend begins to reverse until ultimately, the drag increment is less with the narrow spacing. The Mach number for the crossover increases with C_L.

The oil flow patterns in Fig 2c offer a partial explanation for the change in sign of $\Delta(\Delta C_{D_1})$ between low and high Mach number, eg between $M = 0.75$ and 0.80 at $C_L = 0$. Irrespective of the spacing, the main feature of these flow patterns is the near-unswept shock below the wing between the pylons. With the narrow spacing, this quasi-one-dimensional flow is already established at $M = 0.75$ with the terminal shocks and flow separations behind the shock extending from one pylon to the next. With the wide spacing, this type of pattern does not become fully established until $M = 0.80$ but then, the shock waves in the wider gullies between the stores appear to be stronger. The pictures therefore help to explain why ΔC_{D_1} increases more rapidly above $M = 0.75$ with the wide spacing, the increase being .icient to give higher ΔC_{D_1} than with the narrow spacing above $M = 0.80$. There is an obvious similarity between these effects of spacing and the effects of store depth as already described.

For configurations of the type discussed here, store spacing is clearly a significant parameter, the optimum value would depend on the aircraft operating requirements. It is possible however to envisage how the adverse interference, ie the values of ΔC_{D_i} might be reduced by either changes in pylon design or store relative longitudinal position, ie store stagger. In the present case, the pylons were of simple design with symmetrical slab-sided sections; the shocks between the pylons tended to be unswept because they extended from the peak suction on the outboard side of the inner pylon (aft of its maximum thickness) to the peak suction on the inboard side of the outer pylon (ahead of its maximum thickness), changes in design might improve the shock sweep. The store longitudinal positions were chosen with the aim of minimising the cg shifts for partial and full store loads; these considerations may be less vital in the future with the advent of active controls and acceptance of relaxed stability.

3.4 Effect of Wing Design: Multiple Carriage on Separate Pylons

The influence of wing design has already been discussed in §2 with reference to the drag increments for an underwing tank installation on wings A and B (same planform, different sections, Fig 1d). Comparative tests were also made [7] on these wings and three stores of shape Y mounted on three separate pylons. Results and oil flow patterns from these tests are presented in Fig 3. The upper graphs compare the $C_D - M$ variation for $C_L = 0.2$ for (a) the clean wings, (b) the wings with 3 bare pylons per wing and (c) the fully loaded configurations. It should be noted that the false zeros on the ordinate scales have been staggered by amounts corresponding to the estimated low speed profile drag of respectively, the pylons and the pylons plus stores: in other words, if there were no interference drag, the three pairs of curves would start at low Mach number at the same levels.

The addition of the pylons and then the stores reduces the drag-rise Mach number and by implication, the penetration speed by significant amounts, at least 0.1 in Mach number. This is only to be expected and to some extent at least, is an inevitable consequence of carrying a heavy store load underwing in what has generally been accepted as a 'standard' arrangement. In passing, it should be noted that in this and succeeding sections up to §4.2, we are only concerned with the multiple carriage of stores on separate pylons at different stations across the span. 'Standard' underwing carriage of a multiple store load can in practice imply the use of a triple carrier, eg as on the F-4 Phantom, or a twin carrier as on the Harrier but these cases are not considered here because of the difficulty of separating the store-wing interference from the interference within the multiple carrier.

It is clear that the relative assessment of wings A and B depends on whether the pylons/stores are fitted or not. Clean, the reduction in the Mach number for the steep drag-rise for wing B relative to wing A is about $\Delta M = 0.035$ but with pylons, it is as much as $\Delta M = 0.06$ and with pylons/stores, about $\Delta M = 0.055$. The unexpected feature of these results is the striking effect of the bare pylons. This is a significant conclusion because the aircraft will still be carrying its pylons on the return from the target and hence this is a configuration that should if possible be optimised. Also, the shape of a pylon is probably less sacrosanct - or less constrained by other factors - than the shape of most stores.

Fig 3 also shows the wing lower surface pressure distributions for stations at 0.60 and 0.72 x semi-span on wing A and at 0.64 and 0.74 x semi-span on wing B, for $C_L = 0.2$, $M = M_X$. The stations are between the middle and outer pylons, the outer stations being very close to the outer pylons. For the clean wings, the flow is subcritical in both cases although it is significant that the values of $(-C_p)$ near 0.3c are almost twice as great for wing B as for wing A. Adding the pylons on wing A leads to a local supersonic region inboard of the outer pylon while on wing B, this region appears to extend across the whole panel to the middle pylon. Adding the stores produces a strong shock wave in the gully between the stores as already seen in Fig 2c with poor flow behind the shock particularly on wing B. Near the outer pylon on wing B, the separation is already sufficient to degrade the supersonic region, this is hardly surprising bearing in mind that $M = M_X$, $C_L = 0.2$ is far up the drag-rise for this configuration.

These pressure distributions do not however tell the full story. Fig 3 also contains photographs of oil flow patterns for $M = M_X$, $C_L = 0.2$ for wings A and B with three bare pylons. Weak shocks and fairly narrow pylon wakes are evident in the picture for wing A but generally, the flow is relatively well behaved compared with wing B where there are substantial flow separations both inboard of the outer pylon and downstream and outboard of the inner and middle pylons. These pictures suggest that the drag creep in the results for wing B with bare pylons must be largely associated not with premature wave drag but with gross viscous effects particularly downstream of the pylons.

The full assessments of wings A and B including factors not discussed here could still favour wing B. It is a more advanced wing with notable advantages in usable lift and fuel volume. In designing wing B, it was accepted that there would be some loss in drag rise Mach number at low C_L, a reduction of 0.03 was deemed acceptable. It must be emphasised strongly that the fact that the reduction is about 0.06 with pylons fitted does not destroy the concept of the advanced wing design. It merely shows that one should design the wing-pylons and if possible, the wing-pylons-stores as an entity. The simple pylons that were adequate on wing A

are no longer acceptable on wing B. Aerodynamically, as isolated pylons, they were respectable designs 6.5% thick, symmetrical, slab-sided, elliptic nose, tapered aft section. Looking at the oil flow picture, however, it seems inconceivable that one would not be able to modify the pylon design to reduce the viscous interference effects on the wing

4 UNDERWING STORES OTHER ASPECTS OF INTERFERENCE

4.1 Aircraft Stability and Usable Lift

It is of course self-evident that underwing stores will interfere with the flow over the wing lower surface. Until recently, however, it has not been fully realised that the stores can modify the flow over the wing upper surface and that this can have serious consequences, particularly when the flow is supercritical. To start with a simple example, Fig 4 presents results from tests at $M = 0.85$ on a model of an aircraft with a wing of moderate sweepback and moderate aspect ratio tested with and without two underwing stores per wing. Fig 4a shows the wing upper surface pressure distribution for a station near mid-semi-span and it will be seen that the addition of the stores increases the suctions in the supersonic region and hence, the shock strength. Two factors can contribute to this interference. an increase in upwash and an increase in local velocity. The shock strength is increased - but by varying amounts - across the complete span and thus, the shock-induced separation leading to a forward movement of the shock occurs at a lower incidence. This is shown in Figs 4b,c for stations at mid-semi-span and 0.85 x semi-span. However, the important point is that these effects were not quite the same at all spanwise stations. The differences appeared trivial at first sight but they were sufficient to modify the $C_m - \alpha$ variation as shown in Fig 4d. The results for the clean wing were marginally acceptable; with stores, however, there was an unacceptable pitch up. This is an aspect of store interference which is clearly very configuration-dependent but it cannot be ignored when seeking to optimise the configuration.

The interference with the upper surface flow has more dramatic consequences at high C_L near the usable lift boundary. Two examples drawn from the results of the experiments [7] on wings A and B are presented in Fig 5. First, at the top of the page, data from incidence traverses at a relatively high subsonic Mach number, $M = M_X + 0.07$, indicate serious adverse interference, eg on the lift break, by about $\Delta C_L = -0.05$ for the bare pylons or $\Delta C_L = -0.25$ for the fully loaded case. Measured pressures are shown for 3 stations at 2 incidences. With and without pylon cases are compared at the same incidence. The distributions show that as might be expected, some of the loss in break C_L is due to the interference with the lower surface flow which is still substantial even at these incidences, particularly near the outer pylon. The significant point however is that the flow breakdown on the upper surface appears to occur at a lower incidence. the deterioration between $\alpha = 4.9°$ and 6.7° at 0.64 and 0.73 x semi-span is certainly much more rapid when the pylons are fitted. Once again, relatively small increases in shock strength have been sufficient to provoke these differences. It is possible that these effects could have been averted or at least postponed to a higher Mach number by moving the pylon-wing intersection further aft. The more dramatic effect from fitting the stores is of somewhat academic interest because it is unlikely that the fully loaded aircraft would have sufficient thrust to reach these conditions.

The results in the lower half of Fig 5 have been included to illustrate that the interference effects of underwing pylons/stores on usable lift are not necessarily adverse. These results for $M = M_X$ again show a reduction in break C_L from both the pylons and the stores but the subsequent reduction in lift-curve slope is less and the development of the stall is then more progressive. Indeed, the very fact that data can be presented for the cases with pylons and with pylons/stores up to a high incidence is itself significant because with the clean wing. the test could not be continued beyond the abrupt lift break because of severe model bounce. Pressure distributions, with and without stores are compared for two stations (between the middle and outer stores as in Fig 3) at three incidences, the lowest being near separation-onset. It will be seen that stores off, there is a lift contribution from the forward supersonic region at both stations at $\alpha = 8°$ and 9.5° followed by a collapse at both stations at 11° whereas stores on, the supersonic region has already completely collapsed at one but only one station at $\alpha = 9.5°$; in other words, an earlier but more progressive stall, stores on. This implies earlier buffet onset but better buffet penetration. The presence of the pylons and the stores is tending to dictate the manner in which the areas of separated flow extend with increasing incidence and as a result, the stall development is likely to be less sensitive to other variables: for example, there is evidence from tests on other wing designs that the presence of underwing stores can alleviate any tendency to lateral problems such as wing drop and wing rock. This statement would not however be true of every wing design, examples could be quoted where the exact opposite would apply.

Speculatively and arguably, a wing design philosophy can be suggested that would exploit this possible favourable interference of the pylons/stores on the stall development. One should design the clean wing to carry as much lift as possible at buffet-onset; there is then the risk that the flow will tend to break down all across the span at almost the same incidence; however, the addition of underwing pylons (and stores) could then slightly degrade the stall onset but give the progressive breakdown that is required for satisfactory flying qualities. This design philosophy has been set out in broad terms; to follow it literally may not be possible with a given design at all Mach numbers. The interference from the pylons/stores is probably due to their effect on the spanwise upwash distribution ahead of the swept leading edge of the wing; the detailed effects could be modified by small changes in the geometry of the wing-pylon leading edge junction.

4.2 Buffet at low C_L

As a final contribution from the results of the tests [7] on wings A and B, Fig 6 presented $C_B - C_L$ curves* for $M = M_X$ and $M = M_X + 0.07$ for wing B with and without pylons/stores. It will be seen that even at $M = M_X$, the stores are tending to provoke a buffet response at low positive C_L while at $M = M_X + 0.07$, with stores, there is no C_L-range that can be described as being free from buffet and even the bare pylons give significant buffet at low C_L. Most modifications introduced to reduce the drag increments should also tend to alleviate the buffet.

* $C_B = \dfrac{\text{tuned rms wing root strain}}{\text{dynamic pressure}}$

4.3 Flow Fields: Store Loads and Release

Various references, eg Ref 12, have concluded that for underwing stores, the flow field about the aircraft with stores may be the most important parameter affecting the store trajectory. Mathews in Chapter 5 of Ref 4 notes that the flowfield is likely to vary with aircraft, store, store position, adjacent stores, flight conditions, and aircraft attitude, eg an underwing flowfield often produces a large nose down aerodynamic pitching moment on the store and, for large diameter stores at high Mach number can, to quote Mathews, 'result in unsatisfactory release trajectories for many weapons'. As an illustration, Fig 7 compares the variation with Mach number of the maximum pitch angle experienced by a store when released, with the same ejection velocity from similar locations under two wings of identical planform, but different section thickness [13]. The pitch disturbance increases significantly with both Mach number and thickness/chord ratio. In this example, with a reduction in t/c from 11% to 5%, the release Mach number can be increased by about 0.15 without exceeding a given level of pitch disturbance. This is consistent with the greater chordwise variation of local velocity and flow angles and the earlier appearance of shock waves and flow separations around the pylon and store which would be expected beneath the thicker wing. It also prompts the suggestion that a benign flow environment for a store release exhibits characteristics similar to those required to minimise the drag penalties of store carriage - a reasonable and happy supposition!

5 WING TIP-MOUNTED STORES

Wing tip carriage is increasingly becoming a favoured option for carriage of slender missiles. There may be practical reasons for this, eg a missile mounted well forward at the tip will have a good unobstructed field of view and it may be the best position to avoid ground clearance problems. However, on many wings, it is also an attractive proposal aerodynamically and it certainly should be discussed in this lecture because it provides a prime example of favourable aerodynamic interference.

The AGARD FDP Working Party Report [4] included two examples [14,15] showing that wing-tip carriage of external stores can reduce the lift-dependent drag. Fig 8 presents some results from a recent series of tests which are of considerable interest because surface pressure measurements are available to help in the interpretation of the favourable interference. Tests were made on a sweptback wing research model fitted alternatively with a curved wing tip and with a cropped square-cut tip on which was mounted a model of a missile and its launcher. The tests covered a wide range of Mach number but the results for $M = 0.7$ presented in Fig 8 are typical of those obtained at Mach numbers up to at least $M = 0.9$. They are non-dimensionalised using the geometry of the wing with the square-cut tip. The drag increment at a given C_L from adding the missile and its launcher decreases with C_L, becoming negative above about $C_L = 0.3$. A prediction based on treating the missile and launcher as an effective extension of the span gives very good agreement with the measured results up to quite high values of C_L. This may suggest a very simple analogy but a detailed study of the pressure distributions measured in these tests shows that this analogy does not entirely represent the physics underlying the favourable interference.

Fig 8 shows that the reduction in the lift-dependent drag collates with an increase in lift at a given incidence; some of this extra lift is generated on the missile itself but mostly, it is produced on the outer wing as shown by the local C_N values for the station at 0.95 x semi-span. Indeed, the local lift at this station is almost as great as for the wing with curved tip and is greater than would be predicted on the effective span analogy. Further, the changes in chordwise loading at this station due to the addition of the missile cannot be explained simply by a change in induced incidence. Comparison of the results from the tests with and without the missile tail fins shows that some of the extra lift even at this station some distance away from the fins is due to local interference between the fins and the rear wing (increased suctions on the upper surface, increased pressures on the lower surface).

The results in Fig 8 and in the earlier comparisons [14,15] are for conventional tip-mounted installations. It does not need much imagination to suggest that it might be possible to exploit the favourable interference further by repositioning the missile. Winglet research is obviously relevant. Not all the interference can be described as favourable: the increased adverse pressure gradients near the leading edge on the upper surface near the wing tip-launcher junction at low Mach numbers and a further forward shock position near the tip at higher Mach numbers could have adverse consequences particularly for wings designed to stall progressively inwards from the extreme tip. However, with care, it should be possible to avoid these local problems and thus reap the benefits of the favourable interference.

6 BASIC CONCEPTS FOR FAVOURABLE INTERFERENCE (OR MINIMISING ADVERSE INTERFERENCE)

The discussion in §§2-5 has concerned wing-store interference. Let us now consider store-store interference and the implications for carrier design and for multiple store arrangements, eg below the fuselage. Three basic concepts [16] are available to reduce adverse or to produce favourable interference, viz

(i) increased lateral spacing of the stores,
(ii) longitudinal stagger between adjacent stores, and
(iii) tandem carriage of the stores.

Fig 9 presents results from tests in the 2ft x 1½ft tunnel at RAE Farnborough in which drag measurements were made [17] on various arrays of stores mounted on 45° sweptback struts from the roof of the tunnel. The pylon extended one store diameter from the roof and so the stores were positioned just clear of the roof boundary layer; in effect, the stores were being tested close to a reflection plane simulating the surface of a wing with zero thickness. Results are shown in Fig 9 for two types of store, one with a pointed nose and the other with a hemispherical bluff nose. The results have been collapsed in the form of three interference drag factors, viz

$$K_y = \frac{\text{Drag of row of 2 stores}}{2 \times \text{drag of individual store}}$$ — for a row of 2 stores at different lateral spacings, y,

$$K_{st} = \frac{\text{Drag of staggered row of 2 stores}}{2 \times \text{drag of individual store}}$$ — for a row of 2 stores at a given lateral spacing (0.25 calibres) but different longitudinal stagger, X_{st},

(ie with zero stagger, $K_{st} = K_y$)

$K_T = \frac{\text{Drag of column of 2 stores}}{2 \times \text{drag of individual store}}$ for a column of 2 stores at different axial separation, X_T

The graphs in Fig 9 give an idea of what might be achieved ideally with these 3 basic concepts. It should be noted that the actual values of K_y, K_{st}, K_T and their variation with Mach number depend considerably on the shape of the store. Some of the main features of the results are described below.

6.1 Lateral Spacing

Two stores side-by-side at the close spacing (y = 0.015 calibres) typical of store carriage on standard twin carriers clearly gives appreciable adverse interference. the values of K_y increase from about 1.5 at low Mach number to maxima of 1.65-1.75 before decreasing to 1.3-1.4 at transonic speeds. The maxima in these curves occur at a Mach number close to the drag-rise Mach number M_{D_S} of the individual store if tested in isolation. Increased lateral spacing rapidly reduces the adverse interference at Mach numbers below M_{D_S}, the decrease with y at low speeds being predicted reasonably by the equation

$$K_y = 1 + \frac{0.42}{\exp(y'/0.42d)}$$

where d = store diameter
and y' = minimum distance between the two stores

Above $M = M_{D_S}$, the benefits of increased lateral spacing become less pronounced, the variation with y tending to disappear first at low values of y. Near and above M = 1, the changes in K_y with y only amount to about 0.1.

When applying this concept to an actual twin or triple carrier, other factors intrude, eg an increase in y will tend to give more surface area on the carrier body and will modify the interference between the stores and this body. On a practical installation, the variation of D/q with y can therefore be non-monotonic particularly at high subsonic speeds. This is yet another example of a phenomenon already noted in other areas, viz if one widens a channel between two surfaces, one can reduce low speed viscous interference but allow the supercritical flow to expand to a higher local Mach number, thus increasing the wave drag. In general, however, for aircraft with a heavy store load, it is probably the results at Mach numbers up to M_{D_S} that are important and thus, increased lateral spacing should be helpful. In addition to the reduction in drag, the increased lateral spacing should improve the release characteristics - less tendency for a collision during release and more opportunity to use an optimum ejection angle.

6.2 Store Stagger

A relatively small amount of stagger, eg X_{st} = 1 calibre is sufficient to displace the peak suction regions near the shoulders of the store and Fig 9 shows that this can reduce the drag significantly, particularly at Mach numbers near M_{D_S}. The values of K_{st} for y = 0.25 calibres are then about 1.2 as compared with maxima in the range 1.4 ~ 1.6 for stores with zero stagger. Having displaced the peak suction regions, there is then little further change in drag until the forward shoulder of the rear store has moved aft of the rear shoulder of the forward store. There is then a further reduction in K_{st}, eg for X_{st} = 4 and 6 calibres for the pointed nose store and X_{st} = 6 calibres for the bluff nose store. Values of K_{st} near 0.8 are then obtained at transonic speeds. The most sensible way of describing this result is to say that the favourable interference to be expected (see below) from carrying stores in tandem can still be achieved to some extent with store centres displaced laterally by 1.25 calibres.

Longitudinal stagger of the stores as a means of reducing the drag of loaded multiple carriers at high subsonic and transonic speeds was being suggested [18] as early as 1966 and again at an AGARD FMP conference [19] in 1973. Tests [4,5] on a 1/4 scale model of a standard triple carrier on the ARA isolated store drag rig showed that staggering the bombs on the shoulder stations by 0.92 calibres forward and aft of the bottom bomb reduced the drag by more than 20% at M - 0 9. These and other results have confirmed that stagger can reduce the adverse interference in a practical installation. The benefits affect more than just drag. forces and moments on both installed and released stores can be reduced, as illustrated in Fig 10.

These results in Fig 10 are taken from tests [20] in which the close interference forces and moments between two Mk 10 bombs mounted underwing on a standard twin carrier have been measured during simulated release of the inboard 'free bomb'. Tests were made with the bombs mounted side-by-side and staggered fore-and-aft, by ±1 calibre, the positive sign denoting that the inboard 'free bomb' is staggered aft. Load measurements were made on the sting-mounted 'free bomb' and the carrier-mounted 'captive bomb' and also pressures were measured on the lower surface of the carrier both along the carrier centre line and above the 'free bomb' centre line. Results for M = 0.80 are presented in Fig 10. The pressure distributions appearing above/below the bomb pictures were taken with the captive bomb respectively present and absent, the free bomb was slightly below its installed position. The bottom graphs show the effect of stagger on the variation of store pitching moment and yawing moment with vertical displacement of the free bomb with and without the captive bomb present.

The pressure measurements on the carrier clearly show that store stagger is effective in reducing the store-store and store-carrier interference. The shock strengths are reduced with both positive and negative stagger, the highest peak local Mach numbers being M_ℓ = 1.41 (1.41) for side-by-side carriage, M_ℓ = 1.30 (1.22) for positive stagger and M_ℓ - 1.26 (1.09) for negative stagger, the values in brackets referring to the single bomb case.

Poor release characteristics are often diagnosed as being due to the magnitude of the aerodynamic yawing moments and nose down pitching moments on the released stores and the results in the lower graphs indicate that positive stagger should be very helpful in both respects. Note. with positive stagger, moments for first bomb to be released are given by X_{st} = 1, captive bomb present and for the second bomb by X_{st} = 0, no captive bomb.

Mathews in Ref 4 also quotes an example where staggering the stores on an MER was found to reduce the installed pitching moments. He draws the conclusion that 'store staggering appears to offer considerable potential for both drag reductions and store separation improvements and that additional research in this area is highly recommended.'

6.3 Tandem Carriage

Returning to Fig 9, the bottom pair of graphs illustrate that carrying stores in tandem is a powerful method of obtaining favourable interference, particularly with bluff-nose stores. If the stores are virtually nose-to-tail, ie X_T = 0.005 calibres, the reduction in overall drag for a column of two stores amounts to about 30% near M = 1.0 for the bluff nose and 20% for pointed nose stores; even at a separation of 3 calibres, these figures are 20% and 15%. In inviscid subcritical flow, one would predict compensating buoyancy effects decreasing the drag of the front store and increasing the drag of the aft store. The actual measurements showed that with the stores close together, these opposing trends were present at $M < M_{D_S}$ but the increase in drag of the rear store was not sufficient to offset the reduction in drag of the forward store. At high Mach number near M = 1.0, the drag of even the rear store could be less than the drag of the store in isolation. Five mechanisms for drag reduction in a tandem arrangement were listed in Ref 4, viz

(i) the rear store is in a stream of reduced mean dynamic pressure,

(ii) at very small spacings, the nose of the rear store is in an essentially dead-air region behind the base of the forward store (this applies to stores with large effective base area),

(iii) the wake of the forward store can modify the flow separation characteristics from the nose of a relatively bluff rear store,

(iv) the rear store is in a stream of reduced Mach number and thus, the onset of wave drag from the rear store is delayed and also, the shock wave on the forward store is probably moved forward thus reducing the wave drag of this store, and

(v) the longitudinal cross-sectional area distribution of the combination is better than for the forward or rear stores in isolation and thus, the wave drag at transonic speeds will be less.

Once again, the concept of tandem carriage is not new. Ref 4 quotes results obtained [18] in 1966 at CAL showing that the drag increments due to adding 3 stores to the rear station of an MER was appreciably less than that from adding the first 3 stores to the empty carrier - by 15% at M = 0.8 or more than 40% at M = 1.2. Drag results for tandem carriers [3] and for tandem arrangements [21] of stores under a fuselage are also quoted in Ref 4; all show large drag reductions broadly consistent with Fig 9, the improvements being frequently about 40% at transonic speeds and particularly noticeable for stores with a completely bluff nose. Methods for the quantitative prediction of these effects are being developed.

In addition to the drag improvements, tandem carriage can also lead to better release speeds. Tests on a model of the Phantom showed that the store installed loads for tandem carriers were of the same order as for a standard twin carrier; the moments were in fact somewhat smaller. Even with the same loads, release from a tandem carrier could be preferable because sideways movement during release does not have to be limited because of the proximity of an adjacent store as with a twin carrier. Cases have however been reported where tandem carriage has introduced additional release problems.

The general case for tandem carriage on grounds of drag and store release is very strong and the concept should be exploited whenever possible. It is appreciated that carrier flexibility, CG/stability considerations can raise problems but it is hoped that the latter will be less serious on future aircraft equipped with active control technology.

7 FEASIBLE DRAG IMPROVEMENTS FOR PRACTICAL STORE ARRANGEMENTS

Research over the past 10 years has shown that large improvements in the drag of multiple external store arrangements are feasible. The improvements are achieved by judicious application of the concepts discussed in §6 and by refining the general aerodynamic cleanliness of the assemblies, eg by fairing of external sway braces. The reductions in drag imply less adverse interference, better flow, weaker shocks, less extensive separations and so in many cases, the reductions in drag should be accompanied by smaller installed loads and better and more predictable release characteristics. Figs 11a-c,e,f, illustrate the reductions in drag thought to be feasible; in all cases, present in-service equipment is taken as the datum for comparison. In most cases the curves labelled 'feasible', 'best conventional' or 'radical' are based on actual test data and are for arrangements that it is thought, could be engineered in practice, eg the carriers were designed to allow space for the ejector release units and are not idealised configurations.

7.1 Carriers

The scales of all the graphs are the same, the stores in all cases are Mk 10, 454 kg bombs. To this extent, the results are specific but the gains are so large that hopefully, this is of little consequence. Summarising the results for say, M = 0.85:

(i) the drag of the fully loaded triple carrier, Fig 11a, can be reduced to only about 33% of the fully loaded standard CBTE. As a measure of the achievement, the drag of the feasible triple carrier at this Mach number is only about 20% greater than the simple sum of the isolated drags of three separate bombs and the empty carrier. Three bombs can be carried for less drag than a single bomb on the present in-service triple carrier or two bombs on the present in-service twin carrier,

(ii) the drag of the empty triple carrier, Fig 11b, can be reduced to less than 25% of the drag of the empty standard triple carrier and in isolation, the drag-rise can be postponed to about M = 0.98,

(iii) the drag of the loaded twin carrier, Fig 11c, can be reduced to less than 60% of that of the standard twin carrier of the type shown. Relative to the practice adopted on some aircraft of carrying two stores on a standard triple carrier, the figure is less than 30%.

These figures are for carriers in isolation. The improvements may be even larger if the carrier is mounted underwing but might not be as great if a number of carriers are installed close together underfuselage (unless the whole array was then designed as a unit).

Many factors enter into the design of a good twin carrier. These include the lateral spacing of the stores, the store ejection angle, the longitudinal stagger of the stores, the surface area, fineness ratio and shape of the carrier itself. The standard twin carrier has a body in the form of a thick faired plate of low aspect ratio but various other possible types of twin carrier can be envisaged as shown in Fig 11d. Oil flow patterns [4] from 1/4 scale model tests at ARA have shown that with poor twin carrier designs

(a) there can be considerable outflow over the bomb nose, rolling up to form a vortex over the top of the bomb with a clearly defined secondary separation line,

(b) the flow diverts downwards and accelerates over the bomb nose leading to a shock in the entry to the bomb-carrier passage, this shock being strong enough to induce a local flow separation,

(c) air is sucked through the gaps between the bombs and carrier body near and between the fixation bolts, thus adding to the confused flow situation further aft.

With a good twin carrier design, however, these features are much less pronounced and indeed, the flow over the bombs can appear to be relatively innocuous [4].

7.2 Underwing Stores

Fig 11e compares four different methods of carrying three underwing stores. The measured data on which the curves are based were actually obtained from tests on more than one wing but they have been converted in an approximate but realistic manner to allow for the effects of wing design and so, Fig 11e can be assumed to be a genuine comparison for a given wing. The four curves refer respectively, in order of increasing merit, to

(i) conventional carriage on a standard in-service triple carrier as on for example, the F-4 Phantom,

(ii) conventional carriage with the same three stores mounted on three separate pylons as in the arrangements discussed earlier in §§3,4,

(iii) 'best conventional' carriage with the stores mounted on a mix of improved carriers and pylons, and

(iv) a 'radical' arrangement based on recent research.

The comparison in Fig 11e is dramatic. For example, at a likely operational Mach number, even the 'best conventional' arrangement is capable of reducing the drag increment to less than 65% of the value for the simple arrangement on three separate pylons and less than 40% of that of the in-service arrangement with a standard triple carrier. The drag increment for the 'radical' arrangement at low Mach number is less than half that with the 'best conventional' arrangement and shows little change with Mach number up to a value far in excess of the incremental drag-rise Mach number with any of the other arrangements.

7.3 Underfuselage Stores

Fig 11f presents a similar comparison for multiple arrangements of bombs underfuselage. The three curves relate to

(i) 'current practice' with the bombs mounted on standard multiple carriers,

(ii) a 'best conventional' arrangement in which the store array is designed to exploit stagger and tandem carriage, and

(iii) a radical arrangement exploiting all possible features of conformal carriage (see 8 below).

It should be noted that the model chosen for this comparison is not the same as for the underwing store comparison and to that extent, it may be misleading to present the two figures side-by-side. Nevertheless, the implication that it is preferable to carry a heavy store load in arrays under the fuselage rather than underwing can be accepted as a valid conclusion (although the differences are much less if one can succeed on a new aircraft to adopt a radical approach to underwing carriage). Other examples supporting this conclusion and drawn from US research [21,23] are to be found in Ref 4.

Fig 11f suggests that relative to (i), it is possible with (ii) to reduce the drag by almost 40% and to achieve a gain in drag-rise Mach number of about 0.2. With the radical underfuselage arrangement, the drag increment is less than half that obtained with (ii). With both (ii) and (iii), the drag increment at high subsonic and transonic speeds is less than the free-air drag of the bombs in isolation, ie with (iii), less than half the free-air drag: an outstanding example of configuration optimisation if indeed, the research worker is correct in claiming that the radical approach which produced these results could be engineered in practice. Some radical concepts are described in Ref 22. Ideally, the stores should be mounted tangentially (or semi-submerged if the penalties of empty cavities after the stores have been dropped [23] can be minimised) in tandem with close longitudinal spacing, with due regard to the longitudinal distribution of cross-sectional area for the complete configuration and with the ejector units and indeed, the stores hidden or partially hidden within the fuselage or behind a specially devised fairing. We have therefore now arrived at the theme of conformal carriage which is clearly the prime approach for mounting stores in a way that will exploit favourable aerodynamic interferenc

8 CONFORMAL CARRIAGE

The aim with conformal carriage is to carry the external stores as closely as possible to the external surface of the aircraft. The best way of accomplishing this is to either extend the surface of the aircraft to meet the stores or to enclose the mounting racks within the aircraft so that the stores meet the surface. The primary emphasis to date has been on fuselage mounted arrangements, the advantages of which have been demonstrated in flight on at least the F-4 and F-15 aircraft in the United States. It seems probable that wing-mounted conformal arrangements could also be developed. To date, slipper tanks have been the only common example of this approach.

It should be remembered that the conformal carriage concept has other major advantages apart from drag reductions, eg it allows the use of bluff stores which would give unacceptable performance penalties if mounted on external carriers but which one may wish to use for the sake of their desirable release and trajectory characteristics and second, it allows the use of locations which may have a notable benefit on the aircraft stability, control and handling qualities. Concentrating the loadings closer to the aircraft rotational (stability) axes can improve the inertial qualities to the extent that an aircraft laoded with stores behaves comparably with an unloaded aircraft, the major difference in 'feel' to the pilot being merely that due to the greater vehicle weight. Various practical problems may however make conformal carriage difficult to engineer on some aircraft, these problems are however outside the scope of the present lecture.

The outstanding examples in the published literature of a conformal carriage approach are first, the special stores adaptor, designed, fitted and flight tested [25] on the F-4 Phantom and second, the conformal fuel tank installation, [26] 'Fast Pack' that has now been fitted to the F-15. The results from the F-4 programme have been extensively reported elsewhere [2,4,5,25] and will not be repeated in detail here. The conformal carriage adaptor provided 49 alternative positions for mounting ejector racks below the fuselage including for example, three rows of four racks side-by-side. The fairing over these racks provided a clean, smooth installation on the underside of the fuselage and both flight and tunnel tests showed that the subsonic drag of the F-4 with the conformal adaptor was less than the drag of the clean aircraft. A similar result was obtained with the F-15 'Fast Pack'. It would be easy to dismiss these as particular, somewhat coincidental achievements but in fact, it could be claimed that they show the potential usefulness of the conformal arrangements in improving the aerodynamic cleanliness of an overall combat aircraft configuration.

Nichols [2,4,24,25] highlights the value of combining the concepts of conformal carriage and the use of bluff stores which are likely to have superior store separation, trajectory and impact characteristics. To carry these stores in any fashion other than conformal carriage would produce very large drag increments but in the F-4 tests, flying with a compact array of 9 bluff stores (ordnance almost 40% greater than 12 Mk 82) gave a specific range at low altitude greater than for the clean F-4 up to a Mach number of $M = 0.85$. Tests were made with an additional fairing installed on the forward ramp ahead of the stores, and this improved the performance, stores on.

The main conclusion [24] from the F-4 programme was that the performance advantages of conformal carriage had been convincingly demonstrated in both the flight and the supporting wind tunnel tests. Obviously, the precise quantitative results were a function of the aircraft design and it would not be possible on all aircraft to design retrospectively arrangements that would give such large performance advantages. However, the results should provide the spur to design new aircraft with conformal carriage in mind from the outset.

Turning to the second example, the flight test programme [26] undertaken by McDonnell Douglas Corp, showed that two fuel pallets mounted in the wing-fuselage junction of the F-15 as shown in Fig 12a could provide an additional 5808 litres fuel capacity without undue compromise to the air superiority capability of the basic aircraft. Each pallet, or tank, had a streamline shape designed with regard to the longitudinal cross-sectional area distribution of the complete aircraft-tank combination. Fig 12a also illustrates that the conformal pallet could be used not only for fuel storage but also to carry electronics, weapons or guns. Additional payload could be tangentially attached externally. Fig 12b showed that the addition of the pallets reduced the subsonic drag level and delayed the drag-rise, at supersonic speeds, it allowed the carriage of 5808 litres of fuel for a drag increment that was only about 40% and 65% respectively of the drag increments for 4828 litres carried conventionally underwing or 6791 litres carried partly underwing and partly underfuselage: a major achievement fully justifying the suggestion that on new aircraft in the future, the aim should be to design with these radical ideas for store carriage in mind from the outset.

9 CONCLUDING REMARKS

The two main aims of this lecture have been first to describe the nature of the major adverse and favourable aerodynamic interference encountered with external store installations and second, to present some examples of the improvements that should be feasible. The main conclusions are as follows:

1) With existing external store arrangements, the drag increments can be very large and the release characteristics can pose serious problems.

2) Research has already shown how major improvements could be achieved. Many of the proposals should be feasible even on existing aircraft. Larger improvements should be possible on new aircraft types provided the external store requirements are specified and borne in mind in the early phases of the design.

3) To obtain the full benefit from advanced wing design, the wings should be designed with due regard to store carriage. In particular, the wing/underwing pylons should be considered together. If this is done, it should be possible to alleviate adverse interference at low C_L and to achieve some favourable interference on the flow breakdown at high C_L at moderate and high subsonic speeds.

4) Research should be undertaken to exploit further the favourable interference possibilities of wing tip carriage of slender missiles.

5) New multiple carriers and underfuselage arrays of stores should aim to exploit the concepts of tandem carriage and store stagger and should avoid very close lateral spacing of the stores.

6) For new aircraft, the complete configuration should be designed as an entity with due regard to its longitudinal cross-sectional area distribution and with the stores mounted either in conformal packages or from conformal pallets.

Research to date on conformal carriage has pointed the way. The theoretical methods now available provide the means. It is hoped that this lecture will have helped to stiffen the resolve to develop new radical approaches to store carriage.

10 ACKNOWLEDGEMENTS

The author wishes to thank MOD(PE) and RAE for permission to use some of the material contained in this lecture. Most of the results of tests in the ARA transonic tunnel quoted in the lecture were obtained in research funded under MOD(PE) research contracts. Parts of this lecture are based directly on Chapter 2 of the AGARD FDP Working Party Report [4] on 'Drag and Other Aerodynamic Effects of External Stores', for which Mr J H Nichols Jr of DTNSRDC and the present author were joint editors.

REFERENCES

1 Haines, A B, The reduction of the installed drag of multiple store carriers, 1975, Paper no 7, JTCG Aircraft/Stores Compatibility Symposium Proceedings, Arlington.
2 Evaluation of the conformal carriage concept on the performance and basic static longitudinal stability of the F-4E aircraft, 1971, AFATL-TR-71-76.
3 Haines, A B, Drag of external stores: present standards and possibilities for reduction, 1975, ARA Report 40.
4 Drag and other aerodynamic effects of external stores, 1977, AGARD-AR-107.
5 Haines, A B, Prospects for exploiting favourable and minimising adverse aerodynamic interference in external store installations, 1980, Paper no 5, AGARD CP 285.
6 Whoric, J M, Effect of various external stores on the static longitudinal stability, longitudinal control, and drag characteristics of the model F-4C airplane, 1973, AEDC-TR-73-186.
7 Berry, J B, Stanniland, D R, Haines, A B, The implications of wing/store interference on wing design, Unpublished ARA communication.
8 Day, J, Berry, J B, Measurements of the incremental drag due to various combinations of Mk 10 1000 lb bombs installed on the Z29/2 combat aircraft wing research model, Unpublished ARA communication.
9 Berry, J B, Hutton, P G, Haines, A B, The drag of external stores. An analysis of some experimental data and a proposed framework for the prediction of installed drag increments, 1969, ARA Report 11.
10 Ottensoser, J, Some effects of longitudinal and vertical store position variation on a 0.10-scale F-8 aircraft model, 1968, NSRDC Test Report AL-46.
11 Berry, J B, Pressure plotting and drag measurements on store-pylon installation on a swept wing half model, 1978, ARA Report 47.
12 Marshall, J B, Summers, W E, An analysis of the relative importance of parameters required for the simulation of store separation trajectories, 1971, Vol 2, JTCG Aircraft/Store Compatibility Symposium Proceedings, Dayton, Ohio.
13 Wood, M E, ARA unpublished communication.
14 Silvers, H N, King, T J Jr, Investigation at high subsonic speeds of bodies mounted from the wing of an unswept-wing-fuselage model, 1952, NASA RM L52J08.
15 Bucciantini, G, Private communication, 1975.
16 Hoerner, J F, Fluid-dynamic drag, New York, Hoerner, 1965.
17 Lee, P, Drag measurements at transonic speeds of individual stores within multiple store arrangements, Unpublished RAE memo.
18 Analysis of high speed wind tunnel tests on single and multiple carriage bomb racks, 1966, Douglas Aircraft Co Inc Report No LB-32647.
19 Pugh, P G, Hutton, P G, Aerodynamic drag, 1973, Paper no 19, AGARD CP 124.
20 Jordan, R, Measurement of close interference forces between bombs on a twin carrier during simulated release. Effects of stagger and bomb incidence, Unpublished ARA communication.
21 Ottensoser, J, Drag effects of various methods of carrying fuselage mounted stores, 1968, NSRDC Aero Report 1150.
22 Gough, M N, Carlson, D R, Advanced weapons carriage concepts through integrated design, 1979, AIAA Paper 79-0092.
23 Furey, R J, Martin, C J, A study of captive flight drag and separation characteristics of lifting body (half-bomb and half-pod) store configurations, 1970, AGARD CP 71.
24 Nichols, J H Jr, Martin, C J, Conformal weapons carriage - Joint Service Development Program, 1971, DTNSRDC Report 4027, AL-1188.
25 Nichols, J H Jr, The conformal carriage Joint Service Development Program, 1973, JTCG Aircraft/Stores Compatibility Symposium, Sacramento.
26 F-15 weapon/fuel carriage improvements with Fast Pack conformal pallets, 1975, McDonnell Douglas Report MDC A 3507.

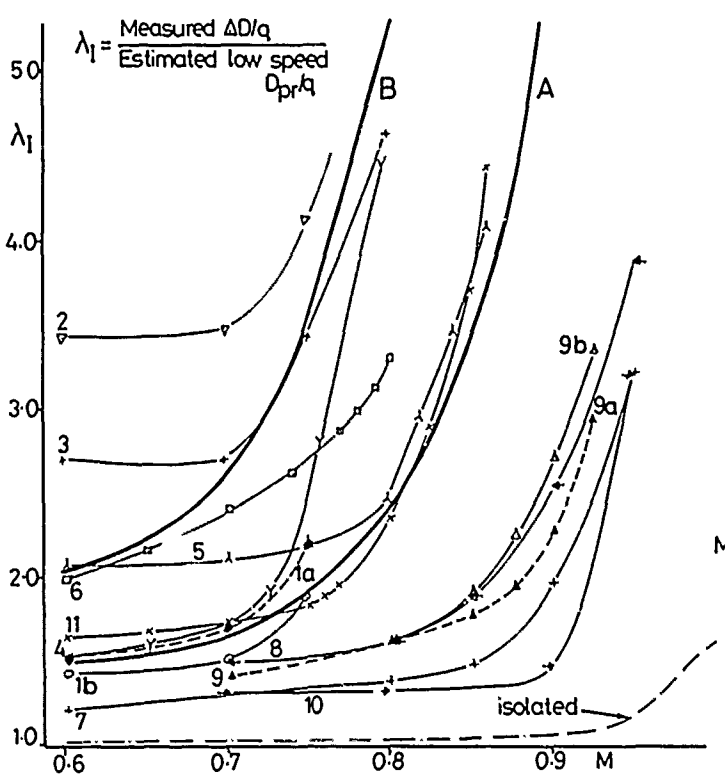

a. INSTALLED DRAG FOR 15 EXAMPLES : $C_L = 0$

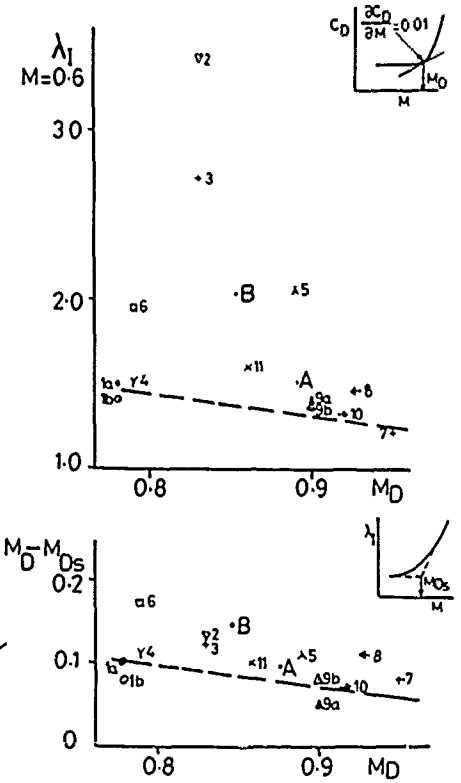

b. ANALYSIS OF INSTALLED DRAG
$C_L = 0$

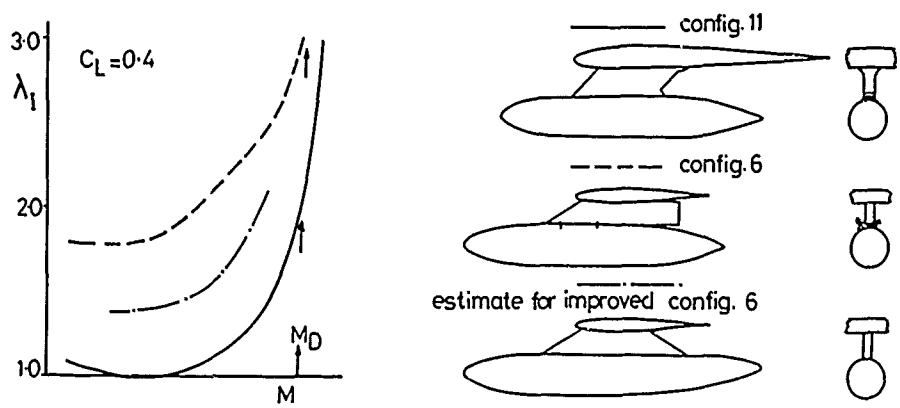

c. EFFECT OF TANK INSTALLATION

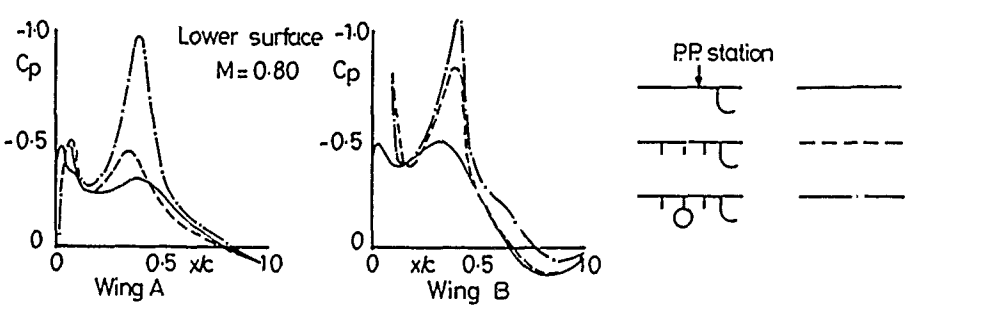

d. EFFECT OF WING DESIGN (TWO WINGS OF SAME PLANFORM)
$C_L = 0$

FIG. 1 EFFECT OF UNDERWING TANKS

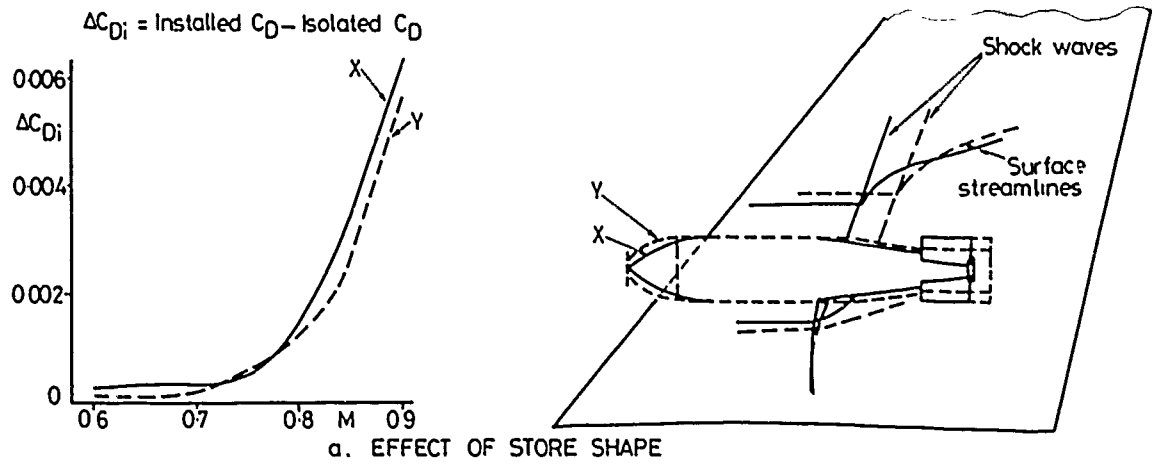

a. EFFECT OF STORE SHAPE

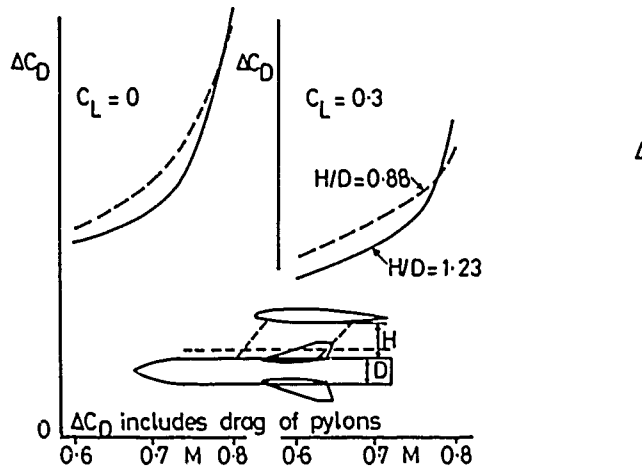

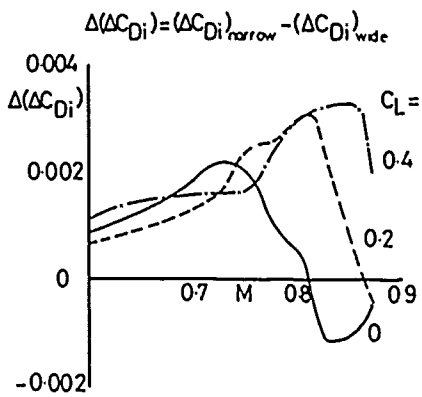

b. EFFECT OF STORE VERTICAL POSITION

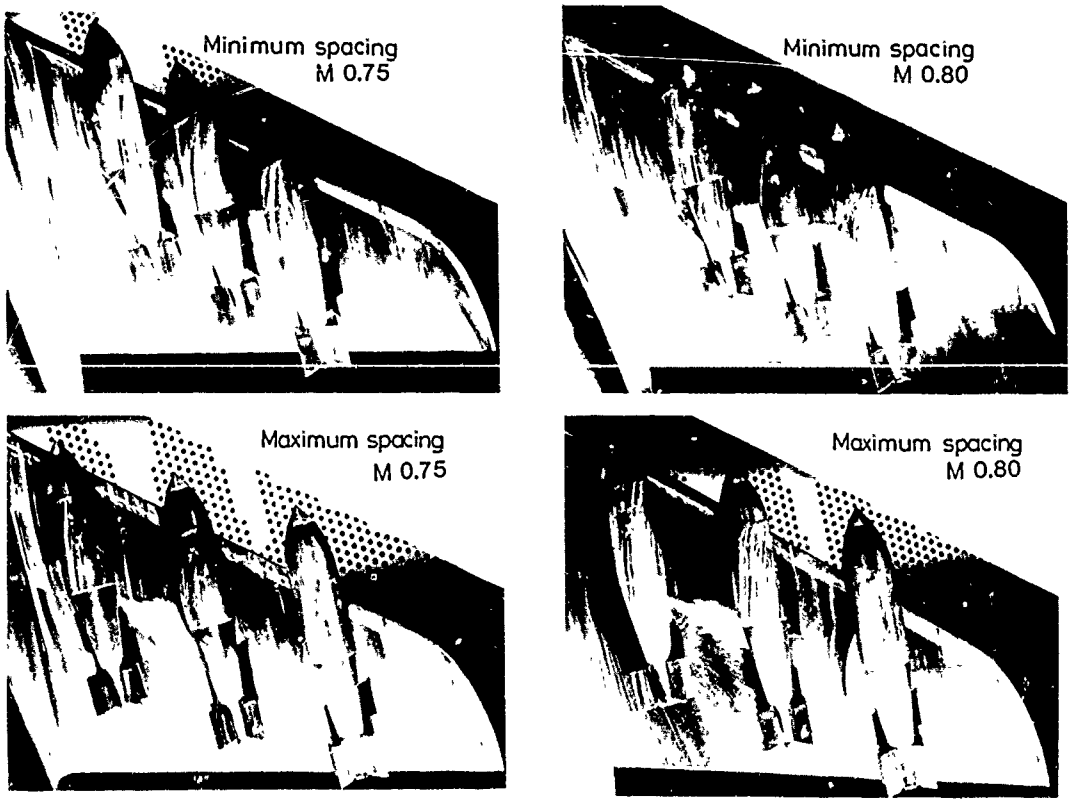

c. EFFECT OF LATERAL SPACING (3 STORES ON SEPARATE PYLONS)

FIG.2. EFFECT OF UNDERWING STORES AT LOW C_L

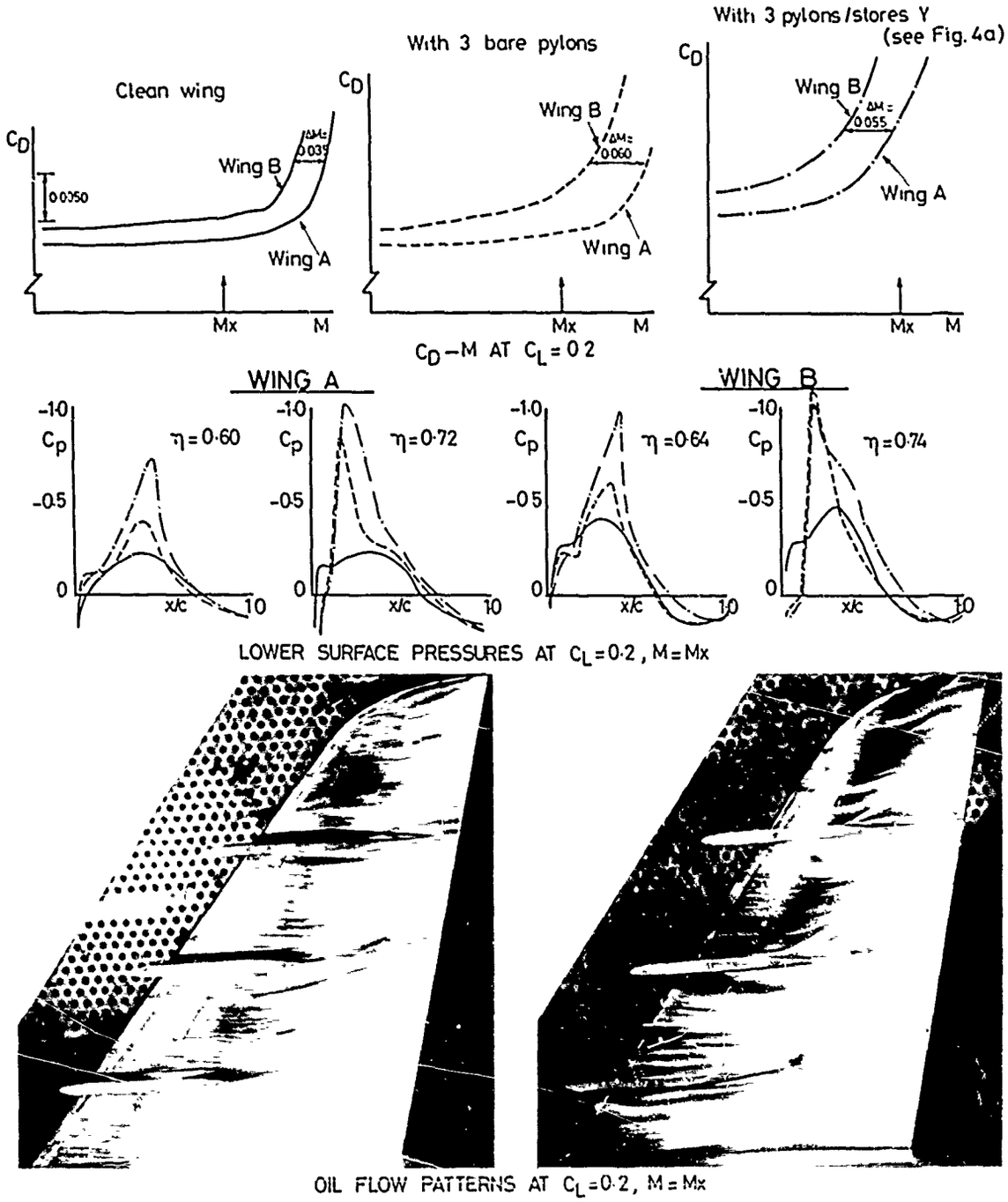

FIG.3. INFLUENCE OF WING DESIGN ON UNDERWING STORES/PYLONS AT LOW C_L

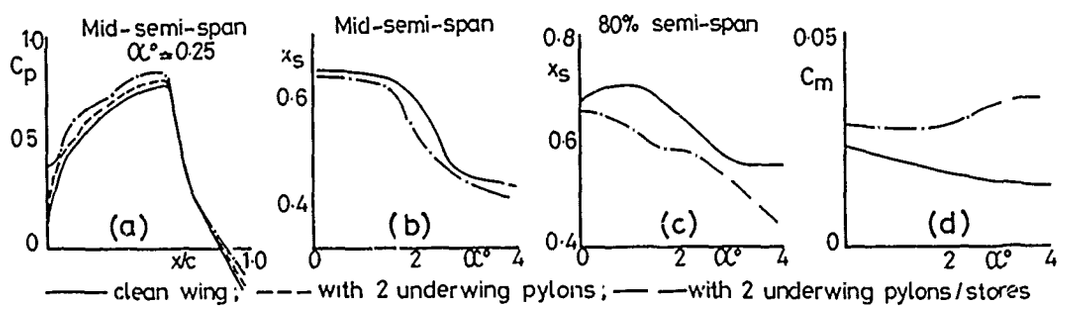

FIG.4. EFFECT OF UNDERWING STORES ON UPPER SURFACE FLOW

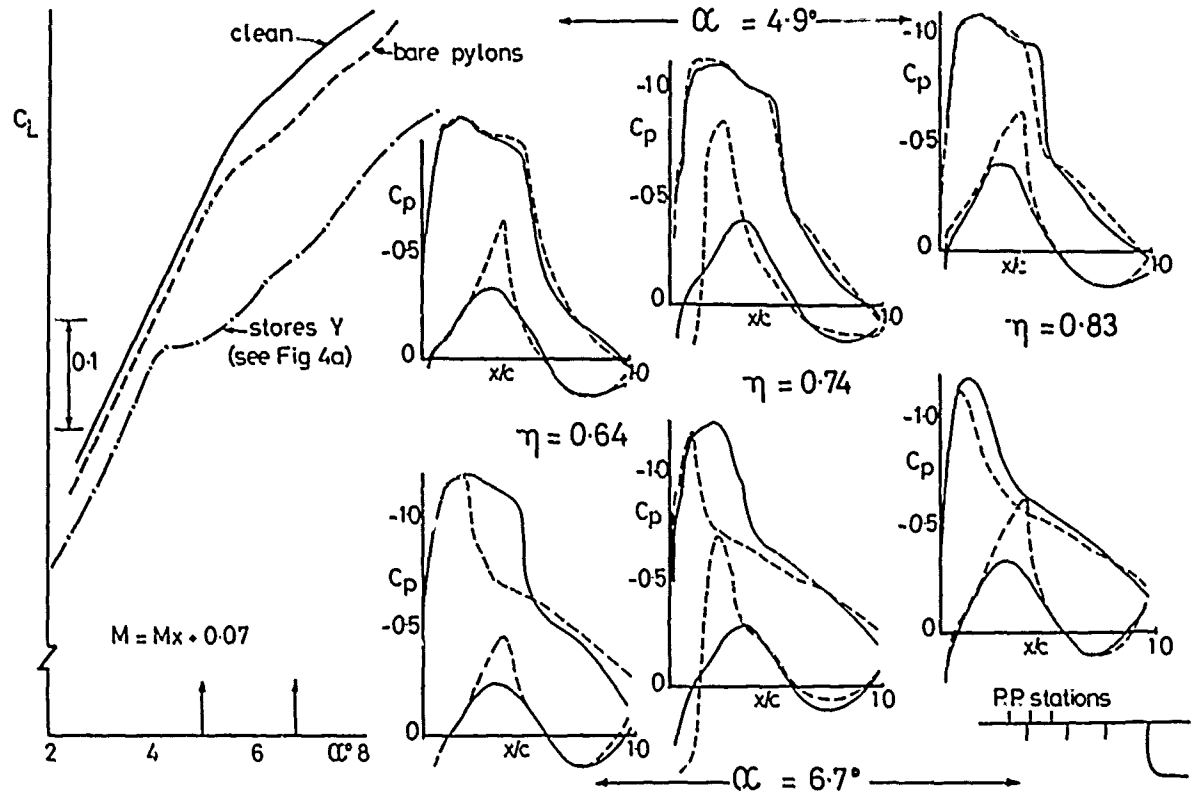

EXAMPLE OF ADVERSE INTERFERENCE

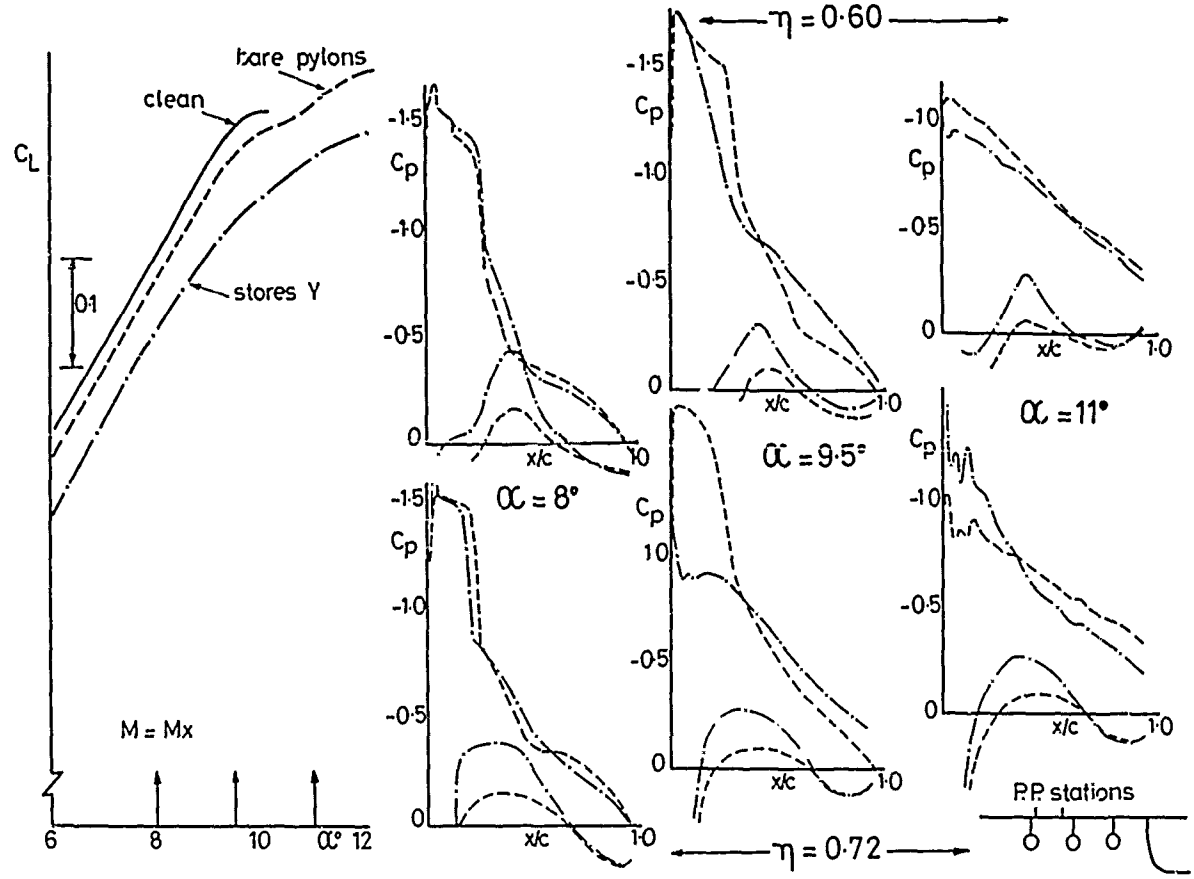

EXAMPLE OF FAVOURABLE INTERFERENCE (see text)

FIG.5. EFFECT OF UNDERWING STORES AT HIGH C_L

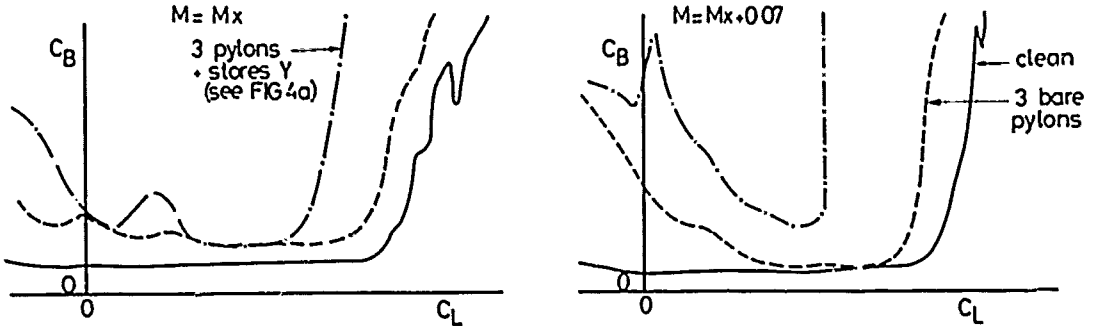

FIG. 6. EFFECT OF UNDERWING STORES ON BUFFET

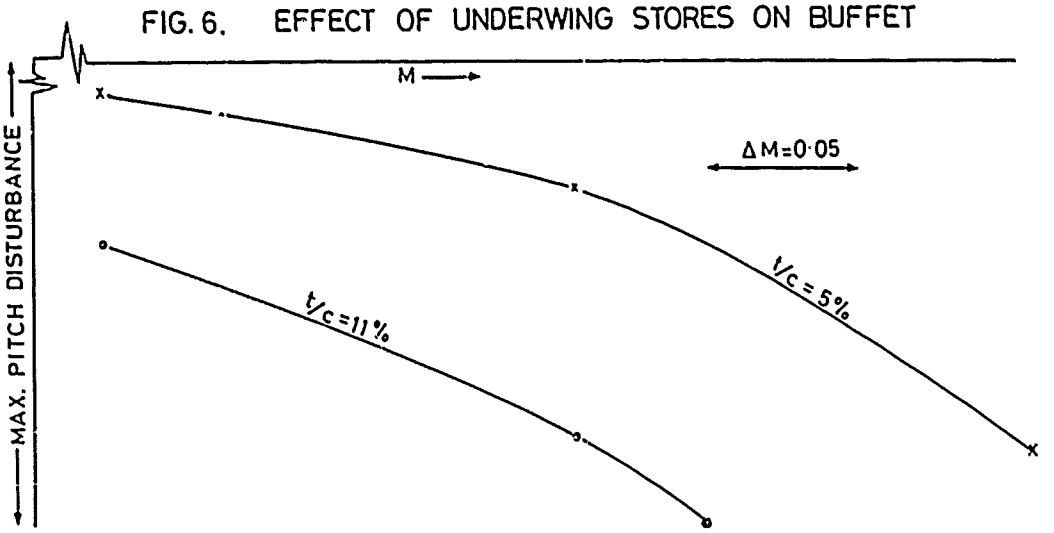

FIG.7. EFFECT OF WING THICKNESS ON THE RELEASE DISTURBANCE OF A STORE

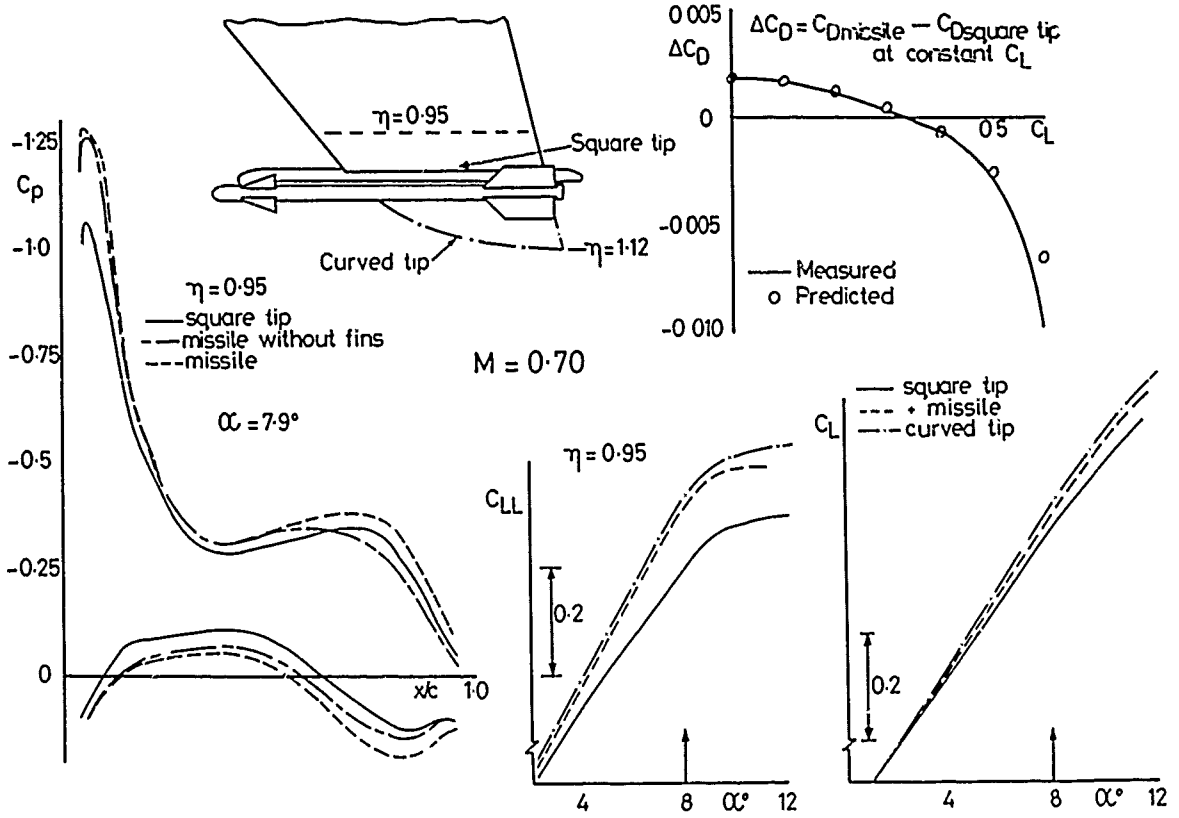

FIG.8. EFFECT OF WING TIP-MOUNTED STORES

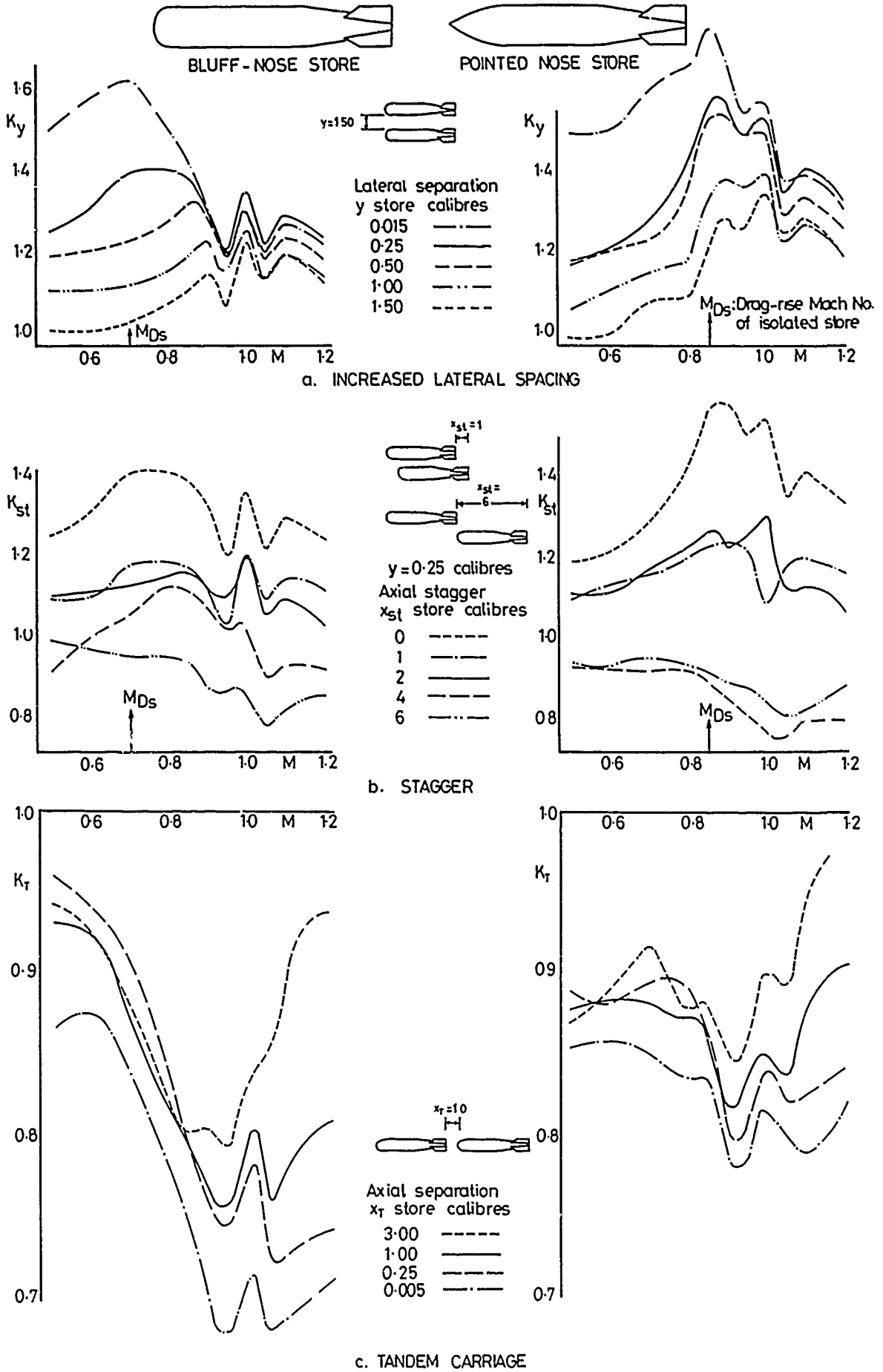

FIG.9. FAVOURABLE INTERFERENCE CONCEPTS

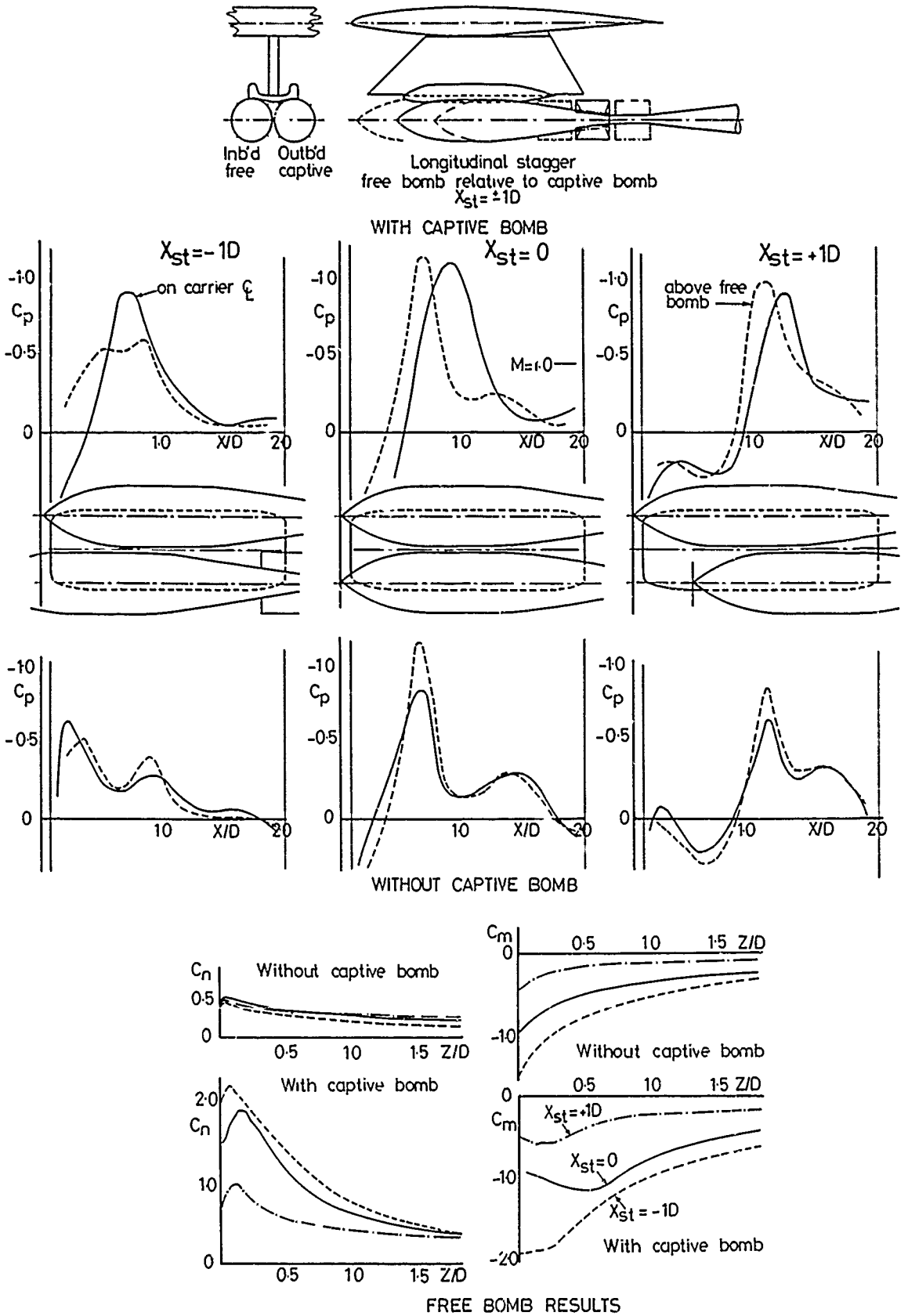

FREE BOMB RESULTS

FIG.10 EFFECT OF STAGGER ON STORE RELEASE LOADS FROM TWIN CARRIER : M=0·80

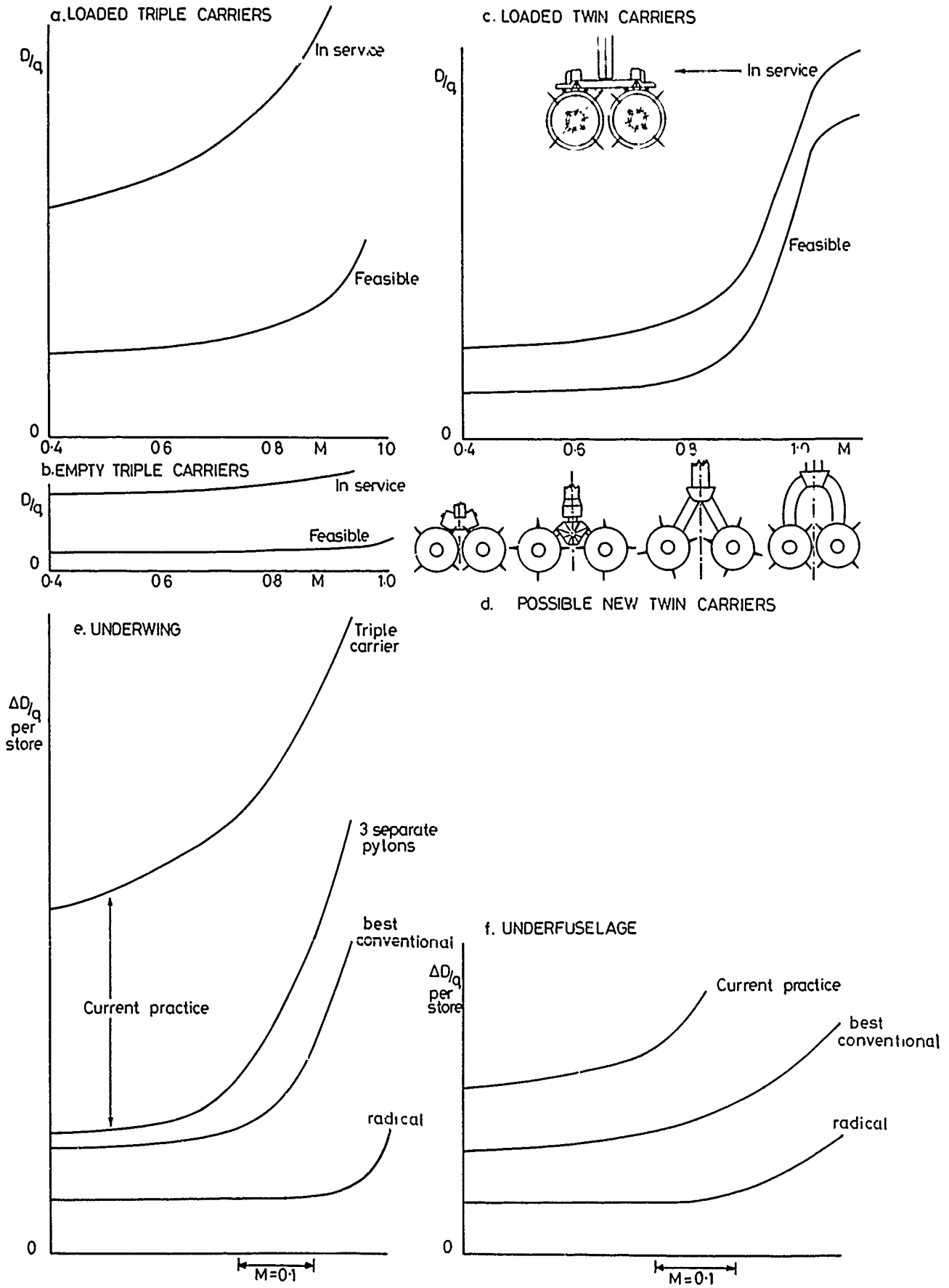

FIG. 11. FEASIBLE DRAG IMPROVEMENTS

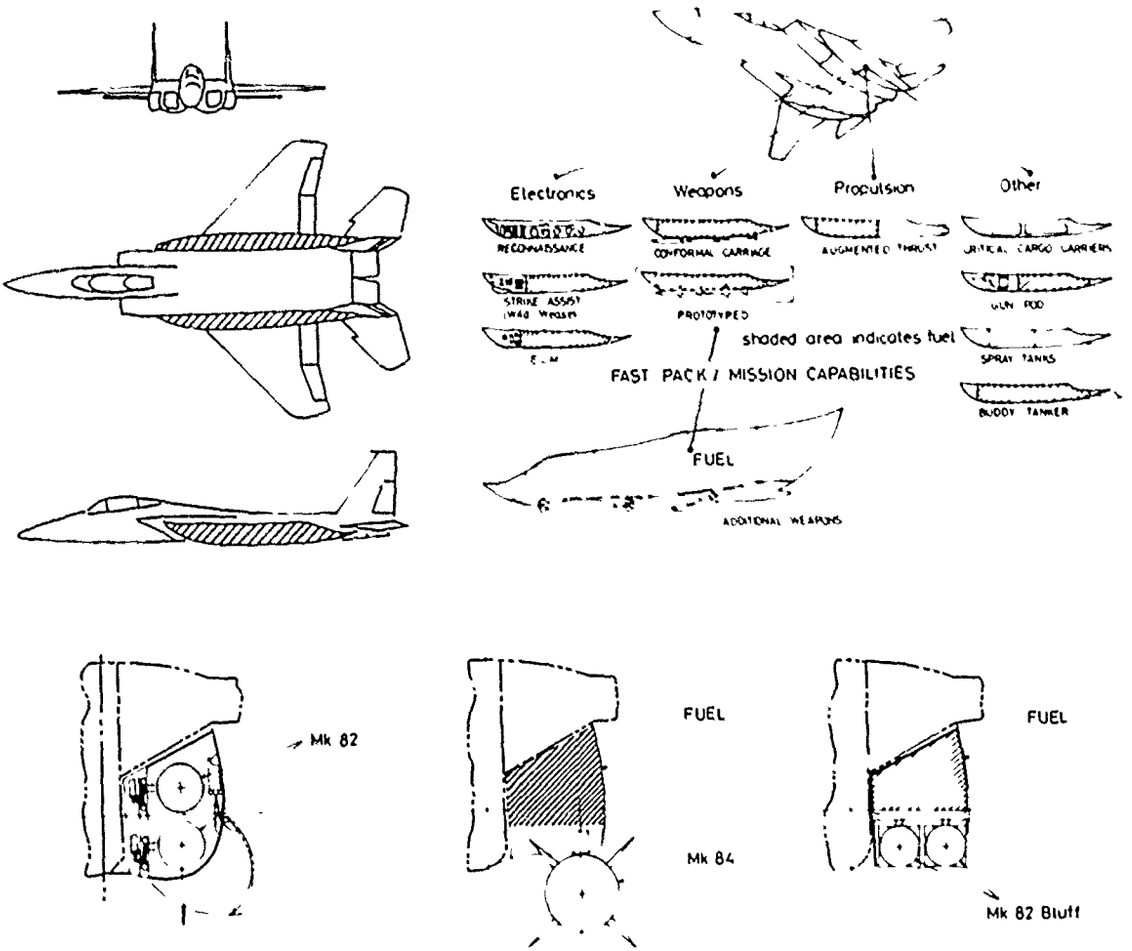

a. POSSIBLE FUEL/STORE ARRANGEMENTS

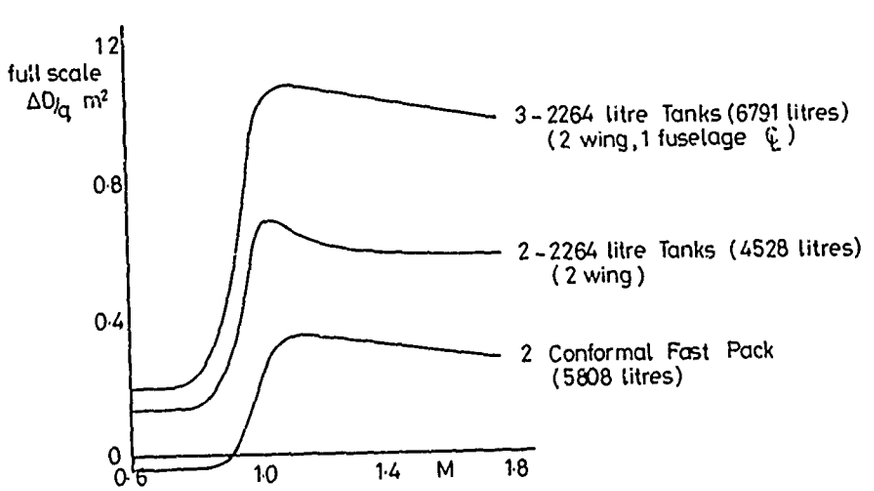

b. TYPICAL REDUCTIONS IN DRAG INCREMENT

FIG. 12 F15 – CONFORMAL CARRIAGE STUDY

INTERFERENCE PROBLEMS IN AIRCRAFT DESIGN

I. H. Rettie
Unit Chief Aero Research and Development
The Boeing Commercial Airplane Company
P.O. Box 3707 M/S 79-93
Seattle, Washington, 98124 - U.S.A.

SUMMARY

The nature of aerodynamic interference among the components of an aircraft is examined. Some of the flow mechanisms involved are studied with the help of theoretical flow models with the objective of identifying design guidelines for the avoidance of performance or other penalties. The possible achievement of favorable interference in some cases is also discussed. Emphasis is placed upon the growing capability of computational methods which allow the designer to explore interference effects during the early phase of a design prior to wind tunnel tests.

INTRODUCTION

Interference flows in aerodynamics represent both a source of major development problems and an opportunity for performance improvement. To take appropriate action, the designer requires in both cases a good physical understanding of the flow processes involved and also an adequate theoretical model of the flow so that quantitative modifications can be made. The recent developments in high-speed digital computing enable the modelling of quite complex flows including many viscous flow phenomena. It is therefore very timely to review current experience of interference flow phenomena and to explore the ways in which Computational Fluid Dynamics (CFD) has been used to understand, cure and exploit the situation as required in each case.

Each type of air vehicle exhibits its own class of interference problem. Basically, however, these are of the same nature. Flow direction and velocity over one component is affected by the flow field of another. In supersonic flows the interference effects are usually very evident from the patterns of shocks and other waves. At high supersonic Mach numbers the effects can become very localized and the opportunities for favorable interference are clearly seen from, for example, the impingement of compression waves from an engine air inlet cowl on the aft facing surface of a rear fuselage. At subsonic speeds the effects are more subtle, but fundamentally similar and it is often the case that an aerodynamicist trained in supersonic flow design work will find it easier than most to appreciate the interference mechanisms involved. In general, the so-called "area rule" approach is a valuable tool at all speeds, but away from a Mach number of unity in both directions (subsonic and supersonic) the spacial relationship of components is important.

An important type of interference occurs as a result of vortex flows. These are, of course, very important in the wake of an aircraft and separation minimums are now required in landing patterns particularly when a small aircraft is following a jumbo jet. Aircraft designers are today much more aware of the effects of part-span vortices from the wing on the horizontal tail. Recently a great deal of attention has been drawn to the handling characteristics of commercial aircraft in conditions beyond normal attitudes in the region of buffet onset and mild buffet. In some cases, vortices shed from components such as engine nacelles can be controlled so as to enhance the wing flow. In other cases small vortices can be created in the flow so as to inhibit separation of the boundary layer. Small vortex generators are frequently mounted on the upper surfaces of wings and on aft bodies. On the Short Bros. and Harland Belfast Freighter, vanes were used on the highly upswept body. On most recent jetliners with large, high-bypass-ratio engines, "ears" can be seen on the upper nacelle cowls which direct the vortices to pass low over the wing upper surface and so avoid premature flow separation. The inboard ear can in fact be tuned so as to allow separation at a given lift coefficient in order to improve handling characteristics at incidences near stall.

A good example of an aircraft design in which interference problems had to be carefully investigated at all stages of the design is the Boeing YC14 prototype military freighters (Figure 1). The flow over the inboard wing is dominated by the effects of upwash generated by the body and nacelles. At low speeds the suction induced by the engine air inlet has an important effect. For this reason, care was taken during the development program to represent the inlet flow in wind tunnel tests by means of turbine powered simulators. In most other testing, the nacelle was domed over and the exhaust flow simulated by blowing. The reasons for this are the greater accuracy of the blown nacelle and the unreliability of turbine powered simulators. This latter problem is one which is now being satisfactorily resolved as a result of design development.

The interference between the nacelle exhaust flow and the wing trailing edge is really a very wide issue which will not be explored here in detail. Attachment of the engine exhaust flow to the wing trailing edge skin and flap system (the "Coanda" effect) enhances the lift of the wing at all forward speeds. Another important effect on the

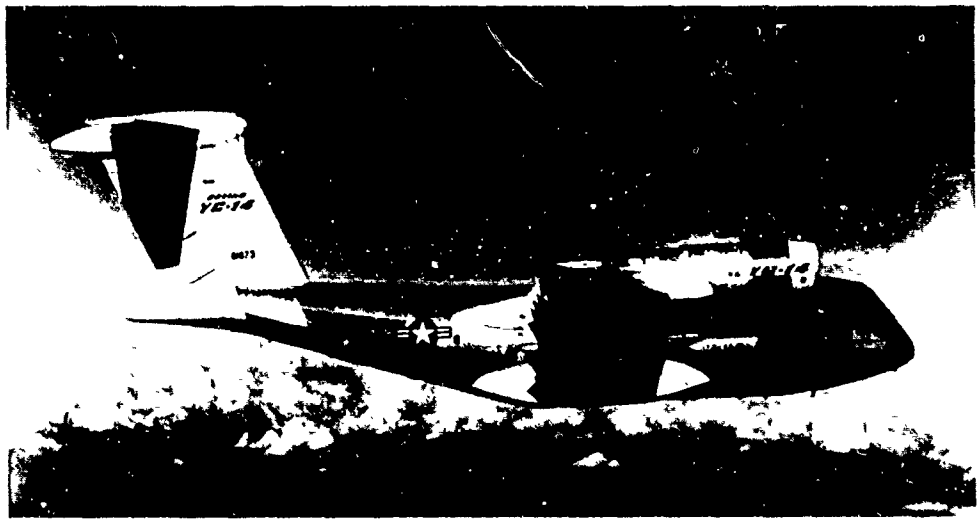

Figure 1: Boeing YC-14

wing, particularly in cruise, is that of the landing gear fairings on the lower corners of the body. Such interference may be expected to be adverse simply on the basis of an area rule computation. In fact, what happens is that the acceleration of the flow induced by the landing gear fairings reduces the levels of pressure on the lower surface of the wing thus causing a loss of lift. Attitude has to be increased in order to recover this, resulting in an increase of drag.

Perhaps the most obvious aerodynamic interference flow in a conventional configuration is the downwash associated with the wing wake over the horizontal tail and aft body. The effect on the horizontal tail is well known from elementary stability theory. At first sight, the effect on the aft body appears favorable since the downwash tends to offset the crossflow over the aft body caused by body incidence. However, particularly in the case of an upswept aft body with the generally flattened underbelly typical of a military transport, the flow along the keel line is relatively unaffected by the downwash. This flow and the flow along the side of the body are bounded by a separation line on the lower part of the body side. From this line, vortex flows emanate which contain significant amounts of energy or drag. Strakes such as those referred to earlier on the Short Belfast are effective in controlling and reducing the drag of these vortices.

Figure 2 shows a typical flow problem on a more conventional aft body. There are three flow mechanisms: the basic flow over the body at incidence, the wing downwash and the junction flow between the body and the horizontal tail. Such junction problems are usually suppressed by a small strakelet at the leading edge. This does not eliminate the junction vortex which is determined by the span loading, but it reduces consequential effects by improving smoothness of the flow.

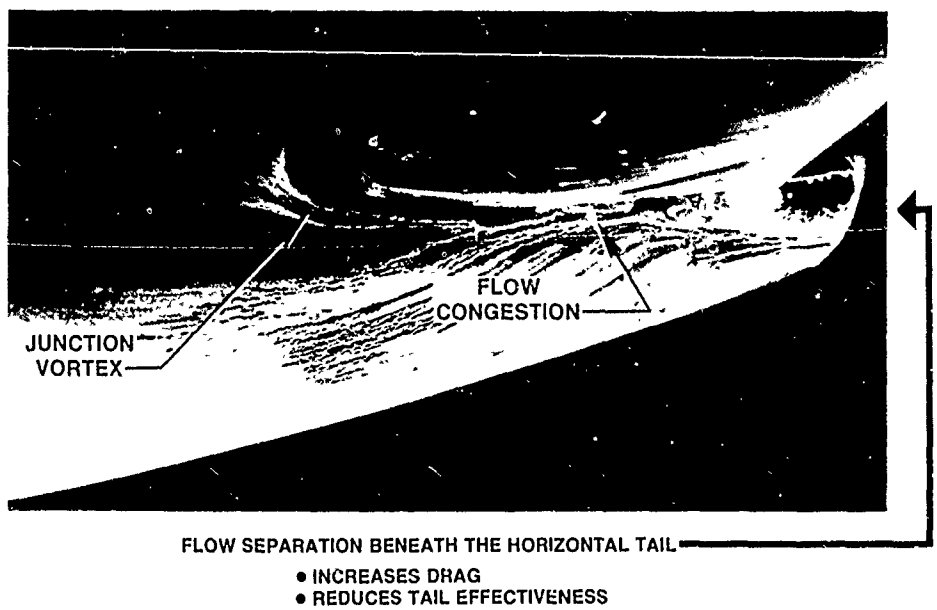

Figure 2: Typical Aft Body Flow Problem

WING INTERFERENCE SITUATIONS

Interference with wing flow characteristics provides some of the most noteworthy examples upon which to draw for a talk of this nature. Consider first the effect of a vertical surface such as a nacelle side or a strut. A good example is an overwing nacelle installation similar to that of the YC14, but on a swept wing. Figure 3 shows a typical installation. It has been studied extensively on transport aircraft to provide jet noise shielding or improved ground clearance, for example with a turboprop installation. A forward location of the nacelle places the boat-tailling so that its effect can be offset by the acceleration of flow around the leading edge of the wing. Thus the peak suction on the wing can be locally reduced. However, the plan view shows the problem of flow constriction which occurs in the inboard junction. This must be relieved by adjusting the inboard nacelle lines in the region of the wing leading edge so as to regain a streamline flow similar to that of the wing alone. The principles involved are explained in Figure 4. Typical wing upper surface pressure gradients are shown to deflect an approaching streamline in a manner different to that of the lower surface pressure gradients. Figure 4 illustrates the effect on the flow field of adding an infinite vertical plate aligned with the freestream approaching an infinite swept wing. Before the plate is added, two undisturbed streamlines approach the wing and follow the paths indicated on the upper and lower wing surfaces. If the plate is then added midway between these two approaching streamlines, the wing span load distribution is perturbed as shown in the lower half of the figure. The portion of the plate over the wing upper surface is at an angle of attack to the flow of the undisturbed streamlines. Negative pressures develop on the left side of the plate and positive pressures on the right side. On the wing lower surface, the effect of the plate is not as pronounced, since its angle of attack to the undisturbed lower surface streamlines is much smaller. Therefore, the wing loading is increased to the left of the plate and decreased to the right. From consideration of the plate as one side of a fuselage or of a nacelle, it is apparent that failure to streamline-countour such a surface would result in undesirable changes in the chordwise and spanwise pressure distributions. The deterioration would include isobar and shock unsweeping and more adverse pressure levels, pressure gradients, and load distribution.

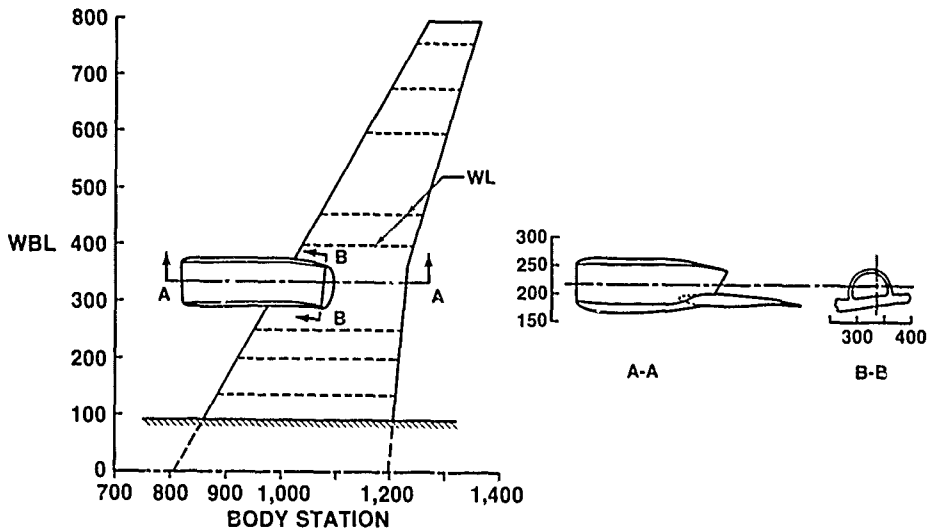

Figure 3: Overwing Engine Configuration Geometry

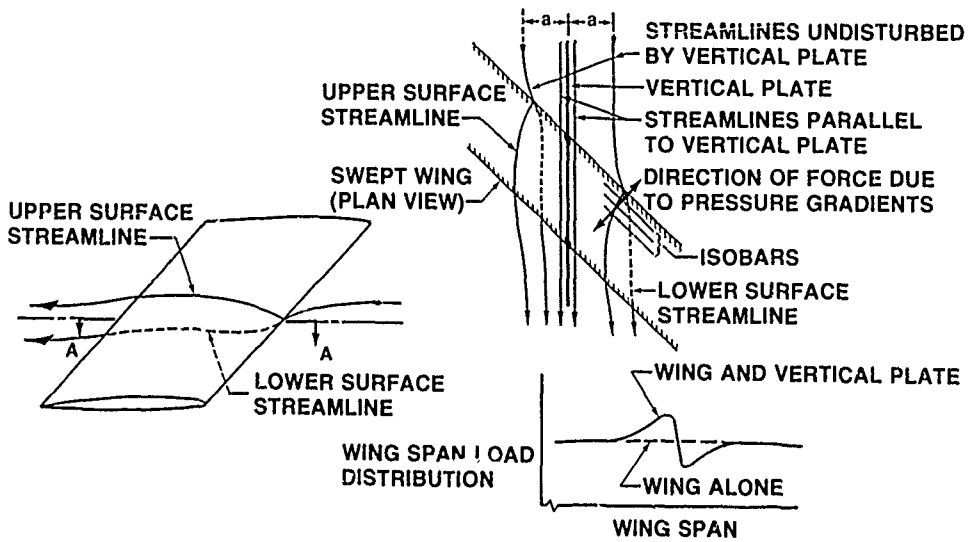

Figure 4: Effect of a Vertical Plate on the Flow Field of a Swept Wing

The objective at a given high-speed cruise condition should be to achieve local Mach numbers no higher than those of the wing alone in the inboard junction and lower than those of the wing alone in the outboard junction. Care must be taken to minimize any lift loss by mounting the pod as low in relation to the wing as is practicable. Then the final result should demonstrate a degree of favorable interference similar to that obtained in an early Boeing test and shown in Figure 5. The effect of the nacelle on the wing shock pattern is shown in Figure 6, Note that with contouring, the sweep of the shock is reasonably well maintained across the wing span so that the associated losses in energy return to about the level for the wing alone.

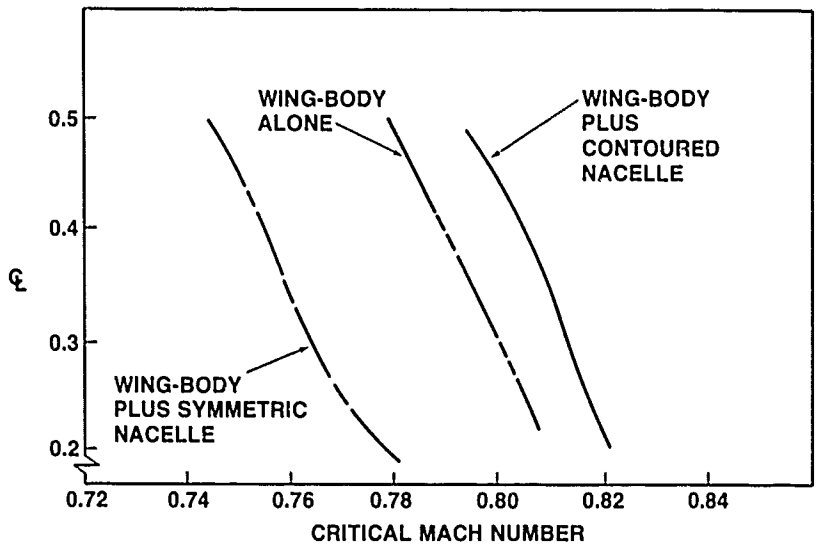

Figure 5: Drag Effect of Contouring Overwing Nacelles

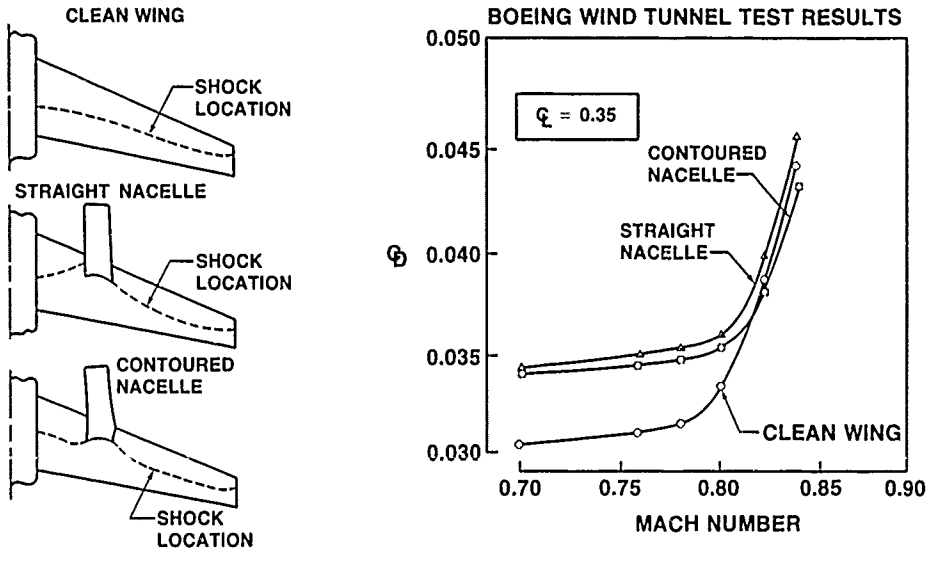

Figure 6.: Installation of Overwing Engine on High-Speed Wing

The winglet interference problem exhibits similar and some different characteristics. Referring to Figure 7, it can be seen that the basic effect of the winglet must be to inhibit flow around the wing tip thus increasing the lift carried by the wing near the tip and reducing induced drag at a given value of lift. A close examination of the winglet environment shows (Figure 7) that it is immersed in a cross flow. If the winglet is loaded in the same sense as the wing the vertical sheet of trailing vortices causes a cross flow in the opposite direction thus creating opportunities for favorable interference. Expressing this in another way, the cross flow induced by the wing rotates the vector of force on the winglet forward thus reducing the net drag increment.

In this way, a well designed winglet will be significantly more successful than would be indicated by the "endplate effect" alone. A secondary interference problem exists in the junction between wing and winglet. Care must be taken to avoid excessive adverse pressure gradients which might arise from the superposition of the two thickness forms. In this regard note that a winglet mounted downwards might be easier to design and offers the same opportunities for reduction of drag. Also, the existence of a dihedral angle on the wing or an outward cant of the winglet will be beneficial.

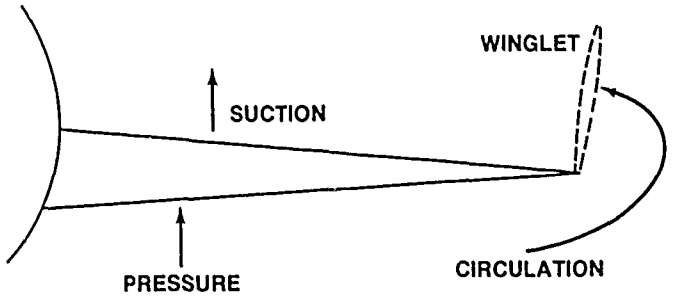

Figure 7: Winglet Flow Environment

Comparisons between winglets and wing tip extensions involve the complete aerodynamic and structural design of the wing. On the basis of purely aerodynamic considerations the increase in span will probably always be superior. Wing bending moments may, however, be greater for a given performance improvement. Note that the bending moment induced by the lateral force on the winglet is relatively small, particularly over the inboard part of the wing. Trade studies of the aerodynamic and structural effects have led to consideration of winglets canted in front elevation in order to determine the best compromise between the penalty in wing bending moment and the improvement in induced drag.

The application of winglets to existing airplanes as product improvement items is obviously very important since in such cases the tolerable increases in wing bending moments are strictly limited. Careful design may therefore maximize the performance benefits available within a given wing strength.

A typical result of winglet studies is shown in Figure 8. This shows the trade between tip extension and winglet. Tip extensions and winglets of equal area and length are compared on the basis of performance improvement and bending moment increase. Figure 8 shows that for a given reduction in induced drag the winglet produces a significantly lower increment in bending moment. In any study of this nature care must be taken to identify all the elements of the trade and to undertake an exact bookkeeping of their effects. In the winglet case the breakdown of performance effects is shown in Figure 9.

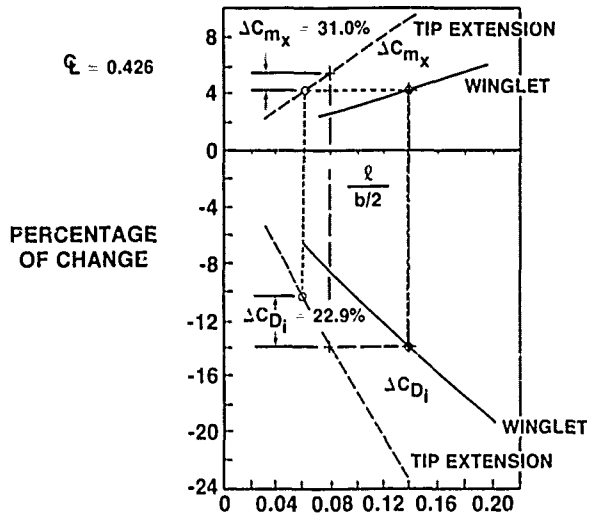

Figure 8: Comparison of Induced Drag and Wing-Root Bending Moment Increments Between Winglets and Tip Extensions

USE OF CFD IN INTERFERENCE PROBLEMS

Modern high-speed computers are capable of describing flows over very complex configurations. Two basic approaches are used. At low speeds singular solutions to the Laplace equation (i.e. source, doublet and vortex singularities) are distributed so as to satisfy the condition of zero flow through the prescribed surface of the body or vehicle being studied. Compressibility corrections are made by the Prandtl-Glauert or other rule so that this approach can be used in flows where the free stream Mach number is of the order of 0.7/0.8. This approach can also be used at supersonic speeds with equivalent formulation of the flow due to singularities. At transonic speeds the compressibility effects must be included correctly in the basic flow equation. Here what are called the Full Potential Equations are commonly used today. They are solved by relaxation techniques using a three-dimensional grid which is fitted to the surface of the body and must be defined throughout the flow field. Construction of these grids is a real barrier to the study of complicated shapes. The tendency is, therefore, to use the panel methods unless the definition of shock strength and location is important.

Four examples of the use of CFD are shown in Figure 10. Two are taken from studies associated with the modification of a 747 for carriage of the NASA Space Shuttle. One is a study of mounting systems in a wind tunnel. The fourth is an analysis of forces on a weapon during the initial stages of its trajectory after release.

$$\Delta C_{D_{NET}} \quad \Delta C_{D_{i_{winglets}}} + C_{D_{\substack{parasite \\ winglets}}} + \Delta C_{D_{\substack{profile \\ airplane}}} + \Delta C_{D_{trim}} + \Delta Wt_{winglets} \frac{\Delta C_D}{\Delta Wt}$$

where

$\Delta C_{D_{NET}}$ = Total drag change due to winglets including weight penalty

$\Delta C_{D_{i_{winglets}}}$ = Change in wing induced drag due to the addition of winglets

$C_{D_{\substack{parasite \\ winglets}}}$ = Winglet parasite drag (skin friction, form drag and interference drag)

$\Delta C_{D_{\substack{profile \\ airplane}}}$ = The change in airplane drag (less the airplane induced drag) due to a change in airplane angle of attack

$\Delta C_{D_{trim}}$ = Change in trim drag due to the addition of winglets

$\Delta Wt_{winglets}$ = Total winglet plus wing installation weight penalty

$\frac{\Delta C_D}{\Delta Wt}$ = Drag-weight trade factor for equal fuel burned

Figure 9: Breakdown of Performance Effects of Winglets

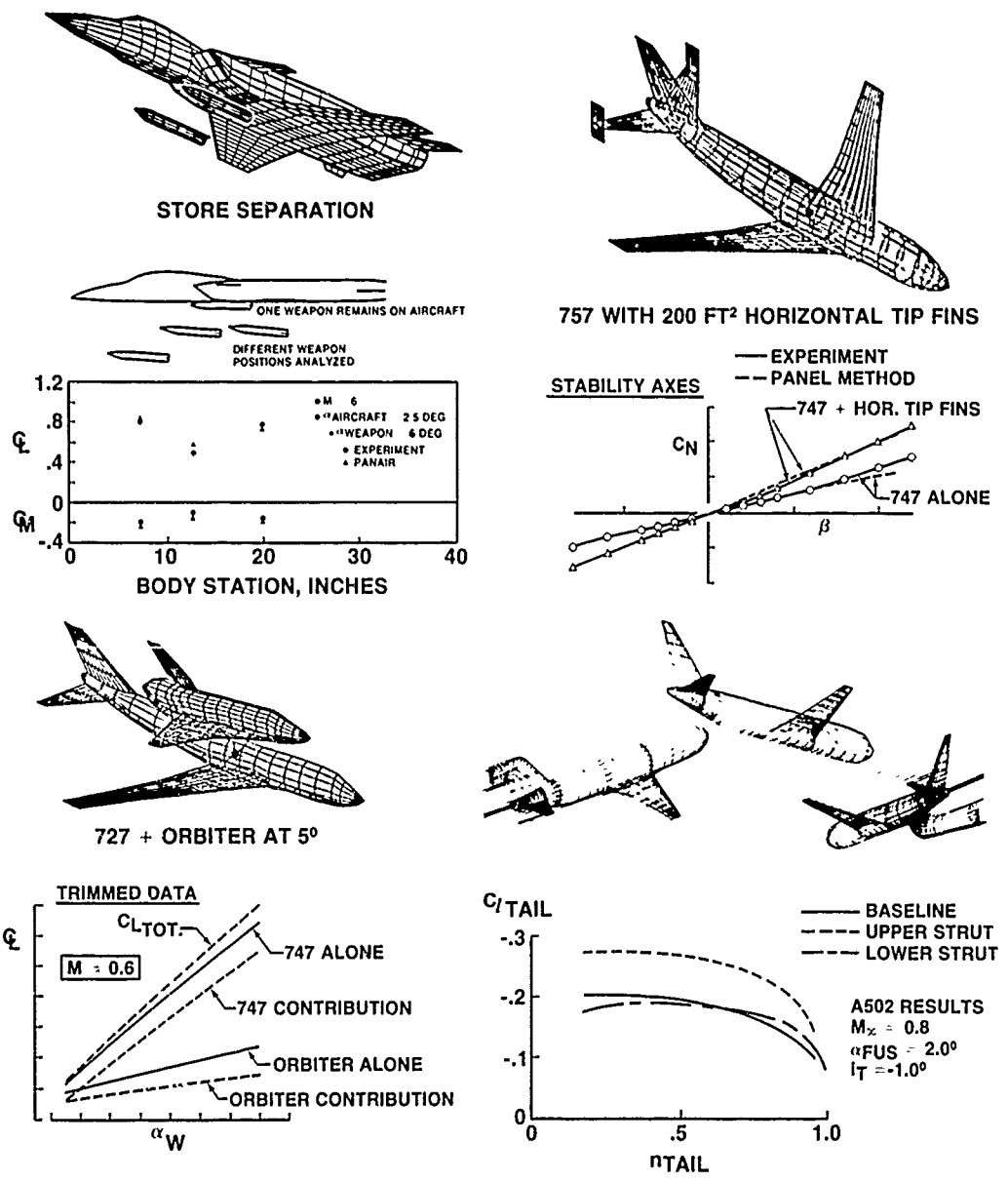

Figure 10: Use of CFD to Investigate Interference Problems

The first 747 study concerned the lifting capability of the 747/Orbiter combination. One purpose was to suggest a suitable attitude for the orbiter. The calculations are shown with the orbiter at five degrees to the body axis of the 747. The total lift is increased, but is less than the sum of the two bodies taken separately. The second 747 study arose from a deficiency which was observed during initial wind tunnel studies of the combination. One effect of the orbiter was a shielding of the vertical tail of the 747 which led to insufficient lateral stability. Several possible modifications were studied on the computer leading to the selection of the horizontal tip fins shown in the figure. Wind tunnel tests confirmed the predicted effectiveness of these. This is a case where the use of the computer provided a good solution more quickly and less expensively than would have the wind tunnel.

The mounting strut interference study was undertaken to indicate which type of mount and what design should be used for particular purposes. In general, the lower strut is not good for drag because of interference with the aft body. The upper strut is difficult for control and stability tests because it provides a poor model of the vertical tail and because it does not properly represent inteference effects on the horizontal tail.

The store separation problem is one which has been studied in many ways. The object is to avoid an untoward maneuver on the part of the weapon while in the flow field of the airplane. The chart shows the capability of the panelling approach in predicting forces and moments on the weapon. Supersonic studies have also been accomplished with similar good agreement.

Examples of the use of the transonic Full Potential Equations are discussed below in relation to nacelle inteference studies.

USE OF FLOW VISUALIZATION IN INTERFERENCE PROBLEMS

While some viscous effects are included in CFD calculations (e.g. boundary layer displacement thickness) we are many years from a realistic capability of describing separated or vortex flows. This is one area in which wind tunnel test techniques are being improved to enable us to explore and understand interference effects. A technique developed at Boeing is known as the Wake Imaging System (WIS). It is a device which records variations in total pressure and converts them to a colour coded light output. By traversing the wake of a separated or vortex flow, a picture in colour of the gradation of total pressure can be compiled and printed.

Two examples of this technique are shown in Figures 11 and 12. The first shows the clear imprint of the nacelle wakes at a incidence of four degrees on the 747 aircraft. At eight degrees it shows a fairly large separation on the outboard wing which is apparently controlled to a large degree by the addition of the outboard nacelle. Presumably, the strut of the nacelle installation interupts the spanwise flow on the upper wing surface causing a part span vortex which collects the bulk of the boundary layer and leaves a relatively cleaner flow over the outer wing.

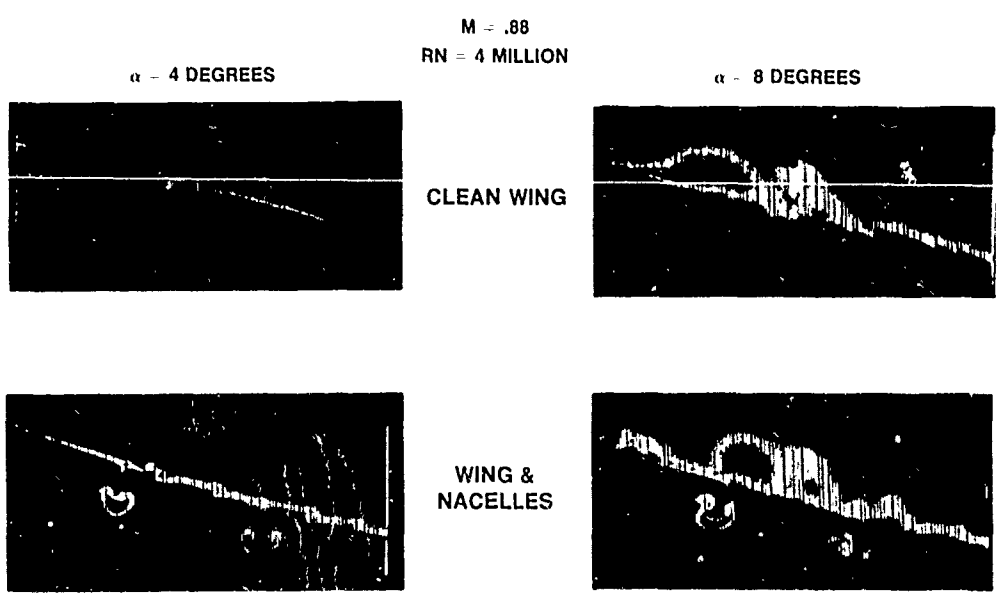

Figure 11: Wake Imaging Results

The second example is from the re-engining of the Boeing 737. This was described in my previous talk on Aerodynamic Design. The CFM-56 engine is housed in a nacelle mounted under the wing. This replaces the more integrated installation of the current JT8D engine. A difficulty of the new installation was the presence of a vortex flow emanating from the inboard side of the nacelle which would cause an early separation of the inboard

wing. By attaching a large vane or "ear" to the nacelle, the vortex was brought down closer to the wing and the separation was delayed. The vane is commonly referred to as a Vortex Control Device (VCD).

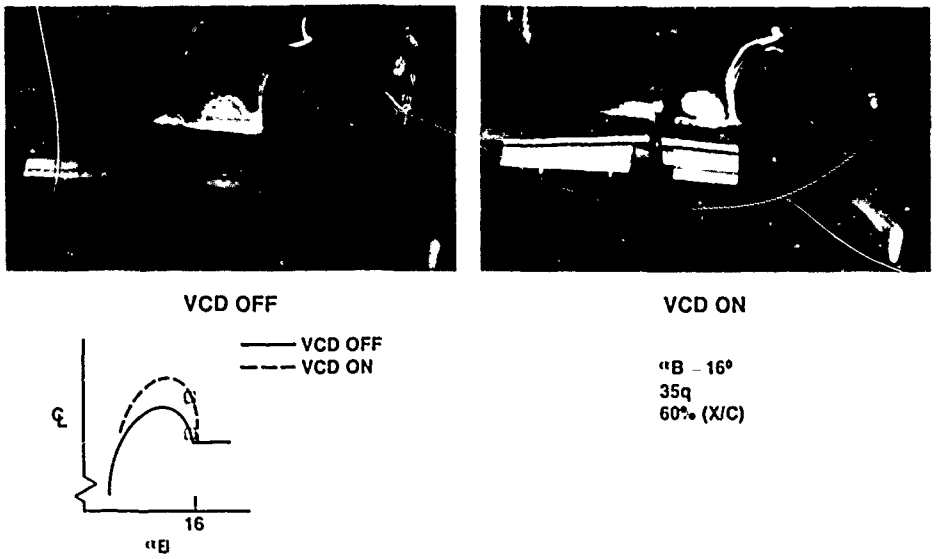

Figure 12: Effect of Vortex Control Device

Further development of the WIS will increase its capability of traversing the flow field both in the wake behind the model and forward on to the surface of the wing. The aim is to be able to visualize not only the downstream effects of vortex or separated flows, but also to help understand and modify the configuration features which give rise to them. The system is particularly useful in exploring the flow field around horizontal and vertical stabilizers. It affords a valuable means of identifying and correcting the causes of undesirable stability characteristics.

NACELLE INTERFERENCE PROBLEMS

Nacelle installations are notoriously fraught with interference problems. These arise from spillage around the engine air inlet, flow problems in channels formed by a nacelle, strut and the airplane wing or body, scrubbing of the airplane structure by the engine exhaust and interference between the exhaust plume and, for example, the wing. This last effect has received particular attention in recent years because of the trend towards twin engine transport installations with high bypass ratio engines. In order to maintain ground clearance and avoid severe penalties in landing gear weight, there is pressure on the aerodynamicist and installation engineer to reduce the separation between the nacelle and the wing. Because of the channel flow problem mentioned above the nacelle is usually mounted on a strut forward of the wing. The variety of installations analyzed at Boeing in recent years is indicated on Figure 13. Of these probably the most critical is the 737-300/CFM-56 where the necessity to keep modifications of the airplane to a minimum, forced the fan cowl exit very close indeed to the leading edge of the wing. Some upward tilt and a flattening of the lower surface of the nacelle are also evident.

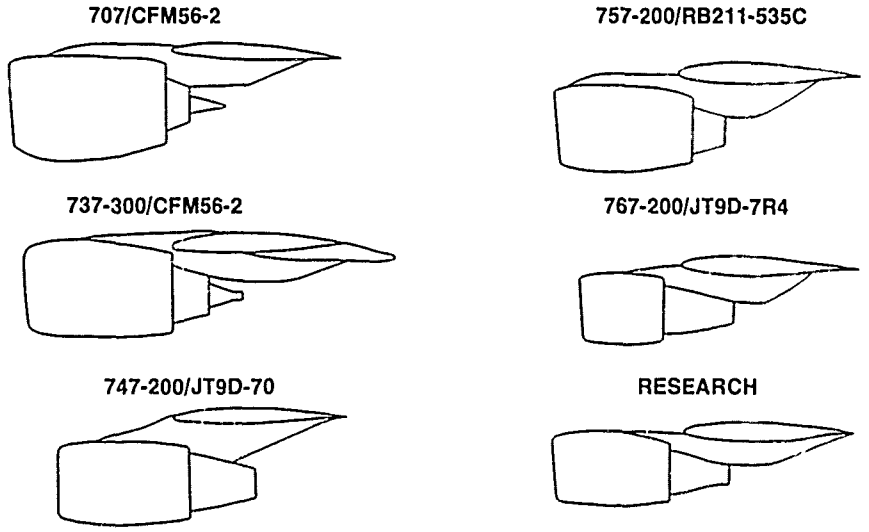

Figure 13: Variations of Engine Installation Scaled to Constant Chord

Wind tunnel tests of nacelle installations to measure drag penalties have to be done with great care and, with proper simulation of the power effects, can be very costly. They are therefore seldom completed before the final stages of project design when it is too late to make many changes. Therefore, the use of CFD for early analysis and prediction of flow phenomena is very valuable in this instance. Typically, calculations are accomplished using the Full Potential Equations since supersonic flows on the wing surface are important. A surface fitted grid is used as shown in Figure 14 and the plume is represented by a prescribed solid shape. Now the physics of the plume flow are very complex involving as they do viscous effects at the interface between the core and fan flows and between the fan and external flows (see Figure 15). A separate model of the plume is therefore usually constructed and iterated with the model shown in Figure 14 to obtain consistent solutions. At the time of writing at Boeing, a complete viscous, non-axisymmetric plume model is being developed and should be operational early in 1983.

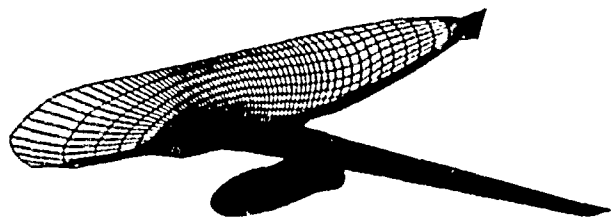

BOUNDARY CONDITIONS

INLET, NACELLE, STRUT, PLUME: $\vec{q} \cdot \vec{n}$

WAKE: KUTTA CONDITION, PRESSURE CONTINUOUS

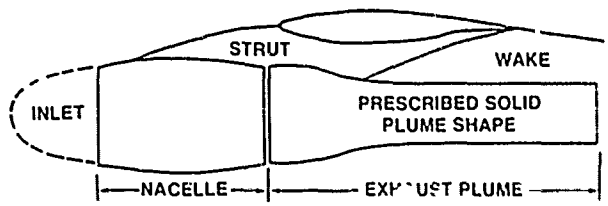

Figure 14: Twin Engine Transport - Surface Grid

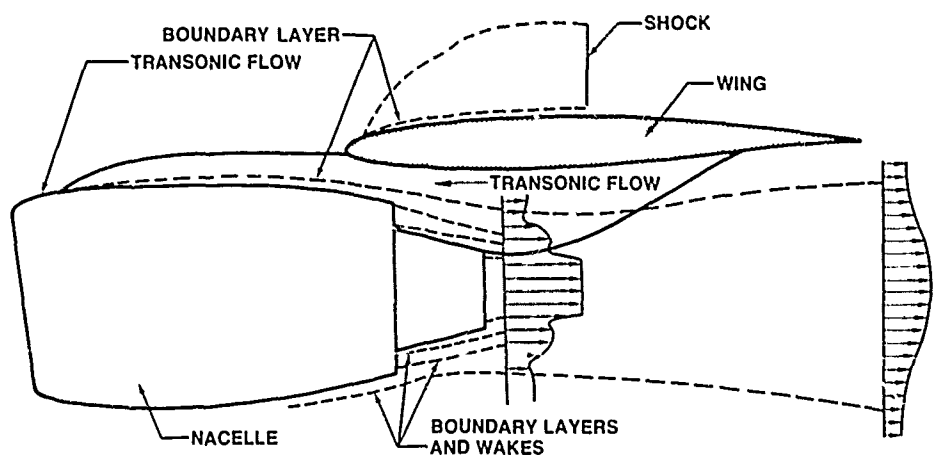

Figure 15: Physics of the Real Flow

In general, experience with this computing model has been very good. Figure 16 shows the effect of the nacelle on the wing lower surface pressure. Note the high suction peak just inboard of the nacelle. Figure 17 shows a case where agreement with theory is less than perfect. Addition of the cowl boundary layer provided better prediction of the suction peak on the lower surface, but did not move the peak forward to the location it had in the experiment. It is hoped that a plume model will better help improve this case where the cowl exhaust is some distance aft of the leading edge of the wing. Figure 18 shows an interesting effect of core cowl shape where the suction on the cowl geometry is modified by interaction between the core cowl and the underwing surface.

Data such as are shown in these last few figures allow the aerodynamicist to judge the presence and possible magnitude of blowing drag. This is defined as the installation penalty associated with power effects which has to be added to the installation penalty measured with flow-through nacelles. It is an item which requires expensive simulation in the wind tunnel. Either blown nacelles or turbo-powered simulators are used and calibration is very critical in each case. The blowing drag arises from a strengthening of the shock on the underwing surface, from increased suction on the aft facing surfaces of the fan and core cowls and from increased flow velocities over the strut surface.

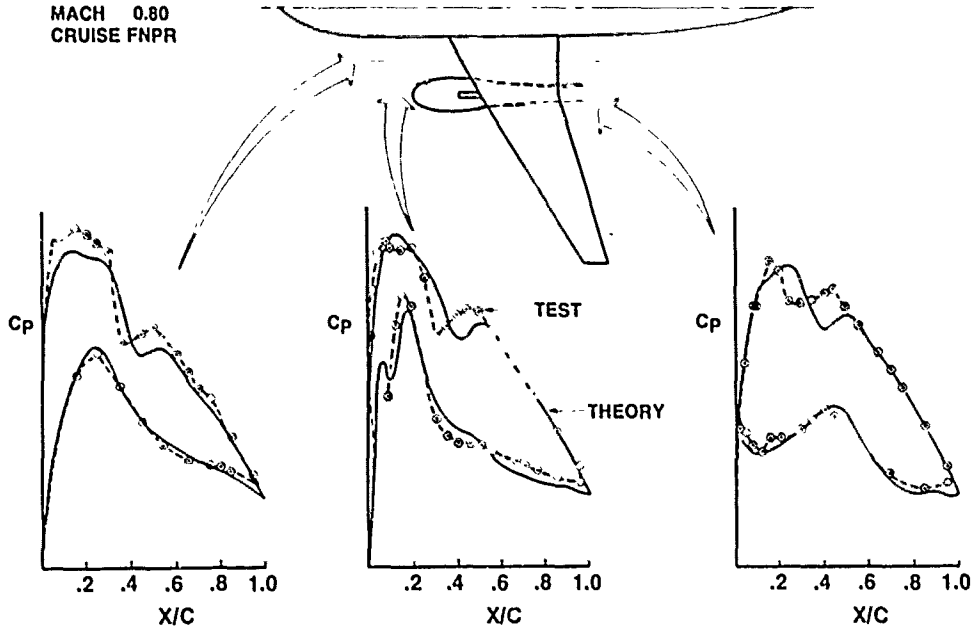

Figure 16: Transonic Wing/Body/Nacelle/Strut Analysis

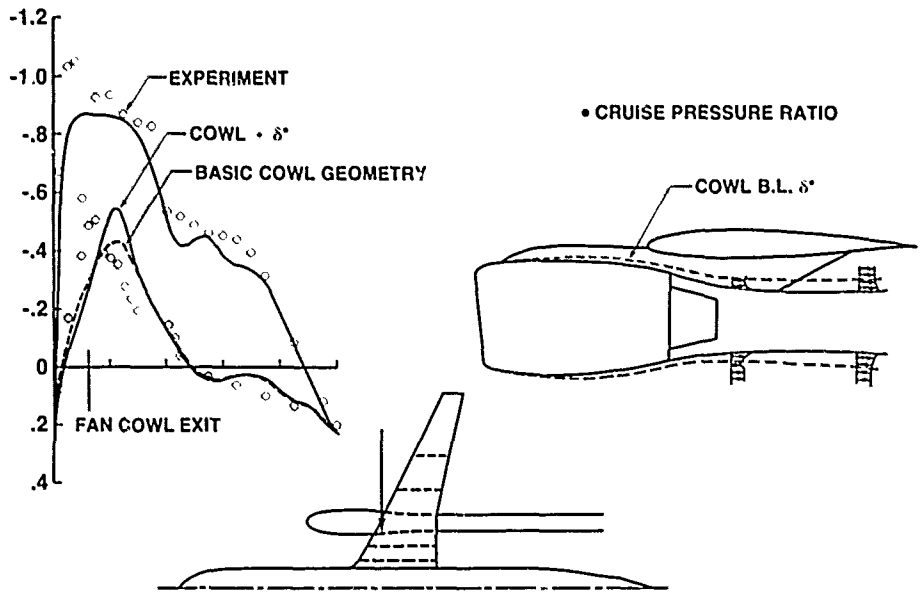

Figure 17: Effect of Boundary Layer

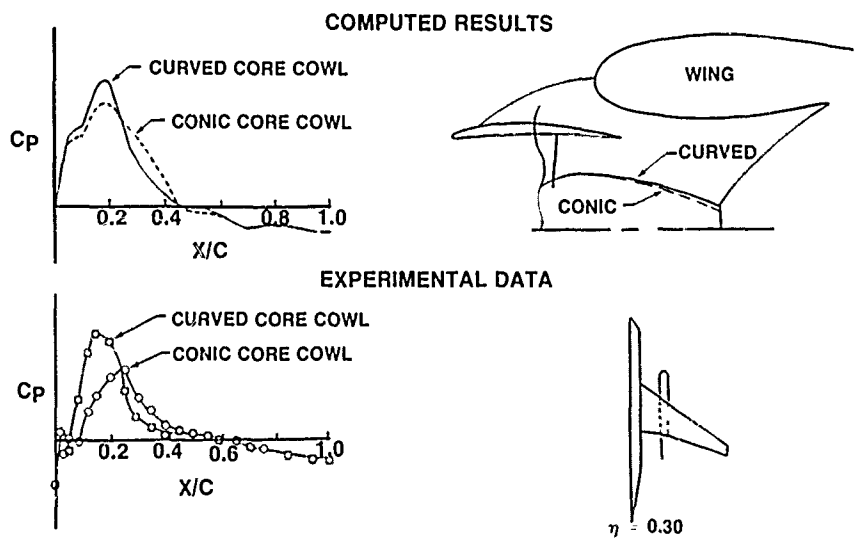

Figure 18: Effect of Core Geometry

ENGINE / AIRFRAME INTERFERENCE

by
G. Krenz
MBB / Vereinigte Flugtechnische Werke GmbH
D 2800 Bremen
Germany

SUMMARY

The history of airframe/engine integration shows quite different aircraft configuration designs, especially since the turbojet engines entered the market of civil aviation. The present paper, therefore starts with a short review about typical aircraft representatives with different types of engine housing and discusses the reasons why current commercial transport aircraft designed for the transonic flight regime prefer conventional engine locations under the wing. On first sight this type of configurations has rarely changed over the past 25 years, however, the strength of flow interference has been increased considerably due to the rapid progress in engine as well as wing technology. On the engine side mainly the enlarged massflow and fan diameter contribute to the stronger interaction, while the wing tends to thicker, higher loaded designs with supercritical flow in the transonic flight regime. The increasing effects of wing/engine interference are studied by MBB/VFW in several transonic wind-tunnels like the NLR-HST in Amsterdam and the ONERA S1 MA in Modane. Results including those of varying engine distances from the transonic wing are presented.

The wind-tunnel measurements employing through flow nacelles and partially plug nozzles to adapt the desired mass flow of the pod are conducted without adequately simulating the real engine jet. For better engine representation, therefore the turbine powered simulators (TPS) should be used. This is done during Airbus design and development studies by Aerospatiale and British Aerospace for cruise flight conditions. However, it was found from flight tests that at low speeds there is also a strong demand for proper engine simulation. Therefore the TPS-test technique was introduced in the MBB/VFW Low Speed Tunnel in Bremen. Tests were performed with different engine types and configurations to evaluate the one engine out second segment climb performance. Measurements of forces and pressures on the wing as well as in the wake at several stations behind the nacelle in the area of wing-pylon-engine were carried out. These results are discussed in the present paper.

The wind-tunnel measurements with turbine powered simulators require a tremendous amount of working time and expenses in the model-shops and wind-tunnel facilities. Hence there is a need for theoretical aerodynamics, to reduce the numerous engine positions, pylon shapes and junctions to be studied during an aircraft design. However, wing-fuselage-pylon-nacelle just represents the configuration, for which the designer has to know the aerodynamic characteristics, and is most complex and difficult regarding the theoretical approach. Therefore at MBB/VFW a simplified method was developed, to calculate the potential flow at transonic speeds around complex configurations including pylon and engine. Results obtained with the method are shown in comparison with wind-tunnel test data.

Although today the conventional aircraft configuration with under-the-wing engine mounting is still in favour for commercial transport aircraft, many other designs with sometimes exotic engine positions were investigated and built to fulfil stringent design requirements or to improve aircraft performance with respect to airframe-engine interference. One concept was the VFW 614, so far the only civil aircraft flying with engines mounted to the upper wing side. Some specific flow characteristics, resulting in a limited cruise flight Mach number due to increasing interference effects, are presented. Since the VFW 614 extensive studies have been carried out concerning different engine positions above the wing. As a result it was found that there is no engine location on the upper wing surface without penalties. However, when the engine above the wing was not connected to the wing, high improvements in the low speed regime were experienced. Also wind-tunnel measurements with a metric nacelle were conducted, using a typical transport aircraft semi-span model where the engine was represented by a turbine powered simulator supported on a canard type of wing. Results are presented in the paper showing improvements in low speed performance characteristics.

LIST OF SYMBOLS

C_D	drag coefficient
C_L	lift coefficient
c_p	pressure coefficient $(p-p_\infty)/q_\infty$
c (l)	local wing chord
D	nozzle diameter
h_p	distance from wing lower surface to fancowl upper side
M	Mach number
p	local static pressure
q	dynamic pressure
R_N	Reynolds number
v	velocity
v_N	normal velocity
x, y, z	body axis system
x_T	distance from nozzle exit to wing leading edge
α	incidence angle
η	spanwise coordinate in relation to half wing span

Abbreviations

I/B	inboard
O/B	outbord
l.e.	leading edge
l/s	lower side
u/s	upper side
MTO	maximum take-off power
TFN	through flow nacelle

Subscripts

j	jet
t	total (local)
t_o	total (indefinite)
∞	indefinite
*	sonic condition

1. INTRODUCTION

The history of engine-airframe integration since turbojets entered the market of commercial transport aircraft reflects a large amount of ideas and work spent in aeronautical research and engineering to find the best engine housing and, the story is not at the end. - The reason is the tremendous progress of both engine and airframe technology with changes in geometry, materials and flow characteristics. The strong interest in these problems is explained by the demand for improved economy. Thus the cruise flight had to be limited to high subsonic Mach numbers in the course of increasing fuel prices and this focussed the aerodynamic work - as far as commercial airplanes are concerned - to a number of major subjects, two of them being presented in the present lecture series: "Transonic Configuration Design" and "Engine-Airframe Interference".

FIG. 1 shows some basic concepts of engine housing since the appearance of turbojets. The designers of Comet presumably did not expect an aircraft family concept with large turbofan engines since the airframe does not provide enough volume at the wing root. The French Caravelle and the B 707 coming into operation 25 years ago are representatives of current aircraft design as far as the engine location is concerned. FIG. 2 presents some newer concepts with engines sitting above the wing. The Sabre Liner being in service, is not far away from the Caravelle concept, but the VFW 614, designed as a short haul aircraft to operate from undeveloped runways, is an exotic configuration with respect to the engine position. A limitation of cruise Mach number is obviously due to the increase of wing-engine interference with speed. The Boeing AMST YC 14 presents a big step in the USA towards advanced configurations with respect to engine housing tested in wind-tunnel and flight. Some problems and merits of the configuration are reported in [1].

Regarding the different engine-airframe concepts, shown in FIG. 1 and FIG. 2, we can recognize that for commercial transports two solutions for fitting the enginges to the airframe are still in favour, these are the positions under the wing and at the rear fuselage. - They fulfil more than others basic conditions for todays commercial aircraft design:

- The flow interaction of both components, engine and airframe, is relatively low and hence is applicable without major technical problems.
- The possibility to install engines of different manufacturers at the same location, if feasible at the same common pylon.
- Taking advantage of improved engine technology, i.e. with changes in geometry and flow characteristics, without penalties for the aircraft which may result from increased engine-airframe interference.

These conditions are more than ever before vital for an aircraft manufacturer because, the airlines decide which engine they want to operate, the engine manufacterer continously offers improvements resulting in cnanges of engine geometry and flow characteristics and, the airframe manufacturer develops a family concept with commonality among the many airframe parts as far as possible.

2. WING-ENGINE INTERACTION OF COMMERCIAL TRANSPORT AIRCRAFT

2.1 Overall design aspects

The large transport aircrafts like the Airbus, seen in FIG. 3, or the Boeing 767 prefer engine positions under the wing. For long range aircraft the number of engines have to be increased to four as for the Boeing 747 or to three like the Mc Donnell Douglas DC 10 or Lockheed 1011. Regarding the wing-engine interaction the problems are basically the same.

Some general design aspects can be mentioned for this classical engine position, see FIG. 4. The vertical distance "z" between wing and engine is often a comprimise between ground and wing clearance for the engine, connected with the main landing gear height. One meter distance from the lower engine side to ground, as we have for the Airbus, ensures reliable operation. The distance from the wing depends on the forward engine position as well as on the pylon and wing shape, and hence is the result of extensive design studies including wind-tunnel measurements. Some solutions for new transonic aircrafts like A 300, B 767 and B 757 are shown in FIG. 5. We see differences in x/z position as well as in pylon planform. The pylon leading edge and its intersection with the wing leading edge is a specific design task in the transonic cruise flight regime and at take-off and landing as well, where the interference with the leading edge devices has to be taken into consideration.

The main target during the engine installation design and development process is to avoid drag increase either on the wing or on the pylon and engine by interference between those components. The direct contribution of the engine to the aircraft lift is negligible at cruise speed. However, unfavourable flow across the area of wing-pylon-engine junction can increase the drag and decrease the lift as shown in FIG. 6. These results we found in the Civil Component Research Programme (ZKP) when testing through-flow nacelles on a transonic wing. The lift loss produces additional drag, an experience we always had to make when we started with a proper wing design and added pod/pylons or flap-track fairings inducing lift losses. There are convincing explanations about the flow mechanism, but a simple rule for the daily work in the wind-tunnel is, that for the recovery of lift loss the angle of attack has to be increased and this is associated with higher drag.

2.2 Wing-engine interference at transonic speed

One of our main tasks from the beginning of the Research Programme ZKP, sponsored by the German Ministry of Research and Technology, was the propulsion-wing integration as sketched in FIG. 7. For accurate performance evaluations in a specific aircraft development programme, the "turbo powered simulator (TPS)" technique is the most reliable tool in todays wind-tunnel work. However it is laborious, time consuming and expensive and therefore has to be connected to and supported by other techniques like ejector engine and through-flow nacelle simulation. Especially testing the effect of different engine positions on wing aero-

dynamics is difficult and costly employing the TPS technique, and therefore we measured some of those effects with through-flow nacelles on a large scale half model in the ONERA S1 MA and with complete models at the NLR-HST. In FIG. 8 test results obtained in the NLR with double-body nacelles and research wings are presented. Forces and static wing pressures on both sides of the pylon were measured at a Reynolds number of $2.5 \cdot 10^6$ in the range $0.3 \leq M \leq 0.86$. The lower wing surface inboard of the engine is considerably effected while outboard the engine pod both surfaces are influenced. In order to separate the combined pylon-nacelle effects, test were conducted with the large ZKP-model at ONERA S1 MA, where the nacelle was mounted on a sting at the tunnel floor. The results in FIG. 9 show, that the main influence on the upper wing pressure distribution is induced by the pod alone. Therefore the change of pod position relative to the wing can be taken as measure for the change of pressure distribution on the upper wing surface, which is important for the wing design. FIG. 10 shows the corresponding results for a more rearward and slightly lower nacelle position. The effect is quite similar though slightly smaller. Starting from this position the nacelle was moved closer to the wing in three steps with the results presented in FIG. 11. The Δcp over the wing chord upstream the shock location is recorded as difference of the pressure at the new positions ②, ⑦, ⑥ and the pressure at position ⑧. At the shock, Δcp increases strongly with small changes of the shock position and is therefore not representative for nacelle-wing interference. Aft of the shock region, the change of the wing pressure distribution caused by the nacelle is small and is therefore omitted in FIG. 11. A comparison with FIG. 10 shows, that the main effect on the forward part of the wing, is the increase of upper surface pressure by the same order of magnitude (10 %), as produced by the pod in its lowest position. The maximum vertical shift in nacelle position from ⑧ to ⑥ is one half of the wing thickness at the pod station. Although this leads to a rather close engine position of 5 % fan diameter to the wing lower side, local modifications in the wing-pylon-nacelle area may be sufficient to compensate for adverse interference effects.

For better engine representation, jet simulation has to be included. For the transonic flight regime this is the responsibility of our partners Aerospatiale and British Aerospace during the design process for actual Airbus programmes. At VFW we concentrate on more accurate tests and better understanding of engine-airframe interference during take-off and landing. Therefore we developed in our Bremen wind-tunnel the low speed TPS-technique. Some results and the experience gained with this technique will be presented in the next chapter.

2.3 Low speed wing-engine interference of transport aircraft

Development and flight testing during the last years have clearly shown the importance of interference effects at take-off and landing conditions of commercial transport aircraft. In case of twin-engined aircraft the one engine out second segment climb performance is a dominant design case with large effect on overall aircraft economy. As different engines mounted to the same aircraft and different nozzles, i.e. long and short core fan nozzles, resulted in changes of the take-off performance, the decision was made at Airbus Industrie, to introduce more accurate test techniques for clarification of the discrepancies. Hence the TPS, developed by Tech Development Inc. Dayton Ohio, was introduced in the VFW low speed wind-tunnel at Bremen. Here the first steps with the new technique were done within the ZKP research programme. Up to that time TPS were never used for testing low speed configurations because

- engine interference effects were considered to be less important for low speed performance;
- the relation between the large simulator thrust (to be calibrated) and the small interference drag increments (to be evaluated) is much more unfavourable at take-off than at transonic cruise flight in the sense that it is more difficult to achieve accurate test results at low speed.

The different engines at the Airbus leading to scattered low speed performance data and the appearance of TPS in Europe have changed the attitude toward low speed wing-engine interference. Some results, partially obtained in comparison with flight test data are presented in the following chapters[2].

2.3.1 Low speed TPS-test in the Bremen wind-tunnel

The basic test set-up in the VFW wind-tunnel is shown in FIG. 12. The model is a half model of the Airbus A 300 B4, the model scale is 1 : 16. The model is mounted to the overhead mechanical balance, which is equipped with a force free air supply bridge.

FIG. 13 shows the simulator without cowling. The simulator is equipped with measuring rakes behind the fan and behind the turbine which gather all data necessary for thrust calibration and evaluation. The thrust calibration is achieved by a simple static thrust measurement: the test set-up is shown in FIG. 14. The concept of this calibration without the use of the conventional tank is outlined in Ref. [3] and [4] .

Some general problems with TPS engine simulation are:

- More staff is needed for the operation of the engine.
- Additional energy is needed to drive TPS.
- The high loaded bearings of the TPS must be changed in certain intervals to avoid a distruction of the system.
- To overcome the problem of ice build-up on the outer and inner contours of the engine due to the very low temperatures in the primary core (a consequence of the expansion of the compressed drive air in the turbine), the dryer for the drive air was replaced by an improved system allowing longer testing periods. Further on, the cowls for the primary core which were made of aluminium alloy were provided with heating wires or exchanged by pieces made of other materials (phenolic resin or glass fibre plastics). Further on, a purging system was installed to keep the pressure tubes in primary core and the static orifices on the outer side of the core cowl and plug free of ice and lubrica-

tion oil.

- During the first test periods, a manifolding system of pressure orifices was used on the fan rake. Three orifices on one radius (I/B or O/B-halfcircle) each were connected to one scani part at the beginning (FIG. 15). The disadvantage of that system was, that it was impossible to detect a leakage or blockage of a single orifice.
- Due to aerodynamic instabilities, oscillations of the tunnel balance and small thrust variations during the data acquisition time of one test point, a certain scatter band of test results is unavoidable. To be able to draw a mean line through the scattering data points, each point is gathered three times, before the test condition is changed (e. g. incidence angle). To shorten the time for this procedure, each orifice of the TPS pressure-rakes was connected to three different ports on one scanivalve (1 between port 1 and 16, a second between port 17 and 32 and a third between port 33 and 48). So, it is possible to registrate 3 data points with all pressure, temperature and balance signals during one turnaround of the scanivalve.
- The pressure and temperatures, which are used for the TPS thrust calculation, are shown on an online display in the tunnel control room. So, a failure in the data acquisition system can immediately be seen and test points can be repeated or - if necessary - a repair can be initiated.
- Additional TPS-data (static pressures behind the fan and turbine) are registrated in order to have a better control of the main data and to have a back-up system for the thrust calculation if necessary.
- Finally, several improvements of the computer programme have been made in order to accelerate the data reduction and test analysis.

2.3.2 Some test results and comparison with flight tests

In order to get as much information as possible from the wind tunnel tests, all available and useful test methods have been used, i. e.

- oilflow-visualizations on wing, pylon and engine
- force measurements
- measurements of static pressure distributions on wing and nacelle
- wake flow investigations behind the engine using a total pressure rake.

In the following sections, some characteristic results of these different test techniques and - as far as possible - their comparison with flight test results will be shown. Most of the tests done so far at VFW were concentrating on jet effects during take-off and second-segment climb of the aircraft, i.e. with one engine failed and one at MTO-power. These tests proved as very useful to show the areas of power effects, to predict the magnitude of modifications in these areas and to compare the jet induced drag effects of different aircrafts under similar conditions.

2.3.2.1 Oilflow visualizations

A zone of major power effects found during 2nd segment climb investigations was the upper side of the fan cowl. FIG. 16 shows the very small area of flow unsteadiness on the I/B-side, while under Ground Idle conditions (FIG. 17) - which would be a typical condition, if a through flow nacelle would be used - two zones of larger dimensions I/B and O/B of the pylon can be seen. An other zone of major jet effects are the I/B and O/B-sides of the pylon. FIG. 18 and 19 show the behaviour during a wind-tunnel test.

The good agreement between the flow visualizations in the wind tunnel and the full scale A/C are shown on FIG. 20 - 22. On FIG. 20 the cross flow over the pylon and the field of flow unsteadiness on the fan cowl at MTO-power setting can be seen which is identical with the model test (FIG. 16). The result of the W/T-test showing the pylon flowfield is the same as on FIG. 21 and FIG. 22 for the A/C.

These examples show,

- that the TPS is useful to simulate a representative flowfield and
- the use of other engine simulation techniques (e. g. through flow nacelles or blown nacelles with blocked intakes) may lead to wrong predictions for the full scale aircraft.

2.3.2.2 Force measurements

An example for the importance of a proper jet simulation even in the low speed region is shown on FIG. 23. The diagram shows the drag differences due to a modification in the pylon nacelle area for engine conditions Windmill, Ground Idle and MTO. Assuming, this test would have been done with a through flow nacelle only (mass flow ratio normally corresponding with TPS running at Ground Idle), it would have been concluded, that the modification were uneffective. The result with MTO-power simulation by a TPS, however, shows the contrary. So, taking into account the second segment climb case with one engine running at MTO-power and one windmilling, the TPS-test leads to the prediction, that the modification will have a favourable effect on drag. A corresponding flight test proved not only this tendency, but also the amount of drag reduction was very similar.

An other task is the prediction of jet induced drag effects for the second segment climb performances. Using the reference method the prediction of second segment jet interference drag for a A/C no. 2 can be made by a comparison with the wind-tunnel results of A/C no. 1. An example for this is given on FIG. 24. This diagram shows the wind-tunnel results of jet induced drag for the relevant lift coefficients and corresponding slat/flap settings for A/C no. 1, whose relation to full scale results is known. The wind-tunnel

results for the new A/C no. 2 are also shown, and the difference between these two sets of curves is used to predict the behaviour of A/C no. 2.

One more field for jet effects on drag is e. g. the influence of different engine configurations. Even here the TPS-tests at VFW showed an agreement with full scale conditions, which could not be shown with other types of engine simulation, neither with through flow nacelles nor with blown nacelles. It should be noted here, however, that successful force measurements with TPS engine simulators in the low speed region can only be achieved, if the whole data acquisition and reduction system is built up on the basis of highest possible accuracies. We retained a repeatability of $\pm$ 4 counts in the take-off test range.

2.3.2.3 Static pressure distributions

These tests, as well as flow visualizations and the wake flow measurements, described below, mainly were done to get more details about the very complex flow field in the wing/pylon/nacelle region. Static pressure orifices were located on the wing I/B and O/B of the pylon and on the nacelle. The locations are shown in FIG. 25.

A typical result for the jet influence on the wing pressure distribution is shown on FIG. 26. From this it can be seen, that due to influence of the fan nozzle jet the static pressure on the wing lower side is increasing. This increase is more pregnant on the O/B side of the pylon than on the I/B side. This result is astonishing on the first view, because one would expect, that the fan jet velocity is higher than the Mach number and correspondingly a suction effect should exist leading to lower pressures under the wing. This mystery found its explanation in the results of the wake flow measurements, described below, from which it can be seen, that the velocity of the fan jet close to the pylon is much closer to tunnel velocity than expected. So, there is no suction due to the jet, while the massflow in the wing/pylon/nacelle area is increasing with increasing engine thrust. These two effects together may indeed lead to increasing pressures below the wing, as the test results show.

FIG. 27 gives an example of static pressures on the core cowl of the engine at MTO-power setting. This diagram gives an impression of the influence of the fuselage and wing flowfield on the nacelle pressures. Comparing the results for α = 0 and 11° it can be seen, that with increasing angle the static pressures on the core cowl I/B of the pylon are increasing, while those of O/B and on the bottom of the nacelle are not influenced. From this result the conclusion may be drawn, that the jet is not to be assumed as a fixed wall, like this is done if a socalled "skirted" through flow nacelle is used. Summarizing the results of the static pressure measurements, it must be stated as from the force measurements, that representative wing/pylon/nacelle interferences will not be got unless a proper jet simulation is used.

2.3.2.4 Wake flow investigations

The wake flow investigations mainly were done, to get more detailed informations about the flowfield of the model jet and its behaviour under different conditions, such as changes due to

- variation of incidence angle,
- different power settings,
- modifications of the nacelle geometry or
- increasing distance from the nozzle exit.

Comparing the TPS results with a real engine, it is to be noticed, that the temperature and hence the velocity of the primary flow are much lower for the TPS (due to expansion of pressurized air in the Turbine), while the pressure ratio of the primary nozzle is comparable to full scale. The more important point, however, is that the TPS can completely simulate the fan flow (i. e. pressures, temperatures, velocities, mass flow and - to a certain distinct - also swirl), which is responsible for the interference with wing, pylon and tailplane.So, the behaviour of the fan flowfield of the TPS can also be used as an input for the development of theoretical 3-D-computer programmes including jet effects.

For the wakeflow investigations in the tunnel a rake with pitot pressure orifices was used. Some examples in FIG. 28 to FIG. 31 show the behaviour of the jet at different power settings and various distances from the nozzle exit. Each diagramme shows the isobaric lines of total pressure ratios in the measuring plane and the corresponding 3-D total pressure ratio mountain.

These diagrammes show, that - except for the well known increasing size of the flowfield and the decaying pressure ratio - at a position where the tailplane may be located, the mixing of fan and primary flow has resulted in a flowfield showing no more unsymmetries, neither due to the pylon nor due to the lower pressure of the primary flow.

2.3.3 Low speed TPS testing in DNW

To overcome the disadvantage of low Reynolds number and lacking asymmetric effects as mentioned above, the concept of complete model TPS testing in the DNW (German/Dutch Low Speed Tunnel) was developed. The typical model scale of Airbus type aircraft in this tunnel is about 1 : 10. FIG. 32 shows the tail sting installation of an A 300 B4 model in 6 x 8 m² test section of this tunnel. The Reynolds number for these tests is $Re_{\bar{c}} \approx 3 \cdot 10^6$.

For the model turbine driven simulators have been developed and delivered to DNW by Tech Development, Dayton (Ohio).

The complete Airbus model, the TPS-cowlings, pylons, the internal instrumentation and the internal air duct system were designed and built by VFW under contracts of the German Ministry of Research and Technology. The tests in DNW start with a reference test phase concerning the A 300 B4 configuration to prove the test technique and the equipment. The model will be mounted with the internal strain gage balance on the tail sting. The internal balance is bridged by a force free air supply with separate feedlines to both simulators.

The TPS nacelles are calibrated in the brand-new NLR calibration tank at the Northeastpolder. This tank closely follows the Boeing calibration tank philosophy and was especially designed and built for engines of this size and type.

The complete model test at DNW will allow to simulate the second segment climb conditions with asymmetric thrust and flow behaviour. Further on the model is prepared to be tested as half model in the pressurized low speed ONERA-tunnel F1 for operation up to 3 bar, to test the effect of Reynolds number up to $Re_c \approx 8 \cdot 10^6$ at a typical take-off Mach number of 0.25.

3. CALCULATION OF WING-BODY-NACELLE INTERFERENCE

The configuration of wing-fuselage-pylon-nacelle is most complex and difficult regarding the theoretical approach. On the other hand it just represents the configuration, for which the designer has to know the aerodynamic characteristics and at least has to predict the performance and loads. Wind-tunnel results are most reliable and so far represent the only tool to estimate counts and percent of the aircraft performance . However, as the last chapter already indicated, these tests require a tremendous amount of working time and money in the model-shops and wind tunnel facilities. Then one objective for theoretical aerodynamics in this case must be, to reduce the numerous engine positions, pylon shapes and junctions to be studied during an aircraft design. This is not a serious task as long as the wing is designed without the engine, however, for new transonic wing concepts, i. e. the A 310, the interference effects have to be taken into consideration.

The theoretical methods we use at MBB/VFW for a transonic wing design are described in the paper "Transonic Configuration Design" [5] . The advantage of such methods, where complex flows like the pylon-engine interference, can be treated sectionwise is obvious. All the efforts made in 2-D calculations for shock-boundary layer interaction and viscid-inviscid flow interference at the trailing edge can be applied. As the calculations are based on the panel method, which is first used to find the subsonic characteristics of the configuration, a large amount of low speed experience enters the design and, hence the transonic and low speed tasks merge to a more homogenious design work.

The MBB/VFW Hybrid Method described in [5] was applied to a wing-pylon-nacelle configuration, as shown in FIG. 33. The nacelle wake is simulated by a cone having empirically determinded non-vanishing normal velocities. For this case correct knowledge of the wake contour is less important than the normal velocity distribution. The calculated pressure distributions of the clean wing and the wing-pylon-nacelle configuration are presented in FIG. 34. After matching the lift coefficient, agreement was achieved with wind-tunnel tests, FIG. 35, which were carried out with the fuselage present. Also in this case the shock representation was satisfactory, where sometimes the calculation was found to be inadequate, because of the simple normalshock concept in the present theory. Further improvements of the method, specifically in the shock region are being introduced with the boundary layer interaction model of Bohning-Zierep, which was discussed in the paper "Transonic Configuration Design".

4. ADVANCED CONCEPTS WITH RESPECT TO ENGINE-AIRFRAME-INTERFERENCE

One of the most advanced and worldwide known programmes in the field of propulsion airframe interaction was the AMST in the USA, performed by Boeing (YC 14) and MD-Douglas (YC 15) in cooperation with NASA. Many publications from this programme appeared, i. e. [1] , and are being discussed at the present VKI-lecture series.

Another concept with strong engine-airframe interference was the VFW 614 , FIG. 36, so far the only civil aircraft flying with engines mounted to the upper wing side. The programme is cancelled, however. three aircraft are still in service of the Bundeswehr and one is in hand of the DFVLR for aeronautical research in cooperation with industry. Some specific flow characteristics resulting in a limited cruise flight Mach number by increasing interference effects are explained in FIG. 37. There is a strong change of pressure distribution on the upper wing surface near the pylon depending on velocity ratio v_{int} over v_∞ and on cruise Mach number as well. The increasing adverse pressure gradient leads to separation and thus sets the boundary for cruise flight operation at M = 0.65. The pylon-engine location induced no adverse effects on the performance or flight characteristics within the certificated flight regime. The low speed performance on undeveloped runways was excellent, because of the continous trailing edge flap without unfavourable interaction with the engine flow.

Ever since the VFW 614 design, we made extensive studies concerning different engine positions above the wing. As a result we found, that there was no location for the engine to be fixed at the upper wing surface without penalties or limitations like in maximum cruise flight Mach number, as for the VFW 614, or drag increase due to airframe-propulsion interference. However, when the engine above the wing was not connected to the wing-body, we experienced very high improvements in the low speed regime. There were some early reports about these results [6], using a powered nacelle supported on the wind-tunnel wall in variable positions above the wing whereby only the forces on the model were measured.

In the meantime we conducted wind-tunnel tests, using a typical transport aircraft semi-span model where the engine was represented by a turbine powered simulator supported on a canard type of wing [7] . The experimental set-up is shown in FIG. 38. Tests were performed with two wing configurations clean (cruise)

and take-off, at jet/freestream velocity ratios ranging from windmilling v_j/v_∞ = 0.8 to maximum take-off v_j/v_∞ = 3.6. In FIG. 39 the variable positions of the engine are sketched. The wing as well as the stub-wing are not designed with respect to each other, thus only approximate interference effects could be measured when the engine was fitted to the non-optimized configuration. In FIG. 40 and FIG. 41 we see, that adding the engine in windmilling condition increases the lift as well as the drag, the increments becoming smaller with higher angle of attack. Running the TPS then up to max T.O. power improves the lift and reduces the drag considerably. The lift/drag ratio for clean and slat-out configurations is plotted in FIG. 42, showing noticable improvements of the performance parameter.

However, the negative aspects of this type of concept must be mentioned: Cabin noise with limited passenger view; ground handling and engine maintenance, fuel flow to the engines, toward wing wake effects and jet influence on the tail.

Further work is necessary with engine simulation (TPS) in the high speed and low speed regimes to fathom the implications and the limitations of the encouraging low speed test results. For this purpose the design of an optimum stub-wing/wing configuration and measurements are proposed with TPS in the transonic flight regime.

REFERENCES

1	I. H. Rettie	Theoretical and experimental studies of aerodynamic interference effects. AGARD-CP-285, May 1980.
2	B. Ewald W. Burgsmuller	Experimental investigations of transport aircraft low speed engine interference effects and flight correlation. AGARD Ground/Flight Test Techniques and Correlation, Cesme, Turkey, Oct. 1982.
3	B. Ewald R. Smyth	The role and implementation of different nacelle/engine simulation concepts for wind-tunnel testing in research and development work on Transport Aircraft. AGARD-CP-301, May 1981.
4	W. Burgsmuller	Halbmodellmessungen mit Triebwerkssimulation durch TPS im VFW-Niedergeschwindigkeitskanal (Grundsatzuntersuchung). VFW-Kurzbericht Ef-980, ZKP-IFAS-Bericht Nr. 10.
5	G. Krenz	Transonic configuration design. AGARD FDP VKI Special Course "Subsonic/Transonic Aerodynamic Interference for Aircraft", 2-6 May, 1983, Brussels and 16-20 May, 1983, Dayton, Ohio.
6	G. Krenz B. Ewald	Airframe-engine interaction for engine configurations mounted above the wing. part 1: Interference between wing and intake/jet. part 2: Engine jet simulation problems in wind tunnel tests. AGARD-CCP-150, September 1974.
7	J. Szodruch	On the aerodynamics of over-the-wing-nacelles supported on stub-wings. AIAA 21st Aerospace Sciences Meeting, Reno, Nevada, AIAA-83-0538, January, 1983.
8	G. Krenz	Transonic Wing Design for Transport Aircraft. AIAA "Advancing Technology", Williamsburg, Virginia, USA, March 1979.
9	W. Burgsmuller	Grundlagen zur Triebwerkssimulation mittels TPS im Windkanal. VFW-Kurzbericht Ef-826, ZKP-Flügelsektion-Bericht Nr. 38.
10	G. Anders G. Giacchetto A. Gravelle	Philosophy and results of steady and unsteady test techniques on a large scale transport aircraft model in the ONERA Transonic Tunnel S1 MA. AGARD-CP-285, May 1980.
11	K.D.Klevenhusen H. Jakob H. Struck	Calculation of wing-body-nacelle interference in subsonic and transonic potential flow. AGARD-CP-301, May 1981.
12	J. Barche	Beitrag zum Interferenzproblem von über dem Tragflügel angeordneten Triebwerken. DGLR-Jahrestagung 1969, Bremen, Vortrag Nr. 34.
13	F. Fischer, R. Hilbig	Gegenseitige Beeinflussung von Zellen- und Triebwerksströmung. BMFT-Bericht IB 3-8391 LFF 6, Dezember 1973
14	F. Fischer, H.-P. Franz, R. John, K. Kaszemeik	Auftriebs- und Vortriebskonzepte bei zukünftigen Transportern. ZTL-Bericht FAG 4, Rü IV 1, Auftrags-Nr. T/R421/70003/72401, Januar 1978

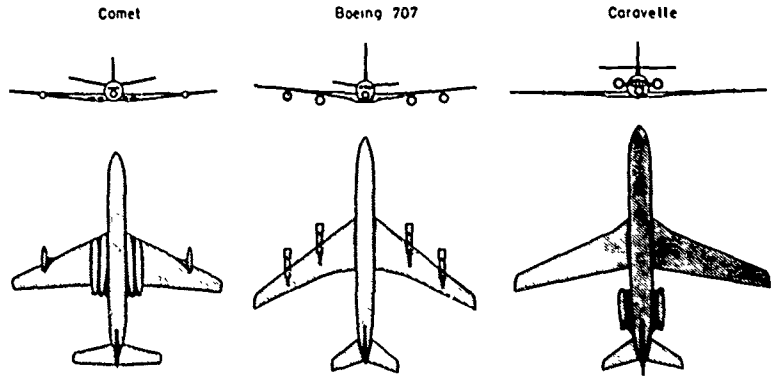

Fig. 1: Different Concepts of Engine Location

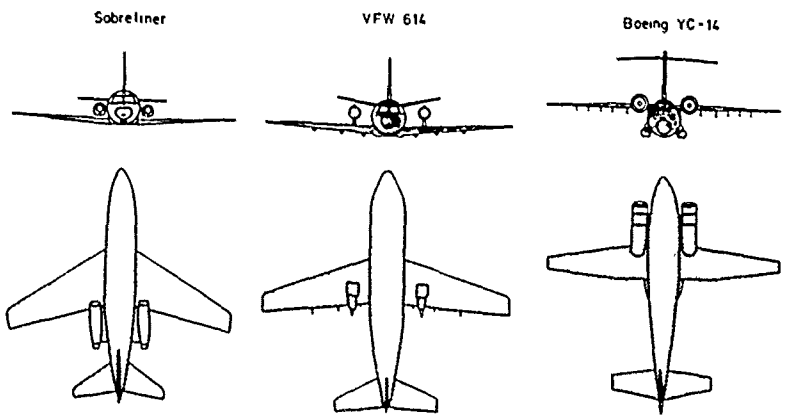

Fig. 2: Aircraft with Engines above the Wing

Fig. 3: Airbus A300-B4 on Ground

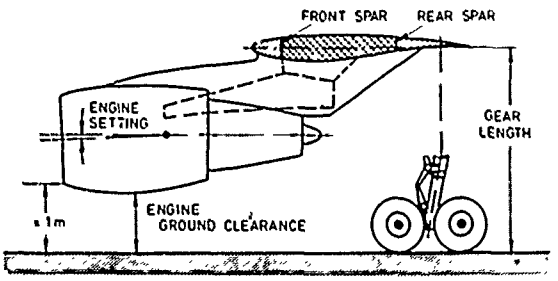

Fig. 4: General Design Aspects of Engine Position

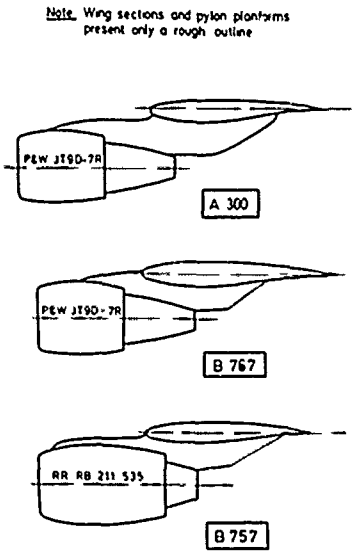

Fig. 5: Pylon Planform and Nacelle Position

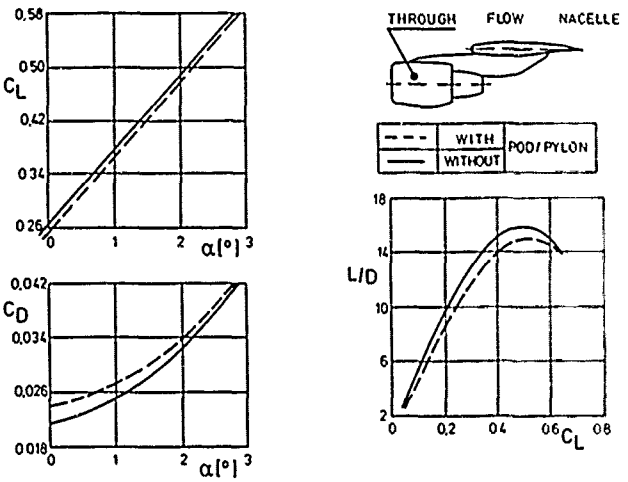

Fig. 6: Effect of Pod/Pylon on Lift and Drag

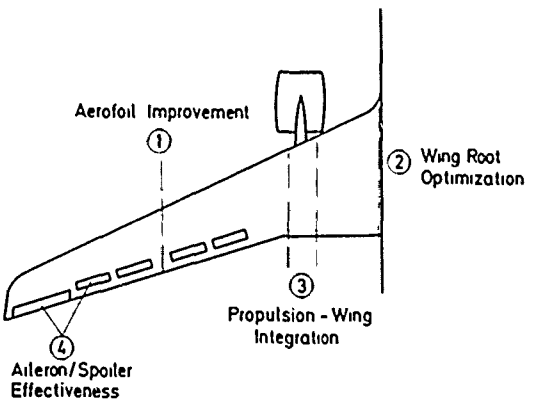

Fig. 7: Future Research in Transonic Aerodynamics

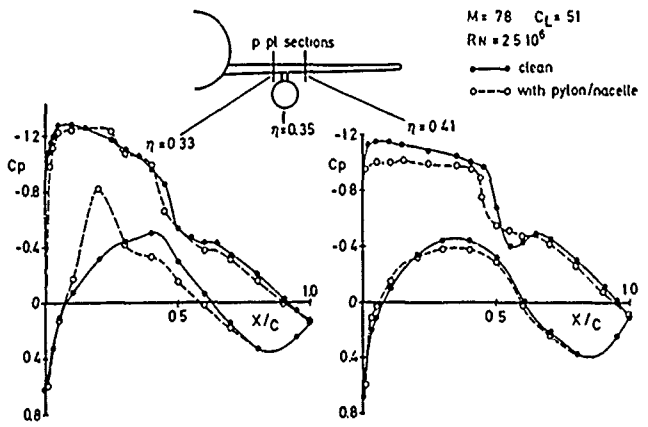

Fig. 8: Windtunnel Tests at NLR-HST, Wing B10.3U

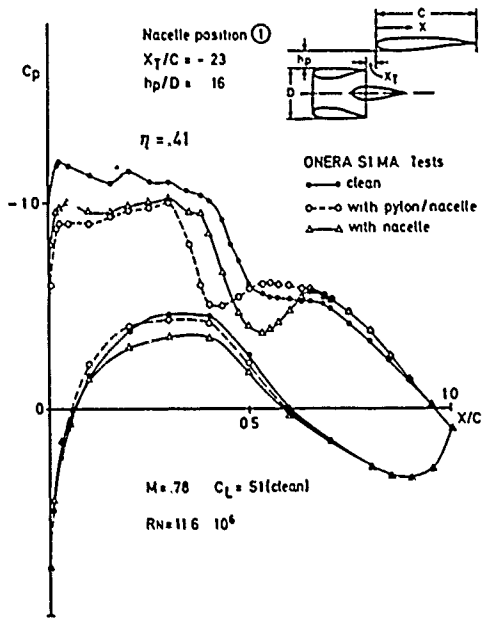

Fig. 9: Pylon/Nacelle Influence on Wing B10.3V Pressure Distribution

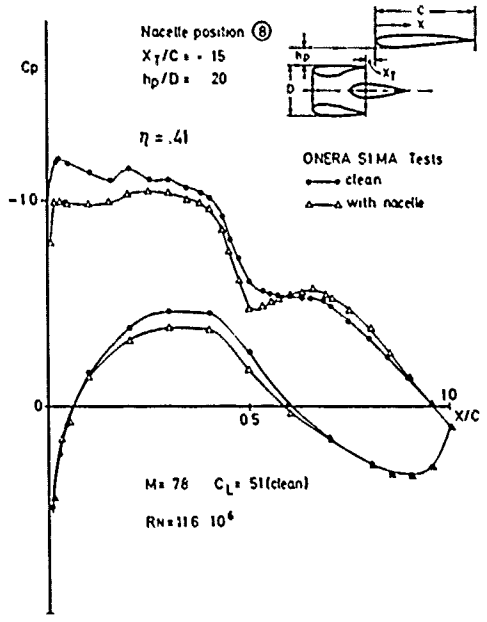

Fig.10: Pylon/Nacelle Influence on Wing B10.3V Pressure Distribution

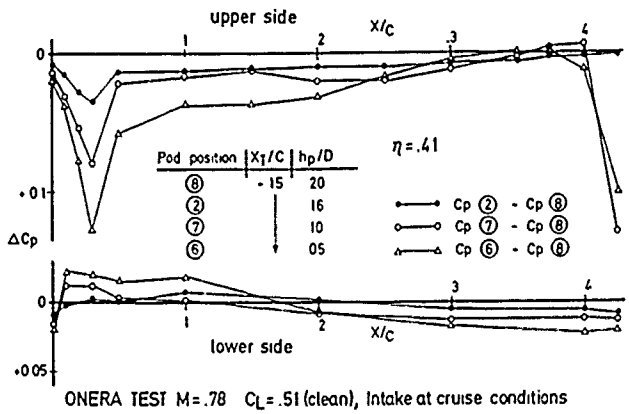

ONERA TEST M=.78 C_L=.51 (clean), Intake at cruise conditions

Fig.11: Change of Wing Pressure Distribution due to decreasing Nacelle Distance from Wing

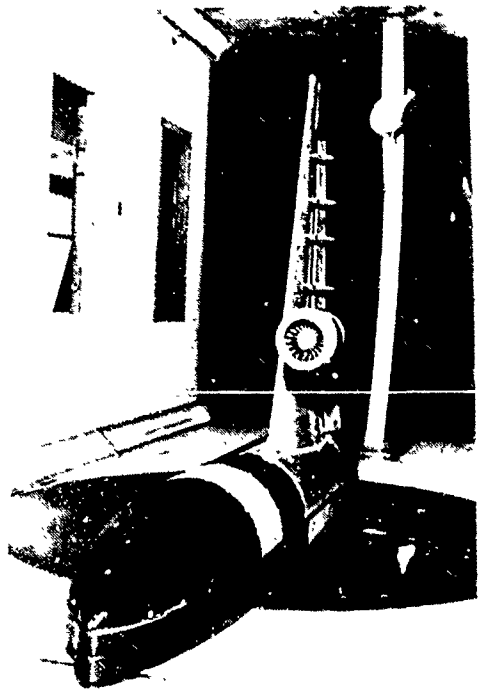

Fig.12: Low Speed Half Model with TPS (Scale 1:16)

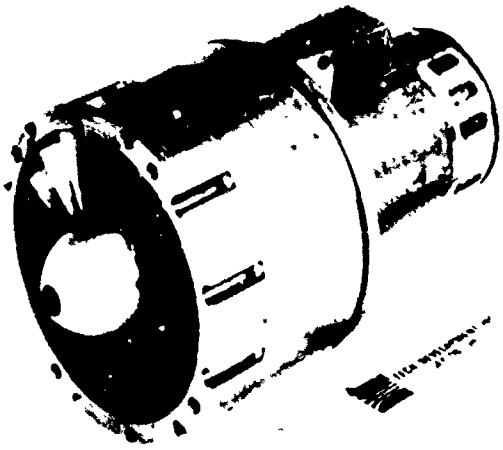

Fig.13: Turbine Powered Simulator

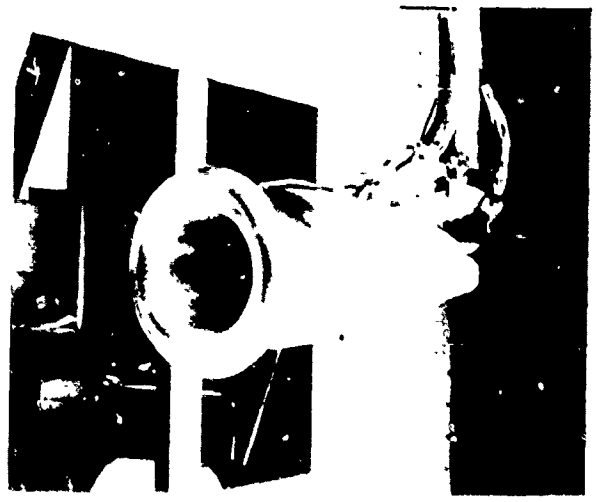

Fig.14: Static Thrust Calibration of TPS

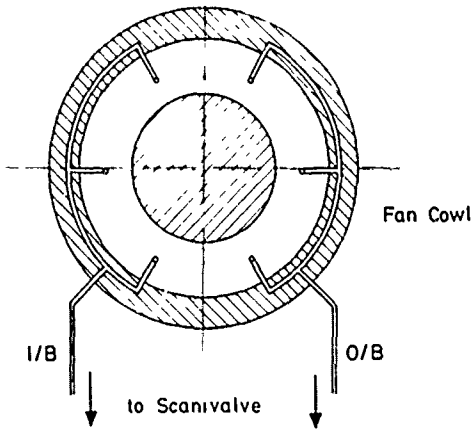

Fig.15: Manifolding of Pressure Orifices

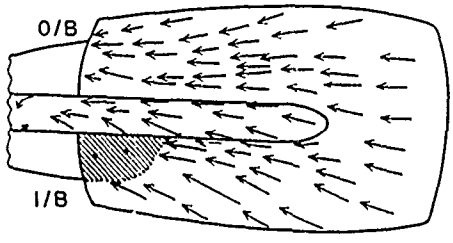

Fig.16: Oilflow on Fan Cowl u/s at MTO-Power Cond. (W/T-Test)

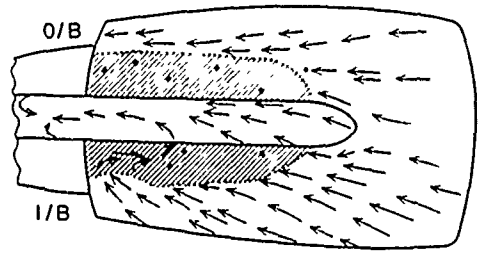

Fig.17: Oilflow on Fan Cowl u/s at Ground-Idle-Power Cond. (W/T-Test)

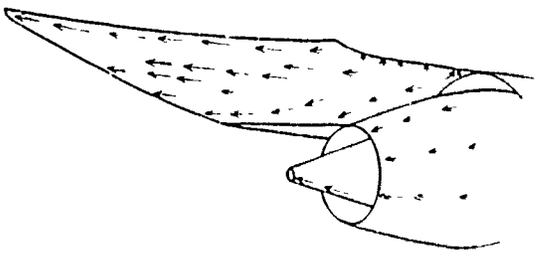

Fig.18: Oilflow on I/B Side of the Pylon, MTO Power Condition (Wind Tunnel)

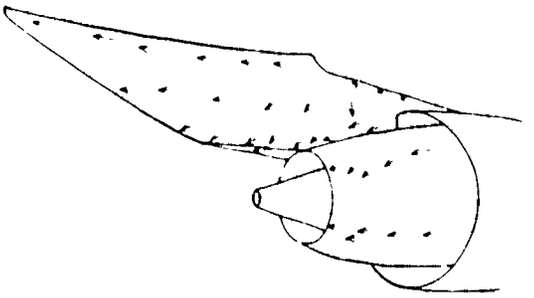

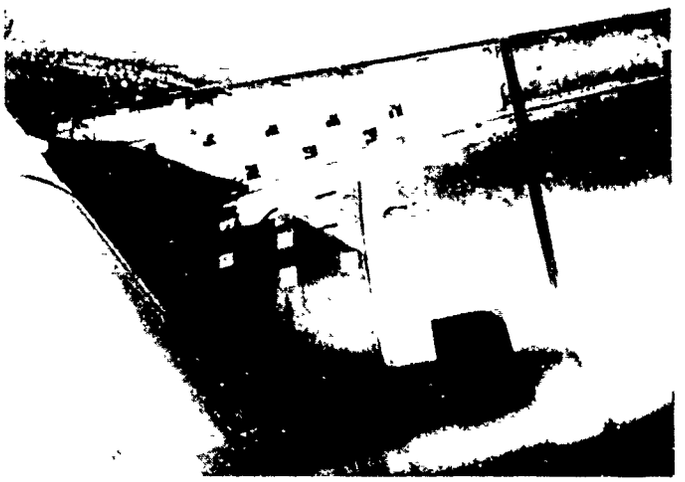

Fig.20: Flight Test with Tufts on I/B Side of Fan and Pylon (MTO-Power Condition)

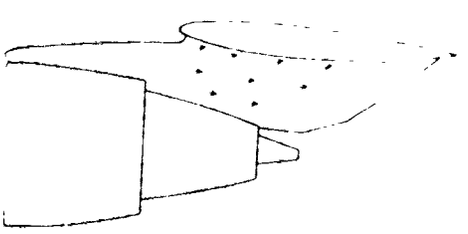

Fig.21: Flight Test with Tufts on I/B Side of Pylon (MTO-Power Condition)

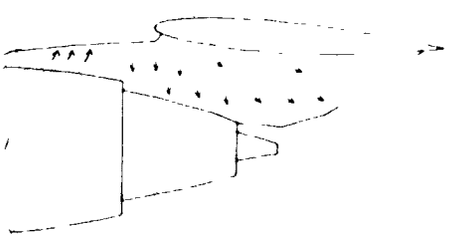

Fig.22: Flight Test with Tufts on I/B Side of Pylon (Windmill Condition)

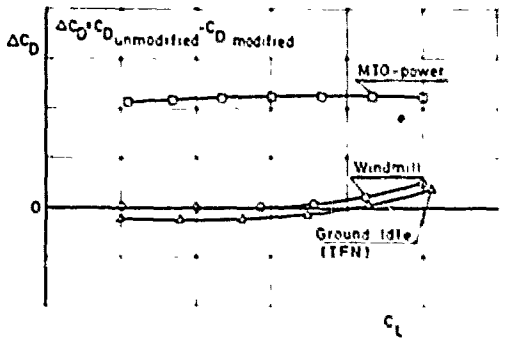

Fig.23: Influences of Power Setting on Modification in the Wing-Pylon Area

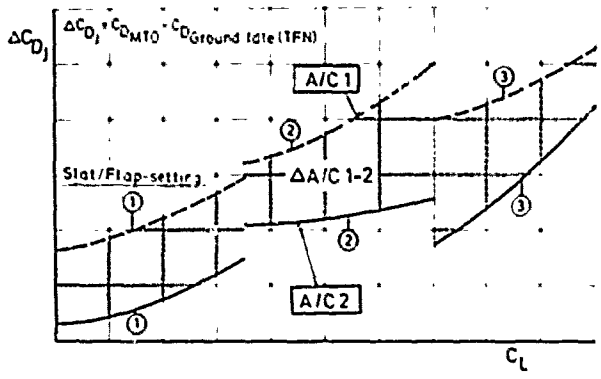

Fig.24: Comparison of Jet Induced Drag for Similar A/C-Configurations

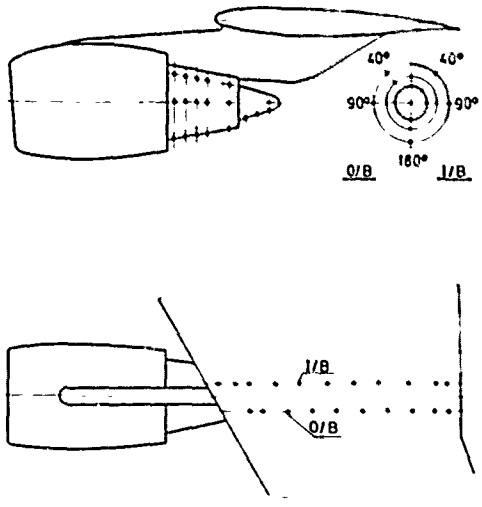

Fig.25: Pressure Points on Wing and Nacelle for W/T-Test

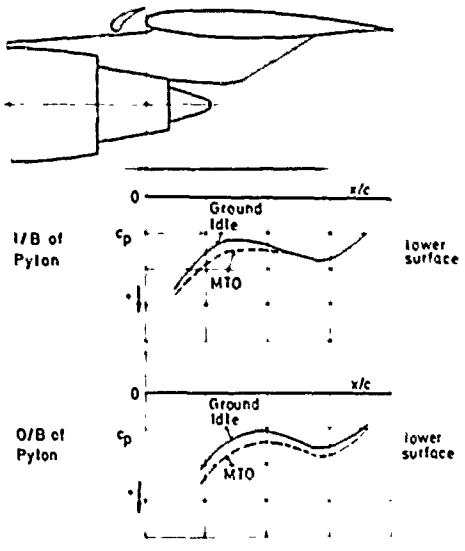

Fig.26: Jet Effects on Wing Pressures (W/T-Test)

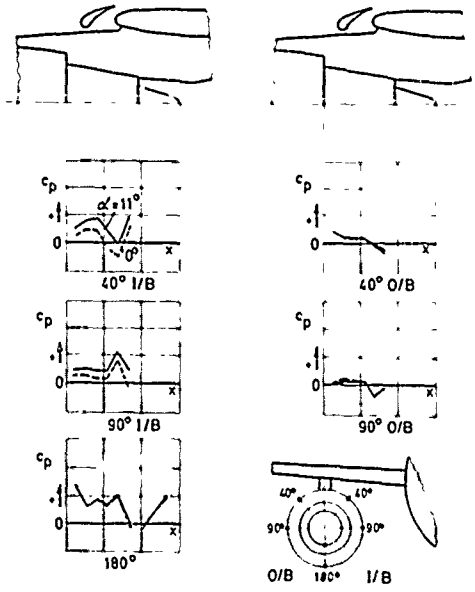

Engine condition MTO

Fig.27: Influence of Incidence Angle on Nacelle Pressures (W/T-Test)

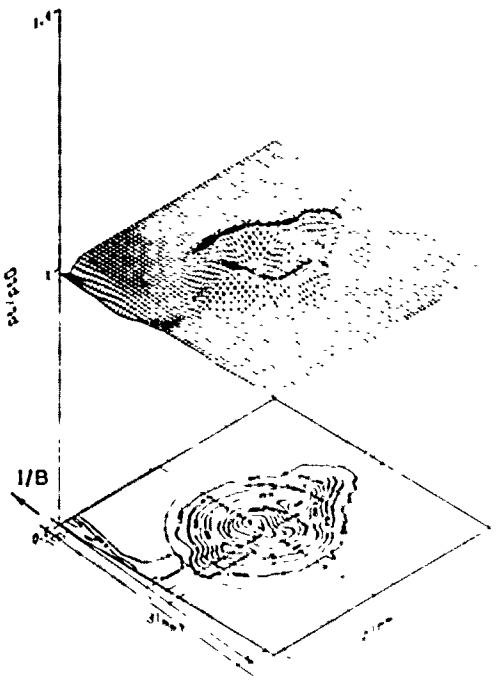

Fig.28: Wake-Flow, Flight-Idle, α = 0°
X/D = 3.2, Core Nozzle 2

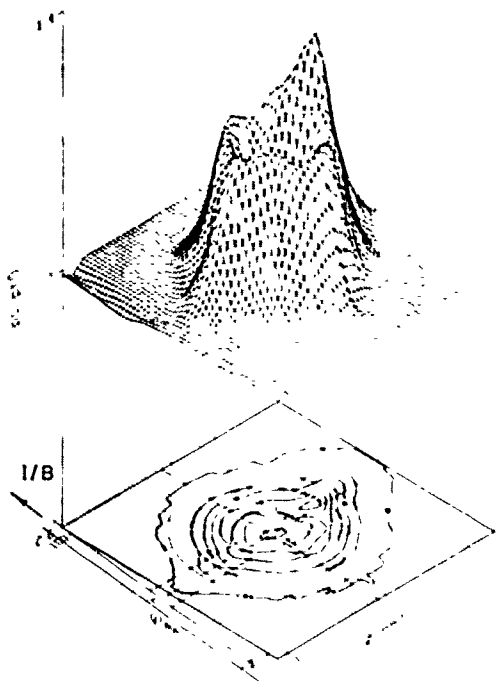

Fig.29: Wake-Flow, MTO-Power, α = 0°
X/D = 3.2, Core Nozzle 2

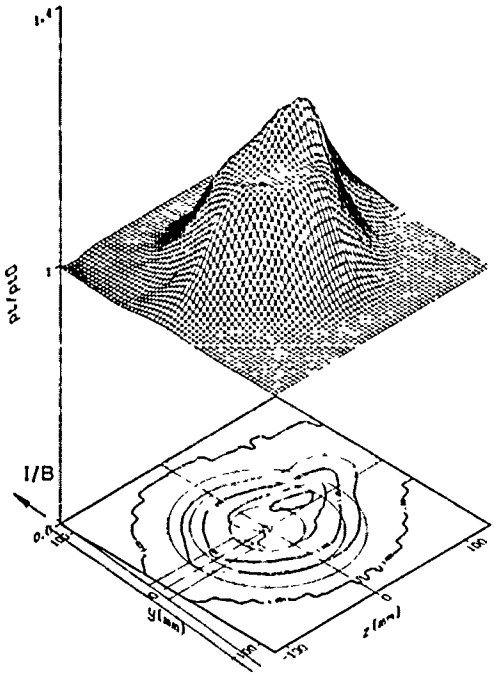

Fig.30: Wake-Flow, MTO-Power, α = 0°
X/D = 5.2, Core Nozzle 2

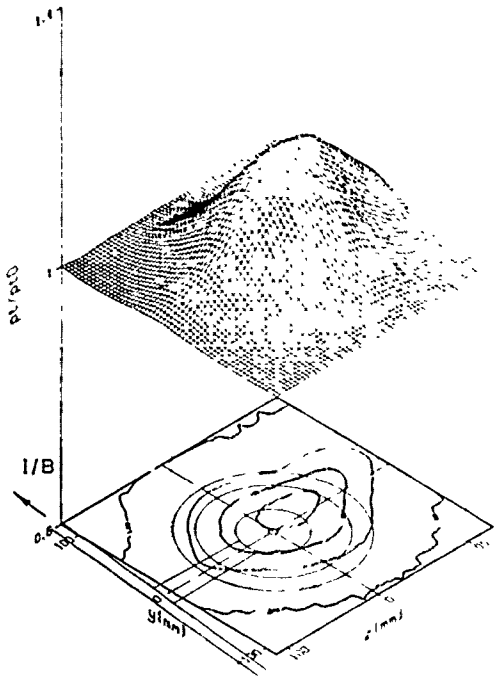

Fig.31: Wake-Flow, MTO-Power, α = 0°
X/D = 7.2, Core Nozzle 2

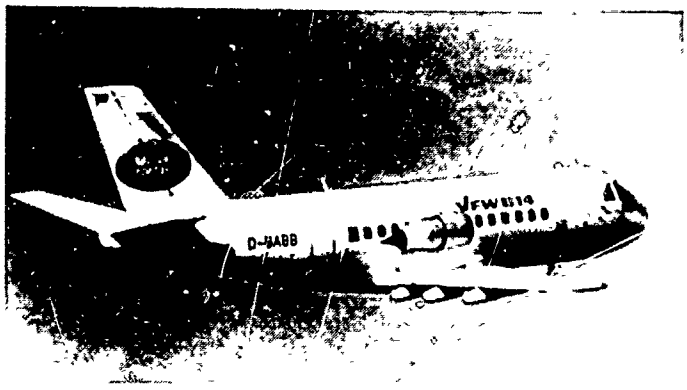

Fig.36: Shorthaul Aircraft VFW 614

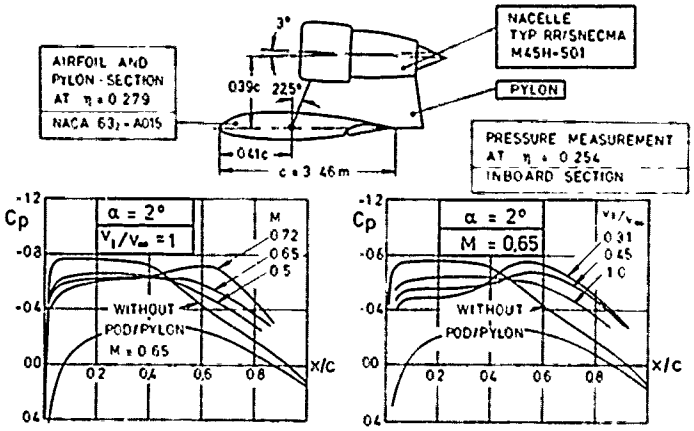

Fig.37: Engine Influence on the Surface of the Upper Wing

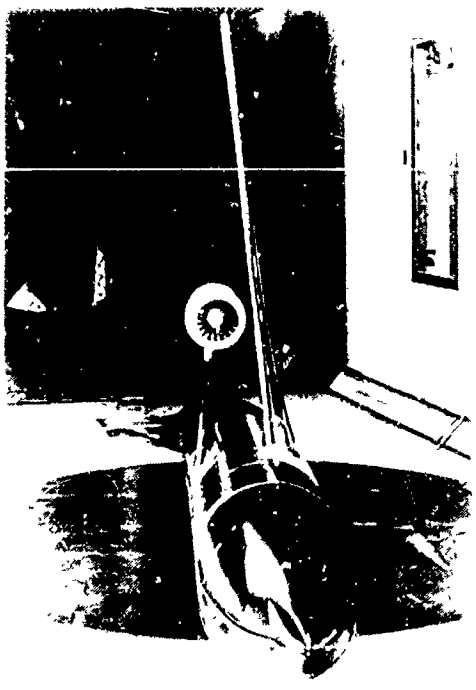

Fig.38: Half Model with Over-the-Wing Nacelles Installed in VFW Low Speed Wind Tunnel

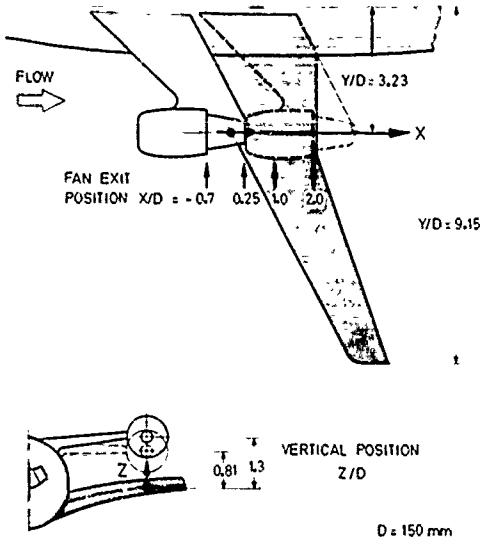

Fig.39: Over-the-Wing Nacelle Positions and Coordinate System Normalized to Fan Exit Diameter D

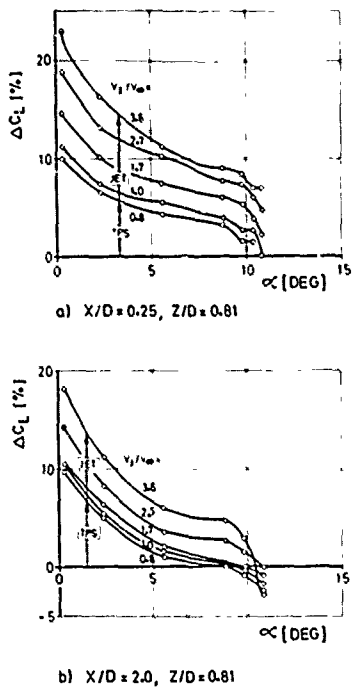

Fig.40: Influence of Engine Simulator on Lift

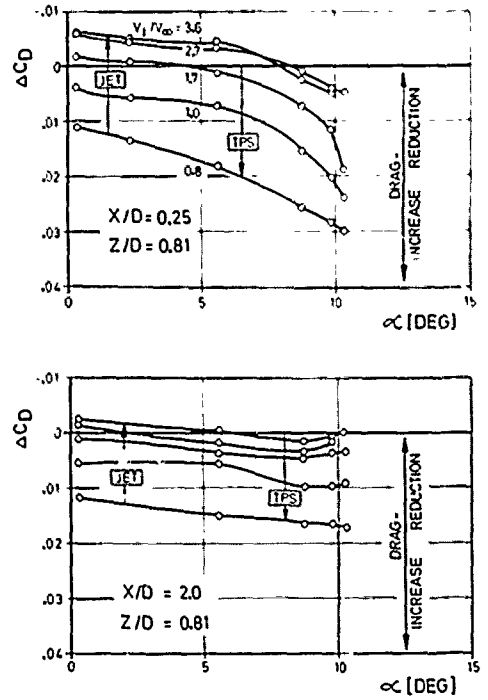

Fig.41: Influence of Engine Simulator on Drag

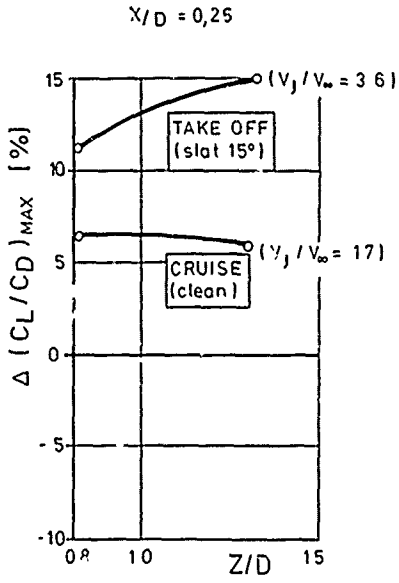

Fig.42: Lift-Drag Ratio for Different Vertical Nacelle Positions

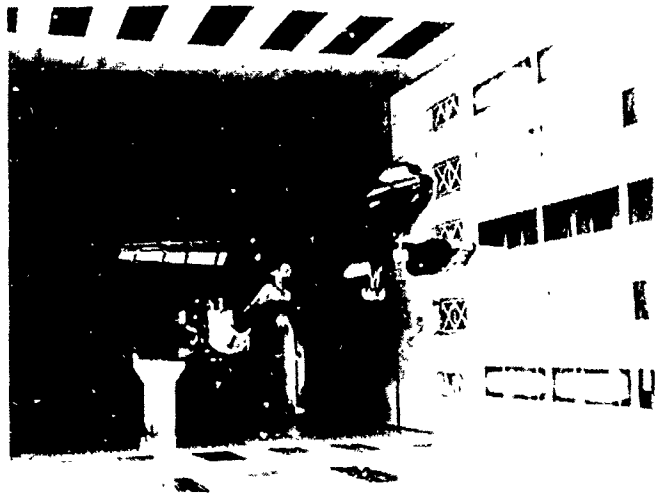

Fig.32: A300-B4 Model in DNW
(Scale 1:9.5)

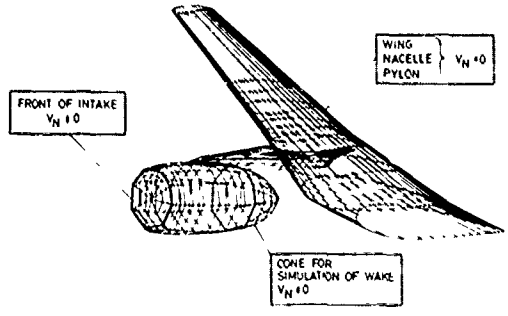

Fig.33: Wing/Nacelle/Pylon Configuration
Panel Half Span Model

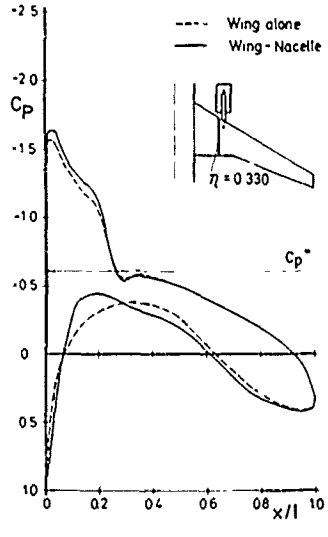

Fig.34: Wing/Nacelle Interference
Calculation Hybrid Method
($\alpha = 0.4°$, $M_\infty = 0.75$)

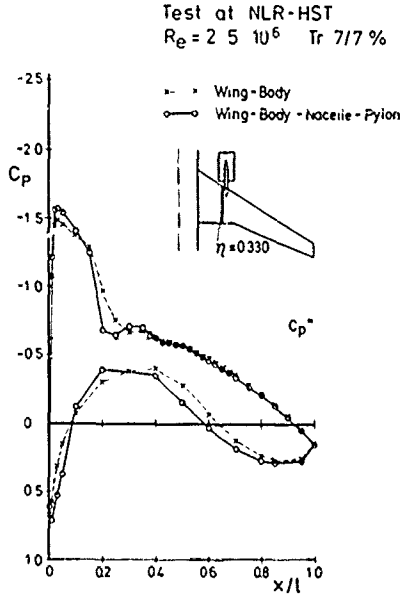

Fig.35: Comparison of Pressure
Distributions Experiment
($\alpha = 0.4°$, $M_\infty = 0.75$)

ENGINE - AIRFRAME INTERFERENCE EFFECTS

BY
Alan Vint
Principal Aerodynamicist
British Aerospace PLC
Warton Division
Preston, Lancashire
England

SUMMARY

The various types of interference between a turbo-jet or turbo-fan engine and the airframe as applicable to military aircraft are described in detail. Examples of the effects on overall aircraft aerodynamics are given, including, where possible, simple means for their evaluation. It is shown that the interference may give either significant benefits or penalties and that relatively minor geometric changes can have profound effects. Above all it is shown that the effects of all aspects of engine airframe interference must be known early in the design process so that pitfalls can be avoided or beneficial effects included in the initial aircraft design.

1. INTRODUCTION

Aerodynamic interference between the jet engine and the airframe of military aircraft has long been recognised as playing a major role in overall vehicle performance. As a result considerable research has been conducted over the years, see for example ref. 1, aimed at achieving optimum engine installation by enabling detailed consideration of the various effects to be carried out early in the design stage.

First consideration, after the size and number of power plants required has been established, is: where best to put the engine? The choice is by no means easy due firstly to the number of locations available and secondly, to the various inter-related yet different effects associated with each. Most locations have in fact been tried: in fuselage (Tornado fig. 1), over fuselage (V1 fig. 2), fuselage mounted semi-podded (Alpha-jet fig. 3), rear fuselage podded (A10 - fig. 4), fin mounted (DC10 fig. 5), under-wing podded (B58 fig. 6), under wing integrated (YC 15, fig. 7), mid wing (Canberra fig. 8) and wing tip mounted (VJ101, fig. 9). It remains to be seen if designers can find good reason for placing engines in the few remaining spaces which have not so far been used e.g. podded on tailplane!

Aerodynamic interference aspects would appear to play a small part in the final choice of engine position (fig. 10). However the designer must be kept fully aware of the aerodynamic implications of each particular contender. Only then can a position be chosen which results in an optimum installation for a particular aircraft role, or, at the very least, a satisfactory overall compromise.

Once the engine location has been established the task of evaluating the associated aerodynamic interference effects starts in earnest. Broadly the sources of interference can be divided into three groups (fig. 11):

a) the installation bulk - obvious for podded installations but still present for engines buried in fuselage or wing,

b) the intake

and c) the exhaust.

Each of these sources influences the engine/airframe interference in a variety of ways, and the paper will attempt to deal with them in turn, listing the detailed sources of interference in each group and giving, where possible, simple means by which the interference effects may be evaluated. Areas which in general have significant development risks are highlighted as well as those which can lead to significant beneficial effects. An example of a possible aircraft deliberately configured to take maximum benefit of engine/airframe interference is given along with an evaluation of one aspect of the performance improvements achieved.

2. ENGINE AIRFRAME INTERFERENCE DUE TO BULK

2.1 Buried Installations

Buried installations may or may not be seen as giving rise to engine/airframe interference in the true sense. For the purposes of this paper however a short discussion is included primarily to show that the choice of buried as against podded - which does give rise to true aerodynamic interference - still has significant aerodynamic effects.

2.2 Buried In Fuselage

The primary effect of burying the engine in the fuselage is the increase in fuselage size required to envelop the complete engine installation, generally resulting in a very large

increase in fuselage drag at both sub- and super-sonic speeds. The increase in drag is from three sources; firstly the increase in fuselage wetted area giving increased friction drag, secondly the increase in fuselage cross-sectional area giving increased form drag (subsonic) and wave drag (supersonic) and thirdly the effects of detailed engine installation requirements.

As an example, the fuselages of two different configurations, designed for the same performance capability, may be considered. 1 has fuselage buried engines, 2 has wing mounted engines. Comparison of the isolated fuselage zero-lift drag for each gives a measure of the effect of burying engines in the fuselage. Note that the discussion of wing-mounted engines is here limited to that with a nacelle integral with the wing. Pylon mounting is more associated with civil aircraft use and will not therefore be considered.

2.2.1 Subsonic Effects on Fuselage Zero-Lift Drag

At subsonic speeds the effect of fuselage installation on the fuselage zero-lift drag is very large. Fig. 12 for example shows that if full consideration is given to all components, the total fuselage drag goes up by a factor of 2.5 to 3.0 relative to that for a fuselage without engines. The increase is built up as follows:

- Friction drag, increases by 40-45% due to the increase in wetted area.
- Canopy form drag remains unchanged in this example. Increases are possible, however, associated with fuselage mounted engines if, for instance, the pilot/seat/canopy has to be raised to clear inlet ducting or to maintain pilot view over a nose inlet.
- Fuselage form drag, or more specifically afterbody drag, becomes an extremely large term when fuselage engines are incorporated. For a twin-engined aircraft afterbody drag can easily double the basic fuselage drag: in the example shown for instance the afterbody drag is actually greater than the friction drag of the basic (no-engine) fuselage. Afterbody drag associated with engine installation therefore ranks high in the overall drag breakdown and will be dealt with in detail later in the lecture.
- Diverter form drag, non-existent for the fuselage without engines, adds a significant amount of zero-lift drag when engines are added. The diverter, which is required to move the intake sufficiently away from the fuselage to be clear of the fuselage boundary layer, increases the drag of the fuselage by about 20% and is approximately 60% of the basic fuselage friction drag. Diverter drag also gives a significant contribution to overall aircraft drag and, again, will be dealt with in more detail later in the lecture.

2.2.2 Transonic Effects On Fuselage Zero-Lift Drag

The transonic effects on fuselage zero-lift drag of installing engines buried in the fuselage are shown in fig. 13. Here it can be seen that the overall fuselage drag change is much smaller (at approximately x 1.5) than occurred subsonically. As can be seen there are still significant increases in friction drag and there is also the presence of the diverter adding similar percentages of drag to those shown for the subsonic case. The main item having a different effect at transonic speeds is however the fuselage wave drag, equivalent to subsonic form drag. For the transonic case both fuselages have large amounts of wave drag, including that due to the afterbody. However, the increase due to installing the engine in the fuselage is relatively small (~15%) due partly to the effect of the intakes and exhaust stream tubes effectively reducing the nett frontal area but also due to the very favourable jet interference on wave drag. The latter effect is very important and will be dealt with later.

2.2.3 Transonic Effects On Total Aircraft Zero-Lift Drag

The previous sections showed the effects of fuselage mounted engines on fuselage drag only. The effects on zero-lift drag of the alternative engine installation must also be considered, however. For military airacraft, due to the physical size of the engine, it is generally not possible to bury the engine in any other component such as the wing and this case will not be considered. The designer is therefore forced into positioning the engine within a nacelle mounted on the wing or fuselage.

Considering a wing-mounted nacelle, the overall effect on aircraft zero lift drag is shown in fig. 14, indicating that the resulting total drag is approximately the same for either fuselage or wing mounted installations. Specifically the breakdown shows:

- When the nacelle is included, nacelle plus fuselage friction drag is greater than the fuselage with buried engines. This is partly through the increase in wetted area and partly through the higher friction coefficient for the nacelles.
- Nacelle plus fuselage wave drag is greater than that of the fuselage with buried engines, including diverter. This is due partly to the disproportionately higher wave drag of the nacelles, which, in general, have a lower fineness ratio than the fuselage, and partly to adverse fuselage/wing/nacelle interference drag.

. For the nacelle case, part of the wing is masked leading to a reduction of exposed wing wave and friction drag.

Moreover note that, with respect to zero-lift interference wave drag at transonic and supersonic speeds, significant benefits may be achieved by the use of area-ruling. The area-ruling concept, discovered many years ago (refs. 1 to 3), basically requires that for minimum drag of an aircraft configuration the total area distribution must be smooth and of the lowest possible cross-sectional area. These points are shown in figs. 15 and 16:

. Cuts are taken through the complete aircraft using planes at angle (the Mach angle) relative to freestream. The total area of the configuration intersected by the plane is then calculated and given as a distribution in the X-direction. The excercise is repeated for small rotation angles up to = 360°, and a series of area distributions formed. The drag of each area distribution is calculated, using in this case slender body theory. The wave drag of the configuration is then the mean value of the drags calculated for each area distribution. An example of the technique applied to a nacelle on wing configuration is shown in fig. 16 indicating the significant "waisting" required in the fuselage area distribution to allow for the effect of the nacelle to minimise total wave drag. The benefits which can be gained are shown in fig. 17: the reduction in zero-lift wave drag at a low supersonic Mach number was found to be approximately 15% for the case studied.

2.2.4 Effect of Wing-Mounted Nacelle On Sub- And Trans-Sonic Drag Due to Lift

The effects dealt with so far have been restricted to comparisons of the effects on zero-lift drag of fuselage with buried engines relative to wing-mounted nacelles. A further effect which fuselage buried engines do not have (apart from that due to the increased fuselage width) is that of interference with the lifting wing.

Recent measurements made at BAe Warton at low speed indicated significant increases in induced drag, due to the presence of a wing mounted nacelle. Fig. 18 illustrates the effects obtained. The expected increase in drag due to lift is approximated by the amount of exposed wing leading edge masked by the nacelle, as indicated. The measurements show, however, that at low lift the penalty on induced drag is lower than expected.

At higher lift coefficients (C_L 0.55, C_L^2 0.3) the presence of the nacelle increases the induced drag by a much greater amount than that expected. The reason for this can be found from consideration of the surface flow patterns obtained (fig. 19). It can be seen that on the inboard side of the nacelle the flow becomes almost perpendicular to the free stream wind direction presenting impossible local angles of attack for the wing leading edge in that region. The flow thus separates from the upper wing surface at the inboard nacelle/wing junction creating a large vortex and region of flow separation. Addition of a large amount of wing leading edge droop locally (fig. 19) has a significant beneficial effect (fig. 20) giving, in this case, of the order of 6% improvement in induced drag and returning the penalty at moderate to high lift coefficients to the value expected (fig. 18). Significant improvements may therefore be obtained by altering the wing leading edge geometry over only a relatively small region.

At transonic speeds, minimisation of induced drag penalties at relatively low lift and hence low angles of attack requires great care in positioning and local shaping of the nacelle in relation to the wing. As an example fig. 21 shows a typical nacelle-wing installation along with the isolated and combined pressure distributions obtained, calculated using a 3D-subsonic panel program (ref. 4). It can be seen that both nacelle and wing have strong suction peaks close to their respective leading edges. The nacelle must therefore be positioned such that the pressure distributions are staggered, minimising both the coalescence of the suction peaks and the local Mach numbers. Even with stagger significant interference between nacelle and wing leading edge will still be found which can only be alleviated by detail shape changes at the wing leading edge nacelle junction (fig. 21). At present it is necessary to use an iterative procedure of shape change followed by panel program calculation until satisfactory pressure distributions are achieved.

3. ENGINE/AIRFRAME INTERFERENCE DUE TO INTAKE

The interference between the engine intake and the airframe can be divided into the following sub-groups:

. DIVERTER EFFECTS)
. SPILLAGE EFFECTS) INTAKE TO AIRFRAME

. ENGINE FACE FLOW DISTORTION)
. ENGINE FACE FLOW SWIRL) AIRFRAME TO ENGINE VIA INTAKE
. ENGINE FACE PRESSURE RECOVERY)

Of these sub-groups the last three come more under the heading of intake/engine compatability than engine/airframe interference. Although the external aircraft aerodynamics can give significant effects on the intake flow, in general, specific design modifications to the intake will attenuate their effects considerably. Inlet design for engine compatibility is a large subject in its own right and will not be dealt with here apart from one or two observations concerning type and position. Diverter and spillage effects on the airframe which can be easily recognised as true engine/airframe interference effects will be dealt with in some detail. The effects are significantly influenced by choice of intake type and choice of intake location.

3.1 Choice of Intake Type

For military aircraft the choice of intake type is in general determined by the Mach number range of the aircraft and the emphasis required on supersonic performance. For a purely subsonic aircraft or one with limited supersonic capability a pitot type of inlet is generally acceptable (Fig. 22). For higher Mach numbers increasingly complex intake types may be chosen depending on the emphasis placed on supersonic operation. (fig. 23). The actual choice is governed by an acceptable compromise between engine compatability, external effects, cost, weight etc. The external effects are in general due to spillage and the associated cowl bluffness and will be dealt with later.

3.2 Choice of Intake Location

The dominant locations available for the intake are:

a. fuselage side)
b. underfuselage (CHIN)) fig. 24
c. overfuselage (DORSAL))
d. nacelle)

Though other positions have been used e.g. at junction between fuselage and lower wing surface (Armpit), these are generally only small variations on the above.

Each location has associated with it many different non-aerodynamic effects e.g. adverse pilot view for a and c, increased height of cockpit above ground/reduced wheelbase for b etc. There are, however, several major aerodynamic effects which must be considered:

3.3 Airframe to Inlet Interference Gross Effects

3.3.1 Side Inlet

In general the side fuselage position gives reasonable overall characteristics for normal intake operation. Providing care is taken to avoid very bad fuselage shaping or large excrescences ahead of the inlet then few problems are likely to occur.

This is, however, only true for up to moderate incidences: as incidence increases two effects are apparent from flow vizualisation studies (fig. 25).

- body upwash increases the incidence on the lower cowl, as shown in fig. 26.
- body outwash increases the "incidence" on the inner cowl side, also shown in fig. 26, exacerbated by sideslip.

The effect of body upwash on the lower cowl can in general be dealt with by reducing the loading on the intake lower lip e.g. by scarfing, by drooping of the lower lip, or even by rotating the whole of the front of the inlet as on F15. Any of these measures provides significant alleviation of the adverse body upwash effects.

Body side-wash effects are much more difficult to alleviate, however. The proper choice of vertical location of the intake combined with careful design of the lower fuselage cross-sectional shape are means of achieving satisfactory overall performance.

3.3.2 Chin Inlet

The underfuselage or chin position offers an aerodynamically favourable location though can be constraining on general configuration layouts. Primarily this is due to the beneficial effect of the fuselage in "shielding" the inlet from incidence effects (figs 25, 26) whilst giving little amplification of sideslip.

Adverse effects can become apparent at transonic speeds and low incidence, however, especially if the aircraft incorporates a drooped radome to maintain pilot view. As speed increases towards M = 1 the suction peak at the lower shoulder increases until eventually a local pocket of supersonic flow occurs. At some stage a shock wave will form, and give rise to a significant increase in boundary layer thickness or, in extreme cases, to complete flow separation (fig. 27). Either of these, if ingested by the intake, can lead to significant losses of engine thrust and care must be taken during design to avoid the situation.

3.3.3 Overfuselage Inlet (Dorsal)

Dorsal inlets would appear at first sight to offer little if any benefits over the previous two configurations, on the grounds that even at moderate incidence the thickening and possible separation of the fuselage boundary layer aft of the canopy would result in significant loss of pressure recovery at the inlet face. However the location offers such significant benefit in other areas e.g. large reduction in hot gas reingestion effects for V/STOL operation, masking of inlet from lower front quadrant with respect to radar reflections etc, that it is worth further consideration of the actual aerodynamic effects.

A recent study (ref. 6) suggests that the suspected adverse effects of incidence may not in fact be present and, indeed, that at the higher incidences the Dorsal intake may give some advantages. The possible reason for this is shown in fig. 28, illustrating that the fuselage vortex flow, augmented perhaps by strake vortices, sweeps away the boundary layer from the fuselage top surface, allowing clean flow to enter the intake. However, the possible adverse effects of low incidence boundary layer thickening or separation at transonic speeds, similar to those encountered for the chin inlet configuration (fig. 27) still exist and must be seriously considered prior to final intake location selection.

3.3.4 Nacelle Inlet

The interference at the nacelle inlet is obviously dependent on nacelle position. Positioning close to the fuselage will result in the interference types illustrated above. For the case of a wing mounted nacelle the inlet can be taken to be free of interference to a first order, ie. acting as an isolated intake. Achievement of the required performance then rests on localised design of the inlet itself and will not be considered here.

3.3.5 Overall Effects Of Inlet Location On Inlet Performance

Demonstration of the overall effects of airframe interference on intake performance may best be done by consideration of the pressure recoveries which may be achieved by intakes at each of the positions described above. The effects at high subsonic speeds are shown in fig. 29 which combines data from BAe Warton in-house studies (side, chin and isolated) with those of reference 6 (dorsal or top-mounted).

It can be seen that, at the conditions chosen, all the inlets give similar performance at low incidence. As incidence increases the performance of the inlet improves: from side location, to isolated, to chin, to dorsal. In fact, but for the "bucket" at around 10^{0} for the dorsal intake where the thick/separated boundary layer effects have not yet been eliminated by the beneficial vortices, the dorsal inlet would appear, perhaps surprisingly, to be the best location.

The effects shown are typical of those normally associated with the choice of inlet location. Significant changes in the order of ranking are possible through careful inlet design, however, so the effects shown must not be considered definitive. Many examples are given in the literature and it is up to the student of engine/airframe installation aerodynamics to judge each intake type/location combination on its own merits. In addition a large amount of dedicated wind tunnel testing and development must take place to ensure satisfactory engine-intake compatibility over the whole of the required flight envelope.

3.4 Intake to Airframe Interference

3.4.1 Diverter Flow

Intake diverters are normally used, rather than internal bleed, whenever the intake is in close proximity to an upstream surface, in order to stand the intake a sufficient distance away to ensure the surface boundary layer is not ingested into the engine. The presence of the diverter has two effects on the airframe: the primary one of increased drag, the secondary one of diverter vortex formation which may have a significant influence if it impinges or comes close to downstream surfaces such as the vertical tail fin. The latter effect is extremely configuration dependent however and will not be considered here.

The primary effect of the diverter, ie increased drag, is very significant, however, (figs. 12 and 13) and is only amenable to alleviation at supersonic speeds. At subsonic speeds the drag coefficient of the diverter is essentially fixed at approximately 0.25 based on frontal area, though minor reductions are possible (down to C_D of 0.2) with well rounded shapes (ref. 7).

At transonic and supersonic speeds the diverter drag coefficient based on frontal area is a strong function of the wedge angle and of Mach number (fig. 30), with increasing Mach number or reducing wedge angle giving significant reductions. The importance of reducing wedge angle is clear but it should be noted that the more slender the diverter the more difficult it becomes to shape the inlet duct to pass in to the main fuselage. From a construction point of view the tendency is to high diverter angles and hence high diverter drag.

3.4.2 Spillage

Spillage effects occur because the engine intake is sized for maximum entry streamtube which, in general, occurs at transonic speeds. At sub- or super-sonic speeds, or at reduced power settings the engine non-dimensional mass flow requirements reduce. The excess air which the intake is capable of delivering is then "spilled" around the intake cowl lips (fig. 31) giving rise to primary (drag) and secondary (vortex) effects similar in some ways to those for diverter flow.

.4.2.1 Spillage Drag

The term spillage drag is actually introduced to balance the accounting between external and internal flow. Engine thrust is conventionally defined as the difference between nozzle gross thrust and ram drag, the latter being calculated in the free stream ahead of the intake (As fig. 31) rather than at the structural entry. There is therefore a so-called pre-entry force equal to the stream-force change between free-stream and the intake which has to be accounted in the basic aircraft drag. However, when spillage occurs, there is a change in the flow over the external surface of the intake cowl producing a thrust which can completely offset the pre-entry force, if the inlet cowl is bluff. For military aircraft, with some emphasis on supersonic performance, a compromise has to be reached. In general, a relatively thin cowl is used in order to give low wave drag; full cowl force is not developed and the net result is spillage drag.

Calculation of spillage drag is relatively straight forward for a pitot intake (fig. 32). Pre-entry force may be calculated as shown fig. 32 and 33. The spillage drag may then be obtained by applying a factor (K_{ADD}) to the pre-entry drag which is a function primarily of the cowl bluffness. In general terms a shallow cowl such as that used for a military aircraft will have a K_{ADD} of approximately 0.6 whilst that designed for subsonic operation may have K_{ADD} of 0.2 coupled with a critical mass flow (Ao/Ac $_{CRIT}$ fig. 32) above which no spillage drag is incurred. Further guidance on values for K_{ADD} may be obtained from ref. 9; example of spillage drag effects at sub-, trans-, and supersonic speeds are given in ref. 10. For a fuller disertation on spillage drag and its prediction at transonic speeds see ref. 18, though note that spillage drag values for a pitot intake at trans- and super-sonic speeds are given in Fig. 33.

3.4.2.2 Other Spillage And Mass Flow Effects

There are two causes of the secondary spillage and mass flow effects ie. cowl separation and/or vortex production at high spillage, and the change in local flow directions at the other components of the aircraft due to changes in engine mass flow.

Of the two, the former ie. cowl separation and/or vortex production is by far the potentially more serious but is very dependent on inlet location if precise effects are to be determined. With an underfuselage inlet, for instance, if the upper cowl lip is outside the fuselage side, spill vortices can interact with the wing leading edge flow to produce unusual effects. As an example fig. 34 shows the different sideslip characteristics of a configuration having an underfuselage but only semi-shielded inlet with and without spillage present. It can be seen that the spillage leads to an adverse change in the rolling moment due to sideslip above about 25^{o}.

Other examples may be quoted but in general it is best that the aerodynamicist is aware of the potential influences so that thorough investigation, preferably in the wind tunnel, can be carried out early in the aircraft design process.

The effects of mass flow changes on flow directions around the aircraft are, apart from separation effects, generally quite small giving only minor changes in the forces from, say, a foreplane close to the inlet face. At high speed (M > approx. 0.5) the effects are in fact completely negligible with respect to forces on surfaces in close proximity.

However, recent improvements in flight control systems such that the aerodynamic benefits of increased aircraft instability may be realised has led to increased emphasis on obtaining very accurate aircraft incidence and sideslip data. At present the information is obtained from flow direction detectors in general mounted on the front fuselage some distance from the inlet. Recent tests carried out at Warton have shown that even for distances of 1 to 2 metres in front of the inlet the mass flow effects at the air direction detector positions are significant at low speed (fig. 35) and must be accounted for if optimum aircraft control is to be realised.

4. ENGINE/AIRFRAME INTERFERENCE DUE TO EXHAUST

The interference between the engine exhaust and the airframe can be divided into two different but closely related groups:

- NOZZLE INSTALLATION EFFECTS
- JET INTERFERENCE

Influences from the aircraft into the exhaust affecting basic engine thrust are, in general, negligible on military aircraft due to the high jet pressure ratios ie. nozzle choked, even at cruise conditions. The interference of the exhaust flow with the airframe can be very large, however, and is significantly influenced by the nozzle type, location and deflection as well as the basic jet characteristics themselves.

4.1 Nozzle Type

Many types of nozzle now exist or have been considered for reheated military aircraft engines and a few are illustrated in fig. 36, showing the means by which the area variation required for reheat operation is obtained. The more important types, at present, are the convergent moving shroud nozzle (fig. 37), the translating iris nozzle - either convergent (fig. 38) or con-di - and the aerodynamic or variable flap ejector nozzle (fig. 39). Each of these is currently in use on production engines and each has advantages and disadvantages relative to the others in terms of weight, cost, complexity as well as internal and external performance.

The final choice of nozzle type has to be by a thorough consideration of all factors, however, and is generally a lengthy and complex business. For example early in the design process for Tornado two contender nozzle types had been identified as the simple moving shroud and the iris nozzle. A study was put in hand to identify the overall effects on one of the proposed missions ie. low level interdiction, involving high speed flight at low level. The results of the trade study are illustrated in fig. 40 and show that although the iris nozzle gave significant reductions in installed drag, the effect of the higher mass resulted in no overall advantage relative to the moving shroud nozzle. In view of the extra cost and complexity of the iris nozzle and because no overall benefit could be identified the moving shroud nozzle was seen as the best choice - in fact thorough studies examining all contender nozzles showed similar effects and as a result led to the adoption of the moving shroud nozzle for Tornado.

In the following paragraphs the external characteristics of the different nozzles will be dealt with in more detail through the primary effect on drag. It should be noted, however, that other external effects can be very significant. Internal effects ie. the effect of nozzle type on the gross engine thrust, are given in general terms (fig. 41) to allow the reader to balance in his own mind the overall performance effects of each.

4.2 Interference Effects Of Nozzle Installation : Base Area

The effect of base area on nozzle installation drag can best be appreciated by examination of typical subsonic boattail pressure distributions (fig. 42). Here several effects can be seen:

- at the start of the boattailing there is a negative pressure peak giving a large axial force contribution in the "drag" direction.
- as distance downstream increases, the flow recompresses giving a large axial force contribution in the thrust sense.
- due to real effects of the boundary layer the actual pressures achived are less negative at the start of the boattailing but also less positive at the rear or base region.
- if flow separation occurs the pressure at the base is dramatically reduced.

Overall the drag of the afterbody is a balance between the thrust and drag components of the boattail axial force in addition to the base force. In fact the total afterbody drag can be correlated very well against effective base area as shown in fig. 43 which shows that, at subsonic speeds the afterbody drag coefficient is approximately 0.13 of the base to maximum area ratio. The data used in the correlation is for several types of nozzle installation (single, twin at rear, twin part way along fuselage) indicating that the correlation may be regarded as very general.

The only difficulty in using the correlation is in the determination of the separated flow area associated with any particular nozzle installation. Normally, iris nozzles, when set at their smallest (dry engine) area, have high boattail angles which tend to cause large areas of separated flow on the nozzles themselves. Of the order of 15° of boattail angle for high speed (M up to 0.9) operation is the maximum which can normally be tolerated on the rear fuselage/nozzle of axisymmetric type bodies before significant areas of separated flow form. In the gully regions associated with the space between the nozzles on twin-engined aircraft the maximum angle is much reduced and can be 10° or even lower.

If the above limiting angles are exceeded flow separation will appear. Determination of the actual area of separation is practically impossible at this stage however due to the extreme complexity of the flow field in the rear fuselage region. In addition, other adverse effects of rear fuselage flow separation at subsonic speeds - primarily vibration, but including reduced fin power etc - are so severe that it is far better to design for no separated flow at all. Theoretical methods to allow the design of the rear fuselage to enable separation free flow combined with low installed nozzle drag are likely to be available in the not too distance future. Until such time as the methods have been proven, however, great reliance has to be placed on proper wind tunnel model testing, though even then full simulation is not yet possible and development during flight tests may still be required.

In summary, the overall objective of any rear fuselage nozzle installation are two-fold:

- minimisation of base area, to minimise drag.
- elimination of separations on nozzle/boattail to minimise drag, vibration, adverse influences on rear fuselage mounted flying surfaces.

The reader is referred to reference 11 for a more detailed apraisal of nozzle installation effects.

4.3 Interference Effects Of Jet Efflux

The interference effects of the jet efflux from the nozzle are due to the following causes:

- entrainment
- modification of potential flow field
- jet impingement/attachment onto downstream structure

4.3.1 Zero-Lift Drag

A typical curve of the variation of subsonic (and to some extent transonic/supersonic) afterbody drag with nozzle pressure ratio is given in fig. 44 illustrating the effect of each of the above. In the absence of base area, entrainment effects tend to be minimum, potential flow effects a maximum. If structure occurs downstream there is in general little influence on the curve until some critical pressure ratio, at which jet attachment to structure occurs. As pressure ratio is increased above the critical value, drag rises rapidly.

The different effects of jets issuing from convergent (ie. under-expanding) and convergent-divergent (ie. fully-expanding nozzles) is shown in fig. 45. In general at transonic speeds the aircraft are operating with afterburners on ie. with increased nozzle area. For a moving shroud type of nozzle this only means that the nozzle base area is reduced. For a fully expanding convergent-divergent nozzle however the jet area is increased significantly leading to a significantly lower boattail angle. Without jets on, the wave drag component of the nozzle is therefore considerably less than that of the moving shroud type nozzle. As jet pressure ratio increases, however, the underexpanded jet from the moving shroud nozzle plumes and causes the boattail terminal shock to move forward, reducing afterbody drag considerably; with the con-di nozzle no such drag relief occurs. In the example given in fig. 45 the jet-effect on drag for the moving shroud nozzle is so powerful that, at operating pressure ratios, there is little to choose between the drag of the two installations.

Temperature also influences the effect of the jet on installed drag, and significant work has been carried out in the past to better quantify the effects (eg. refs. 12, 13). An example, taken from ref. 13 is given in fig. 46. At dry power settings the jet temperature is generally so low that the effect on drag can be neglected. With maximum afterburner, however, jet temperature is extremely large and the effect on drag must be accounted for. It is interesting to note that here at least is one item which actually benefits aircraft performance!

4.3.2 Lift And Drag Due To Lift

One other area in which jet interference can give substantial beneficial interference is in improvements in both lift and drag due to lift. In order to achieve the benefits it is necessary to have the aircraft configured such that the nozzle is at or close to the wing trailing edge. Recent reports have shown a revival of interest in the phenomenon (e.g. refs. 14, 15, 16) possibly due to the likely availability of deflecting nozzles, for the main propulsive nozzle.

An investigation carried out at BAe Warton examined the overall effects of the improvement of lift and of drag due to lift on combat performance. The studies showed that there were substantial gains to be made in the combat applicable regions of the flight envelope (ref. 17). Also included in ref. 17 was a simple method for estimating the jet interference effects a lift, drag and pitching moment.

The configuration examined (fig. 47) was a close coupled canard with the engines under wing such that the jet emerges via a deflecting nozzle at the trailing edge. The presence of the jet at the wing trailing edge enables a substantial proportion of the potential jet flap effect (fig. 48) to be realised giving significant increases in lift. Consideration of the theory shows that drag due to lift also improves and this is confirmed by comparison with experiment (fig. 49). Pitching moments are also influenced, however: the jet effect increases the nose down pitching moment from the wing significantly (fig. 50), such that it may easily be demonstrated that a canard configuration is required if the potential improvements, primarily in the low speed, low level region of the flight envelope (fig. 51) are to be achieved.

4.3.3 Other Jet Interference Effects

Jet interference effects can be many and unexpected and are very much configuration dependent. The engine installation designer must at all times be aware of the possible influences of the jet when located in certain positions. Reference must be made to the available literature to identify if the proposed installation has been previously considered, and literature surveys similar to ref. 1 are invaluable in this respect.

It must also be borne in mind that any new aircraft design will have a unique rear fuselage nozzle installation and early wind tunnel testing of a detailed facsimile of the aircraft are required to ensure that there are no major adverse effects. Only with the model data available can the designer feel reasonably sure that such effects are unlikely to appear in flight. Even if difficulties are encountered, significant assistance as to necessary modifications for their alleviation can normally be quickly generated by properly conducted testing.

Some unexpected jet effects that have been encountered during model and flight testing are

- sudden change in tailplane jack loads with application of reheat.
- power dependence of yawing moment due to sideslip such that at maximum power aircraft directionally stable with fin OFF.
- reduced longitudinal stability due to effect of jet on downwash flow field.

Many other different effects will have been encountered at some stage with different aircraft designs. It must be emphasised that only through designer awareness of the likelihood of such effects can their possible presence be anticipated and avoided, if necessary, in the early design stages.

5. CONCLUDING REMARKS

The various aspects of engine airframe interference effects have been dealt with in some detail in the report, including simple estimating procedures where possible. The effects have been shown in many cases to be far reaching. Emphasis has been put on designer awareness coupled with early model testing as a means of reducing the risk of one or more of the many avoidable adverse effects carrying through on to a production aircraft; similarly for the exploitation of beneficial interference effects which are, as may be expected, rather limited in number.

REFERENCES

1. NICHOLS, M. R. NASA TM 81814 NOVEMBER 1980 — Bibliography on Aerodynamics of airframe/engine integration of high speed turbine powered aircraft.
2. HARRIS, R. V TMX 947 MARCH 1964 — An analysis and correlation of aicraft wave drag.
3. WHITCOMB, R. T. NACA 1273 1956 — The study of zero-lift drag rise characteristics of wing-body combinations near the speed of sound.
4. WHITCOMB, R. T. and FICHETTI, T. L. NACA TIB 3912 — Development of a supersonic area rule and an application to the design of a wing body combination having high-lift to drag ratios.
5. BUTTER, D. J., HUNT, B., & HARGREAVES, G. R — A survey on boundary integral methods (Numerical Methods in Aeronautical Fluid Dynamics - Roe, P. L. 1982)
6. WILLIAMS, T. L. et al PAPER 2 AGARDOGRAPH CP301 MAY 1981 — Top-mounted inlet system feasiblity for transonic-supersonic fighter aircraft.
7. DAVENPORT, C. S&T MEMO 7/68 SEPTEMBER 1968 — A further investigation of the drag at subsonic speeds of side intake boundary layer diverters.
8. PEAKE, D. J. and RAINBIRD, W. J. PAPER 18 AGARD CP124 APRIL 1973 — The drag resulting from 3D separations caused by boundary layer diverters and nacelles in subsonic and supersonic flow.

9. MOUNT, J. S. AGARDOGRAPH 103 1965 — Effects of inlet additive drag on aircraft performance.

10. HAWKINS, J. E. JOURNAL OF AIRCRAFT VOL 13 NO 6, 1976 — YF16 Inlet design and performance.

11. LEYLAND, D. C. NOVEMBER 1979 — Some aspects of nozzle installation. (Proceedings of the 4th Seminar on Gas Turbines held in Bangalor during November 1979. ARDB-PROC-703).

12. KENNEDY, T. L. AEDC TR-80-8 NOVEMBER 1980 — An evaluation of wind tunnel test techniques for aircraft nozzle afterbody testing at transonic Mach numbers.

13. HENRY, B. Z. and CAUN, M. S. NACA/TIL/5250 JUNE 1956 — Additional results of an investigation at transonic speeds to determine the effects of a heated propulsive jet on the drag characteristics of a related series of afterbodies.

14. BOWER, D. L. and BUCHAN, F. AIAA 78-1082 JULY 1978 — An investigation of the induced aerodynamic effects of a vectored non-axisymmetric exhaust nozzle.

15. THOMAS, J. L., PAULSON, J. W. and YIP, L. P. JOURNAL OF AIRCRAFT MAY 1978 — Deflected thrust effects on a close-coupled canard configuration.

16. HUTCHINSON, R. A. CAPONE, F. J., and WHITTAKER, R. W. AIAA 80-1159 JULY 1980 — Investigation of advanced thrust vectoring exhaust systems for high speed propulsive lift.

17. VINT, A. AGARD CP 285 MAY 1980 — Jet-wing interaction to give improved combat performance.

18. MIDAP STUDY GROUP AGARDOGRAPH 237 JANUARY 1979 — Guide to in-flight thrust measurement of turbo-jet and turbo-fan engines, AGARD 237.

ACKNOWLEDGEMENTS

The author would like to take this opportunity to formally thank his colleagues at BAe Warton for their help and advice during the preparation of this paper, with special thanks to MR. M. J. BRIERS for the contribution of certain figures and guidance on part of text.

FIG. 1 TORNADO ADV

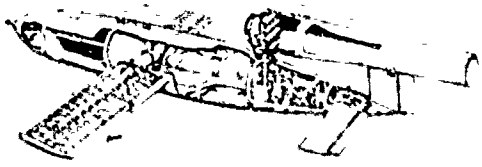

FIG. 2 V1 DOODLE BUG

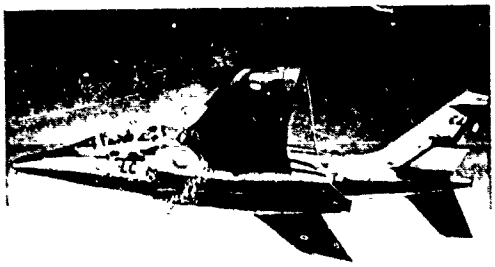

FIG. 3 ALPHA-JET

FIG. 4 A10

FIG. 5 DC10

FIG. 6 B58

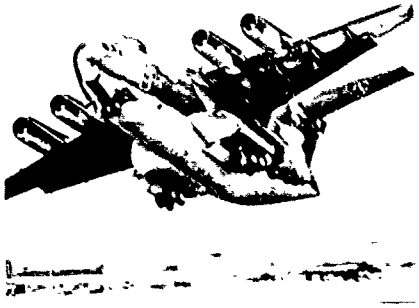

FIG. 7 YC15

FIG. 8 CANBERRA

FIG. 9 VJ101

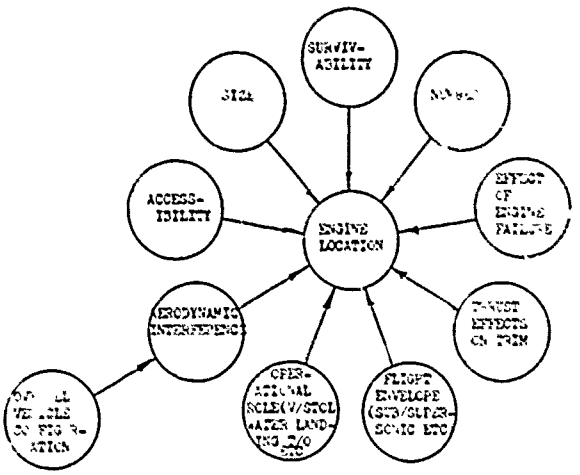

FIG. 10 - FACTORS INFLUENCING CHOICE OF ENGINE LOCATION - MILITARY AIRCRAFT

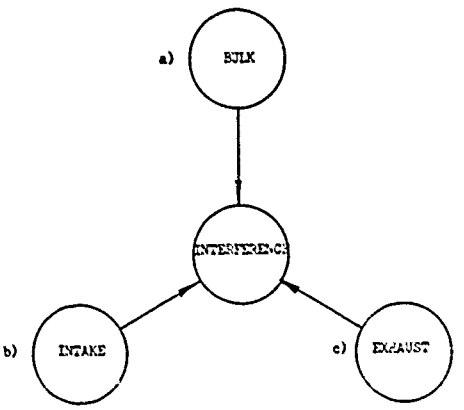

FIG. 11 SOURCES OF ENGINE AIRFRAME INTERFERENCE

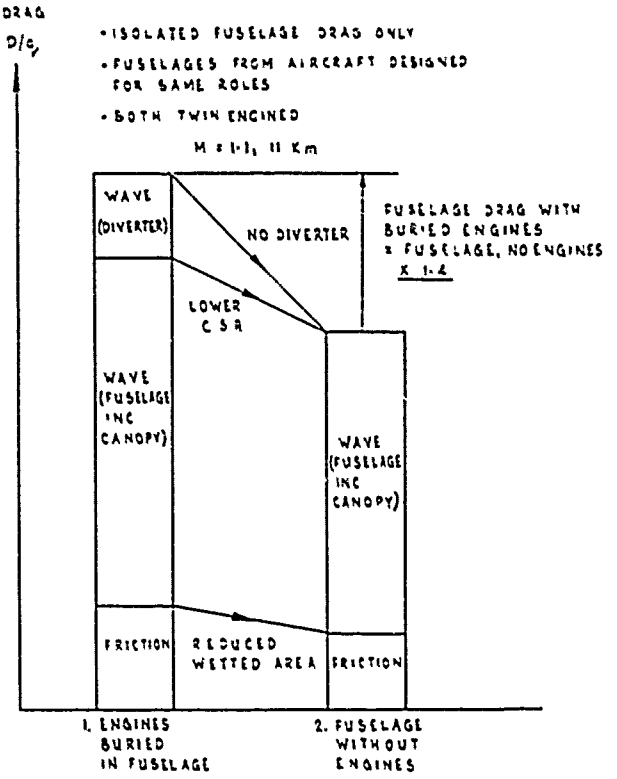

FIG 13 CHANGE IN TRANSONIC ZERO-LIFT DRAG OF FUSELAGE DUE TO BURYING ENGINES

•ISOLATED FUSELAGE DRAG ONLY
•FUSELAGES FROM AIRCRAFT DESIGNED FOR SAME ROLES
•BOTH TWIN-ENGINED

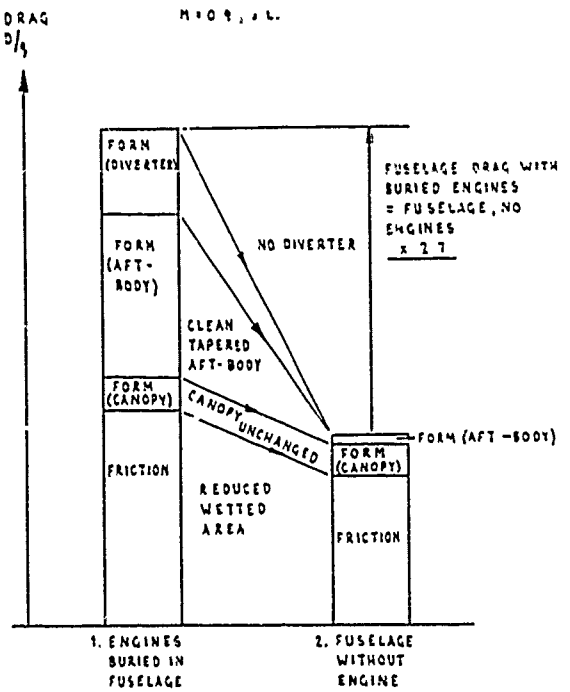

FIG 12 CHANGE IN SUBSONIC ZERO-LIFT DRAG OF FUSELAGE DUE TO BURYING ENGINES

FUSELAGE, WING, NACELLE DRAG INC. INTERFERENCE
AIRCRAFT DESIGNED FOR SAME ROLES
TWIN-ENGINES
WING-MOUNTED NACELLE-NO PYLONS

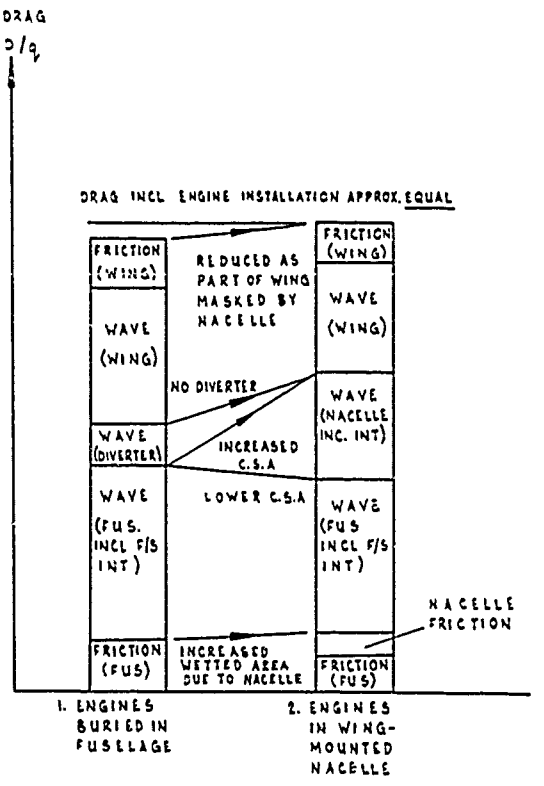

FIG 14 OVERALL CHANGE IN TRANSONIC ZERO LIFT DRAG BURIED Vs NACELLE MOUNTED ENGINES

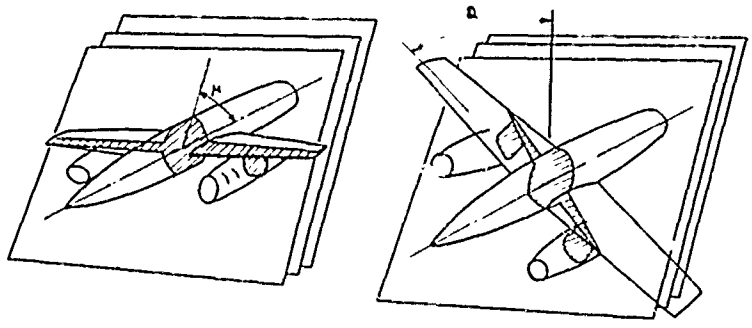

$$\frac{D(\theta)}{q} = -\frac{1}{2\pi}\int_0^{\ell}\int_0^{\ell} S''(x_1)\,S''(x_2)\,\log_e|x_1 - x_2|\,dx_1\,dx_2$$

$$\frac{D}{q} = \frac{1}{2\pi}\int_0^{2\pi}\frac{D(\theta)}{q}\,d\theta$$

FIG 15 AREA RULING WING MOUNTED NACELLES

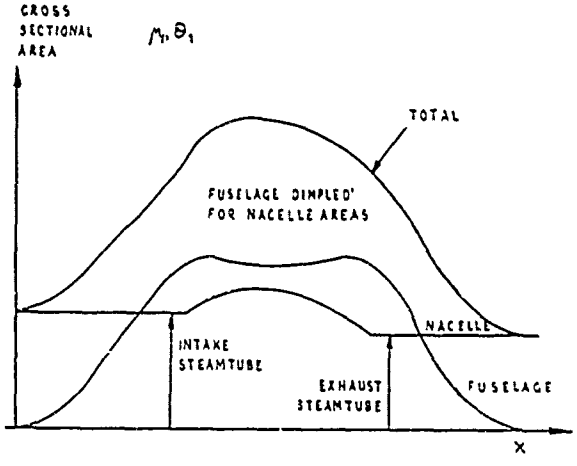

FIG 16 AREA DISTRIBUTION FOR CONFIGURATION WITH WING MOUNTED NACELLE

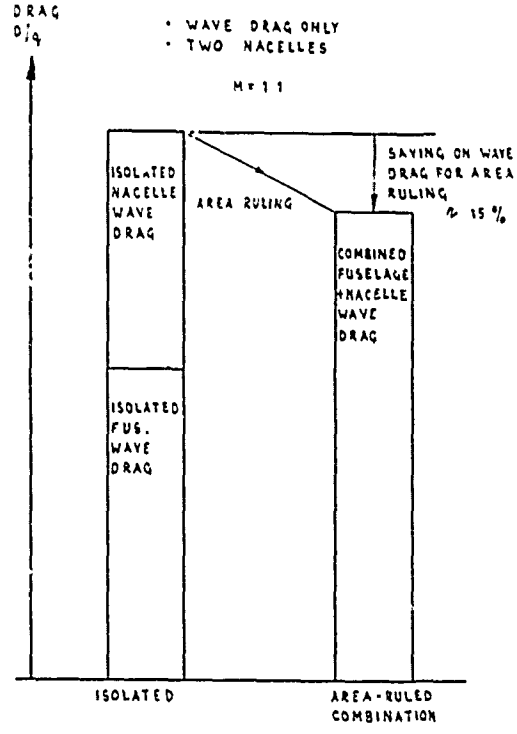

FIG 17 EFFECT OF AREA RULIN. ON TRANSONIC ZERO-LIFT DRAG FOR NACELUCD AIRCRAFT.

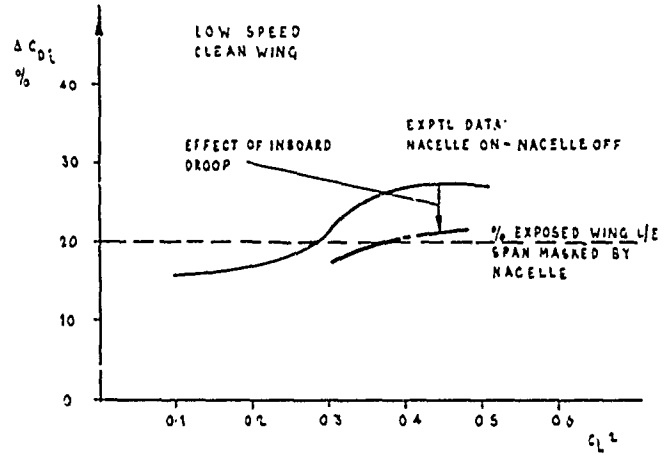

FIG. 18 EFFECT OF WING MOUNTED NACELVE ON DRAG DUE TO LIFt.

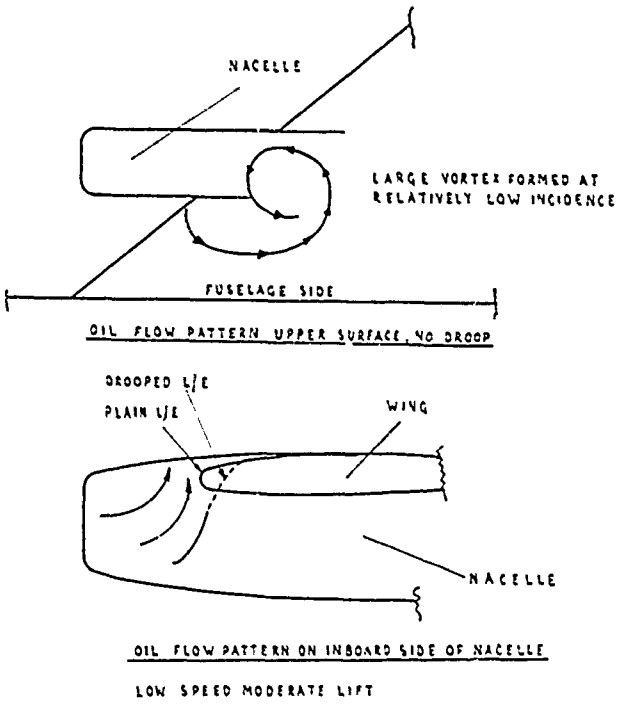

FIG 19 FLOW PATTERN EFFECTS OF NACELLE OF WING

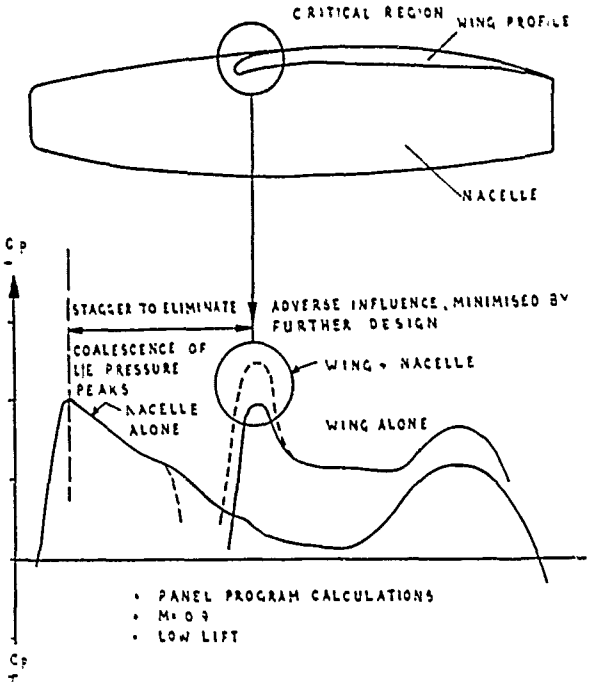

FIG 21 TRANSONIC WING-NACELLE EFFECTS

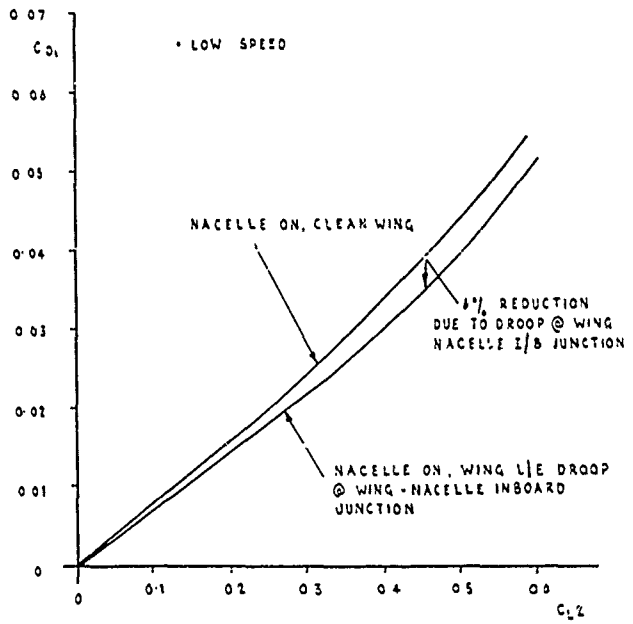

FIG 20 INFLUENCE OF LOCAL INBOARD NACELLE WING JUNCTION L/E DROOP ON INDUCED DRAG.

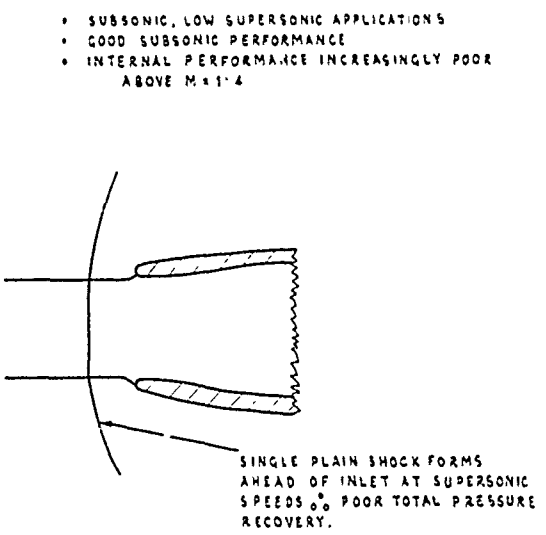

FIG. 22 PITOT INLET

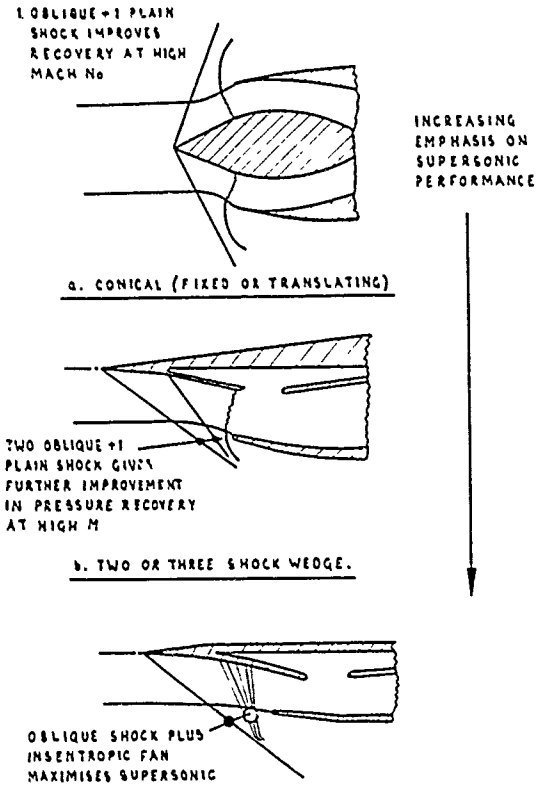

FIG 23 INTAKES FOR SUPERSONIC OPERATION

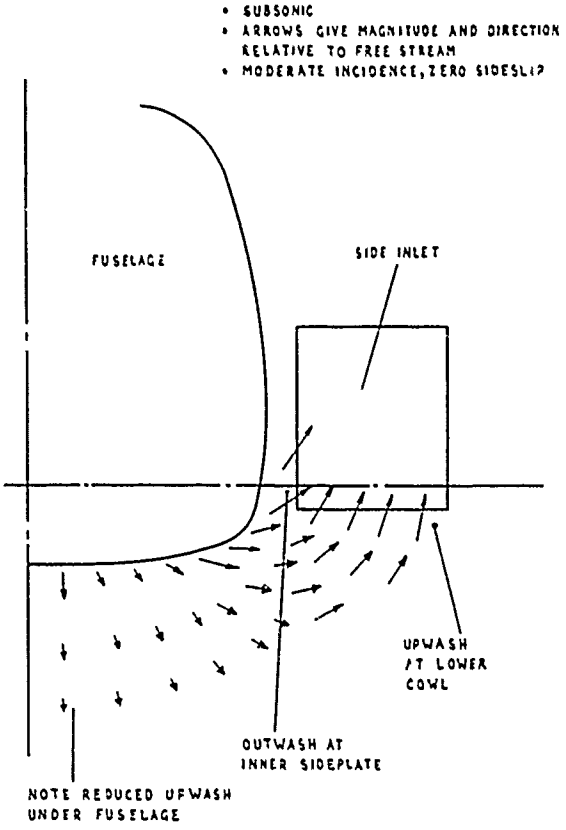

FIG.25 EFFECT OF FUSELAGE FLOW ON SIDE INLET LOCAL INCIDENCE

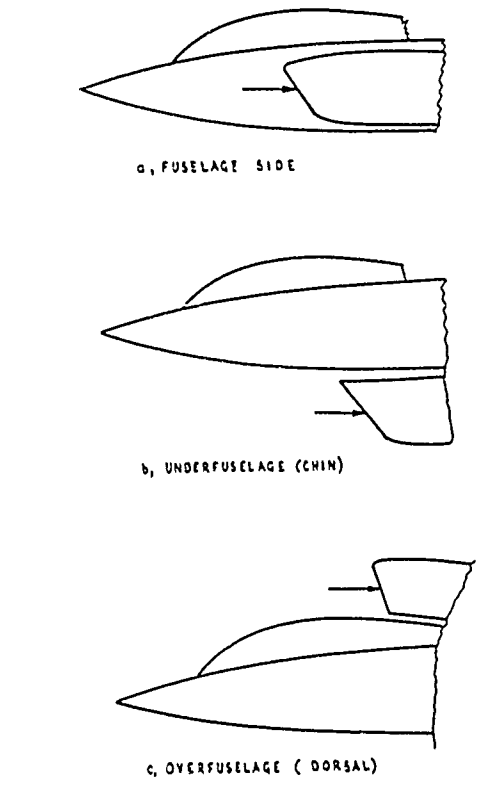

FIG. 24 INTAKE LOCATIONS ON FUSELAGE

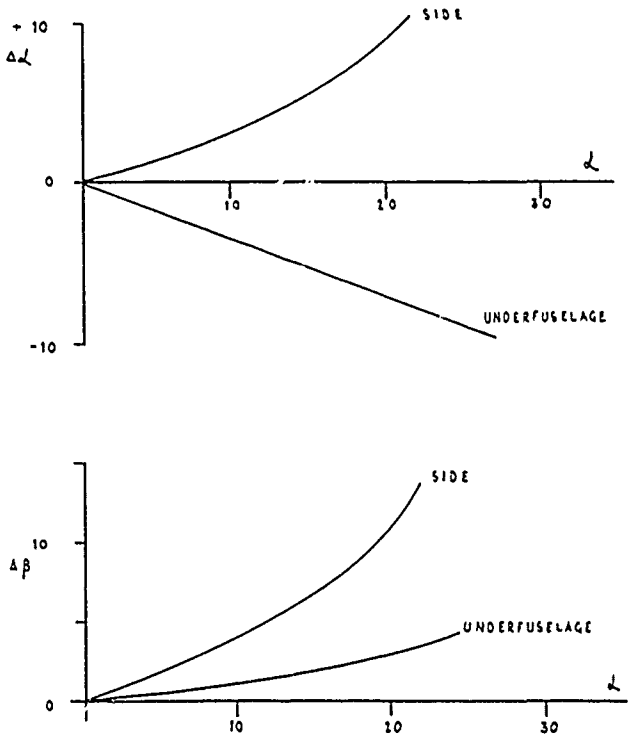

FIG 26 VARIATION IN LOCAL FLOW DIRECTION FOR SIDE AND UNDERFUSELAGE INTAKES

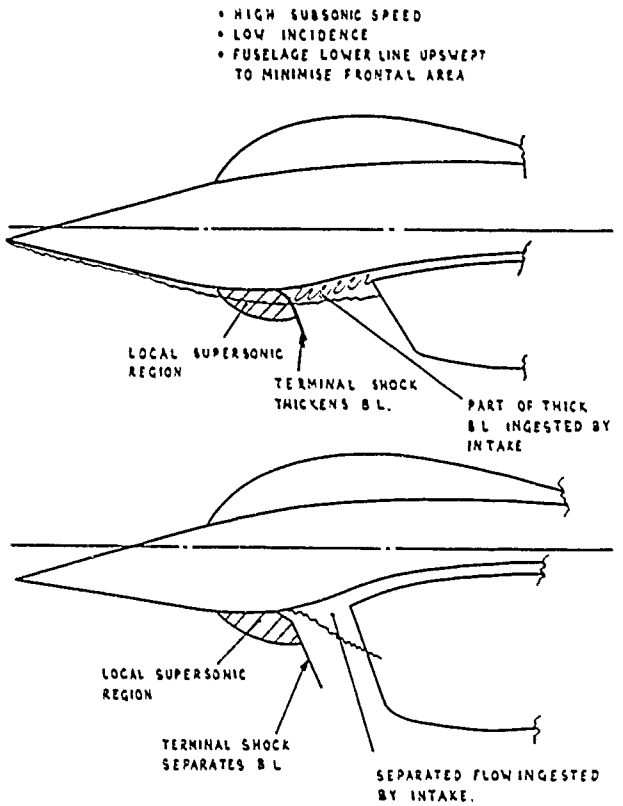

FIG. 27 POSSIBLE ADVERSE TRANSONIC EFFECTS OF UNDERFUSELAGE (CHIN) INTAKE POSITIONS

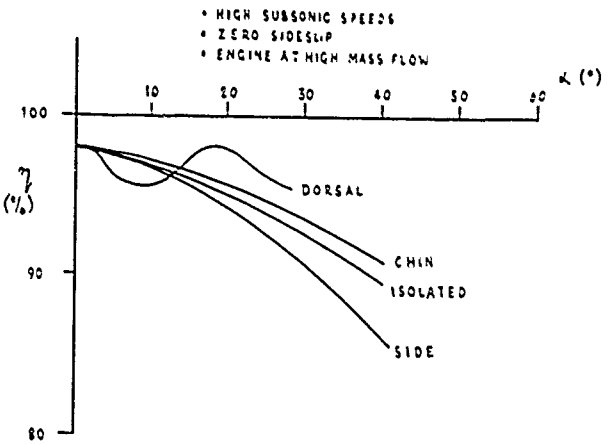

FIG 29 COMPARISON OF PRESSURE RECOVERY ACHIEVED WITH DIFFERENT INTAKE LOCATIONS

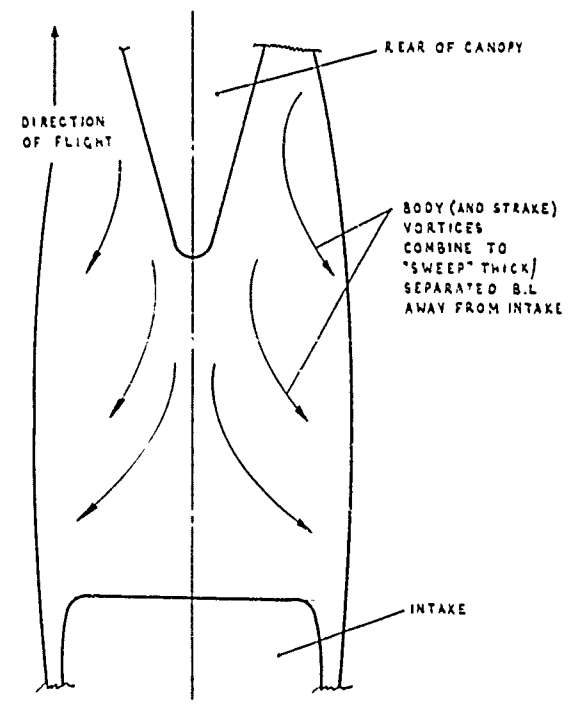

FIG 28 OVERFUSELAGE (DORSAL) INTAKE FLOW IMPROVEMENT EFFECT AT MODERATE TO HIGH INCIDENCE

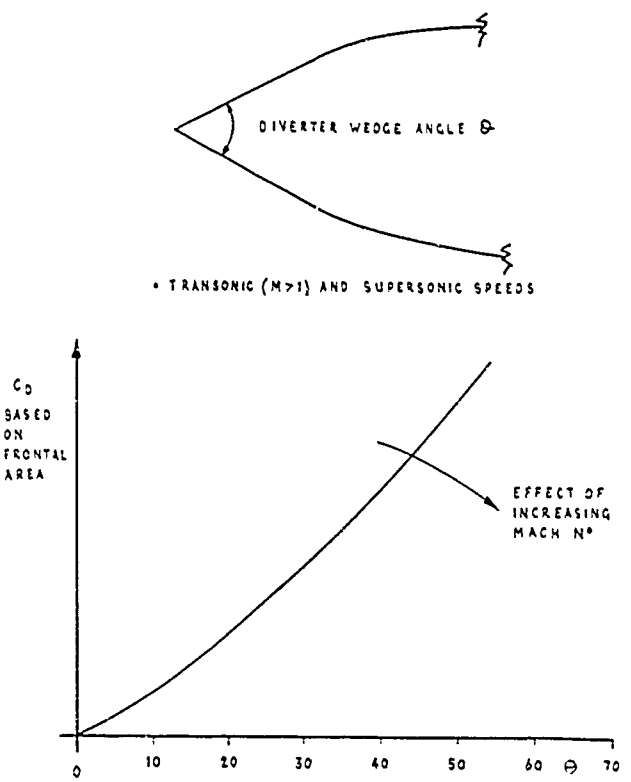

FIG 30 EFFECT OF SUPERSONIC MACH NUMER AND WEDGE ANGLE ON DIVERTER DRAG

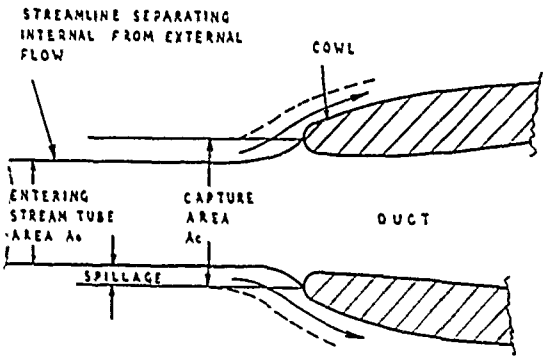

FIG.31 INTAKE SPILLAGE DEFINITION

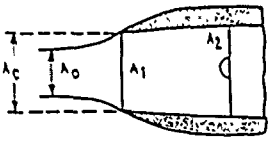

$$\phi_{pre} = F_{G1} - F_{G0}$$
$$F_G = P_T A_G - P_0 A$$
$$C = P/P_T\,(1 + \gamma M^2)$$
$$C_{\phi\,pre} = \frac{2}{\gamma M_0^2}\left[\frac{\eta_1 C_1}{\left(P/P_T\right)_0} - 1\right] - 2\frac{A_o}{A_c} = \left(1 - \frac{A_o}{A_c}\right)^2 \text{ IN COMPRESSIBLE FLOW}$$
$$\frac{A_o}{A_c} = \frac{\eta_2}{A_c}\,\frac{\left(\frac{W\sqrt{T_T}}{P_T}\right)_2}{\left(\frac{W\sqrt{T_T}}{AP_T}\right)_0}$$

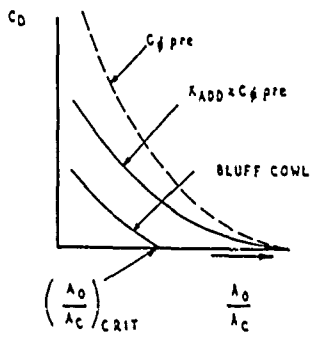

PITOT INTAKE AT SUBSONIC SPEEDS

FIG.32 ORIGIN OF SPILLAGE DRAG

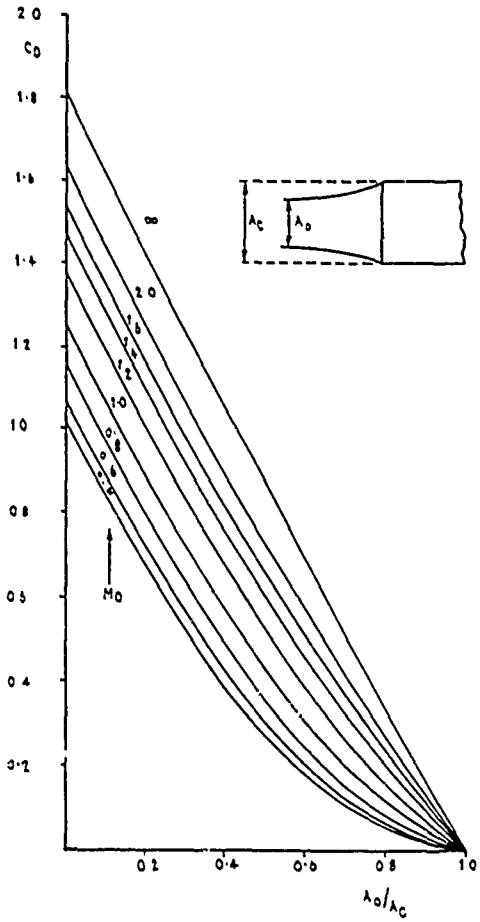

FIG. 33 PITOT INTAKE PRE-ENTRY DRAG

* LOW SPEED DATA
* INLET LIP AHEAD OF WING BODY JUNCTION LEADING EDGE.

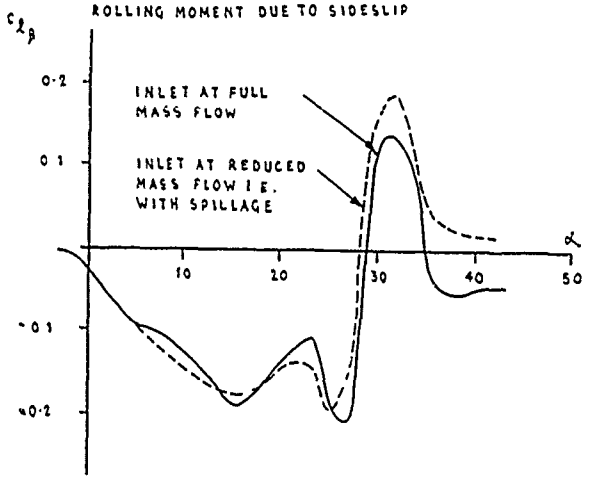

FIG. 34 EFFECT OF UNDERFUSELAGE INLET SPILLAGE FLOW ON ROLL CHARACTERISTICS

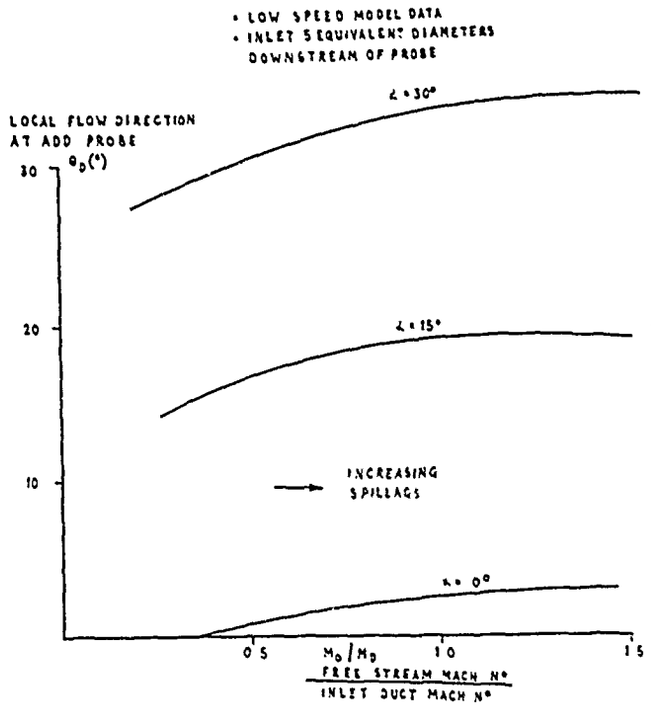

FIG. 35 EFFECTS OF ENGINE INLET MASS FLOW ON AIRFLOW DIRECTION AT AIR DATA PROBE POSITIONS

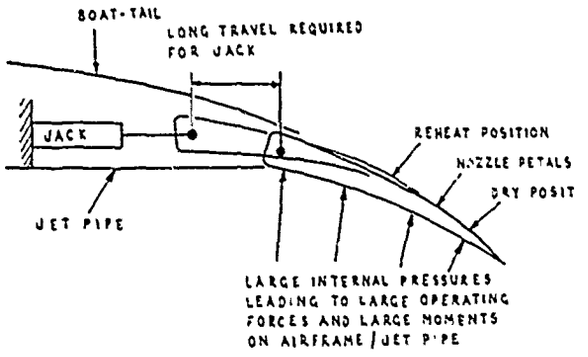

FIG 38 TRANSLATING IRIS NOZZLE

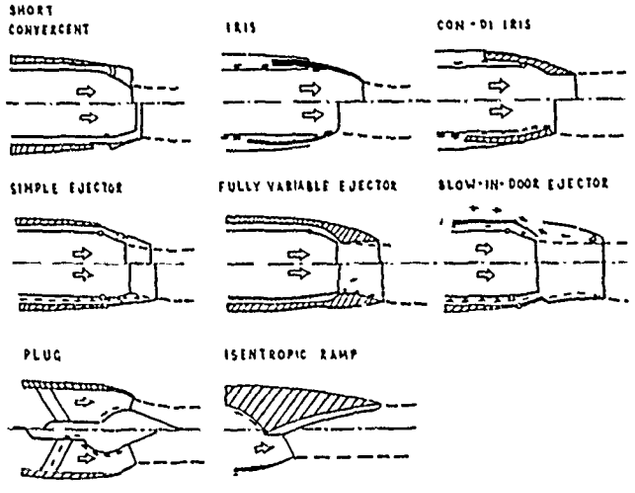

FIG. 36 TYPICAL NOZZLE TYPES FOR REHEATED MILITARY ENGINES

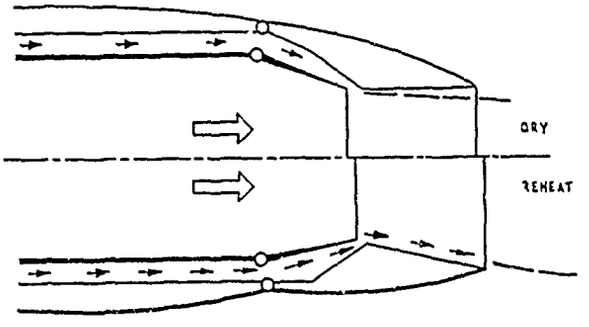

FIG 39 VARIABLE FLAP EJECTOR NOZZLE

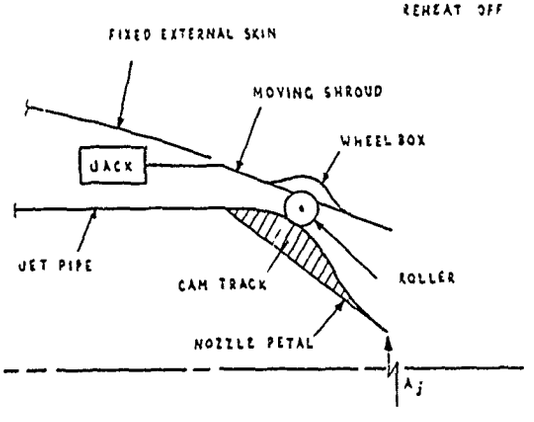

FIG. 37 SCHEMATIC OF MOVING SHROUD NOZZLE

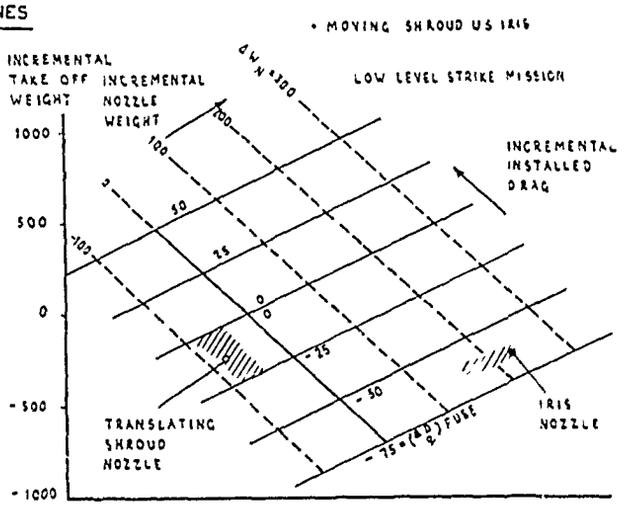

FIG 40 CHOICE OF NOZZLE STUDY

* ALL NOZZLES ARE SIMPLE VARIATIONS OF THOSE FOR WHICH THE THRUST CHARACTERISTICS ARE GIVEN

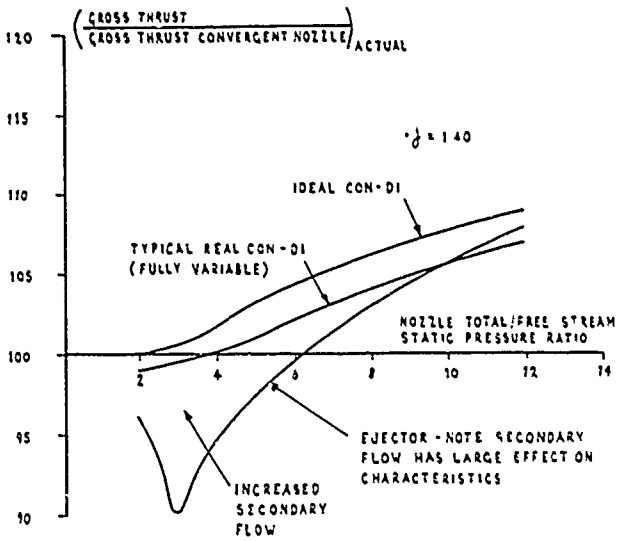

FIG 41 GROSS THRUST EFFECTS OF DIFFERENT NOZZLE TYPES

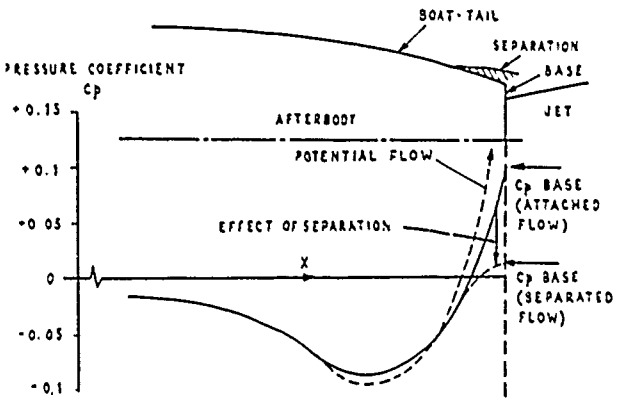

FIG 42 TYPICAL SUBSONIC BOAT-TAIL PRESSURE DISTRIBUTION

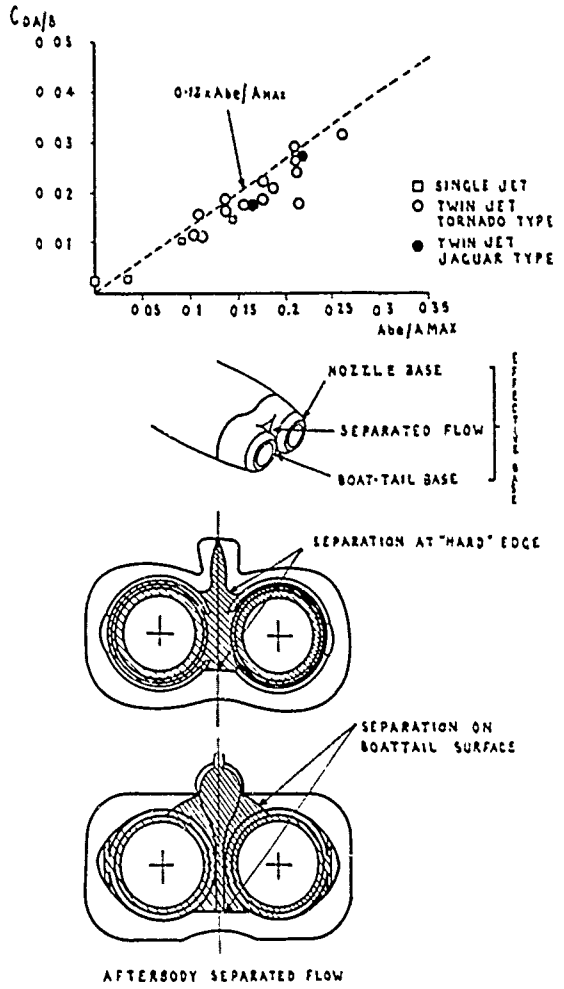

FIG 43 EFFECT OF EFFECTIVE BASE AREA ON MEASURED AFTERBODY FORCE

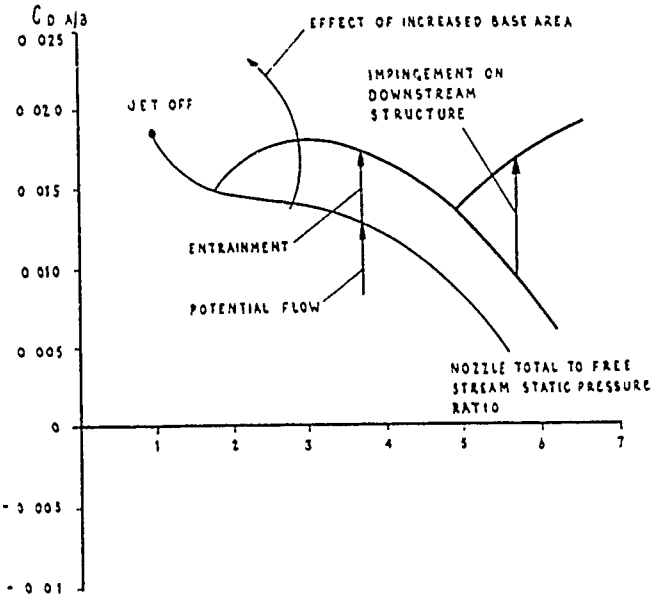

FIG. 44 INFLUENCE OF JET PRESSURE RATIO ON SUBSONIC AFTERBODY DRAG

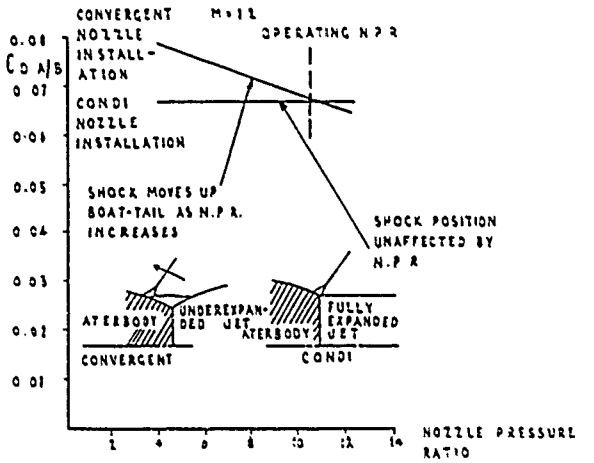

FIG 45 EFFECT OF JET ON CONVERGENT AND CONDI NOZZLE AFTERBODY DRAG

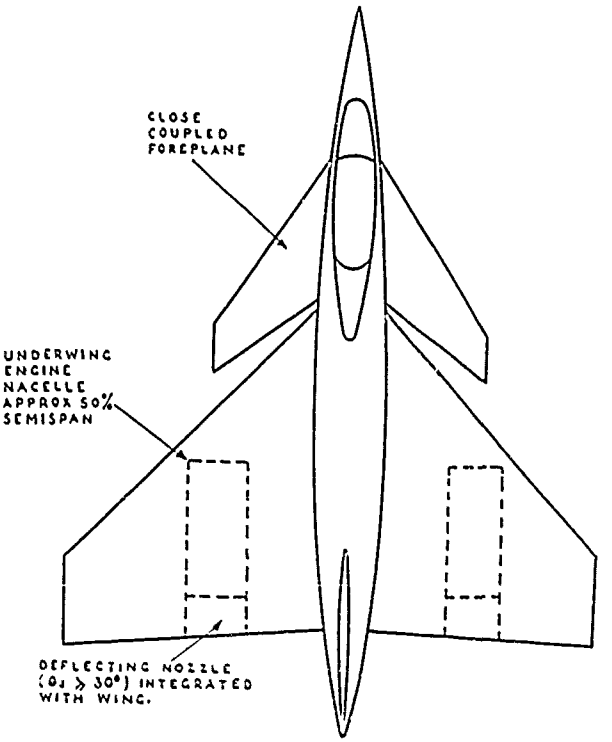

FIG 47 CANARD CONFIGURATION FOR JET WING INTERACTION STUDIES

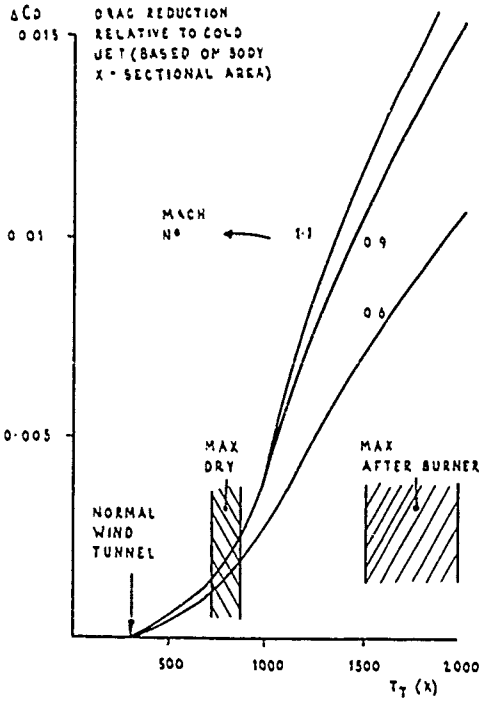

FIG.46 INFLUENCE OF JET TEMPATURE ON AFTERBODY DRAG

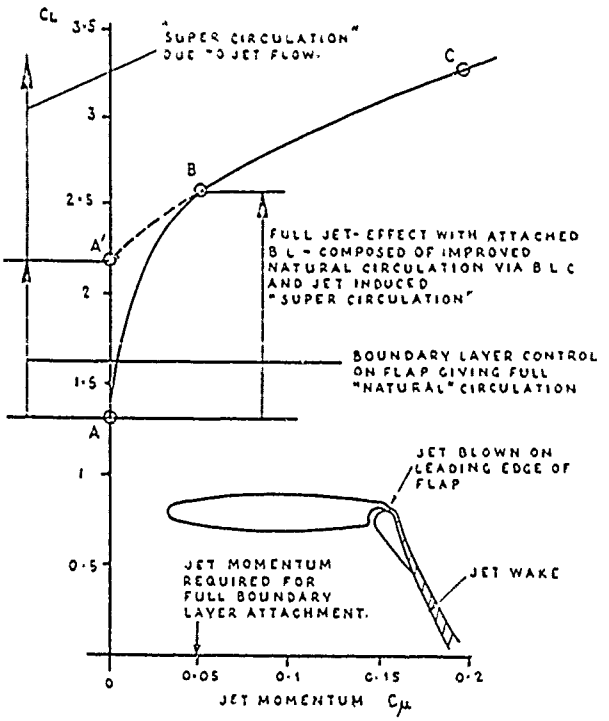

FIG 48 JET FLAP EFFECT ON LIFT

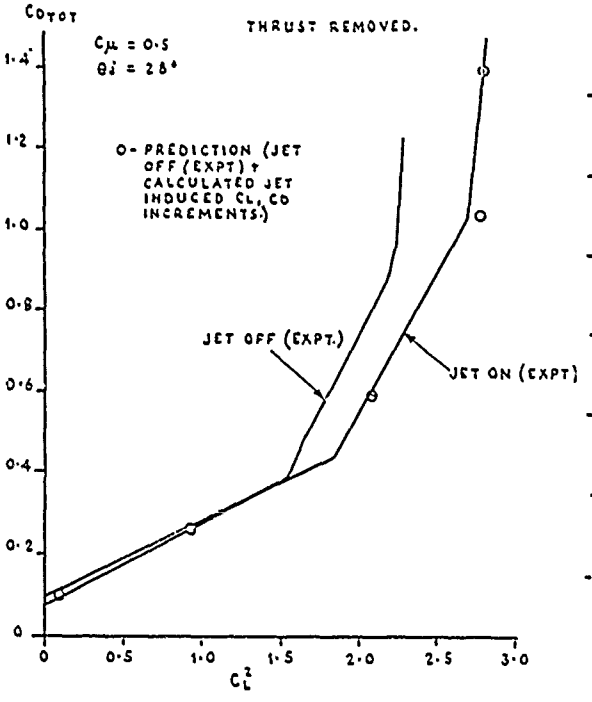

FIG 49 COMPARISON OF PREDICTED AND MEASURED JET INDUCED EFFECTS ON INDUCED DRAG POLAR

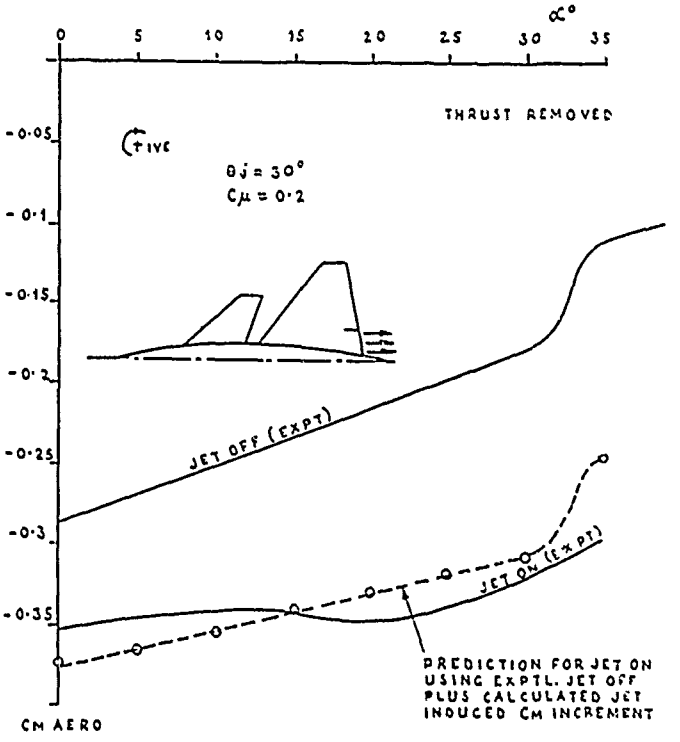

FIG. 50 COMPARISON OF PREDICTED AND MEASURED JET INDUCED PITCHING MOMENT

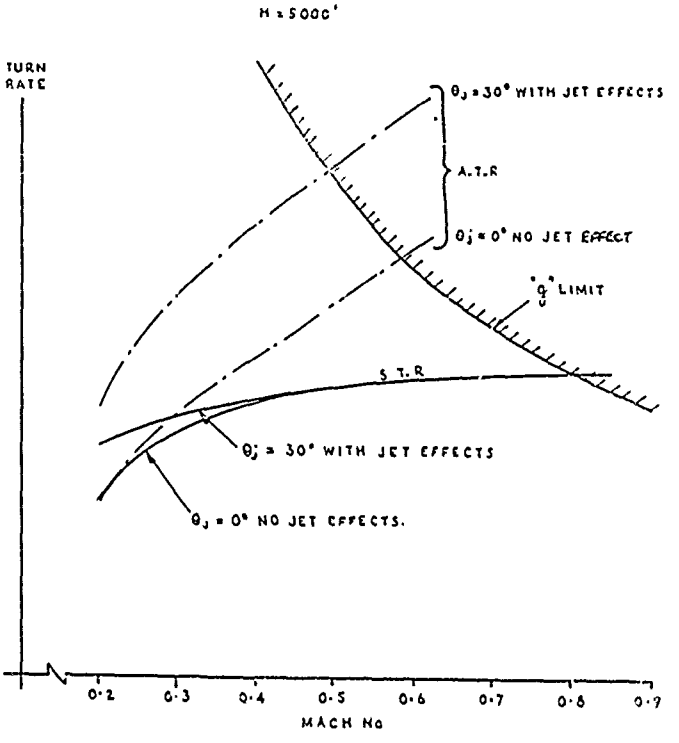

FIG 51 PREDICTED EFFECT OF JET ENHANCEMENT ON SUSTAINED/ATTAINED TURN RATE

IDEES NOUVELLES POUR LA CONCEPTION D'AVIONS FUTURS

par

Ph.Poisson-Quinton
ONERA
29 Ave de la Division Leclerc
92320 Châtillon, France

RESUME

Dans cette introduction préliminaire à la table ronde prévue sur la recherche de configurations nouvelles bénéficiant d'interférences aérodynamiques favorables, on passe en revue quelques formules nouvelles d'avions susceptibles d'être développées avec succès dans les prochaines années.

Ces configurations nouvelles bénéficieront de progrès majeurs réalisés non seulement en aérodynamique mais également dans les autres disciplines intéressant l'Aviation:

- Propulsion: meilleure intégration du moteur à la cellule,
- Structures/Matériaux: prise en compte de déformations aéroélastiques favorables,
  Electronique. introduction du contrôle actif pour l'optimisation de la configuration à l'ensemble de sa mission.

Ces progrès seront appliqués pour des objectifs différents suivant qu'il s'agit d'un avion de transport (optimisation à l'économie du vol) ou de combat (recherche de la manoeuvrabilité et de l'efficacité militaire).

En ce qui concerne *la forme géométrique de l'avion*:

l'utilisation d'un plan Canard proche de la voilure permet déjà de bénéficier d'une interaction tourbillonnaire favorable au vol à grande incidence pour un avion de combat, son rôle sera étendu aux controles directes de portance et de force latérale;

la mise en flèche inversée de la voilure permettra également de meilleurs performances aux grands angles, le risque de divergence structurale étant évité par l'emploi de matériaux composites fibreux convenablement orientés,

cette adaptation aéroélastique permise par les matériaux composites sera d'ailleurs etendue à l'optimisation de la cambrure et du vrillage, aussi bien pour l'aile élancée d'un avion de combat que pour celle de grand allongement sur un avion de transport, simultanément le risque de flottement structural sera contrôlé par volet actif lié à l'ordinateur de bord;

l'application de ce contrôle actif à la stabilisation artificielle de l'avion en longitudinal et en transversal va permettre de réduire sensiblement la dimension des empennages ou de développer la formule "ailes volantes", d'où réduction des traînées parasites et de frottement, pour des tonnages importants, il devient intéressant de rendre cette aile volante habitable, avec une répartition de la charge utile le long de l'envergure, d'où une sensible réduction de sa masse structurale;

la forme et l'emplacement des prises d'air, en particulier pour les avions de combat manoeuvrants, influent considérablement sur leurs performances et elles sont directement interactionnées par le champ de l'aile et/ou du fuselage, des emplacements inhabituels (et aérodynamiquement délicats) sont étudiés pour les rendre moins sensibles à la détection par l'adversaire.

En ce qui concerne *l'intégration du propulseur à la cellule*, de très nombreuses recherches sont actuellement entreprises pour réduire les interactions défavorables, mais aussi pour bénéficier d'interactions favorables liées à l'orientation variable du jet propulsif (effet "jet flap" pour l'hypersustentation).

Dans le domaine des avions de transport, il s'agit de choisir des emplacements de nacelles de turbo-fans qui ne provoquent pas d'interactions aérodynamiques défavorables avec l'aile en croisière transsonique, tout en bénéficiant de cet effet "jet flap" pour réduire les vitesses de décollage et d'atterrissage.

Un autre cas difficile d'interaction aérodynamique apparait également lorsqu'il faut étudier la mise en place d'hélices "transsoniques" adaptées au vol de croisière rapide (Mach de 0,7 à 0,8). les survitesses induites par leur flux sur la voilure doivent être minimisées à partir d'études théoriques et expérimentales sophistiquées, par ailleurs, l'hélice transsonique multipales très chargée pose des problèmes d'aérodynamique et d'aéroélasticité complexes nécessitant des études

pluridisciplinaires approfondies (aérodynamique/acoustique, structure/matériaux). Cependant, le coût/efficacité du développement d'une nouvelle génération d'avions à hélices, très économique d'utilisation, peut apparaitre intéressant au cours de la prochaine décennie.

Un second domaine de l'intégration du propulseur à la cellule concerne les avions de combat manoeuvrant, où une orientation variable de jet propulsif permet de faire participer le moteur à la sustentation de l'avion (et également à son freinage par inversion de poussée).

Ici encore on retrouve des problèmes de fortes interactions aérodynamiques avec les différentes parties de l'avion, dont l'étude théorique est encore peu avancée et l'expérimentation difficile, mais les avantages aérodynamiques apportés par ce concept peuvent être considérables; en particulier, lorsque le jet propulsif débouche à l'arrière de la voilure, on bénéficie d'une forte hypersustentation par effet "jet-flap" permettant d'améliorer les performances à basse vitesse (capacité STOL) et à grand vitesse (manoeuvrabilité accrue).

Un dernier aspect de l'utilisation d'un jet à l'amélioration de l'écoulement aérodynamique est le soufflage transversal par un jet orienté suivant l'envergure de l'aile qui permet d'engendrer une nappe tourbillonnaire bien organisée au-dessus de l'aile, créant ainsi une portance supplémentaire et retardant le décollement généralisé de la voilure aux grandes incidences; ce concept peut d'ailleurs être avantageusement utilisé chaque fois qu'il y a des zones d'écoulement décollé difficiles à résorber (diffuseurs de prises d'air, retreints, etc.).

REPORT DOCUMENTATION PAGE

1. Recipient's Reference	2. Originator's Reference	3. Further Reference	4. Security Classification of Document
	AGARD-R-712	ISBN 92-835-0332-5	UNCLASSIFIED

5. Originator: Advisory Group for Aerospace Research and Development
North Atlantic Treaty Organization
7 rue Ancelle, 92200 Neuilly sur Seine, France

6. Title: SPECIAL COURSE ON SUBSONIC/TRANSONIC AERODYNAMIC INTERFERENCE FOR AIRCRAFT

7. Presented at:

8. Author(s)/Editor(s)	9. Date
Various	July 1983
10. Author's/Editor's Address	**11. Pages**
Various	294

12. Distribution Statement: This document is distributed in accordance with AGARD policies and regulations, which are outlined on the Outside Back Covers of all AGARD publications.

13. Keywords/Descriptors

Aerodynamics	Aerodynamic configurations
Subsonic characteristics	Commercial aircraft
Transonic characteristics	Military aircraft

14. Abstract

The present Special Course was a follow-up of an AGARD Fluid Dynamics Panel Symposium on Subsonic/Transonic Configuration Aerodynamics held in Neubiberg (Munich) in May 1980. The emphasis of the course was on the configuration optimization in the transonic regime were both military and commercial aircraft must cruise efficiently and where military aircraft must maneuver in an agile but stable manner. The course material has been updated and was presented in a more structured fashion emphasizing the fluid dynamic interference mechanisms that are the keys to the optimization. In addition some aspects of subcritical interference were also covered including those arising in the takeoff and landing phase of the flight with high lift devices deployed.

Lectures 1 to 5 form background material describing the computational and testing tools.

Lectures 6 to 14 cover the whole range of interference phenomena arising in the optimization of both military and commercial aircraft starting from the simple airfoil and wing and extending to the complete configuration.

The material assembled in this book was prepared under the combined sponsorship of the Fluid Dynamics Panel, the von Kármán Institute and the Consultant and Exchange Program of AGARD and was presented as an AGARD Special Course at the von Kármán Institute, Rhode-St-Genèse, Belgium on 2–6 May 1983 and at the Wright-Patterson Air Force Base, Ohio on 16–20 May 1983.

AGARD Report No.712 Advisory Group for Aerospace Research and Development, NATO SPECIAL COURSE ON SUBSONIC/TRANSONIC AERODYNAMIC INTERFERENCE FOR AIRCRAFT Published July 1983 294 pages The present Special Course was a follow-up of an AGARD Fluid Dynamics Panel Symposium on Subsonic/Transonic Configuration Aerodynamics held in Neubiberg (Munich) in May 1980. The emphasis of the course was on the configuration optimization in the transonic regime where both military and commercial aircraft must cruise efficiently and where military aircraft must maneuver in an agile but stable manner. The P.T.O	AGARD-R-712 Aerodynamics Subsonic characteristics Transonic characteristics Aerodynamic configurations Commercial aircraft Military aircraft	AGARD Report No.712 Advisory Group for Aerospace Research and Development, NATO SPECIAL COURSE ON SUBSONIC/TRANSONIC AERODYNAMIC INTERFERENCE FOR AIRCRAFT Published July 1983 294 pages The present Special Course was a follow-up of an AGARD Fluid Dynamics Panel Symposium on Subsonic/Transonic Configuration Aerodynamics held in Neubiberg (Munich) in May 1980. The emphasis of the course was on the configuration optimization in the transonic regime where both military and commercial aircraft must cruise efficiently and where military aircraft must maneuver in an agile but stable manner. The P.T.O	AGARD-R-712 Aerodynamics Subsonic characteristics Transonic characteristics Aerodynamic configurations Commercial aircraft Military aircraft
AGARD Report No.712 Advisory Group for Aerospace Research and Development, NATO SPECIAL COURSE ON SUBSONIC/TRANSONIC AERODYNAMIC INTERFERENCE FOR AIRCRAFT Published July 1983 294 pages The present Special Course was a follow-up of an AGARD Fluid Dynamics Panel Symposium on Subsonic/Transonic Configuration Aerodynamics held in Neubiberg (Munich) in May 1980. The emphasis of the course was on the configuration optimization in the transonic regime where both military and commercial aircraft must cruise efficiently and where military aircraft must maneuver in an agile but stable manner. The P.T.O	AGARD-R-712 Aerodynamics Subsonic characteristics Transonic characteristics Aerodynamic configurations Commercial aircraft Military aircraft	AGARD Report No.712 Advisory Group for Aerospace Research and Development, NATO SPECIAL COURSE ON SUBSONIC/TRANSONIC AERODYNAMIC INTERFERENCE FOR AIRCRAFT Published July 1983 294 pages The present Special Course was a follow-up of an AGARD Fluid Dynamics Panel Symposium on Subsonic/Transonic Configuration Aerodynamics held in Neubiberg (Munich) in May 1980. The emphasis of the course was on the configuration optimization in the transonic regime where both military and commercial aircraft must cruise efficiently and where military aircraft must maneuver in an agile but stable manner. The P.T.O	AGARD-R-712 Aerodynamics Subsonic characteristics Transonic characteristics Aerodynamic configurations Commercial aircraft Military aircraft

AGARD Report No.712 Advisory Group for Aerospace Research and Development, NATO SPECIAL COURSE ON SUBSONIC/TRANSONIC AERODYNAMIC INTERFERENCE FOR AIRCRAFT Published July 1983 294 pages The present Special Course was a follow-up of an AGARD Fluid Dynamics Panel Symposium on Subsonic/Transonic Configuration Aerodynamics held in Neubiberg (Munich) in May 1980. The emphasis of the course was on the configuration optimization in the transonic regime where both military and commercial aircraft must cruise efficiently and where military aircraft must maneuver in an agile but stable manner. The P.T.O	AGARD-R-712 Aerodynamics Subsonic characteristics Transonic characteristics Aerodynamic configurations Commercial aircraft Military aircraft	AGARD Report No.712 Advisory Group for Aerospace Research and Development, NATO SPECIAL COURSE ON SUBSONIC/TRANSONIC AERODYNAMIC INTERFERENCE FOR AIRCRAFT Published July 1983 294 pages The present Special Course was a follow-up of an AGARD Fluid Dynamics Panel Symposium on Subsonic/Transonic Configuration Aerodynamics held in Neubiberg (Munich) in May 1980. The emphasis of the course was on the configuration optimization in the transonic regime where both military and commercial aircraft must cruise efficiently and where military aircraft must maneuver in an agile but stable manner. The P.T.O	AGARD-R-712 Aerodynamics Subsonic characteristics Transonic characteristics Aerodynamic configurations Commercial aircraft Military aircraft
AGARD Report No.712 Advisory Group for Aerospace Research and Development, NATO SPECIAL COURSE ON SUBSONIC/TRANSONIC AERODYNAMIC INTERFERENCE FOR AIRCRAFT Published July 1983 294 pages The present Special Course was a follow-up of an AGARD Fluid Dynamics Panel Symposium on Subsonic/Transonic Configuration Aerodynamics held in Neubiberg (Munich) in May 1980. The emphasis of the course was on the configuration optimization in the transonic regime where both military and commercial aircraft must cruise efficiently and where military aircraft must maneuver in an agile but stable manner. The P T.O	AGARD-R-712 Aerodynamics Subsonic characteristics Transonic characteristics Aerodynamic configurations Commercial aircraft Military aircraft	AGARD Report No.712 Advisory Group for Aerospace Research and Development, NATO SPECIAL COURSE ON SUBSONIC/TRANSONIC AERODYNAMIC INTERFERENCE FOR AIRCRAFT Published July 1983 294 pages The present Special Course was a follow-up of an AGARD Fluid Dynamics Panel Symposium on Subsonic/Transonic Configuration Aerodynamics held in Neubiberg (Munich) in May 1980. The emphasis of the course was on the configuration optimization in the transonic regime where both military and commercial aircraft must cruise efficiently and where military aircraft must maneuver in an agile but stable manner. The P.T.O	AGARD-R-712 Aerodynamics Subsonic characteristics Transonic characteristics Aerodynamic configurations Commercial aircraft Military aircraft

course material has been updated and was presented in a more structured fashion emphasizing the fluid dynamic interference mechanisms that are the keys to the optimization. In addition some aspects of subcritical interference were also covered including those arising in the takeoff and landing phase of the flight with high lift devices deployed.

Lectures 1 to 5 form background material describing the computational and testing tools.

Lectures 6 to 14 cover the wide range of interference phenomena arising in the optimization of both military and commercial aircraft starting from the simple airfoil and wing and extending to the complete configuration.

The material assembled in this book was prepared under the combined sponsorship of the Fluid Dynamics Panel, the von Kármán Institute and the Consultant and Exchange Program of AGARD and was presented as an AGARD Special course at the von Kármán Institute, Rhode-St-Genèse, Belgium on 2–6 May 1983 and at the Wright-Patterson Air Force Base, Ohio on 16–20 May 1983.

ISBN 92-835-0332-5

course material has been updated and was presented in a more structured fashion emphasizing the fluid dynamic interference mechanisms that are the keys to the optimization. In addition some aspects of subcritical interference were also covered including those arising in the takeoff and landing phase of the flight with high lift devices deployed.

Lectures 1 to 5 form background material describing the computational and testing tools.

Lectures 6 to 14 cover the wide range of interference phenomena arising in the optimization of both military and commercial aircraft starting from the simple airfoil and wing and extending to the complete configuration.

The material assembled in this book was prepared under the combined sponsorship of the Fluid Dynamics Panel, the von Kármán Institute and the Consultant and Exchange Program of AGARD and was presented as an AGARD Special course at the von Kármán Institute, Rhode-St-Genèse, Belgium on 2–6 May 1983 and at the Wright-Patterson Air Force Base, Ohio on 16–20 May 1983.

ISBN 92-835-0332-5

course material has been updated and was presented in a more structured fashion emphasizing the fluid dynamic interference mechanisms that are the keys to the optimization. In addition some aspects of subcritical interference were also covered including those arising in the takeoff and landing phase of the flight with high lift devices deployed.

Lectures 1 to 5 form background material describing the computational and testing tools.

Lectures 6 to 14 cover the wide range of interference phenomena arising in the optimization of both military and commercial aircraft starting from the simple airfoil and wing and extending to the complete configuration.

The material assembled in this book was prepared under the combined sponsorship of the Fluid Dynamics Panel, the von Kármán Institute and the Consultant and Exchange Program of AGARD and was presented as an AGARD Special course at the von Kármán Institute, Rhode-St-Genèse, Belgium on 2–6 May 1983 and at the Wright-Patterson Air Force Base, Ohio on 16–20 May 1983.

ISBN 92-835-0332-5

course material has been updated and was presented in a more structured fashion emphasizing the fluid dynamic interference mechanisms that are the keys to the optimization. In addition some aspects of subcritical interference were also covered including those arising in the takeoff and landing phase of the flight with high lift devices deployed.

Lectures 1 to 5 form background material describing the computational and testing tools.

Lectures 6 to 14 cover the wide range of interference phenomena arising in the optimization of both military and commercial aircraft starting from the simple airfoil and wing and extending to the complete configuration.

The material assembled in this book was prepared under the combined sponsorship of the Fluid Dynamics Panel, the von Kármán Institute and the Consultant and Exchange Program of AGARD and was presented as an AGARD Special course at the von Kármán Institute, Rhode-St-Genèse, Belgium on 2–6 May 1983 and at the Wright-Patterson Air Force Base, Ohio on 16–20 May 1983.

ISBN 92-835-0332-5

AGARD
NATO OTAN
7 RUE ANCELLE · 92200 NEUILLY-SUR-SEINE
FRANCE
Telephone 745.08.10 · Telex 610176

DISTRIBUTION OF UNCLASSIFIED AGARD PUBLICATIONS

AGARD does NOT hold stocks of AGARD publications at the above address for general distribution. Initial distribution of AGARD publications is made to AGARD Member Nations through the following National Distribution Centres. Further copies are sometimes available from the National Centres, but if not may be purchased in Microfiche or Photocopy form from the Purchase Agencies listed below

NATIONAL DISTRIBUTION CENTRES

BELGIUM
Coordonn
Etat-Majo
Quartier I
Rue d'Ev

CANADA
Defence
Departr
Ottawa

DENMARK
Danisl
Østerl
Cope

FRANCE
O.N
29,
922

GERMA
Fa
Phy...
Kernforschungszen...
D-7514 Eggenstein-Leopoldshafen

GREECE
Hellenic Air Force General Staff
Research and Development Directorate
Holargos, Athens

ICELAND
Director of Aviation
c/o Flugrad
Reykjavik

ITALY
Aeronautica Militare
...Delegato Nazionale all'AGARD

...hment

...e

TUR...
Department of ... ...velopment (ARGE)
Ministry of National Defence, Ankara

UNITED KINGDOM
Defence Research Information Centre
Station Square House
St. Mary Cray
Orpington, Kent BR5 3RE

UNITED STATES
National Aeronautics and Space Administration (NASA)
Langley Field, Virginia 23365
Attn: Report Distribution and Storage Unit

THE UNITED STATES NATIONAL DISTRIBUTION CENTRE (NASA) DOES NOT HOLD STOCKS OF AGARD PUBLICATIONS, AND APPLICATIONS FOR COPIES SHOULD BE MADE DIRECT TO THE NATIONAL TECHNICAL INFORMATION SERVICE (NTIS) AT THE ADDRESS BELOW.

PURCHASE AGENCIES

Microfiche or Photocopy

National Technical
Information Service (NTIS)
5285 Port Royal Road
Springfield
Virginia 22161, USA

Microfiche

Space Documentation Service
European Space Agency
10, rue Mario Nikis
75015 Paris, France

Microfiche or Photocopy

British Library Lending
Division
Boston Spa, Wetherby
West Yorkshire LS23 7BQ
England

Requests for microfiche or photocopies of AGARD documents should include the AGARD serial number, title, author or editor, and publication date. Requests to NTIS should include the NASA accession report number. Full bibliographical references and abstracts of AGARD publications are given in the following journals:

Scientific and Technical Aerospace Reports (STAR)
published by NASA Scientific and Technical
Information Facility
Post Office Box 8757
Baltimore/Washington International Airport
Maryland 21240, USA

Government Reports Announcements (GRA)
published by the National Technical
Information Services, Springfield
Virginia 22161, USA

Printed by Specialised Printing Services Limited
40 Chigwell Lane, Loughton, Essex IG10 3TZ

ISBN 92-835-0332-5